

UNIVERSITY OF
BIRMINGHAM

DRILLING OF CARBON FIBRE REINFORCED PLASTIC (CFRP) AND METAL MATRIX COMPOSITES (MMC)

by

MAOJUN LI

A thesis submitted to
The University of Birmingham
for the degree of
DOCTOR OF PHILOSOPHY

School of Mechanical Engineering
College of Engineering and Physical Sciences
The University of Birmingham
November 2014

UNIVERSITY OF
BIRMINGHAM

University of Birmingham Research Archive

e-theses repository

This unpublished thesis/dissertation is copyright of the author and/or third parties. The intellectual property rights of the author or third parties in respect of this work are as defined by The Copyright Designs and Patents Act 1988 or as modified by any successor legislation.

Any use made of information contained in this thesis/dissertation must be in accordance with that legislation and must be properly acknowledged. Further distribution or reproduction in any format is prohibited without the permission of the copyright holder.

SYNOPSIS

Three main phases of experimental work were conducted to evaluate the drilling of carbon fibre reinforced plastic (CFRP) and Al/SiCp metal matrix composite (MMC) workpiece materials following a comprehensive literature review. The latter focused on current state-of-the-art relating to machinability of both CFRP and MMCs, with high tool wear rates found to be a prevailing challenge due to the abrasive nature of the composite materials. Fibre pull out, matrix burning / degradation, hole entry / exit delamination as well as uncut fibres were the typical damage modes observed following cutting of CFRP. In contrast, workpiece material adhesion, built up edge, poor surface roughness due to pits and voids together with subsurface damage were the primary issues encountered when machining MMCs. The performance of various cutting tool materials such as tungsten carbide (WC) and polycrystalline diamond (PCD) as well as coatings including hardmetal (e.g. TiN, TiCN and TiAlN), CVD-diamond and diamond like carbon (DLC) have been assessed for machining CFRP and MMC materials.

The first phase of experiments was divided into 2 sections, with Phase 1A studying the influence of operating conditions (cutting speed, feed rate and cutting environment) and tool materials / coatings when drilling CFRP using a Taguchi fractional factorial experimental design (L12). Advanced CVD-diamond coated tungsten carbide (WC) and novel domed PCD drills were benchmarked against uncoated WC tools. Both the diamond coated and domed PCD drills achieved 512 holes with corresponding minimum flank wear of 111 and 73 µm respectively, while the uncoated WC tools suffered severe tool wear in the form of cutting edge rounding after machining < ~200 holes, leading to burning of fibre dust and matrix materials. In general, the domed PCD tools produced holes with low delamination levels, clean hole edges and superior surface integrity compared with the CVD-diamond coated tools due to the greater wear resistance and smaller cutting edge radius (4.6 µm vs. 23.8 µm for new tool) in the former. Uncut fibres hanging across the hole exit was however prevalent at test cessation irrespective of tool materials and operating conditions. According to statistical analysis for flank wear, tool material / coating, cutting speed and feed rate were the main contributing factors with percentage contribution ratios (PCR) of 77.4%, 3.8% and 16.5%, respectively.

Phase 1B (preliminary / benchmarking) and Phase 2A work investigated the effect of varying feed rate strategy (feed rate reduced to 0.01 mm/rev for final 2 mm of hole) on tool

life and hole quality when drilling CFRP. The 'critical' thrust force at hole exit ranged between 100 and ~120 N as feed rate was constant (0.01 mm/rev) in the final 2 mm of drilling operations in all tests, and decreased by up to ~80% compared with the maximum thrust force recorded when using the primary feed rate (0.1-0.3 mm/rev) in the initial drilling stage. When applying the variable feed rate strategy, uncut fibres were significantly reduced (~30%) at hole exit compared to results in Phase 1A at the same cutting parameters. In addition, hole surface quality near the exit location improved with limited voids / fibre pull out observed when utilising new tools. In Phase 2B experiments, the effect of workpiece layup configuration / fibre orientation and elevated feed rates (up to 0.6 mm/rev) were evaluated with respect to hole quality and surface integrity. Results indicated that drilling at feed rates of up to 0.4 mm/rev together with the variable feed rate strategy was feasible without exacerbating hole damage and compromising surface integrity. Cavities / flaws due to fibre loss / pull out were largely observed in plies orientated at 135º while 0º, 45º and 90º plies were generally free of damage for the sections analysed. Surprisingly, surface damage was also evident at the exit location despite the use of reduced feed rate (0.01mm/rev) at test cessation, which suggested that tool wear / edge sharpness rather than feed rate was the dominant factor affecting hole surface quality. Evaluation of CVD-diamond coated and domed PCD tools when drilling CFRP at elevated / high cutting speeds of up to 280 and 360 m/min respectively was undertaken in Phase 2C trials. Flank wear on the CVD-diamond coated and PCD drills was lower by 26% (~86 µm) and 11% (~71µm) respectively after 384 holes when machining at the higher cutting speeds compared to 180 m/min (117 and 80 µm). Chatter / vibration was observed up to ~2.5 mm beneath hole entry when operating at high cutting speed (>240 m/min) using CVD-diamond coated drills resulting in deposition / adhesion of fibre dust on the hole surface.

Phase 3A research involved an evaluation of the performance of tool materials and coatings including uncoated and TiAlN+TiN coated WC as well as brazed PCD tools when drilling Al/SiCp MMC's at varying cutting speed and feed rate. The brazed PCD tools showed superior performance compared to both the uncoated and coated WC drills in terms of tool wear, productivity, hole quality and surface integrity. The hardmetal coating provided no appreciable benefits over the uncoated WC drills as both only lasted for ~10 holes (VB_{max} at 300 µm), while flank wear of the PCD drills was only ~60 µm after machining 300 holes. The influence of cutting speed (80 and 160 m/min) and feed rate (0.1 and 0.2 mm/rev) under high pressure (70 bar) and low pressure flood (3 bar) coolant environments using brazed and domed PCD drills were assessed in Phase 3B. In general, brazed PCD drills exhibited lower

flank wear levels (up to 38 µm) compared with the domed products, which was most likely due to the protection offered by the formation of a stable built up edge (BUE) at the cutting lips in the former. Conversely, the domed PCD drills produced holes with superior geometrical accuracy with relatively lower burr heights (~60 µm) at hole exit. Surface integrity analysis showed that workpiece microhardness increase was between 50 and 60 $HV_{0.05}$ above the bulk hardness (~125 $HV_{0.05}$) irrespective of cutting parameters, which extended up to ~100 µm beneath the machined surface. Hole surfaces were generally smooth (<0.51 µm Ra) with limited damage in the form of smearing, voids / cavities in all tests, although minor vibration / chatter marks were visible in holes produced using brazed PCD drills. Based on results from Phase 3B, the impact of elevated cutting speed of up to 360 m/min on the performance of brazed PCD tools when drilling MMCs was assessed in Phase 3C. Differences in tool flank wear in all tests was marginal with maximum deviation of ~17 µm after drilling 300 holes. Built up edge however was prevalent even from the first hole. The difference in thrust force was limited to 14 N (~4%) while torque values were constant at ~115 N.cm, irrespective of cutting parameters. Drilling at higher cutting speeds (>160 m/min) did not improve surface roughness in terms of Ra, although both Rt and Rz values increased with cutting speed possibly due to the loss / pull out of SiC particles. Irregular exit burrs occurred randomly when operating at 360 m/min.

ACKNOWLEDGEMENTS

First and foremost, the author would like to thank Dr. Sein Leung Soo (Senior Lecturer and Head of the Machining Research Group) and Professor David Keith Aspinwall, both in the School of Mechanical Engineering, University of Birmingham for their dedicated academic supervision and guidance over the course of the research. Thanks are also due to Dr. Richard Hood (Lecturer) and Elaine Aspinwall (Honorary Senior Lecturer) for their generous time and help relating to test setup, statistical experimental design and subsequent analysis.

My sincerest appreciation is due to Andy Loat (Technical Engineer in the Machining Research Group), Richard Fasham (formerly Senior Technical Engineer) and other technical staff within the School of Mechanical Engineering for their invaluable assistance with the experimental work, preparation of workpiece materials and equipment maintenance. I would also like to thank members of the Machining Research Group for the useful discussions and generous counsel as well as kind friendship over the past few years.

Special thanks go to David Pearson (Seco Tools, UK) and Dr. Wayne Leahy (Element Six Ltd.) for their helpful technical communications as well as provision of fabricated drills and PCD tool materials for the research. Thanks are also due to the School of Mechanical Engineering, University of Birmingham for the provision a PhD studentship and partial stipend.

Last but certainly not least, I would like to express my deepest love and gratitude to my parents and sister for their unflinching support, endless encouragement and understanding throughout my PhD studies.

TABLE OF CONTENTS

SYNOPSIS II
ACKNOWLEDGEMENTS V
TABLE OF CONTENTS VI
LIST OF FIGURES XI
LIST OF TABLES XXI
NOMENCLATURE XXII
Chapter 1: INTRODUCTION 1
1.1 Background to the project 1
1.2 Project collaborators 2
1.3 Aims and objectives 2
Chapter 2: LITERATURE REVIEW 3
2.1 Carbon fibre reinforced plastic (CFRP) composites 3
2.1.1 Introduction and properties 3
2.1.2 Industrial applications 9
2.2 Metal matrix composites (MMCs) 11
2.2.1 Introduction and properties 11
2.2.2 Industrial applications 14
2.3 Ceramic matrix composites (CMCs) 16
2.3.1 Introduction and properties 16
2.3.2 Industrial applications 17
2.4 Drilling of CFRP composite materials 18
2.4.1 Introduction 18
2.4.2 Tool wear and life 19
2.4.3 Thrust force, torque and cutting temperature 23
2.4.4 Drilled hole geometrical accuracy and surface integrity 28
2.4.5 Non-conventional hole making processes 34
2.5 Machining of MMC materials 37
2.5.1 Introduction 37
2.5.2 Tool wear and life 38
2.5.3 Cutting conditions 42
2.5.4 Chip formation and surface integrity 45

2.5.5 Non-conventional machining processes....51
2.6 Cutting tool materials / coatings....52
2.6.1 Introduction....52
2.6.2 Cutting tools used for drilling CFRP composite materials....53
2.6.3 Cutting tools used for machining MMC materials....55
Chapter 3: EXPERIMENTAL WORK....59
3.1 Workpiece materials....59
3.1.1 Carbon fibre reinforced plastics (CFRP) used in Phase 1 and 2....59
3.1.2 Metal matrix composites (MMCs) used in Phase 3....62
3.2 Equipment....64
3.2.1 Machining centre and fixtures....64
3.2.2 Chilled air and cutting fluid application....65
3.2.3 Tool wear / life evaluation analysis....66
3.2.4 Force and torque measurement....67
3.2.5 Hole entry and exit delamination analysis....68
3.2.5 Workpiece geometrical accuracy measurement....69
3.2.6 Workpiece surface roughness and integrity assessment....70
3.3 Tool geometries, materials and coatings....72
3.3.1 Tools used for drilling CFRP....72
3.3.1.1 CVD-diamond coated drills....72
3.3.1.2 Uncoated drills....73
3.3.1.3 Domed PCD drills....74
3.3.2 Tools used for drilling MMCs....76
3.3.2.1 Uncoated and TiAlN+TiN coated drills....76
3.3.2.2 PCD drills....77
3.4 Experimental design, procedures and test arrays....79
3.4.1 Phase 1A: Influence of operating conditions and tool materials / coatings when drilling CFRP....79
3.4.2 Phase 1B: Preliminary / benchmarking trials in drilling CFRP with variable feed rate operation....81
3.4.3 Phase 2A: Evaluation of hole quality when drilling CFRP with variable feed rate operation....82

3.4.4 Phase 2B: Influence of workpiece configuration / fibre orientation and elevated feed rates on hole quality when drilling CFRP 83

3.4.5 Phase 2C: Evaluation of diamond coated and domed PCD tools when drilling CFRP at elevated / high cutting speeds 85

3.4.6 Phase 3A: Preliminary / benchmarking trials in drilling MMCs with different tool materials / coatings 87

3.4.7 Phase 3B: Evaluation of PCD tools and cutting parameters when drilling MMCs 89

3.4.8 Phase 3C: Drilling of MMC using PCD tools at elevated / high cutting speeds 90

Chapter 4: RESULTS AND DISCUSSION 91

4.1 Phase 1A: Influence of operating conditions and tool materials / coatings when drilling CFRP 91

4.1.1 Tool wear and life 91

4.1.2 Cutting edge radius 96

4.1.3 Thrust force and torque 99

4.1.4 Hole entry and exit quality 105

4.1.5 Hole size and geometrical accuracy measurement 109

4.1.6 Hole surface integrity analysis 112

4.1.7 Chip analysis 115

4.1.8 Confirmation test 117

4.2 Phase 1B: Preliminary / benchmarking trials in drilling CFRP with variable feed rate operation. 118

4.2.1 Thrust force and torque 118

4.2.2 Hole exit quality 120

4.3 Phase 2A: Evaluation of hole quality when drilling CFRP with variable feed rate operation 123

4.3.1 Tool wear and life 123

4.3.2 Thrust force and torque 124

4.3.3 Hole entry and exit quality 127

4.3.4 Hole size 130

4.3.5 Hole surface integrity analysis 130

4.4 Phase 2B: Influence of workpiece configuration / fibre orientation and elevated feed rates on hole quality when drilling CFRP 132

4.4.1 Tool wear and life 132

4.4.2 Thrust force and torque 133

4.4.3 Hole entry and exit quality 136
4.4.4 Effect of fibre cutting angle on workpiece delamination / uncut fibre damage 138
4.4.5 Two and three dimensional (2D and 3D) surface topography analysis 139
4.4.6 Hole size, out of roundness and cylindricity 143
4.4.7 Hole surface integrity analysis 146
4.5 Phase 2C: Evaluation of diamond coated and domed PCD tools when drilling CFRP at elevated / high cutting speeds 150
4.5.1 Tool wear and life 150
4.5.2 Thrust force and torque 152
4.5.3 Hole entry and exit quality 154
4.5.4 Hole roundness and cylindricity 156
4.5.5 Hole surface integrity analysis 157
4.6 Phase 3A: Preliminary / benchmarking trials in drilling MMCs with different tool materials / coatings 161
4.6.1 Tool wear and life 161
4.6.2 Thrust force and torque 164
4.6.3 Hole entry and exit quality 166
4.6.4 Chip analysis 166
4.6.5 Hole geometrical accuracy 169
4.6.6 Hole surface integrity analysis 170
4.7 Phase 3B: Evaluation of PCD tools and cutting parameters when drilling MMCs 172
4.7.1 Tool wear and life 172
4.7.2 Thrust force and torque 175
4.7.3 Burr size and morphology 178
4.7.4 Chip morphology 180
4.7.5 Hole size and geometrical accuracy 182
4.7.6 Microhardness analysis 184
4.7.7 Surface roughness analysis 185
4.7.8 Hole surface integrity analysis 187
4.8 Phase 3C: Drilling of MMCs using PCD tools at elevated / high cutting speeds 190
4.8.1 Tool wear / life, thrust forces and torque 190

4.8.2 Surface roughness analysis 192
4.8.3 Microhardness analysis 193
4.8.4 Hole edge quality 194
4.8.5 Chip morphology 196
4.8.6 Hole surface integrity analysis 197
Chapter 5: CONCLUSIONS 200
5.1 Literature review 200
5.1.1 Drilling of CFRP 200
5.1.2 Machining of MMCs materials 200
5.2 Experimental work – drilling of CFRP composites 201
5.2.1 Phase 1A: Influence of operating conditions and tool materials / coatings when drilling CFRP 201
5.2.2 Phase 1B and 2A: Evaluation of hole quality when drilling CFRP with variable feed rate operation 202
5.2.3 Phase 2B: Influence of workpiece configuration / fibre orientation and elevated feed rates on hole quality when drilling CFRP 203
5.2.4 Phase 2C: Evaluation of diamond coated and domed PCD tools when drilling CFRP at elevated / high cutting speeds 204
5.3 Experimental work – drilling of MMCs mateirals 205
5.3.1 Phase 3A: Preliminary / benchmarking trials in drilling MMCs with different tool materials / coatings 205
5.3.2 Phase 3B: Evaluation of domed PCD tools and cutting parameters when drilling MMCs 206
5.3.3 Phase 3C: Drilling of MMC using PCD tools at elevated / high cutting speeds 207
5.4 Overall conclusions and recommended operating conditions 208
5.4.1 Drilling of carbon fibre reinforced plastic composite materials 208
5.4.2 Drilling of metal matrix composite materials 209
Chapter 6: RECOMMENDATIONS FOR FUTURE WORK 211
REFERENCES 212
APPENDIX A 224
APPENDIX B 225
APPENDIX C 226
APPENDIX D 232

LIST OF FIGURES

Figure 2.1:	(a) Schematic of a prepreg, (b) setup in an autoclave to fabricate laminated composite, (c) lay up of plies with different fibre orientation and (d, e) micrographs of plies with different fibre orientation [7]	7
Figure 2.2:	Change in composite application in aircraft over time[12]	9
Figure 2.3:	CFRP composite components used in Airbus A380 airplane (courtesy of Airbus)	10
Figure 2.4:	Composite materials used in Boeing 787 Dreamliner airplane (courtesy of Boeing)	10
Figure 2.5:	Composite fan blades used for GEnx-1B engine which powers Boeing's Dreamliner 787 (maximum diameter: ~2822mm) (courtesy of General Electric Co.)	11
Figure 2.6:	Stress-strain curves for (a) variable volume fractions of SiC particles (6 μm) in Al matrix and (b) different particle sizes in a fixed volume fraction (20% by volume) [7]	13
Figure 2.7:	Schematic of the spray deposition and forming process to fabricate metal matrix composites [7]	14
Figure 2.8:	Discontinuously reinforced MMCs for electronic packaging applications: (a) SiCp/Al electronic package for a remote power controller (photo courtesy of Lockheed Martin Corporation) and (b) cast SiCp/Al components (photo courtesy of MMCC. Inc.) [19]	15
Figure 2.9:	Racing motorcycle brakes made from MMCs (photo courtesy of Swan Metal Composites)	15
Figure 2.10:	Development of high temperature materials for turbine components [31]	17
Figure 2.11:	Major ceramic matrix composites components used for automotive ceramic gas turbine [34]	18
Figure 2.12:	SEM micrographs of tool wear at the cutting speed of 235 m/min and feed rate of 0.1 mm/rev: (a) aggressive abrasive wear at chisel edge, (b) abrasion of flank wear, (c) corner edge rounding and (d) adhesion of carbon fibres on the flank face [43]	20
Figure 2.13:	Tool wear at the cutting speed of 179 m/min and feed rate of 0.05 rev under the observation of (a) tool maker microscope and (b) SEM [44]	20
Figure 2.14:	SEM micrographs of tool wear after drilling 1728 holes at a cutting speed of 200 m/min and feed rate of (a) 0.04 mm/rev and (b) 0.1 mm/rev [46]	21

Figure 2.15:	Delamination at hole exit with corresponding cutting edge radius [50]	21
Figure 2.16:	Delamination as a function of tool cutting edge radius [51]	22
Figure 2.17:	(a) Cutting edge profile of uncoated carbide drill corresponding to number of drilled holes and (b) SEM micrographs of cutting edge of AlTiN coated drill [49]	22
Figure 2.18:	(a) Variations of maximum thrust force and (b) torque against number of drilled holes with different tool materials and cutting conditions [42]	24
Figure 2.19:	Schematic showing drilling tools: (a) standard twist drill and (b) double cone tool type M2 [61]	25
Figure 2.20:	Progression of thrust force against number of drilled holes [61]	25
Figure 2.21:	Experimental setup for temperature measurement [62]	26
Figure 2.22:	Cutting temperature and feed force when drilling CFRP at the feed rate of (a) 0.1 mm/rev and (b) 0.3 mm/rev [62]	27
Figure 2.23:	Experimental setup for temperature measurement using pyrometer [66]	27
Figure 2.24:	Cutting temperature and feed force against cutting speed in drilling CFRP [66]	28
Figure 2.25:	Hole diameter variations in drilling CFRP/Al with different cutting specifications (A: Ø16 mm uncoated conventional drill; B: Ø15.4/16 mm uncoated, TiB_2 and diamond coated step drills) [67]	29
Figure 2.26:	SEM micrographs of surface damage [55]	31
Figure 2.27:	Entry and exit delamination at the cutting speed of 20 m/min [54]	31
Figure 2.28:	SEM micrographs with corresponding surface roughness profile showing delamination at (a) hole entrance and (b) hole exit [54]	32
Figure 2.29:	SEM micrographs with corresponding surface profiles produced by new and wore drill [83]	32
Figure 2.30:	Micrographs of hole surface layers in drilling CFRP [66]	33
Figure 2.31:	Micrographs of subsurface with various fibre orientations [85]	34
Figure 2.32:	(a-b) Schematic and kinematics of wobble milling, (c) double cone geometry of the hole after wobble milling [92]	35
Figure 2.33:	(a) Interior cracks and (b) HAZ induced by laser cutting [102]	36
Figure 2.34:	Thrust force comparison between conventional drilling and vibration assisted drilling [103]	37
Figure 2.35:	Characteristics / factors relating to the machinability of MMCs [20]	38
Figure 2.36:	Variation of tool wear against machining time at (a) feed rate of 0.1 mm/rev and (b) cutting speed of 300 m/min [120]	40
Figure 2.37:	SEM micrographs of tool wear after machining (a) Al-SiC/100 µm MMCs and (b) Al-SiC/45 µm MMCs at a cutting speed of 100 m/min	41

	and feed rate of 0.12 mm/rev [124]	
Figure 2.38:	Tool wear progression with variable cutting parameters (a) feed rate at 0.1 mm/rev and (b) cutting speed at 50 m/min [125]	41
Figure 2.39:	SEM micrographs of tool wear on rake face of PCD tool after removing BUE with NaOH solution (cutting speed: 670m/min, feed rate: 0.15 mm/rev, DOC: 1.5 mm) [128]	42
Figure 2.40:	Chip morphology of turning MMC with different feed rate (cutting speed: 400 m/min, DOC: 1 mm) [145]	46
Figure 2.41:	Chips produced at the cutting speed of 26.4 m/min and feed rate of 0.0635 mm/rev with (a) 20 vol.% MMCs, HSS drill, (b) 10 vol.% MMCs, carbide drill, (c) 20 vol.% MMCs, carbide drill, (d) 10 vol.% MMCs, PCD drill and (e) 20 vol.% MMCs, PCD drill [119]	47
Figure 2.42:	Chip morphology at different cutting speeds (feed rate: 0.2 mm/rev, DOC: 1 mm) [148]	48
Figure 2.43:	SEM micrographs of machined surface/sub-surface (cutting speed: 670 m/min, feed rate: 0.45 mm/rev, DOC: 1.5 mm): (a) overview topography, (b) voids around SiC particles, (c) pulled-out particles and (d) fractured SiC particles [151]	49
Figure 2.44:	SEM micrographs of machined sub-surface of 10% Al/Al_2O_3 MMCs with the average particle size of (a) 20 µm and (b) 9.5 µm [152]	50
Figure 2.45:	(a) Schematic of LAM experimental setup and (b) actual setup [156]	51
Figure 2.46:	Hardness and toughness relationship for cutting tool materials [12]	52
Figure 2.47:	Variations of maximum thrust force, torque and flank wear against number of holes drilled [168]	53
Figure 2.48:	SEM micrographs of inserts after turning Al-12 wt.% Si alloy for 1400 m with (a) thick diamond brazed and (b) chamfered diamond coated Si3N4 [183]	56
Figure 2.49:	Variations of surface roughness Ra against cutting distance in turning 20 vol.% Al-SiC MMCs with PCBN and PCD tools at the cutting speed of 400 m/min [187]	57
Figure 2.50:	Tool wear progression in turning MMCs with (a) CVD diamond coated inserts (feed rate: 0.2 mm/rev, DOC: 1 mm) and (b) brazed PCD inserts (feed rate: 0.1 mm/rev, DOC: 1 mm) [190]	58
Figure 3.1:	Optical and SEM micrographs of plies oriented at different orientations	61
Figure 3.2:	Dimension of workpiece specimens and schematic of drilled hole array	62
Figure 3.3:	Prepared MMCs workpieces for testing	63
Figure 3.4:	Optical micrograph of the workpiece before etching in (a) transverse	63

	and (b) longitudinal extrusion direction	
Figure 3.5:	Microstructure of workpiece materials after etching in (a) transverse and (b) longitudinal extrusion direction	64
Figure 3.6:	Matsuura FX-5 high speed machining centre	64
Figure 3.7:	(a) Fibre dust extractor and (b) high pressure pump system	65
Figure 3.8:	(a) Fixture was for securing CFRP and (b) clamping plate used for holding MMC workpieces	65
Figure 3.9:	(a) Chilled air generator and (b) working schematic	66
Figure 3.10:	(a) Tool wear measurement setup and (b) tilting table for accommodating tool holder	67
Figure 3.11:	(a) Alicona G4 InfiniteFocus (IF) microscope system and (b) setup for cutting edge radius measurement	67
Figure 3.12:	(a) Rotating dynamometer measuring system [193], (b) rotating dynamometer and (c) multichannel signal conditioner	68
Figure 3.13:	(a) Force and torque measurement setup and (b) Kistler 5011 charge amplifiers	68
Figure 3.14:	Hole delamination measurement	69
Figure 3.15:	(a) Taylor Hobson Talyrond series 300 and (b) setup for hole geometrical accuracy assessment of strip sample	69
Figure 3.16:	Illustration of (a) EXTEC Labcut 300 disc cutting machine, (b) Buehler grinder/polisher and (c) Leica DMLM microscope	70
Figure 3.17:	Illustration of (a) JEOL 6060 SEM and (b) Emscop SC500 gold sputter	71
Figure 3.18:	Illustration of (a) Taylor Hobson Form Talysurf series 120 L and (b) Mitutoyo MVK-H1 Vickers microhardness tester	72
Figure 3.19:	(a) Dimensions [198] and (b) image of Seco CVD-diamond coated C1 geometry drill	73
Figure 3.20:	CVD-diamond coated drill tip: (a) side view, (b) end view and (c) cutting lip	73
Figure 3.21:	Microstructure of WC tool material used for uncoated C1 geometry drill [199]	74
Figure 3.22:	Image of Seco uncoated WC C1 geometry drill	74
Figure 3.23:	Uncoated Seco C1 geometry drill tip: (a) side view, (b) end view and (c) cutting lip	74
Figure 3.24:	Image of Seco domed PCD CX1 geometry drill	75
Figure 3.25:	Seco domed PCD CX1 geometry drill tip: (a) side view, (b) end view and (c) cutting lip	75
Figure 3.26:	Microstructure CTM302 grade PCD [200]	75
Figure 3.27:	(a) Dimensions [198], images of (b) Seco uncoated WC T-type drill	76

	and (c) TiAlN+TiN coated M-type drill	
Figure 3.28:	(a) Cutting lip of coated drill, (b) cutting lip of uncoated WC drill and (c) magnified view of cutting edge	77
Figure 3.29:	Microstructure of WC tool material used for Seco M and T-type drills [157]	77
Figure 3.30:	(a) Dimensions [198] and (b) image of Seco brazed PCD CX31 geometry drill	78
Figure 3.31:	Tip geometry of Seco brazed PCD CX31 drill: (a) end view and (b) cutting lip	78
Figure 3.32:	Microstructure of CTB002 grade PCD [200]	78
Figure 3.33:	Setup for drilling CFRP in Phase 1A	80
Figure 3.34:	(a) Experimental correlation between thrust force and delamination extent, (b) experimental critical thrust force for produce delamination against feed rate [201]	81
Figure 3.35:	Schematic of variable feed rate drilling strategy	83
Figure 3.36:	Experimental setup for Phase 2B tests	84
Figure 3.37:	Cutting speed and feed rates typically employed when drilling CFRP and GFRP using tungsten carbide drills	86
Figure 3.38:	Experimental setup for Phase 2C tests	87
Figure 3.39:	Drills used in Phase 3A experiment (a) overview and (b) side view	88
Figure 3.40:	(a) Setup of high pressure through tool cutting fluid application and (b) setup for external high pressure cutting fluid application	88
Figure 3.41:	Setup for applying (a) high pressure cutting fluid and (b) low pressure flood	90
Figure 4.1:	Tool wear progression against number of drilled holes	91
Figure 4.2:	Tool wear scars at test cessation (last hole) in all trials	92
Figure 4.3:	Tool wear evolution for Test 5 (uncoated WC, 90 m/min, 0.05mm/rev and dry)	93
Figure 4.4:	Fibre dust burning in Test 1 after drilling 192 holes	93
Figure 4.5:	Drill condition at test cessation in Test 5 after drilling 192 holes	94
Figure 4.6:	Sample SEM micrographs of drill cutting edge at test cessation	94
Figure 4.7:	Main effects plot for maximum flank wear (Tests 5-12)	95
Figure 4.8:	Cutting edge morphology at test cessation in all trials	97
Figure 4.9:	Cutting edge radius values recorded at new and worn (at test cessation) conditions	98
Figure 4.10:	Main effects plot for cutting edge radius at test cessation	98
Figure 4.11:	Sample thrust force and torque profiles	100
Figure 4.12:	Maximum thrust force progression against number of drilled holes	101
Figure 4.13:	Maximum torque progression against number of drilled holes	102

Figure 4.14:	Main effects plot for maximum thrust force at the first hole in Phase 1A	103
Figure 4.15:	Main effects plot for maximum thrust force at the last hole (hole 512) in Phase 1A	104
Figure 4.16:	Main effects plot for maximum torque at the last hole (hole 512) in Phase 1A	104
Figure 4.17:	Hole entry micrographs at the first and last hole in Phase 1A	106
Figure 4.18:	Hole exit micrographs at the first and last hole in Phase 1A	107
Figure 4.19:	Delamination factor at hole entry and exit for both the first and last holes	108
Figure 4.20:	Main effects plot for exit delamination factor for the first hole drilled	109
Figure 4.21:	Hole diameter results against number of drilled holes	110
Figure 4.22:	Out of roundness measurement results against number of drilled holes	111
Figure 4.23:	Cylindricity measurement results against number of drilled holes	111
Figure 4.24:	Sample SEM micrographs of hole surface drilled with uncoated WC tools	113
Figure 4.25:	Sample SEM micrographs of hole surface drilled with diamond coated and domed PCD tools	114
Figure 4.26:	Entangled fibres were found in (a) Test 5 and (b) Test 12 after drilling 64 holes	115
Figure 4.27:	(a) Fibre dust / swarf produced in Test 5 and (b) cutting tool condition at test cessation	116
Figure 4.28:	SEM micrographs of fibre dust / swarf morphology	116
Figure 4.29:	(a) Cutting edge morphology, (b) cutting edge profile and (c) hole entry and exit quality at test cessation (hole 512)	117
Figure 4.30:	Tool cutting edge condition at test cessation of (a) Test 6 and (b) Test 8 used for current experiment	118
Figure 4.31:	Thrust force and torque profiles in Phase 1B when drilling with chilled air at cutting speeds of (a, b) 90 m/min and (c, d) 180 m/min	119
Figure 4.32:	Maximum thrust force and torque values in different cutting environment	120
Figure 4.33:	Hole exit quality when drilling at 90 m/min	121
Figure 4.34:	Hole exit quality when drilling at 180 m/min	122
Figure 4.35:	Flank wear curves for all tests against number of drilled holes	123
Figure 4.36:	Tool wear scar at test cessation in (a) Test 2 and (b) Test 5	124
Figure 4.37:	Force and torque profile of the last hole (hole 384) in Test 4	124
Figure 4.38:	Thrust force and torque progression against number of drilled holes at the principal feed rate	125
Figure 4.39:	Thrust force and torque progression against number of drilled holes at	125

	the reduced feed rate	
Figure 4.40:	Main effects plot for thrust force at last hole (hole 384)	126
Figure 4.41:	Main effects plot for torque at last hole (hole 384)	127
Figure 4.42:	Hole entry and exit quality at the first and last holes in all tests	128
Figure 4.43:	Delamination factors for at hole entry and exit for the first and last holes in all trials	129
Figure 4.44:	Hole diameter progression against number of drilled holes	130
Figure 4.45:	SEM micrographs of hole surface at the first hole in (a) Test 1 (0.1 mm/rev), (b) Test 3 (0.2 mm/rev) and (c) Test 5 (0.3 mm/rev)	131
Figure 4.46:	SEM micrographs of hole surface at the last hole in (a) Test 3 (0.2 mm/rev) and (b) Test 5 (0.3 mm/rev)	131
Figure 4.47:	Tool wear scar when drilling the first hole at feed rate of 0.6 mm/rev taken at (a) lip 1 and (b) lip 2	132
Figure 4.48:	Maximum flank wear results recorded at test cessation	133
Figure 4.49:	Tool wear scar at test cessation in (a) Test 3 and (b) Test 4	133
Figure 4.50:	Thrust force and torque progression against number of drilled holes when machining with the reduced feed rate	134
Figure 4.51:	Thrust forces recorded for the first and last holes when drilling with the principal feed rate level	134
Figure 4.52:	Main effects plot for thrust force recorded at the last hole (hole 384)	135
Figure 4.53:	Torque values recorded for the first and last holes when drilling with principal feed rate level	136
Figure 4.54:	Hole entry and exit quality at the first and last holes in all tests	137
Figure 4.55:	(a) Hole entry with feed rate of 0.6 mm/rev in the preliminary trial, (b) hole exit with constant feed rate of 0.2 mm/rev and (c) 0.4 mm/rev	138
Figure 4.56:	Fibre cutting angle definition	138
Figure 4.57:	Hole exit quality at (a) Type 1workpiece material with feed rate of 0.1 mm/rev, (b) unidirectional (UD) workpiece at 0.2mm/rev and (C) UD at 0.4mm/rev	139
Figure 4.58:	Schematic of uncut fibres relating to fibre cutting angles with (a) Type 1WP having 45^{o} orientation for the last / exit ply and (b) unidirectional WP	139
Figure 4.59:	Surface roughness (Ra) results for hole entry and exit section of the first and last holes in all tests	140
Figure 4.60:	Surface roughness Rsk and Rku results for the first and last holes in all tests	140
Figure 4.61:	Surface roughness (Sa and St) results at the first and last hole in for all tests	141

Figure 4.62:	Three dimensional (3D) topography maps for the first and last holes in all tests	142
Figure 4.63:	Main effects plot for surface roughness (Sa) at the first hole	143
Figure 4.64:	Hole diameter progression against number of drilled holes	144
Figure 4.65:	Out of roundness results against number of drilled holes	145
Figure 4.66:	Cylindircity results against number of drilled holes	145
Figure 4.67:	SEM micrographs of the first hole surfaces drilled at a feed rate of 0.4 mm/rev	146
Figure 4.68:	SEM micrographs of the last hole surfaces drilled at a feed rate of 0.4 mm/rev	147
Figure 4.69:	Sample SEM photograph of the first hole in Test 1 observed at ply / fibre orientation of (a) 0º and (b) 135º	148
Figure 4.70:	Cutting mechanism in machining of CFRP at various ply / fibre orientations [4]	148
Figure 4.71:	Sample SEM micrographs observed at hole exit location with low feed rate operation (0.01 mm/rev)	149
Figure 4.72:	Tool fracture in (a) overview, (b) end view and (c) picture of the third drilled hole	150
Figure 4.73:	Tool wear scar at the cutting speed of (a) 280 m/min with diamond coated tool and (b) 360 m/min with domed PCD tool	151
Figure 4.74:	Maximum flank wear values at test cessation in all tests	151
Figure 4.75:	Maximum thrust force and torque values recorded at the first and last holes in all tests	153
Figure 4.76:	Sample picture showing fibre dust adhered in drill flute	153
Figure 4.77:	Thrust force and torque profiles recorded at various cutting conditions	154
Figure 4.78:	Hole entry and exit quality for the first and last holes in all tests	155
Figure 4.79:	Out of roundness and cylindricity values recorded at the first and last holes in all trials	156
Figure 4.80:	Sample out of roundness (1.5 mm beneath hole entrance) and cylindricity profiles measured at last hole (hole 384)	157
Figure 4.81:	SEM micrographs taken at the last hole (hole 384) in Tests 1 and 2	158
Figure 4.82:	Sample SEM micrographs of hole surface machined with CVD-diamond coated tools	159
Figure 4.83:	Sample SEM micrographs of hole entry and exit	160
Figure 4.84:	Flank wear progression against number of drilled holes in all tests	161
Figure 4.85:	Tool wear scar at new tool, the first and last holes (hole 300) in all tests	162
Figure 4.86:	Tool wear scar following soaking in 25% NaOH solution to remove	163

	the BUE / workpiece adhesion in (a) Test 5 and (b) Test 6	
Figure 4.87:	SEM and EDS analysis of worn cutting lips for (a) Test 1 and (b) Test 3	163
Figure 4.88:	Thrust force and torque profiles for the first hole in (a) Test 1, (b) Test 4 and (c) last hole (hole 300) in Test 5	164
Figure 4.89:	Maximum thrust force and torque against number of drilled holes	165
Figure 4.90:	Maximum thrust force and torque for the first and last hole	165
Figure 4.91:	Hole edge quality for the last hole drilled	166
Figure 4.92:	Burr morphology at hole entry and exit of the hole	166
Figure 4.93:	Chips / swarf produced following each test	167
Figure 4.94:	SEM micrographs of chip morphology following different drilling tests	168
Figure 4.95:	Schematic of chip formation in drilling [209]	168
Figure 4.96:	Hole diameter results for the first and last holes in all tests	169
Figure 4.97:	Hole out of roundness and cylindricity measurement results	170
Figure 4.98:	SEM of machined hole surface quality	171
Figure 4.99:	Micrographs of hole subsurface at last holes in (a) Test 1, (b) Test 3 and (c) Test 6	171
Figure 4.100:	Tool wear progression in all trials	172
Figure 4.101:	Tool wear scar for the first and last hole in all tests	173
Figure 4.102:	Top view of drills at test cessation in (a) Test 2 and (b) Test 6	174
Figure 4.103:	Main effects plot for maximum flank wear	174
Figure 4.104:	Maximum thrust force and torque values recorded at the first and last holes	176
Figure 4.105:	Main effects plot for maximum thrust force at the last hole (hole 306)	176
Figure 4.106:	Main effects plot for maximum torque at the last hole (hole 306)	177
Figure 4.107:	Hole exit quality in all tests	178
Figure 4.108:	Micrographs of burr formation at hole entry and exit	179
Figure 4.109:	Chip morphology in all tests	181
Figure 4.110:	Sample long spiral chips generated in Test 8 (domed PCD, 160 m/min, 0.2 mm/rev and 3 bar low pressure flood)	182
Figure 4.111:	Hole diameter progression against number of drilled holes	183
Figure 4.112:	Out of roundness progression against number of drilled holes	183
Figure 4.113:	Cylindricity progression against number of drilled holes	184
Figure 4.114:	Microhardness results for both the first and last holes	185
Figure 4.115:	Surface roughness (Ra and Rt) measured at the first and last holes in all tests	186
Figure 4.116:	Main effects plot for surface roughness Ra measured at the last hole	186
Figure 4.117:	Overview of (a) the first hole surface in Test 3using brazed PCD tool	187

and (b) the last hole surface in Test 7 using domed PCD tool
Figure 4.118: SEM micrographs of last hole (hole 306) surface in Test 3 with overview and (b, c) higher magnification of hole surface 188
Figure 4.119: Sample pictures showing stacked / adhered chips / swarf at drill flute with (a) side view and (b) cutting lip at hole 234 in Test 3 188
Figure 4.120: SEM micrograph observed at the last hole (hole 306) in Test 7 189
Figure 4.121: Sample micrographs observed at hole sections 189
Figure 4.122: Sample pictures of tool wear scar at test cessation 191
Figure 4.123: Maximum flank wear, thrust force and torque values at test cessation 191
Figure 4.124: Hole surface roughness of Ra, Rt, Rz and Rsk measured at the first and last holes in all tests 192
Figure 4.125: SEM micrograph observed at the last hole (hole 300) in Test 3 193
Figure 4.126: 2D topography trace recorded in Test 2 (200 m/min) 193
Figure 4.127: Microhardness profiles against distance from machined workpiece surface 194
Figure 4.128: Hole exit quality at the first and last holes in all tests 195
Figure 4.129: Irregular burrs observed in Test 4 (360 m/min) 195
Figure 4.130: Sample micrographs of burr morphology at hole entry and exit 196
Figure 4.131: Chip morphology at the cross section observation 197
Figure 4.132: SEM micrographs of hole surfaces 198
Figure 4.133: SEM micrographs of machined subsurface 199

LIST OF TABLES

Table 2.1:	Properties of reinforcement fibres [4, 6]	4
Table 2.2:	Room temperature mechanical properties of matrix materials [4,6]	5
Table 2.3:	Room temperature thermal properties of matrix materials [4]	6
Table 2.4:	Properties of typical fibre reinforced epoxy composites [11]	8
Table 2.5:	Material properties of unidirectional metal matrix composites for space applications [19]	12
Table 2.6:	Properties of discontinuous reinforced aluminium metal matrix composites [19]	12
Table 2.7:	Room temperature mechanical and thermal properties of some matrix materials [4]	16
Table 2.8:	Vickers' microhardness of various tool materials / coatings [117]	39
Table 2.9:	Summary of cutting parameters in drilling MMCs	44
Table 2.10:	Properties of PCBN and PCD materials used in the experiment [187]	57
Table 3.1:	Summary of the CFRP layup configurations used in Phase 1 and 2	60
Table 3.2:	Fibre and CFRP composite laminate properties [191]	60
Table 3.3:	Buehler grinding / polishing route for aluminium alloy	71
Table 3.4:	Mechanical and physical properties of CTM302 grade PCD [159]	75
Table 3.5:	Mechanical and physical properties of CTB002 grade PCD [159]	78
Table 3.6:	Test matrix involving L12 modified Taguchi fractional factorial array for Phase 1A experiments	80
Table 3.7:	Test matrix for Phase 1B experiments	82
Table 3.8:	Full factorial array for Phase 2A experiments	83
Table 3.9:	Test matrix for Phase 2B experiments	85
Table 3.10:	Test matrix for Phase 2C experiments	86
Table 3.11:	Test matrix for Phase 3A experiments	88
Table 3.12:	Test matrix for Phase 3B experiments	89
Table 3.13:	Test matrix for Phase 3C experiments	90
Table 4.1:	ANOVA results for maximum flank wear (Tests 5-12)	96
Table 4.2:	ANOVA results for maximum thrust force at the first hole in Phase 1A	103
Table 4.3:	ANOVA results for thrust force at last hole (hole 384)	126
Table 4.4:	ANOVA results for thrust force recorded at the last hole (hole 384)	135
Table 4.5:	ANOVA results for surface roughness (Sa) at the first hole	143
Table 4.6:	ANOVA results for maximum flank wear	175
Table 4.7:	ANOVA results for maximum thrust force at the last hole (hole 306)	177
Table 4.8:	ANOVA results for maximum torque at the last hole (hole 306)	177
Table 5.1:	List of recommended / preferred operating parameters / strategy when drilling CFRP	209
Table 5.2:	List of recommended / preferred operating parameters / strategy when drilling MMCs	210

NOMENCLATURE

%	:	Percentage
<	:	Less than
>	:	More than
ºC	:	Degree Celsius
µm	:	Micrometre
Al	:	Aluminium
Al_2O_3	:	Aluminium oxide
ANOVA	:	Analysis of variance
BUE	:	Built up edge
BUL	:	Built up layer
C	:	Carbon
CFRP	:	Carbon fibre reinforced plastic
cm	:	Centimetre
CMC	:	Ceramic matrix composite
CMM	:	Coordinate measuring machine
Co	:	Cobalt
COF	:	Coefficient of friction
C_p	:	Specific heat (kJ/kgºC)
CTE	:	Coefficient of thermal expansion (10^{-6} K^{-1})
CVD	:	Chemical vapour deposition
DF	:	Degree of freedom
DLC	:	Diamond like carbon
D_{max}	:	Maximum damage zone diameter (mm)
D_0	:	Drilled hole diameter (mm)
EDM	:	Electrical discharge machining
EDX	:	Energy dispersive x-ray spectroscopy
Exp SS	:	Expected sum of squares
F	:	f-test value
F_d	:	Delamination factor
FEM	:	Finite element modelling
GFRP	:	Glass fibre reinforced plastic
GPa	:	GigaPascal
HAZ	:	Heat affected zone
HM	:	High modulus carbon fibre
HS	:	High strength carbon fibre
HSS	:	High speed steel

HV	:	Vickers' hardness
K	:	Kelvin
kg	:	Kilogram
m	:	Metre
max.	:	Maximum
min.	:	Minimum
min	:	Minute
mm	:	millimetre
MMC	:	Metal matrix composite
MQL	:	Minimum quantity lubrication
MRR	:	Material removal rate (mm^3)
N	:	Newton
NaOH	:	Sodium hydroxide
PCD	:	Polycrystalline diamond
PCR	:	Percentage of contribution ratio
PVD	:	Physical vapour deposition
Ra	:	Roughness parameter, arithmetic mean deviation of the assessed profile (µm)
rpm	:	Revolutions per minute
Rt	:	Total surface roughness (µm)
Sa	:	Areal surface parameter, arithmetic mean deviation of the surface (µm)
SEM	:	Scanning electron microscopy
SiC	:	Silicon carbide
SS	:	Sum of squares
T_g	:	Glass transition temperature (ºC)
Ti	:	Titanium
TiAlN	:	Titanium aluminium nitride
TiC	:	Titanium carbide
TiCN	:	Titanium carbon nitride
TiN	:	Titanium nitride
UD	:	Unidirectional
USM	:	Ultrasonic machining
VB_{max}	:	Maximum flank wear (µm)
V_c	:	Cutting speed (m/min)
WC	:	Tungsten carbide
WEDM	:	Wire electrical discharge machining

Chapter 1: INTRODUCTION

1.1 Background to the project

The use of carbon fibre reinforced plastic (CFRP) composites has been steadily increasing in recent years as an alternative to traditional metallic materials in a wide range of industrial applications. Within the aerospace sector, components in the latest generation of commercial aeroplanes from Airbus and Boeing have already incorporated substantial levels of composite based materials (up to 50% in the Boeing 787), which provide benefits in terms of increased strength to weight ratios leading to enhanced aircraft operational efficiency and associated fuel cost savings. Joining of parts such as wing and tail plane sections are still primarily mechanical based requiring the production of fastener holes and therefore drilling operations to meet component dimensional tolerances are still necessary. Metal matrix composites (MMCs) are a class of material that consists of ceramic particulates or fibres distributed within a metallic matrix (e.g. aluminium, magnesium, titanium and copper), which results in mechanical properties that are superior to conventional homogenous / single phase alloys. Key mechanical / physical property benefits include high specific strength and modulus, superior abrasion and wear resistance together with low sensitivity to temperature variations. Other advantages, particularly in comparison to polymer matrix composites are greater temperature resistance (~500ºC), no moisture absorption, higher electrical and thermal conductivities as well as being non-flammable. Despite the attractive properties of MMC materials, their utilisation in industry remains largely limited to specialised, high value applications in the premium automotive and defence sectors. This is partly attributed to the materials' relatively poor machinability due to the highly abrasive reinforcement phase (typically SiC or Al_2O_3), which generally demands the use of ultra-hard tooling such as PCD.

While there is considerable rsearch literature relating to the cutting of composites, prevailing challenges in drilling include high tool wear rates, limited productivity together with poor hole quality and surface integrity, which are influenced in part by the inhomogeneous and anisotropic nature of composites as well as dissimilar mechanical / physical properties of the matrix and reinforcement. Therefore, the selection of appropriate tool materials / coatings, operating parameters and cutting environment is essential to improve hole surface quality / integrity and achieve greater productivity when drilling CFRP or MMCs. Recent developments in tool design, coatings and tool materials have the potential to significantly improve machinability performance, hence the motivation for the present project.

1.2 Project collaborators

The research was carried out as part of a Doctor of Philosophy (PhD) degree programme based within the Machining Research Group in the School of Mechanical Engineering at the University of Birmingham. The project involved collaboration with industrial organisations including Seco Tools (UK) Ltd. and Element Six Ltd., who provided considerable in-kind support in the form of fabricated drills, advanced polycrystalline diamond tool materials, analysis facilities and technical knowledge. Details of the contact person in the respective companies are listed in Appendix A. A PhD studentship from the School of Mechanical Engineering, University of Birmingham provided further financial support.

1.3 Aims and objectives

The overall aim of the project is to assess the performance when drilling epoxy based CFRP and Al/SiCp MMC composites used in the manufacture of aerospace components and understand its effects on feature quality and workpiece integrity. Specific objectives of the project relate to:

- Comprehensive literature review on current state-of-the-art relating to machinability of carbon fibre reinforced plastic and metal matrix composites.
- Establishing preferred / optimum operating parameters (cutting speed, feed rate and drill strategies) and the influence of cutting environment (dry, chilled air, high pressure internal / external supplied coolant and low pressure flood) for drilling specific composite material systems. Key response measures include tool wear / life, thrust force / torque, hole size and geometrical accuracy, hole edge quality (delamination, uncut fibres and burrs) and surface integrity (surface roughness, microhardness, fibre / particle pullout, surface damage, etc.)
- Evaluation of the latest cutting tool materials and advanced diamond coatings, drill geometry and design (e.g. domed PCD) to provide improved levels of productivity, tool life and hole quality.
- Identification of tool wear mechanisms and develop correlation of subsequent effects on hole surface quality.
- Minimisation / elimination of workpiece surface defects.

Chapter 2: LITERATURE REVIEW

2.1 Carbon fibre reinforced plastic (CFRP) composites

2.1.1 Introduction and properties

A composite material is made by combining two or more materials to give a unique combination of properties. The final properties of composite materials are superior to the constituent material properties [1-3]. The main concept of a composite is that it contains matrix materials and reinforcements. The reinforcements, which determine the principal mechanical characteristics of the composite, can be fibres, particulates, or whiskers. The matrix materials usually determine the characteristics of the composite according to the field of application, together with its usable temperature and weight, and can be a plastic, metal, or ceramic. The important functions of a matrix material include its ability to bind fibres together and transfer the load to the fibres, to provide a good surface finish quality and to protect reinforcing fibres against chemical attack [1]. Based on the characteristics of the matrix materials, composites can be divided into fibre reinforced plastics (FRP), metal matrix composites (MMC) and ceramic matrix composites (CMC). The selection of specific fibre and matrix to be used in the composite is not arbitrary, the two phases of a composite must be carefully chosen if the composite material is to be structurally as well as commercially efficient. The composite generally must be resistant to debonding at the fibre / matrix interface, and also to fibre breakage and matrix cracking [2].

Fibres are most commonly used in a soft matrix as reinforcement and glass, carbon and aramid fibres are generally employed. Glass fibres are produced by drawing molten glass through numerous tiny orifices in a gravity-fed tank to form continuous filaments which are gathered together in a strand or tow [2]. Glass fibres are the cheapest among all types of fibres and come in several types with E (electrical) and S (high strength) being the most common. E-glass offers excellent electrical properties and durability and is a cheap general-purpose reinforcement. S-glass offers improved strength, stiffness and high temperature tolerance, and is considerably more expensive than E-glass [4]. Glass fibre reinforced composites are strong, low in cost, nonconductive, and corrosion resistant. Their disadvantages include low tensile modulus, relatively high specific gravity, sensitivity to abrasion with handling, relatively low fatigue resistance and high hardness [5].

Aramid fibres (sold as Kelvar) are organic fibres manufactured from aromatic polyamides by solution spinning. Aramid fibre is used as a higher performance replacement for glass fibre in industrial applications and sporting goods as well as in protective clothing [4]. The filaments are small in diameter (~12 μm) and very flexible. Additionaly, aramid fibres tend to have high tensile strength but only intermediate modulus and also exhibit significantly lower strength in compression [2]. However, they provide good impact strength and a negative coefficient of thermal expansion. Consequently, aramid fibres are widely used in the automotive industry for tire cords, timing belts, and brake friction materials. They are also used as concrete reinforcing materials and in high-performance ropes.

Carbon fires are widely used for advanced composites in aerospace and some sporting goods applications due to their relatively high specific stiffness and strength. They are classified as high modulus (HM), intermediate modulus (IM) and high strength (HS) grades. The latter two grades are mostly made from a PAN (polyacrylonitrile) precursor [4]. The properties of typical fibres are listed in Table 2.1.

Table 2.1: Properties of reinforcement fibres [4, 6]

Characteristics	PAN*-based carbon		Kelvar 49	E-glass	S-glass
	HM*	HS*			
Diameter (μm)	5-8	6-8	8-14	10-20	10-20
Density (kg/m^3)	1.81	1.78	1.44	2.62	2.46-2.49
Young's modulus (GPa)					
Parallel to fibre axis	400	230	131	80-81	88-91
Perpendicular to fibre axis	12	20	70	-	-
Tensile strength (GPa)	2.5-4.5	3.8-4.2	3.6-4.1	3.1-3.8	4.38-4.59
Strain to failure (%)	0.6	2.0	2.8	4.6	5.4-5.8
Coefficient of thermal expansion ($10^{-6}K^{-1}$)					
Parallel to fibre axis	-0.5	-0.6	-4.3	6.0	2.9
Perpendicular to fibre axis	7.0	10.0	41	-	-
Thermal conductivity (W/m K)	70	11	0.04-1.4	10-13	1.1-1.4
Specific heat (kJ/kg K)	0.7-0.9	-	0.769	0.45	0.41

*PAN: Polyacrylonitrile; HM: high modulus; HS: high strength

The role of the matrix in a composite is to transfer stresses between the fibres; to provide a barrier against an adverse environment; and to protect the surface of the fibres from mechanical abrasion [5]. Polymeric matrix materials can be further subdivided into thermoplastics and thermosets. Polymers which will soften or melt on heating are called thermoplastic polymers and are suitable for liquid flow forming, whereas molecules in a polymer that are cross-linked in the form of network and will not soften on heating are termed thermosetting polymers [7]. The most common thermoset polymer matrix materials are polyester, epoxies and polyimides. Polyesters are used extensively with glass fibres. They are normally inexpensive and lightweight with an application temperature range up to 100℃, and somewhat resistant to environmental exposures. Epoxies are more expensive but have better moisture resistance and suffer lower shrinkage on curing. Their maximum operating temperature is ~175℃. Polyimides have a higher operating ceiling of ~300℃ but are more difficult to fabricate [2]. Common thermoplastic resins used as matrix materials in composites include polypropylene, nylon, polyamide imide, polyphenylene sulphide (PPS), polyarylsulfone, and polyetherether ketone (PEEK). PEEK is a very attractive matrix material due to its high melting temperature (343ºC) and good oxidation stability [7]. Potential problems with the use of polymer matrix materials relate to their limited temperature range; susceptibility to environmental degradation due to moisture, radiation, and atomic oxygen (in space); low transverse strength; and high residual stresses due to the large mismatch in coefficients of thermal expansion between fibre and matrix [2]. The specific mechanical and thermal properties of matrix materials at room temperature are detailed in Table 2.2 and 2.3, respectively.

Table 2.2: Room temperature mechanical properties of matrix materials [4, 6]

	Density (g/cm^3)	Young's modulus (GPa)	Tensile strength (MPa)	Strain to failure (%)
Polymers – Thermosets				
Unsaturated polyester, UP	1.10-1.23	3.1-4.6	50-75	1.0-6.5
Epoxy, EP	1.10-1.20	2.6-3.8	60-85	1.5-8.0
Phenolics (Bakelite)	1.00-1.25	3.0-4.0	60-80	1.8
Polymers – Thermoplastics				
Polypropylene, PP	0.90	1.1-1.6	31-42	100-600
Polyamide (nylons), PA	1.10	2.0	70-84	150-300
Poly (phenylene sulfide), PPS	1.36	3.3	84	4.0
Poly (ether ether ketone), PEEK	1.26-1.32	3.2	93	50

Table 2.3: Room temperature thermal properties of matrix materials [4]

	K (W/m ºC)	C_p (kJ/kg ºC)	α (10^{-6} ºC)	T_g (ºC)	T_m (ºC)
Polymers – Thermosets					
Unsaturated polyester, UP	0.17-0.22	1.3-2.3	55-100	70-	-
Epoxy, EP	0.17-0.20	1.05	45-65	65-175	-
Phenolics (Bakelite)	0.12-0.24	1.4-1.8	25-60	300	-
Polymers – Thermoplastics					
Polypropylene, PP	0.11-0.17	1.8-2.4	80-100	-20-5	165-175
Polyamide (nylons), PA	0.24	1.67	80	55-80	265
Poly (phenylene sulfide), PPS	0.29	1.09	49	85	285
Poly (ether ether ketone), PEEK	0.25	1.34	40-47	145	345

K: Thermal conductivity; C_p: Specific heat; α: Coefficient of thermal expansion; T_g: Glass transition temperature; T_m : Melting temperature.

Manufacting techniques for composites include hand / automated lay-up (laminating) and autoclave processing processes (bag molding process), filament winding, pultrusion and liquid composite molding. The prepreg lay-up process, also called autoclave processing or vacuum bagging processing, is very common in the aerospace industry as well as for making small batch prototype parts [8]. Complicated shapes with very high fibre volume fractions can be manufactured using this process, which is suitable for making a wide variety of shapes [1]. With increasing production volumes hand lay-up is uneconomic and necessitates the use of new automated technology [9]. The term ‘prepreg’ refers to pre-impregnated fibres, which can be unidirectional or woven to form a polymer composite lamina protected on both sides with easily removable separators, as shown in Figure 2.1(a). Figures 2.1(b) and 2.1(c) show schematics of an autoclave to fabricate a laminated composite and lay-up plies with different fibre orientations. Optical micrographs of laminated composites are shown in Figures 2.1(d) and 2.1(e) [7]. The lay-up geometry of a composite strongly affects not only crack initiation but also crack propagation, with the result that some laminates appear highly notch sensitive, whereas others are totally insensitive to the presence of stress concentrators [10]. An autoclave is a closed vessel for controlling temperature and pressure and is used for curing polymeric matrix composites. The composite to be cured is prepared either through hand lay-up or machine placement of an individual laminate in the form of fibrous tape which has been impregnated with resin. The component is then placed in an autoclave and subjected to a controlled cycle of temperature and pressure [2].

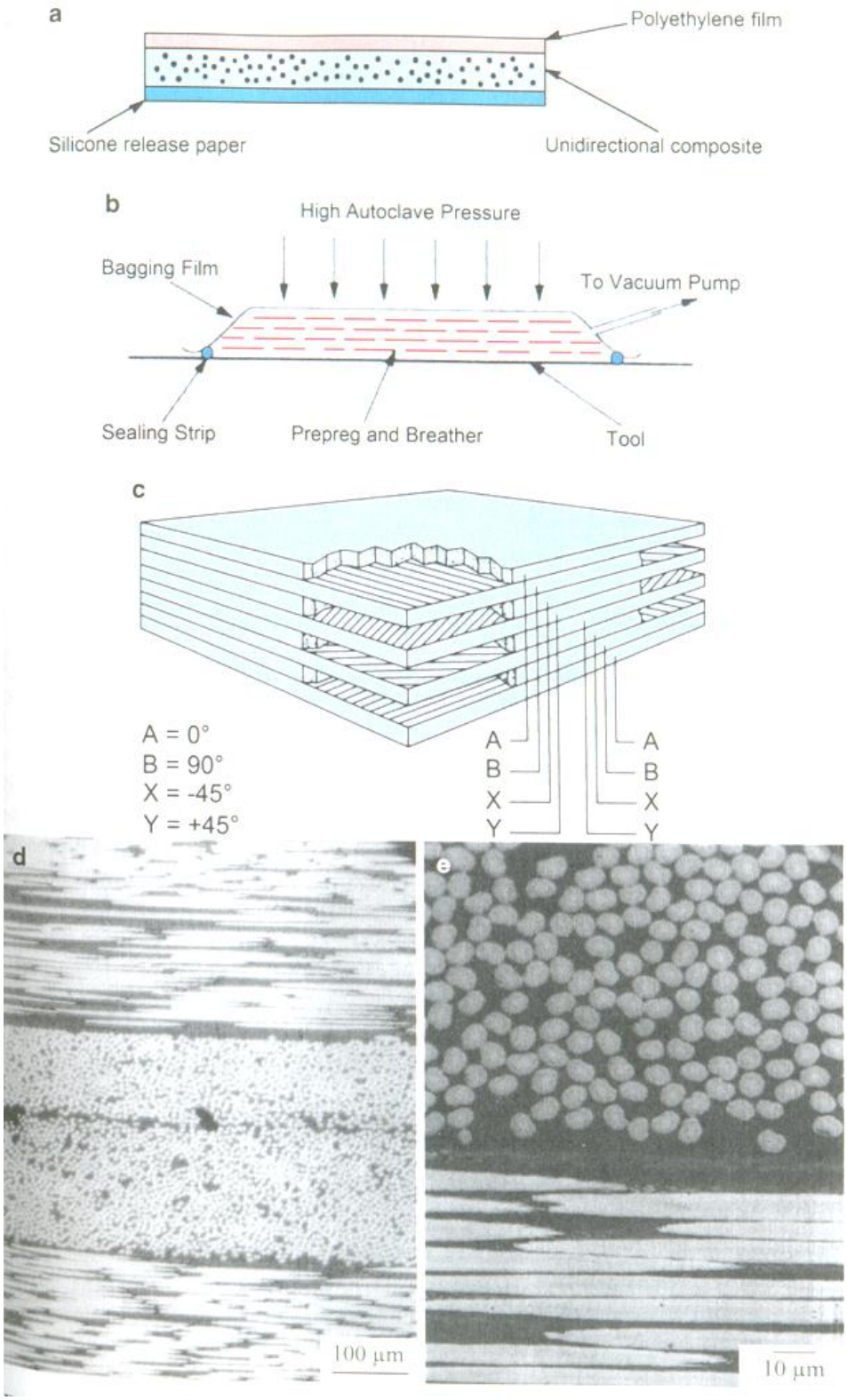


Figure 2.1: (a) Schematic of a prepreg, (b) setup in an autoclave to fabricate laminated composite, (c) lay up of plies with different fibre orientation and (d, e) micrographs of plies with different fibre orientation [7]

Composite materials offer increased design flexibility. Available options include the choice of fibre and matrix material, the volume fraction of both, fabrication method, layer orientation, the number of layers in a given direction, the thickness of individual layers and type of layer, and the layer stacking sequence [1]. The most often cited advantages of fibrous composites are their high specific stiffness and high specific strength (strength to density ratio) as compared with traditional engineering materials. These properties lead to improved performance and reduced energy consumption [2]. Their specific strength is typically in the range of 3 to 5 times that of steel and aluminum alloys [1]. Improved fatigue life is one of the major reasons why there has been a shift to composites by the aircraft industry [2]. Unidirectional carbon / epoxy composites have good fatigue strength, up to almost 90% of their static strength [1]. Table 2.4 presents properties of continuous and aligned glass, carbon and aramid fibre reinforced epoxy matrix composites in longitudinal and transverse directions. In all cases the fibre volume fraction is 60% [11]. Although composite materials offer many benefits, they suffer from the following disadvantages. Material cost is very high compared to that of steel and aluminium and while large design databases are available for metals, much less information is available for composites. Additionaly, the temperature resistance of composite parts depends on the temperature resistance of the matrix materials and composites absorb moisture, which affects their properties and dimensional stability [1].

Table 2.4: Properties of typical fibre reinforced epoxy composites [11]

Properties / Composites	E-glass/epoxy	High strength carbon/epoxy	Kevlar 49 (aramid)/epoxy
Density (g/cm^3)	2.1	1.6	1.4
Tensile modulus (GPa)			
Longitudinal	45	145	76
Transverse	12	10	5.5
Tensile strength (MPa)			
Longitudinal	1020	1240	1380
Transverse	40	41	30
Ultimate tensile strain (%)			
Longitudinal	2.3	0.9	1.8
Transverse	0.4	0.4	0.5

2.1.2 Industrial applications

The use of CFRP materials has shown a marked increase in recent years, particularly in the aerospace industry for next generation aircraft components. Figure 2.2 shows the development of composite applications in aircraft. The most significant benefits / advantages of using CFRP composites compared with conventional metallic alloys are mass and part reduction as a consequence of their high specific strength and modulus, good fatigue life and vibration damping properties [10].

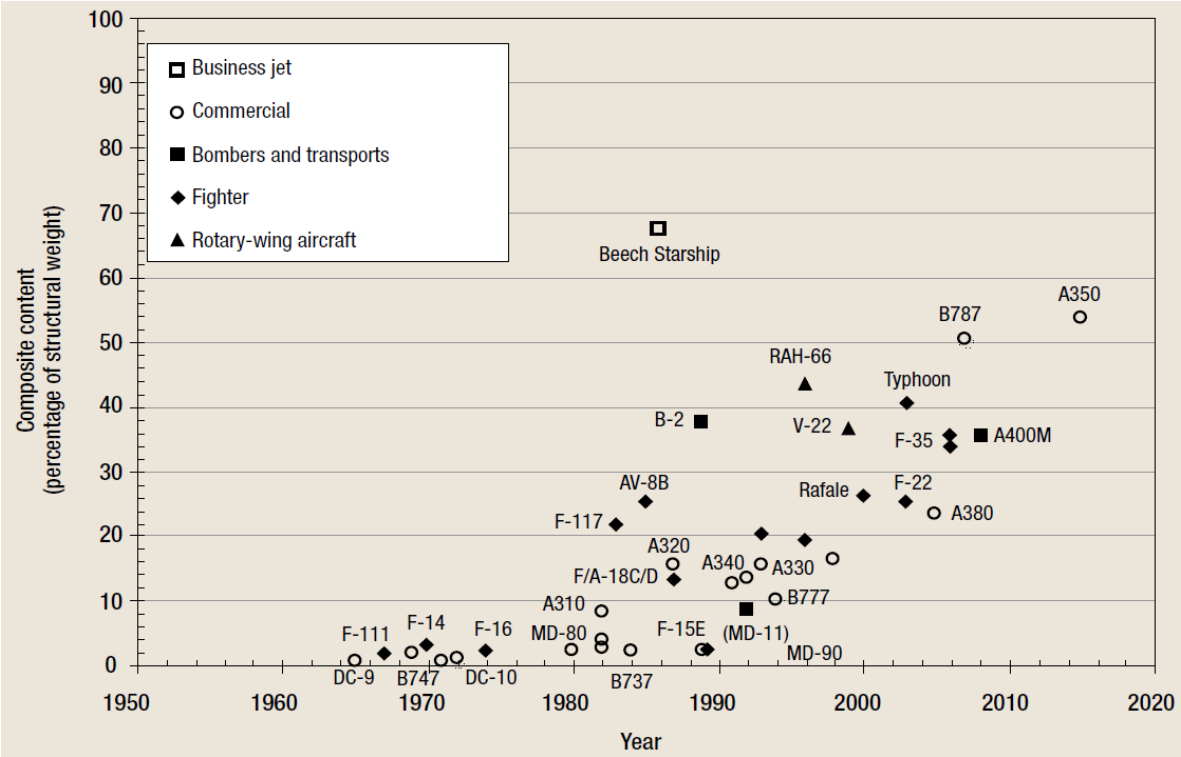


Figure 2.2: Change in composite application in aircraft over time [12]

The newly designed Airbus A380, the world's largest aircraft with a capacity of 550 to 700 passengers, has horizontal stabilizers, ailerons, wing boxes and leading edges, fuselage secondary mounting brackets, and deck structures made of composite materials employing carbon fibres, thermosetting resins, and thermoplastics [13]. The centre wing box in the A380 weights ~8.8 tonnes, of which 5.3 tonnes is composite material [14]. Figure 2.3 shows the application of CFRP in the Airbus A380. Composite materials are also widely applied by Boeing. Composites use has increased from less than 5% of total weight in the Boeing 757/767 (1980s) to almost 50% in the new Boeing 787 Dreamliner for the centre wing box's primary structure, wing ribs, and rear fuselage section, as shown in Figure 2.4. It has been predicted that weight savings approaching 40% are feasible by replacing light metals with composites for aircraft secondary structures, and about 20% for primary structures including wings and fuselages [10, 15]. Composite technology is also employed in the fan case. The

General Electric GEnx engine uses third-generation composite fan blades to deliver superior aerodynamic performance and durability, see Figure 2.5. The light weight composite fan case reduces aircraft weight by 1200 lbs., eliminates corrosion and lowers maintenance costs [16].

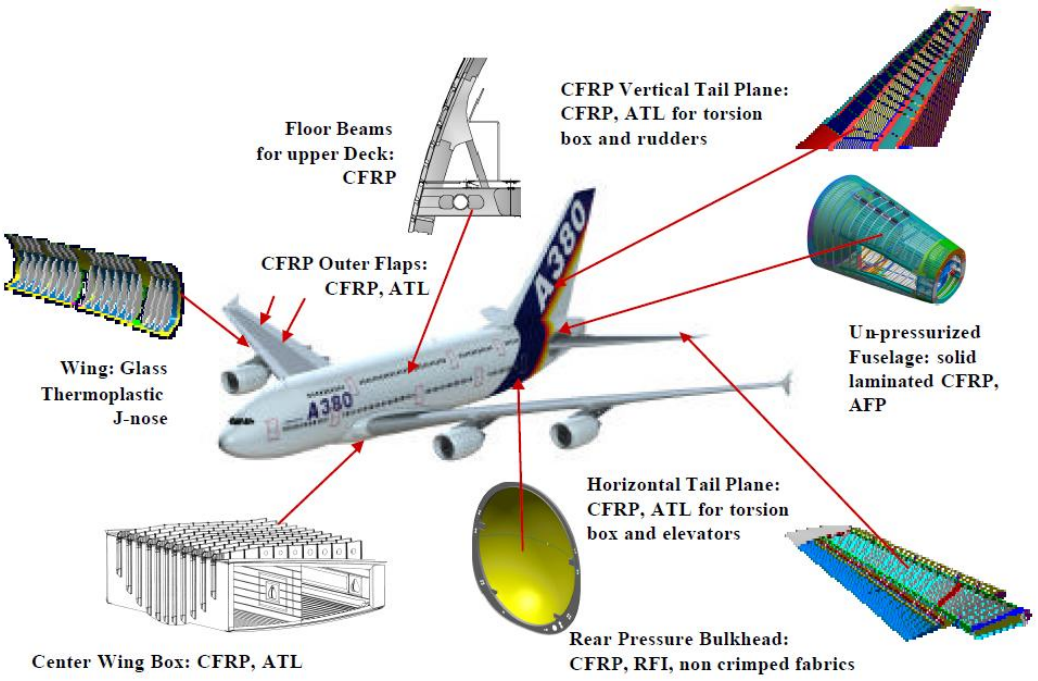


Figure 2.3: CFRP composite components used in Airbus A380 airplane (courtesy of Airbus)

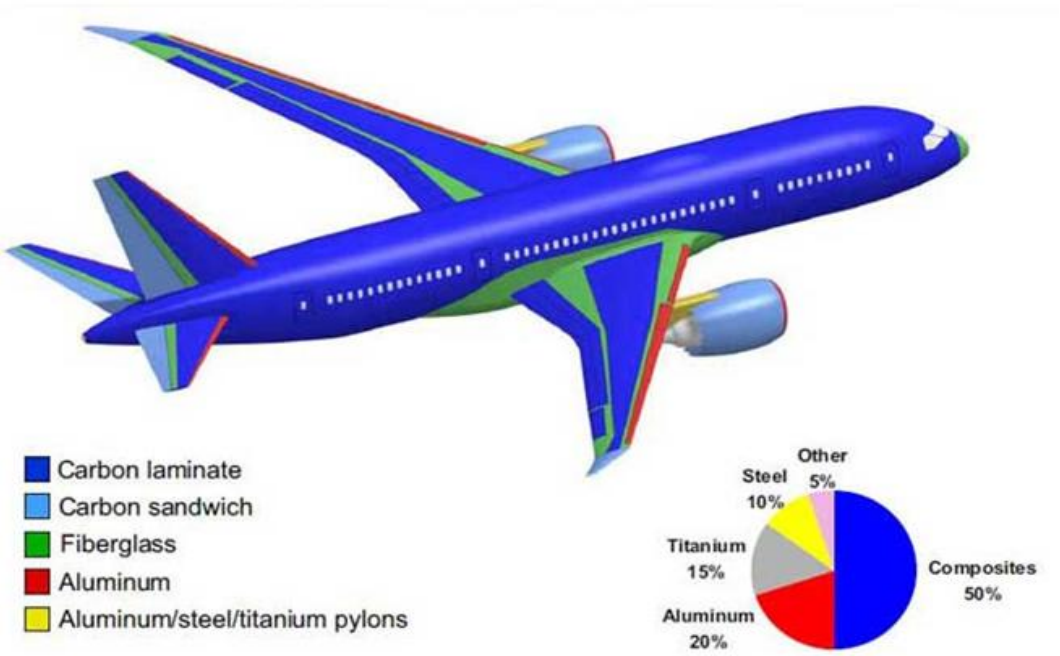


Figure 2.4: Composite materials used in Boeing 787 Dreamliner airplane (courtesy of Boeing)



Figure 2.5: Composite fan blades used for GEnx-1B engine which powers Boeing's Dreamliner 787 (maximum diameter: ~2822 mm) (courtesy of General Electric Co.)

Carbon reinforced polymer composites are also currently being utilized extensively in sports and recreational equipment (fishing rods, golf clubs, etc.), filament wound rocket motor cases and pressure vessels [11]. The main challenges restricting their use include material and processing costs, damage tolerance, repair and inspection, dimensional tolerances, and conservatism associated with uncertainties about relatively new materials [10]. Since composite materials cannot be welded, and gluing is quite complex, mechanical joining, involving rods, pins, fasteners and rivets, is the solution commonly adopted to assemble a composite part to other parts. The holes required by mechanical joining are generally drilled and as many as 55,000 holes are required in the Airbus A350 aircraft [6, 17]. Therefore, improving the productivity and machinability when drilling CFRP composite materials is the key issue in order to facilitate industrial application.

2.2 Metal matrix composites (MMCs)

2.2.1 Introduction and properties

The matrix materials of metal matrix composites are normally ductile alloys including aluminium, magnesium, titanium and copper. As with polymer matrix composites, the reinforcement can be continuous and discontinuous fibres, particulates and whiskers. In MMCs, the matrix and reinforcement are physically mixed together, while a second phase forms as a particular eutectic or eutectoid reaction in a dual phase alloy [18]. MMC materials can be classified as continuous or discontinuous depending on the form of reinforcement materials used. Continuous reinforcement is typically long fibres (carbon, boron, etc.) while discontinuous reinforcement is commonly particulates / particles, whiskers and chopped fibres. Continuous fibre reinforced MMCs show superior mechanical properties and good thermal

conductivity, however anisotropy can present problems and their high cost make them prohibitive. Table 2.5 details properties of some sample MMCs reinforced with unidirectional fibres (P100: graphite fibre). In contrast, particulate reinforced MMCs are essentially isotropic and cheaper to produce, and therefore more widely used for commercial products. Table 2.6 presents properties of sample discontinuous reinforced Al based MMCs.

Table 2.5: Properties of unidirectional metal matrix composites for space applications [19]

Properties	P100/6061 Al (0°)	P100/AZ91C Mg (0°)	Boron/Al (0°)
Volume of reinforcement (%)	42.2	43	50
Density (g/cm^3)	2.5	1.97	2.7
Poisson ration	0.295	0.3	0.23
Specific heat, C_p (kJ/kg K)	812	795	801
Longitudinal			
Young's modulus (GPa)	342.5	323.8	235
Ultimate tensile strength (MPa)	905	710	1100
Thermal conductivity, *K* (W/m K)	320	189	-
Transverse			
Young's modulus (GPa)	35.4	20.7	138
Ultimate tensile strength (MPa)	25	22	110
Thermal conductivity, *K* (W/m K)	72	32	-

Table 2.6: Properties of discontinuous reinforced aluminium metal matrix composites [19]

Properties	Graphite Al GA 7-230	Al6092/SiC/17.5p	Al/SiC/63p
Density (g/cm^3)	2.45	2.8	3.01
Young's modulus (GPa)	88.7	100	220
Compressive yield strength (MPa)	109.6	406.5	-
Ultimate tensile strength (MPa)	76.8	461.6	253
Ultimate compressive strength (MPa)	202.6	-	-
Thermal conductivity (W/m K)	6.89	-	-

For particulate reinforced MMCs, the main factors influencing mechanical properties are the matrix alloy, the volume fraction and size of reinforcements [7, 20, 21]. The strength generally increases with the volume fraction of reinforcement, although beyond ~30% the increase is not apparent. Mechanical properties are typically improved with finer (<~20 μm)

of particulates [20]. Figure 2.6(a) shows the tensile stress against strain curves of Al/SiC metal matrix composites with different volume fraction of SiC reinforcement while Figure 2.6(b) presents stress-strain curves for variable sizes / dimensions of SiC particulates. In general, the strength of the composite increases with increasing particle volume fraction, while the ductility decreases. The stress increases ~30% up to ~650 MPa with 30% volume fraction of SiC particles in comparison with the unreinforced matrix alloy. With a fixed volume fraction at 20%, the strength increases as the particle size decreases. MMCs reinforced with 20 vol.% 5 µm SiC particles showed high strength up to ~600 MPa which increased ~20% compared with unreinforced conventional material [7]. One of the main limitations of MMCs is the reduction / restriction in ductility / elongation caused by the addition of reinforcements, see Figure 2.6(a). For SiC reinforced Al (AA2124) MMC, the elongation is below 3% when reinforcement volume fraction increases above ~10%.

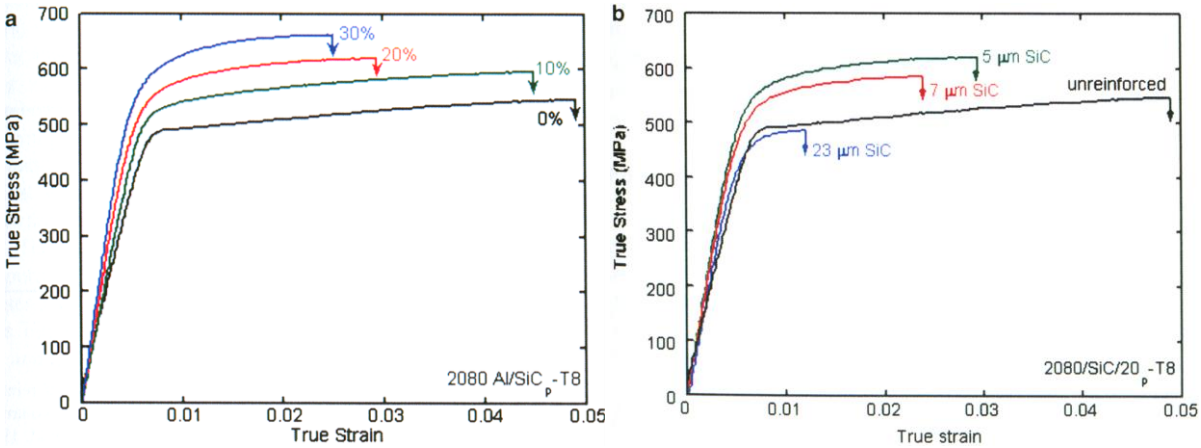


Figure 2.6: Stress-strain curves for (a) variable volume fractions of SiC particles (6 µm) in Al matrix and (b) different particle sizes in a fixed volume fraction (20% by volume) [7]

The processing techniques / methods for producing MMCs generally comprise primary materials production and secondary consolidation or forming operations. Many primary processes are available / feasible to fabricate metal matrix composites including centrifugal casting, spray deposition and forming as well as diffusion bonding techniques [7]. In the spray deposition process (see the schematic in Figure 2.7), alloys are melted by induction heating and then subsequently pressurised and ejected through a nozzle into an atomiser. The atomised stream is collected on a substrate placed in the line of flight and a solid deposit is built up on the collector. Particles are introduced into the metal spray leading to co-deposition with the atomised metal on the substrate. An even / uniform distribution of reinforcement can be achieved in this process, however directionality of the particles can be observed in the microstructure after extrusion [7].

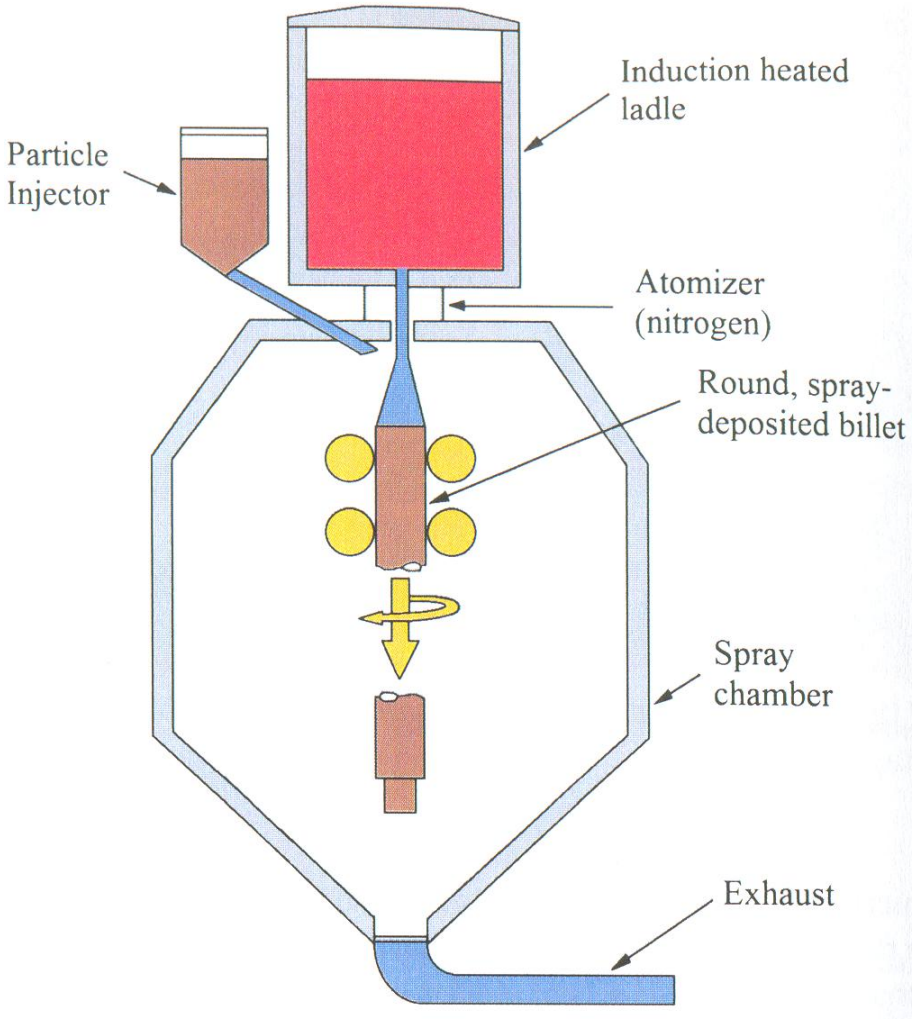


Figure 2.7: Schematic of the spray deposition and forming process to fabricate metal matrix composites [7]

2.2.2 Industrial applications

Metal matrix composites have received considerable attention over the past 20 years due to their attractive strength, stiffness, fatigue and thermal properties [19]. The advantages of these materials over polymer matrix composites include higher operating temperature, noflammability, better conductivity and greater resistance to degradation with organic fluids [5]. Figure 2.8 shows the sample applications of discontinuous reinforced MMCs in electronic components. MMCs have also been developed / investigated for space application with reported use for fuselage structures in the Space Shuttle Orbiter, high gain antenna for the Hubble Space Telescope and structural components for liquid rocket engines [19, 22, 23]. The application of MMCs for missile fins and tank components in military defense have also proved successful [24].

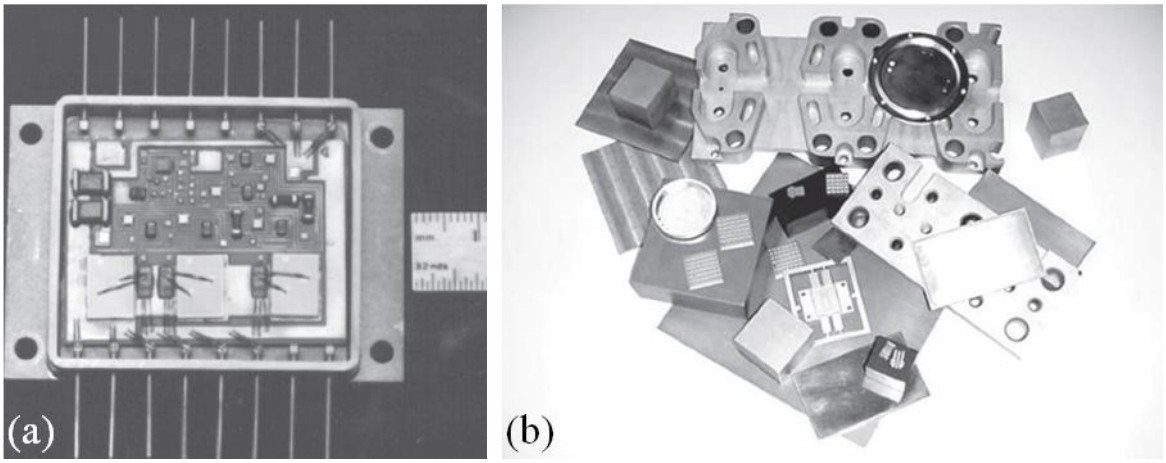


Figure 2.8: Discontinuously reinforced MMCs for electronic packaging applications: (a) Al/SiCp electronic package for a remote power controller (photo courtesy of Lockheed Martin Corporation), (b) cast Al/SiCp components (photo courtesy of MMCC. Inc.) [19]

Traditionally automotive brake rotors, drums and pads are made of cast irons, but recently SiC reinforced Al metal matrix composites have been employed. Figure 2.9 shows a typical application of MMCs for racing motorcycle brakes. The benefits of applying MMCs in the automotive area relate to the reduction in weight of cars and improving balance due to a reduction in the rotating unsprung mass. Duralcan has manufactured MMC disks used extensively in USA racing cars [5]. The rotors made of Al/SiC MMCs demonstrate better wear resistance and higher durability compared with conventional cast iron components. More importantly, MMCs rotors weigh only 33-60% of equivalent cast iron parts. The weight reduction not only improves petrol consumption but also reduces vibration and improves handling as the unsprung weight is reduced [5].

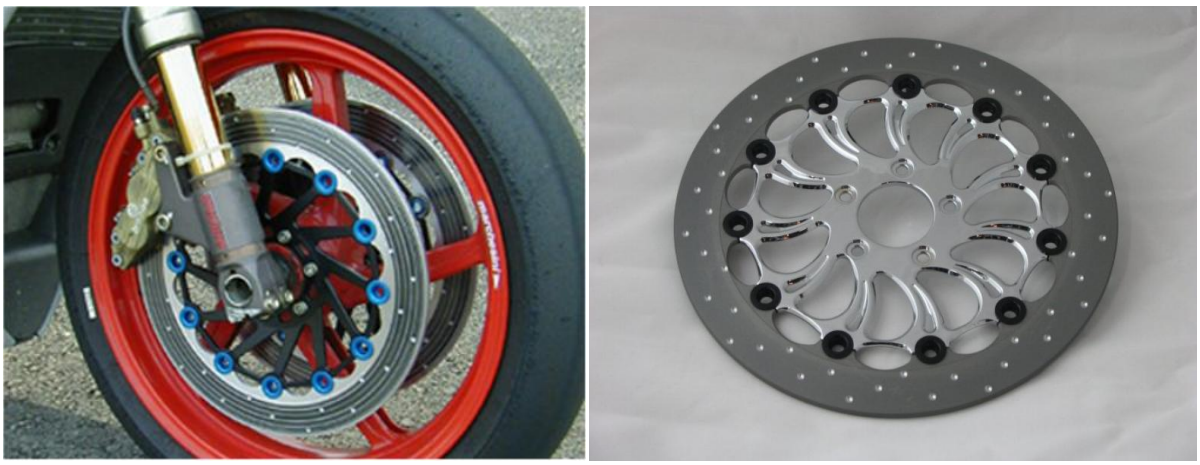


Figure 2.9: Racing motorcycle brakes made from MMCs (photo courtesy of Swan Metal Composites)

2.3 Ceramic matrix composites (CMCs)

2.3.1 Introduction and properties

The main reasons for choosing ceramics as the matrix include a high application temperature range (up to ~2000℃), high elastic modulus, chemical inertness and low density. Table 2.7 details the mechanical and thermal properties of ceramic matrix materials compared with plastic and metal matrix materials. CMCs posses higher specific modulus and elevated temperature mechanical properties than metals [25, 26]. The use of ceramic materials in structural applications however is limited, due to their susceptibility to catastrophic brittle failure, low fracture toughness, flaw sensitivity, and their relatively low bulk tensile strength. By reinforcing with fibres or whiskers, CMCs fail gradually rather than catastrophically [27]. The main disadvantage of ceramic matrix materials is their brittleness [2, 28]. Small surface flaws, such as scratches and nicks, or internal flaws including pores, microcracks and inclusions can lead to disastrous results [7]. CMCs can be processed by conventional powder processing techniques used for making polycrystalline ceramics, such as cold pressing and sintering, hot pressing, reaction bonding and infiltration. Chemical vapour infiltration, liquid polymer infiltration and liquid silicon infiltration are currently used for the production of carbon fibre reinforced SiC ceramic composites [7, 29].

Table 2.7: Room temperature mechanical and thermal properties of some matrix materials [4]

	ρ (mg/m^3)	E (GPa)	σ_u (MPa)	Strain to failure (%)	K (W/m℃)	C_p (kJ/kg℃)	α (10^{-6}℃)
Thermoset Epoxy	1.10-1.20	2.6-3.8	60-85	1.5-8.0	0.17-0.20	1.05	45-65
Thermoplastic PEEK	1.26-1.32	3.2	93	50	0.25	1.34	40-47
Ceramic Alumina Al2O3	3.98	380	282-551	-	39	0.775	7.4
Ceramic Silicon carbide SiC (sintered)	3.20	207-483	96-520	-	71	0.59	4.1
Metal Aluminium alloys (7075)	2.80	71	572	11	130	0.96	23.4
Metal Steel alloy (1020 Cold drawn)	7.85	207	420	15	51.9	0.486	11.7

ρ: Density; E: Young's modulus; σ_u: Tensile strength; K: Thermal conductivity; C_p: Special heat; α: Coefficient of thermal expansion.

2.3.2 Industrial applications

Due to their attractive mechanical and thermal properties, ceramic matrix composites are suitable for a range of aerospace applications requiring high temperature performance and reliability. They can be used to replace CFRP and MMCs in relatively high temperature working environments (up to ~2000℃) [27, 30]. Industrial uses of CMCs include furnace materials, energy conversion conponents, gas turbines, and heat engines [5]. CMCs have excellent potential as structural materials in aerospace applications offering high tensile and flexural strength, high temperature capability, damage tolerance, dimensional stability, good chemical and oxidation resistance and great thermal shock resistance [30]. For example, carbon fibre reinforced CMCs have good resistance to oxidation degradation in air at temperature of up to 400℃, whereas SiC reinforced CMC can operate up to 1000℃ in air [30]. Ohnabe [31] studied the potential applications of CMCs for aero-engine components including blisks (bladed disk for rotating parts), nozzle flaps, exhaust nozzles, combustor and turbine nozzle vanes. Figure 2.10 shows the trends in development of high temperature materials for turbine components.

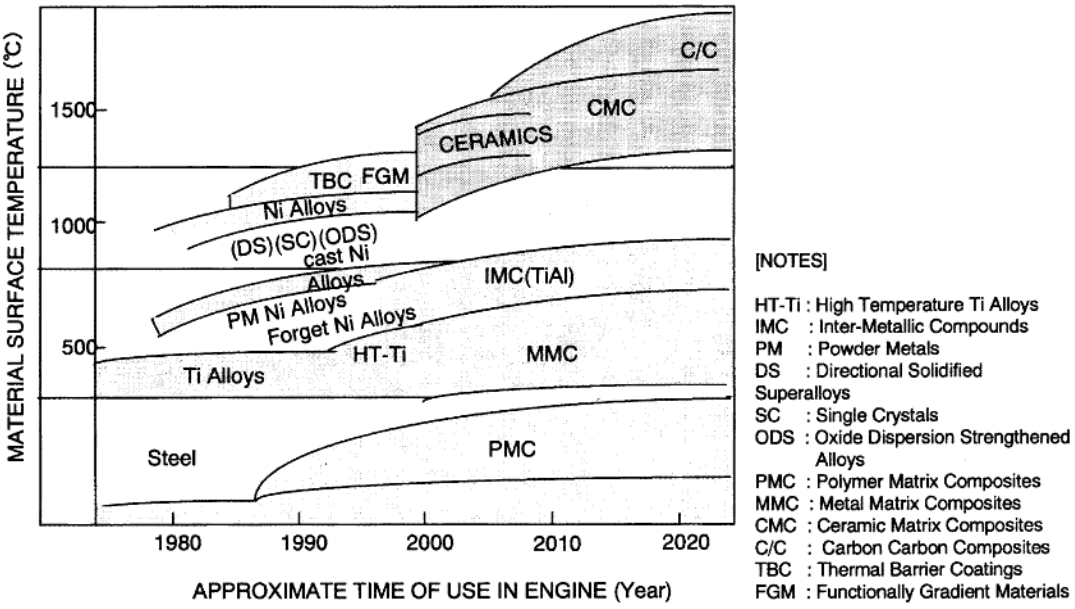


Figure 2.10: Development of high temperature materials for turbine components [31]

Ceramic matrix composites have become first choice for components subjected to high temperature in the aerospace industry and in advanced vehicles, such as nose caps, nozzle jet vanes, engine flaps and brake discs [32]. Rosso [33] stated that the development of CMCs has lagged behind other composites for two main reasons, the first being that the processing routes for CMCs involve high temperatures and can only be employed with high temperature reinforcements, while the second concerns the high temperatures employed in production.

Kaya [34] outlined the use of ceramic matrix composites in automotive ceramic gas turbines and claimed that the thermal efficiency was increased by over 40% at a turbine inlet temperature of 1350℃ as well as reduced exhaust emissions. Figure 2.11 shows the major CMC components used for automotive ceramic gas turbines. Sommers et al. [35] detailed the application of CMCs for heat exchangers in advanced thermal systems, due to their high temperature stability and shock resistance, high hardness, good corrosion resistance and non-magnetic properties.

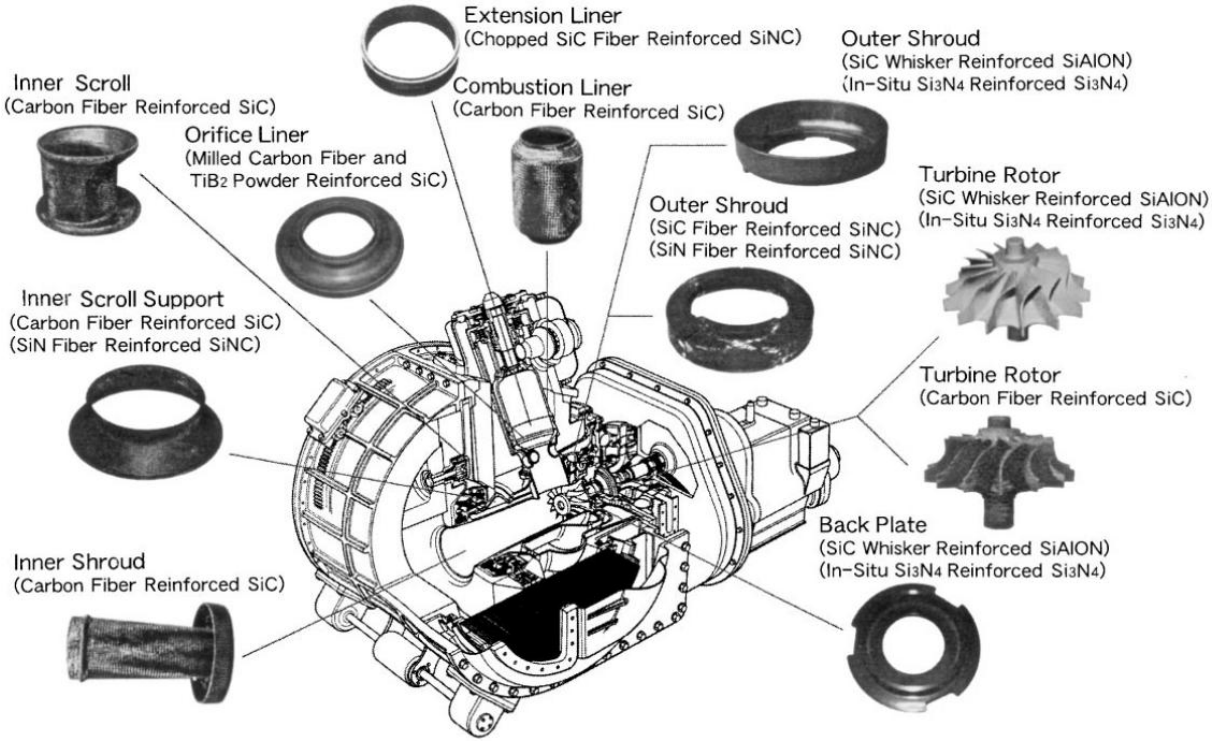


Figure 2.11: Major ceramic matrix composites components used for automotive ceramic gas turbine [34]

2.4 Drilling of CFRP composite materials

2.4.1 Introduction

Carbon fibre reinforced plastic composites are commonly used for structural aerospace components including floor beams and frame panels, as well as the majority of vertical and horizontal sections of the tail. Joining of such parts is mainly dependent on mechanical bolting / riveting, which depends critically on the quality of machined holes. Consequently, the quality of drilled fastener holes in CFRP is paramount, with metrics relating to hole surface roughness, out of roundness and cylindricity as well as the level of workpiece delamination / flaws. However, CFRP composites have relatively poor machinability mainly due to the abrasive nature of the fibres leading to rapid tool wear, inhomogeneous and

anisotropic properties relating to different fibre orientation and the lay up process, and dissimilar thermal properties of the matrix and fibre [36-38]. Damage such as delamination, fibre pull out and matrix burning which occur by drilling operations can significantly reduce strength / fatigue life [39]. It has been reported that the rejection rate for composite laminate parts due to damage / defects induced by drilling during final assembly in the aircraft industry is up to 60% [40, 41]. Therefore, it is essential to study / understand machinability when drilling CFRP composite materials and improve drilling efficiency / productivity with minimum hole damage / defects.

2.4.2 Tool wear and life

When drilling CFRP composites, tool wear is primarily the result of abrasion due to the highly abrasive nature of fibres, with chipping a characteristic feature of coated tools. The tool life criteria widely used to determine end of tool life is maximum flank wear (VB_{max}), which is typically between 0.3-0.6 mm. It is common to observe that the wear on WC tools is generally smooth and uniform along the entire cutting edge due to abrasion between the hard carbon fibres and tool [42]. Rawat and Attia [43] experimentally investigated tool wear mechanisms of WC drills when drilling woven CFRP. They found that cutting edge rounding and abrasion were the main wear mechanisms, as shown in Figure 2.12. Relatively high cutting temperatures (~350ºC) caused by aggressive rubbing of fractured fibres and WC grains against epoxy matrix exacerbated tool wear. The progression in flank wear was divided into three regions; the initial / primary wear region, steady / secondary wear region and severe / catastrophic wear region. The initial / primary wear was caused by chipping and micro-cracking and occurred after drilling a small number of holes (~10). Nor Khairusshima et al. [44] came to similar conclusions when machining CFRP with carbide tools using chilled air as the coolant. Figure 2.13 shows tool wear observations under the microscope and SEM. The shiny and worn area was detected with the microscope while a corresponding smooth and polished surface was found under SEM. This was due to the abrasive carbon fibres and powdery chips which acted as polishing elements continually rubbing the cutting edge during the machining process. A polished and shiny tool surface was apparent at test cessation. Masuda et al. [45] studied tool wear mechanisms and the influence of WC grain size as well as Co content on tool wear rate when machining CFRP with uncoated WC tools. They pointed out that the main failure was due to loss of WC particles leading to the probability of brittle fracture as the Co binder was subject to severe wear when cutting abrasive CFRP materials. Tool wear decreased with the increase of WC grain size (varied from 1.11 to 2.93 μm) while

lower Co content (ranged from 4 to 10%) led to better tool performance. Therefore, larger WC grain size integrated with lower Co content was preferable for machining CFRP materials.

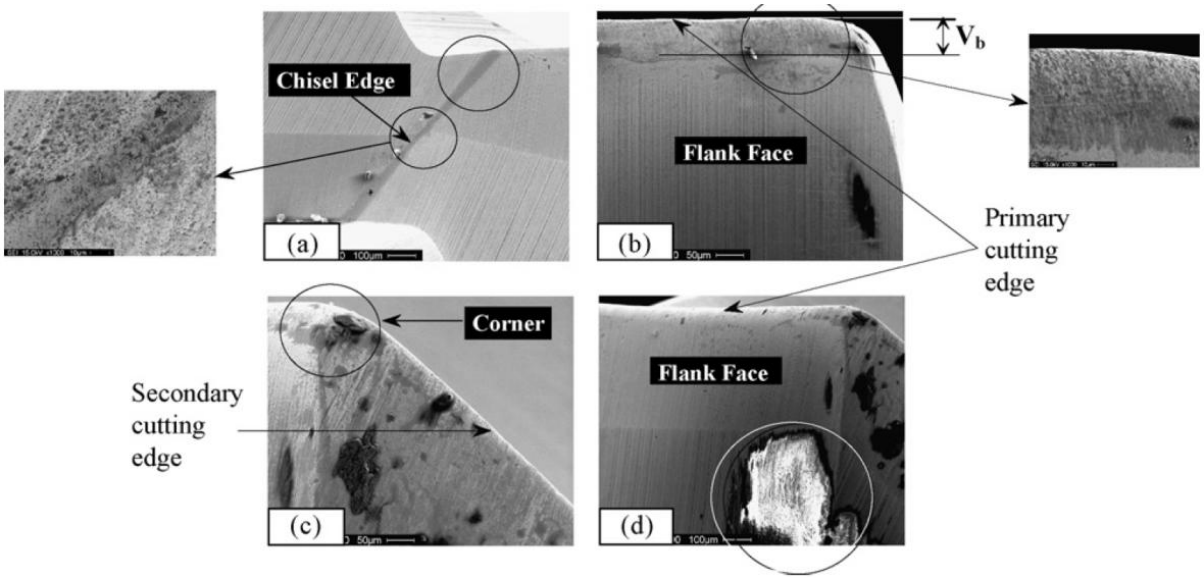


Figure 2.12: SEM micrographs of tool wear at the cutting speed of 235 m/min and feed rate of 0.1 mm/rev: (a) aggressive abrasive wear at chisel edge, (b) abrasion of flank wear, (c) corner edge rounding and (d) adhesion of carbon fibres on the flank face [43]

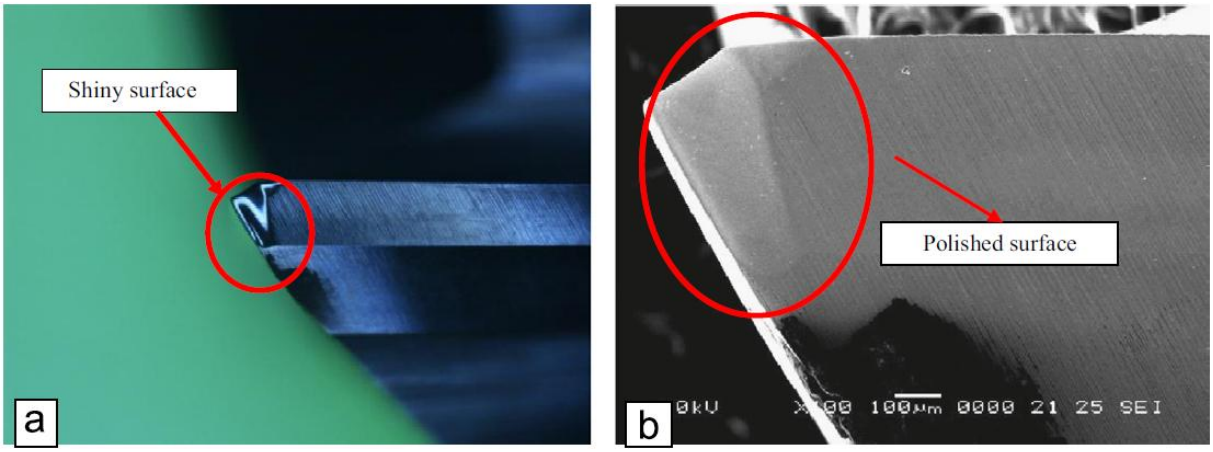


Figure 2.13: Tool wear at the cutting speed of 179 m/min and feed rate of 0.05 mm/rev under the observation of (a) tool maker microscope and (b) SEM [44]

Diamond coated tools were also investigated by researchers. Karpat et al. [46] evaluated the tool wear of diamond coated tools when drilling woven CFRP laminates under dry conditions. As shown in Figure 2.14, drilling at high feed rate (0.1 mm/rev) was shown to be more favourable in terms of tool wear as severe damage was observed at low feed rate (0.04 mm/rev). This was due to the longer contact time (2.5×) at low feed rate compared with drilling at high feed rate. After drilling 1728 holes, coating fracture was observed at both high

and low feed. Iliescu et al. [47] compared tool life of uncoated and diamond coated drills. They concluded that diamond coated tools gave 10~12 times longer tool life than uncoated carbide drills even though the cutting speed was 3 times higher (170 m/min instead of 56 m/min) at the feed rate of 0.05 mm/rev. Abrasion and chipping of the coating were the main tool wear modes.

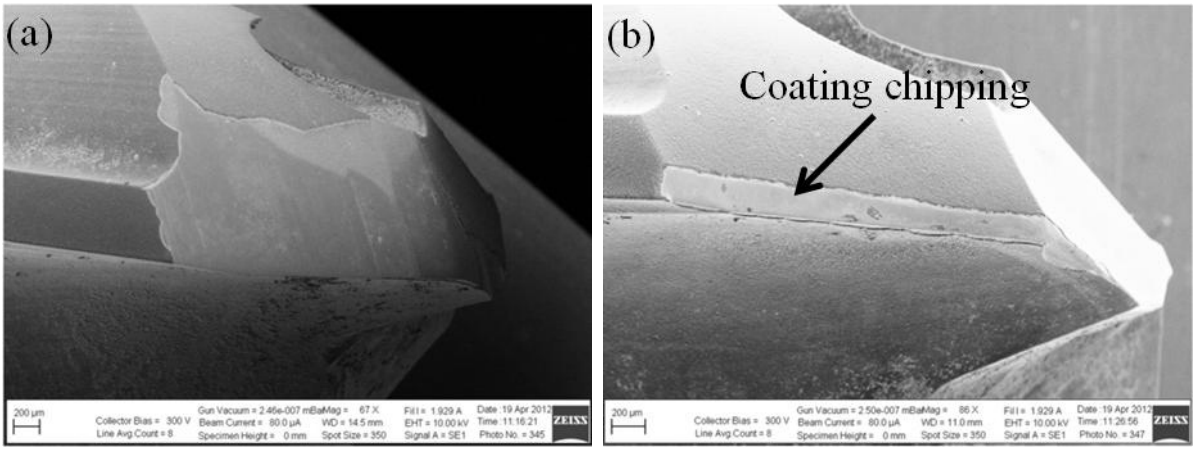


Figure 2.14: SEM micrographs of tool wear after drilling 1728 holes at cutting speed of 200 m/min and feed rate of (a) 0.04 mm/rev and (b) 0.1 mm/rev [46]

Another typical wear pattern commonly observed when cutting CFRP composites is severe cutting edge rounding [4, 17, 48]. The influence of cutting edge radius / sharpness on drilled hole quality was investigated by several researchers [17, 49-51]. Figure 2.15 shows the effect of cutting edge radius on delamination when drilling GFRP with fibres having a diameter of approximately 15 µm. Hole exit delamination significantly deteriorated with growing cutting edge radius, as shearing was severely impeded when the cutting edge radius was larger than fibre diameter [50]. Faraz et al. [17] firstly recommended using cutting edge radius (CER) as an innovative tool wear criterion when drilling CFRP. The applicability of the new wear form was successfully tested on four drills with different geometries and good correlations were observed between thrust force and CER as well as between the size of hole entry / exit delamination and CER.

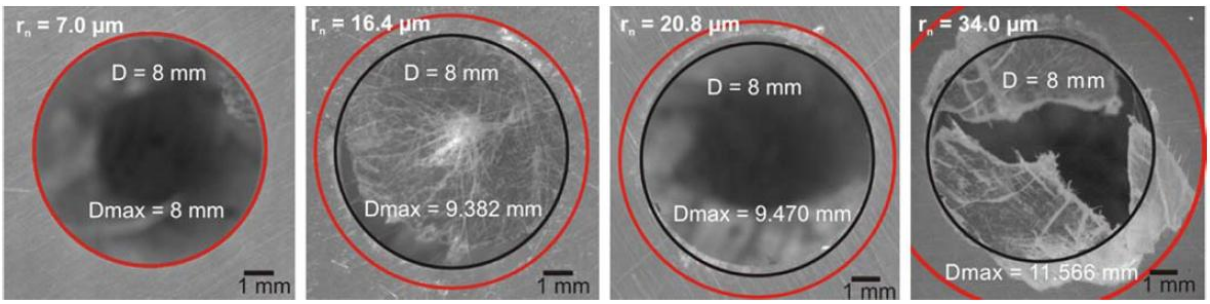


Figure 2.15: Delamination at hole exit with corresponding cutting edge radius [50]

Results from other research studies also indicated that the occurrence of delamination was highly dependent on tool sharpness (cutting edge radius). As shown in Figure 2.16 when milling CFRP, there was no delaminnation and uncut fibres observed when using a sharp tool (cutting edge radius r_n=9 µm), whereas small fibre overhangs were observed after using a tool having medium wear (r_n=45 µm). Significant fibre overhang and breakout occurred when increasing cutting edge radius to 90 µm.

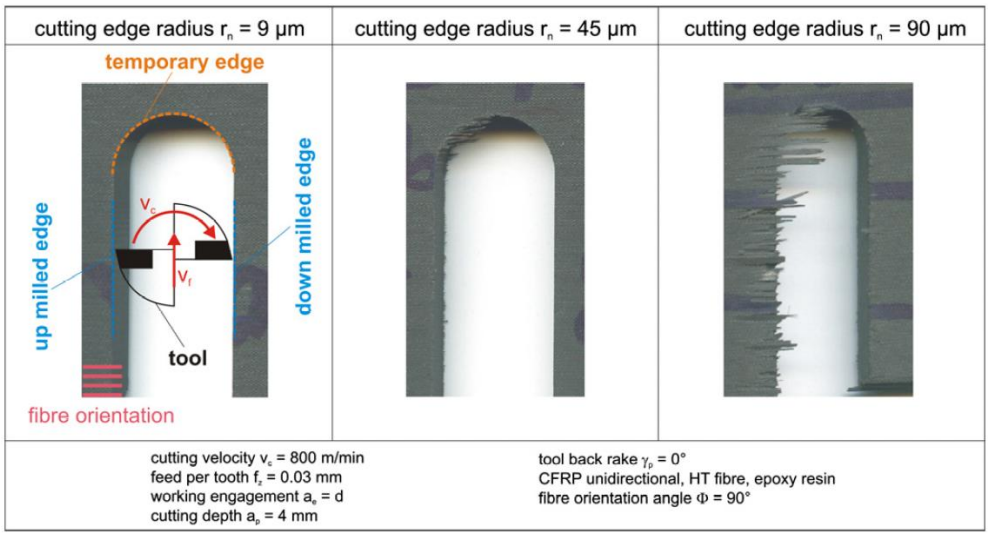


Figure 2.16: Delamination as a function of tool cutting edge radius [51]

Wang et al. [49] investigated tool wear in drilling CFRP using uncoated, diamond coated and AlTiN coated tools at 180 m/min with a feed rate of 0.076 mm/rev. They found that cutting edge rounding or edge recession was the primary wear mode, as shown in Figure 2.17. Drills coated with AlTiN showed no improvement over uncoated carbide drills.

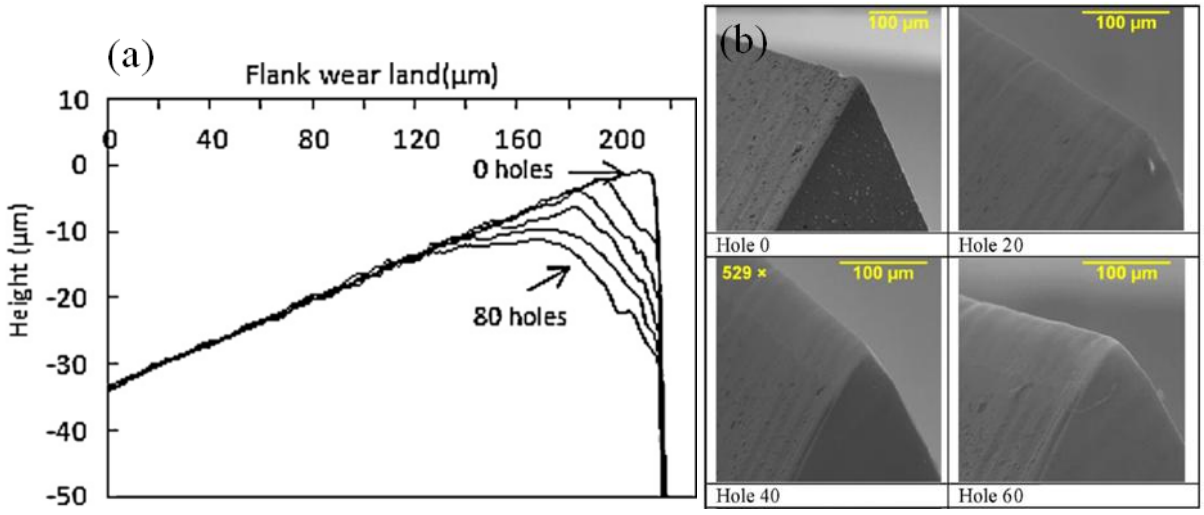


Figure 2.17 (a) Cutting edge profile of uncoated carbide drill corresponding to number of drilled holes and (b) SEM micrographs of cutting edge of AlTiN coated drill [49]

2.4.3 Thrust force, torque and cutting temperature

Thrust force and torque in drilling composite materials have been extensively studied by researchers and they are in agreement that feed rate has significant effect on thrust force while torque normally decreases with increasing cutting speed [52-57]. Monitoring of thrust force was demonstrated as a suitable response to assess tool wear and hole exit quality due to a strong correlation. According to Heisel and Pfeifroth [58], thrust force (from ~100 to 400N) increased almost linearly with feed rate ranged from 0.05 to 0.40 mm/rev at the cutting speed of 42.7 m/min when drilling CFRP with carbide tools. Rawat and Attia [53] explained that the reduction of thrust force when drilling CFRP at high cutting speeds (up to 236 m/min) was due to thermal softening of the matrix resulting from poor heat conductivity of the epoxy, the heat concentration leading to matrix decomposition and even burnout. Zitoune et al. [59] studied the effect of tool materials on thrust force when drilling CFRP/Al stacks at a cutting speed of 38 m/min and feed rate of 0.1 mm/rev with 6 mm uncoated and triple coated (TiN+AlTiN+nanocomposite CrAlSiN) tools. After drilling 70 holes, the thrust force in the CFRP section increased by 72% and 92% with coated and uncoated tools, respectively. The variation in thrust force for the Al section was about 11% irrespective of the tool material. Park et al. [42] carried out experiments in drilling CFRP/Ti stacks using WC and PCD tools with mist water-soluble coolant at a flow rate of 16 ml/min. They found that the thrust forces of both WC and PCD tools increased gradually in the CFRP and Ti, due to the tool wear progression. In the Ti section, the thrust forces generated by WC tools at high speed (24 m/min) increased more rapidly compared with those at lower cutting speed (12 m/min), while the PCD drills with less tool wear produced approximately constant thrust forces (~1500 N), see Figure 2.18. There was marginal difference in thrust forces and torques in the CFRP sections generated at high and low cutting speeds, which was in agreement with Chen's conclusions that cutting speed had little / no significant influence on thrust forces when drilling CFRP with carbide tools [60].

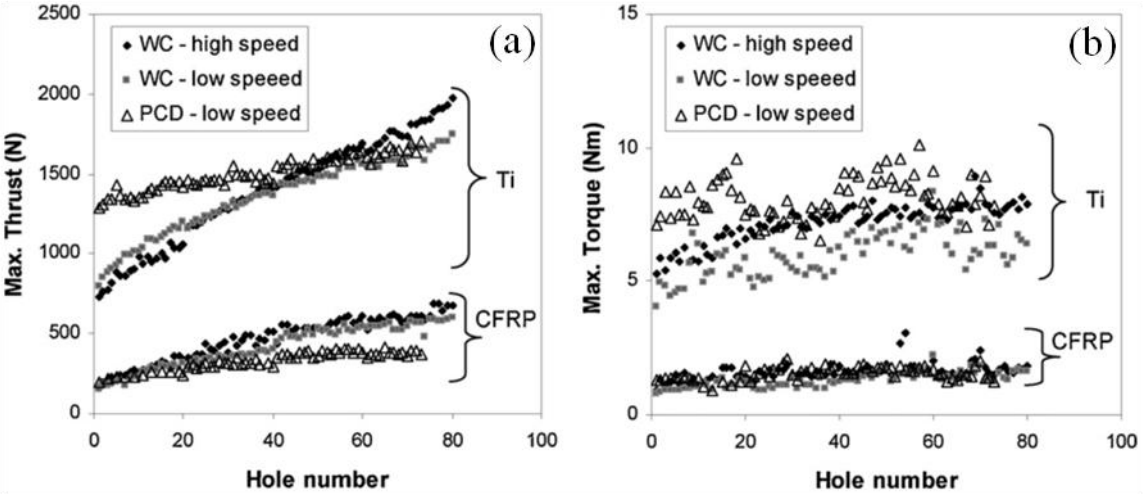


Figure 2.18: (a) Variations of maximum thrust force and (b) torque against number of drilled holes with different tool materials and cutting conditions [42]

Zitoune et al. [61] studied thrust force and torque when drilling copper mesh/CFRP/woven ply using uncoated WC twist and double cone drills. The double cone drill had 90° and 136° point angles with corresponding cutting edge length L1 and L2, as shown in Figure 2.19. Results indicated that double cone drills produced 20-30% lower thrust forces compared with conventional twist drill, see Figure 2.20. This was attributed to the fact that the secondary point angle (90°) reduced the average chip thickness by ~15% at the same machining parameters. A small reduction of thrust force (~20N) was observed when machined at low feed rate (0.05 mm/rev) and high cutting speed (55 m/min) as opposed to 40 m/min, which was due to increased temperature resulting in softening of the materials and a subsequent reduction in thrust force. The torque generated by the double cone drills was generally higher than that produced with twist drills. This was due to the higher cutting length of double cone drills.

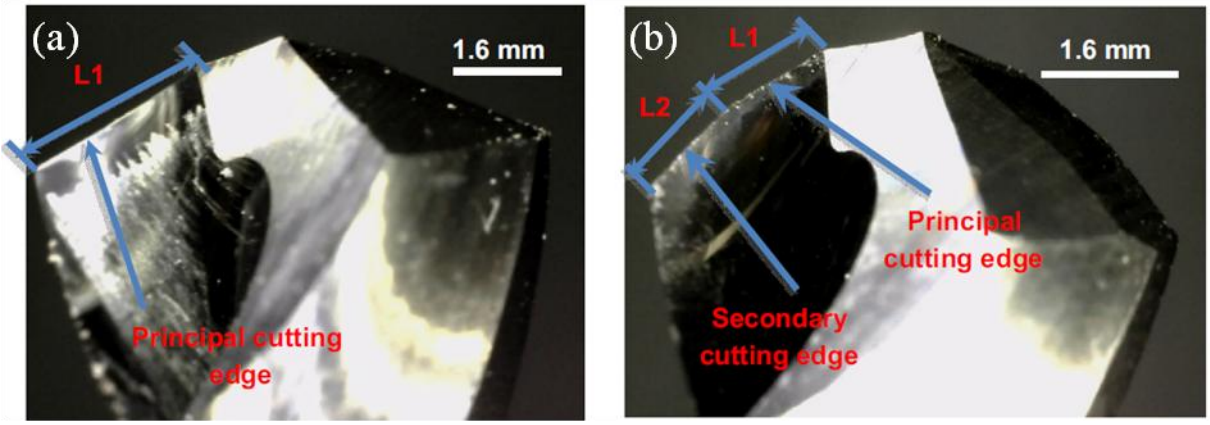


Figure 2.19: Schematic showing drilling tools: (a) standard twist drill and (b) double cone tool type M2 [61]

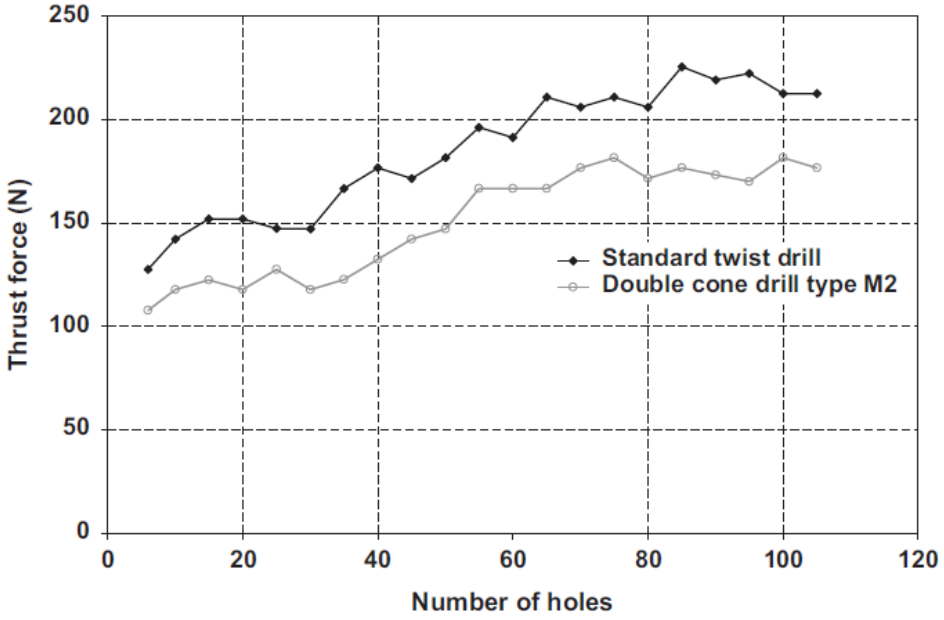


Figure 2.20: Progression of thrust force against number of drilled holes [61]

Cutting temperature has a close relationship with hole quality as relatively high temperatures can lead to matrix degradation / burning and tool wear acceleration. Weinert and Kempmann [62] investigated cutting temperature when drilling CFRP. They used implanted nickel-chromium-nickel thermocouples and performed the tests with a rotating cylindrical specimen and fixed drill, as shown in Figure 2.21. Cemented carbide drills were employed with a diameter of 8 mm. Cutting temperature and feed force against drilling depth at a cutting speed of 180 m/min together with feed rates of 0.1 and 0.3 mm/rev are shown in Figure 2.22. The temperature increased rapidly up to ~180ºC at the beginning of drilling and went up continuously reaching 387ºC when operating at the lower feed rate (0.1 mm/rev). When the feed rate was elevated to 0.3 mm/rev, cutting temperature was approximately constant (~310ºC) which was possibly due to the balance between temperature generation and heat

removal. Weinert et al. [63] also employed implanted thermocouples to measure cutting temperature when drilling polyetheretherketone (PEEK) and 30 vol.% glass and fibre reinforced PEEK (PEEK GF 30 and PEEK CF 30), with PCD tools at a cutting speed of 120 m/min and feed rate of 0.1 mm/rev. The non-reinforced PEEK recorded the highest temperature of ~370ºC after drilling 20 mm due to its lower thermal diffusion coefficient (19.5 $kJm^{-2}h^{0.5}K$) compared with PEEK GF 30 (63 $kJm^{-2}h^{0.5}K$) and PEEK CF 30 (94 $kJm^{-2}h^{0.5}K$). The generated temperature was higher than the materials melting temperature (334ºC) and caused visible unevenness at the surface due to a local adhering and tearing effect of the tool as the material became more ductile and the static friction coefficient increased. The cutting temperature for PEEK GF 30 and PEEK CF 30 after drilling 20 mm was ~310ºC and 290ºC, respectively. Quan and Sun [64] measured cutting temperature with inserted K-type thermocouples (0.25 mm in diameter) between two CFRP (30 vol.% reinforcement) laminates having shallow grooves which were tightly clamped. Carbide tools were used. It was found that the temperature increased up to ~180ºC at 63 m/min and 0.01 mm/rev due to poor heat dissipation associated with poor conductivity of the CFRP composite. The highest temperature was recorded at ~250ºC when drilling CFRP at a cutting speed of 188 m/min and feed rate of 0.005 mm/rev. This method was also employed by Yashiro et al. [65], who measured cutting temperature when milling CFRP.

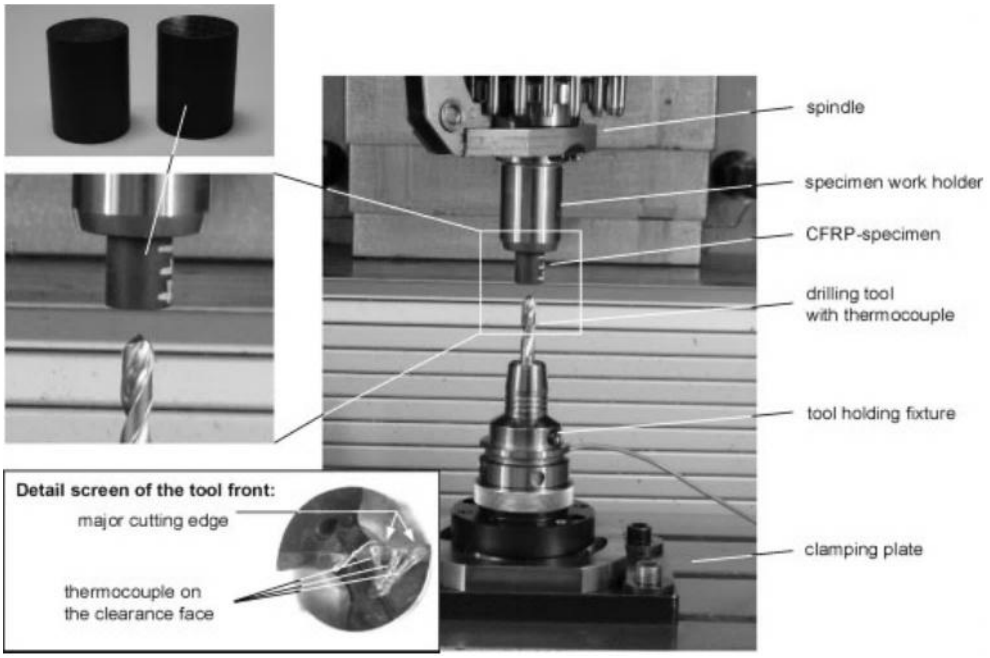


Figure 2.21 Experimental setup for temperature measurement [62]

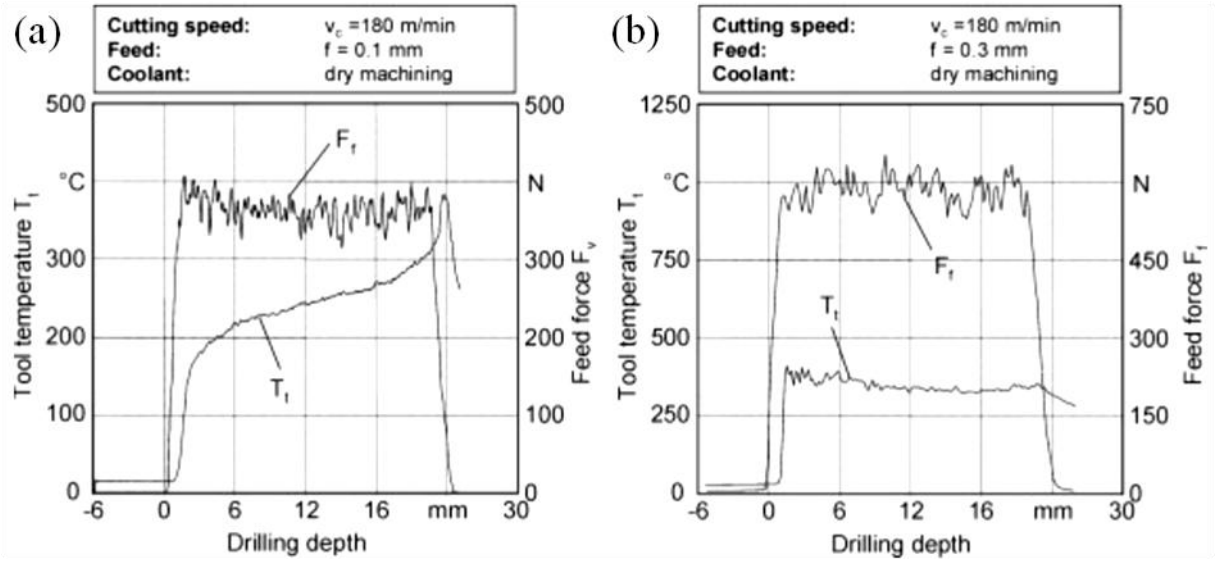


Figure 2.22: Cutting temperature and feed force when drilling CFRP at the feed rate of (a) 0.1 mm/rev and (b) 0.3 mm/rev [62]

Rawat and Attia [53] reported a cutting temperature of ~210ºC when drilling CFRP at a cutting speed of 24 m/min and feed rate of 0.02 mm/rev with carbide tools under dry conditions. The temperature exceeded 290ºC at 133 m/min and 0.2 mm/rev. Brinksmeier et al. [66] employed a pyrometer when measuring cutting temperature during drilling of CFRP composites. The experimental setup is shown in Figure 2.23. It was observed that cutting temperature increased with cutting speed but decreased with an increase of feed rate. The highest temperature of 191.6ºC was recorded at a cutting speed of 120 m/min and a feed rate of ~0.027 mm/rev (200 mm/min). In contrast, both the cutting speed and feed rate had a reverse effect on thrust force, as shown in Figure 2.24.

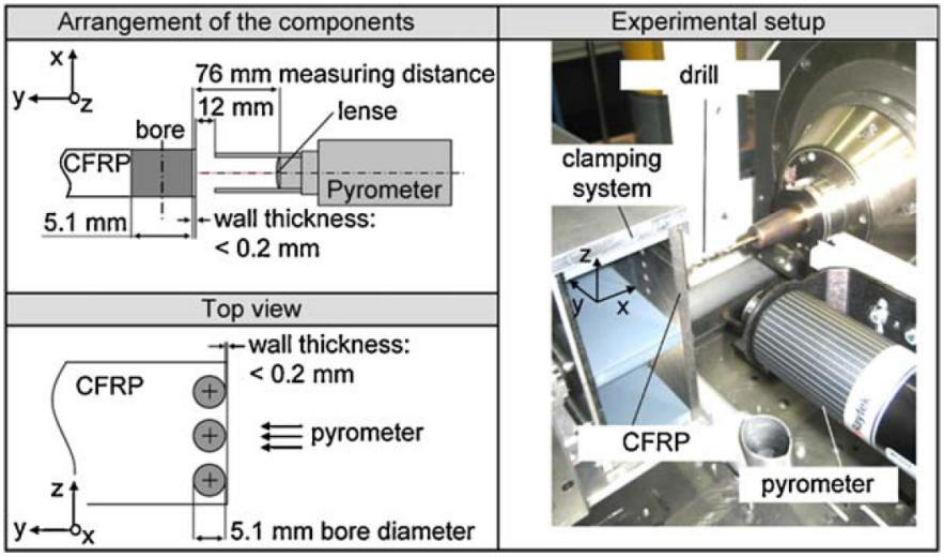


Figure 2.23: Experimental setup for temperature measurement using pyrometer [66]

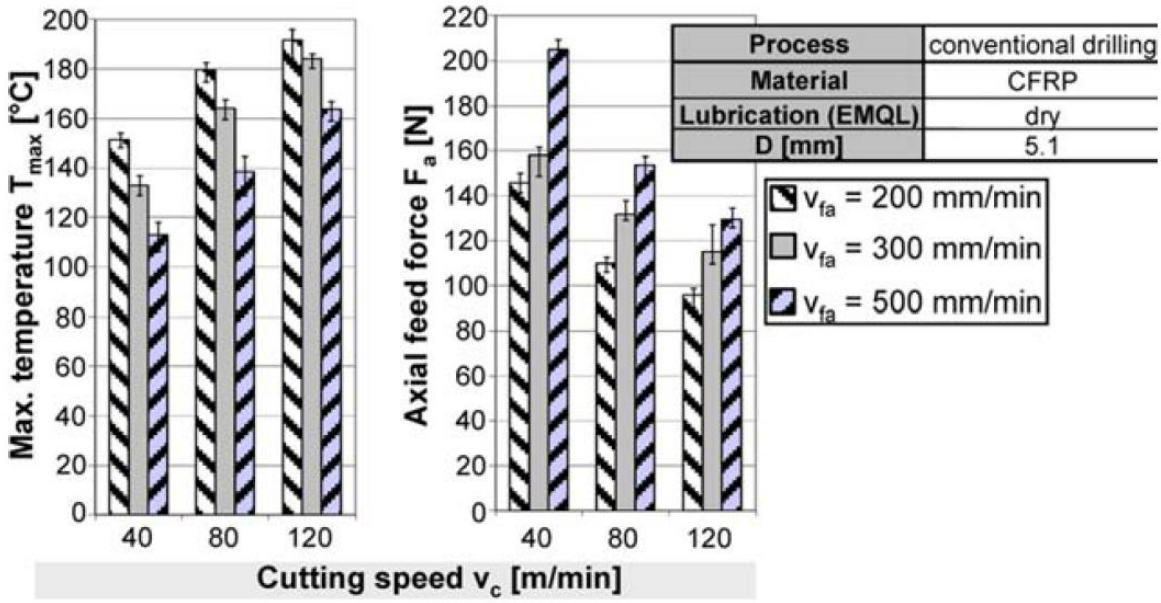


Figure 2.24: Cutting temperature and feed force against cutting speed in drilling CFRP [66]

2.4.4 Drilled hole geometrical accuracy and surface integrity

The diameter tolerance on bolt holes in CFRP wing and tail structures is about 30 µm or lower [67]. Brinksmeier and Janssen [67] studied hole diameter variations when drilling CFRP/Al multi-layer materials with both conventional twist and step drills. The deviations of hole diameter were within ~55 µm and diameter values in the CFRP layer were lower than those in Al layer when using uncoated conventional drills, which was attributed to the low modulus of elasticity of CFRP. Step drills improved hole diameter tolerance as the deviations were ~20 µm, which was due to reduction of mechanical loads by distribution on several cutting edges. Further improvement was observed when using minimum quantity lubricant (MQL) instead of dry machining. The hole diameters produce by diamond coated drills were however unexpectedly high, which was thought to be due to coating chipping and poor cutting lip sharpness. Montoya et al. [68] analysed hole diameter in drilling CFRP/Al multi-layer materials using 6.0 mm diameter tools with different tool materials and coatings including uncoated tools, diamond tools, TiAlCrN and AlTiSiN-G coatings at a cutting speed of 56.5 m/min and feed rate of 0.04 mm/rev. Results showed that the diameter measured in CFRP was bigger than the one recorded in Al, which was possibly due to a thermal effect during drilling. Better results for hole diameter error were observed for uncoated and coated tools with values of 8-9 µm against 16-18 µm for TiAlCrN and AlTiSiN-G coated tools at test cessation (drilling ~100 holes).

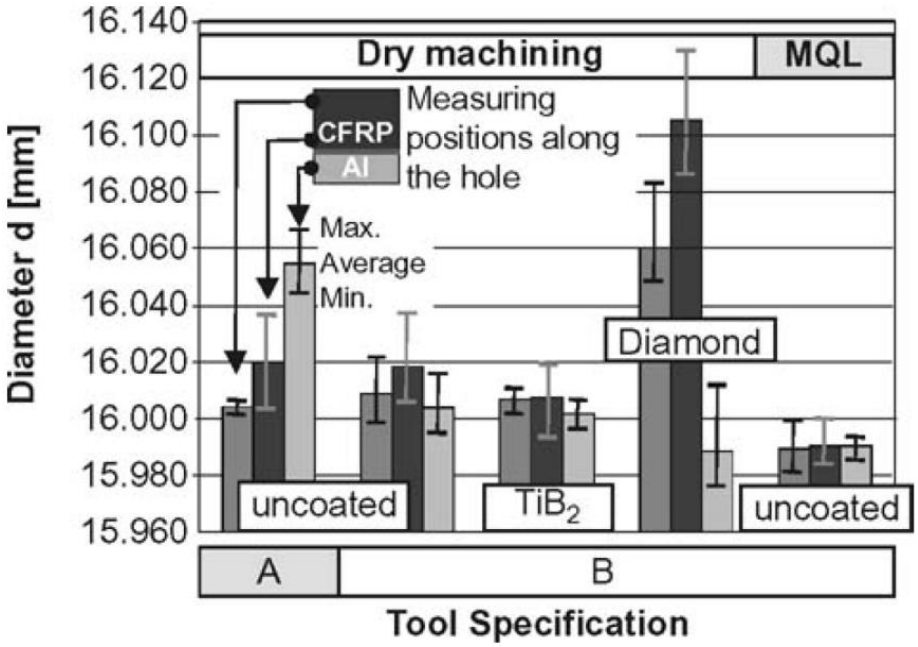


Figure 2.25: Hole diameter variations in drilling CFRP/Al with different cutting specifications (A: Ø16 mm uncoated conventional drill; B: Ø15.4/16 mm uncoated, TiB_2 and diamond coated step drills) [67]

Circularity is a measure of how much a feature deviates from a perfect circle. Zitoune et al. [69] experimentally analysed hole diameter and circularity when drilling CFRP/Al stacks with carbide drills under dry conditions. Hole diameter and circularity were measured using a coordinate measuring machine (CMM) with a 2 mm diameter ruby probe. When machining with a 4 mm diameter drill at cutting speeds of 13 to 35 m/min and feed rates from 0.05 to 0.15 mm/rev, circularity for the CFRP increased with increasing of feed rate and was marginally influenced by cutting speed. Circularity was limited to ~6 µm at low feed rate (0.05 mm/rev) but increased to ~25 µm at high feed rate (0.15 mm/rev). Roundness and cylindricity are two measures that can be used to characterise hole geometrical accuracy. Roundness indicates how the individual circular cross section of a hole approximates a true circle, while cylindricity refers to how much the entire cylinder deviates [70, 71]. The determination of roundness necessitates the measurement of irregularities, which are normally referred to as undulations, peaks, valleys and lobes, while poor cylidricity typically relates to a lack of straightness, poor roundness and taper exhibits either a curved, waisted or barrelled geometric shape [70]. Ramulu and Kim [72-74] studied hole geometric quality and surface integrity when drilling graphite / bismaleimide and Ti6Al4 alloy stacks using HSS and carbide tools. They observed that cutting speed was a major factor affecting cylindricity while feed rate mostly influenced hole diameter and surface roughness values. Shyha et al. [71] assessed hole quality including hole diameter, out of roundness and cylindricity when drilling

metallic-composite (Ti-6Al-4V/CFRP/Al7050) stacks at various cutting parameters in wet / flood and spray mist conditions. The majority of holes in the CFRP layer produced under wet / flood cutting conditions were undersized with a maximum error of 20 µm, while spray mist trials generated oversized holes. This was probably due to thermal expansion of the matrix from increased cutting temperature due to the lack of lubricant / coolant access and poor chip evacuation. Both roundness and cylindricity improved as the tests proceeded in wet / flood cutting conditions with deviations in CFRP roundness of up to 39 µm and cylindricity error over the entire stack 23-120 µm after drilling up to ~300 holes.

It is considered that drilling of composite materials is a critical operation, as the principle drawbacks relating to entry / exit delamination, fibre pullout and poor surface finish are not uncommon [37, 53, 75, 76]. Figure 2.26 shows the typical hole surface damage when drilling CFRP workpiece materials. Various forms of hole defects / damage including porosity / cavities (due to loss / absence of matrix materials between layers), internal cracks (fibre / matrix cracking), resin / fibre loss etc. were observed. The damage was mainly due to the fibrous nature of the workpiece material and the differences in thermal / mechanical properties between fibres and matrix material [56]. Zhang et al. [77] characterised hole exit defects with spalling and fuzzing. The spalling caused by chisel and cutting edge actions developed normally along the fibre direction and outside the cutting region, while fuzzing occurred in the cutting region and was mainly influenced by cutting angle and fibre orientation. Both defects co-existed and had similar variation tendency. Dipaolo and Caprino et al. [78-80] studied damage development / crack growth phenomenon in drilling composite materials and divided it into three stages including plate bulge, spall opening and spall tearing / twisting. All researchers concluded that damage was strongly dependent on feed rate value.

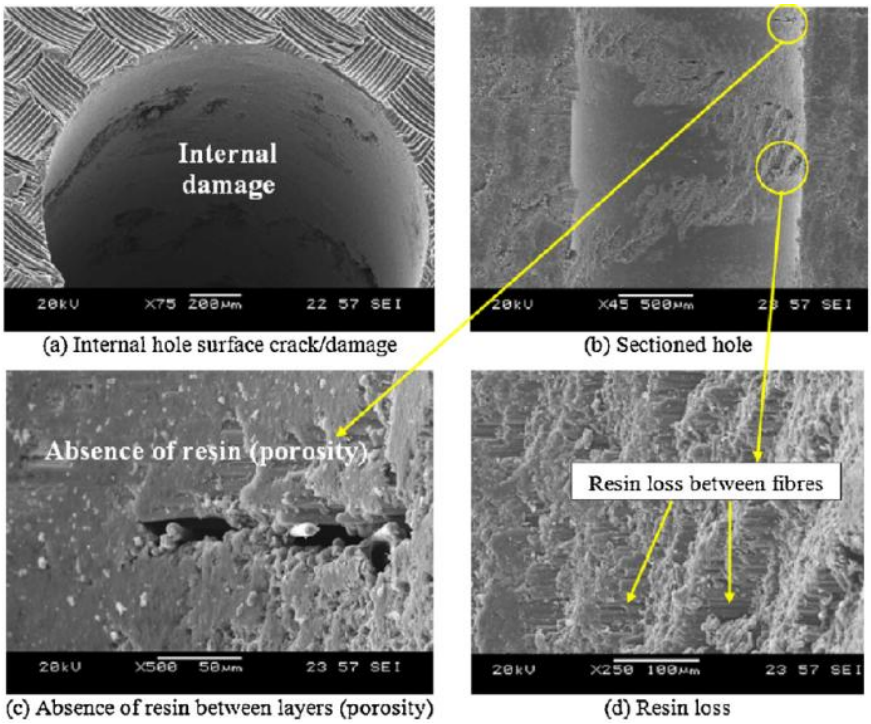


Figure 2.26: SEM micrographs of surface damage [55]

Delamination is not uncommon in drilling composite materials and results in poor structural integrity and assembly tolerance as well as potential deterioration of long term performance. Khashaba et al. [54] reported delamination at both hole entry and exit even at a feed rate as low as 0.056 mm/rev and cutting speed of 20 m/min when drilling GFRP with 13 mm diameter carbide tools, as shown in Figure 2.27. The delamination behaviour is partly related to cutting temperature which can promote softening of the matrix and induce additional delamination [81]. Several authors report that that delamination is sensitive to cutting speed, feed rate and drill point angle [82].

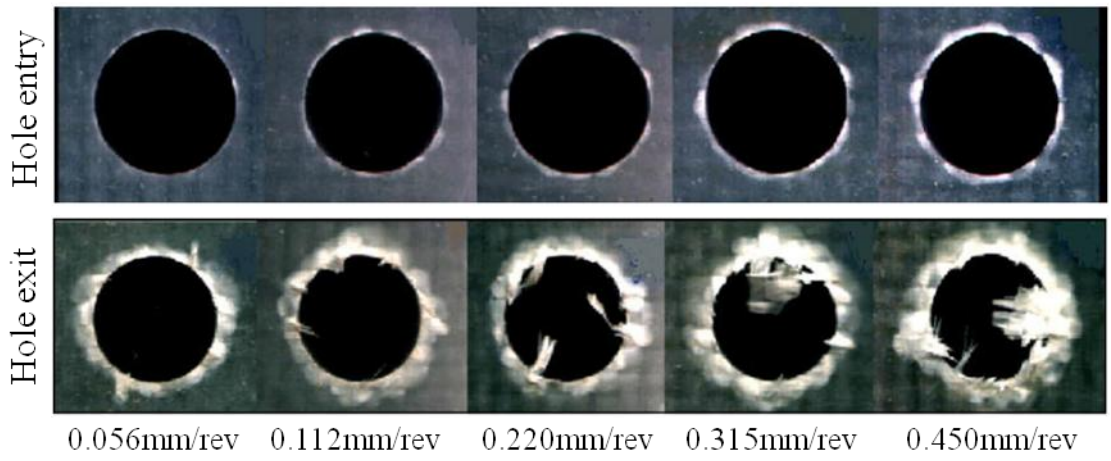


Figure 2.27: Entry and exit delamination at the cutting speed of 20 m/min with various feed rates [54]

Surface roughness measuring instruments which employ a stylus can be used to detect the internal damage in drilling composites [54, 83]. Figures 2.28(a) and 2.28(b) show SEM micrographs of drilled holes in GFRP with corresponding surface roughness profiles. Deep vallies can be seen at the position of internal delamination.

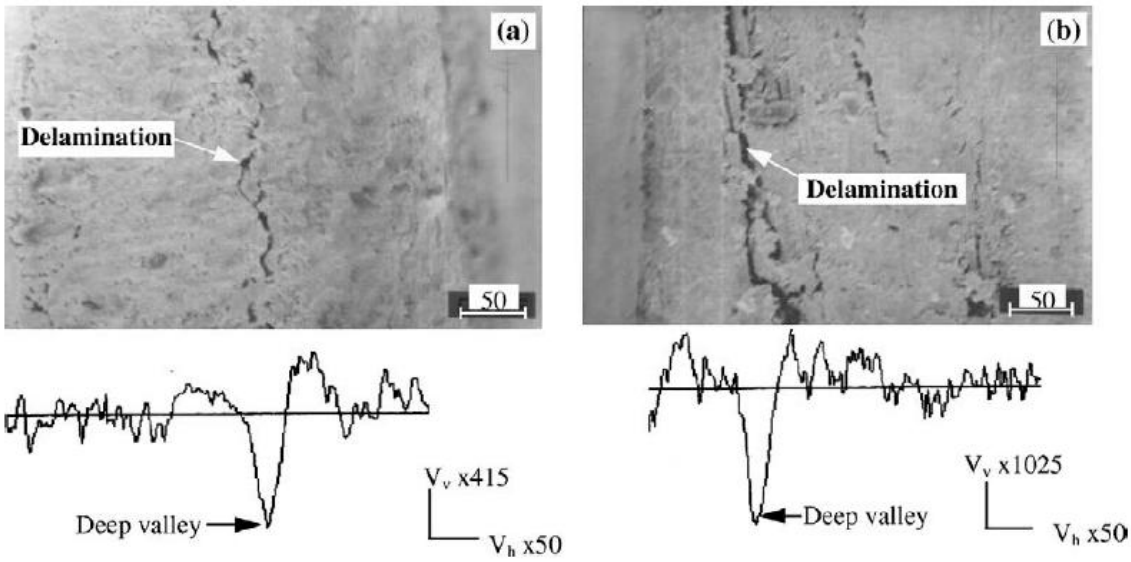
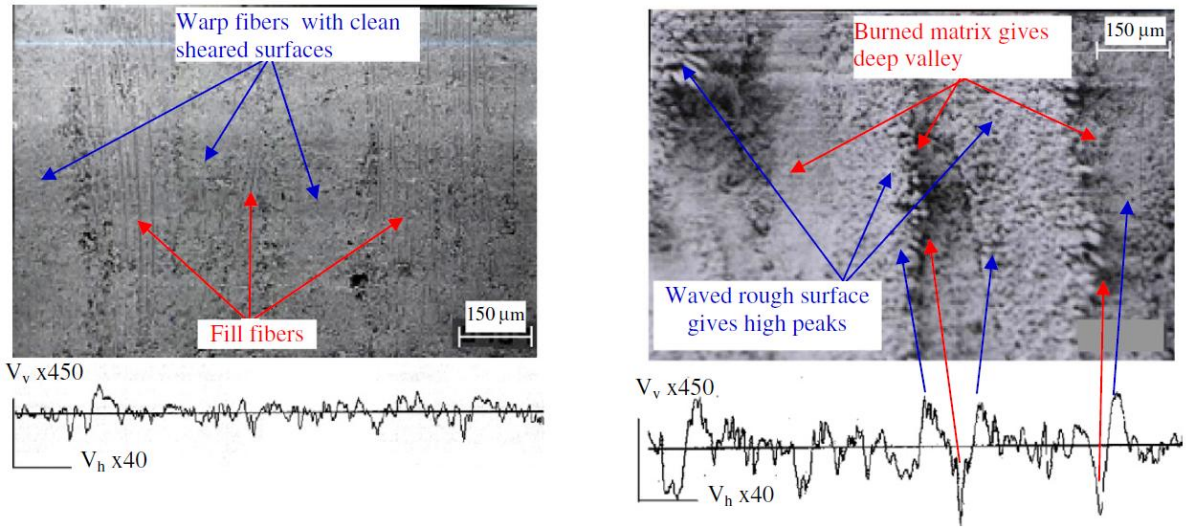


Figure 2.28: SEM micrographs with corresponding surface roughness profile showing delamination at (a) hole entrance and (b) hole exit [54]

Khashaba et al. [83] compared the hole surface roughness produced with new and worn tools when drilling GFRP composites, and concluded that the deterioration of surface roughness was due to higher thrust forces generated by worn drills together with high temperatures resulted from the low conductivity of the composite materials. Surface damage mainly included matrix burning and micro-cracking at the ply interfaces, which could be clearly seen with corresponding surface roughness profiles, as shown in Figure 2.29.



(a) New tool, Ra=2.58µm (b) Worn tool, Ra=8.81 µm

Figure 2.29 SEM micrographs with corresponding surface profiles produced by new and worn drills [83]

Khashaba et al. [54] reported that surface roughness increased up to 50% as feed rate increased from 0.056 to 0.45 mm/rev when drilling woven GFRP composite using carbide tools, however there appeared to be little or no effect when the speed varied from 6.4 to 50.6 m/min. Surface roughness measurement was sufficient for locating damage such as internal delamination and cracking [54, 84]. According to Brinksmeier et al. [66], smooth hole surfaces occurred at low cutting speed (40 m/min) and high feed rate (0.2 mm/rev / 500 mm/min), but subsurface cracks (extended to 50 µm below the surface) were found at high cutting speed (120 m/min) combined with low feed rate of 0.026 mm/rev (200 mm/min), see Figure 2.30. At high cutting speed, hole surface roughness Ra was below 1.6 µm, due to smearing of fibre dust and matrix at high temperature (191.6ºC).

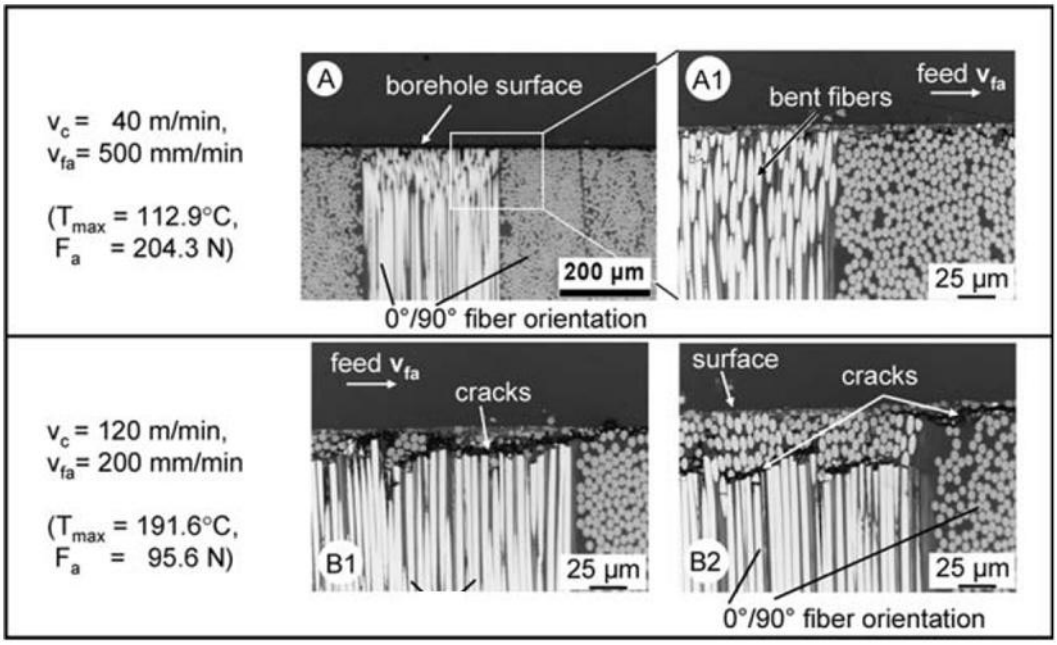


Figure 2.30: Micrographs of hole surface layers in drilling CFRP [66]

Ramulu et al. [84] studied the effect of fibre orientation on surface roughness when edge-trimming graphite/epoxy composite. They found that the surface roughness and breakage of bundles of fibres were highly dependent on fibre direction while crushed fibres were reduced with increasing fibre angle. Pecat et al. [85] evaluated the influence of fibre orientation on surface integrity and forces when milling CFRP with a discmilling cutter equipped with solid carbide inserts. Figure 2.31 shows the various fibre orientations. It was found that damage was visible with fibres oriented at 90° and -45° while the surface for 0° and 45° was smooth and approximately free of cracks or other damage. With fibres oriented at 90°, cracks extended from the machined surface at intervals of ~200 µm, probably as a result of the brittle behaviour of CFRP materials. A large crack parallel to the machined surface was

observed at a fibre orientation of 45°. The depth of the crack extended to about 300 µm beneath the machined surface.

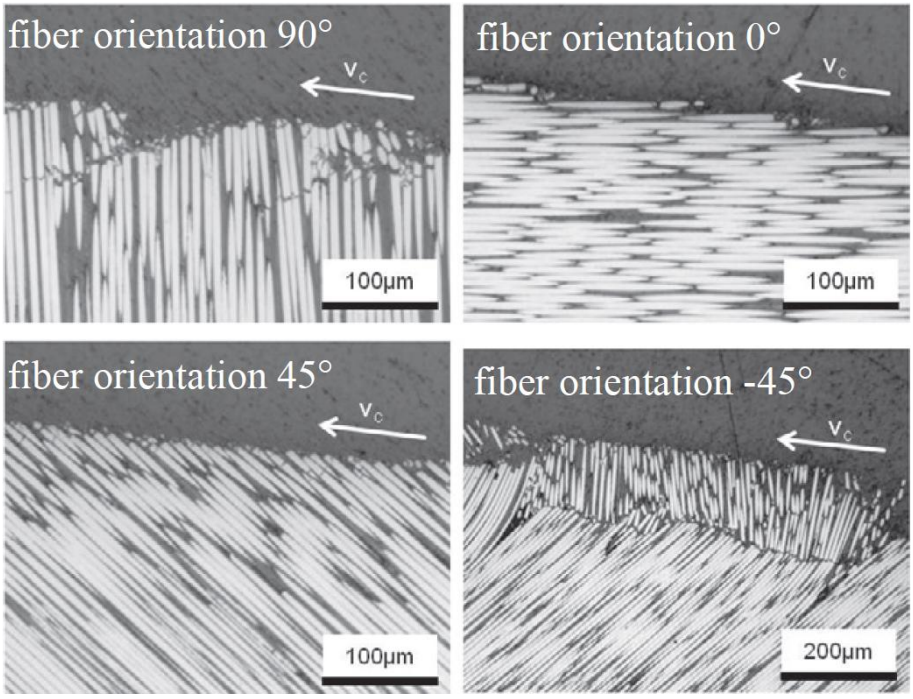


Figure 2.31: Micrographs of subsurface with various fibre orientations [85]

2.4.5 Non-conventional hole making processes

Non-conventional methods such as laser and waterjet cutting, ultrasonic machining, electrical discharged machining and helical / circular milling have been considered for hole making with composite materials. Both laser and waterjet are very flexible in terms of the type of materials to be cut, automation and productivity, with the major concern being severe surface damage and the possibility of introducing delamination [86]. Additionaly, initial investment is comparably high and difficulties can arise when the hole does not penetrate the workpiece material. Other novel approaches have been applied to minimise thrust force induced damage effects [87]. Liu et al. [88] analysed the feasibility of drilling CFRP with diamond coated core drills integrated with ultrasonic vibration in the axial direction. The results demonstrated that hole exit delamination could be prevented and hole precision as well as surface quality were improved in comparison with conventional drilling without vibration, unfortunately material removal rate was as low as ~8.6 mm^3/s.

In helical milling / orbital drilling, a milling tool traverses a helical trajectory to produce a hole with the finished diameter larger than that of the tool. The two major advantages of this approach are the wide range of diameter that can be produced without changing the tool and the possibility of drilling complex tapered holes [89, 90]. Sadek et al. [91] applied orbital

drilling using a four flute 6.35 mm end mill to make 9.50 mm holes. They found that the maximum tool temperature at hole exit with orbital drilling (~120ºC) was reduced by ~60% compared to conventional drilling with a three flute twist drill at a spindle speed of 6000 rpm and axial feed of 360 mm/min. Schulze et al. [92] presented two milling strategies for hole making including a three-axis process combining circular and spiral milling, and a five-axis process named wobble milling as shown in Figure 2.32. In the five-axis wobble milling process, a starter hole was initially drilled and then the tilted tool rotated around the hole centre followed by final machining of uncut material with a vertical tool in a spiral and circular movement. Wobble milling was found to be influenced by the tool's tilt angle, the major disadvantage of the approach being the relatively low feed rate resulting in a long process time. The circular / helical milling technique was also studied by Weinert and Denkena et al. [93, 94]. While commenting on the advantages previously detailed, they also concluded that productivity was poor.

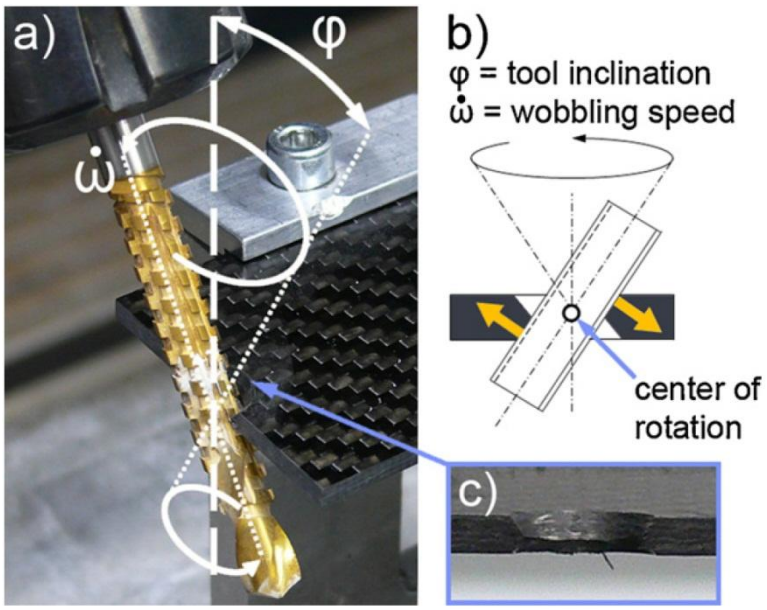


Figure 2.32: (a, b) Schematic and kinematics of wobble milling and (c) double cone geometry of the hole after wobble milling [92]

Riveiro et al. [95] studied the CO_2 laser cutting of CFRP and reported a minimum heat affected zone of 540 µm with a pulsed mode laser. Some other researchers [96-98] also conducted experiments on laser cutting of composites and concluded that epoxy based composite was subject to a large heat affected zone (HAZ). Interior cracks / delamination and a HAZ are quite common in laser cutting of composite materials as shown in Figure 2.33, the results obtained being highly dependent on laser type and operating parameters, fibre orientation and cutting direction, and interaction time between the beam and workpiece. More

research is necessary as there is insufficient knowledge about the influence of thermal machining on the material behaviour. Abrasive water jet machining has also been investigated for cutting composites, key advantages being the absence of thermal distortion, high machining versatility and flexibility as well as low cutting forces [97, 99-101]. However, the relatively high level of machined surface roughness (up to ~30 µm Ra) and water absorption resulting in composite swelling / mechanical property deterioration are the main restrictions in applying this technique [100].

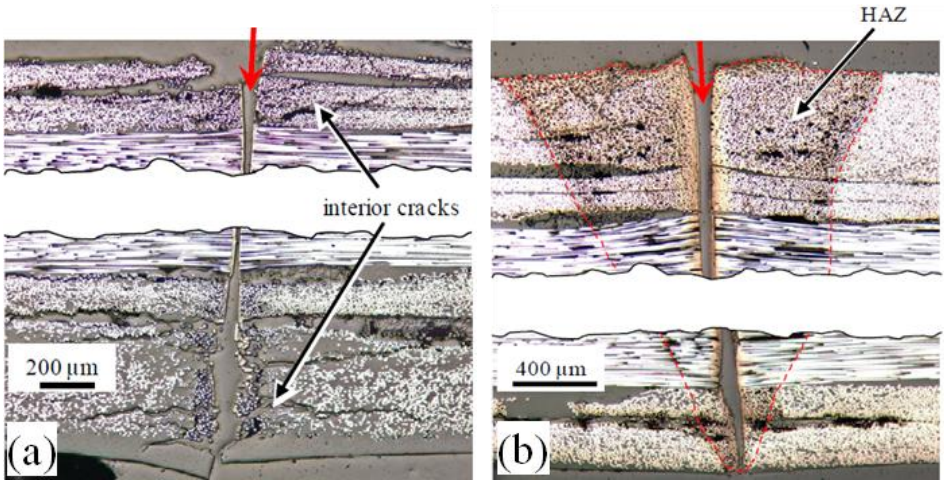
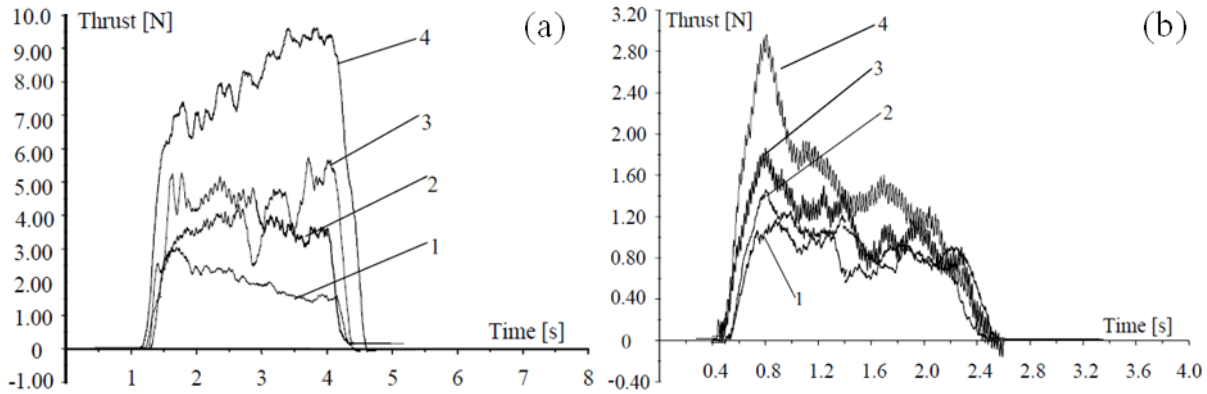


Figure 2.33: (a) Interior cracks and (b) HAZ induced by laser cutting [102]

Vibration assisted drilling (VAD) which is characterised as a pulsed intermittent cutting process, has also been adopted for machining composite materials. A decrease of thrust force, tool wear and delamination was reported when applied the vibratory drilling technique [103-108]. Figure 2.34 shows the thrust force profiles when employing vibration assisted drilling for machining CFRP and GFRP compared with the performance of conventional drills. The decreasing thrust force was attributed to the pulsed / intermittent cutting mode, while reduction in flank wear was possibly due to the reduction in sliding friction and temperature in the cutting zone [104]. Sadek et al. [109] analysed vibration assisted drilling of CFRP and concluded that axial force was reduced by up to 45% compared with conventional drilling. The cutting temperature at the tool lip was recorded by infrared camera and reduced by up to ~20% at a cutting speed of 226 m/min and feed rate of 0.025 mm/rev. Hole exit free of delamination was demonstrated in VAD at a feed rate of 0.025 mm/rev irrespective of cutting speeds (113-226 m/min). According to the experimental work by Jain and Yang [110] as well as Cong et al. [111, 112], it is feasible to use rotary ultrasonic machining techniques for drilling CFRP and CFRP/Ti stacks with metal-bonded diamond core tools. The low feed rate (~0.002 mm/rev) and productivity (< ~30 holes) were the main limitations. EDM has also

been investigated for hole making with CFRP materials, however material removal rate is reported as very low [113-116].



1, 3: vibration assisted drilling, amplitude=2 µm, feed rate=50 mm/min, 100Hz and 300Hz frequency for drilling (a) CFRP and (b) GFRP, respectively

2, 4: conventional drilling, feed rate=50 mm/min

1, 2: Ø0.5mm carbide drill; 3, 4: Ø0.5mm HSS drill

Figure 2.34: Thrust force comparison between conventional drilling and vibration assisted drilling [103]

2.5 Machining of MMC materials

2.5.1 Introduction

Machining of MMC materials is notoriously difficult due to high / extensive tool wear, caused by the hard and abrasive reinforcement (such as SiC particles, carbon fibres, etc.), high dynamic loads caused on the cutting edge, inhomogeneity of workpiece materials and high local cutting temperature generated by intensive microcontact between the cutting edge and reinforcement [36]. Most of the publications related to machining of particulate reinforced MMCs involve turning although some relate to hole production operations and have been evaluated to assess tool wear, surface roughness, cutting forces, subsurface alterations and surface integrity. From the literature, it is apparent that machinability is affected by several factors, such as the type of reinforcement, its volume fraction and matrix properties, see Figure 2.35.

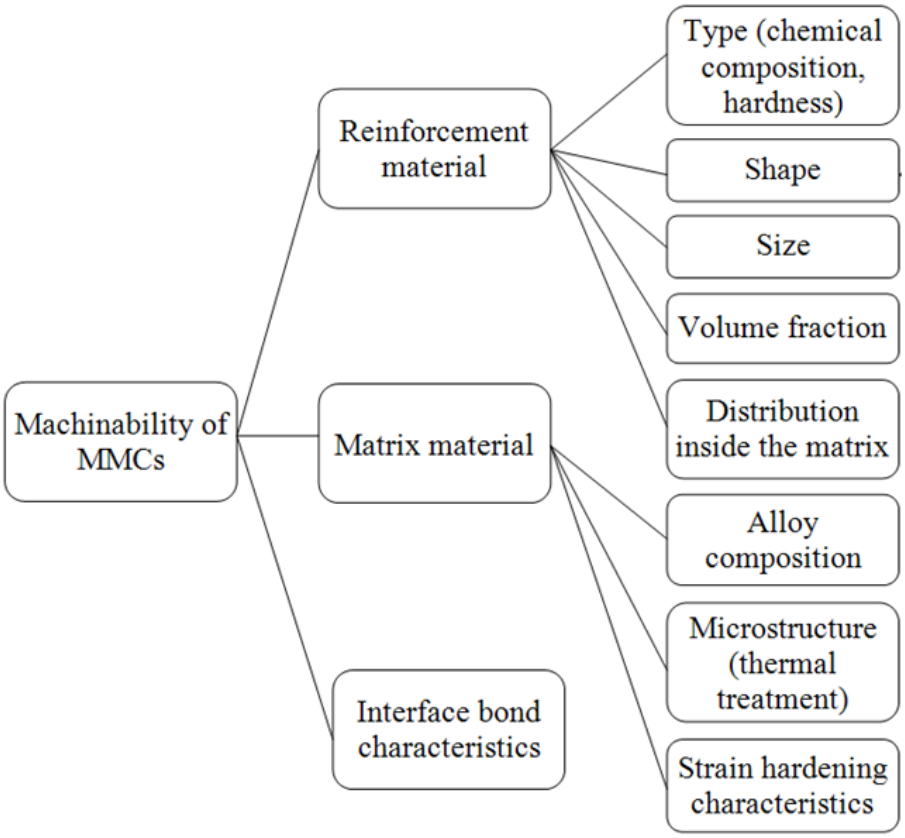


Figure 2.35: Characteristics / factors relating to the machinability of MMCs [20]

2.5.2 Tool wear and life

Tool life / wear investigation of machining MMCs has been the focus of much of the research. Brun and Lee [117] stated that the hardness of tool materials / coatings played an import role in tool wear progression when machining Al/SiC MMCs. The tool wear rate was rapid when the hardness of tool materials / coatings was less than that of SiC. Table 2.8 details the hardness of cutting tool materials / coatings. The drilling of MMCs using conventional carbide tooling is typically characterised by high tool wear rates, poor hole quality and subsurface damage. Polycrystalline diamond (PCD) tool materials show superior hardness compared with other tool materials / coatings and is preferable for machining MMCs.

Table 2.8: Vickers' microhardness of various tool materials / coatings [117]

Material	Microhardness (Test load: 1000 gf)	Material	Microhardness (Test load: 1000 gf)
Polycrystalline diamond (coarse grain)	8000	Polycrystalline diamond (fine grain)	8500
Polycrystalline cubic BN	5000	Hipped alumina-zirconia	2000
Hot-pressed Al_2O_3-TiC	2100	Hot-pressed titanium diboride-boron carbide	3000
Hot-pressed titanium diboride-titanium carbide	3100	SiAlON	1700
Cemented WC-3%Co (medium grain)	1800	Cemented WC-6%Co (fine grain)	1800
Cemented WC-6%Co (medium grain)	1600	Cemented WC-10%Co	1600

Barnes et al. [118] experimentally investigated the effect of matrix heat treatment on tool wear when drilling 18 wt.% Al/SiC MMCs using TiN coated WC tools with 4.5 bar through tool coolant. The four different heat treatment conditions included as-extruded, solution treated (at 530ºC, 2 hours), solution treated and then aged (at 190ºC) for 12 and 20 hours respectively. Results indicated that tool wear at the 100th hole for drilling solution treated and aged MMCs was ~1000 μm compared with ~600 μm for un-aged materials. However, tool wear increased rapidly and only 10 holes were drilled for a flank wear of ~300 μm irrespective of workpiece condition. Ramulu et al. [119] machined Al_2O_3 reinforced Aluminium MMCs with different particle volume fractions (10 and 20%) using HSS, carbide and PCD drills at various cutting speeds (26.4-108.8 m/min) and feed rates (0.0635-0.254 mm/rev). For HSS tools, only one hole could be drilled and flank wear was 0.84 mm after machining 20 vol.% Al/Al_2O_3 at a cutting speed of 26.4 m/min and feed rate of 0.0635 mm/rev. A small number of holes (~15) were drilled with the carbide tool and uniform grooves were observed on the flank face. These grooves showed that Al_2O_3 particles were removed by ploughing rather than abrading or shearing. No obvious wear was found on the PCD tool after drilling ~100 holes due to its superior hardness. Lin et al. [120] analysed tool wear progression when turning 20 vol.% Al/SiC MMCs using PCD inserts at 3 various cutting speeds (300, 500, 700 m/min) together with 3 different feed rates (0.1, 0.2, 0.4 mm/rev) and DOC of 0.5 mm. As shown in Figure 2.36, tool wear increased rapidly with increased cutting speed. Machining time was 4-8 fold longer at the cutting speed of 300 m/min in comparison with 500 and 700 m/min. When machined at a constant cutting speed of 300 m/min, tool wear progressed faster at high feed rate (0.4 mm/rev) while there was

marginal difference when machining at 0.1 and 0.2 mm/rev. This was possibly due to the high temperature generated at high cutting speed and feed rate leading to matrix softening and diffusion wear together with the high kinetic energy of SiC particles accelerating tool wear progress.

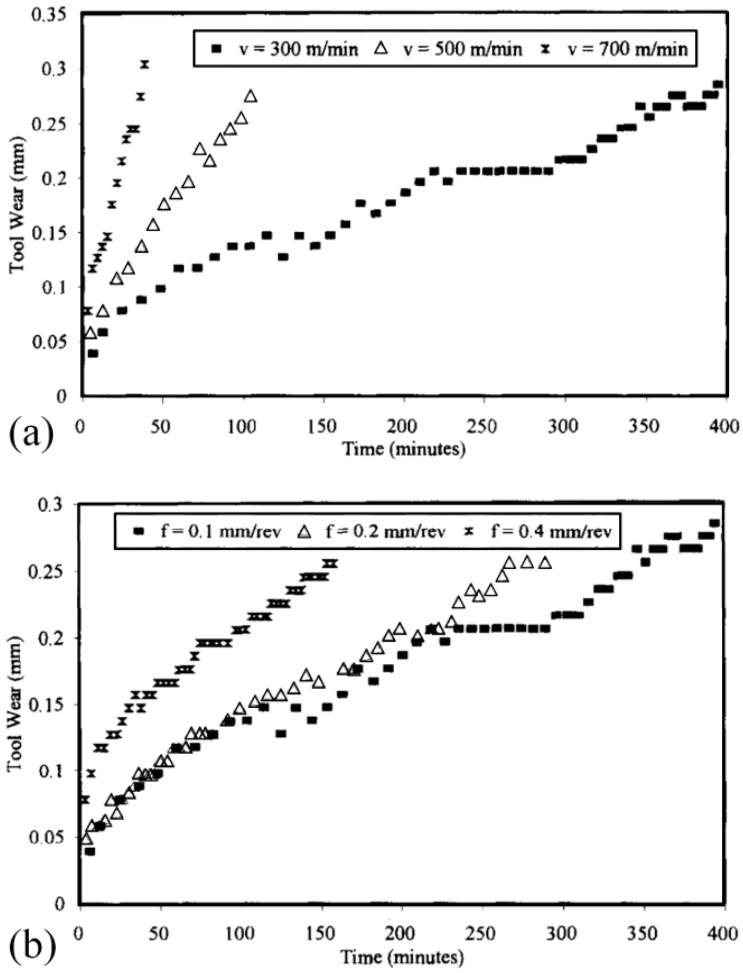


Figure 2.36: Variation of tool wear against machining time at (a) feed rate of 0.1 mm/rev and (b) cutting speed of 300 m/min [120]

Coelho et. al [121, 122] concluded that lower feed rate resulted in increased flank wear due to greater contact time and hence rubbing of the tool against the abrasive particles when drilling MMC under wet conditions. In terms of alternative operations, Ciftci et al [123] evaluated the effect of uncoated and coated (TiC, Al_2O_3 and TiCN triple layer coating) tools when turning MMC, the coated tool giving a ~10% lower tool wear over the uncoated product. This was attributed to the superior wear resistance of the coating and formation of a stable built up edge (BUE) to protect the flank face. Ciftci et al. [124] also evaluated tool wear when turning 16 wt.% SiC/Al MMCs with 3 different average SiC particle size of 30, 45 and 110 µm using CBN inserts. As shown in Figure 2.37, flank wear was the dominant wear mode with abrasion and adhesion the main wear mechanisms when machining the MMCs

containing the 30 and 45 µm SiC particles. When the particles size increased to 110 µm, cutting edge and nose fractures were observed.

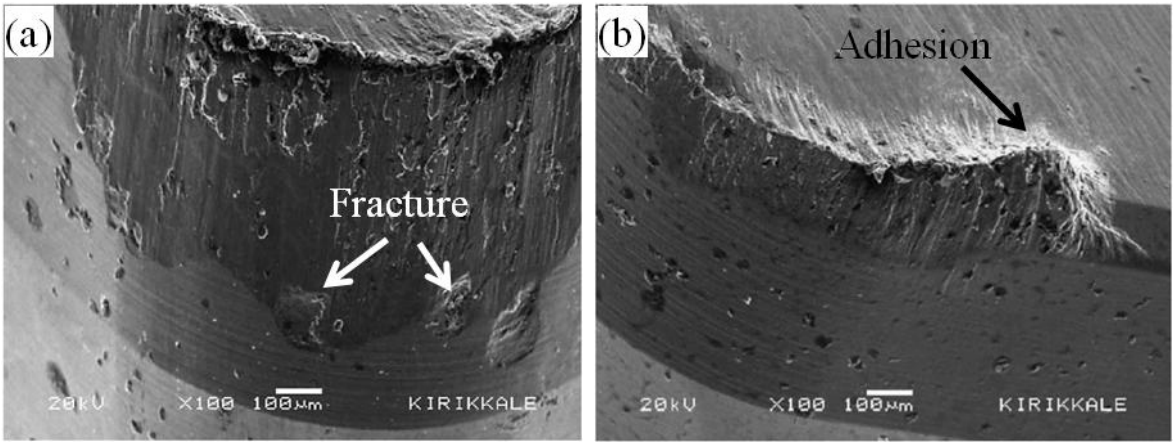


Figure 2.37: SEM micrographs of tool wear after machining (a) Al-SiC/100 µm MMCs and (b) Al-SiC/45 µm MMCs at a cutting speed of 100 m/min and feed rate of 0.12 mm/rev [124]

Davim and Baptista [125] experimentally studied tool wear in turning and drilling 20 vol.% Al/SiC MMCs with PCD tools using emulsion as coolant. They concluded that abrasion was the principle wear mode with adhesion observed occasionally. Figure 2.38 shows the progression of tool wear with various cutting speeds and feed rates. Tool wear increased with increasing cutting time at a constant feed rate of 0.1 mm/rev, however a similar trend was not apparent in the range of tested parameters. There was negligible difference in tool wear with variable feed rates at a cutting speed of 50 m/min, however only a limited number of holes were drilled.

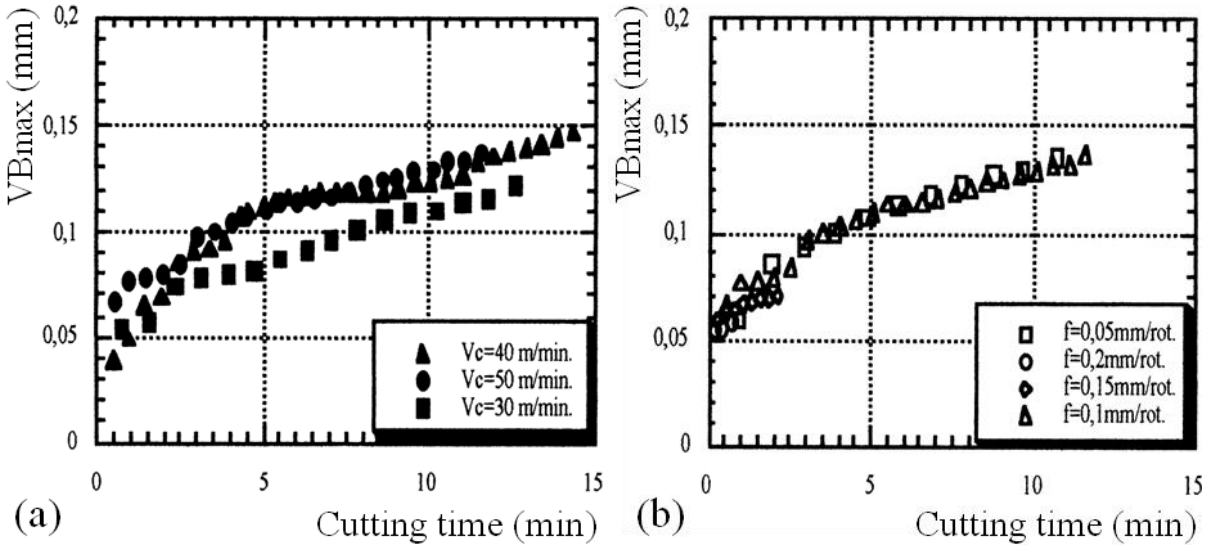


Figure 2.38: Tool wear progression with variable cutting parameters (a) feed rate at 0.1 mm/rev and (b) cutting speed at 50 m/min [125]

Sahin et al. [126] analysed tool wear when turning Al_2O_3 particle reinforced aluminium MMCs with various particle sizes (16, 32, 66 µm) and weight fractions (10, 20, 30%) using TiN coated and triple coated (Ti+Ti(C,N)+TiN) tools. Experimental results showed that tool life decreased with increasing cutting speed (100, 160, 210 m/min) for both coatings. The tool life of the TiN coated tool was slightly longer in comparison with the triple coated one however the tool life was less than 4 min when machining 10 wt.% Al/Al_2O_3 (16 µm) MMCs. It was observed that chipping combined with cutting edge rounding was the main tool wear form. Sahin [127] also used TiC+ Al_2O_3 and Al_2O_3+Ti(C, N)+TiN coated tools when turning Al_2O_3 reinforced aluminium MMCs at cutting speeds of 40, 60 and 80 m/min with a feed rate of 0.12 mm/rev and DOC of 0.6 mm. The cutting time was limited to 15s as flank wear reached 300 µm regardless of cutting parameters and coatings. El-Gallab and Sklad [128] studied tool wear of PCD inserts when turning 20% Al/SiC MMCs at high speeds (670 and 894 m/min). They concluded that the main wear mechanism of PCD was abrasion with micro-chipping / grooves parallel to the chip flow direction. The grooves formed on the rake face were filled with smeared workpiece material characterised as BUE, which protected the tool rake from further abrasion. Figure 2.39 shows the fine grooves which were possibly due to abrasion and the seizure / pull out process of PCD grains.

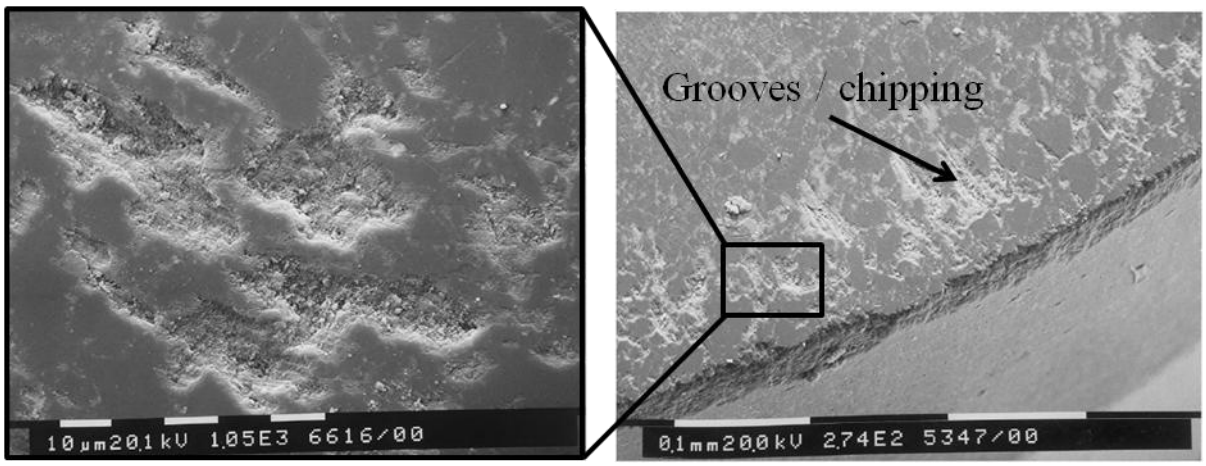


Figure 2.39: SEM micrographs of tool wear on rake face of PCD tool after removing BUE with NaOH solution (cutting speed: 670m/min, feed rate: 0.15 mm/rev, DOC: 1.5 mm) [128]

2.5.3 Cutting conditions

In general, cutting speed, feed rate and the cutting environment play a significant role in the machinability of MMCs materials. Tosun [129, 130] statistically analysed process parameters including cutting speed, feed rate, tool materials / coatings and point angle when drilling 17 vol.% Al/SiC MMC. Results showed that the best surface roughness (0.19 µm Ra)

was obtained at a cutting speed of 4 m/min and feed rate of 0.16 mm/rev with the carbide drill having a 130º point angle. Haq et al. [131] statistically studied surface roughness using grey relational analysis with the Taguchi method when drilling 10 vol.% Al/SiC MMC with TiN coated HSS tools having different point angles (90°, 115°, 140°). The various cutting speeds were 35.2, 56.5, 88.0 m/min and feed rates of 0.05, 0.125, 0.2 mm/rev. The optimisation analysis identified the best hole quality (lowest Ra) when drilling at the highest cutting speed (88.0 m/min) and feed rate (0.2 mm/rev) with the 90° point angle. Barnes and Pashby [132] investigated cutting performance in terms of tool wear, thrust force, surface finish and burr height when drilling 18% Al/SiC MMCs using TiN coated tools under dry, flood and internal through tool coolant (4.5 bar) conditions. They concluded that conventional application of coolant (flood) had no benefits on the cutting operation compared with dry drilling, while through tool coolant even at low pressure gave a significant improvement in all assessed metrics. After drilling 100 holes, flank wear with through tool coolant was ~300 µm while it reached ~700 µm when drilling in dry and flood conditions. This was due to the difficulty in getting the flood coolant to the bottom of the hole and consequently an abrasive slurry around the cutting edges. Ramulu et al. [119] studied cutting performance including tool wear, thrust force, surface roughness, chip shape and burr formation when machined Al_2O_3 reinforced aluminium MMCs with different particle volume fractions (10 and 20%) using HSS, carbide and PCD drills at various cutting speeds (26.4-108.8 m/min) and feed rates (0.0635-0.254 mm/rev). PCD drills outperformed other drills for all the measurements made due to their high wear resistance and were recommended for finish machining of MMCs. Table 2.9 summarises the reported cutting parameters (cutting speed and feed rate) typically employed when drilling MMCs according to the comprehensive literature review. It can be seen that cutting speeds below ~100 m/min are usually employed and feed rate values lower than 0.3 mm/rev are common.

Table 2.9 Summary of cutting parameters in drilling MMCs

Tool material	Workpiece material	Cutting speed (m/min)	Feed rate (mm/rev)	Cutting environment	Reference
PCD	20 vol.% SiC/Al	30, 40, 50	0.05, 0.1, 0.2	Flood	Davim et al. [125]
HSS, TiN coated HSS, carbide	17 vol.% SiC/Al	4, 21	0.08, 0.16	Dry	Tosun et al. [129, 130, 133]
HSS	20 vol.% SiC/Al	35.2	0.16	Not indicated	Morin et al. [134]
Carbide, coated carbide	15 wt.% SiC/Al, 15 wt.% SiC+3 wt.% graphite (15SiC-3Gr/Al)	15.7, 31.4, 47.1	0.05, 0.15, 0.25	Not indicated	Basavarajappa et al. [135-137]
HSS, carbide, PCD	10 vol.% Al_2O_3/Al, 20 vol.% Al_2O_3/Al	26.4, 44.6, 70.0, 108.8	0.0635, 0.127, 0.191, 0.254	Not indicated	Ramulu et al. [119]
HSS, carbide, PCD	15 vol.% SiC/Al	28.6, 40.0, ,56.6, 75.4	0.05, 0.1, 0.2, 0.3	Flood	Coelho et al. [121, 122]
HSS, carbide, PCD	20 vol.% Al_2O_3/Al	45	0.06	Flood	Mubaraki et al. [138]
Carbide, TiN coated carbide, PCD	10 wt.% SiC/Al	19, 38, 57	0.017-0.15	Not indicated	Rajmohan et al. [139, 140]
HSS, TiN coated HSS, carbide, PCD	25 vol.% SiC/Al	4	0.1, 0.2, 0.3	Not indicated	Monahan and O'Reilly [141]
Diamond-like carbide (DLC) coated	20 wt.% SiC+5% Gr/Al, 20 wt.% SiC+10% Gr/Al	55, 63, 71	0.1, 0.13, 0.16	Dry	Altunpak et al. [142]
TiN coated carbide	18 vol.% SiC/Al	30, 40	0.15	4.5 bar through-tool coolant	Barnes and Pashby [118, 132]
HSS	5 wt.% SiC+5 wt.% B_4C/Al	2.5, 5, 10	0.125, 0.2, 0.315	Dry	Ahamed et al. [143]

2.5.4 Chip formation and surface integrity

The size and shape of chips are influenced / governed by tool geometry, cutting parameters and workpiece materials, etc. Generally, small / discontinuous chips are preferable / desirable as they are easily cleared from the cutting area, while long / continuous chips can become entangled with the workpiece and clog the cutting zone particularly when drilling and can result in increased torque requirement and even tool breakage [144]. Pramanik et al. [145] analysed chip shape / morphology when turning 20 vol.% SiC reinforced aluminium MMCs with PCD tools. Figure 2.40 shows various chip morphologies produced at different feed rates with a cutting speed of 400 m/min and DOC of 1 mm. At 0.025 mm/rev, short and irregular chips were observed, while long spiral and straight chips were produced at 0.05 and 0.1 mm/rev, respectively. When increasing the feed rate to 0.2 and 0.4 mm/rev, short C-shape chips were formed. Due to the presence of the reinforcement particles, stress concentrations and local deformations occurred during chip deformation with cracks initiating from bonded particles and work hardening of matrix material making chips brittle and easy to fracture. At low feed rate, chips were deformed homogenously leading to long chips. When reducing the feed to 0.025 mm/rev, chips were thin and easily to break due to fracture of the highly strained particle-matrix interface. Manna and Bhattacharayya [146] also studied chip formation in turning 15 wt.% Al/SiC MMCs using WC inserts at a cutting speed of 100 m/min and feed rate of 0.5 mm/rev. Most of the chips were characterised by a saw tooth profile with high radius curling circle and were broken into small pieces. Cracks initiated from the outside free surface of chips as small voids were formed due to loss of SiC particles and the low ductility of the MMC material. The propagation of the cracks was accelerated by upward and side curling action of the chip resulting in small size chips.

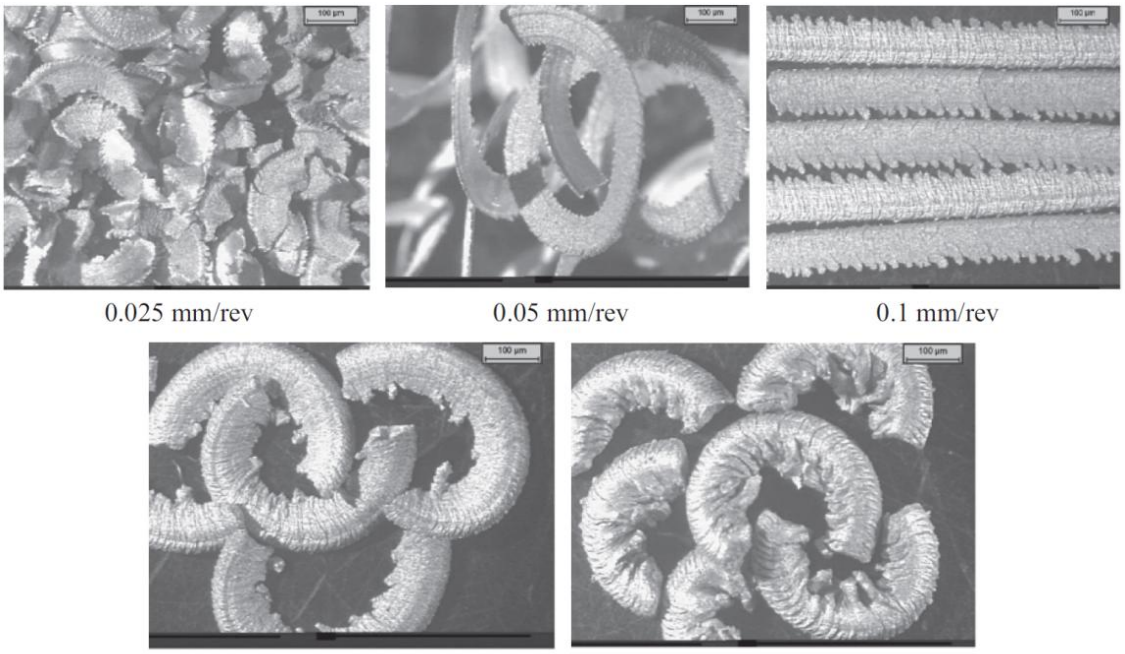


Figure 2.40: Chip morphology in turning MMCs with different feed rate (cutting speed: 400 m/min, DOC: 1 mm) [145]

Ozcatalbas [147] studied chip and BUE formation in turning Al_4C_3 reinforced aluminum based MMCs with a quick stop device. Elemental and arc chips were produced due to the Al_4C_3 particles on the propagation of crack formation on the shear plane. The formation of cracks was attributed to a high stress field and high dislocation density around the Al_4C_3 particles. Ramulu et al. [119] studied surface roughness and chip morphology when machining Al_2O_3 reinforced aluminium MMCs with different particle volume fractions (10 and 20%) using HSS, carbide and PCD drills. They concluded that surface roughness increased with increasing feed rate and decreased with an increase of cutting speed. For PCD tools, Ra was less than 1 μm for both 10 and 20 vol.% MMCs after drilling ~100 holes. Negative skewness was generally observed for all the drilled holes suggesting surfaces suitable for sliding and bearing operations. For HSS and carbide drills, most of the chips were broken into single conical helical shapes although a few were continuous, as shown in Figure 2.41. PCD tools produced uniform single conical helical chips due to the modified cusped flutes as mentioned by the author. Continuous chips are not desirable when drilling as they may damage / destroy the machined surface.

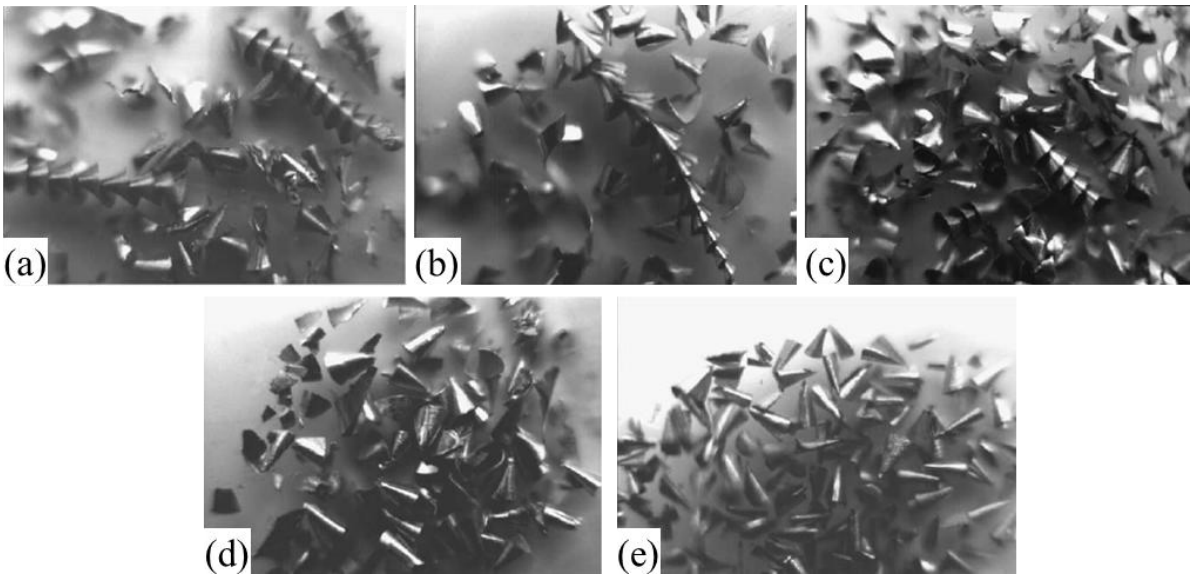


Figure 2.41: Chips produced at the cutting speed of 26.4 m/min and feed rate of 0.0635 mm/rev with (a) 20 vol.% MMCs, HSS drill, (b) 10 vol.% MMCs, carbide drill, (c) 20 vol.% MMCs, carbide drill, (d) 10 vol.% MMCs, PCD drill and (e) 20 vol.% MMCs, PCD drill [119]

Dabade and Joshi [148] studied chip morphology and formation mechanisms when turning Al/SiC MMCs with various particle sizes (coarse: ~65 µm, fine: ~15 µm) and volume fractions (20% and 30%). The experiment was conducted using Taguchi experimental design (L_{27}) with four variables including insert nose radius, tool geometry, feed rate, cutting speed and depth of cut. Each parameter had three levels. Results indicated that feed rate and cutting speed were more significant / dominant in terms of chip morphology. Segmented chips were generated at lower cutting speed (40 m/min) regardless of reinforcement size and fraction. When cutting speeds of 80 and 120 m/min were used, C-type and spring type chips were produced with finer size (~15 µm) reinforcement, while segmented chips were still observed for the coarser (~ 65 µm) reinforcement (see Figure 2.42). The coarse particles acted as chip breakers and produced both segmented and small curled chips. Basavarajappa et al. [137] analysed chip formation when drilling Al/15%SiC and Al/15%SiC-3%graphite (by weight) MMCs using uncoated and coated tools. When drilling Al/15%SiC MMCs, curled and segmented chips were formed regardless of tool material / coatings. This was attributed to the brittleness of the workpiece materials together with loss of SiC particles. The chip regions with particles pulled out acted as crack initiation points. For Al/15%SiC-3%graphite materials, short chips without curl were produced, due to the lubrication effect of graphite and more crack initiation from the loss of both SiC and graphite particles.

Al/SiCp 20 vol.% fine	Al/SiCp 30 vol.% fine	Al/SiCp 20 vol.% coarse	Al/SiCp 30 vol.% coarse
Cutting speed, 80 m/min (Tool nose radius: 0.8 mm, wiper insert geometry)			
			
Connected C-type chips	Connected C-type chips	C-type chips	Small radii C-type chips
Cutting speed, 120 m/min (Tool nose radius: 0.4 mm, wiper insert geometry)			
			
Large radii spring chips	Tubular helix chips	1/2 circle segmented chips	Small radii segmented chips

Figure 2.42: Chip morphology at different cutting speeds with feed rate of 0.2 mm/rev and DOC at 1 mm [148]

A manufacturing process produces a surface consisting of topography and metallurgy, which will influence the surface functional performance, reliability and longevity / fatigue life for industrial / commercial applications [70, 149, 150]. Rajmohan et al. [139] analysed surface integrity in terms of hole surface finish and microhardness when drilling 10 wt.% Al356/SiC MMCs using carbide, TiN coated and PCD tools at cutting speeds ranging from 18 to 57 m/min and feed rates from 50 to 150 mm/min. SEM micrographs showed that microcracks, grooves and pits were the typical surface damage. The grooves were due to SiC particles which had been pulled out and then dragged over the machined surface. It was observed that microhardness increased up to 30HV beneath the machined surface extending to 150-200 µm due to subsurface plastic deformation and strain hardening. El-Gallab and Sklad [151] evaluated surface integrity in terms of surface roughness, subsurface damage / microstructure and microhardnesss alterations when turning MMCs reinforced with 20% SiC particles using PCD inserts. As shown in Figure 2.43(a), grooves / scratches were observed on the machined surface, which could be attributed to lost SiC particles dragged over the surface causing

scratches. PCD grains were also thought be responsible for the formation of these grooves as abrasion was the main wear mechanism. SEM micrographs of the machined surface / sub-surface are shown in Figures 2.43(b), 2.43(c) and 2.43(d), and detail voids around the SiC particles, lost particles and fracture / crushed particles. Microhardness depth profiles indicated a variation of up to 80HV with plastic deformation / strain hardening confined to 60-100 µm below the machined surface.

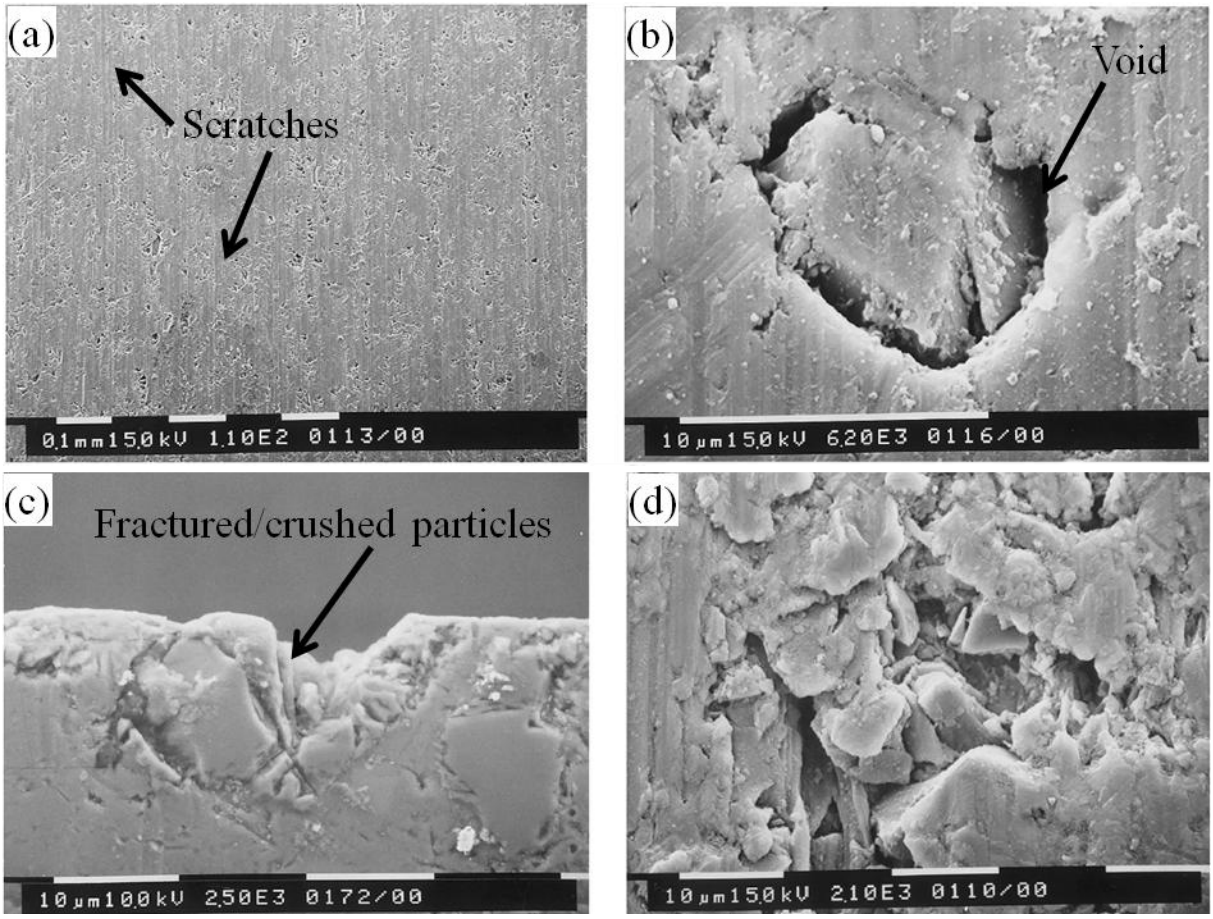


Figure 2.43: SEM micrographs of machined surface/sub-surface (cutting speed: 670 m/min, feed rate: 0.45 mm/rev, DOC: 1.5 mm): (a) overview topography, (b) voids around SiC particles, (c) pulled-out particles and (d) fractured SiC particles [151]

Kannan and Kishawy [152] studied the effect of cutting variables and particle properties (volume fraction and average size) on microhardness profiles when turning Al/Al_2O_3 MMCs with uncoated WC tools. Microcracks, voids, pits and craters were generally observed on the machined surface. A microhardness variation of up to ~40HV was recorded and alterations in microhardness extended up to ~60 µm from the machined surface. They found that microhardness variations increased with an increase of particle size and decrease of volume fraction. Figure 2.44 shows SEM micrographs of workpiece sections. Work hardened / deformed matrix materials were observed within ~60 µm beneath the machined surface.

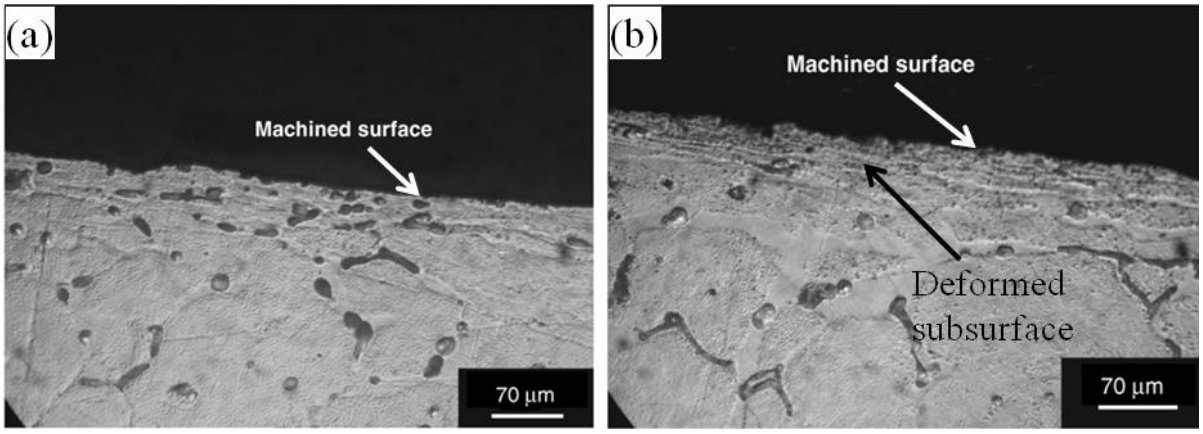


Figure 2.44: SEM micrographs of machined sub-surface of 10% Al/Al_2O_3 MMCs with the average particle size of (a) 20 µm and (b) 9.5 µm [152]

Reddy et al. [153] analysed surface integrity in terms of surface roughness, microhardness and microstructure when machining 20 wt.% Al/SiC MMCs using TiAlN coated tools. Surface roughness values (Ra) reduced from ~1.9 to ~1.1 µm when cutting speed increased from 100 to 200 m/min. In contrast, feed rate (0.1-0.3 mm/rev) had only a marginal influence on surface finish. Surprisingly, microhardness was ~40HV below bulk hardness (160HV) up to the depth of 20 µm irrespective of cutting parameters. This was attributed to thermal softening and loss of SiC particles due to particle pull out and fracture / cracks. Microstructure was analysed by TEM and dislocation pile-ups were observed. Tosun and Muratoglu [133] analysed subsurface microstructure after drilling 17 vol.% Al/SiC MMCs using HSS, TiN coated HSS and WC tools under dry conditions. Cutting speeds of 4 and 21 m/min and feed rates of 0.08 and 0.16 mm/rev were employed. Subsurface microstructure and microhardness profiles indicated that deformation / microstructural alteration extended to ~100-200 µm beneath the machined surface. This was possibly due to severe tool wear leading to relatively high cutting temperature. Tomac et al. [154] studied surface finish when turning Al/SiC MMCs and concluded that the surface roughness deteriorated with increasing cutting speed. This was due to the generation of fine grooves on the machined surface caused by ploughing of SiC particles. With an increase of cutting speed the cutting temperature increased resulting in softening / weakening of the bond between SiC particles and the Al matrix. The reinforcement particles were easily removed / pulled out rather than cut and broken to make grooves on the machined surface. In experimental investigation of drilling Al 2219/15%SiC and Al 2219/15% SiC+3%graphite at cutting speeds of 15.7, 31.4, 47.1 m/min and feed rates of 0.05, 0.15, 0.25 mm/rev with carbide tools, Basavarajappa et al. [135] observed that thrust force and surface roughness were primarily influenced by feed rate while burr height (recorded at up to 120 µm) was affected by both

cutting speed and feed rate. The incorporation of 3% graphite in Al/SiC composite reduced thrust force by up to 25% irrespective of cutting parameters, which was due to the natural lubricant property of graphite.

2.5.5 Non-conventional machining processes

Various nonconventional machining techniques have been investigated to minimise surface / subsurface damage in machining MMCs, including laser assisted machining (LAM), electrical discharge machining and ultrasonic vibration assisted machining. With laser assisted machining, research has shown that reinforcement particles are more easily disloged / moved by the thermally softened matrix [155-158]. Yang et al. [155] investigated laser assisted turning of 25 vol.% Al_2O_3 reinforced MMC. The 0.8 mm average focus diameter of laser point was applied 10 mm ahead of the cutting point. Results showed that cutting force and tool wear were reduced by 30-50% and 20-30% respectively in comparison with conventional turning. The Al matrix became more ductile when heated by laser and Al_2O_3 particles were pushed into the matrix rather than being cut. According to Bejjani et al. [156], tool life increased by up to 180% with laser assisted turning of titanium metal matrix composite (10-12% TiC reinforced Ti6Al4V) compared with conventional machining at the same cutting speed (100 m/min). The workpiece surface roughness however increased by up to 15%. The experimental setup is detailed in Figure 2.45.

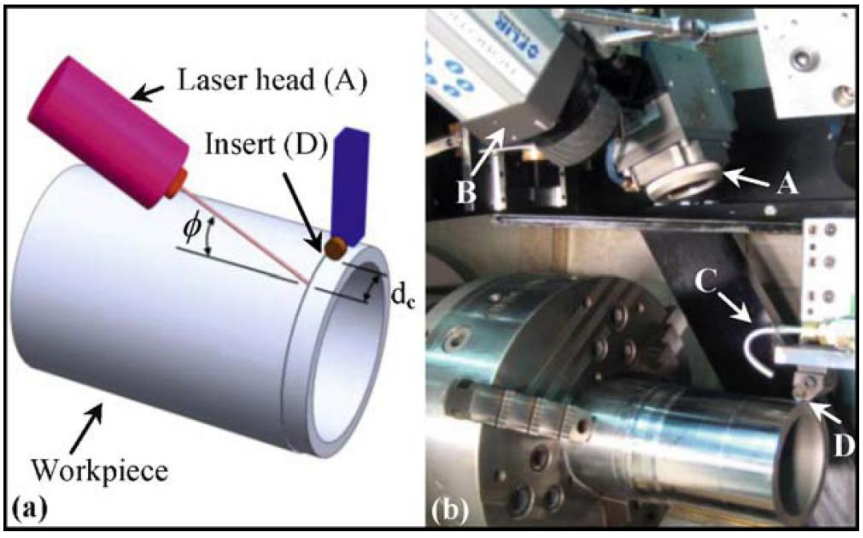


Figure 2.45: (a) Schematic of LAM experimental setup and (b) actual setup [156]

The feasibility of employing electrical discharge machining to cut MMCs has also been studied / evaluated, however low efficiency / productivity and generally high surface roughness (~10 µm) were the main impediments [159-163]. Ultrasonic vibration assisted machining of MMCs was investigated by Kadivar et al. [164] and Liu et al. [165]. Compared

with conventional drilling, burr height was reduced by ~2 mm (to ~0.5 mm) while surface roughness (Ra) dropped ~1.5 µm (to ~2.0 µm) when applying classical ultrasonic vibration during the drilling process [164]. Hocheng et al. [166] claimed that it was possible to apply ultrasonic drilling for hole making using B_4C, SiC and Al_2O_3 mixed with water as abrasive slurry. The highest material removal rate was ~10 mm^3/s and was significantly influenced by static load, vibration amplitude and grain size of the particles in the slurry.

2.6 Cutting tool materials / coatings

2.6.1 Introduction

Due to the highly abrasive nature of composite materials, selecting the appropriate tool material is very critical to achieve acceptable machinability. In general, selection is determined by workpiece properties, tool geometry, cutting parameters, machined surface quality and productivity requirements as well as tooling cost. The balance of tool material toughness / bending strength with wear resistance and hardness is also paramount [167]. Figure 2.46 details toughness and hardness correlations for specific tool materials / coatings. Generally, high speed steel and uncoated tungsten carbide tools are not suitable for volume production of composites due to rapid tool wear (limited wear resistance), even though they are widely used for the machining of conventional alloys (such as aluminium, cast iron, titanium and stainless steels).

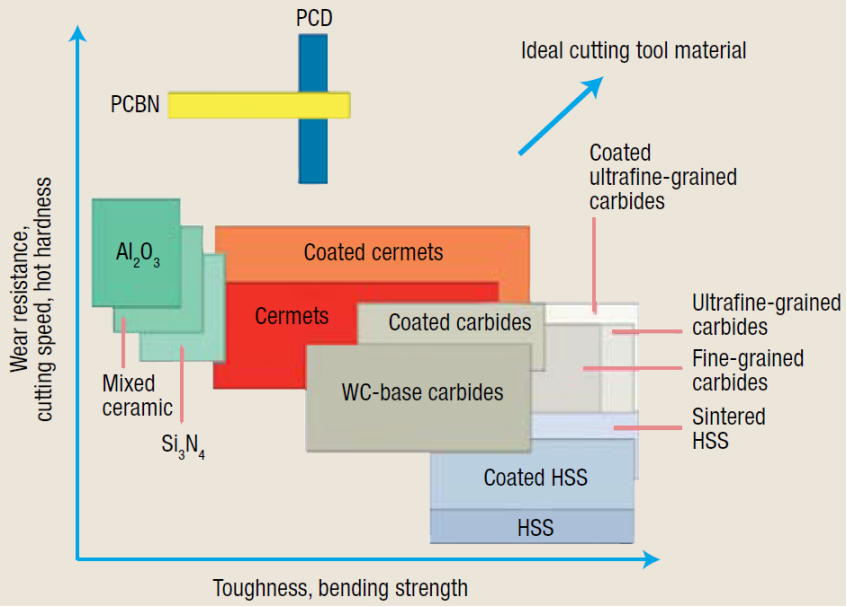


Figure 2.46: Hardness and toughness relationship for cutting tool materials [12]

2.6.2 Cutting tools used for drilling CFRP composite materials

Murphy et al. [168] compared the performance of different tool materials / coatings for the drilling of CFRP. These included uncoated WC, TiN coated and diamond-like carbon (DLC) coated WC operating at a cutting speed of 60 m/min and feed rate of 0.0485 mm/rev. The coatings were observed to be of no benefit in terms of both tool wear and hole quality. According to the experimental results presented in Figure 2.47, the maximum thrust force, torque and flank wear showed similar trends. Flank wear increased rapidly within drilling a small number of holes (<10) which corresponded to the transition between primary and secondary wear stages defined by Rawat and Attia [43]. Arul et al. [169] also studied the influence of tool material in drilling GFRP with high speed steel (HSS), TiN coated HSS and WC drills at a cutting speed of 18.85 mm/min and feed rate of 0.02 mm/rev. Results showed that ~100 holes could be produced before flank wear reached 300 µm while it increased rapidly in the first 30 holes with WC and TiN coated drills.

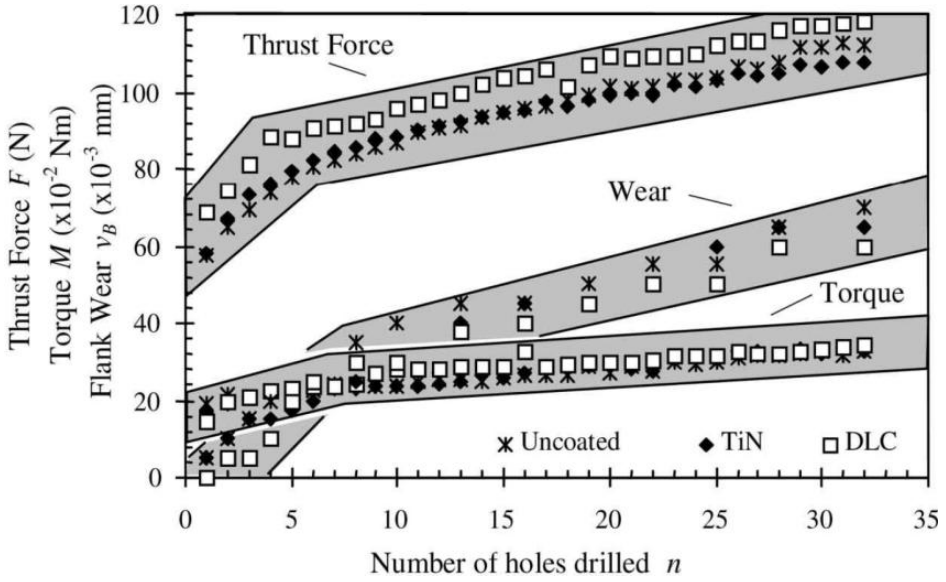


Figure 2.47: Variations of maximum thrust force, torque and flank wear against number of holes drilled [168]

Zitoune et al. [59] investigated the performance of a new nano-coated tool compared with uncoated WC (K20) when drilling CFRP/Aluminium stacks. The nano-coating designated as nc-CrAlN/a-Si3N4 was present in a nanocrystalline form, which was characterised by single crystals of nanometer size (10 nm) and exhibited a high degree of hardness. It was observed that the thrust forces recorded with the uncoated tools were generally 20-25% higher than those recorded with nano-coated drills at cutting speeds from 19.8 to 51.8 mm/min and feed rates from 0.05 to 0.15 mm/rev. This was attributed to the fact

that the coating significantly reduced the friction between the tool and machined surface as well as the friction between the chips and flutes of the cutting tool. The improved thermal conductivity of the nano-coating was also cited. Davim and Mata [170] investigated the performance of CVD-diamond coated tools when machining CFRP. Their results showed that CVD-diamond coated tools compared favorably with PCD tools in terms of surface roughness (4 µm Ra as opposed to 3.5 µm Ra), however it had a number of advantages including lower production costs (<30% of PCD) and easy to manufacture chip breakers on inserts as PCD tools were difficult to grind. Montoya et al. [68] analysed tool wear on uncoated and coated tools including diamond, TiAlCrN and AlTiSiN-G when drilling CFRP/Al stacks at a cutting speed of 56.5 m/min and feed rate of 0.04 mm/rev using mist coolant. They concluded that both TiAlCrN and AlTiSiN-G coatings were not efficient, their flank wear after drilling 75 holes being close to that on the uncoated tool (~70 µm). For the diamond coated tool, chipping occurred after drilling 150 holes, however flank wear was up to 50% lower compared with that of the uncoated tool (~ 250 µm) after drilling 250 holes.

Polycrystalline diamond (PCD) tools are widely used in machining CFRP and GFRP composite materials due to their extreme resistance to abrasion, high thermal conductivity and low coefficient of friction, however most of the published work has focused on turning operations [170-176]. Ramulu et al. [176] pointed out that the wear behaviour of PCD tools in turning CFRP is characterised by small cracks, rounded edges and flank wear. When comparing tool performance of fine (~2 µm), medium (~10 µm) and coarse (~25 µm) grain size PCD products at a cutting speed of 228.6 m/min and feed rate of 0.1778 mm/rev with DOC at 4.76 mm, results showed that coarse grade PCD was more wear resistant than fine grade material as flank wear increased by ~60% with fine PCD (~80 µm) compared with coarse PCD (50 µm) after machining 23 minutes. Park et al. [42] studied tool wear in drilling CFRP/Ti sandwich using WC and PCD tools at a cutting speeds of 60 and 180 m/min and a feed rate of 0.0762 mm/rev with a water-soluble mist coolant. It was observed that cutting edge chipping occurred after drilling 20 holes with tool catastrophic failure at hole 73 due to the brittleness of PCD materials. Cutting edge chipping togehter with abrasion from carbon fibres and hard inclusions in the Ti as well as adhesion of Ti were the main tool wear mechanisms for PCD drills. Ramulu et al. [177] conducted experiments in drilling graphite / bismaleimide composite material using HSS, WC and PCD tools at cutting speeds varying from 13 to 54 m/min and a feed rate of 0.028 mm/rev when drilling a small number of holes (~40 at test cessation). The composite material started burning after drilling ~20 holes with the HSS tool. Unfortunately, as only a few holes were drilled, the PCD tools did not

demonstrate significant advantages in terms of tool life and hole quality compared with uncoated tools.

2.6.3 Cutting tools used for machining MMC materials

Drilling MMCs using conventional carbide tooling is typically characterised by high tool wear rates, poor hole quality and subsurface damage [178]. In a study of workpiece integrity following the drilling of hybrid metal matrix composites (aluminium-SiCp-graphitic) with carbide tools at a cutting speed of 47m/min and feed rate of 0.25mm/rev, Basavarajappa et al. [136] found surface defects such as microcracks, particle pull out and scratches, with subsurface microstructural deformation extending up to a depth of 150µm below the machined surface. Kannan and Kishawy [152] reported similar defects (microcracks, voids, pits and craters) when machining Al based MMCs, which were formed due to particulate fracture and pull out as well as interfacial debonding. More recently, a comprehensive experimental assessment on the influence of key process variables when drilling Al/SiCp MMCs showed that feed rate and tool material were the most significant factors affecting workpiece surface roughness [129]. Kilickap et al. [179] studied tool wear in turning 5 wt.% SiC reinforced aluminium MMC materials with uncoated and TiN coated inserts under dry conditions. They concluded that tool wear increased with increasing both cutting speed (50 to 150 m/min) and feed rate (0.1 to 0.3 mm/rev). At a DOC of 1 mm, TiN coated tools showed marginal benefit in comparison with uncoated tools at low cutting speed (50 m/min), while there was a ~25% reduction in tool wear at high cutting speed (150 m/min) irrespective of feed rate. Ozben et al. [180] used the same parameters and TiN coated tools turning Al based MMC with different SiC particle content (5, 10 and 15 wt.%) and achieved similar results. Carbide tools, either uncoated or coated, sustained high levels of tool wear after a short period of machining. Karakas et al. [181] studied tool wear when machining 20 vol.% B_4C_p reinforced aluminium metal matrix composites using WC, double coated (TiN+TiAlN) and triple coated (TiCN+Al_2O_3+TiN) tools. The triple coated tools showed the best wear resistance in comparison with uncoated and double coated tools over a range of cutting speeds (100, 130, 169, 220 and 286 m/min) with a feed rate of 0.2 mm/rev and DOC of 1.5 mm. Flank wear increased with increasing cutting speeds for all tools. At low cutting speed (100 m/min), chip volumes of 3750, 6000, and 8000 mm^3 were recorded at test cessation (0.3 mm flank wear) for uncoated, double coated and triple coated tools, respectively. With a cutting speed of 286 m/min, chip volumes were reduced to 3000, 3000, and 6000 mm^3 for the three different tools, respectively. Higher cutting speeds resulted in high temperature causing

workpiece softening and reduction of adhered materials (BUE) on the tool, which served as a thin film protecting layer. Quigley et al. [182] also used two different triple coated ($TiCN+Al_2O_3+TiN$ and $TiCN+Al_2O_3+TiC$) tools when turning 25 vol.% Al/SiC MMCs. They noted that flank wear rapidly increased to 0.3 mm after machining only 53 mm even at a cutting speed of ~20 m/min. Castro et al. [183] applied diamond coated ceramics (Si_3N_4) and diamond brazed carbide tools when turning silicon-aluminium (Si-Al) alloys at a cutting speed of 600 m/min and feed rate of 0.1 mm/rev with DOC at 0.5 mm under dry conditions. Figure 2.48 shows micrographs of tools after machining 1400 m, there is no evidence of tool wear on both tools, although some alloy was adhered on the rake face.

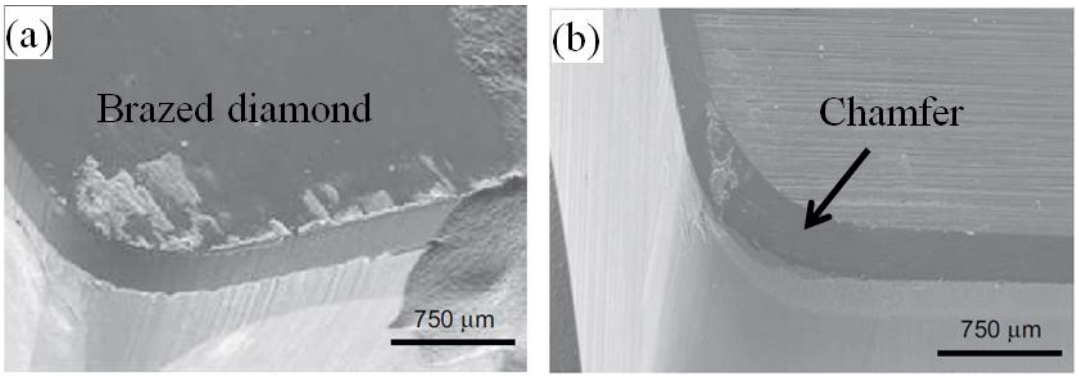


Figure 2.48: SEM micrographs of inserts after turning Al-12 wt.%Si alloy for 1400 m with (a) thick diamond brazed and (b) chamfered diamond coated Si3N4 [183]

Altunpak et al. [142] used diamond-like carbon coated tools in drilling Al/20%SiC+5%graphite and Al/20%SiC+10%graphite hybrid composites at different cutting speeds (55, 63, 71 m/min) and feed rates (0.1, 0.13, 0.16 mm/rev). Results indicated that inclusion of graphite as an additional reinforcement reduced thrust force while surface roughness increased from 0.289 to 0.595 µm for Al/20%SiC+5%graphite and Al/20%SiC+10%graphite respectively. This was attributed to the lubricant effect of graphite, resulting in a reduction of burnishing and honing of the SiC particles. SEM micrographs showed fine grooves, scratches, small valleys, cracks and pits in the machined surface. PCD tools however used by various researchers in turning MMC materials and have proven to be the preferred tool material [120, 125, 145, 184-187]. According to the observation of Bhushan et al. [185], PCD tools showed superior wear resistance compared with carbide tools. The maximum flank wear of a carbide insert was 540 µm compared with only 10 µm for a PCD tool after turning 10 wt.% SiC reinforced 7075 Al MMC for 7 minutes at a cutting speed of 240 m/min and feed rate of 0.4 mm/rev with a depth of cut at 2 mm. Ding et al. [187] evaluated the performance of various type of PCBN and PCD tools in turning 20 vol.%

Al/SiC MMCs with cutting speeds of 50 to 400 m/min, a feed rate of 0.1 mm/rev and DOC at 0.3 mm. Table 2.10 lists the specific properties of PCBN and PCD tools used in the experiment. They concluded that the major wear mechanism of PCBN tools was intergranular fracture, abrasion and workpiece material adhesion. PCD tools showed the lowest tool wear rate due to higher abrasion and fracture resistance combined with lower adhesion. At a cutting speed of 400 m/min, machining in wet conditions improved the surface finish as lower Ra values were recorded compared with dry machining irrespective of the tool material used, as shown in Figure 2.49.

Table 2.10: Properties of PCBN and PCD tool materials used in the experiment [187]

Tool type	Grain size (µm)	Other constituents	CBN or PCD (vol.%)	Hardness (HV)	TRS[a] (kg/mm^2)	λ^b (W/mK)
BN100	3	TiN binder	85% CBN	4000-5000	80	217
BN300	0.5	TiN binder	60% CBN	3300-3600	110-120	54
IZ900	Ultra-fine, <0.5	Compressed cBN	>90% CBN	5100-5610	138	360-400
PCD	0.5	Co binder	90% PCD	7000-11000	80-90	2000

a: Transverse rupture strength, b: thermal conductivity.

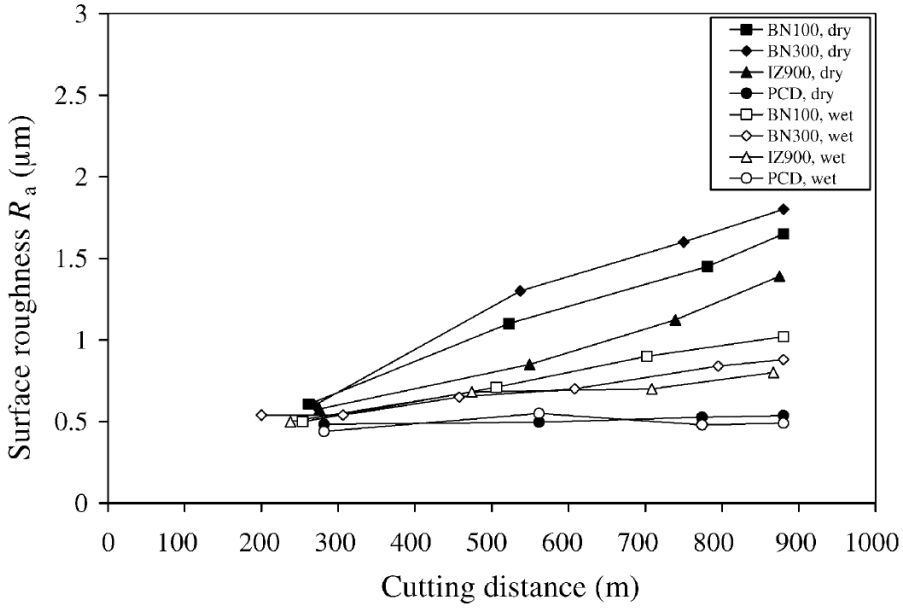


Figure 2.49: Variations of surface roughness Ra against cutting distance in turning 20 vol.% Al-SiC MMCs with PCBN and PCD tools at the cutting speed of 400 m/min [187]

Durante et al. [188] studied the machinability of diamond coated tools in turning MMC and concluded that chipping occurred frequently a few seconds after machining. The same

conclusion was found by Chou and Liu [189], as catastrophic coating failure / peeling was observed after machining ~1 minute at cutting speeds of 120 and 360 m/min and feed rate of 0.2 mm/rev with 20% Al/SiC MMC. Davim [190] employed CVD diamond coated WC and brazed PCD tools when turning 20% Al/SiC MMCs at various cutting speeds and feed rates. Flank wear progression with cutting time is shown in Figure 2.51. For CVD diamond coated tools, a cutting time of only ~4.5 min was achieved before reaching the 0.6 mm flank wear criteria at the lowest cutting speed (50 m/min), while tool life for brazed PCD tools was ~45 min with flank wear of 0.25 mm at a cutting speed of 250 m/min. Chipping of the CVD diamond coated was the typical wear mechanism resulting in a short tool life (<4 min).

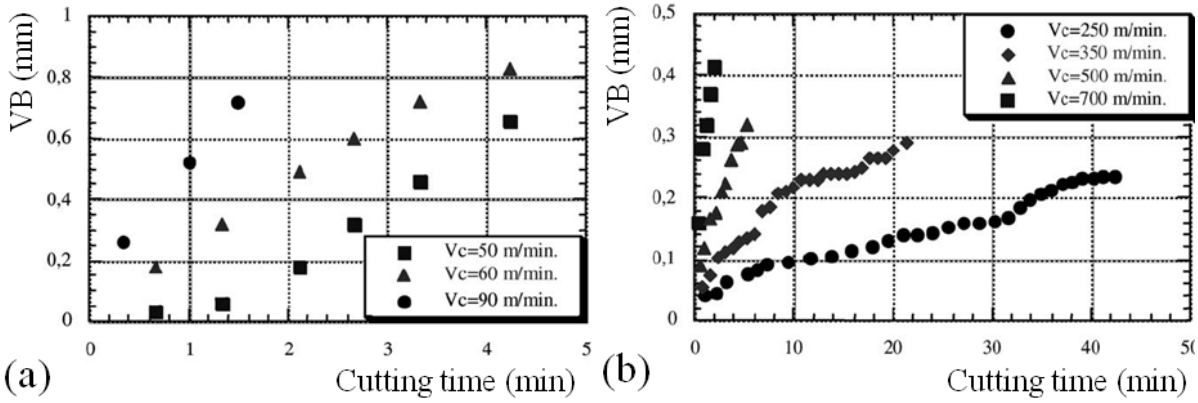


Figure 2.50: Tool wear progression in turning MMCs with (a) CVD diamond coated inserts (feed rate: 0.2 mm/rev, DOC: 1 mm) and (b) brazed PCD inserts (feed rate: 0.1 mm/rev, DOC: 1 mm) [190]

Monaghan and O'Reilly [141] indicated that tool material hardness played the key role in efficient and cost-effective drilling of MMCs. A wide range of HSS, TiN coated HSS, carbide tipped HSS, WC and PCD tipped HSS drills were used for the experiments with low cutting speeds (1, 2, and 3.7 m/min) and feed rates varying from 0.1 to 0.3 mm/rev. They concluded that the PCD tipped tool was superior to other tools in terms of all recorded values of flank wear, thrust force, torque and surface finish. Mubaraki et al. [138] carried out experiments studying tool wear characteristics when drilling 26 vol.% Al/Al_2O_3 MMCs using HSS, WC and brazed PCD tools at a cutting speed of 45 m/min and feed rate of 0.06 mm/rev in wet conditions. They found that the flank wear reached 1000 µm after only drilling one hole using a HSS drill and ~160 µm for a WC drill after drilling 50 holes. The WC drill resulted in chip compaction in the drill flutes which required manual removal leading to some delays. In the case of the PCD drill, flank wear was 120 µm after drilling 184 holes.

Chapter 3: EXPERIMENTAL WORK

The experimental drilling trials were performed over three main phases. Phase 1 and 2 were conducted to evaluate the effect of operating conditions, drilling strategy, tool materials / coatings and workpiece configuration / layup when drilling carbon fibre reinforce plastics (CFRP), while Phase 3 involved a similar assessment for Al/SiCp metal matrix composites (MMCs). Each of the principal phases were divided into several sub-phases as listed below:

- Phase 1A: Influence of operating conditions and tool materials / coatings when drilling CFRP.
- Phase 1B: Preliminary / benchmarking trials in drilling CFRP with variable feed rate operation.
- Phase 2A: Evaluation of hole quality when drilling CFRP with variable feed rate operation.
- Phase 2B: Influence of workpiece configuration / fibre orientation and elevated feed rates on hole quality when drilling CFRP.
- Phase 2C: Evaluation of diamond coated and domed PCD tools when drilling CFRP at elevated / high cutting speeds.
- Phase 3A: Preliminary / benchmarking trials in drilling MMC with different tool materials / coatings.
- Phase 3B: Evaluation of domed PCD tools and cutting parameters when drilling MMCs.
- Phase 3C: Drilling of MMCs using PCD tools at elevated / high cutting speeds.

3.1 Workpiece materials

3.1.1 Carbon fibre reinforced plastics (CFRP) used in Phase 1 and 2

The CFRP workpiece materials used for experiments were autoclave cured laminates with three different configurations / fibre orientations. Type 1 and 3 were manually laid up with 40 unidirectional (UD) prepreg (0.26 mm thick) layers to provide 10.4 mm thick plates, while Type 2 was 9.36 mm thick comprising 36 plies. Type 1, 2 and 3 laminates were stacked according to the sequence $[45/0/135/90]_{5S}$, $[40/0/135/0/90/0/135/0/45]_{2S}$ and $[45/0/135/135/135/90/45/45/45/0/135/135/90/45/45/0/135/135/90/45]_{S}$, respectively. Each type of CFRP layup had a different number of plies oriented at 0°, 45°, 90° and 135°, with details summarised in Table 3.1. The autoclave cured CFRP panels were made of intermediate

modulus (IM), high tensile strength carbon fibres impregnated with epoxy resin and had a fibre weight fraction of between 64 and 68%. The specific mechanical / physical properties of the fibre and cured CFRP composite panels are listed in Table 3.2.

Table 3.1: Summary of the CFRP laminate layup configurations used in Phase 1 and 2

	Type 1		**Type 2**		**Type 3**	
Number of plies	40		36		40	
Cured ply thickness (mm)	0.26		0.26		0.26	
Cured panel thickness (mm)	10.4		9.36		10.4	
Designation	25/50/25		44/44/11		15/70/15	
Ply orientation	**Total plies**	**Percentage (%)**	**Total plies**	**Percentage (%)**	**Total plies**	**Percentage (%)**
0°	10	25	16	44	6	15
45°	10	25	8	22	14	35
135°	10	25	8	22	14	35
90°	10	25	4	11	6	15

Table 3.2: Fibre and CFRP composite laminate properties* [191]

Fibre properties	Tensile strength	5880 MPa
	Tensile modulus	294 GPa
	Elongation	2.0%
	Density	1.80 g/cm^3
	Filament diameter	5 μm
Cured CFRP composite panel properties	Tensile strength	2950 MPa
	Tensile modulus	154 GPa
	Compressive strength	291 MPa

* CFRP composite was cured with Toray 3631 epoxy resin at 60% fibre volume.

Figure 3.1 shows sample cross-sectional optical and SEM micrographs relating to the different fibre / ply orientations. The carbon fibres were observed to be approximately evenly distributed within the epoxy resin matrix of each ply. The autoclave cured CFRP panels were prepared in the form of plates with dimensions of 100 mm×100 mm to fit a previously designed drilling jig. Each plate can accommodate an array 64 holes (8×8) of 6.35 mm in diameter at a pitch distance of 10 mm, see schematic of a workpiece with drilled holes in Figure 3.2. Strip specimens with dimensions of ~17 mm×100 mm were also prepared for thrust force and torque measurements mounted on the drilling dynamometer.

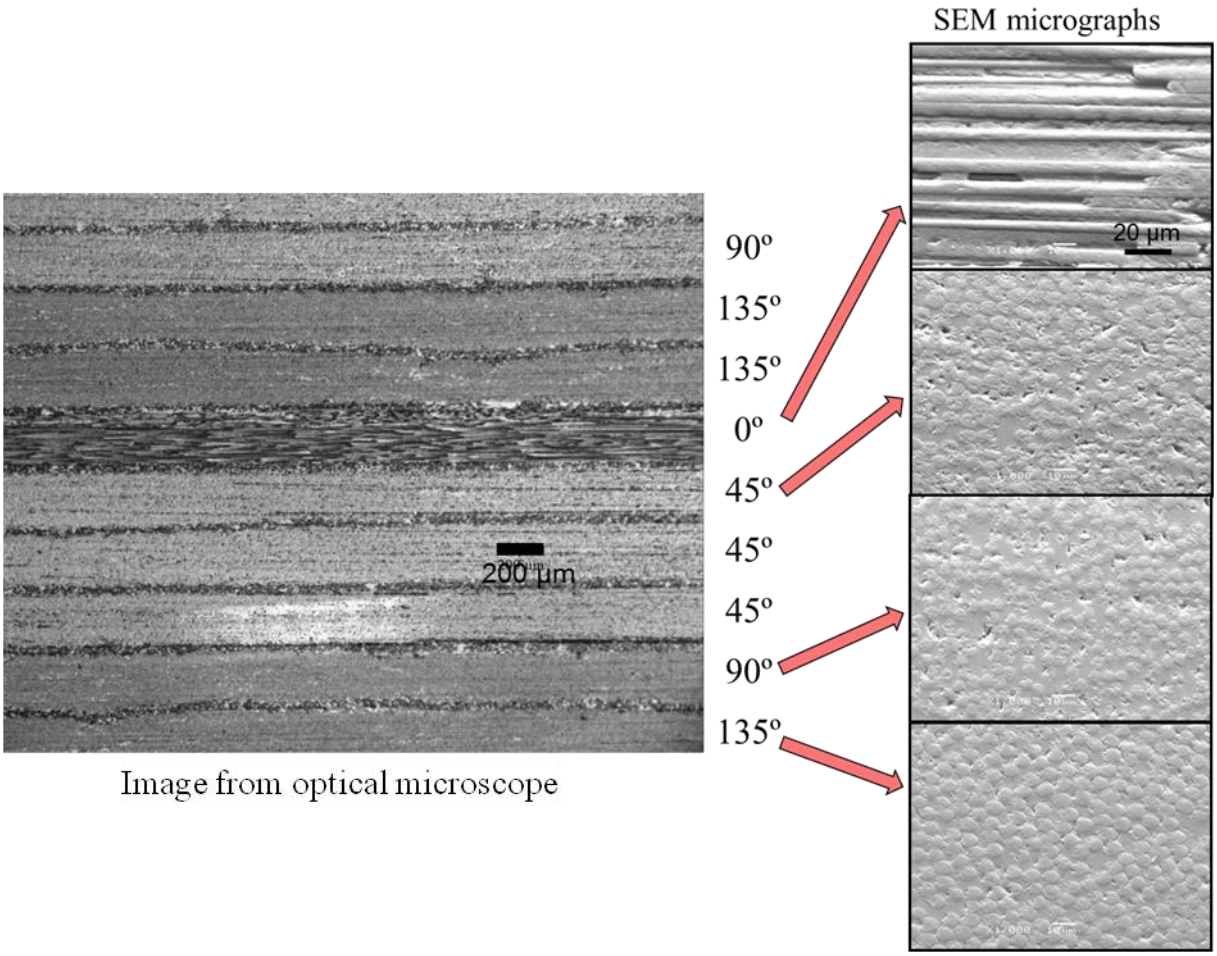


Figure 3.1: Optical and SEM micrographs of plies oriented at different orientations

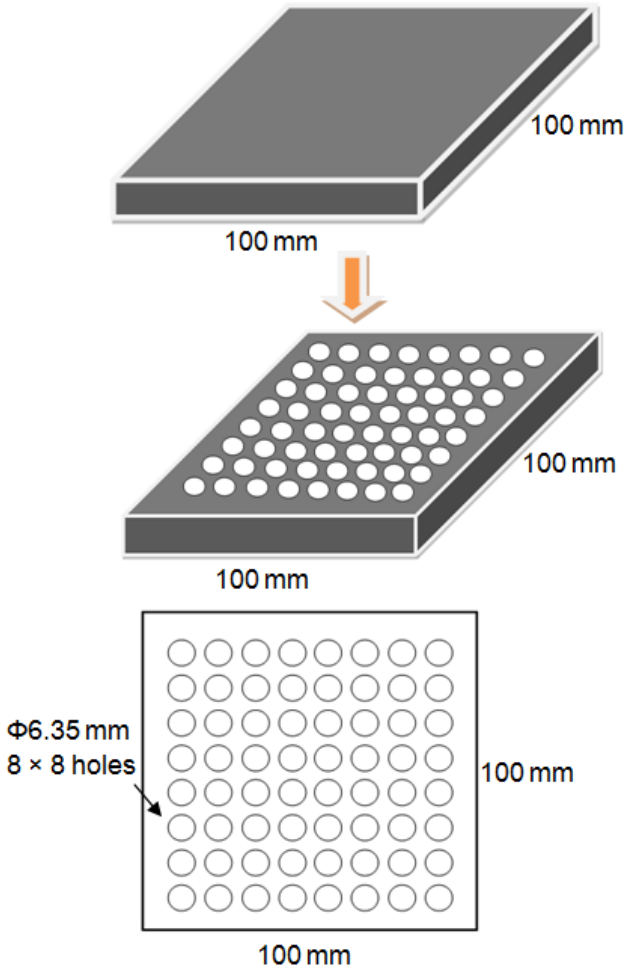


Figure 3.2: Dimensions of workpiece specimens and schematic of drilled hole array

3.1.2 Metal matrix composites (MMCs) used in Phase 3

The MMC workpiece material used for Phase 3 experiments was composed of a wrought aluminium alloy, AA2618 (2.3%Cu, 1.5%Mg, 1.2%Fe, 1.1%Ni) matrix, reinforced with 15% volume fraction of SiC particles (average size of 10-15 μm). The composites were produced by Cospray Ltd., (part of Alcan International Ltd.) using the spray deposition process (see Figure 2.7) and fully consolidated via extrusion. Extruded bars of rectangular section (25 mm×100 mm×1000 mm) provided by the material supplier were then cut into blocks of ~170 mm long and skimmed by facemilling to 19 (~3 mm removed from each side) and 24 mm (~0.5 mm removed from each side) thickness respectively, with a surface roughness Ra ≤ 0.8 μm. Strip specimens with width of ~17mm were prepared for thrust force and torque measurements. All of the tests were undertaken using the 24 mm thick blocks except for Phase 3B, which utilised the thinner workpieces (19 mm) due to the limited drilling length of the domed PCD tools. The workpiece test specimens are shown in Figure 3.3.

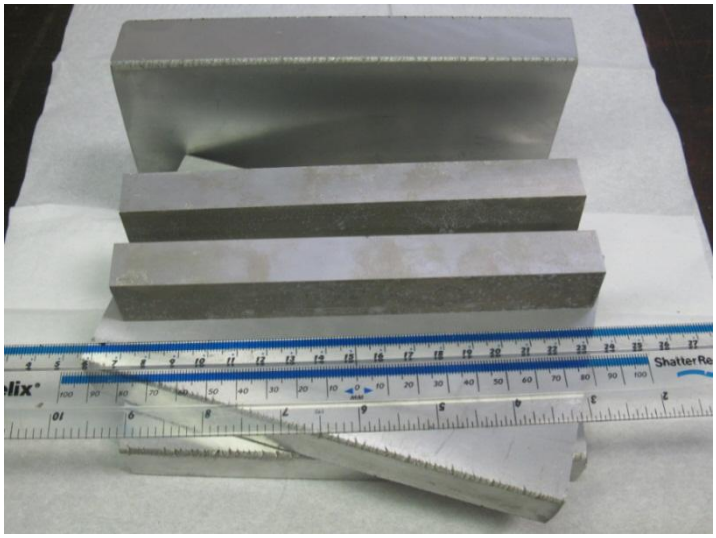


Figure 3.3: Prepared MMCs workpieces for testing

Figure 3.4 shows optical micrographs of the MMC's metallurgical structure sectioned in both transverse and longitudinal directions prior to etching. The SiC particles were seen to be evenly distributed in the aluminium matrix. Following chemical etching using Keller's reagent comprising 1% HF, 1.5% HCl and 2.5% HNO_3 mixed with water (samples soaked for 30s), the fine grain (~5 µm) microstructure of the matrix phase was visible, as detailed in Figure 3.5.

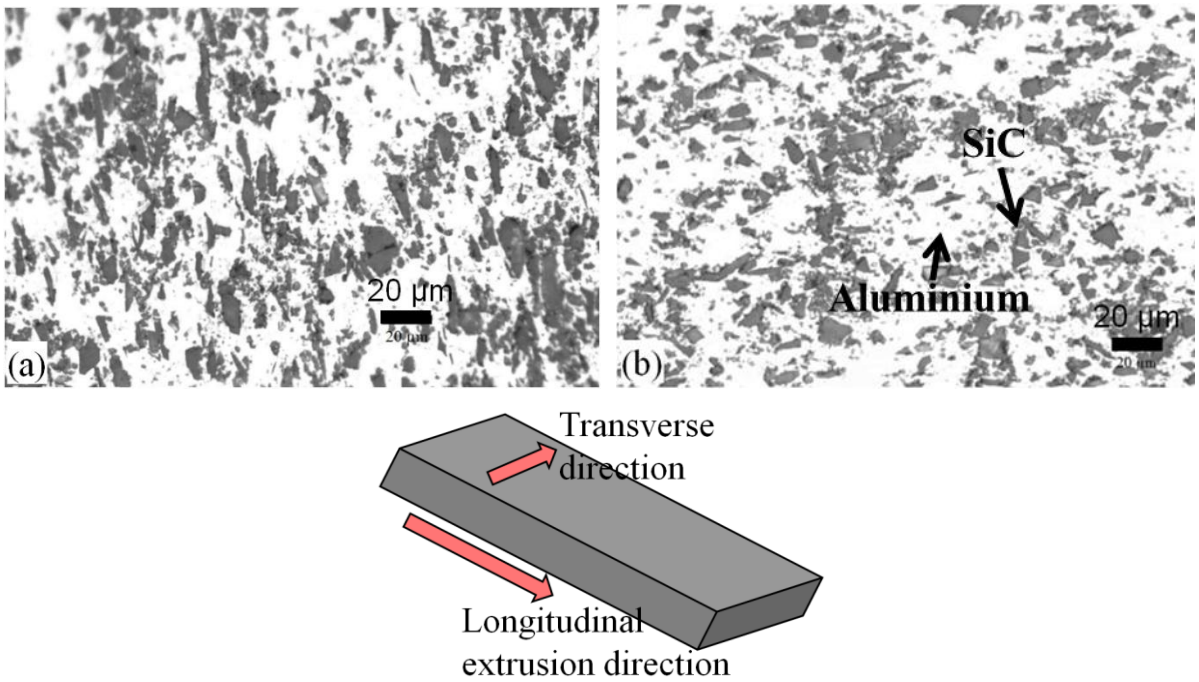


Figure 3.4: Optical micrograph of the workpiece before etching in (a) transverse and (b) longitudinal extrusion direction

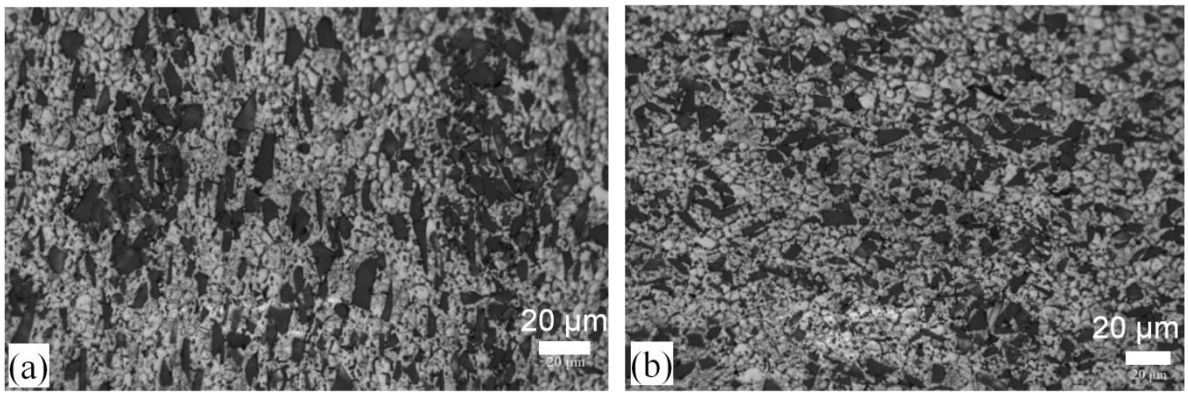


Figure 3.5: Microstructure of workpiece material after etching in (a) transverse and (b) longitudinal extrusion direction

3.2 Equipment

3.2.1 Machining centre and fixtures

All tests were carried out on a Matsuura FX-5 vertical high speed CNC machining centre with the spindle having a maximum rational speed of 20,000 rpm. The maximum feed rate was 15 m/min with a spindle power rating of 15 kW. The machining centre was fitted with a Renishaw probe and tool length setter as well as equipped with a CFRP dust extraction system (Filtermist Dustomat 15), capable of removing particles down to 0.3 µm. A high pressure pumping system by Pumps & Equipment Warwick Ltd. was also connected to the FX-5, which supplied cutting fluid at pressures of up to 300 bar. Figure 3.6 shows the Matsuura FX-5 unit while Figure 3.7 details the integrated fibre dust extractor and high pressure pump system located in the Machining Research Group laboratory at the University of Birmingham.



Figure 3.6: Matsuura FX-5 high speed machining centre



Figure 3.7: (a) Fibre dust extractor and (b) high pressure pump system

The CFRP specimens used for tool wear / life testing were held in a bespoke drilling jig with an array (10×10) of pre-fabricated 9 mm diameter clearance holes together with double side clamps as shown in Figure 3.8(a). In contrast, the MMC workpieces for tool life testing were mounted in a modular clamping plate as shown in Figure 3.8(b), with several flexible and repositionable chucks to accommodate different size plates.

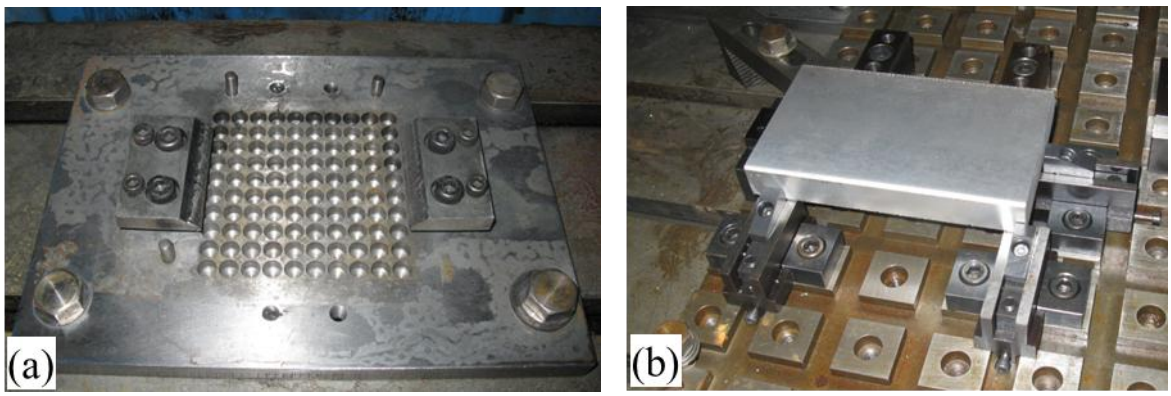


Figure 3.8: (a) Fixture was for securing CFRP and (b) clamping plate used for holding MMC workpieces

3.2.2 Chilled air and cutting fluid application

Chilled air used in Phase 1 and 2 tests for drilling CFRP was generated and delivered by a Nex-Flow vortex tube (type 56030FD), see Figure 3.9(a), while a schematic of the apparatus is shown in Figure 3.9(b). Compressed air initially enters point (A) into the tube component of the device, following which the vortex tube splits the compressed air into a cold (B) and hot (C) stream of air. The hot air is then vented to the atmosphere at point (D), which is also

muffled to reduce noise. Conversely, the cold air enters the muffler (E) and is subsequently pumped through the hose (F) and directed onto the cutting zone. The system is designed to deliver air at a temperature of up to 28ºC below the inlet temperature [192]. For the experiments in Phase 1 and 2, the temperature of the output chilled air was ~8ºC at 0.4 bar pressure.

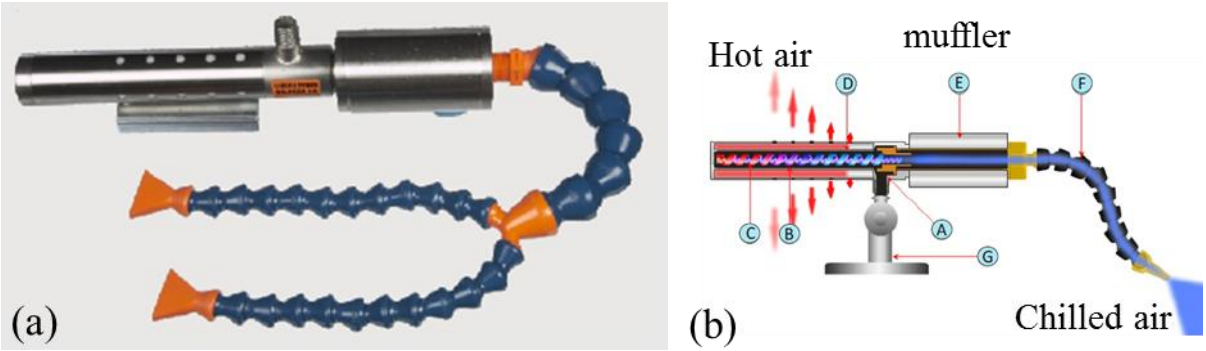


Figure 3.9: (a) Chilled air generator and (b) working schematic [192]

The cutting fluid used when drilling MMCs was a water soluble emulsion containing 6-8% volume solution of Hocut 3380 mineral oil. The concentration of the cutting fluid / coolant was monitored regularly using a refractometer. For the drilling experiments in Phase 3A and 3C, cutting fluid was supplied at a constant flow rate of ~26 litres per minute and corresponding pressure of 70 bar (7 MPa). In Phase 3B, fluid delivery was varied between flood (3 bar) and high pressure (70 bar) conditions, with flow rate of the former at approximately 27 litres per minute.

3.2.3 Tool wear / life evaluation analysis

Drill flank and chisel wear was measured using a WILD M3Z toolmaker's microscope integrated with a X-Y digital micrometer platform having a resolution of 1 µm. A Canon EOS400D digital camera was mounted on the microscope and connected to a laptop for tool image capture, see Figure 3.10(a). In addition, an adjustable tilting table fitted with a bespoke fixture that held the tool holder / adapter was employed to accommodate drills with varying point angles in order to achieve optimal image focus, see Figure 3.10(b). Maximum flank wear / chipping / fracture of each cutting lip was recorded at various intervals of drilled holes. Drill cutting edge radius for both new and worn tools at test cessation were measured in Phase 1A using an Alicona G4 InfiniteFocus (IF) microscope system, which is capable of both dimensional and surface topography evaluation (based on focus variation technology), with a vertical resolution down to 10 nm. Figure 3.11 shows the Alicona G4 IF unit and setup with a rotating chuck for tool geometry / cutting edge radius measurement.

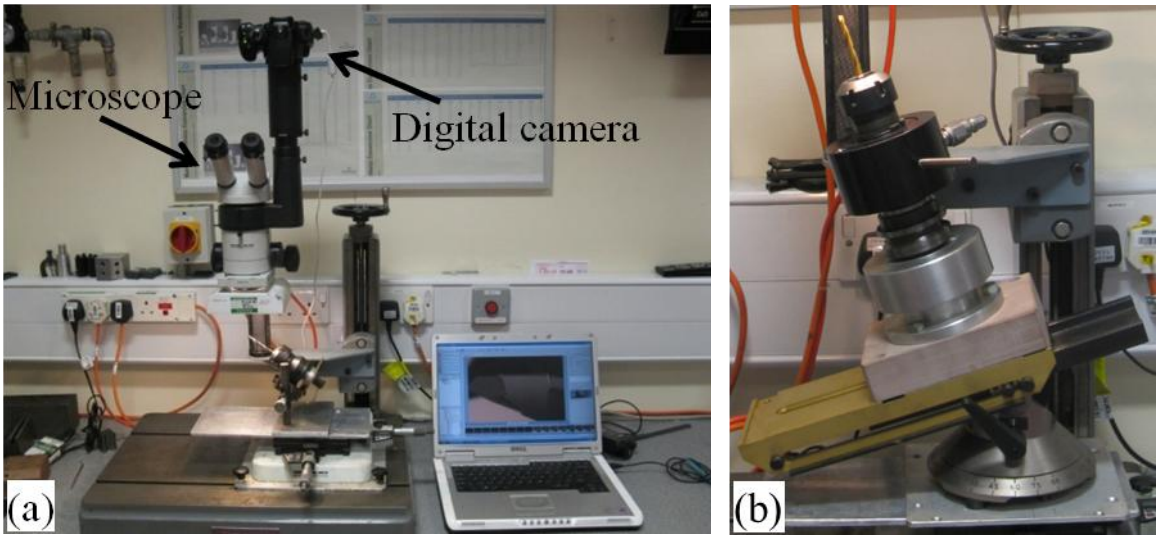


Figure 3.10: (a) Tool wear measurement setup and (b) tilting table for accommodating tool holder

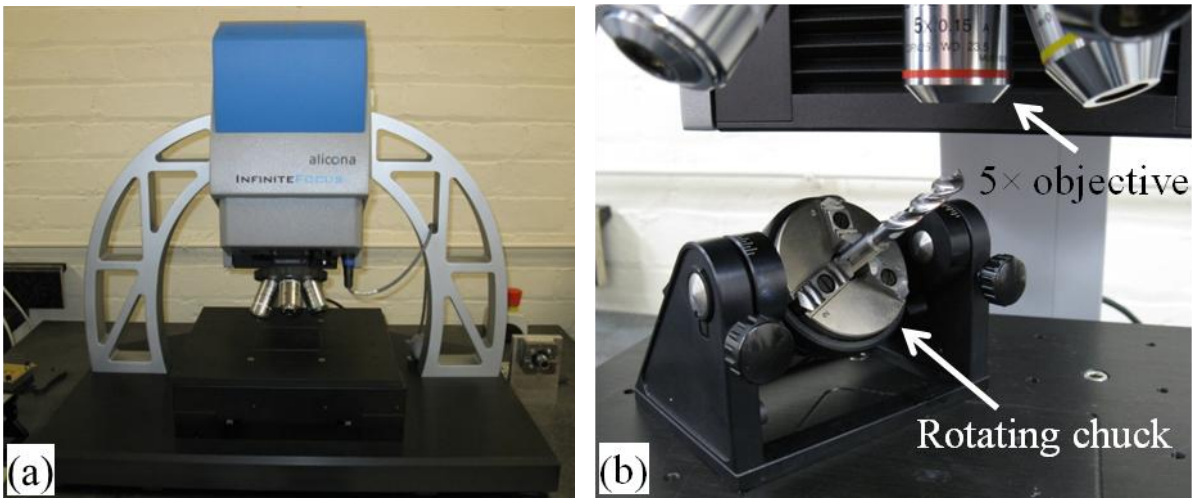


Figure 3.11: (a) Alicona G4 InfiniteFocus (IF) microscope system and (b) setup for cutting edge radius measurement

3.2.4 Force and torque measurement

Drilling thrust forces and torque in Phase 1A, 1B, 2A, 2B and 3B were recorded using a Kistler 9123B 4-component piezoelectric rotating dynamometer with a Sandvik Varilock quick change tool holder. The rotating dynamometer, with a maximum operating speed of 10,000 rpm was connected to a PC with data-logging hardware and Kistler Dynoware software via a Kistler type 5221A stator and type 5223A multichannel signal conditioner, see schematic in Figure 3.12(a). The rotating dynamometer and signal conditioner units are shown in Figures 3.12(b) and 3.12(c), respectively.

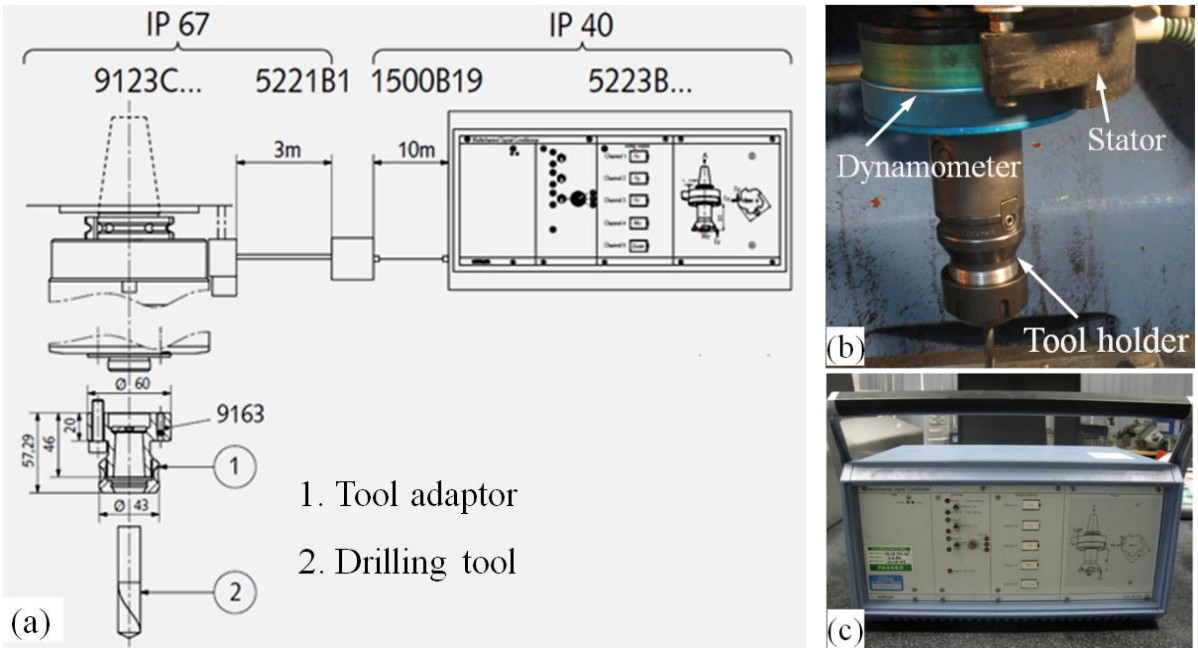


Figure 3.12: (a) Rotating dynamometer measuring system [193], (b) rotating dynamometer and (c) multichannel signal conditioner

Due to the limitation in operating speed of the rotating dynamometer and requirement to accommodate to a through-tool cutting fluid adaptor, a Kistler 9273 4-component drilling dynamometer connected to Type 5011 charge amplifiers was employed for Phase 2C, 3A and 3C, see Figure 3.13. Appropriate strip specimens were mounted on the drilling dynamometer with a specially designed fixture / jig.

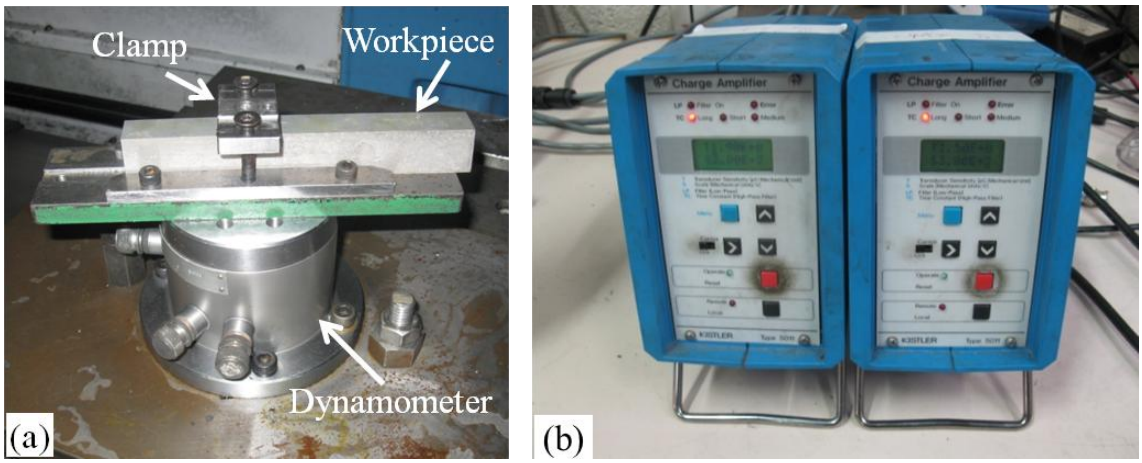
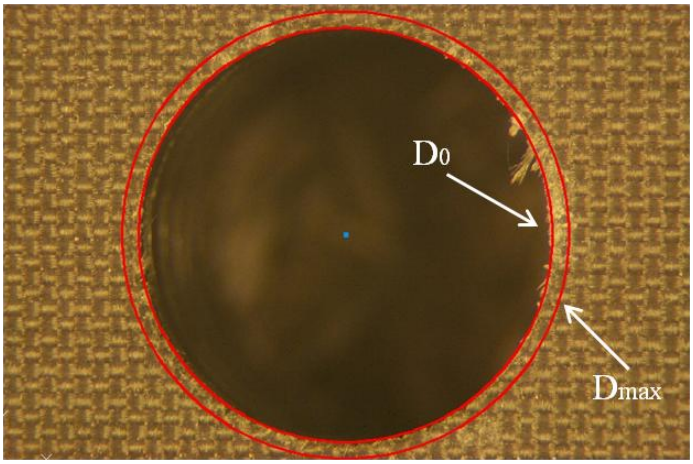


Figure 3.13: (a) Force and torque measurement setup and (b) Kistler 5011 charge amplifiers

3.2.5 Hole entry and exit delamination analysis

The delamination at hole entry and exit locations in CFRP workpieces was quantified using a parameter known as delamination factor (F_d), which is defined as the ratio of maximum damage diameter (D_{max}) to nominal drilled hole diameter (D_0), see Figure 3.14. This definition / parameter has been applied previously by several researchers [55, 60, 81,

194-196]. Images of hole entry and exit were taken using the Wild M3Z toolmaker's microscope, with the respective diameters were measured using Autodesk software (AutoCAD 2013). Entry and exit delamination were evaluated for both the first and last drilled hole.



$$F_d = D_{max} / D_0$$

Figure 3.14: Hole delamination measurement

3.2.5 Workpiece geometrical accuracy measurement

Geometrical parameters of drilled holes including hole diameter, out of roundness and cylindricity were assessed on a Taylor Hobson Talyrond series 300 unit equipped with a 3 mm ruby ball stylus, see Figure 3.15(a). The setup for strip samples is shown in Figure 3.15(b). The system was calibrated with 6.35 mm (1/4 inch) diameter standard ring gauge prior to each measurement. For CFRP workpiece materials, hole diameter, out of roundness and cylindricity were measured at depths of 2, 5 and 8 mm from hole entry with the average (replicated 3 times) recorded, while measurements were taken at 3, 8, 13 and 18 mm positions for the drilled MMC samples.

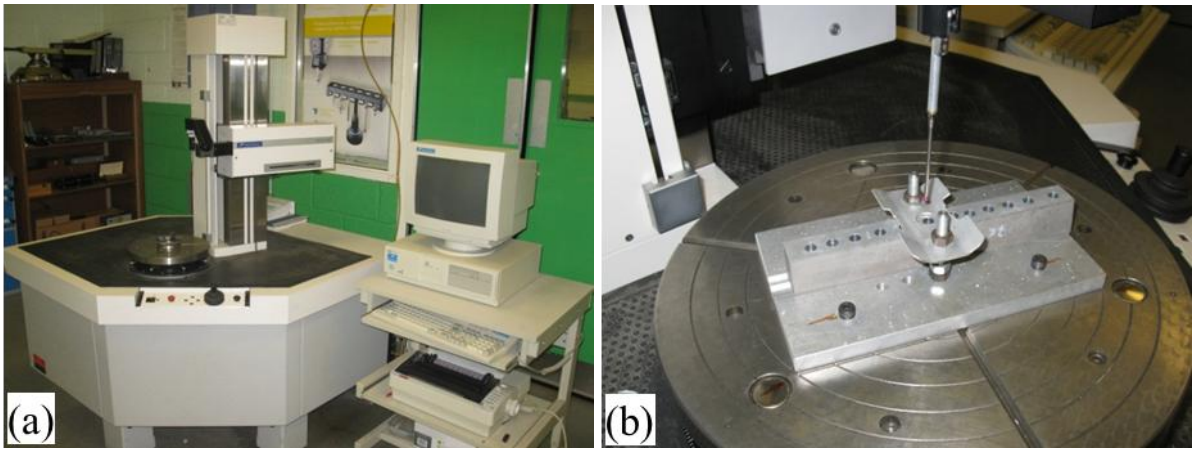


Figure 3.15: (a) Taylor Hobson Talyrond series 300 and (b) setup for hole geometrical accuracy assessment of strip sample

3.2.6 Workpiece surface roughness and integrity assessment

For both CFRP and MMCs samples, drilled holes were initially sectioned ~500 µm away from the hole centreline. As CFRP materials had limited / low electrical conductivity, samples were sectioned using an EXTEC Labcut 300 disc cutting machine equipped with recirculating coolant system, vise set and alumina based abrasive blade, see Figure 3.16(a). Conversely, the MMC specimens were cut using a Charmilles Technologies Robofi 200 wire electrical discharge machining (WEDM) unit. In order to avoid any metallurgical alterations prior to microhardness and microstructure analysis, all of the sectioned samples were cold mounted using Buehler's EpoxiCure epoxy resin and compatible hardener. The mounted samples were then ground and polished according to Buehler's procedure for aluminium alloys using a Buehler Alpha grinder / polisher (see Figure 3.16(b)). The detailed grinding / polishing route for MMCs is outlined in Table 3.3.

Optical assessment of chip morphology, burr formation, hole surface quality, subsurface and microstructural alterations / damage of the samples were performed on a Leica DM LM microscope (see Figure 3.16(c)) and high resolution JEOL 6060 scanning electron microscope (SEM) as shown in Figure 3.17(a). For CFRP materials, specimens were gold coated to increase electrical conductivity using an EMSCOP SC500 gold sputter, see Figure 3.17(b), prior to SEM analysis.

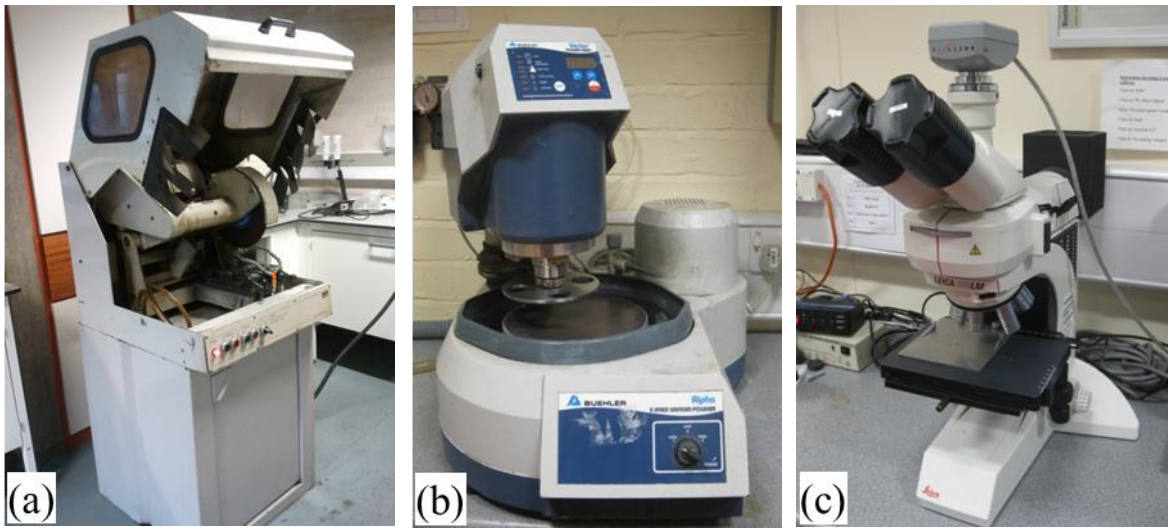


Figure 3.16: Illustration of (a) EXTEC Labcut 300 disc cutting machine, (b) Buehler grinder/polisher and (c) Leica DMLM microscope

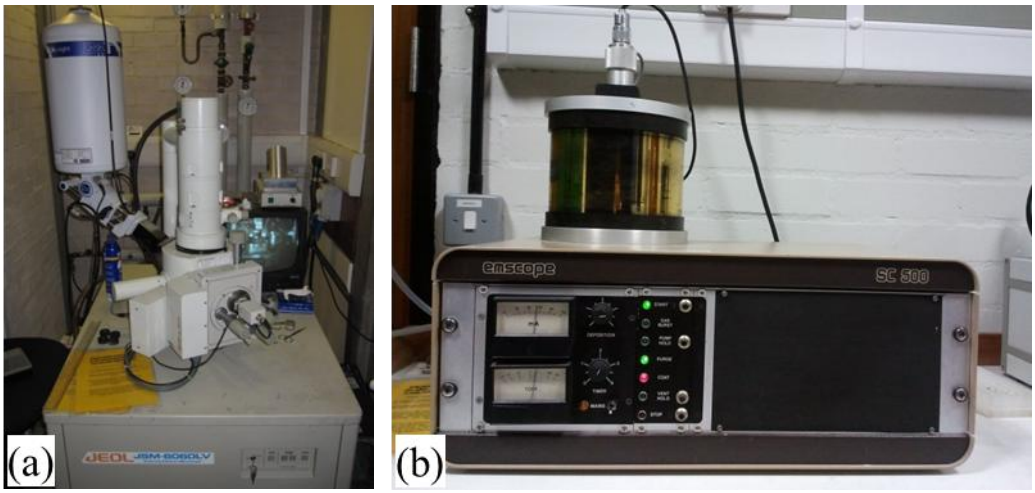


Figure 3.17: Illustration of (a) JEOL 6060 SEM and (b) Emscop SC500 gold sputter

Table 3.3: Buehler grinding / polishing route for aluminium alloy

Surface	**Abrasive / Size**	**Load Lb. (N) / Specimen**	**Base Speed (rpm) / Direction**	**Time (min:sec)**
CarbiMet paper	220 or 320 (P240 or P400) grit SiC, water cooled	5 (22)	240-300 Complementary	Until plane
UltraPol cloth	6 µm MetaDi Supreme diamond suspension	6 (27)	240-300 Complementary	6:00
TriDent cloth	3 µm MetaDi Supreme diamond suspension	6 (27)	240-300 Complementary	4:00
ChemoMet cloth	~0.05 µm MasterMet colloidal silica suspension	6 (27)	120-150 Contra	2:00

Workpiece surface topography (2D and 3D) was characterised using a Taylor Hobson Form 120 Talysurf with a vertical resolution of 10 nm and stylus tip radius of 2 µm, see Figure 3.18(a). A Mitutoyo Suftest 201 portable surface roughness tester was also used for intermediate measurements in Phase 3B. For 2D roughness analysis, a cut-off and evaluation length of 0.8 and 4 mm respectively were utilised with measurements repeated 3 times at different positions (entry, middle and exit location of the hole) and an average calculated. In the case of 3D topography analysis, a sampling area of 8 mm×1 mm was employed. Microhardness depth profile measurements of MMC hole cross sections were carried out on Mitutoyo MVK-H1 Vickers microhardness testing unit with a 50g load and 15s dwell, see Figure 3.18(b). In order to avoid / minimise the influence of plastic deformation from

preceding microhardness indentations on subsequent readings, the distance between the centre of each test-point was larger than 50 µm. The microhardness depth profiles were recorded up to 1000 µm below machined surface, with each position measured three times to improve statistical reliability.

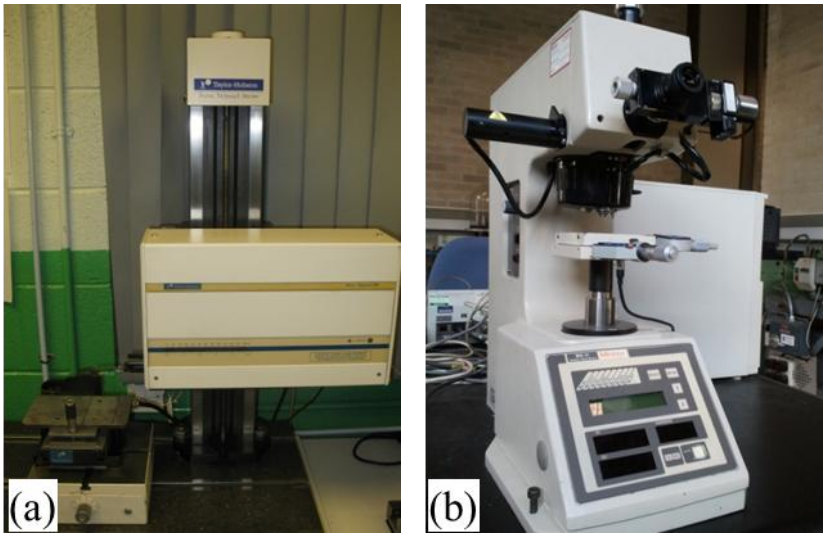


Figure 3.18: Illustration of (a) Taylor Hobson Form Talysurf series 120 L and (b) Mitutoyo MVK-H1 Vickers microhardness tester

3.3 Tool geometries, materials and coatings

3.3.1 Tools used for drilling CFRP

3.3.1.1 CVD-diamond coated drills

All of the diamond coated drills employed for the experimental work were fabricated and supplied by Seco Tools, UK. The diamond coating was deposited via a chemical vapour deposition (CVD) process onto 2-fluted tungsten carbide (WC) drills manufactured with a recently developed double point geometry (designated as C1), which was recommended by Seco for drilling CFRP. The coating thickness was ~7-11 µm, providing a hardness of 8000-1000$HV_{0.05}$ with corresponding friction coefficient of 0.02-0.1 and surface roughness of 0.1-0.4 µm Ra [197]. The sharp, double point geometry of the C1 drill was designed to provide excellent chip breaking characteristics with enhanced swarf evacuation for improved surface finish [198]. The dimensions and image of the C1 geometry drill are shown in Figure 3.19, which has a helix angle of 30° and two different point angles (130° and 60°) with corresponding primary and secondary cutting edges. The drills used in Phase 1A, 1B, 2B and 2C were 6.38 mm in diameter while those employed in Phase 2A were 6.00 mm in diameter.

Micrographs of the tool tip detailing the side view, end view and cutting lip are depicted in Figure 3.20.

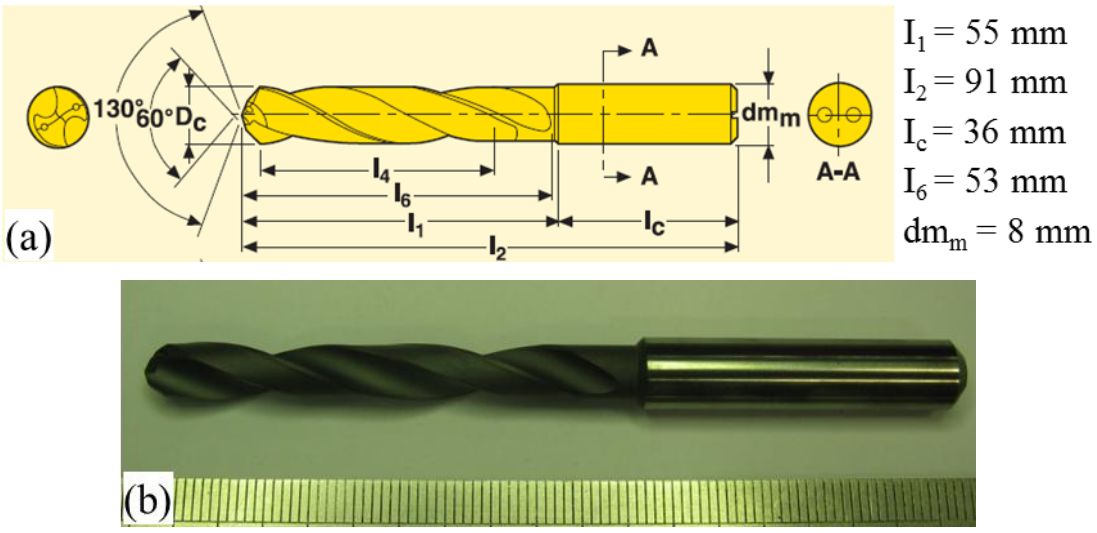


Figure 3.19: (a) Dimensions [198] and (b) image of Seco CVD-diamond coated C1 geometry drill

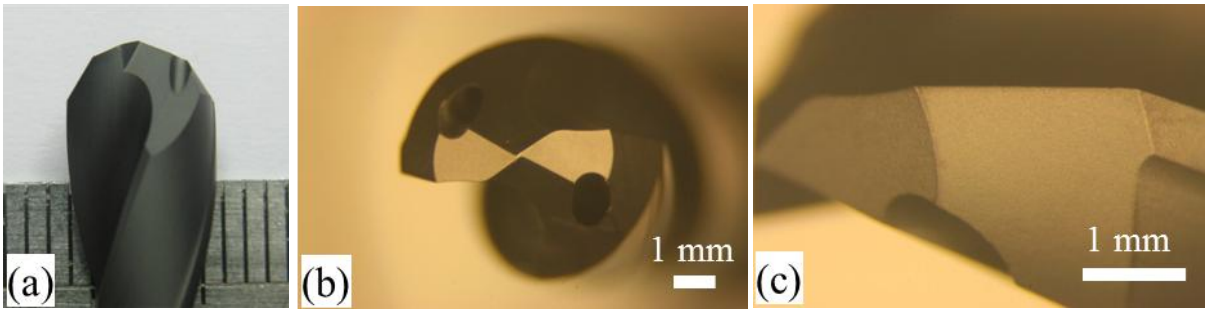


Figure 3.20: CVD-diamond coated drill tip: (a) side view, (b) end view and (c) cutting lip

3.3.1.2 Uncoated drills

In order to evaluate the performance of different tool materials / coatings and avoid / minimise the influence of tool geometry, uncoated WC drills with the same C1 geometry were employed in Phase 1A. The drills were manufactured using ~94% WC with an average grain size of ~0.8 µm and 6% cobalt binder content (K05-K10), giving a bulk hardness of 1790±50 HV_{30} and transverse rupture strength of >3900 N/mm^2 [197, 199], see Figure 3.21 for sample WC microstructure. All of the drills were 6.38 mm in diameter similar to that shown in Figure 3.22, with corresponding images of the tip geometry detailed in Figure 3.23.

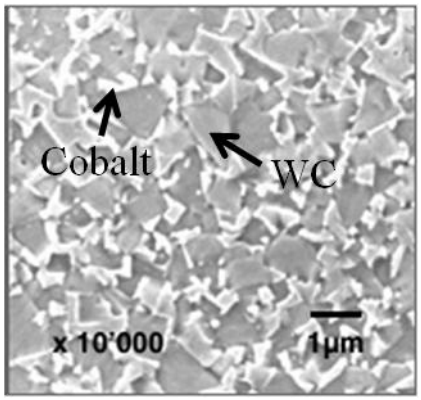


Figure 3.21: Microstructure of WC tool material used for uncoated C1 geometry drill [199]

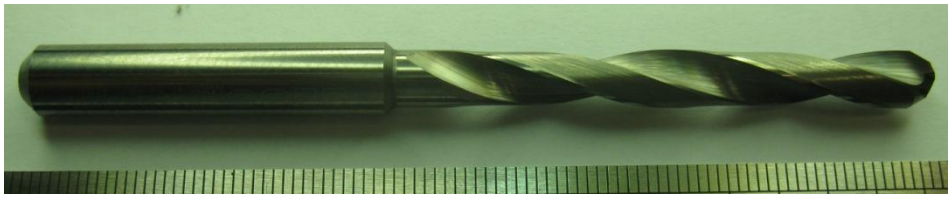


Figure 3.22: Image of Seco uncoated WC C1 geometry drill

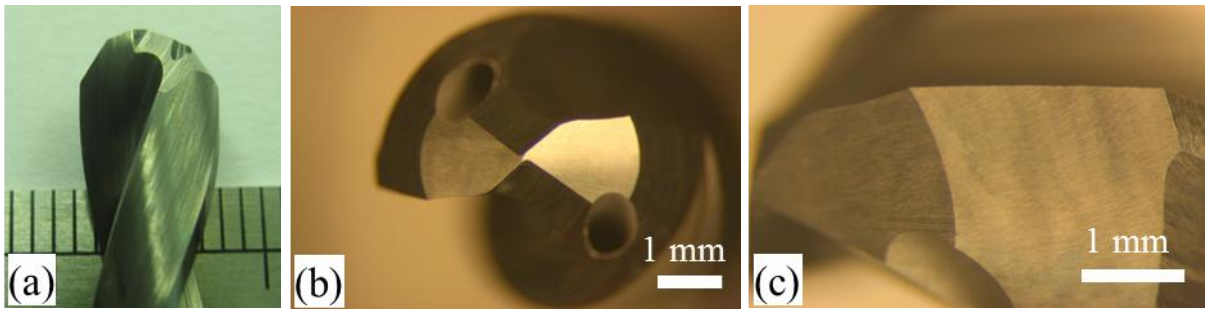


Figure 3.23: Uncoated WC drill tip: (a) side view, (b) end view and (c) cutting lip

3.3.1.3 Domed PCD drills

Novel domed PCD drills (designated as CX1) were evaluated when drilling CFRP in Phase 1A and 2C experiments. The 6.36 mm diameter tools comprised cylindrical PCD blanks (~4.0 mm length) having a hemispherical / domed profile at one end, which was copper-brazed on WC shanks / bodies, see Figure 3.24. The point geometry / cutting lips of the domed PCD drills were fabricated as close as possible to the C1 configuration, as shown in Figure 3.25. The drills however were 3-fluted in order to eliminate delamination / uncut fibres at the hole exit and improve geometrical accuracy. The domed PCD blanks was a multi-modal grade (CTM302) produced by Element Six, with grain sizes varying from 2 to 30 µm, which was designed to provide an excellent combination of wear resistance, thermal stability, edge strength and edge quality [197, 200]. The microstructure and mechanical / physical properties of the CTM302 PCD tool material is detailed in Figure 3.26 and Table 3.4 respectively.



Figure 3.24: Image of Seco domed PCD CX1 geometry drill

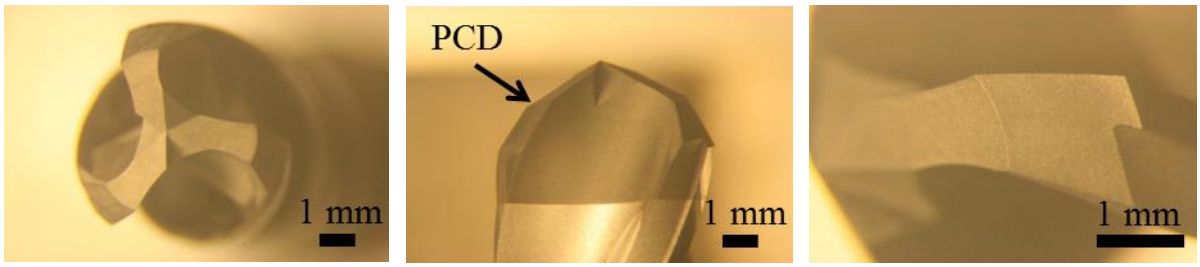


Figure 3.25: Seco domed PCD CX1 drill tip: (a) side view, (b) end view and (c) cutting lip

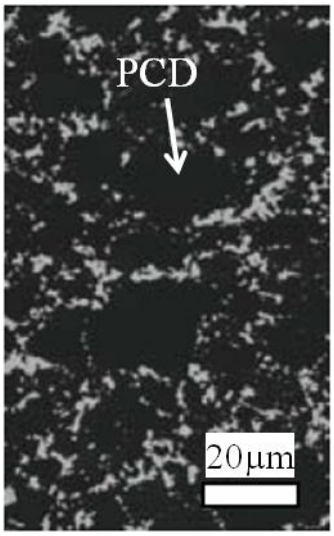


Figure 3.26: Microstructure of CTM302 grade PCD [200]

Table 3.4: Mechanical and physical properties of CTM302 grade PCD [159]

PCD grade	**Density (g/cm^3)**	**Koop hardness (GPa)**	**Young's Modulus (GPa)**	**Fracture toughness ($MPa•m^{1/2}$)**	**Thermal diffusivity ($mm^{-2}s^{-1}$)**	**Thermal conductivity ($Wm^{-1}K^{-1}$)**	**Poisson's ratio**
CTM302	3.99	50	883	9.34	218.0	421.7	0.109

3.3.2 Tools used for drilling MMCs

3.3.2.1 Uncoated and TiAlN+TiN coated drills

Uncoated (designated as T-type) and TiAlN+TiN coated (designated as M-type) WC drills with equivalent geometry were employed in Phase 3A work for the drilling of Al/SiCp MMCs. Both the T and M-type twist drills had diameters of 6.35 mm with a 140° point angle and 30° helix angle as well as through tool coolant holes. Figure 3.27(a) details a schematic showing the key geometrical features of the tool while corresponding images of the T and M-type drills are shown in Figures 3.27(b) and 3.27(c) respectively. Figures 3.28(a) and 3.28(b) show optical micrographs of the cutting lip geometry on the uncoated and coated WC drills respectively. A ~100 µm chamfer was apparent at the peripheral section on both tools, see Figure 3.28(c), which was applied to minimise the risk of chipping / breakage / severe abrasion of the cutting edge corner and maintain good hole geometrical accuracy, as maximum cutting speed occurred at this position in the drilling process. The drills were made from K30-K40 cemented tungsten carbide (90% WC and 10% Co) with an average grain size of 0.6 µm (see microstructure in Figure 3.29), which had a hardness of 1610 HV_{30} and transverse rupture strength of >3600 N/mm^2 [157, 197]. The TiAlN+TiN coating was deposited via physical vapour deposition (PVD) process.

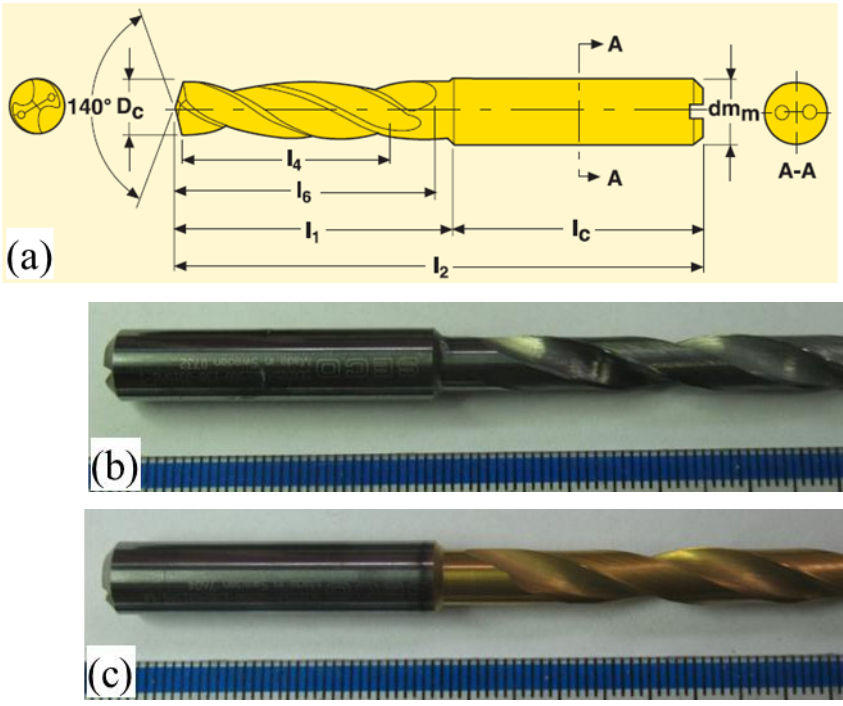


Figure 3.27: (a) Dimensions [198] and images of (b) Seco uncoated WC T-type drill and (c) TiAlN+TiN coated M-type drill

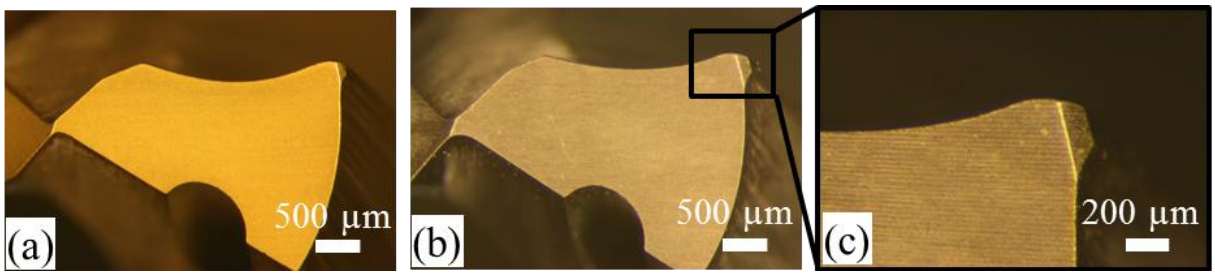


Figure 3.28: (a) Cutting lip of coated WC drill, (b) cutting lip of uncoated WC drill and (c) magnified view of cutting edge

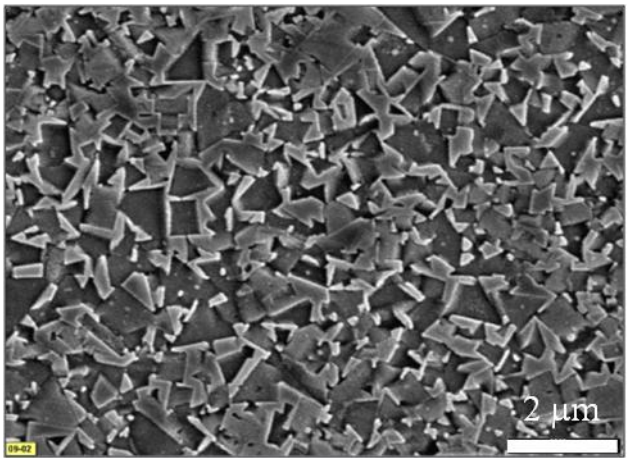


Figure 3.29: Microstructure of WC tool material used for the Seco M and T-type drills [157]

3.3.2.2 PCD drills

The domed PCD drills with CX1 geometry detailed previously in Section 3.3.1.3 were similarly utilised for the drilling of MMCs in Phase 3B experiments. An alternative brazed PCD drill design was also evaluated in Phase 3 trials, having a single point angle of 120° and helix angle of 30° (designated as CX31 geometry), as shown in the schematic and image in Figure 3.30. All of the brazed PCD drills were 6.38 mm in diameter, with the tool tip and cutting lip shown in Figure 3.31. In contrast to the domed PCD drills, the brazed tools employed a fine grained PCD grade, CTB002, which had an average particle size of 2 µm. The microstructure and associated mechanical / physical properties of CTB002 PCD are detailed in Figure 3.32 and Table 3.5 respectively.

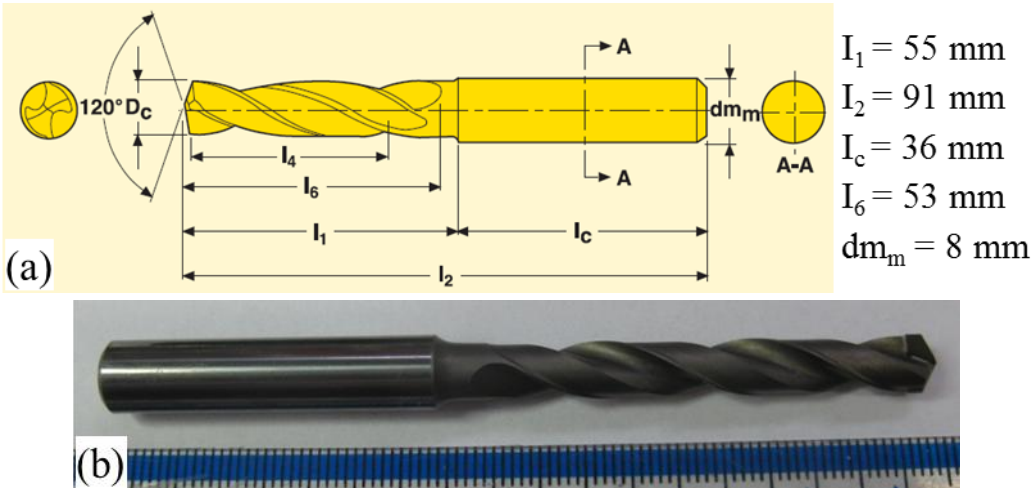


Figure 3.30: (a) Dimensions [198] and (b) image of Seco brazed PCD CX31 geometry drill

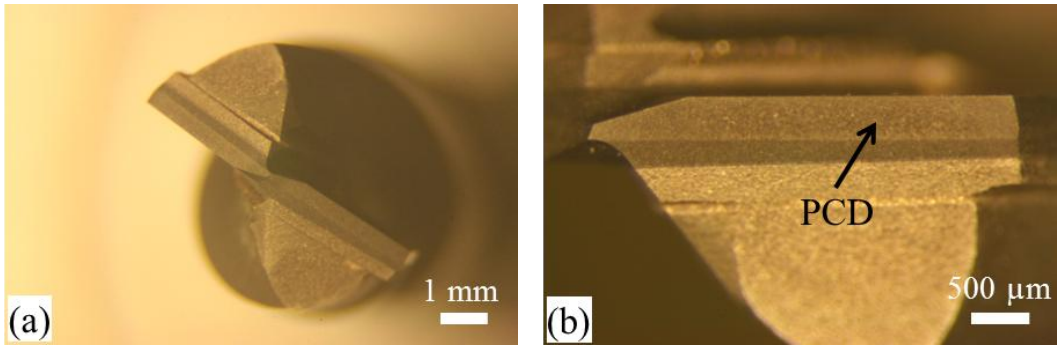


Figure 3.31: Tip geometry of Seco brazed PCD CX31 drill: (a) end view and (b) cutting lip

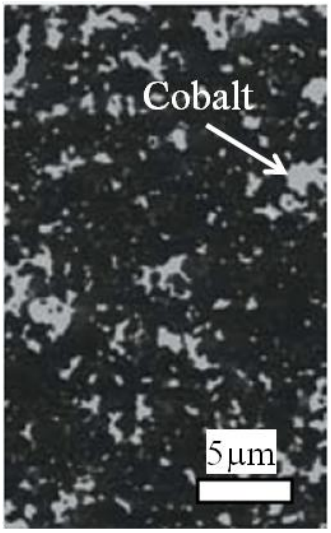


Figure 3.32: Microstructure of CTB002 grade PCD [200]

Table 3.5: Mechanical and physical properties of CTB002 grade PCD [159]

PCD grade	Density (g/cm^3)	Koop hardness (GPa)	Young's Modulus (GPa)	Fracture toughness ($MPa \cdot m^{1/2}$)	Thermal diffusivity ($mm^{-2}s^{-1}$)	Thermal conductivity ($Wm^{-1}K^{-1}$)	Poisson's ratio
CTB002	4.35	50	901	8.05	113.3	239.0	0.100

3.4 Experimental design, procedures and test arrays

3.4.1 Phase 1A: Influence of operating conditions and tool materials / coatings when drilling CFRP

The overall aim of Phase 1A was to investigate the effect of varying operating conditions when drilling CFRP with different tool materials / coatings. More specifically, the objectives of the work related to investigating the influence of tool material / coating, cutting speed, feed rate and cutting environment on thrust force / torque, hole quality, workpiece surface integrity and tool life / wear mechanisms.

A modified Taguchi fractional factorial experimental design (L12 orthogonal array) was employed. The output responses was analysed with Minitab 16 software involving main effects plots and analysis of variance (ANOVA) to identify significant factors / levels, percentage contribution ratios (PCR) etc. The operating parameters selected were based on information derived from the literature review together with recommendations from the tool manufacturers. The experiments involved four variable factors comprising tool material / coating, cutting speed, feed rate and cutting environment with one at three levels and the others at two levels. All of the trials were performed on Type 3 CFRP workpieces according to the test matrix listed in Table 3.6. Thrust force / torque and tool wear was measured at the first hole and then at intervals of 32 holes. The end of test criteria was a maximum flank wear (VB_{max}) of 0.3 mm or after drilling 512 holes.

Figure 3.33 shows the experimental setup for Phase 1A. The dual hose nozzles for supplying chilled air was directed towards the cutting zone and located approximately 15 mm away from the drill tip. The extraction point connected to the Filtermist dust extraction system was positioned as close as possible to the cutting area without interfering with the drilling operation. No backup plate was used in the experiment.

Table 3.6: Test matrix involving L12 modified Taguchi fractional factorial array for Phase 1A experiments

Test no.	Tool material / coating	Cutting speed (m/min)	Feed rate (mm/rev)	Cutting environment
1	Uncoated WC	90	0.05	Dry
2	Uncoated WC	90	0.1	Chilled air
3	Uncoated WC	180	0.05	Chilled air
4	Uncoated WC	180	0.1	Dry
5	CVD-diamond coated WC	90	0.05	Dry
6	CVD-diamond coated WC	90	0.1	Chilled air
7	CVD-diamond coated WC	180	0.05	Chilled air
8	CVD-diamond coated WC	180	0.1	Dry
9	Domed PCD	90	0.05	Dry
10	Domed PCD	90	0.1	Chilled air
11	Domed PCD	180	0.05	Chilled air
12	Domed PCD	180	0.1	Dry

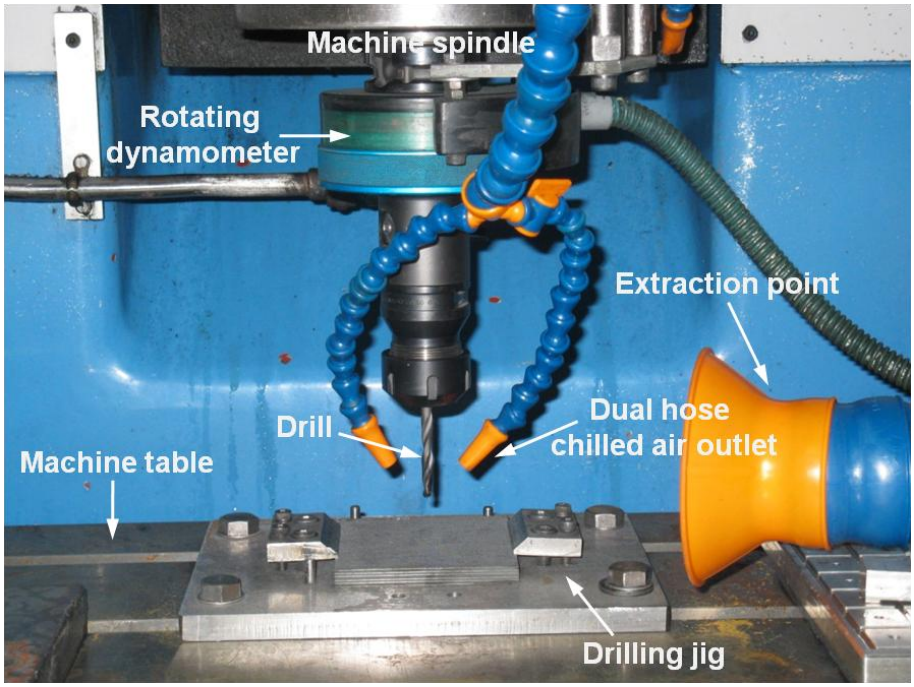


Figure 3.33: Setup for drilling CFRP in Phase 1A

3.4.2 Phase 1B: Preliminary / benchmarking trials in drilling CFRP with variable feed rate operation

Phase 1B trials related to a preliminary investigation on the influence of varying feed rate operation and cutting environment on thrust force / torque and hole exit quality (uncut fibres and delamination). In order to minimise / reduce the number of required tools, worn drills from Tests 6 and 8 in Phase 1A (~110-120 µm flank wear) were utilised in this experiment. According to work reported by Hocheng and Tsao [201], hole exit delamination increases linearly with drilling thrust force, see Figure 3.34(a). For uncoated 10 mm diameter WC twist drills operating at a cutting speed of 31.4 m/min under dry conditions, the 'critical' feed rate (maximum value without the occurrence of workpiece delamination) was 0.0047 mm/rev, as shown in Figure 3.34(b). In the current experiment, a variable feed rate strategy where drill feed was decreased from 0.1 mm/rev to 0.01 or 0.02 mm/rev in the final 2 mm of the plate in order to reduce thrust forces and minimise hole exit damage without severely impacting process productivity. Two cutting speed levels (90 and 180 m/min) were employed while the influence of dry, chilled air and wet cutting environments were also studied. The detailed experimental matrix is shown in Table 3.7 with ~10 holes drilled per test. Similar to Phase 1A trials, Type 3 CFRP panels were used for all tests.

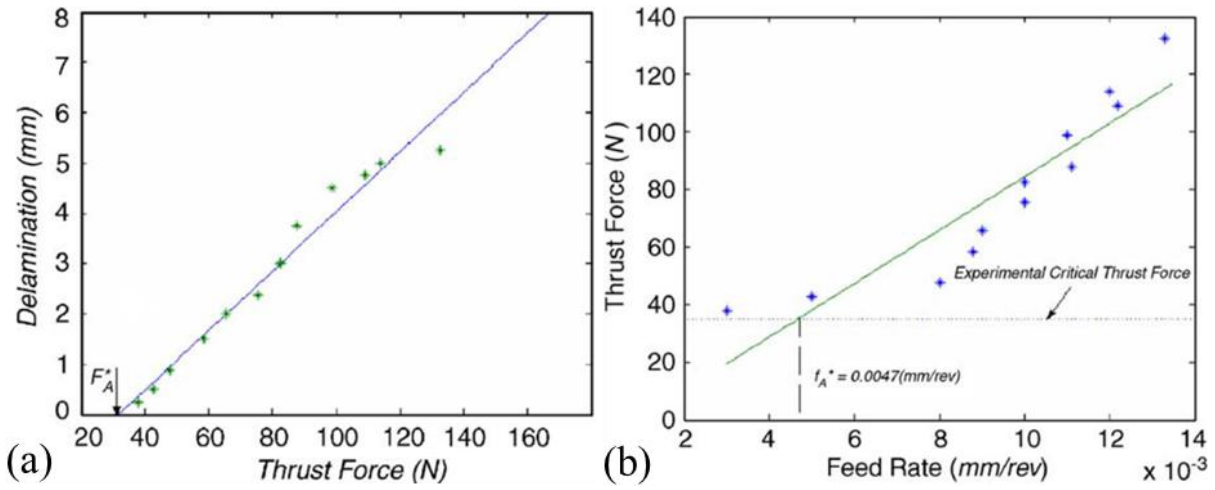


Figure 3.34: (a) Experimental correlation between thrust force and delamination extent, (b) experimental 'critical' thrust force to initiate delamination against feed rate [201]

Table 3.7: Test matrix for Phase 1B experiments

Test no.	Tool material / Coating	Cutting speed (m/min)	Feed rate (mm/rev)	Feed rate in final 2 mm (mm/rev)	Cutting environment
1	CVD-diamond coated WC (Tool from Test 6 in Phase 1A, tool wear: 117 µm)	90	0.1	0.01	Chilled air
2				0.02	Chilled air
3				0.01	Dry
4				0.02	Dry
5				0.01	Flood
6	CVD-diamond coated WC (Tool from Test 8 in Phase 1A, tool wear: 111 µm)	180		0.01	Chilled air
7				0.02	Chilled air
8				0.01	Dry
9				0.02	Dry
10				0.01	Flood

3.4.3 Phase 2A: Evaluation of hole quality when drilling CFRP with variable feed rate operation

Based on results from Phase 1A and 1B trials, a move in-depth investigation on the effects of varying feed rate strategy on hole quality when drilling CFRP was performed in Phase 2A. A full factorial experimental design involving two variable factors (CFRP workpiece configuration at two levels and primary feed rate at three levels) was performed. Cutting speed was constant at 90 m/min with chilled air applied in all tests. The drilling trials were carried out using 6.0 mm diameter drills with the primary feed rate levels (0.1-0.3 mm/rev) reduced to 0.01 mm/rev for the final 2 mm of the hole, see illustration in Figure 3.35. Tool wear (mean from maximum flank wear of both flutes) and thrust force / torque were measured after the first hole and at subsequent intervals of 32 holes. The test cessation criterion was either 384 holes drilled or a maximum flank wear of 300 µm. The detailed test matrix is listed in Table 3.8. Photogaraphs of hole entry and exit both in the first and last hole were taken to evaluate workpiece delamination / damaged, which was quantified using a

parameter known as the delamination factor (F_d). SEM ananlysis was performed for the hole surafecs machined with new and worn tools.

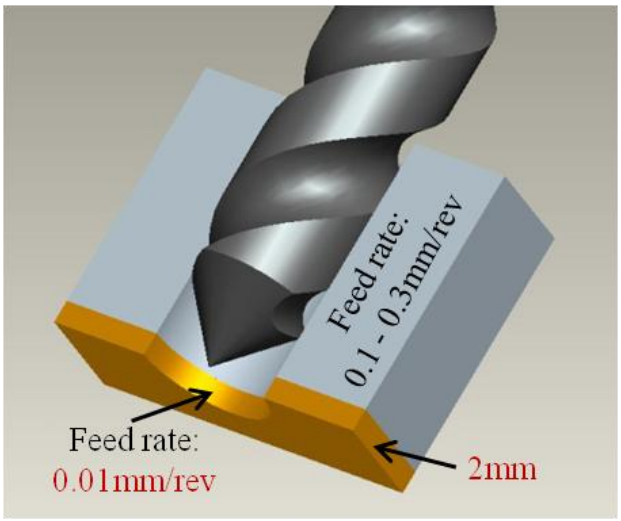


Figure 3.35: Schematic of variable feed rate drilling strategy

Table 3.8: Full factorial test array for Phase 2A experiments

Test no.	Workpiece material	Cutting speed (m/min)	Cutting environment	Feed rate (mm/rev)	
1	Type 2 (44/44/11)	90	Chilled air	0.10	0.01 mm/rev in final 2 mm
2	Type 3 (15/70/15)			0.10	
3	Type 2 (44/44/11)			0.20	
4	Type 3 (15/70/15)			0.20	
5	Type 2 (44/44/11)			0.30	
6	Type 3 (15/70/15)			0.30	

3.4.4 Phase 2B: Influence of workpiece configuration / fibre orientation and elevated feed rates on hole quality when drilling CFRP

Following results from Phase 2A experiments, the effect of workpiece configuration / fibre orientation and elevated feed rate (with variable feed rate strategy) when drilling CFRP was investigated in Phase 2B work. In order to further improve hole exit quality and minimise uncut fibres, an aluminium plate with an array of 7.0 mm diameter clearance holes was positioned beneath the CFRP workpiece, as shown in the setup assembly in Figure 3.36. In a trial, a high primary feed rate of 0.6 mm/rev was applied to obtain benchmark / baseline data.

In contrast to previous tests, feed rate was reduced to 0.01 mm/rev in the final 0.5 mm of the hole to increase productivity. A full factorial experimental design involving three different CFRP laminate layup / fibre orientation (Types 1, 2 and 3) and primary feed rates of 0.2 and 0.4 mm/rev, was utilised in mainstream trials, see test matrix in Table 3.9. Cutting speed was fixed at 90 m/min with chilled air used throughout the entire experiment. The end of test criterion was equivalent to that in Phase 2A (VB_{max} of 300 µm or 384 holes drilled). Limited additional trials (~10 holes) without the variable feed rate strategy were performed on Type 3 and unidirectional CFRP laminates after the cessation of Tests 3 and 6, in order to validate the benefits of reducing feed rate near the hole exit. Tools employed for current work were 6.38 mm diameter CVD-diamond coated WC drills. Hole surface roughness, 3D topographic maps, hole diameter as well as geometrical characteristics (out of roundness and cylindricity) were assessed for all the tests.

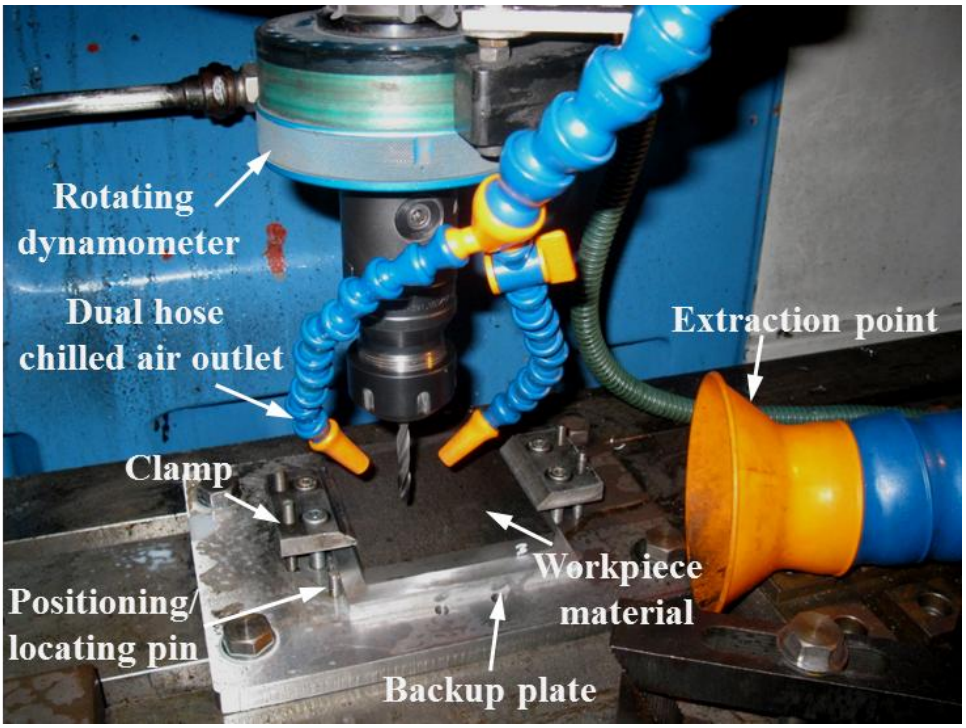


Figure 3.36: Experimental setup for Phase 2B tests

Table 3.9: Test matrix for Phase 2B experiments

Test no.	Cutting speed (m/min)	Workpiece material	Feed rate (mm/rev)		Cutting environment
Initial test	90	Type 3 (15/70/15)	0.6	0.01 mm/rev in final 0.5 mm	Chilled air
1		Type 1 (25/50/25)	0.2		
2		Type 2 (44/44/11)	0.2		
3		Type 3 (15/70/15)	0.2		
4		Type 1 (25/50/25)	0.4		
5		Type 2 (44/44/11)	0.4		
6		Type 3 (15/70/15)	0.4		
Further test after Test 3		Type 3 (15/70/15)	0.2		
Further test after Test 6		Type 3 (15/70/15)	0.4		
Further test after Test 3		Unidirectional (UD)	0.2		
Further test after Test 6		Unidirectional (UD)	0.4		

3.4.5 Phase 2C: Evaluation of diamond coated and domed PCD tools when drilling CFRP at elevated / high cutting speeds

Figure 3.37 summarises the reported cutting parameters (cutting speed and feed rate) typically employed when drilling CFRP and GFRP using tungsten carbide drills based on information in the literature. Cutting speeds typically ranged from 20 to 80 m/min, whereas feed rate values were generally lower than 0.3 mm/rev. The reason for keeping cutting speed below 80 m/min may be explained that higher cutting speed values lead to higher cutting temperature, which in turn may cause the burning of the matrix [37]. The use of feed rates below 0.3 mm/rev may be associated to the delamination damage caused when this parameter is increased.

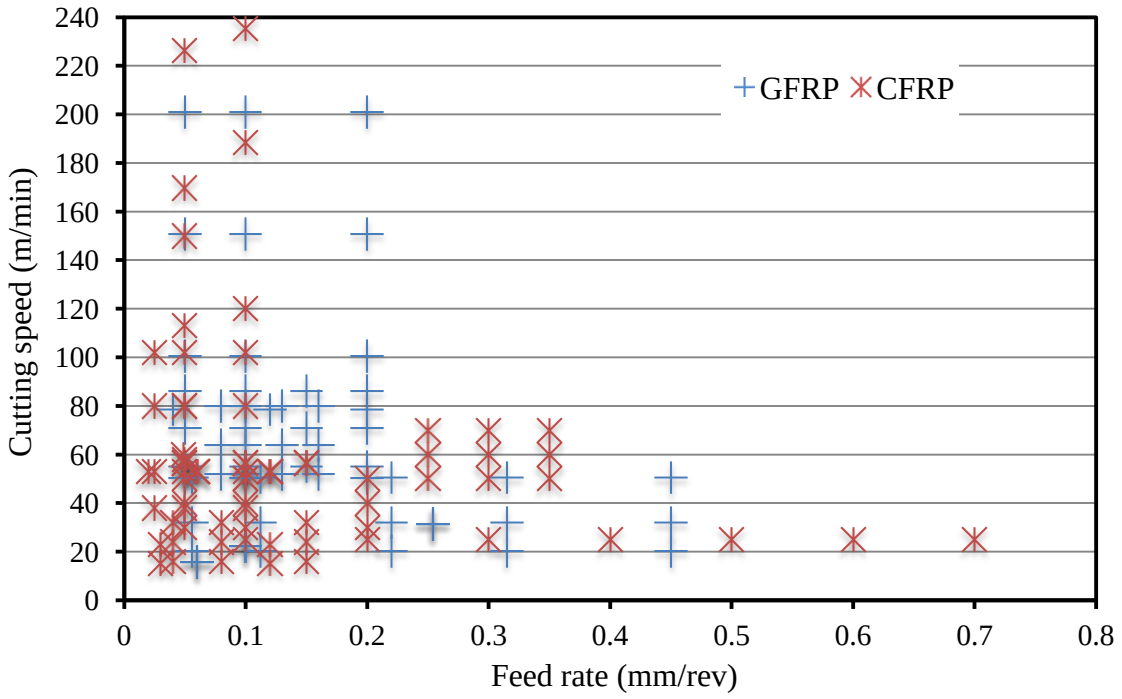


Figure 3.37: Cutting speed and feed rates typically employed when drilling CFRP and GFRP using tungsten carbide drills

The overall aim of Phase 2C tests was to evaluat the performance of CVD-diamond coated and domed PCD tools at elevated cutting speeds when drilling Type 3 CFRP laminates. Cutting speed was varied between 180 and 360 m/min while feed rate was kept constant at 0.05 mm/rev with chilled air used in all trials, see test matrix detailed in Table 3.10. The end of test criterion was equivalent to that specified in Phase 2A and 2B (VB_B of 300 µm or 384 holes were drilled). Thrust force and torque were measured using the drilling dynamometer in accordance with intervals detailed in Section 3.2.4. The experimental setup is shown in Figure 3.38.

Table 3.10: Test matrix for Phase 2C experiments

Test no.	Tool materials	Cutting speed (m/min)	Feed rate (mm/rev)	Cutting environment	Workpiece materials
1	Diamond Coated	180	0.05	Chilled air	Type 3 (15/70/15)
2	Diamond Coated	240			
3	Diamond Coated	280			
4	Diamond Coated	360			
5	Domed PCD	180			
6	Domed PCD	360			

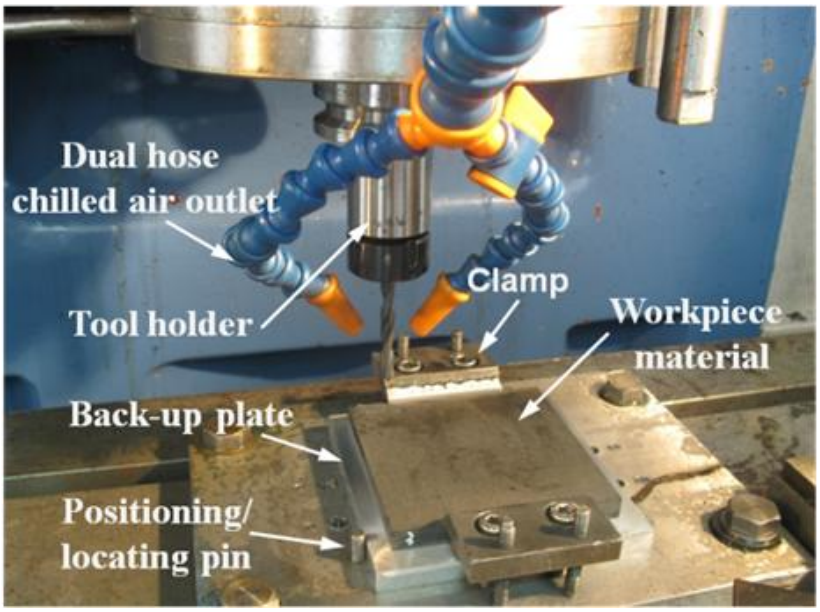


Figure 3.38: Experimental setup for Phase 2C tests

3.4.6 Phase 3A: Preliminary / benchmarking trials in drilling MMCs with different tool materials / coatings

Phase 3A experiments were designed to investigate the effect of different tool materials / coatings and operating parameters when drilling Al/SiCp MMCs and provide benchmark / baseline data for subsequent mainstream testing / analysis. The operating parameter levels selected were based on information in the literature and previous work done in the Machining Research Group at Birmingham [121, 122]. The end of test criteria was a maximum flank wear (VB_{max}) of 0.3 mm or when 300 holes were drilled. Each workpiece block accommodated up to 144 holes (6.35 mm diameter) according to a 9×16 array with 9.0 mm pitch. The workpiece specimens were fixed on a bespoke clamping plate (without pre-drilled clearance holes) for tool life testing. Separate strip specimens with a width of 17 mm were used for thrust force, torque and surface integrity evaluation were held on a Kistler 9273 four-component piezoelectric drilling dynamometer. Drills employed for this phase of work were uncoated (designated as T-type) and TiAlN+TiN coated (designated as M-type) solid carbide as well as brazed PCD tools (designated as CX31 type), see Figure 3.39. For trials utilising the uncoated and coated carbide tools, cutting speed was fixed at 80 m/min while feed rate varied from 0.1 to 0.2 mm/rev with cutting fluid applied internally through the drills. In contrast, the PCD drills were assessed at a constant feed rate of 0.1 mm/rev over two levels of cutting speed (80 and 160 m/min) with coolant supplied externally via standard nozzles. The test array is detailed in Table 3.11 and corresponding experimental setups are shown in Figure 3.40.

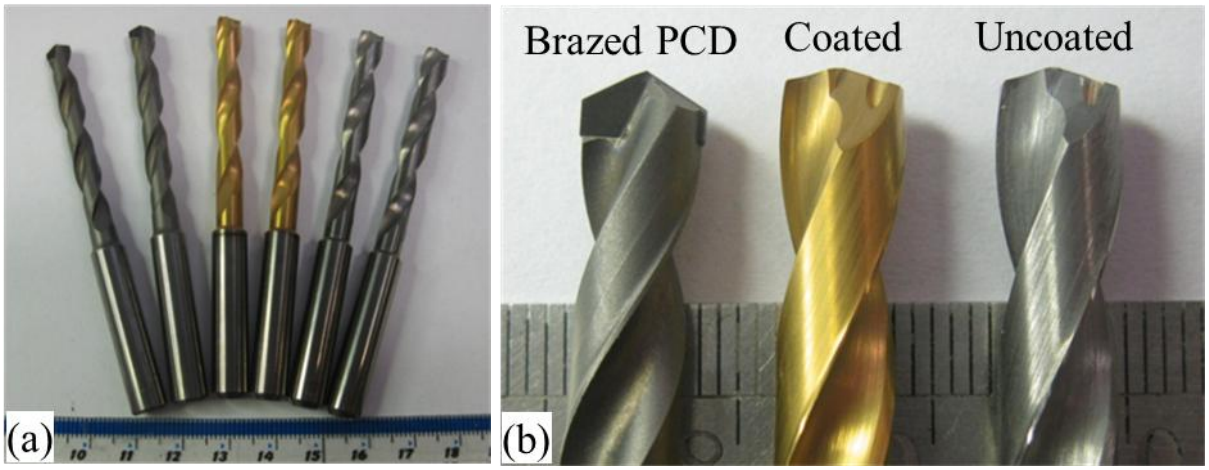


Figure 3.39: Drills used in Phase 3A experiment (a) overview and (b) side view

Table 3.11: Test matrix for Phase 3A experiments

Test no.	Tool materials / coatings	Cutting speed (m/min)	Feed rate (mm/rev)	Cutting environment
1	Uncoated WC	80	0.1	70 bar (internal)
2	Uncoated WC	80	0.2	70 bar (internal)
3	Coated WC	80	0.1	70 bar (internal)
4	Coated WC	80	0.2	70 bar (internal)
5	Brazed PCD	80	0.1	70 bar (external)
6	Brazed PCD	160	0.1	70 bar (external)

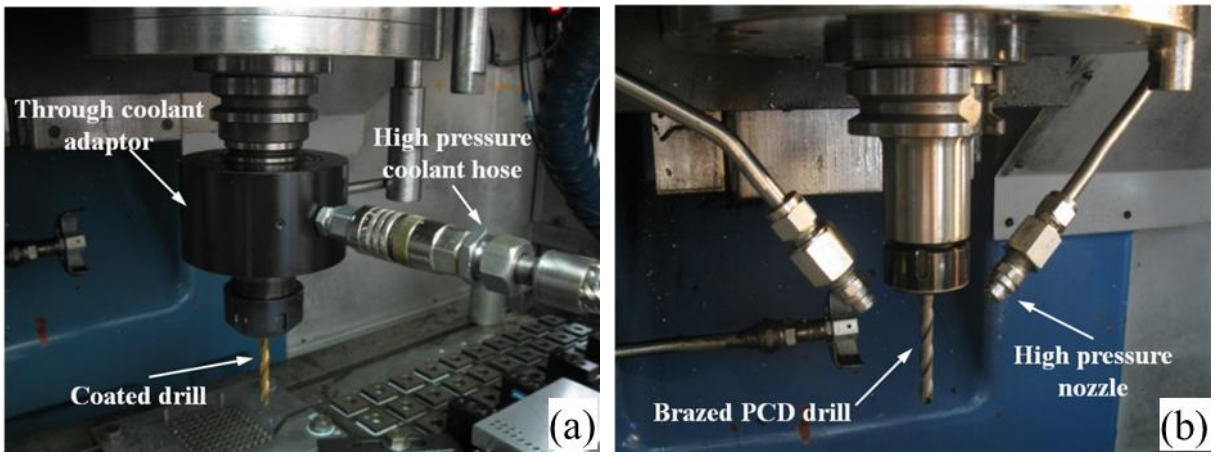


Figure 3.40: (a) Setup of high pressure through tool cutting fluid application and (b) setup for external high pressure cutting fluid application

3.4.7 Phase 3B: Evaluation of PCD tools and cutting parameters when drilling MMCs

Following preliminary work in Phase 3A, the effect of varying cutting speed, feed rate and cutting fluid pressure was evaluated when drilling Al/SiCp MMCs using brazed and domed PCD tools in Phase 3B. Response measures assessed include thrust force / torque, tool wear / life, hole quality (hole diameter, out of roundness, cylindricity etc.) and surface integrity (surface roughness, burr formation, subsurface damage, microhardness etc.). A Taguchi L8 fractional factorial design involving four variable factors, each at two levels was used, see test matrix in Table 3.12. The output responses were analysed using Minitab 16 software, with main effects plots and analysis of variance (ANOVA) employed to identify significant factors / levels and percentage contribution ratios (PCR). Block workpicees of ~170 mm length were held on a clamping plate with accommodating 153 (9×17) holes at a pitch of 9.0 mm. Similar to Phase 3A, the end of test criteria was a maximum flank wear (VB_{max}) of 0.3 mm or when 306 holes (in two blocks) were produced. As shown in Figure 3.41, high pressure (70 bar) cutting fluid at a flow rate of ~26 litres/min was supplied via twin stainless pipes (1.5 mm diameter outlet), while triple loc-line hoses (~3 mm diameter outlet) were utilised for tests at flood (3 bar) conditions. In order to remove BUE / adhered materials, drills were soaked in 25% NaOH solution for ~1 minute prior to flank wear measurement.

Table 3.12: Test matrix for Phase 3B experiments

Test no.	Tool material	Cutting speed (m/min)	Feed rate (mm/rev)	Cutting environment
1	Brazed PCD	80	0.1	70 bar high pressure fluid
2	Brazed PCD	80	0.2	3 bar low pressure flood
3	Brazed PCD	160	0.1	3 bar low pressure flood
4	Brazed PCD	160	0.2	70 bar high pressure fluid
5	Domed PCD	80	0.1	3 bar low pressure flood
6	Domed PCD	80	0.2	70 bar high pressure fluid
7	Domed PCD	160	0.1	70 bar high pressure fluid
8	Domed PCD	160	0.2	3 bar low pressure flood

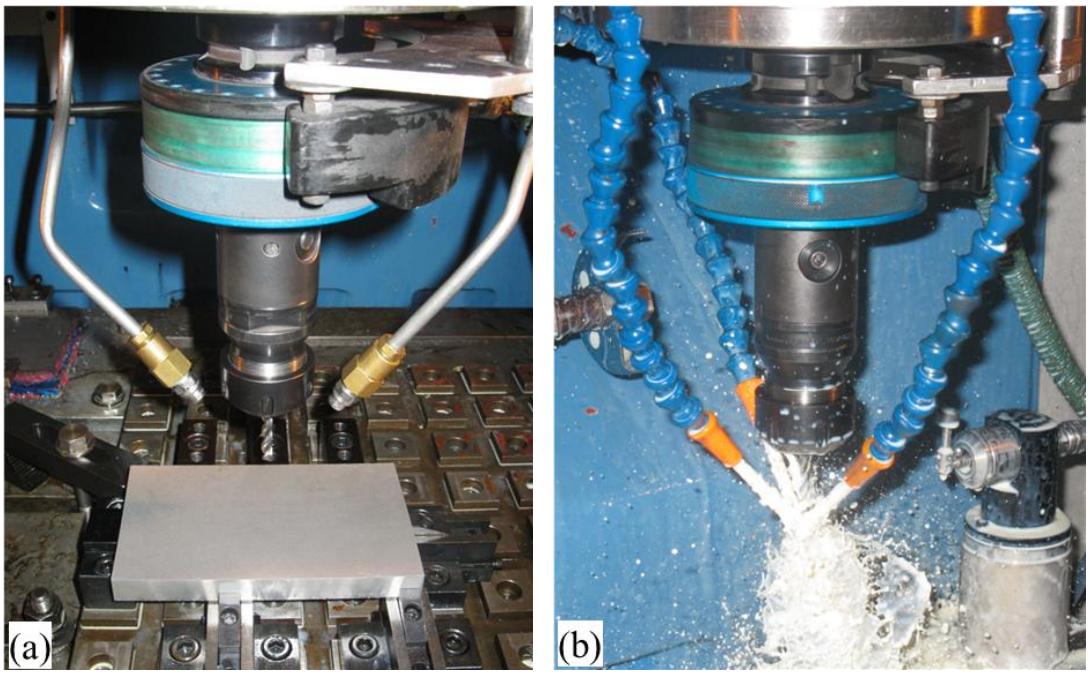


Figure 3.41: Setup for applying (a) high pressure cutting fluid and (b) low pressure flood

3.4.8 Phase 3C: Drilling of MMC using PCD tools at elevated / high cutting speeds

Based on the results from Phase 3A and 3B tests, Phase 3C was carried out to evaluate the performance of brazed PCD tools when drilling Al/SiCp MMCs at elevated cutting speeds. Four levels of cutting speed up to 360 m/min (18,000 rpm) were utilised while feed rate was kept constant at 0.1 mm/rev, see experimental matrix in Table 3.13. High pressure cutting fluid (70 bar) delivered externally was employed throughout the entire experiment, with the end of test criteria equivalent to that used in Phase 3A. Strip workpiece was clamped on drilling dynamometer Kistler 9273 for thrust force / torque and corresponding tool wear measurement. The first and last holes were sectioned and subsequently cleaned for surface roughness measurement, followed by mounted and ground / polished for microhardness and subsurface quality analysis. Chips from each trial were also collected and photographed for evaluation.

Table 3.13: Test matrix for Phase 3C experiments

Test no.	Tool materials	Cutting speed (m/min)	Feed rate (mm/rev)	Cutting environment
1	Brazed PCD	160 (8,000 rpm)	0.1	70 bar high pressure fluid
2	Brazed PCD	200 (10,000 rpm)		
3	Brazed PCD	240 (12,000 rpm)		
4	Brazed PCD	360 (18,000 rpm)		

Chapter 4: RESULTS AND DISCUSSION

4.1 Phase 1A: Influence of operating conditions and tool materials / coatings when drilling CFRP

4.1.1 Tool wear and life

Figure 4.1 shows the tool wear progression plot against number of holes drilled for all trials. In Tests 2 and 3 using uncoated tools, drilling was prematurely terminated with tool flank wear at ~150 µm (instead of the 300 µm criterion) due to severe damage observed at hole entry (fuzzing and uncut fibres). A total of 384 and 320 holes were produced respectively. Similarly, Tests 1 and 4 had to be halted after only 192 holes as a result of fibre dust / matrix burning. In contrast, all of the tests undertaken using CVD-diamond coated and domed PCD drills achieved 512 holes, with the highest flank wear of 144 µm seen in Test 5, while the best performance was obtained in Test 12 (domed PCD drill, 180 m/min, 0.1 mm/rev, dry) with average maximum flank wear of 73 µm. Drill wear progression typically followed a similar trend in every trial except for Test 5 with chipping occurring after ~320 holes, following which flank wear increased rapidly. The wear rate was also somewhat higher in Tests 5, 7, 9 and 11, possibly due to the lower feed rate (0.05 mm/rev) employed, leading to longer contact time between the tool and workpiece material.

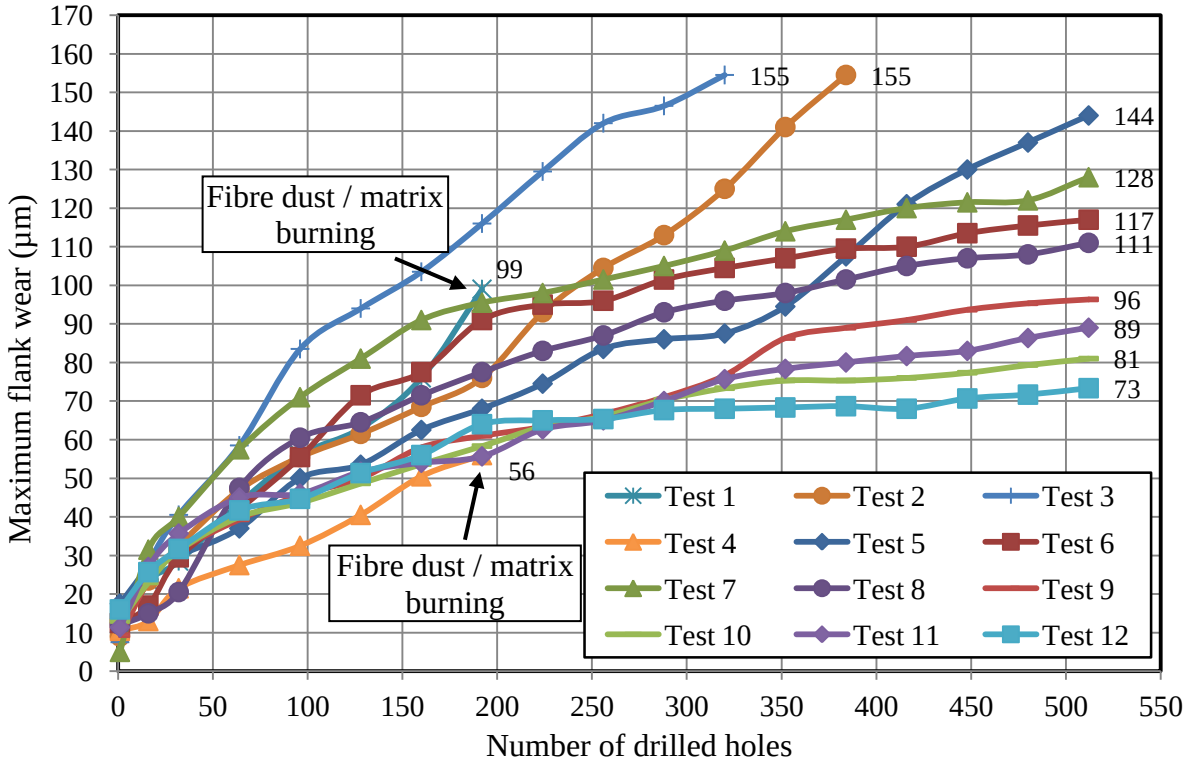


Figure 4.1: Tool wear progression against number of drilled holes

Tool wear scar images for all trials at test cessation are presented in Figure 4.2. The degree of wear on the cutting edges of all flutes were generally consistent, which reflects the good geometrical accuracy of the drills. In general, flank wear was the dominant damage mode, which increased gradually over the test duration, with the maximum level occurring at the drill corner (location of highest cutting speed). Cutting edge rounding and shiny flank surface were evident on the uncoated drills due to prolonged contact with the highly abrasive carbon fibres / powdery chips during machining. This was in agreement with the results of Khairusshima et al. [44] when milling CFRP with WC tools. For domed PCD drills, no signs of chisel or cutting edge chipping / fracture were detected in any of the tests, with all tools displaying comparable wear patterns in the form of abrasion at test cessation. Chipping / delamination of the CVD-diamond coating however was observed in Test 5 after drilling ~320 holes, although only marginal / limited wear on the chisel edge was apparent after 512 holes. The flank wear evolution of the CVD-diamond coated drill used in Test 5 is shown in Figure 4.3. Adhesion of fibre dust / epoxy matrix on the drill tip was prevalent from the first hole, which was most likely due to relatively higher cutting temperatures when machining dry.

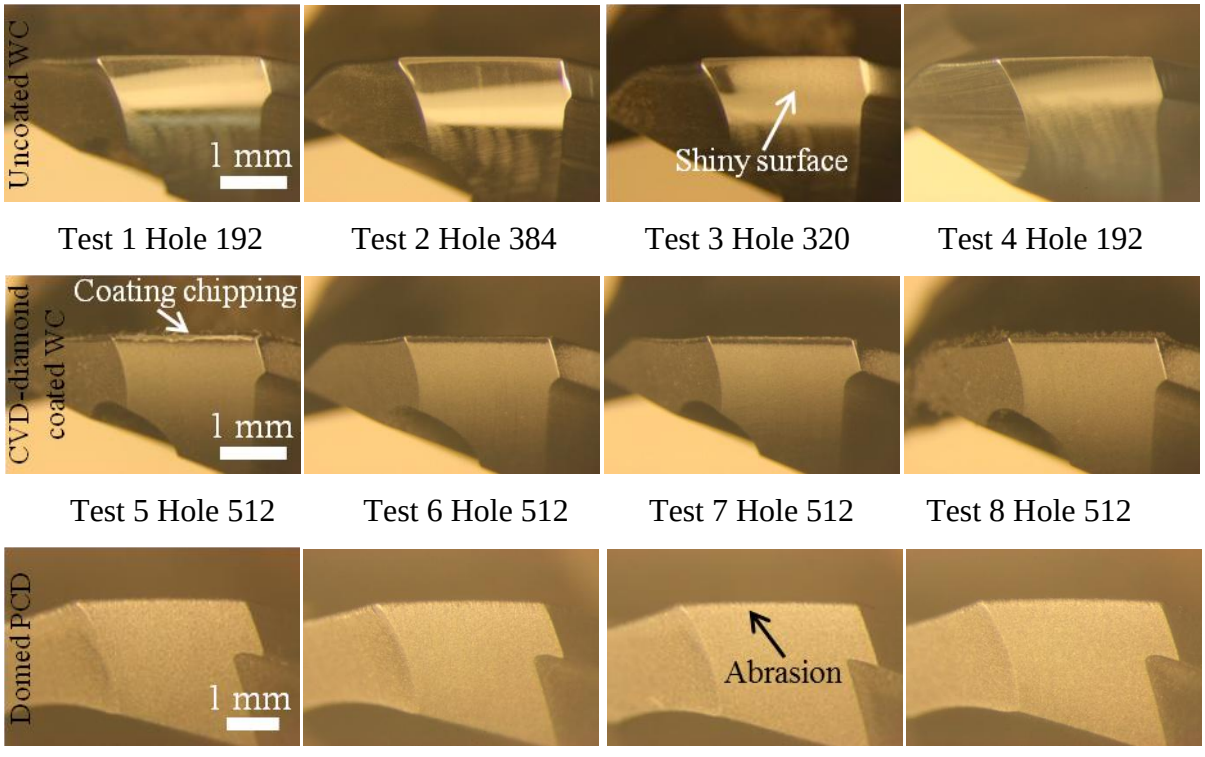


Figure 4.2: Tool wear scars at test cessation (last hole) in all trials

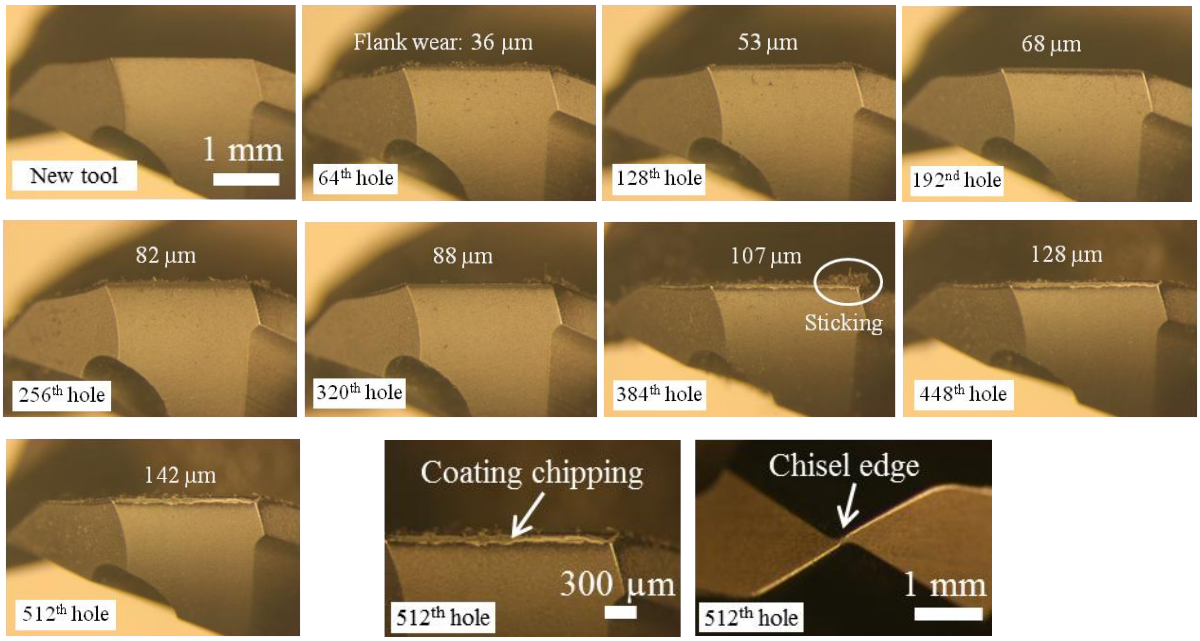


Figure 4.3: Tool wear evolution for Test 5 (uncoated WC, 90 m/min, 0.05mm/rev and dry)

The fibre dust covering the workpiece samples began to burn after drilling ~160 holes using uncoated WC tools in Test 1 (90 m/min, 0.05 mm/rev, dry) and 4 (180 m/min, 0.1 mm/rev, dry). Smoke was clearly visible during drilling (see Figure 4.4) coupled with a strong odour, which was most likely due to the use of either low feed (0.05 mm/rev) or high cutting speed (180 m/min) combined with a dry cutting environment. Severe build-up / accumulation of fibre dust in the drill flutes was also observed as shown in Figure 4.5, which was exacerbated by the poor thermal conductivity (~0.2 W/m^{o}C) and low glass transition temperature of the epoxy resin (<175^{o}C) [4].



Figure 4.4: Fibre dust burning in Test 1 after drilling 192 holes

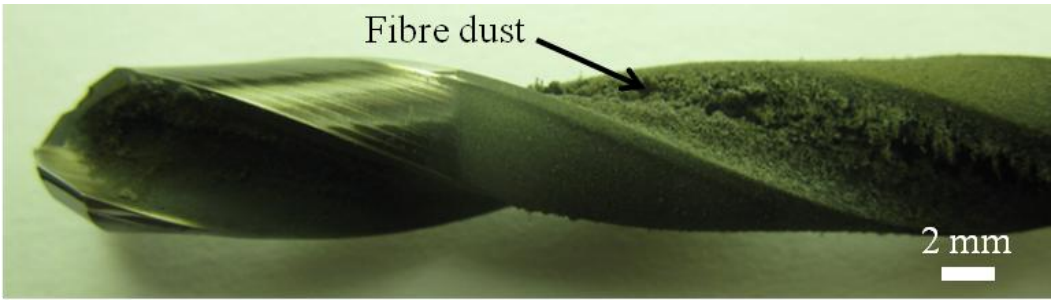
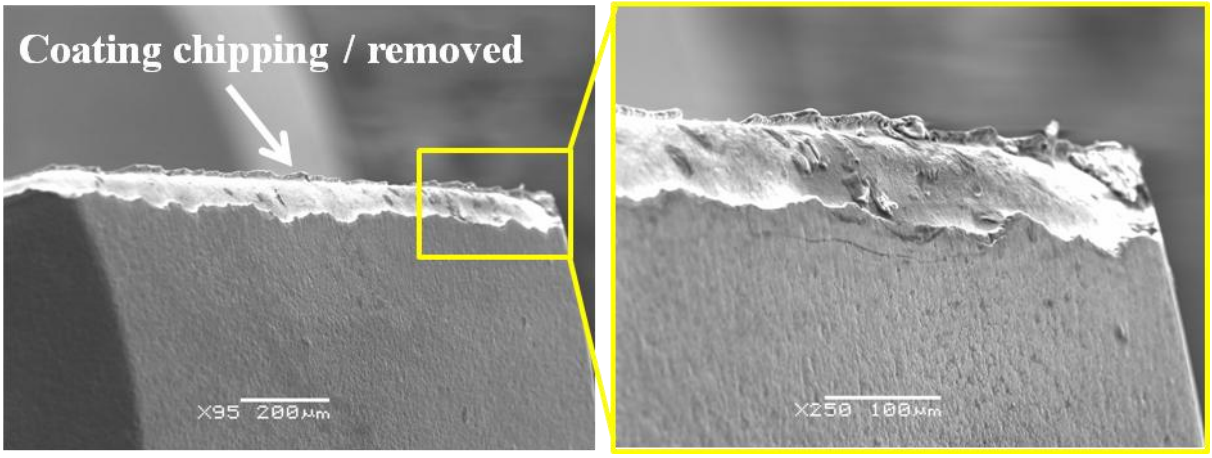
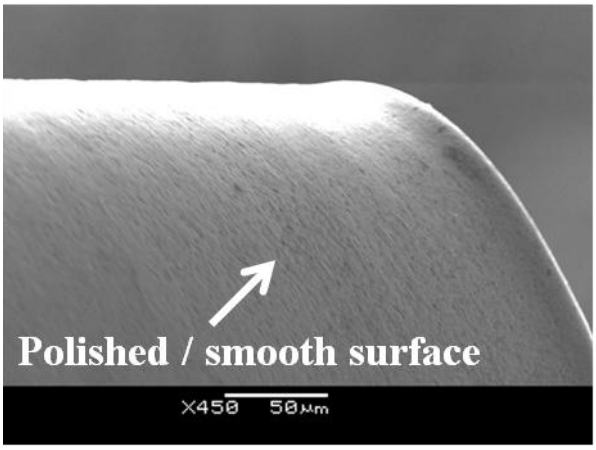


Figure 4.5: Drill condition at test cessation in Test 1 after drilling 192 holes

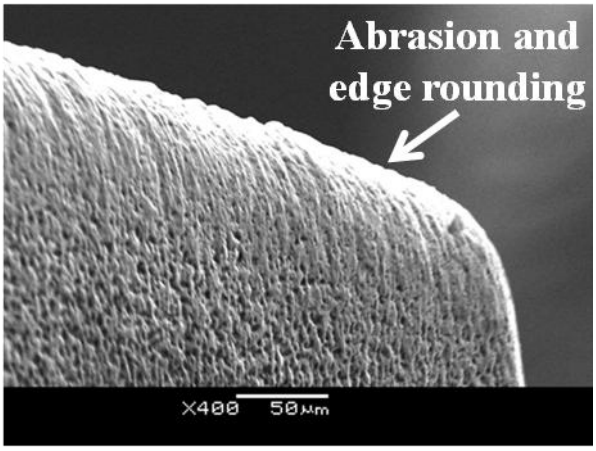
The cutting edges of the worn drills were further analysed using high resolution SEM and sample micrographs are shown in Figure 4.6. Heavy chipping / removal of the CVD-diamond coating along the entire length of the cutting edge / lip was apparent in Test 5. In contrast, abrasion and cutting edge rounding were prevalent when using uncoated WC and domed PCD drills, which were in line with previous optical microscope observations (see Figure 4.2)



(a) SEM micrographs taken in Test 5 (diamond coated WC drill)



(b) Test 2 (uncoated WC drill)



(c) Test 9 (domed PCD drill)

Figure 4.6: Sample SEM micrographs of drill cutting edge at test cessation

Due to the limited number of holes (<192) drilled in Tests 1 to 4 when using uncoated WC tools as well as the poor hole quality and premature trial cessation due to fibre dust burning, only results from Tests 5 to 12 were considered in subsequent statistical analysis, with the modified L12 Taguchi design reduced to a L8 array (orthogonal). Figure 4.7 presents the main effects plot for flank wear while the corresponding ANOVA results are detailed in Table 4.4. Tool material, cutting speed and feed rate were found to be statistically significant factors with PCR's of 77.4%, 3.8% and 16.5%, respectively. Domed PCD drills showed the best performance, with superior wear resistance as well as consistent cutting edge sharpness leading to higher productivity compared with the CVD-diamond coated drills. High feed rate (0.1 mm/rev) was also preferred in terms of minimising flank wear, although this generally resulted in more severe hole entry and exit defects (detailed in the following sections). While machining environment was not significant with respect to tool flank wear, it had a considerable influence on hole quality. Furthermore, the ANOVA calculations indicated a low error level of 2.3%, suggesting that all important factors were considered and the measurements performed accurately.

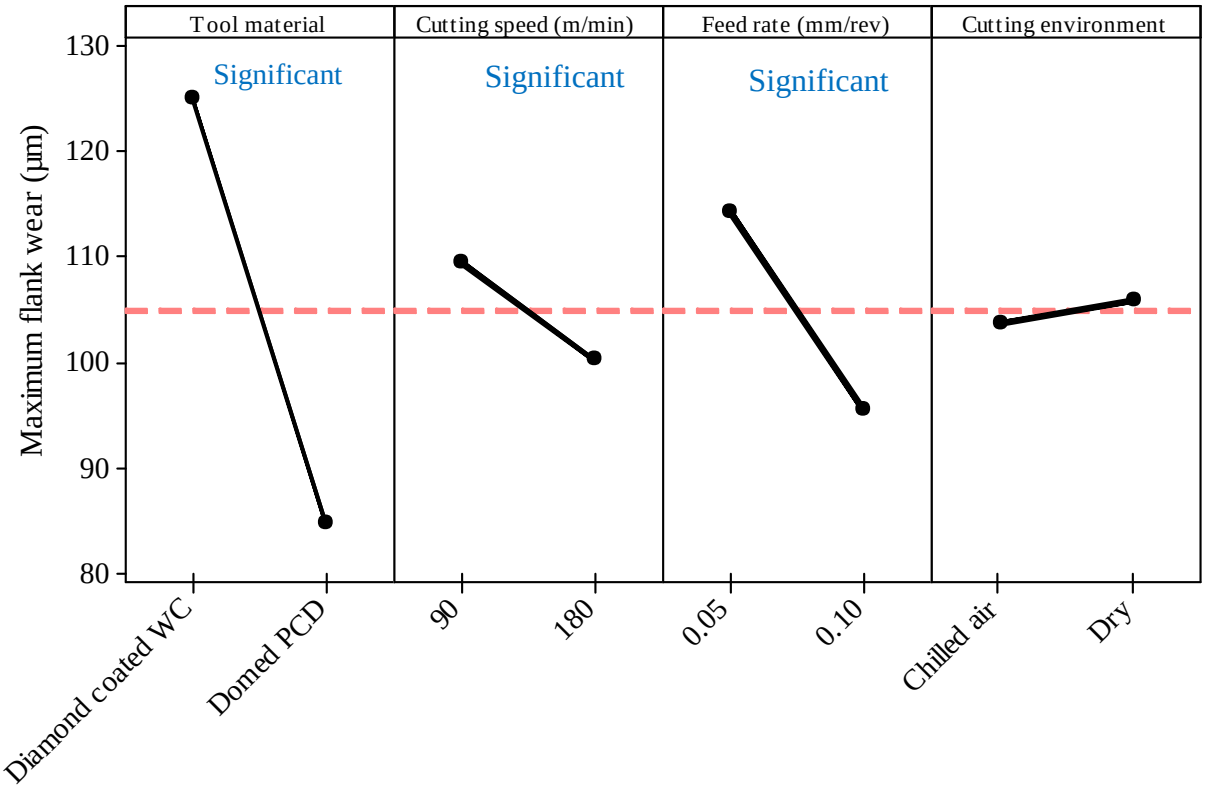


Figure 4.7: Main effects plot for maximum flank wear (Tests 5-12)

Table 4.1: ANOVA results for maximum flank wear (Tests 5-12)

Factor	DF	Seq SS	Adj MS	F	P	PCR
Tool material	1	3240.1	3240.1	229.39	0.001*	77.4%
Cutting speed (m/min)	1	171.1	171.1	12.12	0.040*	3.8%
Feed rate (mm/rev)	1	703.1	703.1	49.78	0.006*	16.5%
Cutting environment	1	10.1	10.1	0.72	0.459	0.0%
Error	3	42.4	14.1			2.3%
Total	7	4166.9				

DF = Degrees of freedom, Seq SS = Sequential sum of squares, Adj SS = Adjust sum of squares, F = 10.1 (F-test value), P = Probability, PCR = Percentage contribution ratio, * Significant at the 5% level.

4.1.2 Cutting edge radius analysis

The drill cutting edge radius was measured at ~200 µm away from the drill periphery corner, which was replicated 3 times and the average recorded. Cutting edge morphologies for both new and worn (at test cessation) tools are displayed in Figure 4.8 with the associated edge radius values detailed in Figure 4.9. When new, the domed PCD drills demonstrated superior sharpness with cutting edge radiuses of <5 µm, followed by the uncoated WC tools with typical values of ~7 µm. Conversely, the CVD-diamond coated tools showed comparably high cutting edge radiuses of up to ~24 µm even in the new condition. Rapid abrasion of the uncoated WC drills was prevalent, which led to dulling of the cutting edges (up to ~70 µm) at test cessation. A relatively large edge radius (67.4 µm) was also observed on the CVD-diamond coated drill in Test 5 (90 m/min, 0.05 mm/rev, dry) at test cessation, which was due to chipping / removal of the coating and subsequent wear of the substrate material (see SEM micrograph in Figure 4.6(a)). The cutting edge radiuses of the domed PCD drills were typically below ~30 µm even after drilling 512 holes irrespective of the operating conditions. In general, the variation of cutting edge radius levels was in line with the flank wear results. Corresponding statistical analysis indicated that tool material and feed rate were significant at the 5% level with respect to tool edge radius at test cessation with PCR's of 49.1% and 25.3% respectively, while the influence of cutting speed and cutting environment was marginal, see the main effects plot in Figure 4.10. During drilling CFRP, when the cutting edge radius becomes larger than the fibre particles, bending / ploughing (rather than shearing) of the fibres dominates, resulting in uncut fibres at the hole exit together with the formation of voids / porosities on the machined surfaces [4].

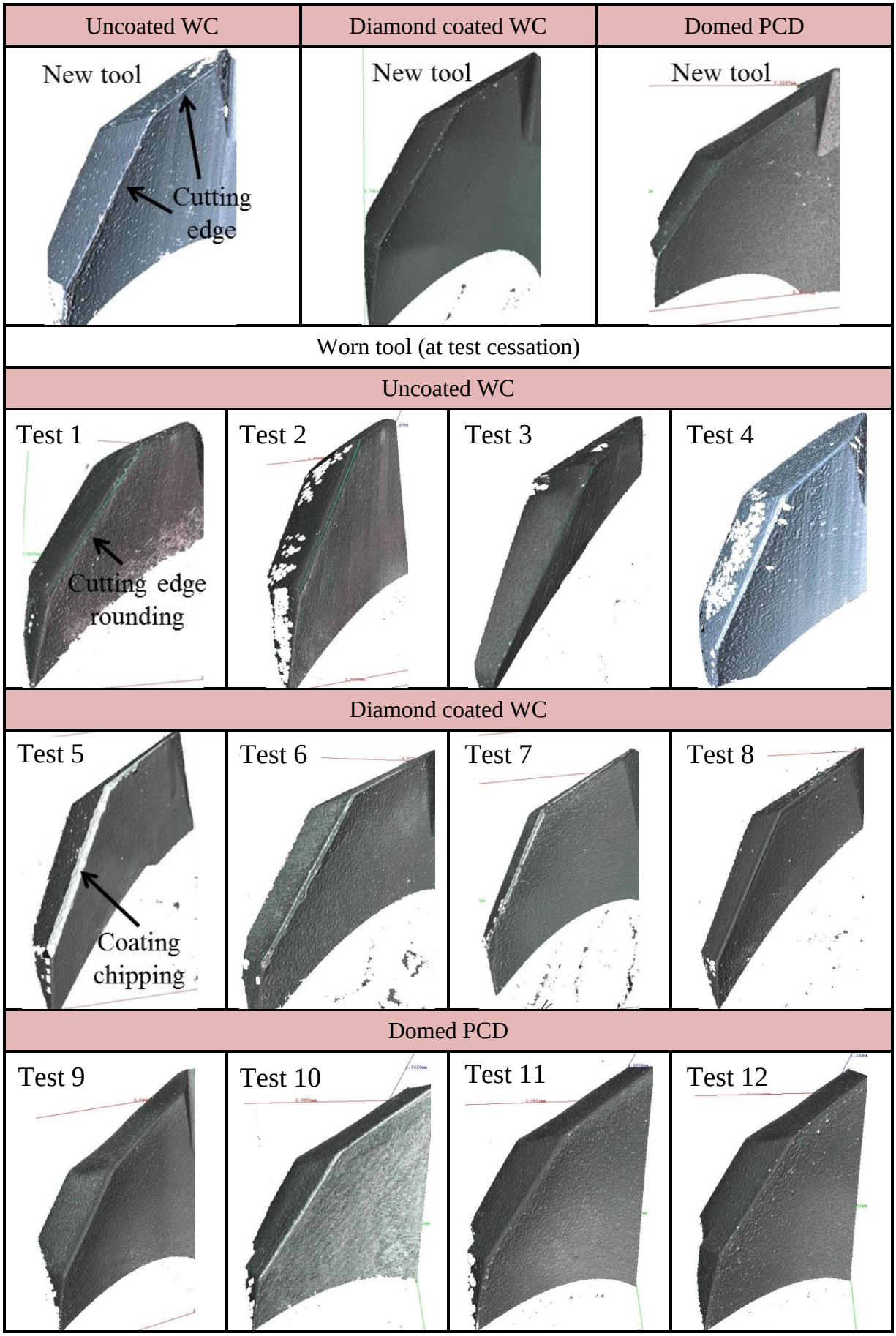


Figure 4.8: Cutting edge morphology at test cessation in all trials

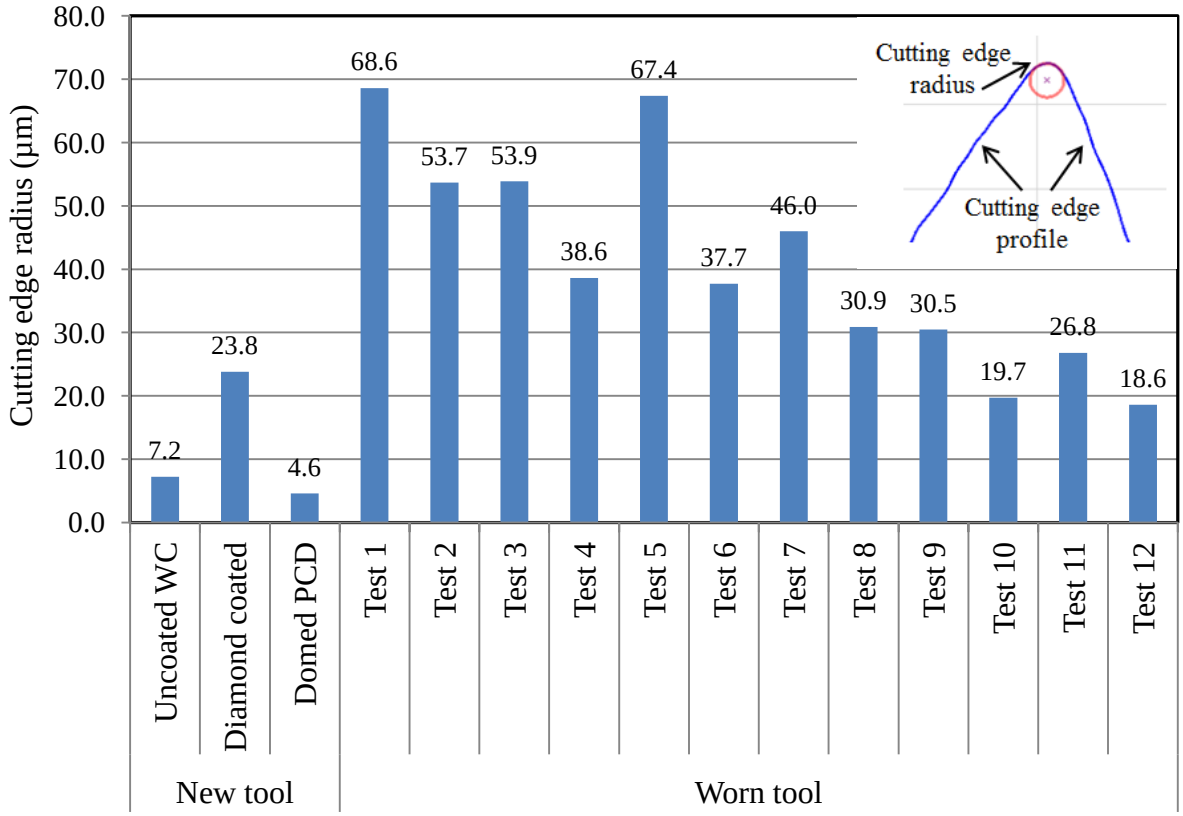


Figure 4.9: Cutting edge radius values recorded at new and worn (at test cessation) conditions

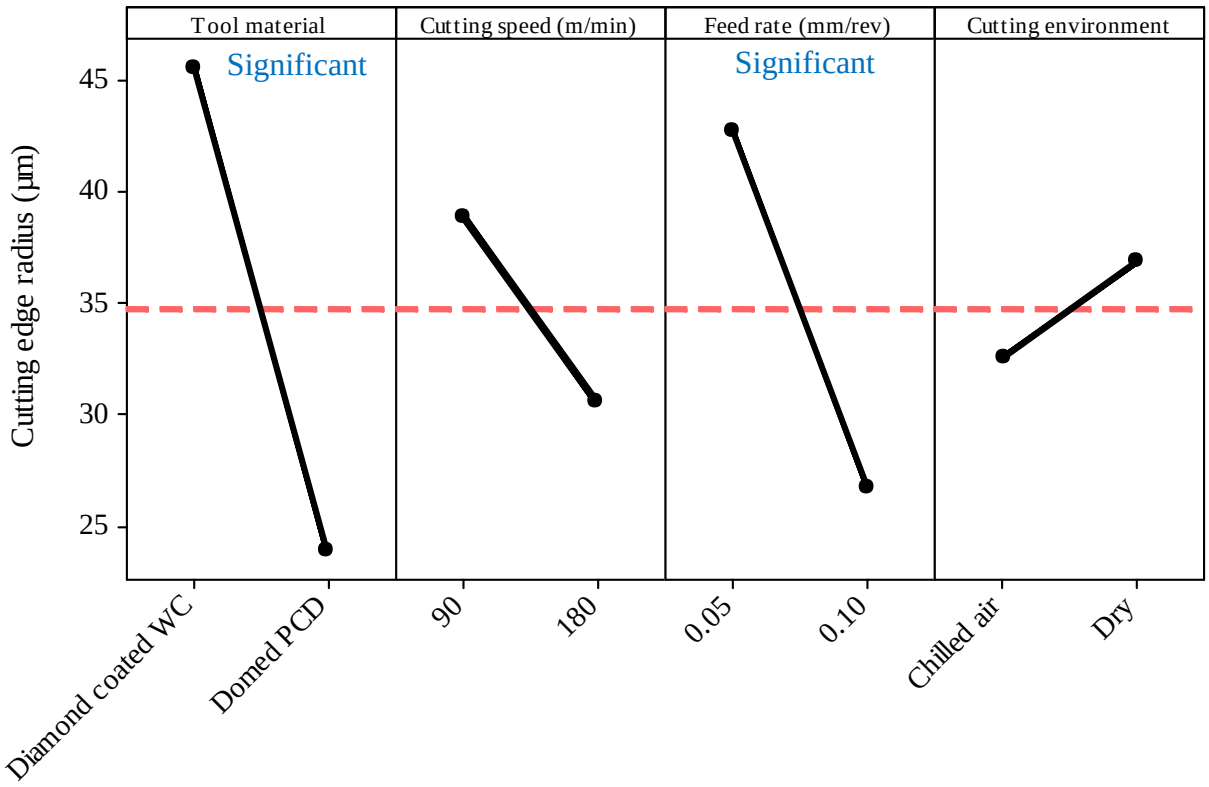
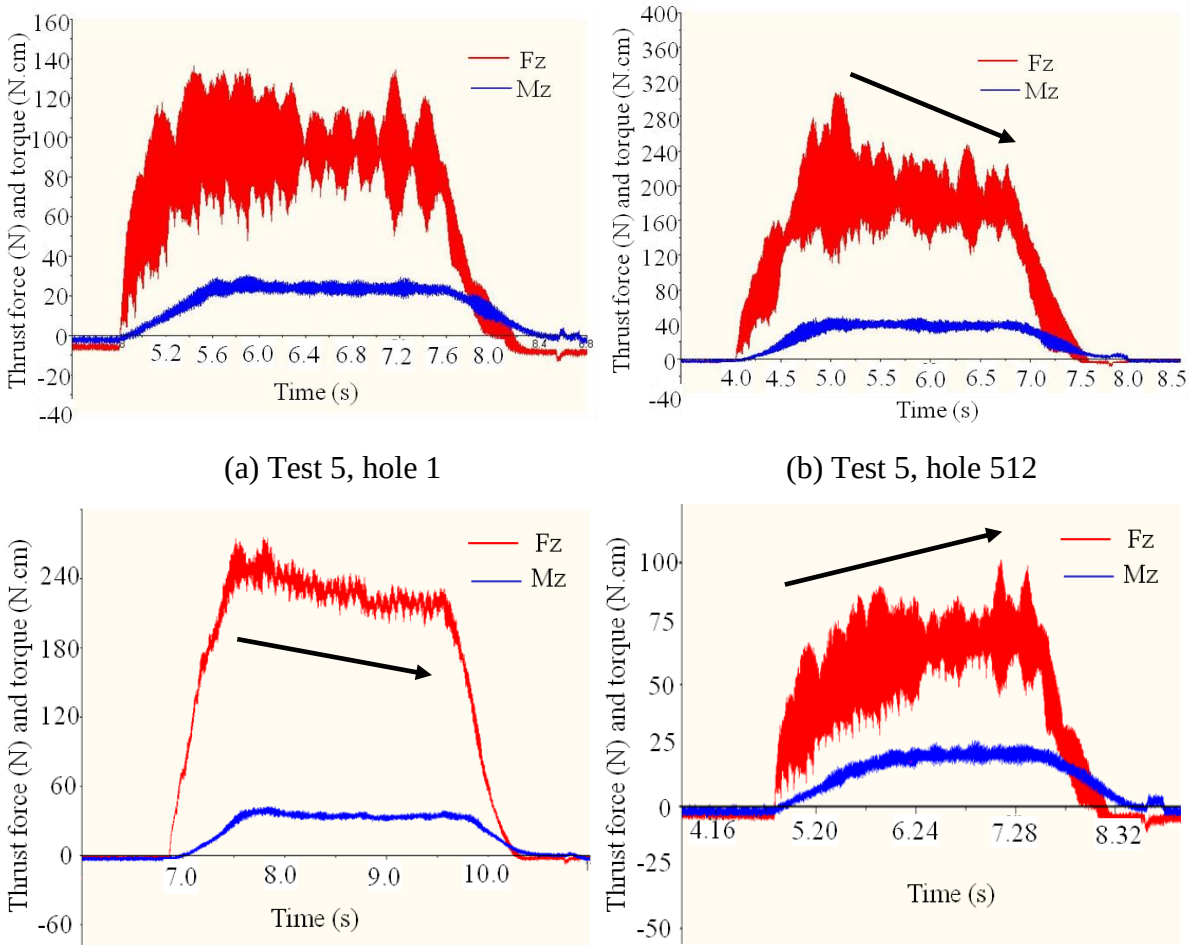


Figure 4.10: Main effects plot for cutting edge radius at test cessation

4.1.3 Thrust force and torque

Figure 4.11 shows sample thrust force and torque profiles for a typical hole drilled with different tool materials at the same operating parameters (90 m/min, 0.05 mm/rev and dry condition). In general, thrust force fluctuations over the hole depth were the result of tool edges passing through the varying fibre orientations within the laminate as well as the different properties between fibre and matrix. Figures 4.11(a) and 4.11(b) were recorded at the first and last hole respectively when using CVD-diamond coated drills. The maximum thrust force and torque increased from 137 N and 31 N.cm in the first hole to 308 N and 49 N.cm respectively after 512 holes. A decreasing trend in thrust force values (by ~40-60N) was apparent for the last hole drilled in Tests 5 and 9, as shown in Figures 4.11(b) and 4.11(c). This was most likely due to the high temperatures generated when drilling dry with worn tools, which led to deterioration / weakening of the epoxy matrix material. Similar results were also reported by Rubio et al. [81] and Velayudham et al. [202] when drilling glass fibre reinforced plastic composites. In contrast, thrust forces when using uncoated WC drills were rising even in the first hole, see profile in Figure 4.11(d), suggesting rapid wear rates of the cutting edges. Furthermore, signs of chatter / vibration were evident in trials involving uncoated and CVD-diamond coated WC drills, which was minimised when utilising the domed PCD tools (see Figure 4.11(c)). This was possibly due to the relatively low wear levels and comparatively sharp cutting edge condition of PCD drills.



(a) Test 5, hole 1

(b) Test 5, hole 512

(c) Test 9, hole512

(d) Test 1, hole 1

Figure 4.11: Sample thrust force and torque profiles

Thrust forces and torque progression against the number of drilled holes are shown in Figures 4.12 and 4.13 respectively. Thrust forces generally increased gradually over the duration of the experiments except when using the uncoated WC drills (Tests 1-4), where steep rises were prevalent irrespective of operating conditons. An unexpected drop in thrust force of up to ~70N after drilling ~100 holes was however observed in Test 1. This was most likely due to high machining temperatures and fibre dust burning degrading the support strength of matrix materials. The thrust forces generated when employing CVD-diamond coated drills at test cessation (~230-300N) were found to be lower than results reported in the literature that employed diamond coated tools and similar cutting conditions [47, 49]. This was possibly due to the optimised double point angle tool geometry used in the present work, which acted as a 'pilot section' to reduce the overall thrust force when machining. The use of tools with similar tip geometry were also reported to reduce thrust forces when drilling composites [61, 203]. Despite lower flank wear levels, the domed PCD drills produced higher thrust forces in comparison to the CVD-diamond coated tools, which was attributed to the

longer primary cutting edge length of the former (~2.46 mm for the domed PCD and ~2.06 mm for CVD-diamond coated WC drills). Maximum thrust forces in the first hole were typically ~20% higher when operating at the elevated feed rate (0.1 mm/rev) for the CVD-diamond coated WC and domed PCD drills.

In general, torque was found to be approximately constant over the test duration, except for trials involving uncoated WC tools, where values increased by up to ~150% from the first to the last hole drilled. Similar to thrust force results, torque increased with feed rate and the levels were typically higher when employing domed PCD in comparison to the CVD-diamond coated drills. This was possibly due to the former having 3 cutting flutes (as opposed to 2 for the latter) together with the longer cutting edge length of the PCD drills as detailed previously.

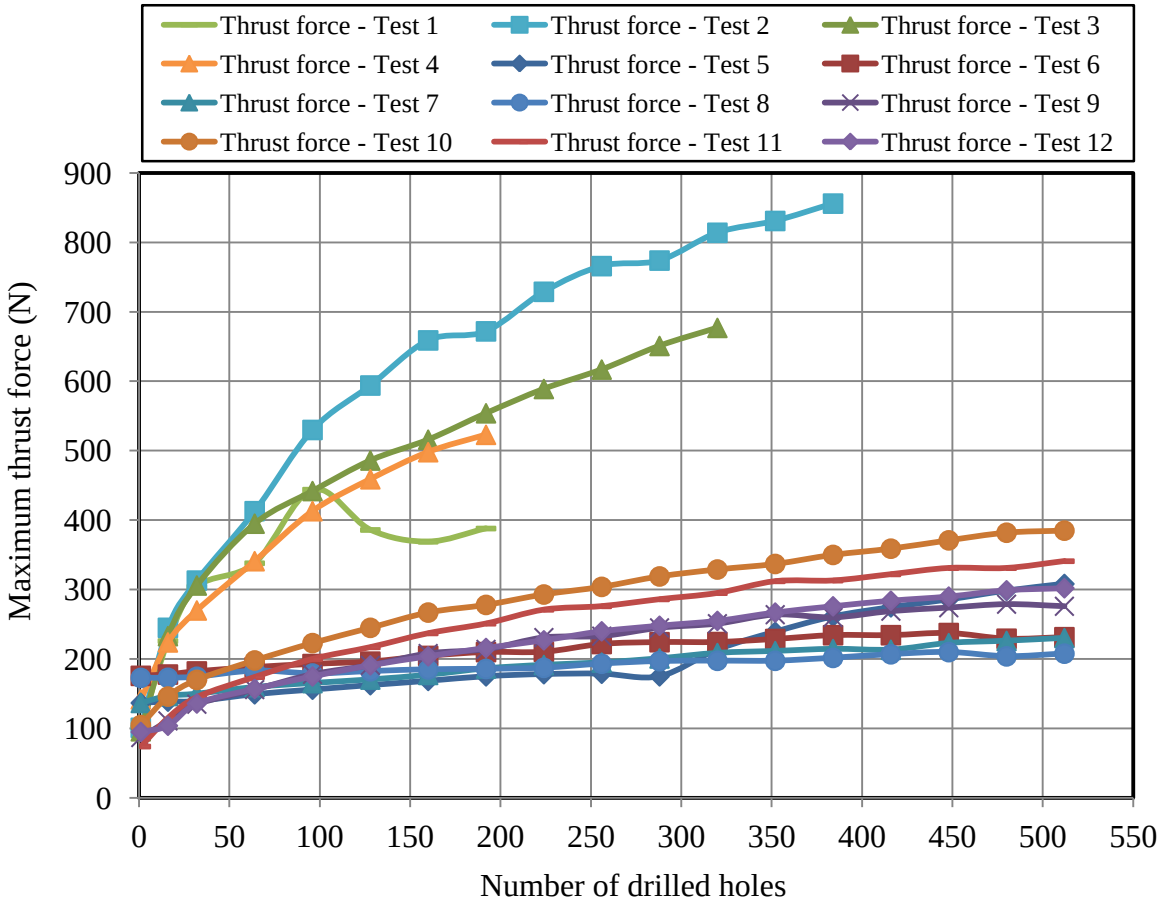


Figure 4.12: Maximum thrust force progression against number of drilled holes

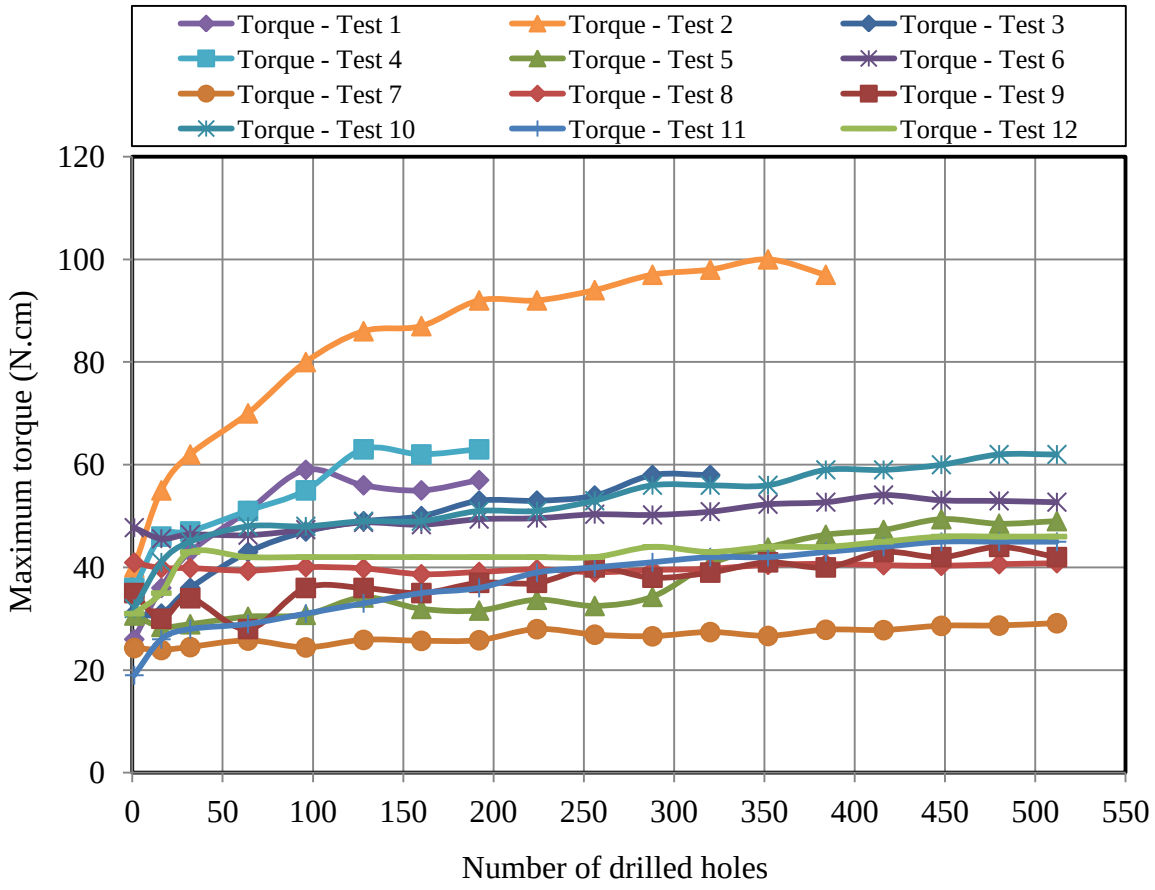


Figure 4.13: Maximum torque progression against number of drilled holes

Figure 4.14 and Table 4.2 show the main effects plot and associated ANOVA results relating to thrust forces for the first hole drilled using CVD-diamond coated WC and domed PCD tools. Tool material was seen to have the strongest effect on thrust forces with an overwhelming PCR of 81.4%, which was most likely due to the differences in the initial cutting edge sharpness / radius of the drills. In addition, feed rate was also found to be significant at the 5% level with a corresponding PCR of 14.5%. This was in line with observations reported by Shyha et al. [55, 56] when drilling CFRP with uncoated step drills. For thrust forces at the last hole (hole 512), tool material was the sole statistically significant factor with a percentage contribution ratio of 39.2%. Variations in the other factor levels including cutting speed, feed rate and cutting environment had relatively limited influence on thrust force, see the main effects plot in Figure 4.15. In terms of torque results at the last hole, none of the factors were found to be significant, although cutting speed and feed rate showed comparatively greater variation (see Figure 4.16) with corresponding PCR's of 32.0% and 19.3% respectively. The ANOVA calculations however indicated high error levels (up to 45.6%) for the torque results in both the first and last holes drilled. This was probably due to interactions between factors that were not considered in the fractional factorial array.

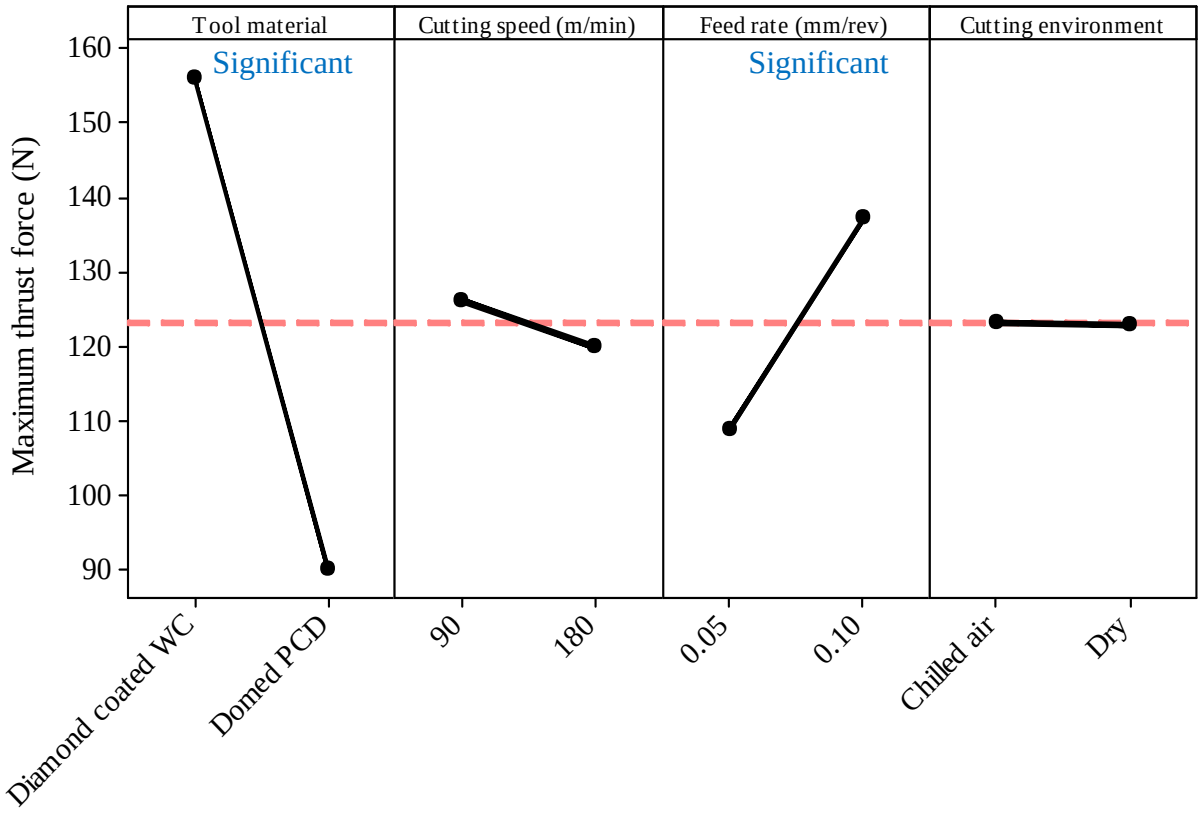


Figure 4.14: Main effects plot for maximum thrust force at the first hole in Phase 1A

Table 4.2: ANOVA results for maximum thrust force at the first hole in Phase 1A

Source	DF	Seq SS	Adj MS	F	P	PCR
Tool material	1	8646.1	8646.1	121.00	0.002*	81.4%
Cutting speed (m/min)	1	78.1	78.1	1.09	0.373	0.1%
Feed rate (mm/rev)	1	1596.1	1596.1	22.34	0.018*	14.5%
Cutting environment	1	0.1	0.1	0	0.969	0.0%
Error	3	214.4	71.5			4.0%
Total	7	10534.9				

* Significant at the 5% level.

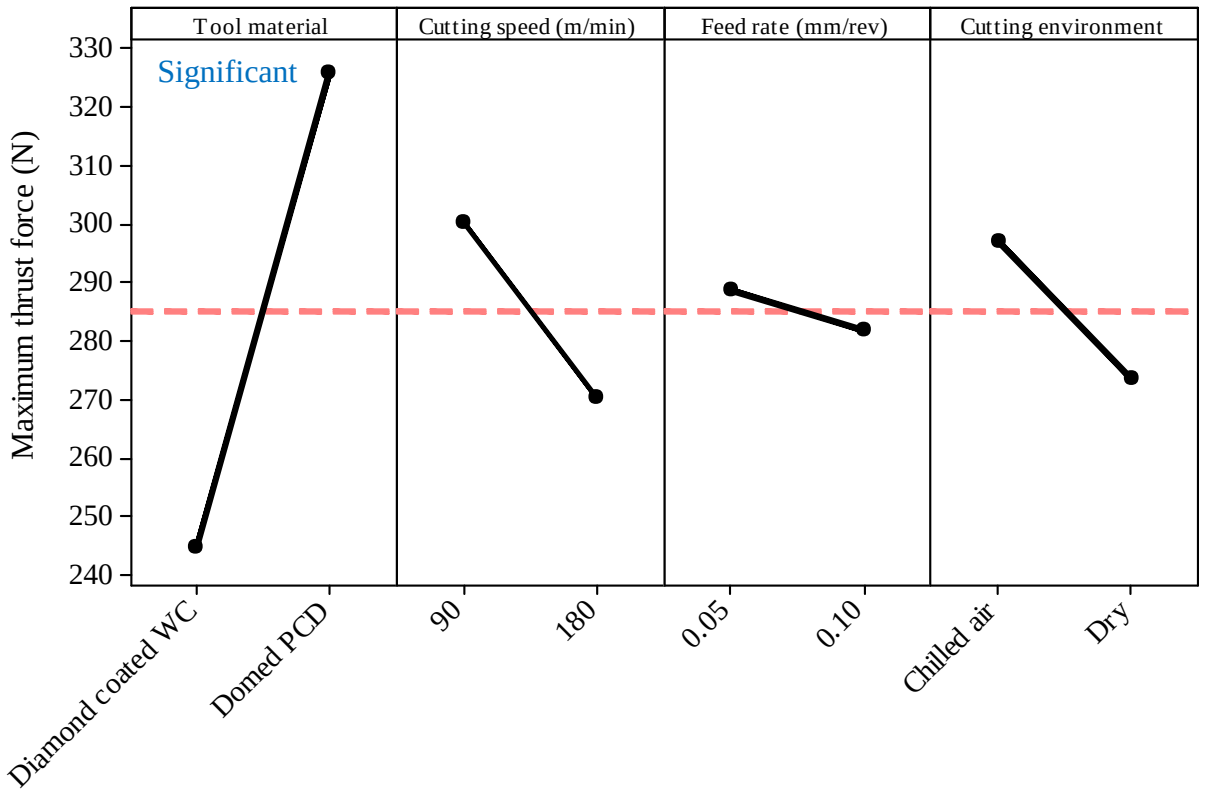


Figure 4.15: Main effects plot for maximum thrust force at the last hole (hole 512) in Phase 1A

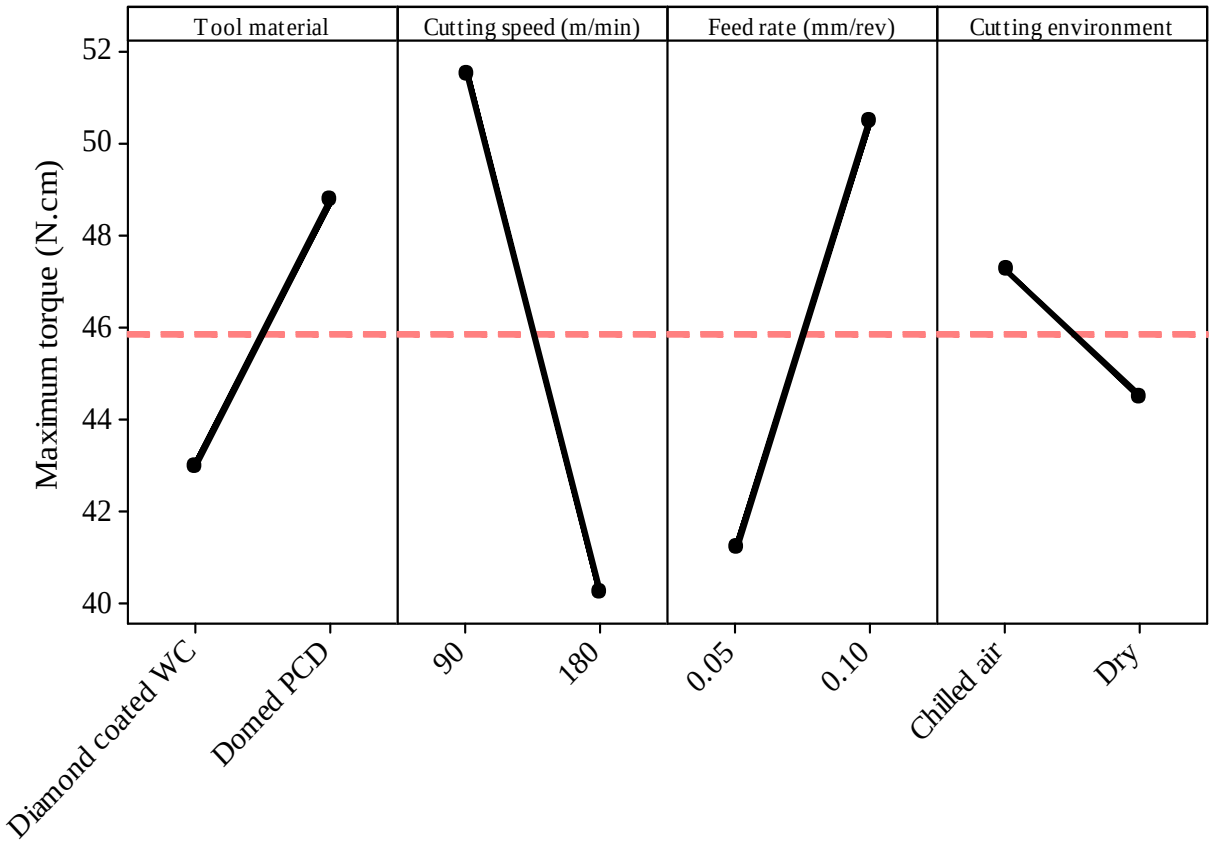


Figure 4.16: Main effects plot for maximum torque at the last hole (hole 512) in Phase 1A

4.1.4 Hole entry and exit quality

Figure 4.17 shows micrographs taken at the entrance location for both the first and last holes drilled in all trials. In terms of hole edge integrity for the first hole, only limited damage in the form of minor fuzzing and uncut fibres was observed when using diamond coated drills, while the hole edges were comparably free of flaws when utilising the uncoated WC and domed PCD tools. The superior hole edge quality was due to the lower thrust force levels (~100 N) and sharper cutting edge conditions (<7 µm cutting edge radius for uncoated WC and PCD tools) in the preliminary stages of the trials. Damage in the form of delamination, fuzzing and uncut fibres however began to develop as drilling progressed and reached substantial levels after ~100 holes in trials utilising uncoated WC tools irrespective of cutting parameters, due to rapid tool wear and fibre dust burning (Tests 1 and 4). Superior edge quality with limited uncut fibres were observed even after drilling 512 holes when using CVD-diamond coated WC and domed PCD tools regardless of cutting parameters / conditions, except in Tests 5 and 9. The poor hole quality in Tests 5 and 9 was attributed to the relatively high flank wear levels when drilling at a cutting speed of 90 m/min and feed rate of 0.05 mm/rev (114 µm for diamond coated drill and 96 µm for PCD drill).

Corresponding hole exit micrographs for both the first and last holes in each test are presented in Figure 4.18. Uncut fibres were apparent even on the first holes in all trials involving uncoated and CVD-diamond coated WC drills irrespective of the operating conditions (Tests 1-8). In contrast, the edge condition of the first holes produced using domed PCD drills were generally defect free except for minor instances of protruding fibres in Test 12, which was carried out at the higher cutting speed and feed rate levels (180 m/min and 0.1 mm/rev) under dry environment. Defects at the exit position of the first hole was surprisingly lower in trials with the uncoated WC compared to the CVD-diamond coated drills. This was possibly due to the relatively larger cutting edge radius (>~24 µm) of the latter in the new condition. The level of uncut fibres generally increased with the number of holes drilled, which was seen to cover the entire hole circumference at test cessation when employing the uncoated WC drills. The deterioration in hole edge quality over the test cessation however was less severe when CVD-diamond coated and domed PCD drills were utilised, with the exception of Tests 5 and 9 due to the relatively higher levels of tool wear recorded.

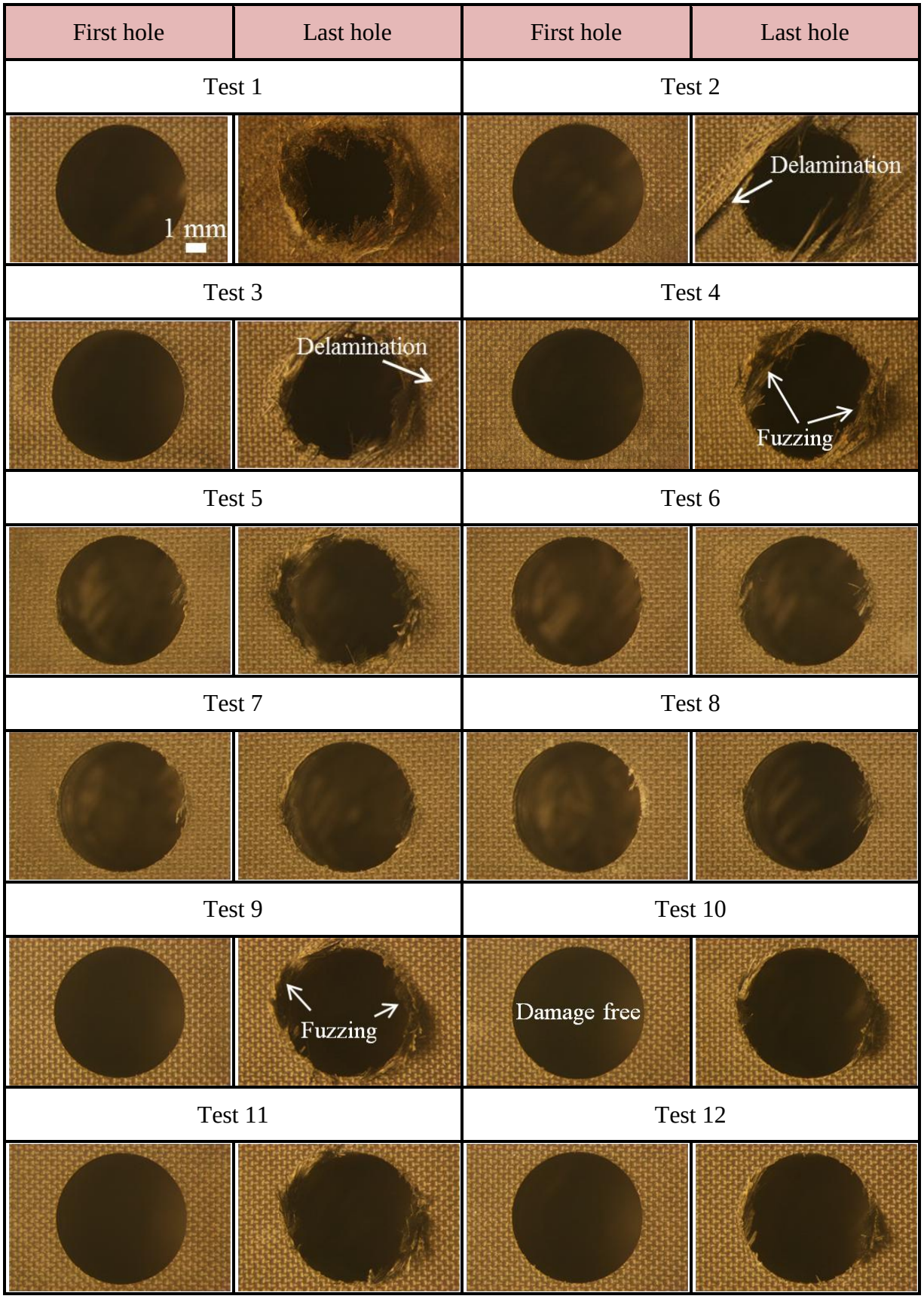


Figure 4.17: Hole entry micrographs at the first and last hole in Phase 1A

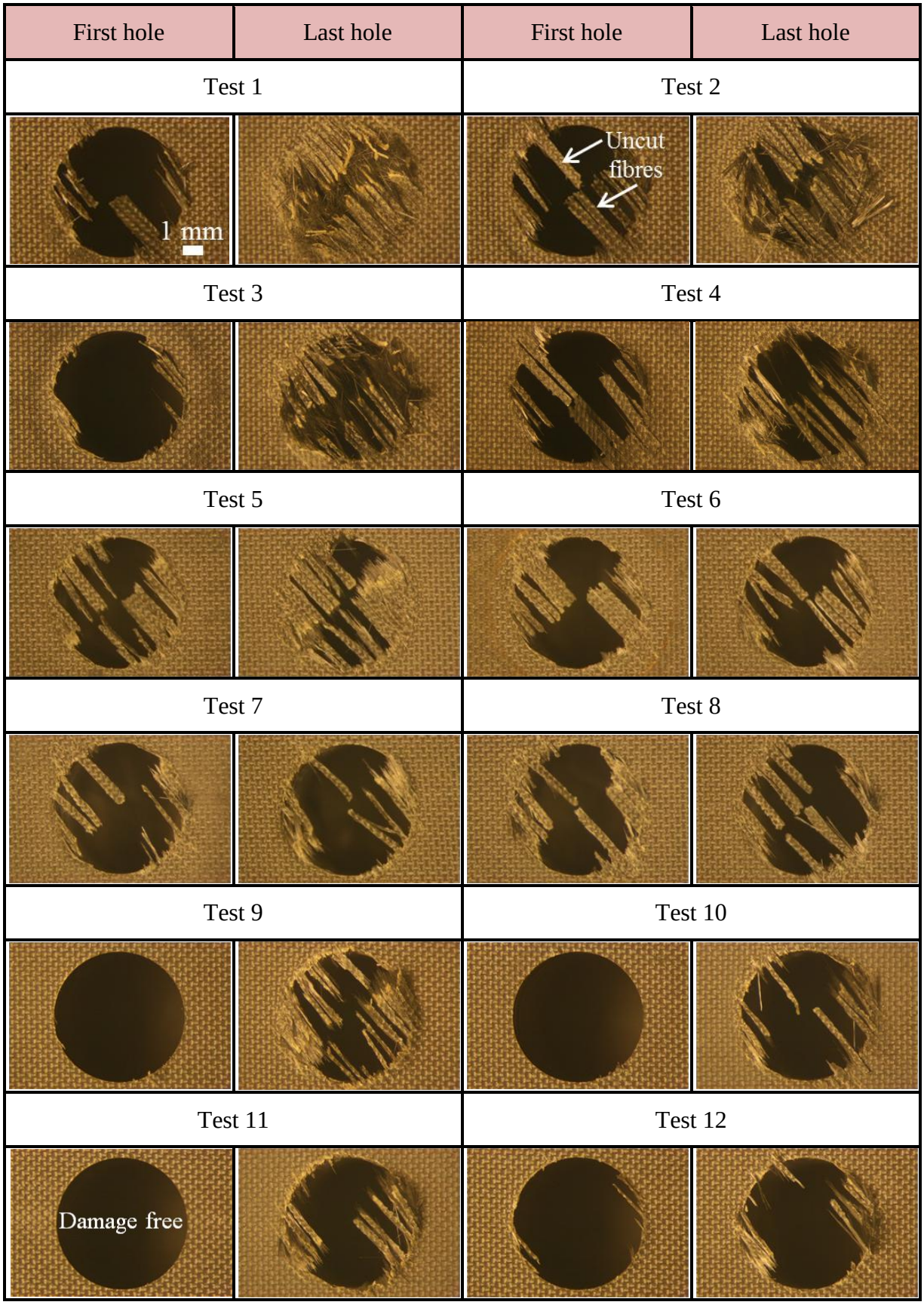


Figure 4.18: Hole exit micrographs at the first and last hole in Phase 1A

Figure 4.19 details the delamination factors calculated at the entry and exit locations for both the first and last holes (hole 512) drilled when using CVD-diamond coated WC and domed PCD tools. In general, the exit delamination factors at hole 1 and 512 were ~50% higher than the corresponding entry delamination factors except for the former produced by domed PCD drills. The low level of workpiece delamination in the first holes was attributed to the high edge sharpness (~4.6 µm cutting edge radius) of the PCD drills allied with the low thrust force levels at the start of the trials. The measured delamination factors at the entry and exit sections were approximately equivalent for both the first and last holes when using the CVD-diamond coated WC drills. Domed PCD tools however generally produced lower exit delamination factors which were up to 33% (~0.49) for the first and 10% (~0.15) for the last holes drilled. This was in agreement with tool wear results. Figure 4.20 shows the main effects plot with respect to exit delamination factor for the first hole machined. Tool material was the dominant parameter affecting exit delamination factor with an associated PCR of 85.3%, while not shown here, the results were similar for the last hole drilled, albeit with a lower PCR of 69.9%. Based on the main effects plot, exit delamination can be minimised by drilling at a cutting speed of 90 m/min and feed rate of 0.05 mm/rev under chilled conditions using domed PCD tools.

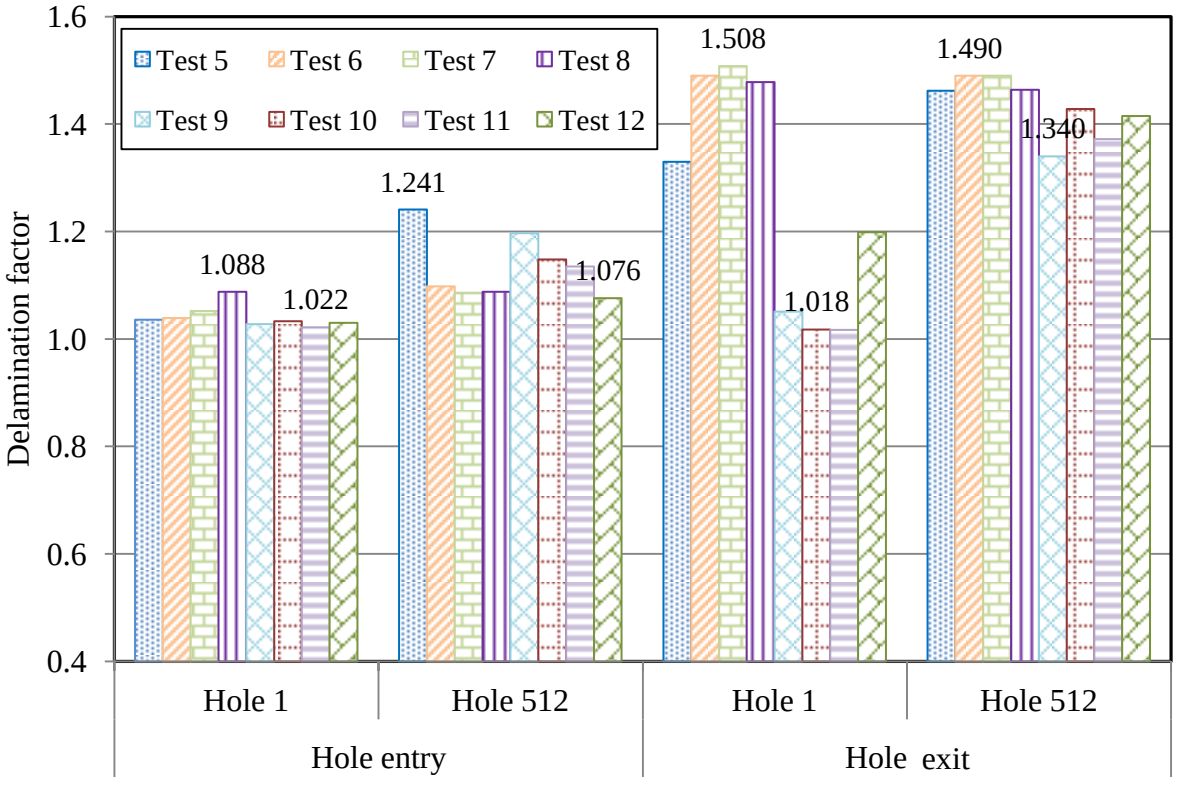


Figure 4.19: Delamination factor at hole entry and exit for both the first and last holes

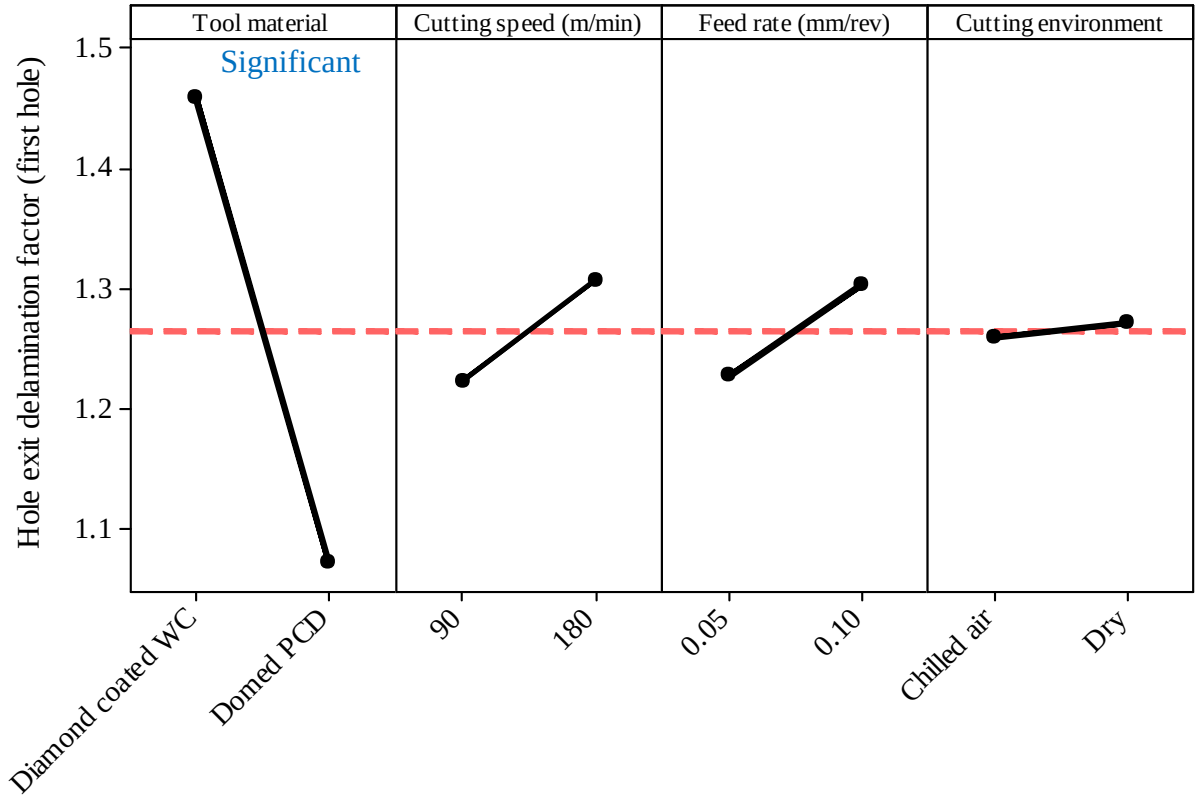


Figure 4.20: Main effects plot for exit delamination factor of the first hole drilled

4.1.5 Hole size and geometrical accuracy measurement

Due to the poor performance of uncoated WC drills which suffered from rapid wear (number of drilled holes <320) leading to fibre dust / matrix burning and adverse hole quality, hole size and geometrical accuracy were only evaluated for specimens drilled with CVD-diamond coated WC and domed PCD tools. The variation in hole diameter against the number of drilled holes is shown in Figure 4.21. All of the holes were found to be oversized when drilling with new tools (hole 1) regardless of the drill material or operating parameters. At test cessation, only holes in Tests 5 and 6 (CVD-diamond coated drills) were observed to be undersized by ~40 µm and ~18 µm respectively (nominal diameter of 6.38 mm). In particular, hole diameter in Test 5 was found to decrease sharply after ~200 holes, most likely due to the heavy chipping / delamination of the tool coating. All of the holes measured in Test 7 were found to be oversized, possibly due to a thicker than expected coating layer, while the deviation in hole diameter did not exceed 10 µm in Test 8, even after drilling 512 holes. In general, the holes produced using domed PCD drills were oversized, but all within a range of ~20 µm from the nominal hole diameter of 6.36 mm, irrespective of the experimental conditions. This was attributed to the superior wear resistance of PCD, which maintained consistent cutting edge conditions.

Hole out of roundness and cylindricity results plotted against number of drilled holes are detailed in Figures 4.22 and 4.23 respectively. For tests using CVD-diamond coated WC drills, the hole out of roundness measurements were within 10-20 µm over the experiment duration except for Test 5, which showed a significant increase up to an average of 47 µm after 512 holes. This was in line with the results of tool wear progression. In addition, Test 5 also indicated higher measurement variation compared to other tests, which suggested possible fluctuations in hole surface quality. Similar results were recorded in Test 9 when using the domed PCD drill, which was undertaken at equivalent machining prameters. The trends in hole cylindricity were comparable to the variation in out of roundness, with values of 55, 18, 27 and 15 µm recorded for the last hole drilled in Tests 5, 6, 7 and 8 respectively. Surprisingly, the out of roundness and cylindricity values were higher (inferior) after 384 and 512 holes when utilising the domed PCD drills, despite the greater wear levels on the CVD-diamond coated WC tools.

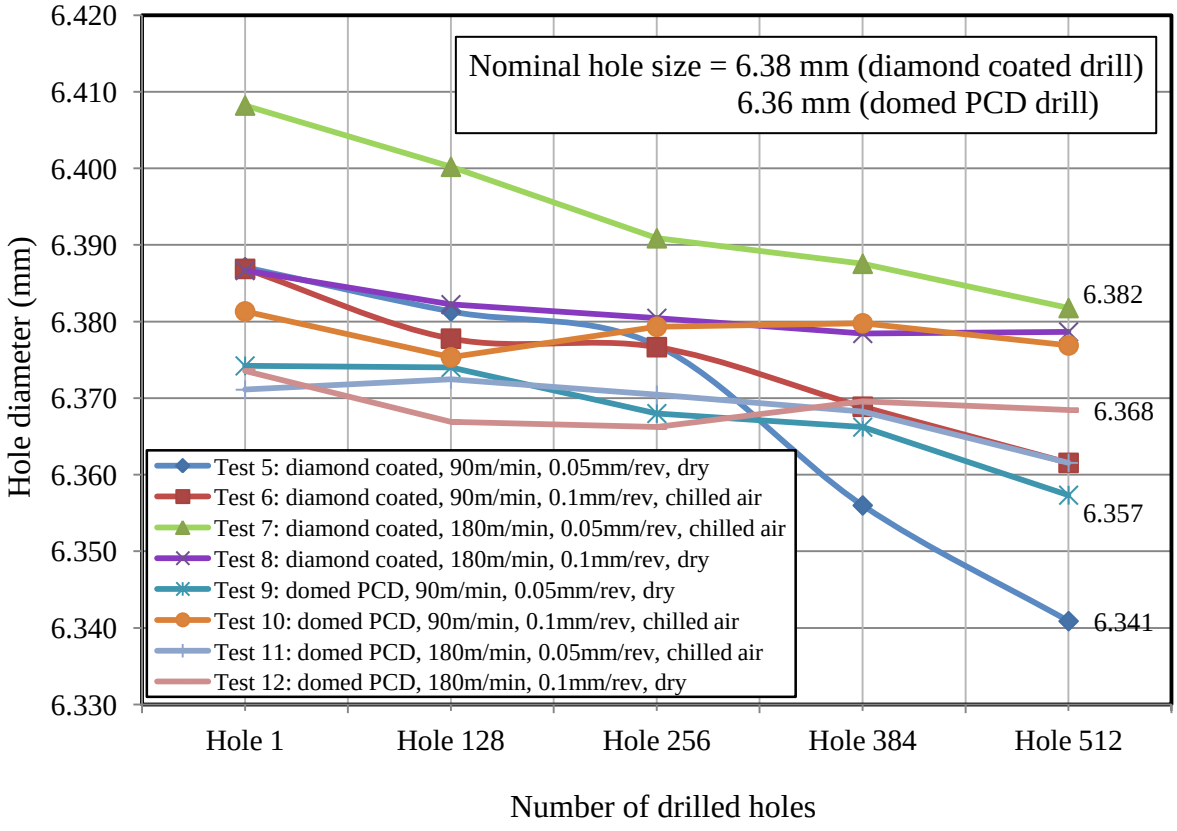


Figure 4.21: Hole diameter results against number of drilled holes

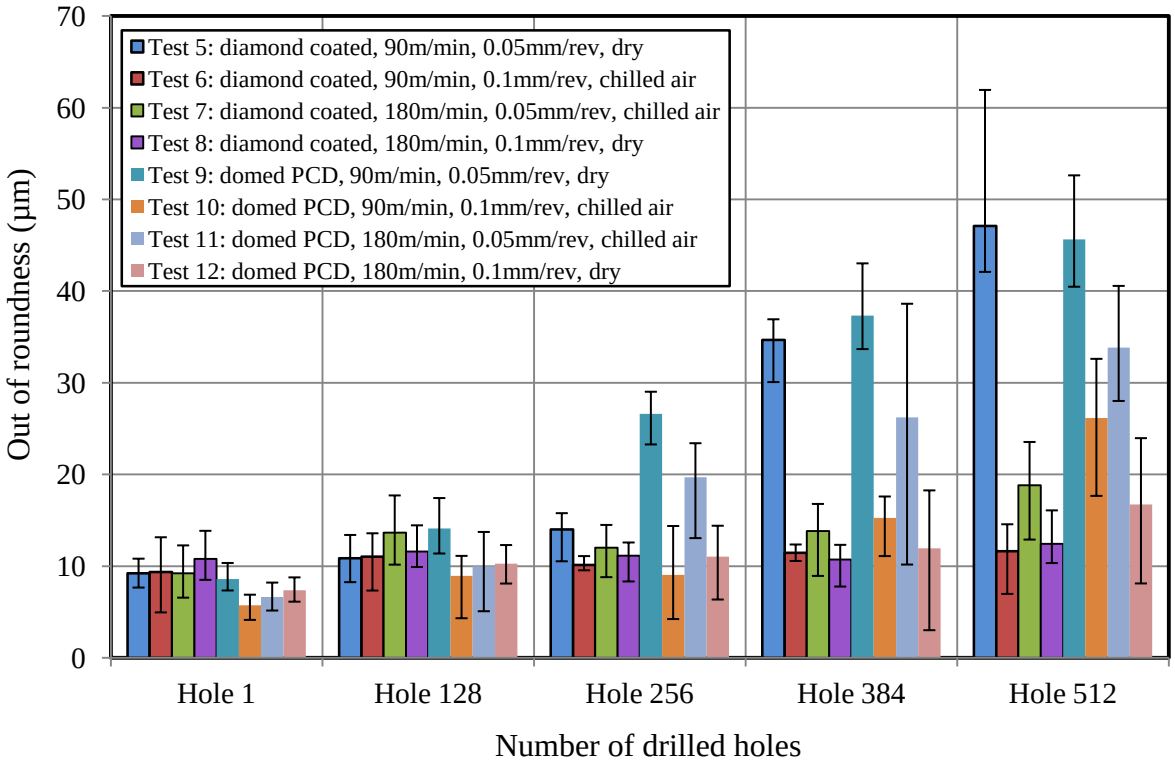


Figure 4.22: Out of roundness results against number of drilled holes

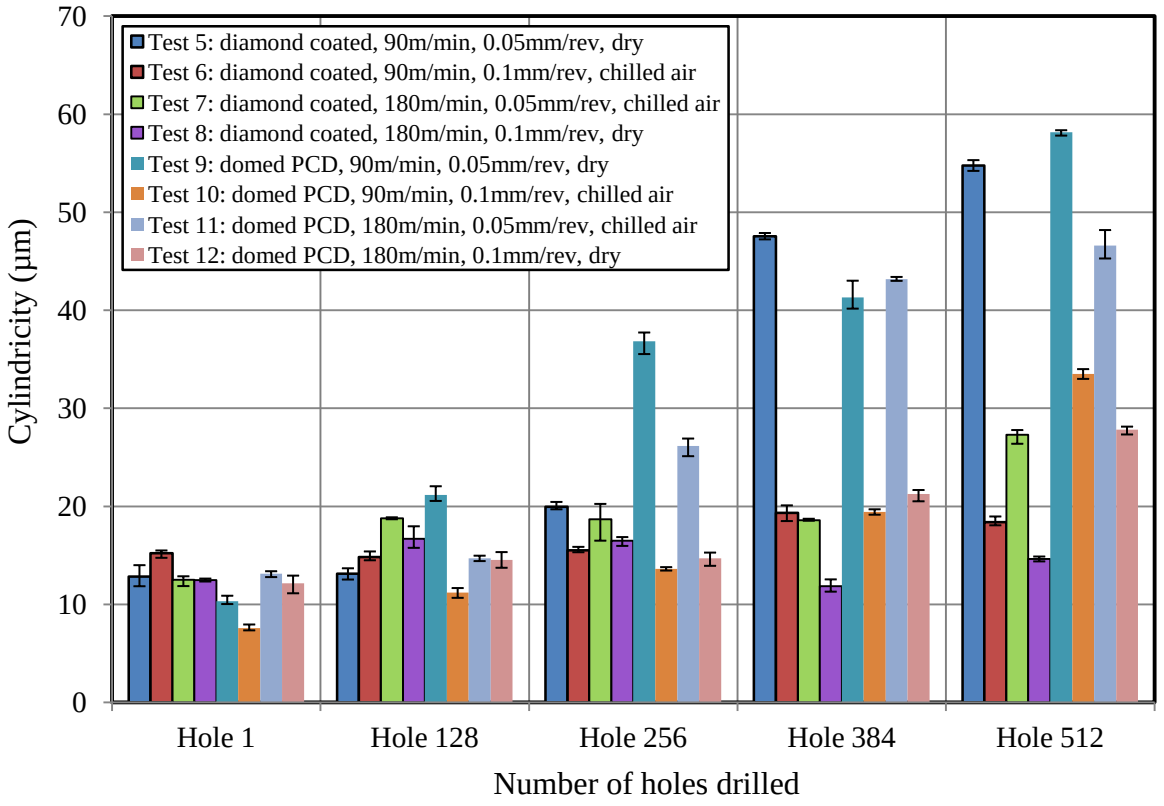
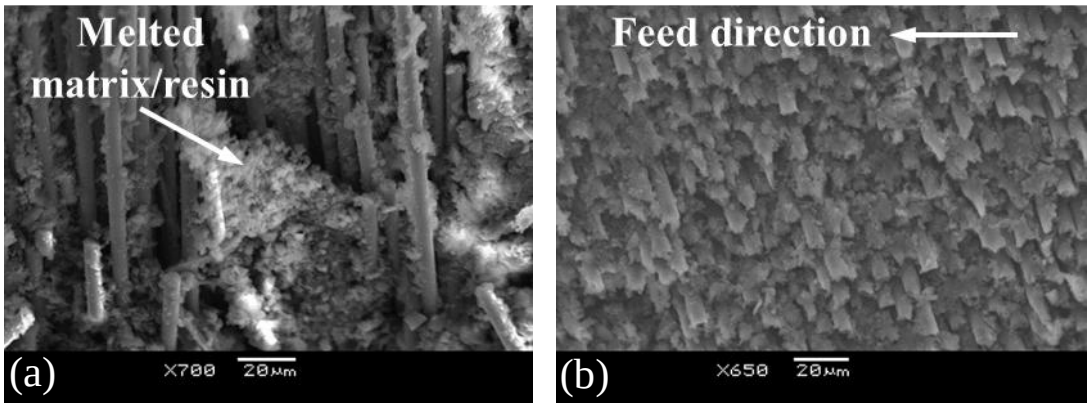


Figure 4.23: Cylindricity measurement results against number of drilled holes

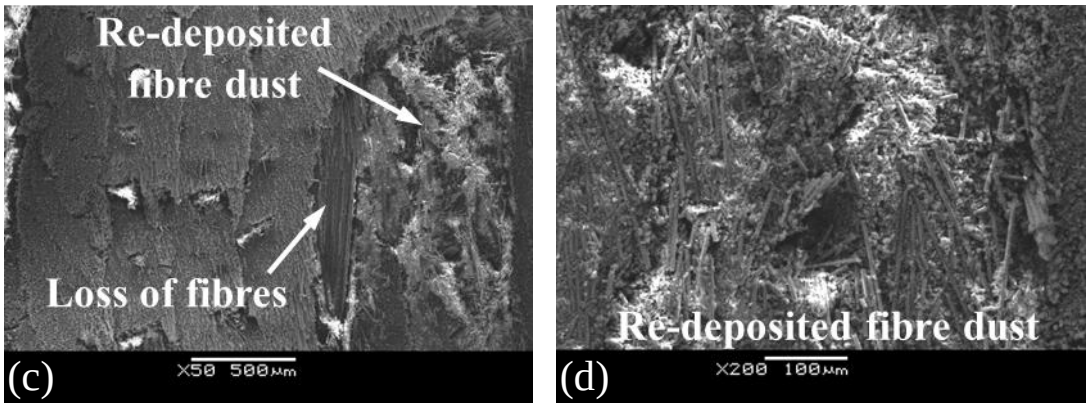
4.1.6 Hole surface integrity analysis

Figure 4.24 shows sample SEM micrographs of hole surfaces drilled with uncoated WC tools. Melted matrix / resin material was apparent on the machined surfaces of the last hole (hole 192) in Test 1 (90 m/min, 0.05 mm/rev and dry), see Figures 4.24(a) and 4.24(b), which typically occurs at temperatures of 300-350ºC [43, 60, 62]. The combination of rapid tool wear, low feed rate and dry cutting environment coupled with the poor thermal conductivity of CFRP were major contributing factors in relation to matrix / resin melting. Severe fibre reorientation / bending, workpiece porosity / cavities, fibre / matrix cracking and ply separation were also observed on the surfaces of the last hole in Tests 1 and 2, see Figures 4.24(c, d, f-h). In addition, smashed fibre dust was common sticking / depositing in the voids / porosities as shown in Figures 4.24(d) and 4.24(h). This was probably attributed to the melted resin materials caused low viscosity of fibre dust and smearing effect. Fibre dust covered on the workpiece plate and stacked in drill flute (see Figure 4.5) further exacerbated the situation (fibre dust evacuation). In contrast, the surfaces of the first hole were damage free, due to the new condition of the drills, see Figure 4.24(e).

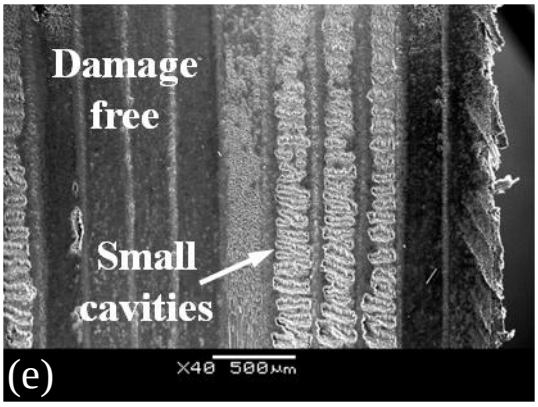
Coversely, no evidence of melted resin was found in Test 5 when using CVD-diamond coated tools even after drilling 512 holes, see Figures 4.25(a) and 4.25(b). This was due to the superior thermal conductivity of the CVD-diamond coating and relatively stable tool wear progression. Fibre dust was however seen lodged in the surface cavities and especially prevalent in tests performed dry, see Figures 4.25(g) and 4.25(h). Limited damage was found in holes at the cessation of Tests 8 and 12 for both the entry and exit sections, as shown in Figures 4.25(c) and 4.25(f). Porosity / matrix pull out occurred typically at specific ply / fibre orientations (135º), which suggests that hole quality is highly influenced by fibre direction. The effect of fibre orientation on hole surface quality is further evaluated in Phase 2 work.



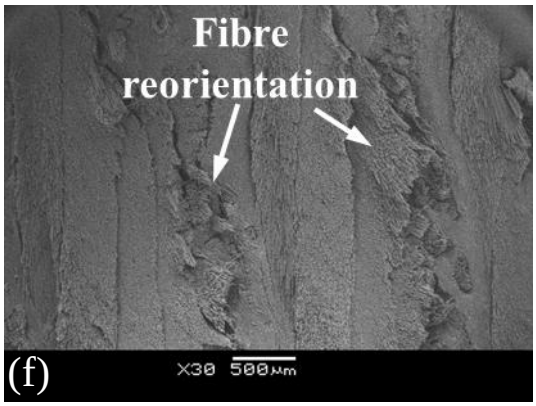
(a, b) Last hole (hole 192) in Test 1



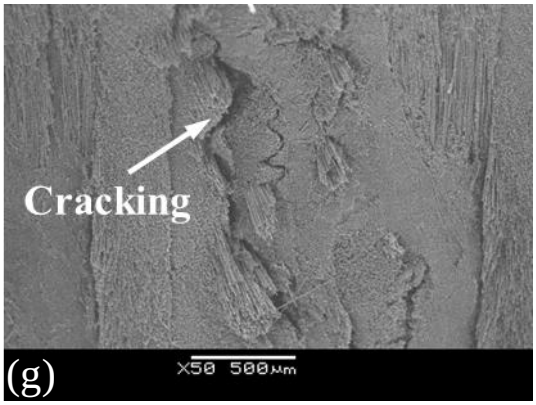
(c, d) Last hole (hole 192) in Test 1

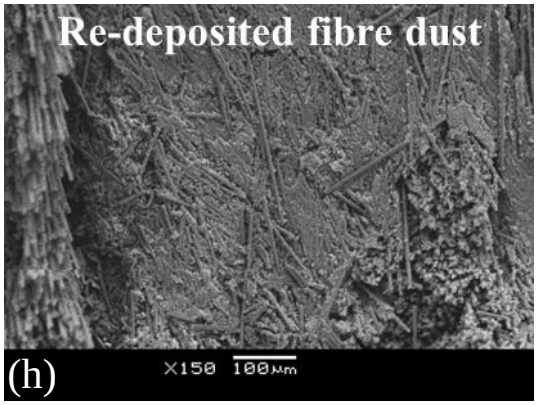


(e) Fist hole in Test 1



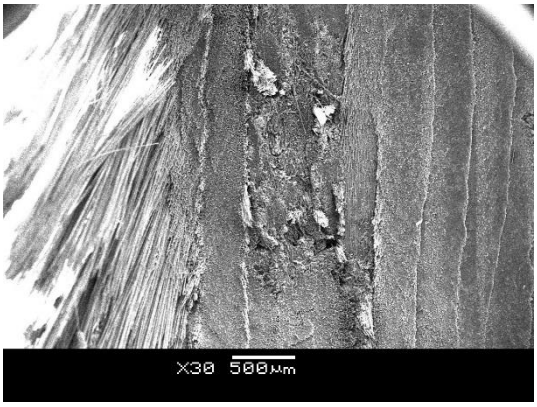
(f) Last hole (hole 384) in Test 2



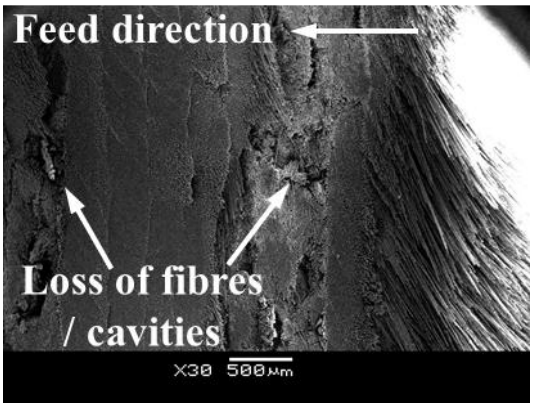


(g, h) Last hole (hole 384) in Test 2

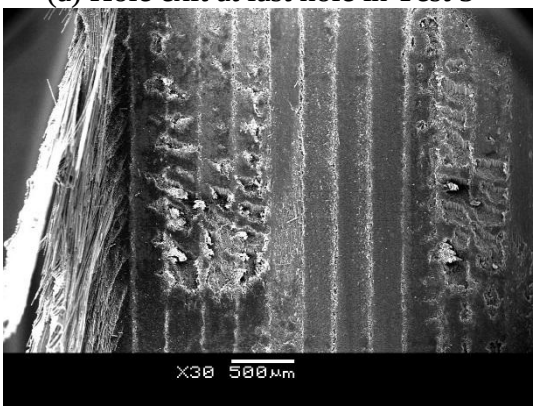
Figure 4.24: Sample SEM micrographs of hole surfaces drilled with uncoated WC tools



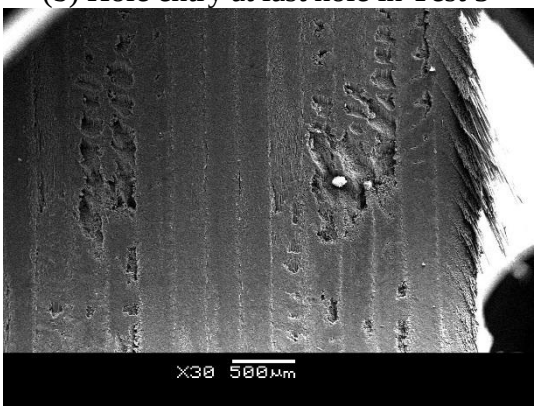
(a) Hole exit at last hole in Test 5



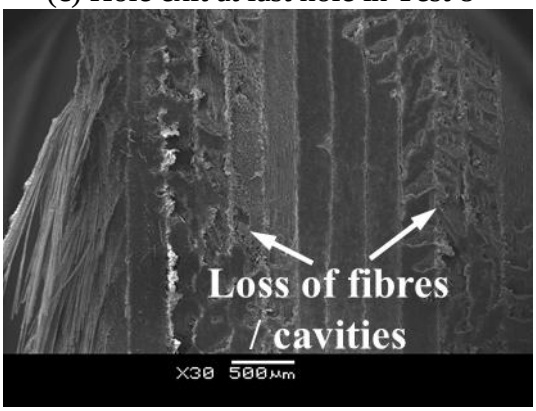
(b) Hole entry at last hole in Test 5



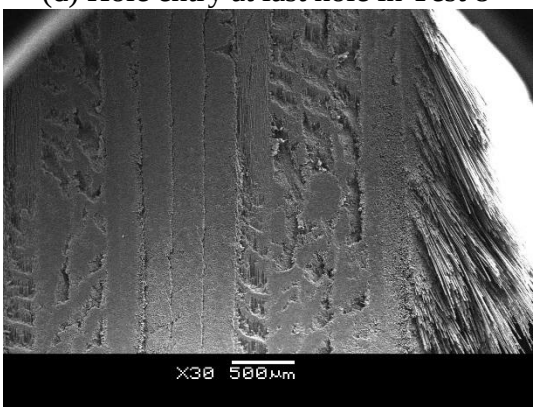
(c) Hole exit at last hole in Test 8



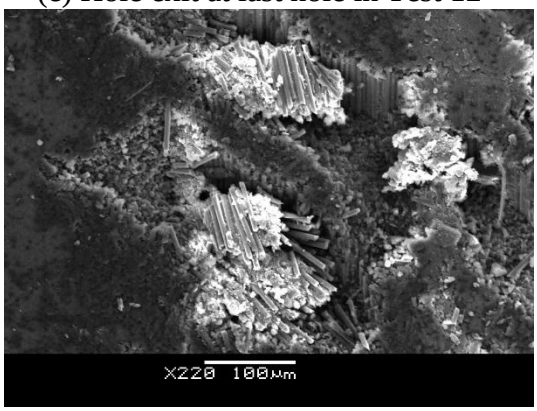
(d) Hole entry at last hole in Test 8



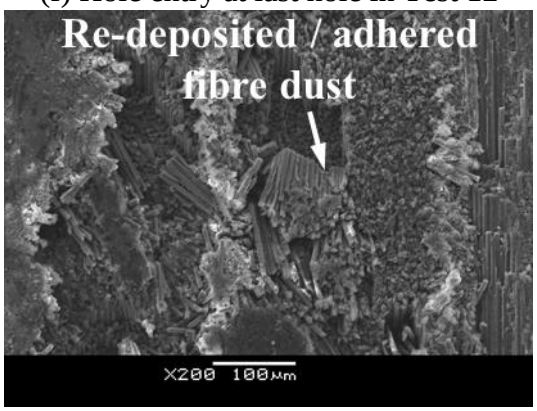
(e) Hole exit at last hole in Test 12



(f) Hole entry at last hole in Test 12



(g) Last hole (hole 512) in Test 8



(h) Last hole (hole 512) in Test 12

Figure 4.25: Sample SEM micrographs of hole surfaces drilled with diamond coated and domed PCD tools

4.1.7 Chip analysis

When drilling at a cutting speed of 90 m/min and feed rate of 0.05 mm/rev in dry conditions, the entanglement of carbon fibres on the drill was predominantly with associated dust particles packing / adhering onto the flutes. This was prevalent from the first hole irrespective of tool materials. A similar occurrence was also observed in Test 12 (domed PCD and 0.1 mm/rev) at the higher cutting speed, where the fibres had to be manually removed after several holes, see sample images in Figure 4.26 after drilling 64 holes. This was possibly due to the lower viscosity of the epoxy resin caused by the high drilling temperatures together with the poor evacuation of carbon fibre swarf. No signs of fibre entanglement however was observed in the remaining tests, most likely due to the application of chilled air. The workpiece debris typically comprised long fibre 'threads', powdery particles, and compacted dust, of which a significant proportion was trapped in the drill flutes, see Figure 4.27(a). Figure 4.27(b) shows an image of the drill condition after 512 holes in Test 5. A change in colour of the coating was visible near the tool tip indicating the likelyhood of high temperatures generated when drilling dry at low feed rates. Additionally, the entangled fibres further exacerbated the situation by inhibiting heat dissipation. Figure 4.28 shows sample SEM micrographs of the swarf morphology from Tests 7 and 8. It was found that fibre clusters were held together by melted resin material forming 'thread' of up to ~100 µm in length. The fibre bundles were generally between two 'threads' and possibly generated via fibre pull out from the hole surface.

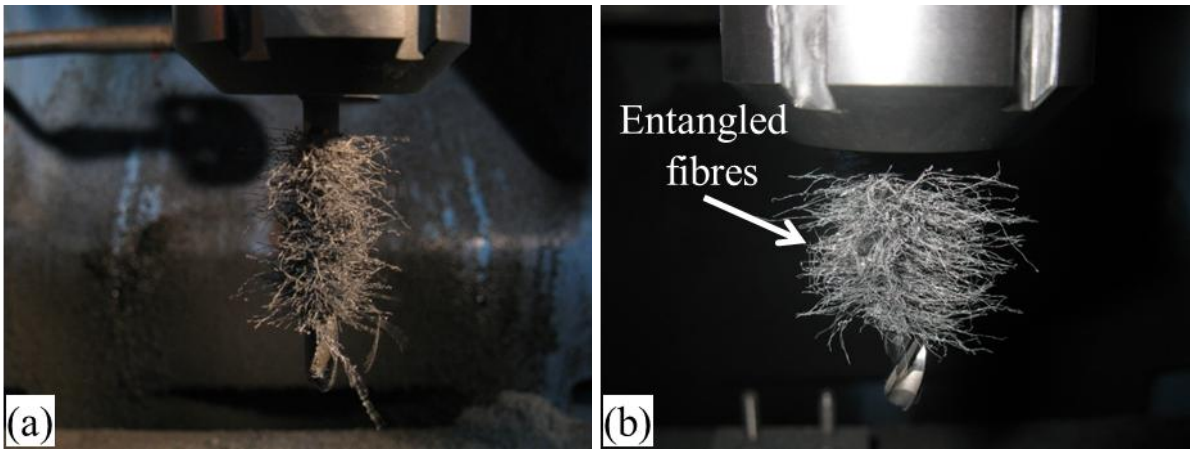


Figure 4.26: Entangled fibres were found in (a) Test 5 and (b) Test 12 after drilling 64 holes

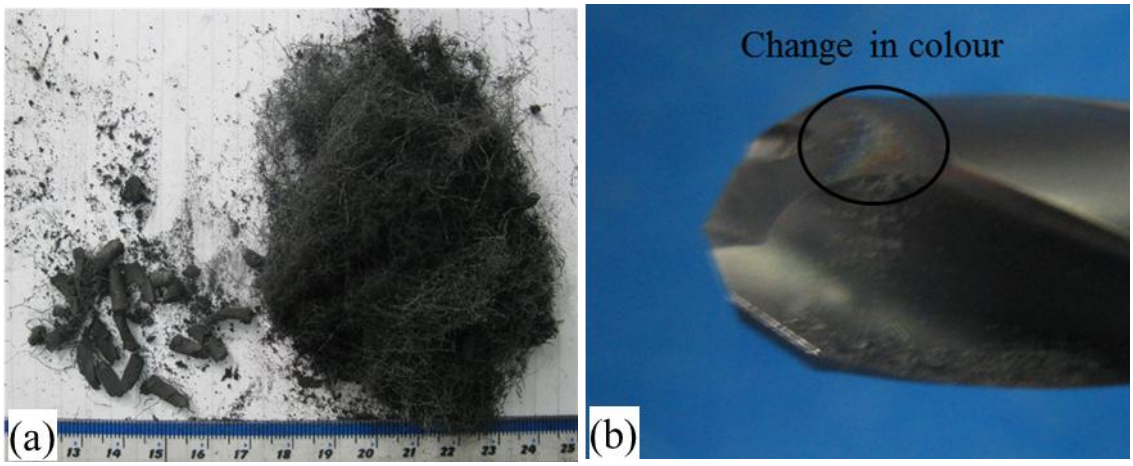
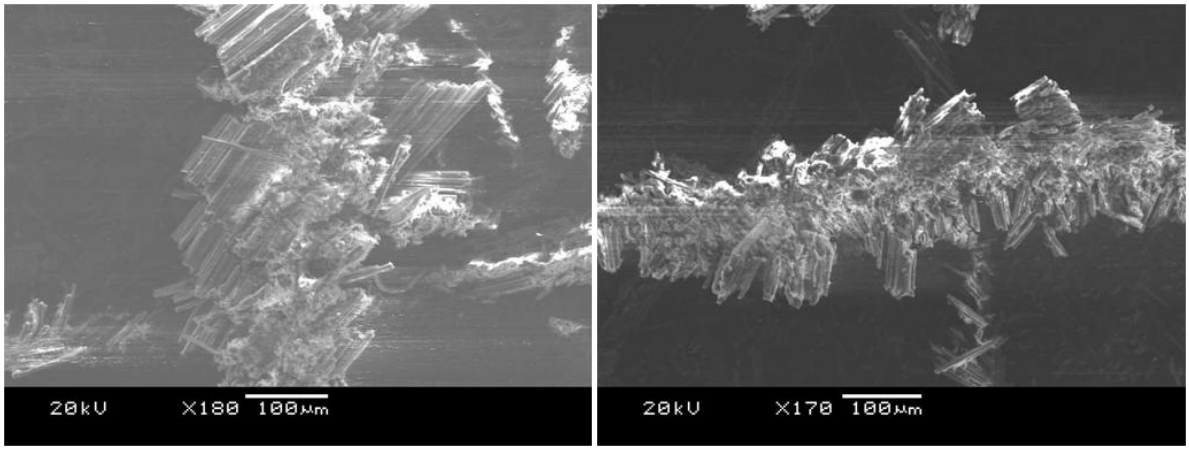
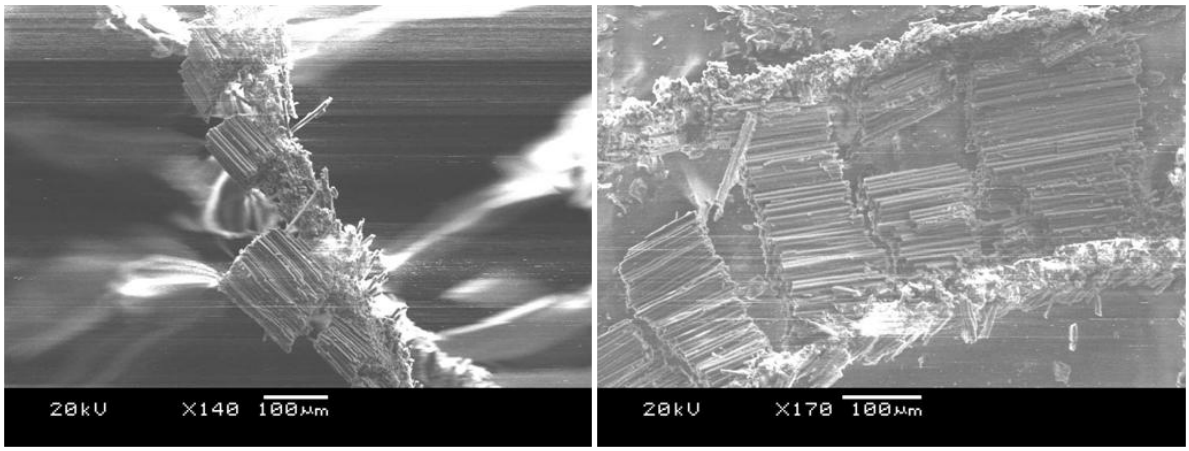


Figure 4.27: (a) Fibre dust / swarf produced in Test 5 and (b) cutting tool condition at test cessation



(a) Fibre dust produced in Test 7



(b) Fibre dust produced in Test 8

Figure 4.28: SEM micrographs of fibre dust / swarf morphology

4.1.8 Confirmation test

A confirmation test was carried out to verify the statistical analysis for minimum tool wear. Based on results in section 4.1.1, the preferred factor level combination to achieve minimum flank wear of 69.6 µm at test cessation was by utilising domed PCD drills at a cutting speed and feed rate of 180 m/min and 0.1 mm/rev respectively under dry conditions. The confidence interval at the 5% level was calculated using the following equation [204]:

$$Confidence\ interval = \sqrt{F_{\alpha;1;\nu_e} V_{ep} [\left(\frac{1}{n_{\text{eff}}}\right) + (1/r)]}$$

F_a = tabulated F value for a 95% confidence interval

ν_e = degrees of freedom associated with the error

V_{ep} = mean sum of square associated with the error

r = sample size for the confirmation test

$$n_{\text{eff}} = \frac{\text{Total number of observations}}{1+[\text{total degree of freedom associated with items used in estimating mean}]}$$

According to the experiment, F_a = 10.1, V_{ep} = 14.1 and $n_{\text{eff}} = 1.6$.

Confidence interval = 69.6 ± 15.2 and confidence limits = 54.4 and 84.8 µm.

Results from the confirmation test showed the flank wear at test cessation (512 holes) was 64 µm, which was within the confidence interval calculated, indicating that the experiment was statistically valid. Corresponding thrust force and torque values recorded at the first hole were 105 N and 34 N.cm respectively, which rose to 390 N and 54 N.cm after 512 holes. The drill cutting edge radius was up to 16.5 µm (see Figures 4.29(a) and 4.29(b)), which was lower than the best result seen in Test 12 (18.6 µm). Hole entry and exit quality following 512 holes was comparable with results observed in mainstream tests, see Figure 4.29(c).

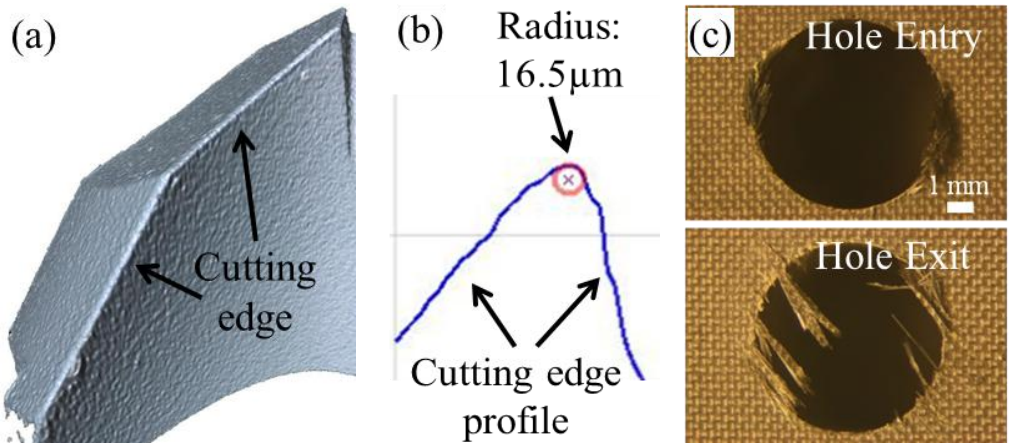
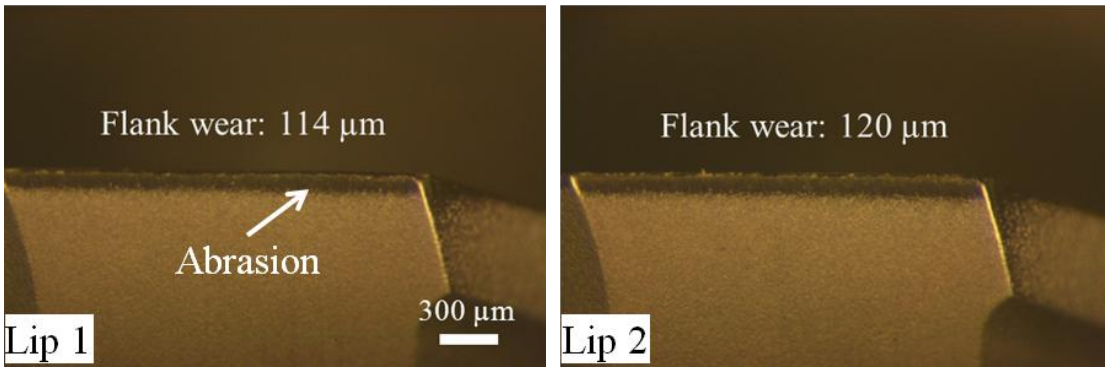


Figure 4.29: (a) Cutting edge morphology, (b) cutting edge profile and (c) hole entry and exit quality at test cessation (hole 512)

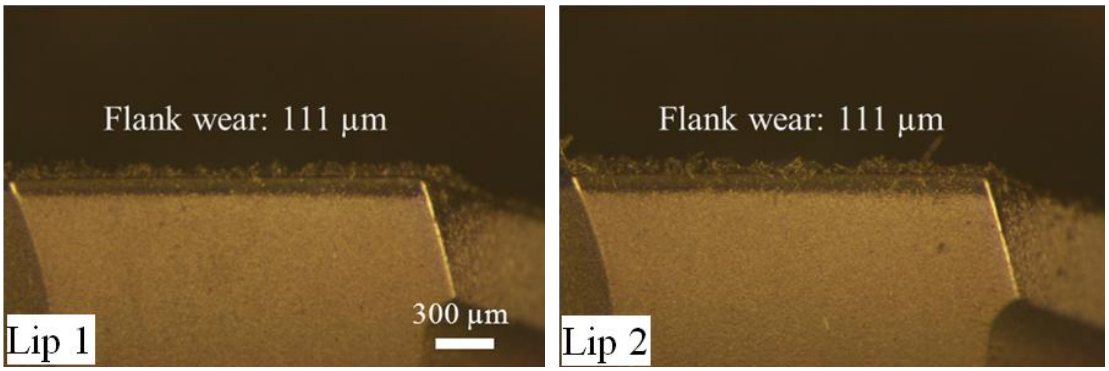
4.2 Phase 1B: Preliminary / benchmarking trials in drilling CFRP with variable feed rate operation.

4.2.1 Thrust force and torque

Due to the limited availability of tools, selected worn drills from Phase 1A experiments were utilised for Phase 1B trials. Figures 4.30(a) and 4.30(b) show the tool wear scars on both cutting lips at test cessation of drills used in Tests 6 and 8 in Phase 1A respectively, with corresponding average flank wear of ~117 and 111 µm. Additionally, no chipping of the coating was observed on the drills after 512 holes. In the current experiment, a series of drilling trials were conducted at cutting speeds of 90 and 180 m/min respectively, with an initial feed rate of 0.1 mm/rev, which was reduced to 0.01 / 0.02 mm/rev for the final 2 mm of the hole, under different environment conditions (flood coolant, chilled air, dry).



(a) Tool wear scar in Test 6 after drilling 512 holes



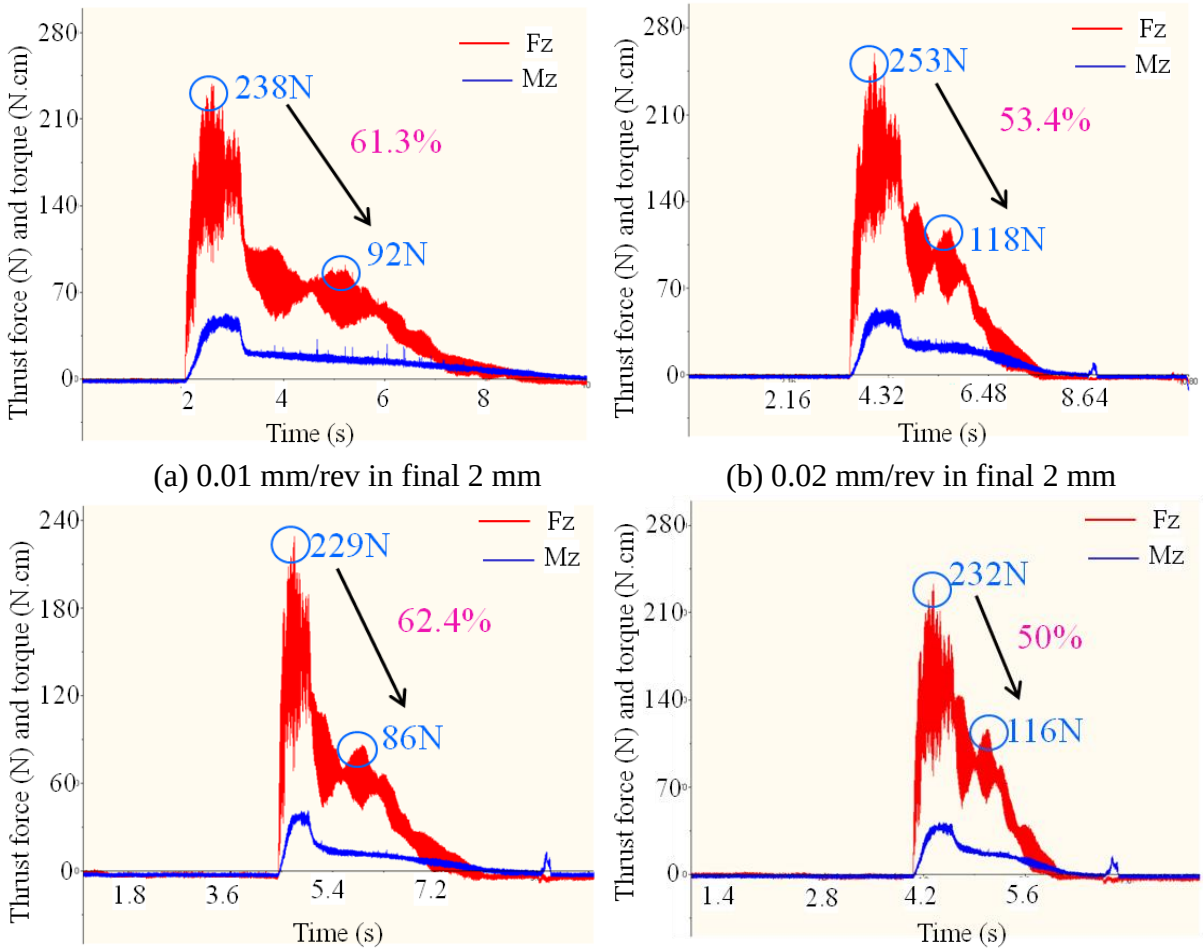
(b) Tool wear scar in Test 8 after drilling 512 holes

Figure 4.30: Tool cutting edge condition at test cessation of (a) Test 6 and (b) Test 8 used for current experiment

Figure 4.31 shows typical thrust force and torque profiles when drilling CFRP at the different operating parameters. At a cutting speed of 90 m/min with chilled air environment, the maximum thrust force recorded decreased by 61.3% from 238N to 92N as feed rate reduced from 0.1 to 0.01 mm/rev. Similarly, the thrust force dropped from 253N to 118N (by 53.4%) when feed rate varied from 0.1 to 0.02 mm/rev near the hole exit. When operating at

the higher cutting speed of 180 m/min with chilled air, thrust forces decreased by 62.4% and 50.0% upon reduction of feed rate to 0.01 and 0.02 mm/rev respectively. The difference of thrust forces (~24N) at the initial stage of drilling was mainly due to the variation in flank wear levels as worn tools were utilised from previous Phase 1A trials.

Figure 4.32 details the maximum thrust force and torque results for tests performed under the different cutting conditions. In general, both thrust force and torque values increased when employing chilled air and flood coolant compared to dry conditions irrespective of cutting speed. Maximum thrust force increased by up to 17.3% when drilling with flood coolant as opposed to dry, which was most likely due to the superior heat removal characteristics of the former that prevented / reduced thermal degradation of the workpiece material. However, the use of water based emulsion is generally restricted for machining CFRP materials due to absorption of fluid by the composite, which can cause swelling as well as induce chemical reactions with certain functional groups of macro molecules, leading to form and geometrical errors [62].



(a) 0.01 mm/rev in final 2 mm

(b) 0.02 mm/rev in final 2 mm

(c) 0.01 mm/rev in final 2 mm

(d) 0.02 mm/rev in final 2 mm

Figure 4.31: Thrust force and torque profiles in Phase 1B when drilling with chilled air at cutting speeds of (a, b) 90 m/min and (c, d) 180 m/min

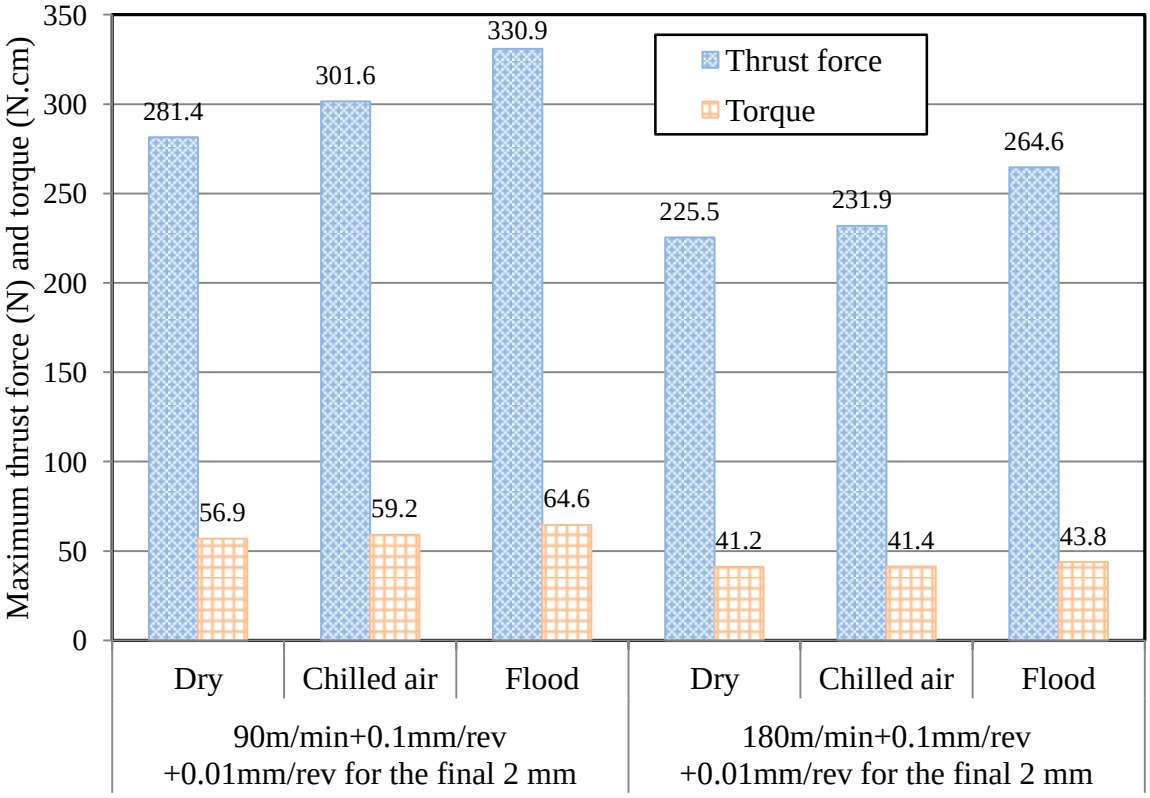


Figure 4.32: Maximum thrust force and torque values in different cutting environment

4.2.2 Hole exit quality

Figure 4.33 shows the typical hole exit defect modes observed in a series of 4 consecutive holes drilled in trials performed at 90 m/min under dry and chilled conditions, which includes signs of spalling, fuzzing, delamination and uncut fibres. These were compared against the first and last holes drilled from Test 6 in Phase 1A, where uncut fibres were prevalent across the hole exit and typically orientated in the same direction. The level of damage however was approximately equivalent in the first and last hole. In the current experiment, the number of uncut fibres at the hole exit were generally lower when drilling with chilled air in comparison to dry environment. Furthermore, use of the variable feed rate strategy with chilled air resulted in superior hole exit quality, where uncut fibres decreased by up to ~65% compared to results from Test 6 in Phase 1A. This was probably due in part to the considerable drop in thrust forces as feed rate was reduced to 0.01 or 0.02 mm/rev, leading to lower workpiece delamination and hole damage. However when operating dry, significant levels of workpiece splintering and uncut fibres remained around the hole exit periphery, despite utilising a lower feed rate in final 2 mm of drilling.

For trials at a cutting speed of 180 m/min with the variable feed rate strategy, no appreciable improvement in hole quality was observed over results in Test 8 (180 m/min, 0.1

mm/rev, dry) from Phase 1A, see Figure 4.34. The level of uncut fibres and splintering were similar regardless of the cutting environment employed. This was possibly attributed to the increased temperatures generated at the higher cutting speed resulting in weakening of the resin matrix.

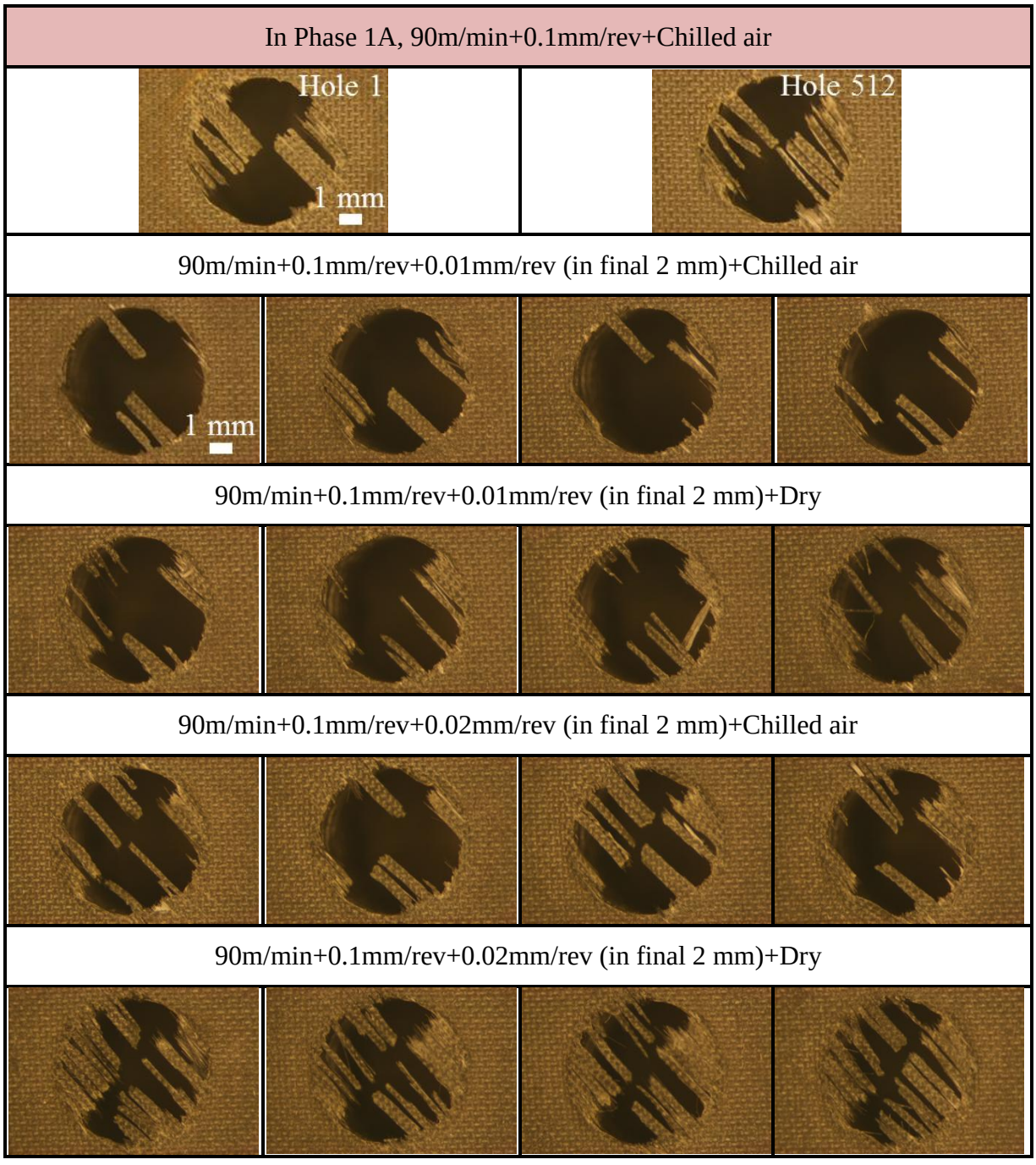


Figure 4.33: Hole exit quality when drilling at 90 m/min

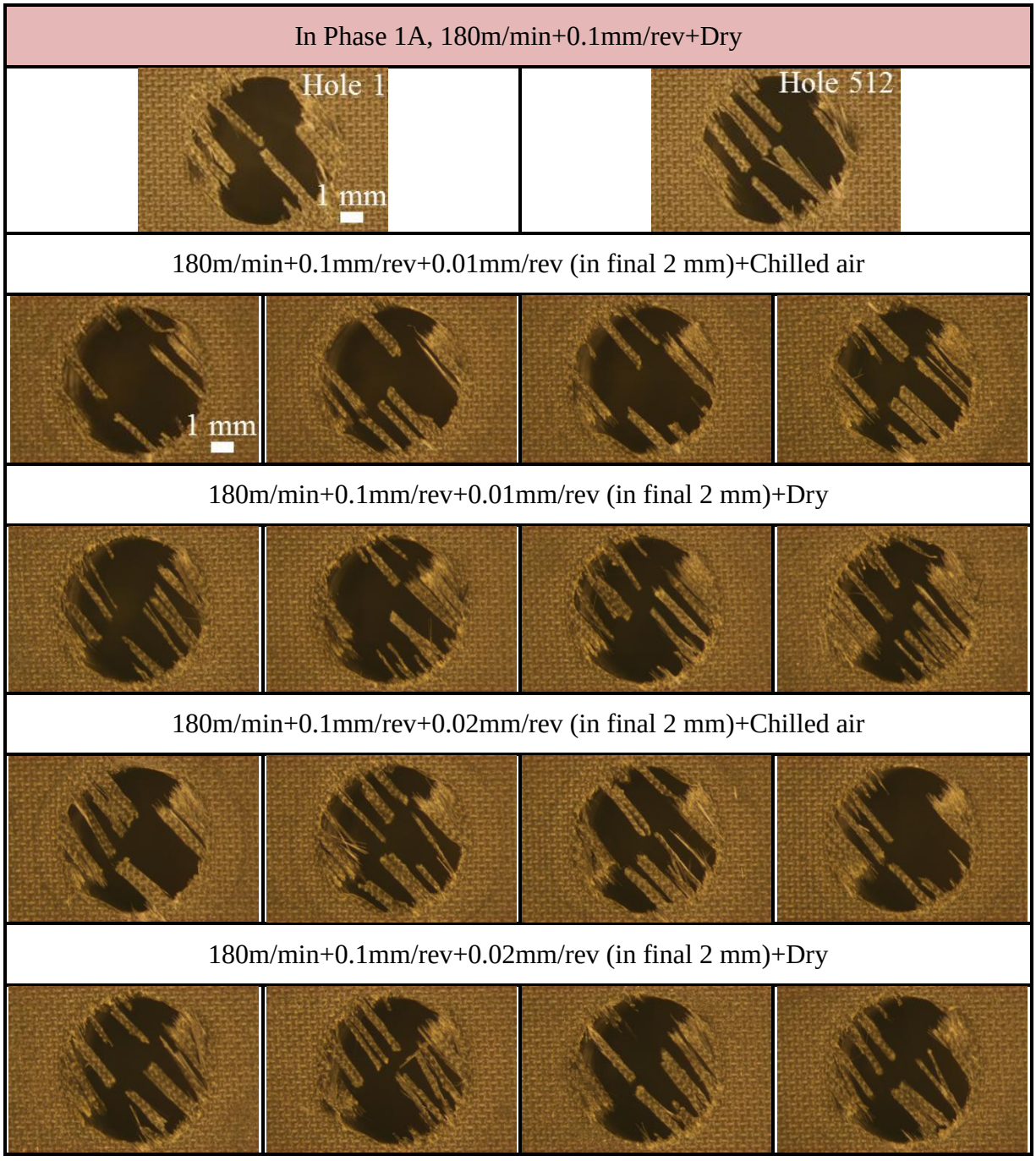


Figure 4.34: Hole exit quality when drilling at 180 m/min

4.3 Phase 2A: Evaluation of hole quality when drilling CFRP with variable feed rate operation

4.3.1 Tool wear and life

Figure 4.35 details the evolution of drill flank wear for all tests, which typically showed 'steady' wear progression until test cessation. All of the drills produced 384 holes, with flank wear ranging between 114 µm (Test 5) and 193 µm (Test 2). Tool wear was lowest when drilling Type 2 laminates at the highest feed rate of 0.3 mm/rev. This was partly due to the shorter contact time between workpiece and tool, although flank wear was up to 57 µm higher when drilling Type 3 CFRP material at equivalent feed rates. Abrasion and chipping of coating were the primary tool wear modes, as shown in Figure 4.36, detailing drill wear scar images at test cessation in Tests 2 and 5.

According to the ANOVA, none of factors were found to be statistical significant with respect to tool wear, although this could have been due to the majority of total tool-workpiece contact time (~70-88%) being confined to the final 2 mm of the hole when the feed rate was reduced to 0.01 mm/rev. This may have also contributed to the relatively high residual level, with workpiece material having a percentage contribution ratio of 24.54% while feed rate showed negligible PCR.

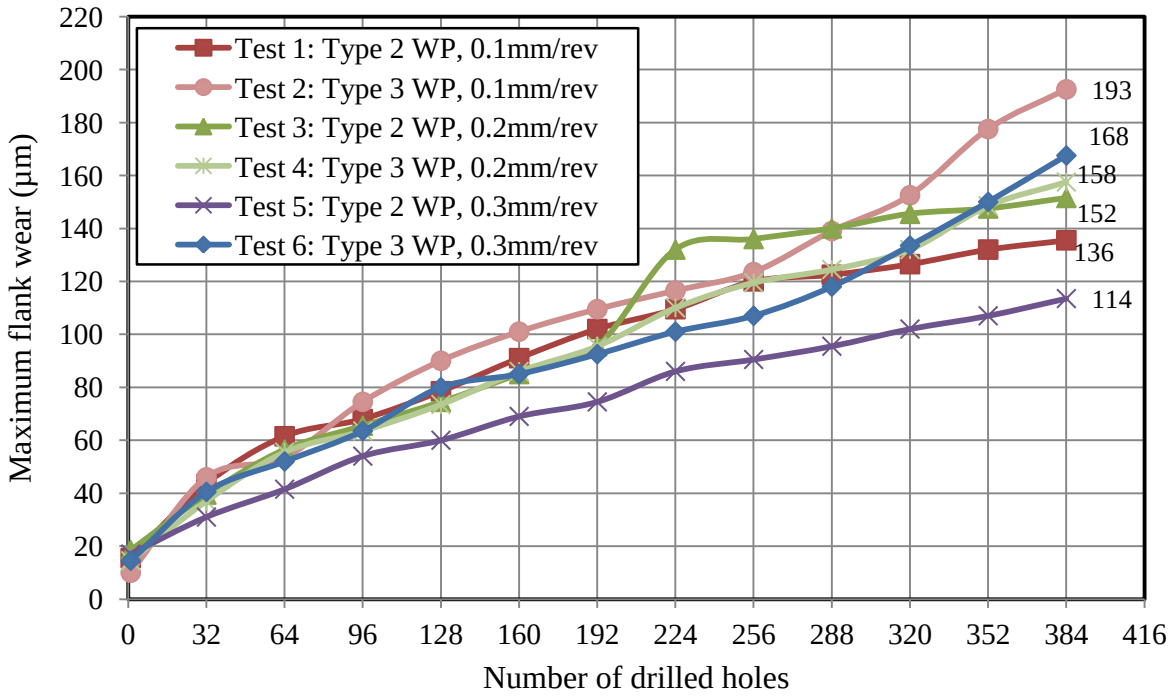


Figure 4.35: Flank wear curves for all tests against number of drilled holes

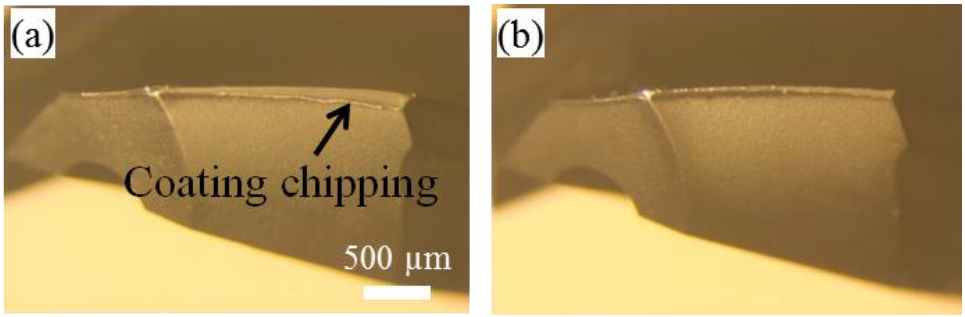


Figure 4.36 Tool wear scar at test cessation in (a) Test 2 and (b) Test 5

4.3.2 Thrust force and torque

Figure 4.37 shows the thrust force and torque profile when drilling the last hole (hole 384) in Test 4. Both parameters increased rapidly during the initial stage of drilling under the principal feed rate of 0.1 mm/rev, which then dropped dramatically with reduction in feed rate. Drilling time over the last 2 mm of the hole was 2.51s as opposed to only 1.05s, 0.57s and 0.35s when operating at the principal feed rates of 0.1, 0.2 and 0.3 mm/rev respectively.

Figure 4.38 shows the maximum thrust force and torque measured during the initial stage of drilling at the principal feed rate for each trial. The former in Tests 2, 4 and 6 (Type 3 workpiece) increased by ~155%,~118% and ~98% respectively from the first to the last hole drilled, while trials involving the Type 2 laminates (Tests 1, 3 and 5) recorded lower increases in thrust force of only ~56-67%. Conversely, torque values remained approximately constant in all tests. Figure 4.39 details the thrust force and torque progression when operating at the reduced feed rate of 0.01 mm/rev. Here, the thrust force values largely ranged between 100 and ~120N over the test duration, with the marginal increasing trend attributed to tool wear.

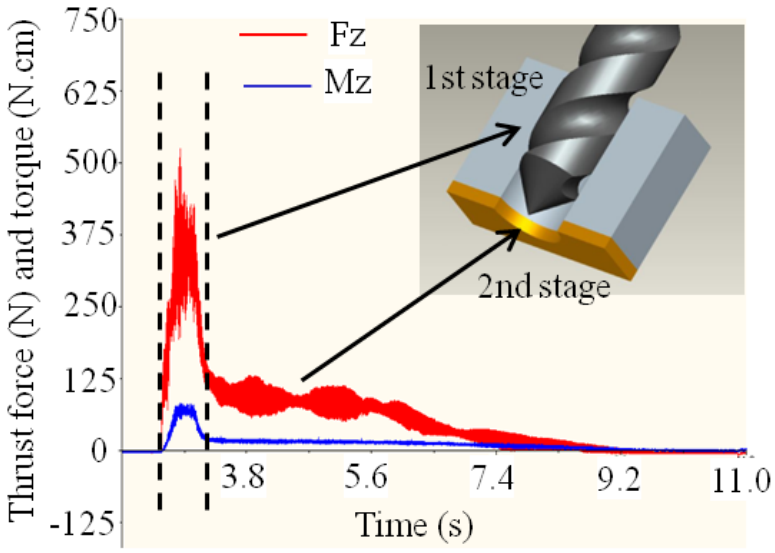


Figure 4.37: Force and torque profile at the last hole (hole 384) in Test 4

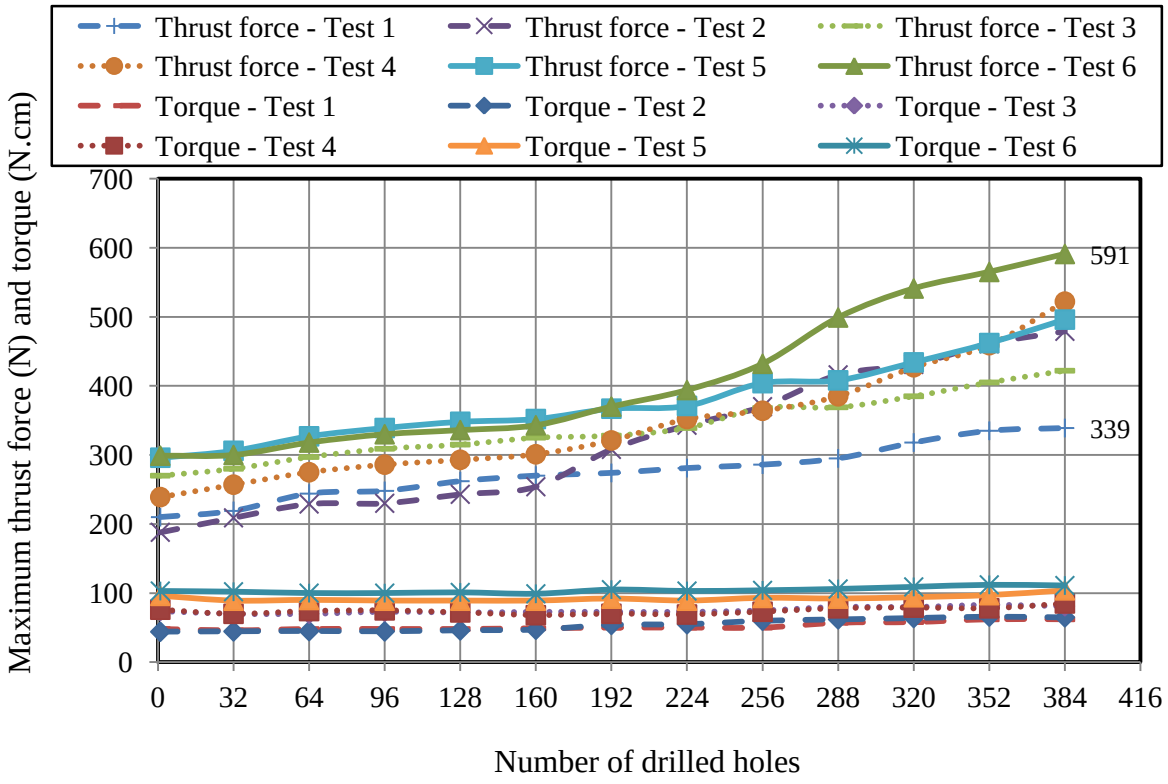


Figure 4.38: Thrust force and torque progression against number of drilled holes at the principal feed rate

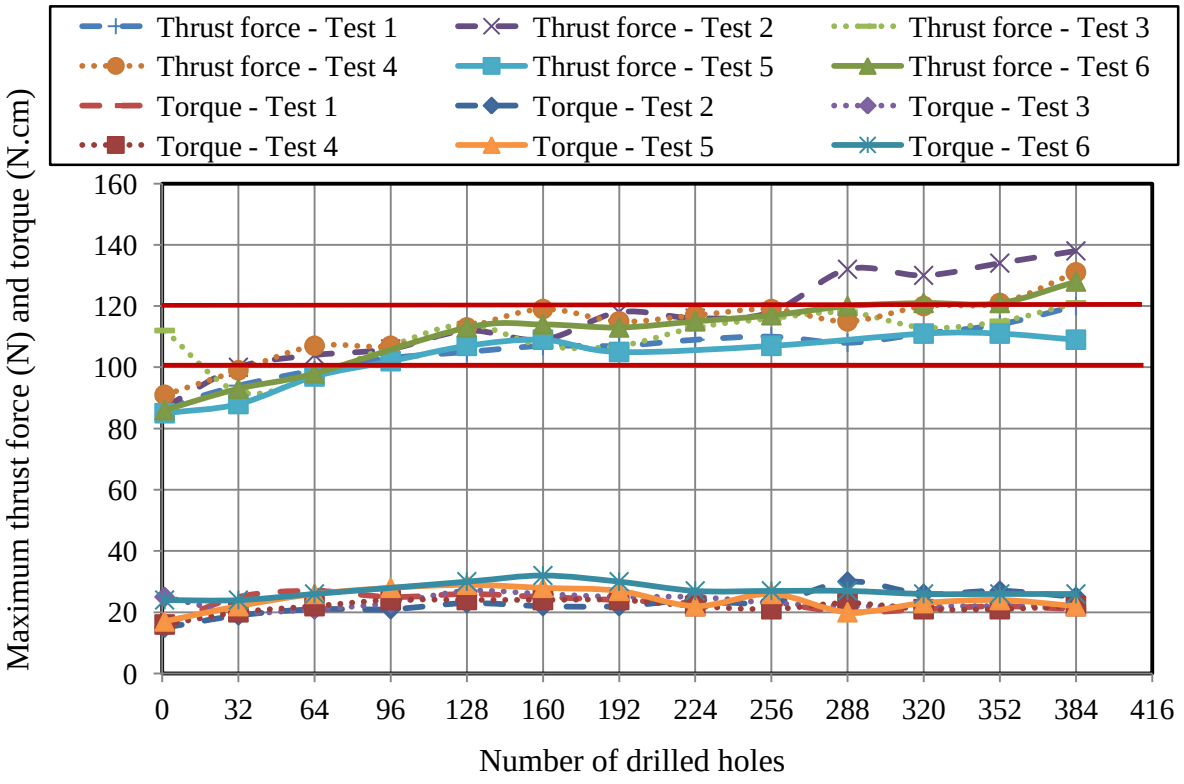


Figure 4.39: Thrust force and torque progression against number of drilled holes at the reduced feed rate

The main effects plot and corresponding ANOVA table for initial stage thrust force measured at the last hole drilled are shown in Figure 4.40 and Table 4.3 respectively. Both workpiece material and feed rate were found to be statistical significant, with associated PCR values of 33.4% and 61.4% respectively. Feed rate also had an overriding influence on torque with a PCR of 96.5% according to the ANOVA analysis, while the effect of workpiece material was negligible, see main effects plot detailed in Figure 4.41. The results generally agreed with published data in the literature [55, 56].

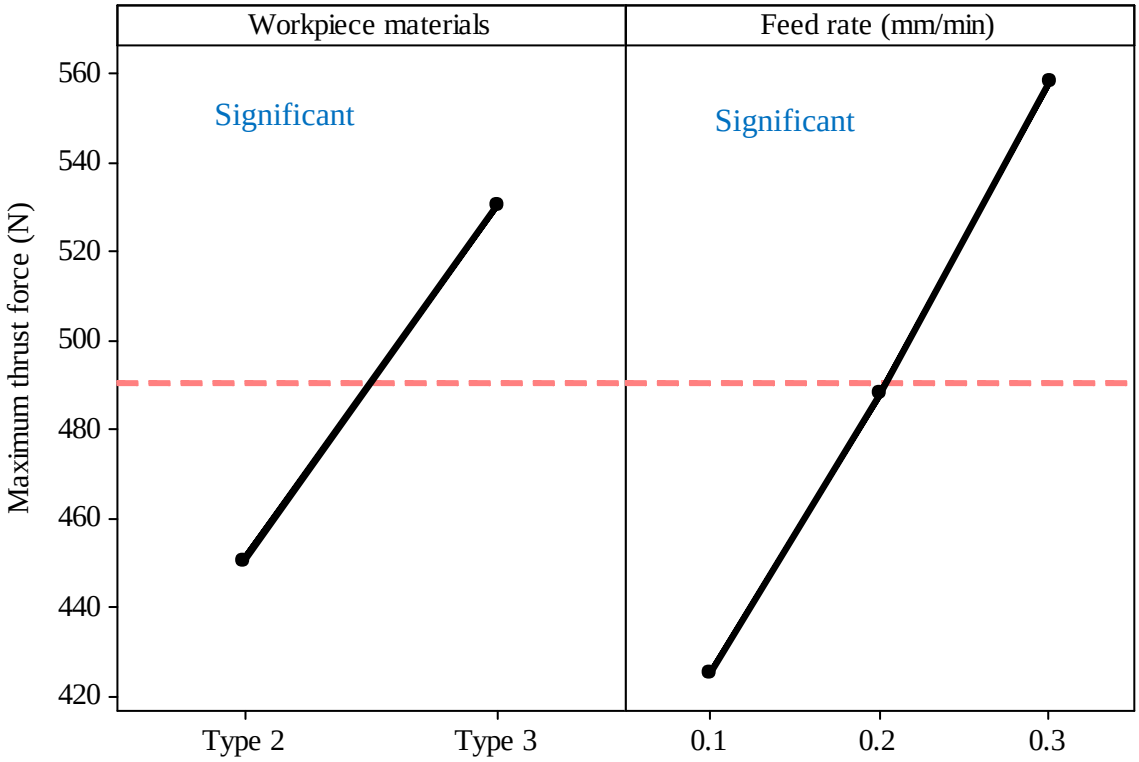


Figure 4.40: Main effects plot for thrust force at last hole (hole 384)

Table 4.3: ANOVA results for thrust force at last hole (hole 384)

Source	DF	Seq SS	Adj MS	F	P	PCR
Workpiece material	1	9680.2	9680.2	33.59	0.029*	33.4%
Feed rate	2	17841.0	8920.5	30.96	0.031*	61.4%
Error	2	576.3	288.2			5.2%
Total	5	28097.5				

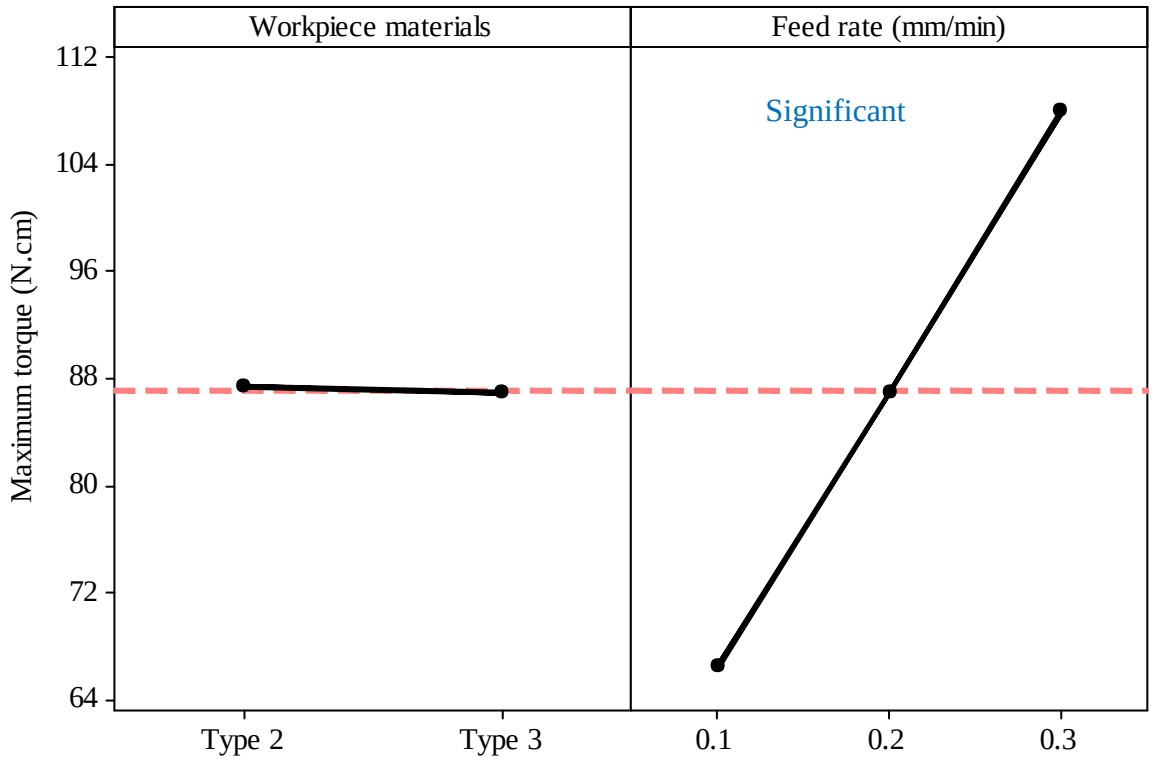


Figure 4.41: Main effects plot for torque at last hole (hole 384)

4.3.3 Hole entry and exit quality

Figure 4.42 shows micrographs of hole entry and exit for the first and last holes drilled in all tests, which are compared against corresponding results from Test 6 performed at constant feed rate in Phase 1A. In terms of hole entry quality, only minor damage in the form of fuzzing and limited uncut fibres was observed at the first hole, while increased fuzzing, uncut fibre and delamination were apparent at the last hole irrespective of feed rate and workpiece type. At the highest feed rate (0.3 mm/rev), uncut fibres were observed even at the first hole.

Compared to hole exit results from Test 6 in Phase 1A (constant feed rate at 0.1 mm/rev), the level of uncut fibres were significantly lower in both the first and last holes when drilling with the variable feed rate strategy. This was attributed to the decreased thrust forces in line with the reduction in feed rate (0.01 mm/rev). The only exception was at the last hole drilled in Test 2, where the highest flank wear of ~193 µm was observed, which likely caused an elevation in thrust force.

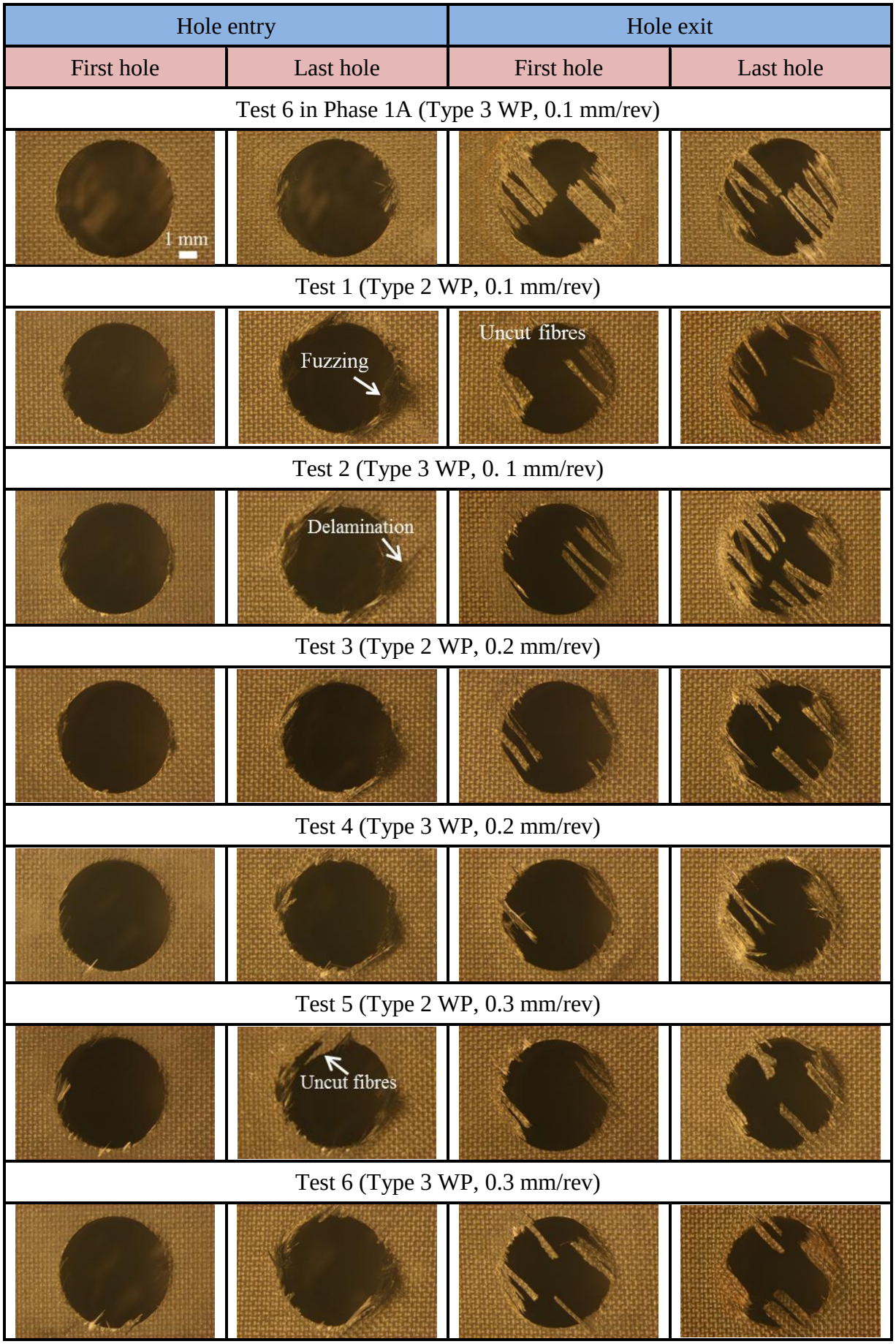


Figure 4.42: Hole entry and exit quality at the first and last holes in all tests

Delamination factor (F_d) results at hole entry and exit for the first and last holes are detailed in Figure 4.43. In general, delamination factor was found to be greater (by up to 0.18) at test cessation compared with the first hole for both entrance and exit positions. Damage was also typically more severe at the hole exit. Delamination factor values at hole entrance generally increased with feed rate where a maximum of 1.35 was observed in Test 5 (Type 2 WP, 0.3 mm/rev). For the exit delamination factor, Type 2 workpiece normally produced lower values (up to 0.16) except for the last hole drilled when operating at 0.3 mm/rev (Test 5). Furthermore, the influence of varying feed rate on exit delamination factor exhibited no apparent trend. According to the associated statistical analysis, feed rate was found to be a significant factor affecting the entrance F_d of the first hole with a PCR of 87.9%, which was in agreement with the observations of several researchers [55, 60, 194, 205]. The discrepancy of exit F_d between the first and last holes however was limited, which was most likely due to the constant reduced feed rate (0.01mm/rev) applied.

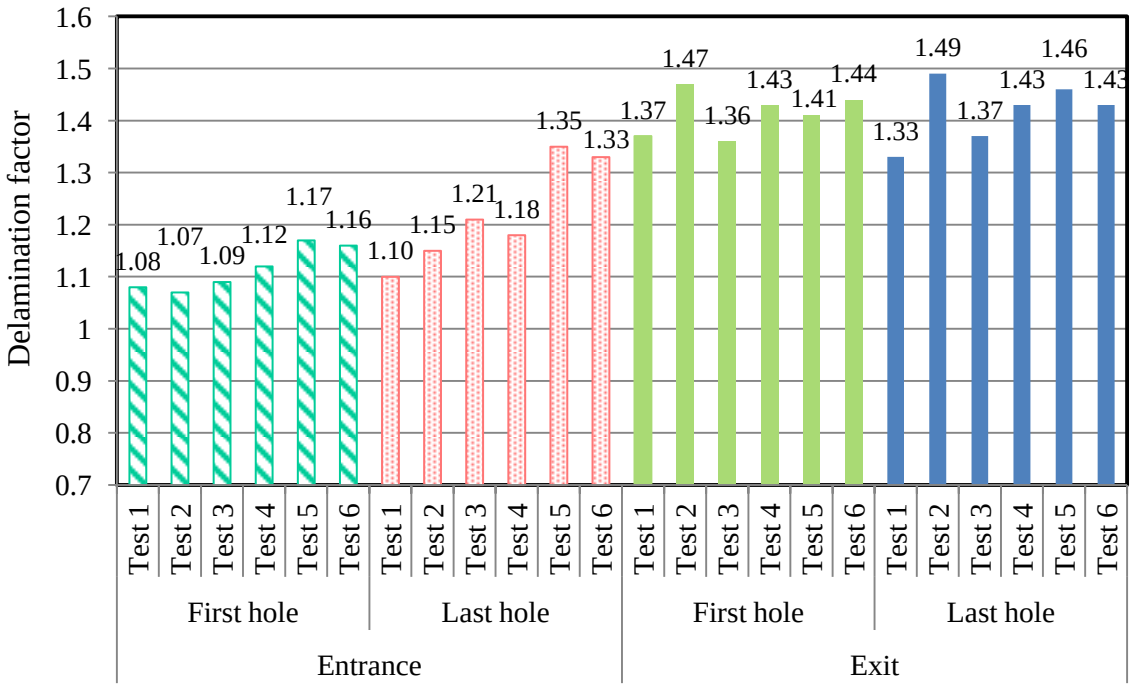


Figure 4.43: Delamination factor at hole entry and exit for the first and last holes in all trials

4.3.4 Hole size

The diameter for each of the measured holes were found to be undersized, with the exception of the first hole drilled in Test 2, see Figure 4.44. The deviation from the nominal hole diameter was up to ~40 µm (~0.7%) at test cessation (after drilling 384 holes). In general, a large proportion of the hole diameter error (up to ~30 µm reduction) occurred within the first 128 holes, followed by a more gradual decrease over the last 256 holes. This was mainly due to rapid loss of the coating layer at the initial stage of drilling, prior to steady abrasion of the WC substrate.

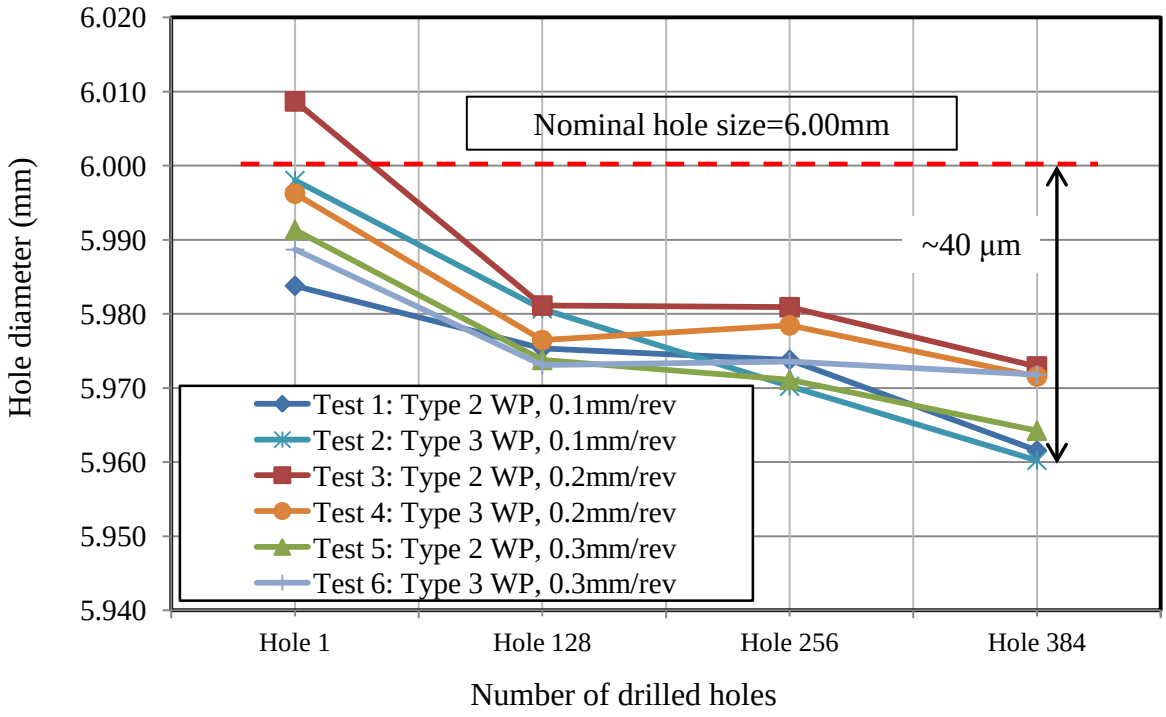


Figure 4.44: Hole diameter progression against number of drilled holes

4.3.5 Hole surface integrity analysis

Figure 4.45 shows SEM micrographs of the machined surface at the first hole in Tests 1, 3 and 5. Type 2 CFRP workpieces were used in all three trials. Even in the first hole, defects in the form of fibre loss / void formation were evident in the vicinity of the hole entry irrespective of the principal feed rate (0.1-0.3 mm/rev) level. In contrast, surfaces with limited damage was observed near the hole exit due to the lower feed rate (0.01 mm/rev) employed over the final 2 mm of drilling. Considerable deterioration in surface quality over the entire hole however was visible at test cessation, see Figure 4.46. Here, reducing feed rate to 0.01 mm/rev near the hole exit provided no appreciable benefits, which suggests that tool condition had a more prominent influence than feed rate during the latter stages of a test. Surprisingly,

increasing principal feed rate to 0.3 mm/rev did not appear to exacerbate the level of damage compared to results at 0.1 mm/rev.

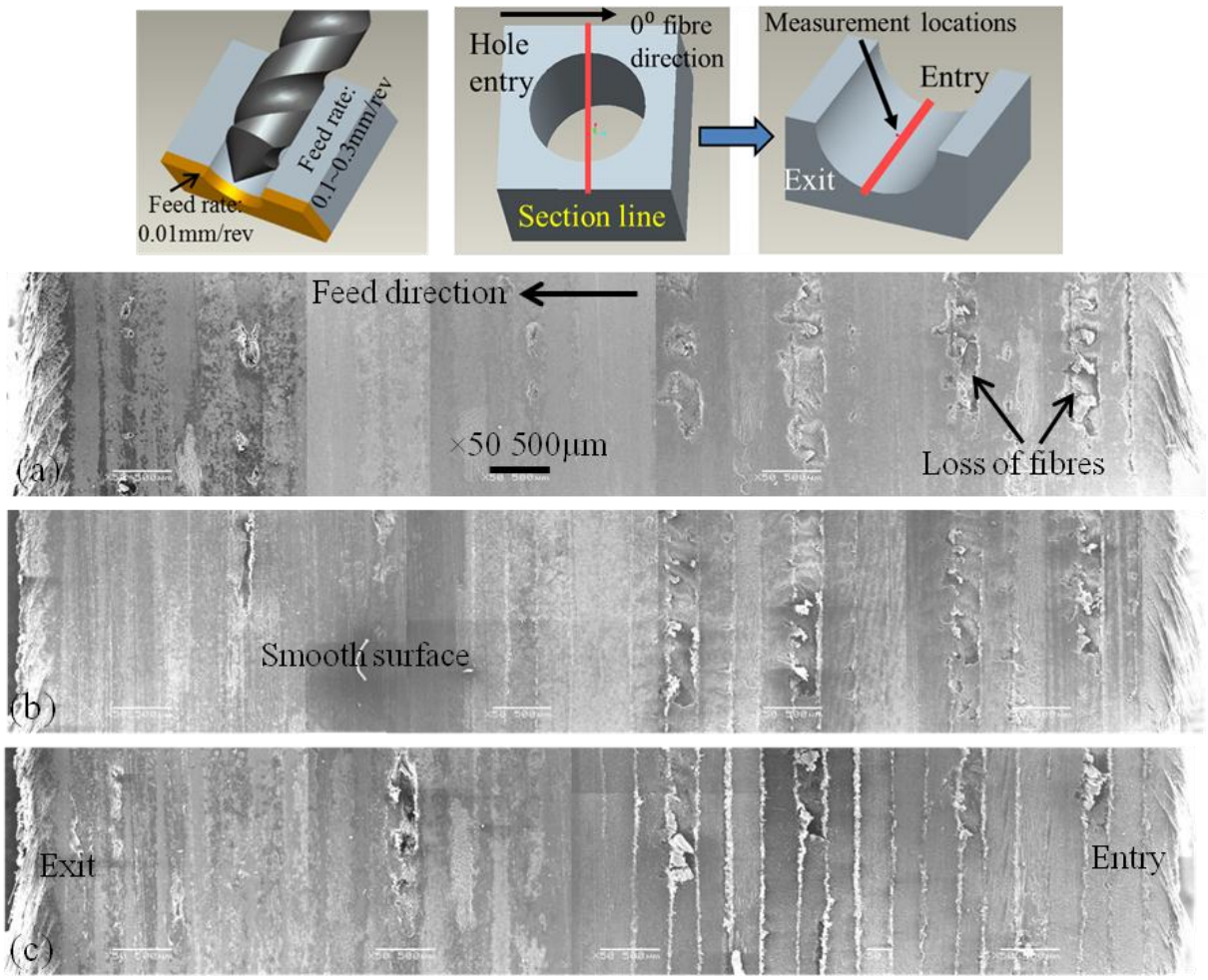


Figure 4.45: SEM micrographs of hole surface at the first hole in (a) Test 1 (0.1 mm/rev), (b) Test 3 (0.2 mm/rev) and (c) Test 5 (0.3 mm/rev)

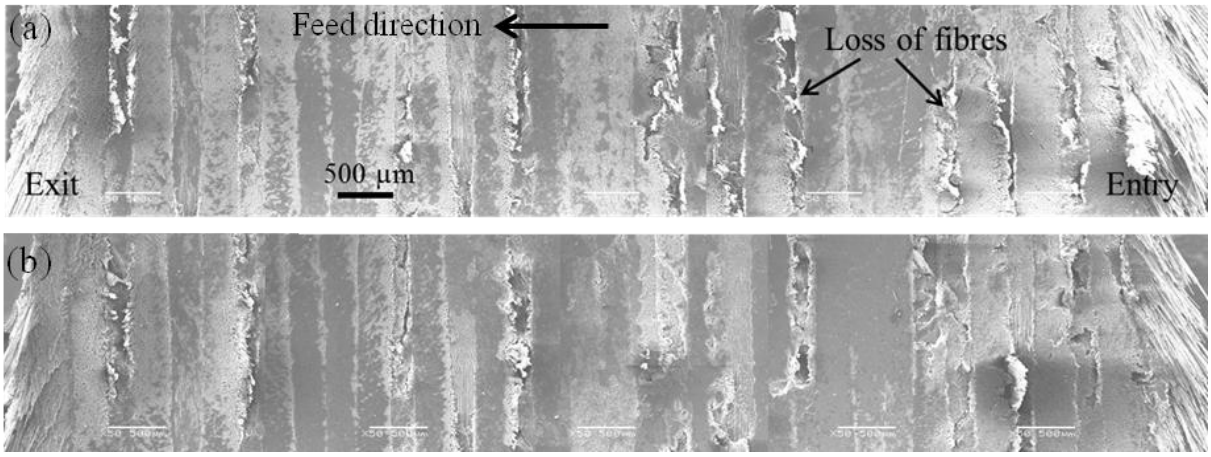


Figure 4.46: SEM micrographs of hole surface at the last hole in (a) Test 3 (0.2 mm/rev) and (b) Test 5 (0.3 mm/rev)

4.4 Phase 2B: Influence of workpiece configuration / fibre orientation and elevated feed rates on hole quality when drilling CFRP

4.4.1 Tool wear and life

In the preliminary test at a feed rate of 0.6mm/rev, both cutting lips experienced catastrophic failure / fracture at the flank surface when drilling the first hole, as shown in Figure 4.47. This was most likely due to the high thrust forces (~1304N) generated at high feed rates. Chipping of both the coating and substrate material at the tool periphery was also prevalent.

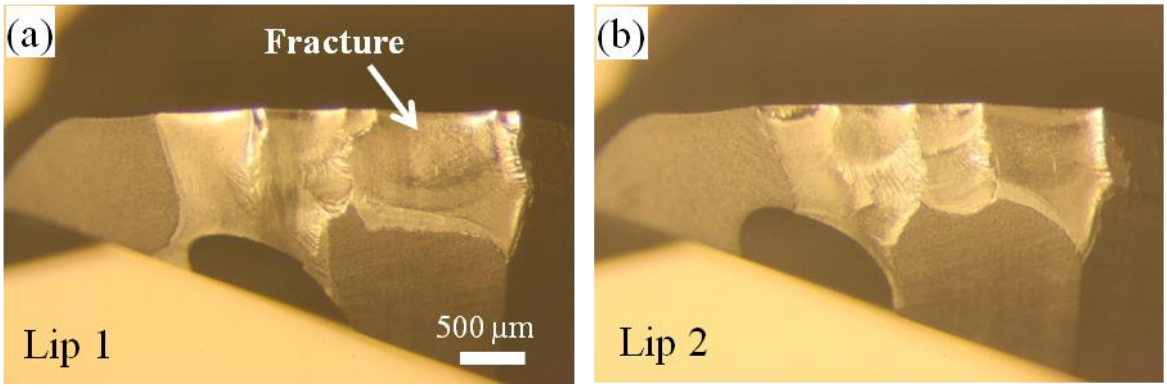


Figure 4.47: Tool wear scar after the first hole at a feed rate of 0.6 mm/rev for (a) lip 1 and (b) lip 2

Figure 4.48 details the maximum flank wear values recorded at test cessation while the corresponding wear progression curves against the number of drilled holes for all tests is presented in Appendix C. Drill wear progression followed a similar trend regardless of feed rate level or workpiece configuration, with all trials achieving 384 holes. The highest flank wear at test cessation was 123 µm in Test 3 (Type 3 WP, 0.2 mm/rev) while the best performance was observed in Test 4 (Type 1 WP, 0.4 mm/rev) with flank wear of 102 µm. There was marginal difference (21µm) in flank wear levels between all tests after 384 holes, as the tool-workpiece contact time per hole was limited to ~1.33 and ~1.00s when operating at 0.2 and 0.4 mm/rev respectively. Sample tool wear scar images from Tests 3 and 4 at test cessation are shown in Figure 4.49, highlighting that abrasion and chipping of the CVD-diamond coating (at the drill corner) were the main tool wear modes.

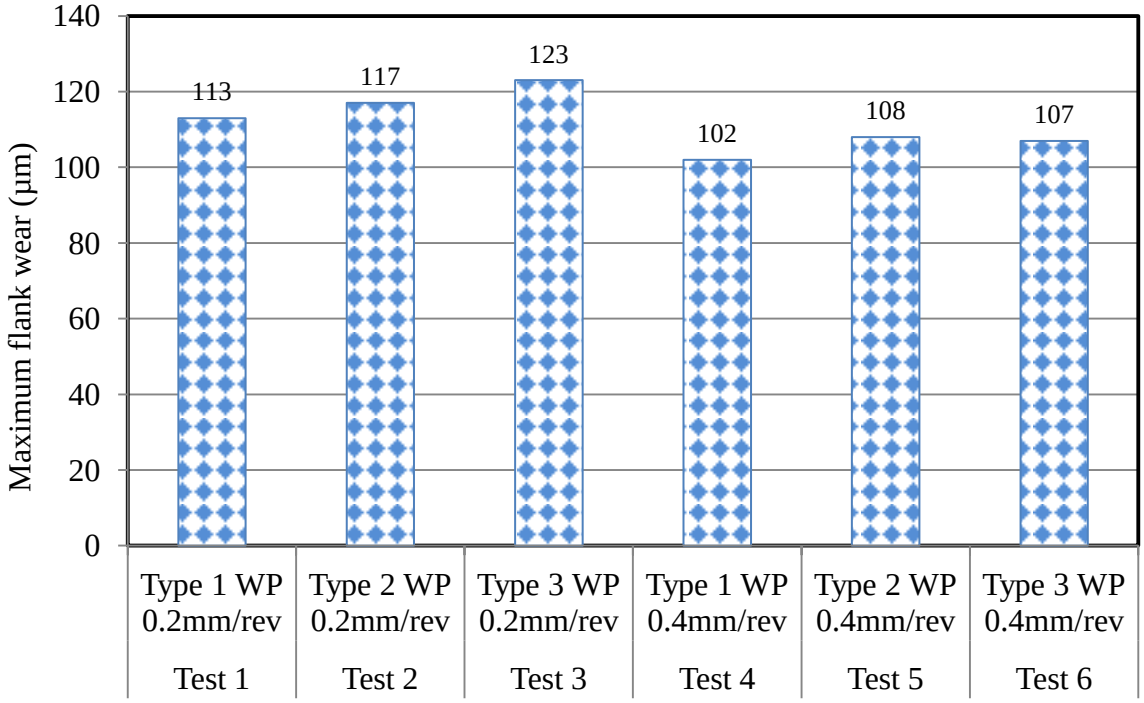


Figure 4.48: Maximum flank wear results recorded at test cessation

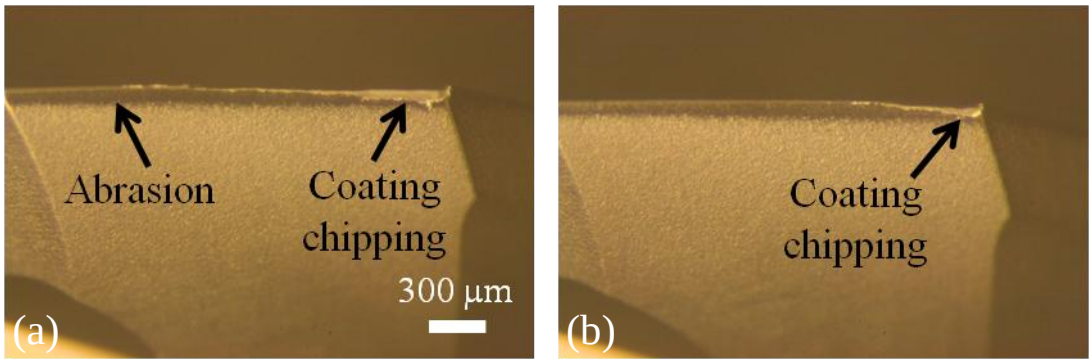


Figure 4.49: Tool wear scar at test cessation in (a) Test 3 and (b) Test 4

4.4.2 Thrust force and torque

Maximum thrust force and torque were recorded both for the first stage of drilling at the principal feed rate (0.2 or 0.4mm/rev) as well as the second stage at the reduced feed rate of 0.01mm/rev. The force / torque progression against number of drilled holes during the initial drilling period is detailed in Appendix C (Figure C2). Generally, thrust force variations were in line with tool wear progression, while there was marginal difference (<10 N.cm) in torque values between the first and last hole drilled (hole 384). Figure 4.50 details the evolution of thrust force / torque when drilling at the lower feed rate. Thrust force values typically varied between ~80 and ~110 N, while torque was approximately constant (~30 N.cm) over the test duration. This was due to the constant feed rate (0.01 mm/rev) applied in the final 0.5 mm of the hole. Maximum thrust forces when drilling at the principal feed rate typically increased by

an average of ~60% from the first to the last hole, see Figure 4.51. The highest thrust force was seen in trials utilising Type 2 workpieces, which was possibly due to the greater number of plies (16) orientated at 0º generating elevated shearing forces. Compared to drilling at a feed rate of 0.2 mm/rev, thrust forces were up to 45% and 36% higher at 0.4 mm/rev for the first and last holes respectively.

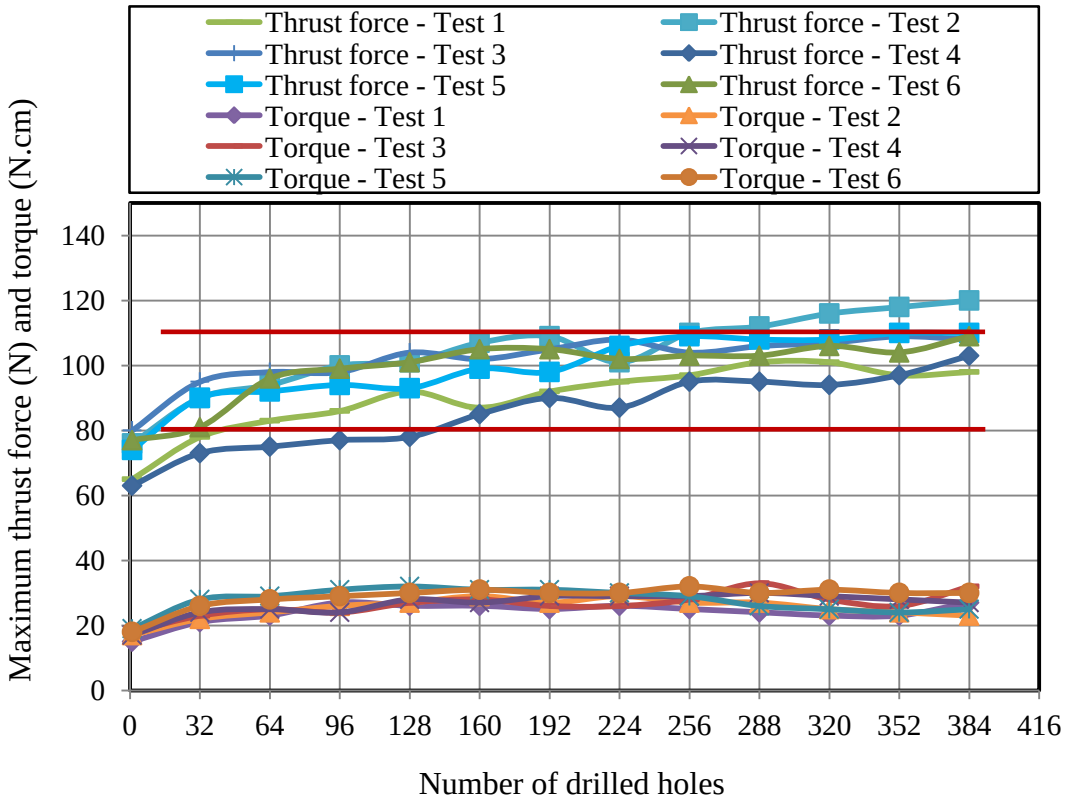


Figure 4.50 Thrust force and torque progression against number of drilled holes when machining with the reduced feed rate

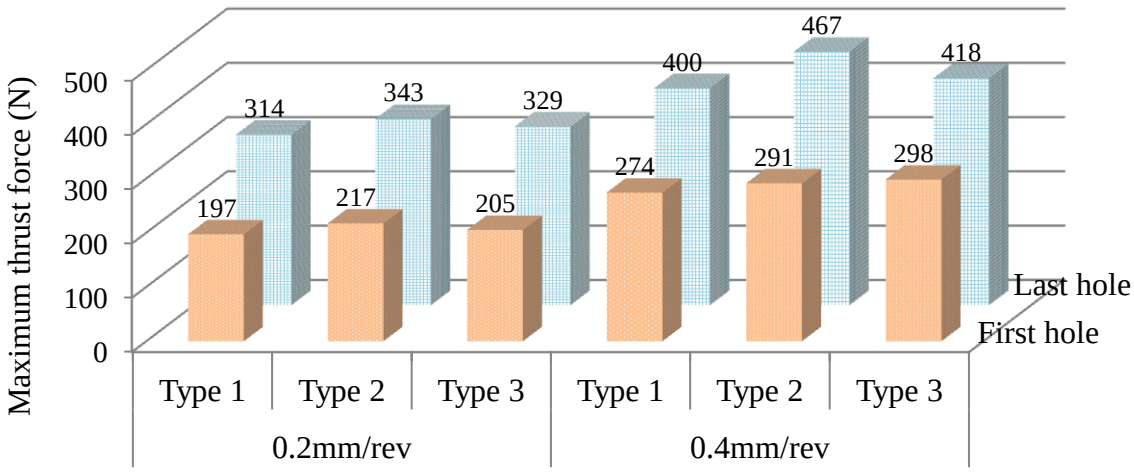


Figure 4.51: Thrust forces recorded for the first and last holes when drilling with the principal feed rate level

According to the statistical analysis, feed rate was found to have a significant influence on thrust force at the first hole with an overwhelming PCR of 94.6%. Conversely, the effect of workpiece configuration was negligible, having a PCR of 2.9%. Similar results were observed from the main effect plots and corresponding ANOVA table relating to thrust force for the last hole, as shown in Figure 4.52 and Table 4.4 respectively. Feed rate had a dominant effect with a PCR value of 82.8%.

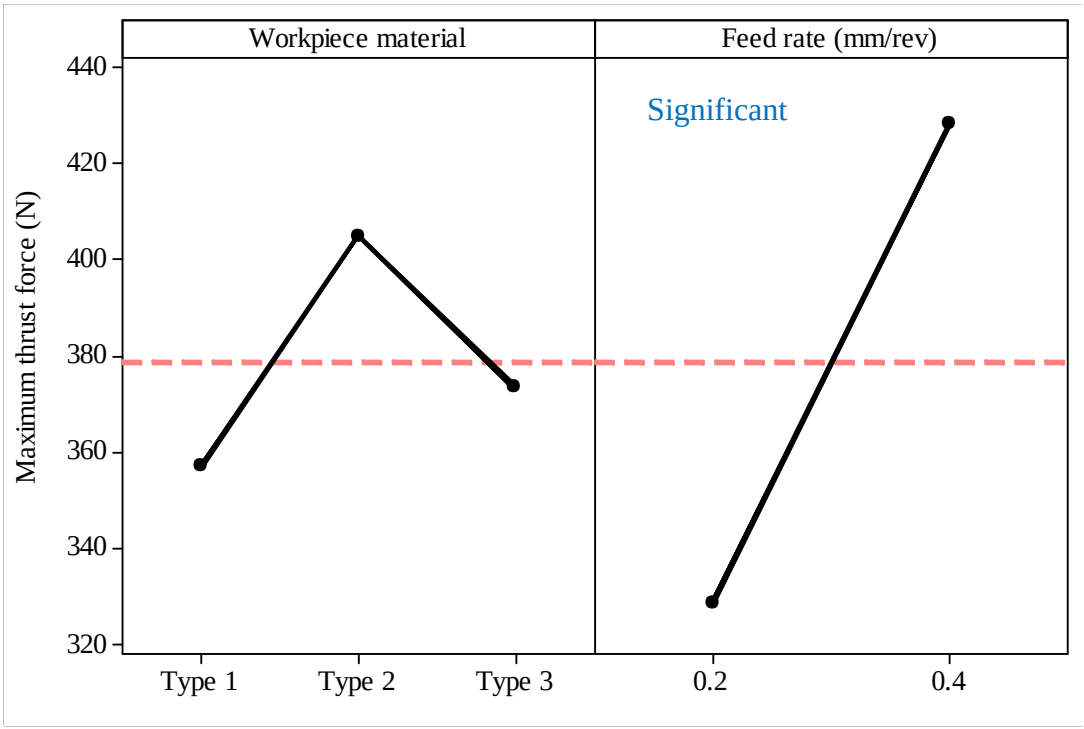


Figure 4.52: Main effects plot for thrust force recorded at the last hole (hole 384)

Table 4.4: ANOVA results for thrust force recorded at the last hole (hole 384)

Source	DF	Seq SS	Adj MS	F	P	PCR
Workpiece material	2	2379.0	1189.5	5.33	0.158	10.9%
Feed rate	1	14900.2	14900.2	66.77	0.015*	82.8%
Error	2	446.3	223.2			6.3%
Total	5	17725.5				

The variation in maximum torque values between the first and last holes did not exceed 10 N.cm irrespective of composite type. The progression of torque against number of drilled holes is detailed in Figure C2 of Appendix C. Increasing feed rate from 0.2 to 0.4 mm/rev however resulted in a considerable rise in torque of up to ~58%, as shown in Figure 4.53. Associated ANOVA calculations indicated that feed rate had an overriding influence on

torque at the last hole with a PCR of 98.4%, while workpiece material type had no appreciable effect.

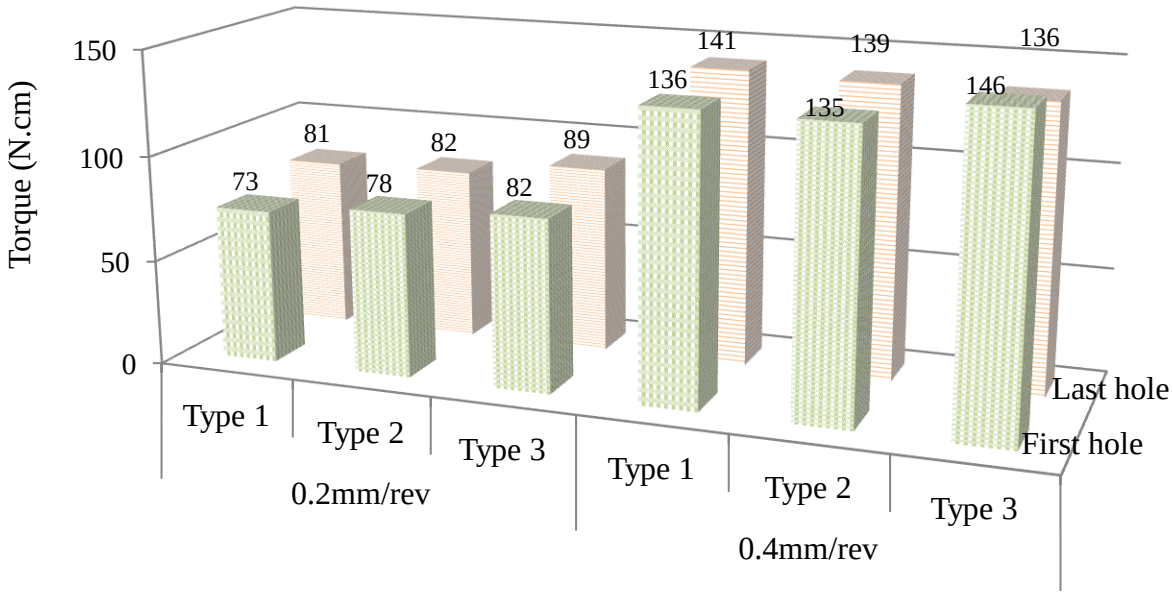


Figure 4.53: Torque values recorded for the first and last holes when drilling with the principal feed rate level

4.4.3 Hole entry and exit quality

Figure 4.54 details optical micrographs of hole entry and exit for both the first and last holes in all tests. Hole entry was largely free of any major flaws over the entire test duration when drilling at a feed rate of 0.2 mm/rev, while uncut fibres and splintering were prevalent from the first hole when feed rate was increased to 0.4 mm/rev. The level of damage was even more pronounced with further increment in feed rate to 0.6 mm/rev, as shown in Figure 4.55(a). This was due to laminate 'peel up' effects as well as increased thrust force at elevated feed rates [75, 194, 206]. In all tests, there were relatively low levels of uncut fibres at the hole exit, due to use of a support jig with 7.0 mm clearance holes that minimised delamination and fibre 'push out' as well as the reduced feed rate of 0.01 mm/rev. The latter most likely kept exit thrust forces below the 'critical' threshold for triggering workpiece delamination, which is the main factor affecting hole exit damage according to Hocheng and Tsao [201]. Additional trials were conducted at constant / fixed feed rates of 0.2 and 0.4 mm/rev in order to investigate the influence of variable feed rate strategy on hole exit quality. In the subsequent tests, a high degree of uncut fibres were prevalent at the exit section of the hole even when utilising the support jig, as shown in Figures 4.55(b) and 4.55(c). This suggests that variable feed rate operation was instrumental in minimising uncut fibres and improving hole exit quality.

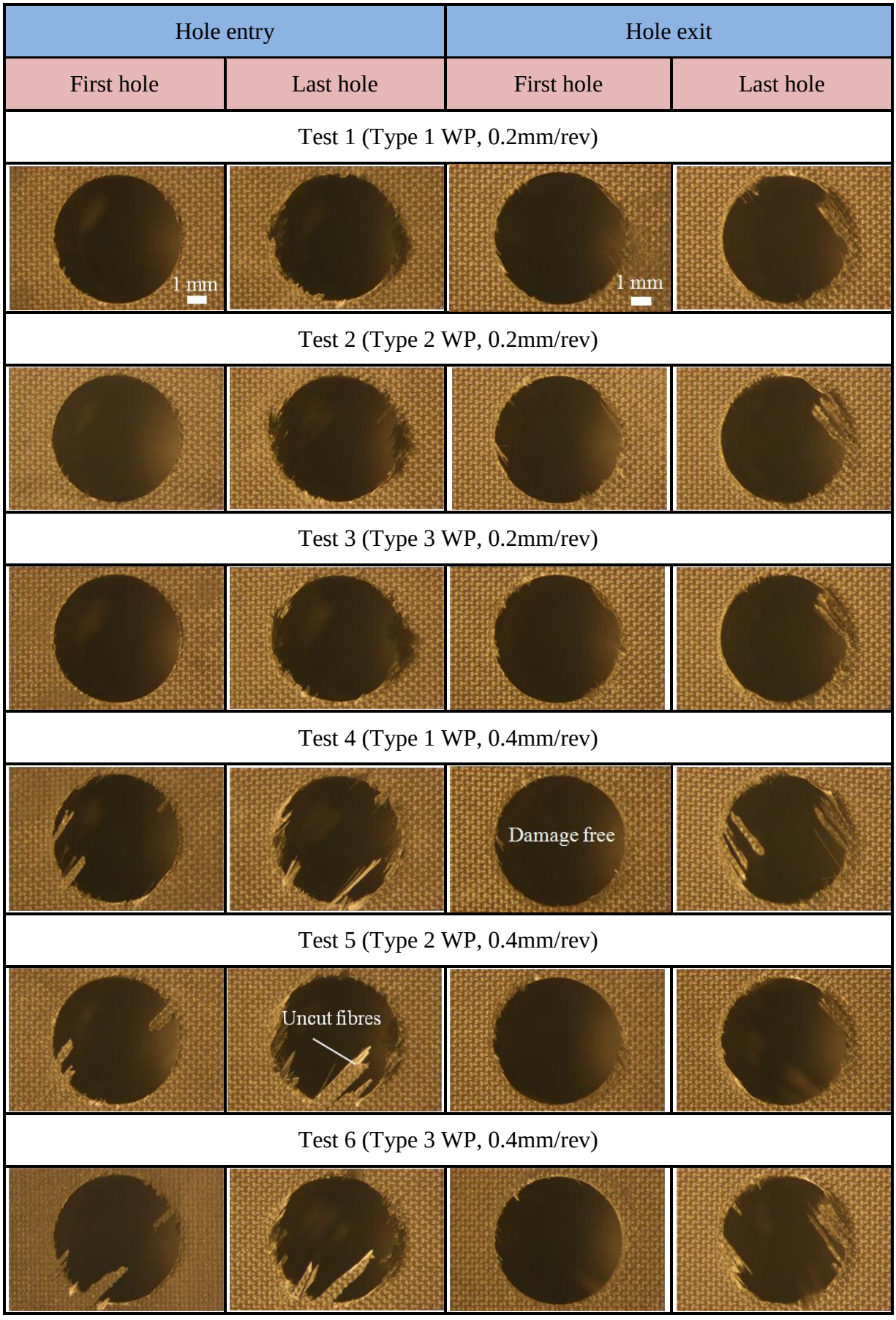


Figure 4.54: Hole entry and exit at the first and last holes in all tests

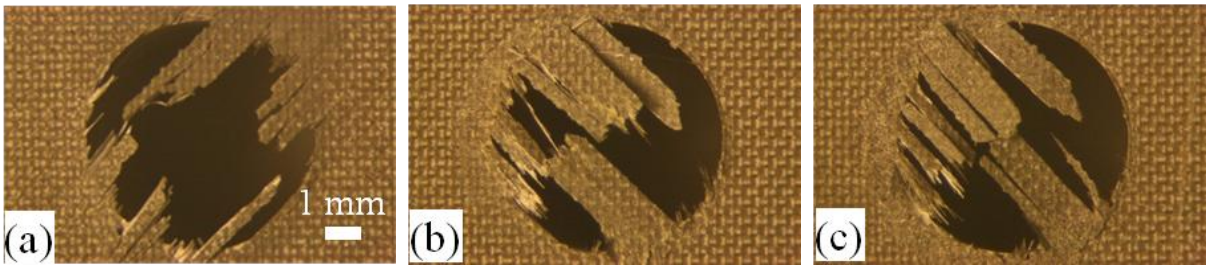


Figure 4.55: (a) Hole entry with feed rate of 0.6 mm/rev in the preliminary trial, (b) hole exit with constant feed rate of 0.2 mm/rev and (c) 0.4 mm/rev

4.4.4 Effect of fibre cutting angle on workpiece delamination / uncut fibre damage

The fibre cutting angle θ is defined as the angle between the tool feed direction and workpiece fibre orientation, as shown in Figure 4.56. In drilling, the angle θ is continuously changing due to tool rotation. From previous experimental results (especially in Phase 1A), uncut fibres are generally prevalent at the hole exit (see sample picture in Figure 4.57(a)). When drilling without workpiece support, uncut fibres / delamination typically formed symmetrically at opposite quadrants of a hole, within critical cutting angles of $90^o \leq \theta < 180^o$, irrespective of fibre lay-up configuration. However, when the cutting angle in the range of $0^o < \theta < 90^o$, no delamination / uncut fibres were observed, as shown in the schematic in Figure 4.58(a). In order to evaluate the occurrence of delamination / uncut fibres in relation to fibre cutting angle, further experiments were conducted at feed rates of 0.2 and 0.4mm/rev when drilling unidirectional CFRP plates. Uncut fibres were visible in a symmetrical pattern regardless of feed rate, as detailed in Figures 4.57(b) and 4.57(c). This was illustrated by the schematic in Figure 4.58(b), where uncut fibres were mainly seen to form within the critical cutting angles of $90^o \leq \theta < 180^o$.

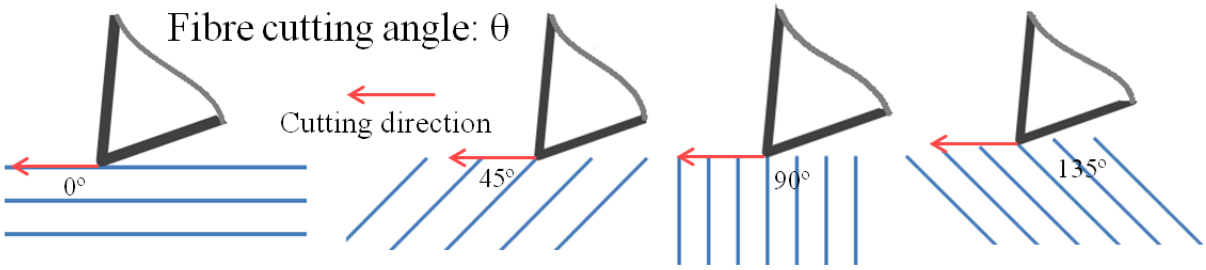


Figure 4.56: Fibre cutting angle definition



Figure 4.57: Hole exit quality at (a) Type 1workpiece material with feed rate of 0.1 mm/rev, (b) unidirectional (UD) workpiece at 0.2mm/rev and (C) UD at 0.4mm/rev

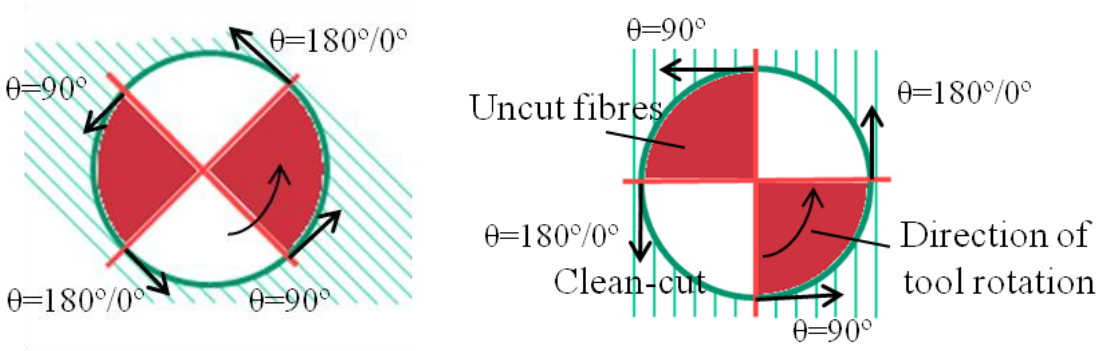


Figure 4.58: Schematic of uncut fibres relating to fibre cutting angles with (a) Type 1WP having 45º orientation for the last / exit ply and (b) unidirectional WP

4.4.5 Two and three dimensional (2D and 3D) surface topography analysis

Figure 4.59 details the surface roughness (Ra) values measured at the entry and exit positions in both the first and last holes for all tests. Hole roughness was generally higher in Type 3 workpieces (Tests 3 and 6) at both feed rate levels, which was due to the larger number of plies (14) orientated at 135º. Increasing feed rate from 0.2 to 0.4 mm/rev led to lower Ra in all of the samples analysed, which was attributed to a decrease in tool wear when operating at higher feed rates, as a result of the shorter interaction period between the tool and workpiece. Furthermore, the Ra measured in the vicinity of the hole exit location was consistently found to be lower (by up to ~ 80%) compared to the entrance section, which was possibly due to a ‘ploughing’ or ‘polishing’ effect when operating at the very low feed rate of 0.01 mm/rev. An analysis of skewness (Rsk) showed that all values were negative, indicating that the machined surfaces were typically dominated by sharp / deep valleys, most likely the result of fibre pull out / matrix loss. Conversely, the relatively high kurtosis (Rku) values recorded (>3) suggests the presence of sharp peaks on the measured profiles, which was likely from uncut / re-deposited fibres on the hole surfaces.

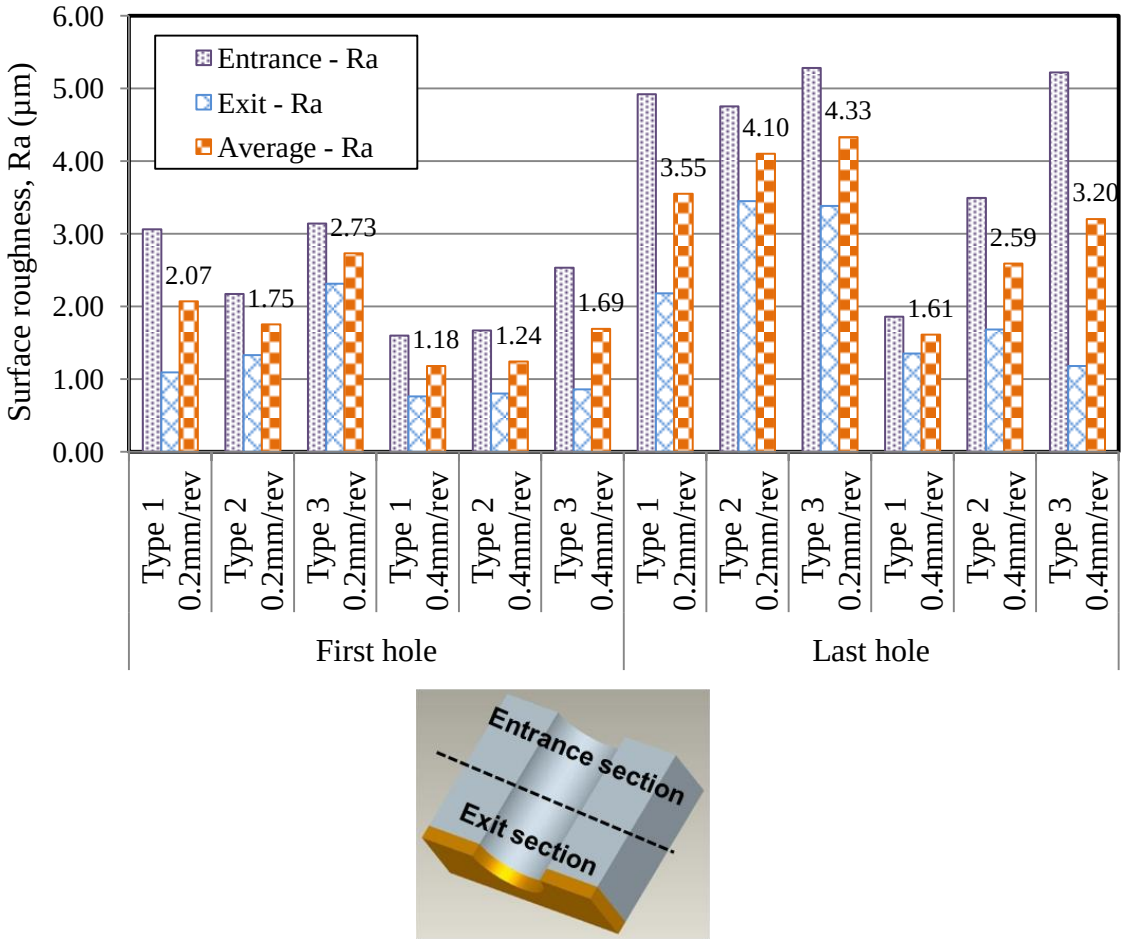


Figure 4.59: Surface roughness (Ra) results for hole entry and exit section of the first and last holes in all tests

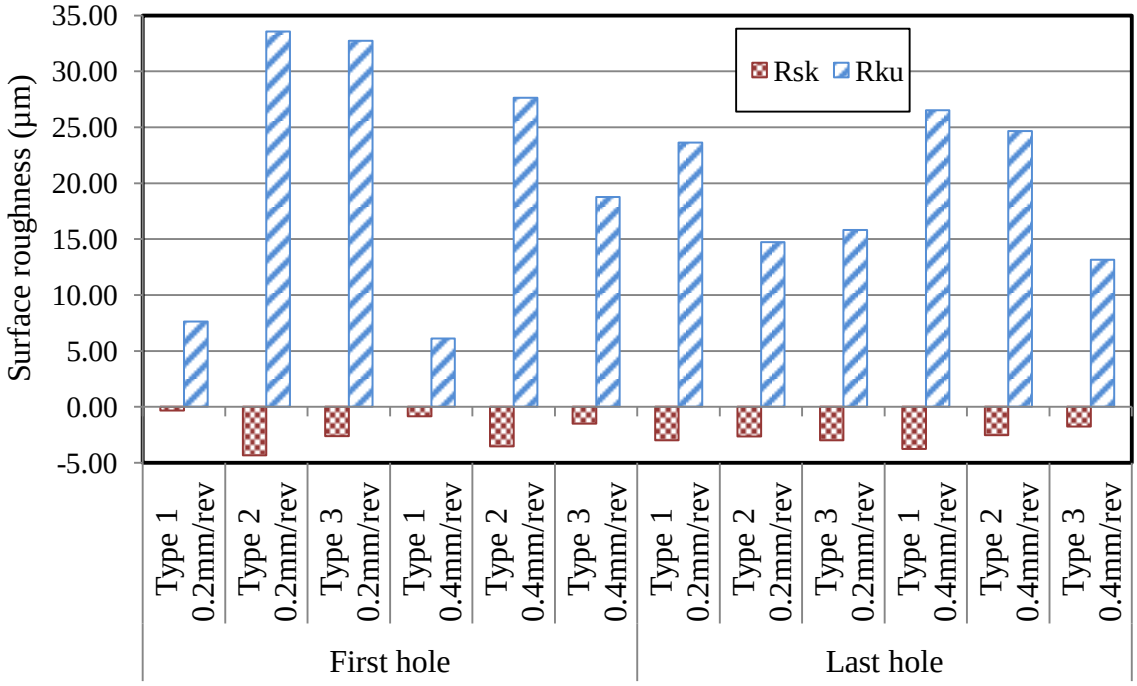


Figure 4.60: Surface skewness (Rsk) and kurtosis (Rku) results for the first and last holes in all tests

Figure 4.61 details 3D surface roughness values (Sa) recorded at the first and last holes in all tests, with associated surface topography maps outlined in Figure 4.62. Substantial grooving / voids were clearly visible particularly at the 135º orientated plies in all workpiece samples despite drilling with new tools. Damage was also more severe in the Type 3 workpiece due to the presence of adjacent 135º plies, which would explain the poorer surface roughness observed in both 2D and 3D measurements. For both the first and last holes, Type 2 workpiece material showed the lowest Sa value (0.46 and 1.16 µm) while Type 3 demonstrated the highest roughness values (up to 2.47 µm). The variation in St (total height of the surface) was similar to that of the Sa parameter. Statistical analysis on results from the first hole showed that both workpiece material and feed rate were significant at the 5% level with respect to Sa, the former having a greater influence with a PCR of 83.7% compared to only 16.2% for feed rate, see main effects plot and corresponding ANOVA results shown in Figure 4.63 and Table 4.5 respectively.

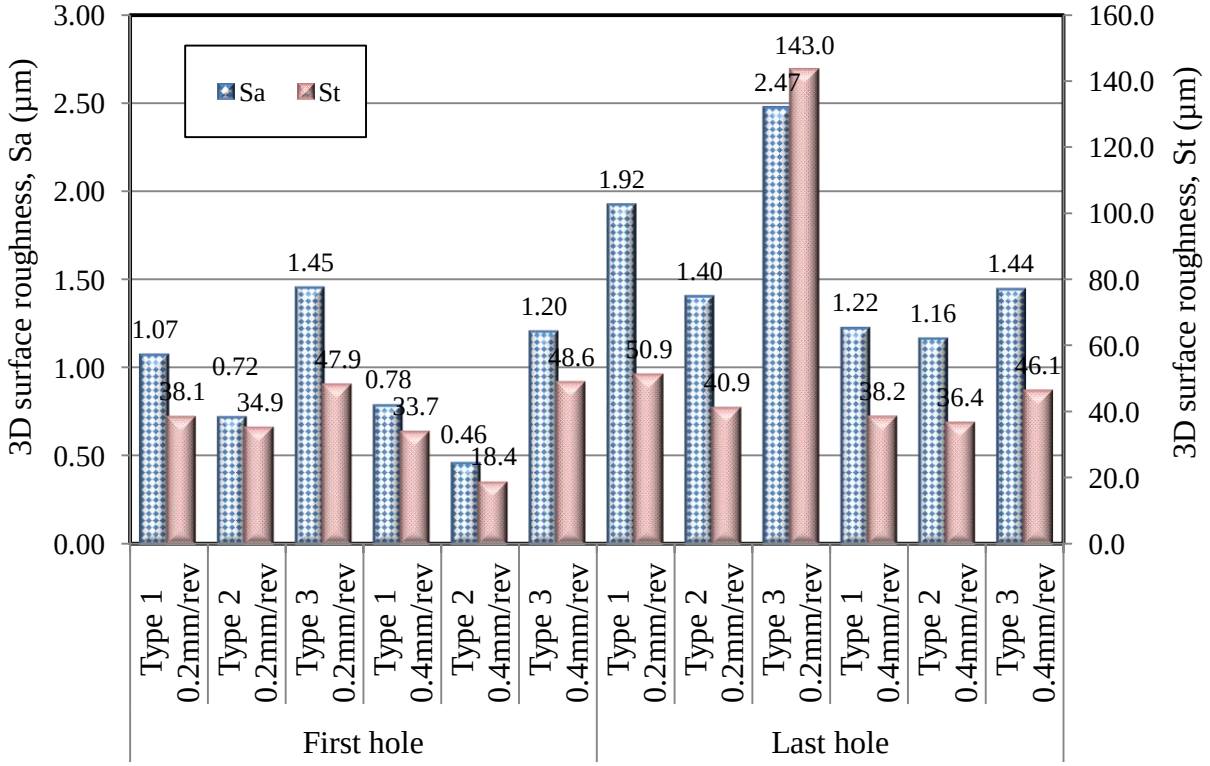


Figure 4.61: Surface roughness (Sa and St) results at the first and last hole in for all tests

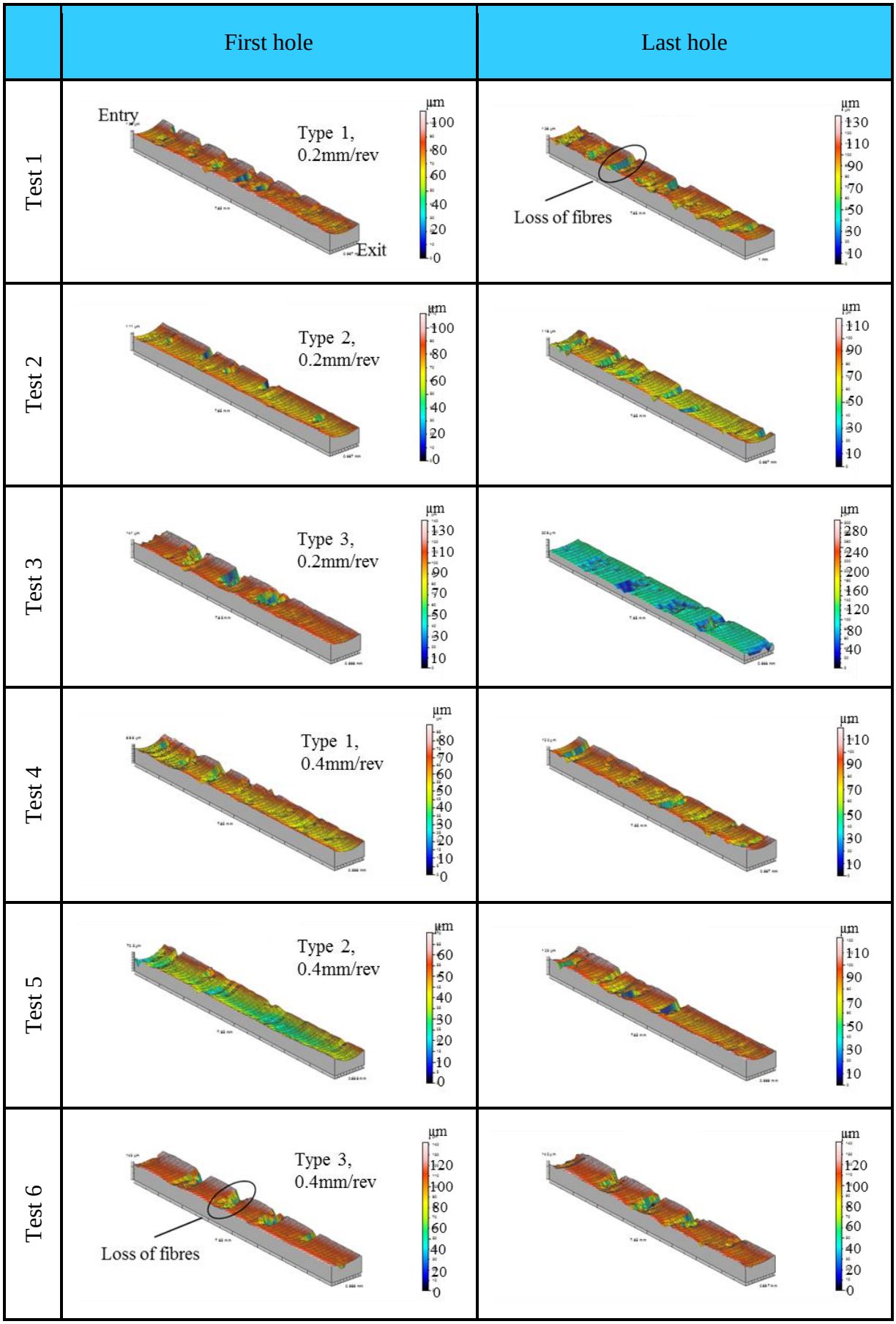


Figure 4.62: Three dimensional (3D) topography maps for the first and last holes in all tests

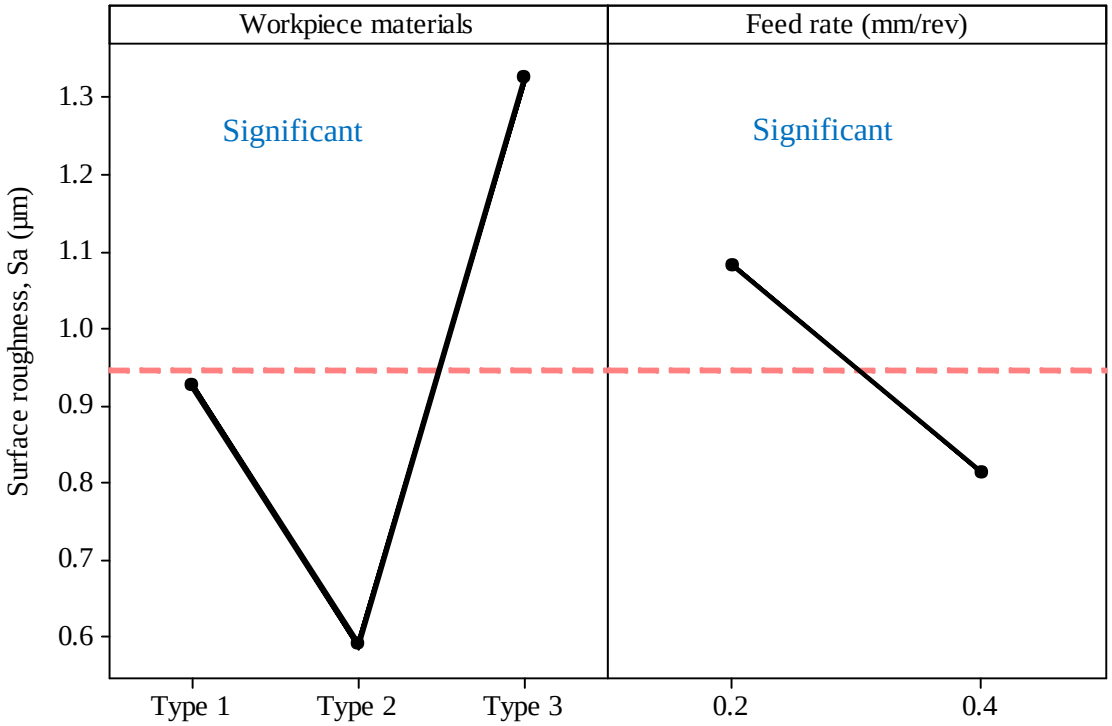


Figure 4.63: Main effects plot for surface roughness (Sa) at the first hole

Table 4.5: ANOVA results for surface roughness (Sa) at the first hole

Source	DF	Seq SS	Adj MS	F	P	PCR
Workpiece materials	2	0.54800	0.27400	1389.7	0.001*	83.7%
Feed rate	1	0.10587	0.10587	537.0	0.002*	16.2%
Error	2	0.00039	0.00020			0.1%
Total	5	0.65426				

4.4.6 Hole size, out of roundness and cylindricity

Figure 4.64 shows the variation in hole diameter against number of drilled holes. In general, all tests produced oversized holes (>6.38 mm) with the maximum deviation from the nominal diameter at test cessation up to 10 µm. The difference in diameter of the last holes between all trials was in line with tool wear results. The influence of feed rate and material type on hole diameter was also largely marginal.

Figures 4.65 and 4.66 detail the average out of roundness and cylindricity measurements at intervals of 128 holes. In general, both the roundness and cylindricity levels showed a rising trend with the number of drilled holes, due to increasing tool wear. Average

out of roundness however did not exceed 20 µm even after drilling 384 holes in any of the trials. Hole cylindricity results were similar, with values of ~15 µm recorded for the first hole, which increased to ~23 µm at test cessation. Variation in feed rate and composite type did not appear to have any significant influence on both out of roundness and cylindricity.

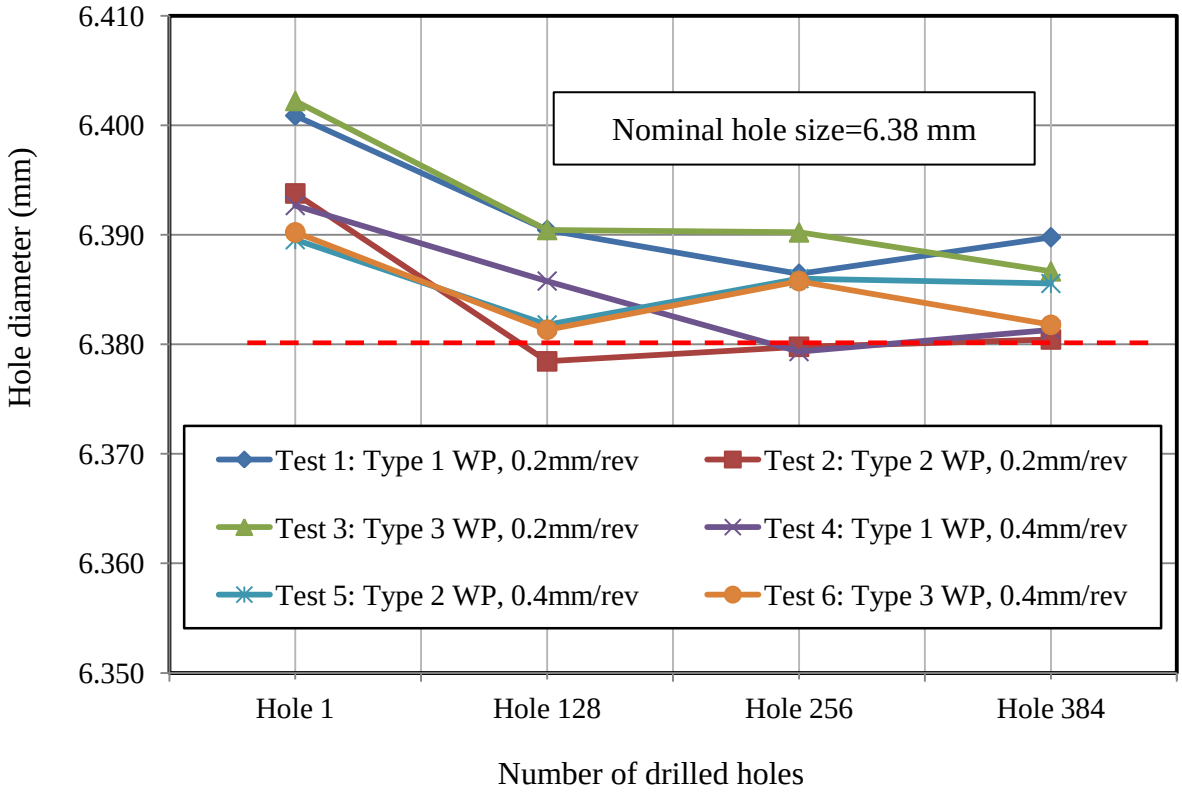


Figure 4.64: Hole diameter variation against number of drilled holes

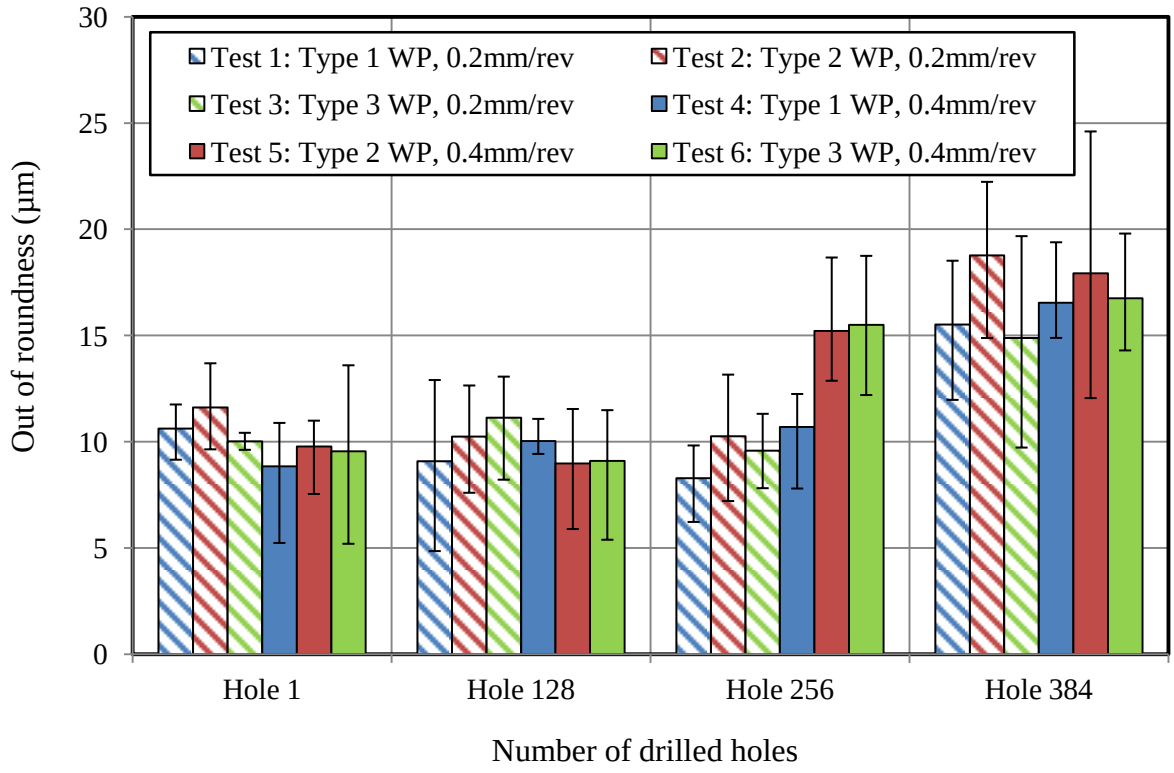


Figure 4.65: Out of roundness results against number of drilled holes

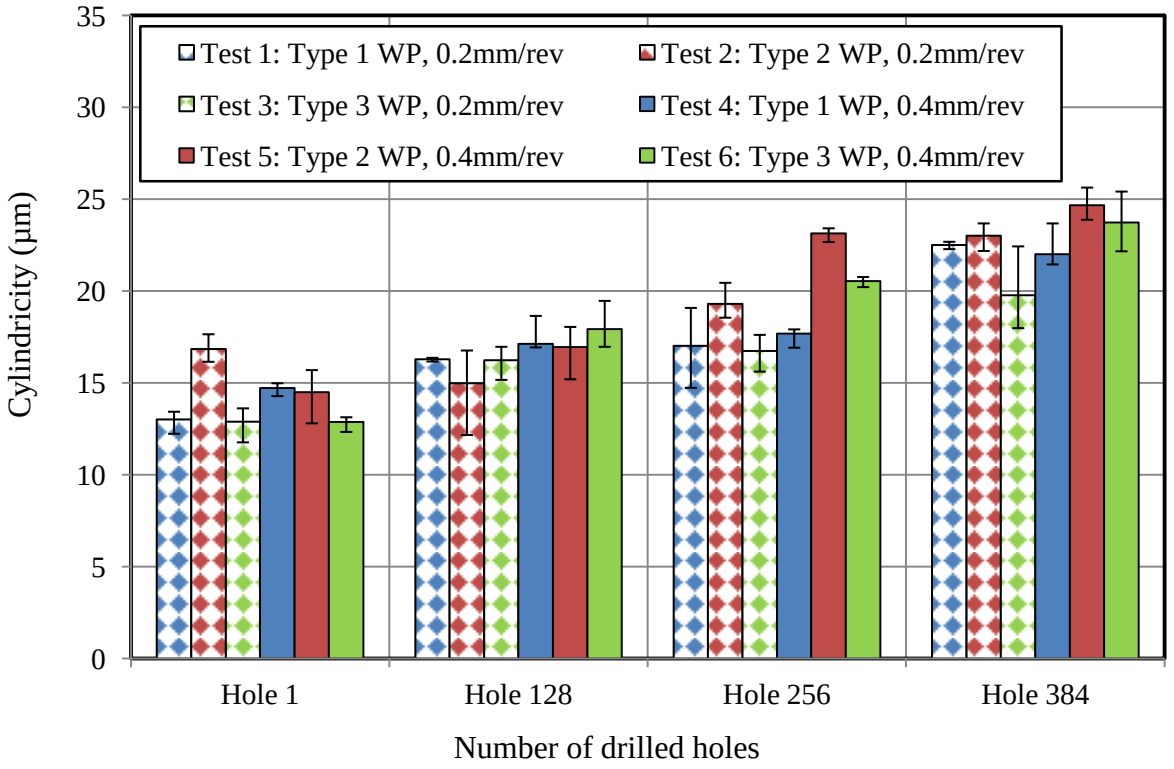


Figure 4.66: Cylindricity results against number of drilled holes

4.4.7 Hole surface integrity analysis

Figure 4.67 presents SEM micrographs of cross sectioned hole surfaces for the first holes drilled at a feed rate of 0.4 mm/rev (Tests 4-6). Cavities / damage were mainly concentrated at plies with 135º orientation while those at 0º, 45º and 90º were generally free of damage for the sections analysed. Defects were typically caused by fibre loss / pull out, which were significantly more adverse in tests involving Type 3 workpieces, due to the presence of adjacent 135º plies. Reducing feed rate to 0.01mm/rev towards the exit location significantly improved hole surface quality in terms of eliminating cavities / fibre pull out, which was attributed to the lower thrust force generated together with a ploughing / polishing effect resulting from the extended tool-workpiece contact time.

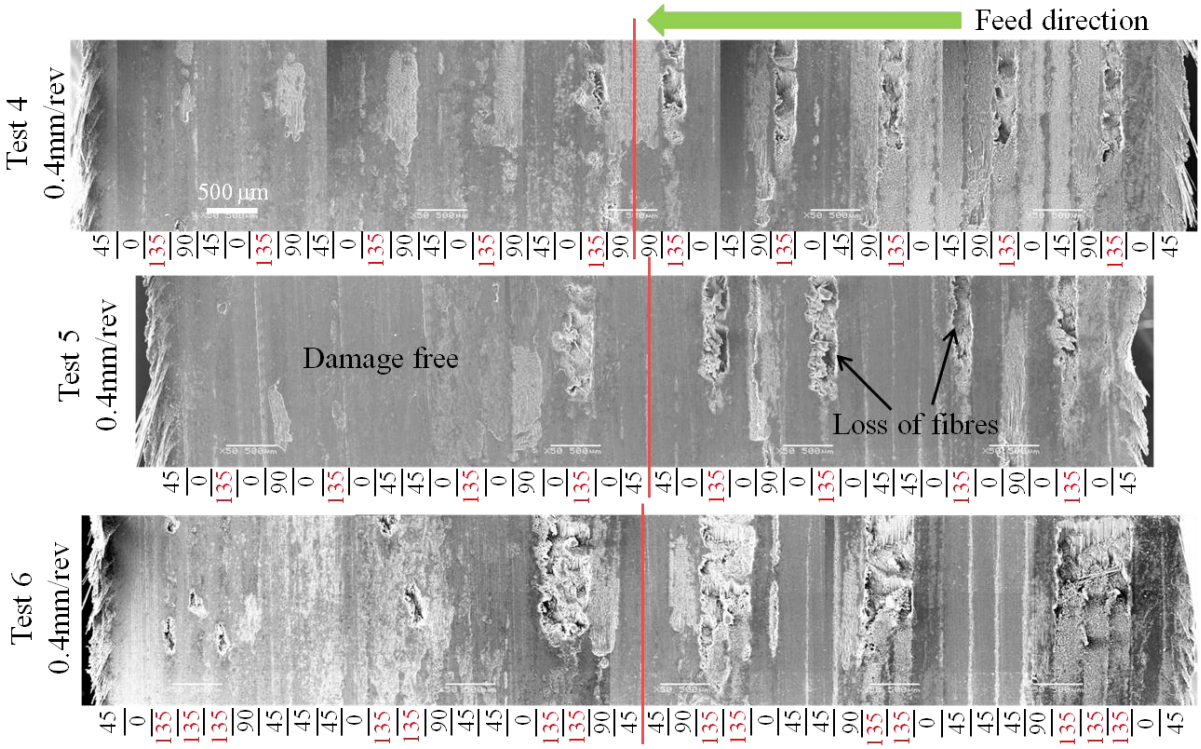


Figure 4.67: SEM micrographs of the first hole surfaces drilled at a feed rate of 0.4 mm/rev

Corresponding SEM micrographs of surfaces on the last hole (hole 384) drilled at 0.4 mm/rev are shown in Figure 4.68. In addition to increased levels of damage, fibre loss / cavities were also evident at the exit location despite the reduced feed rate (0.01mm/rev), which suggests that tool wear / edge sharpness was the dominant factor affecting hole surface quality.

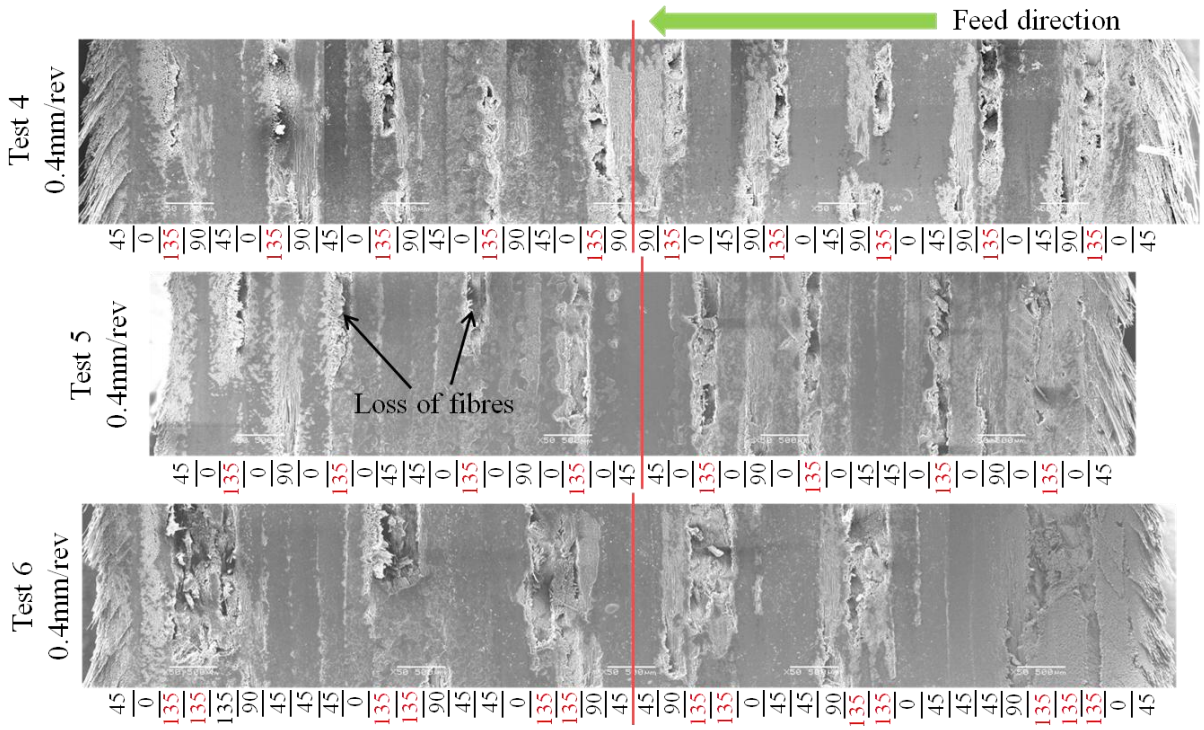


Figure 4.68: SEM micrographs of the last hole surfaces drilled at a feed rate of 0.4 mm/rev

Typical hole surface damage in terms of fibre pull out was further analysed via higher magnification SEM microscopy, see Figure 4.69 showing the machined surface at ply / fibre orientations of 0º and 135º respectively. Schematics of the cutting mechanisms when machining CFRP at specific fibre orientations are detailed in Figure 4.70. Generally, when machining fibres at 0º orientation, 'peeling' of the laminates occurs due to buckling, which slides up the tool rake face leading to limited / marginal defects. Fibre fracture initiating at the tool point (without elastic bending) is prevalent for plies in the 45º and 90º orientations, resulting comparably smooth surface. In contrast, fibres in the 135º direction are typically subjected to intense elastic bending caused by the cutting edge being pressed against the fibres. As the pressure exceeds the strength of the fibres, fracture occurrs below the cutting plane followed by elastic recovery, which generates a stepped surface [4]. Understandably, high feed rates and worn tools with large cutting edge radii generally exacerbate damage at the 135º orientated plies.

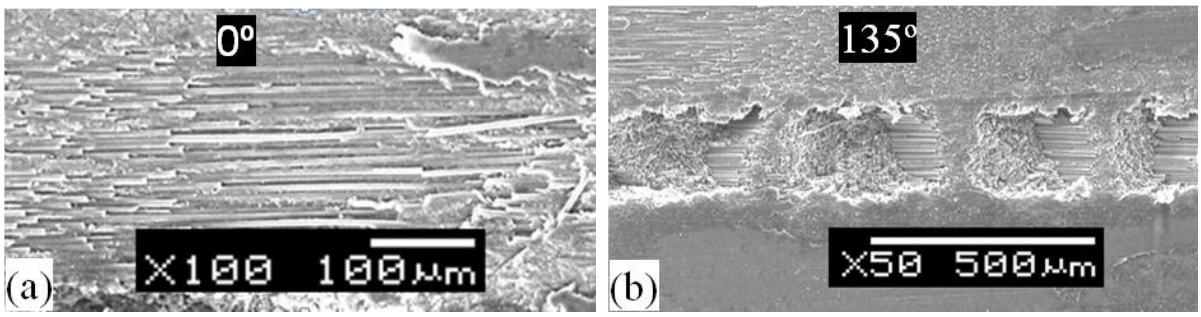


Figure 4.69: Sample SEM micrographs of the first hole in Test 1 at ply / fibre orientation of (a) 0º and (b) 135º

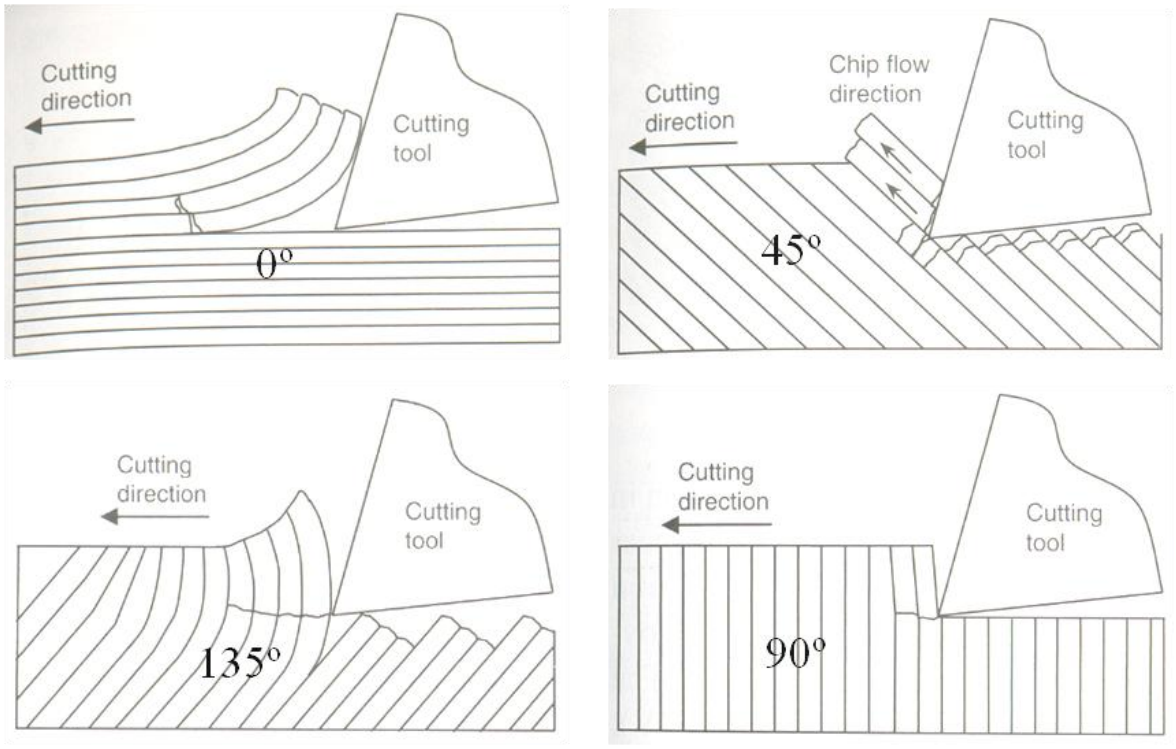
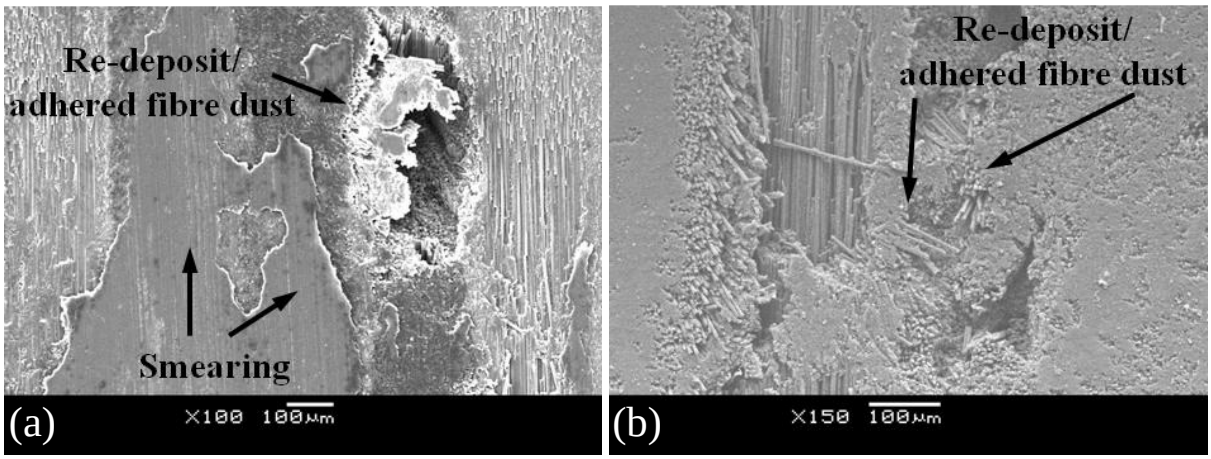
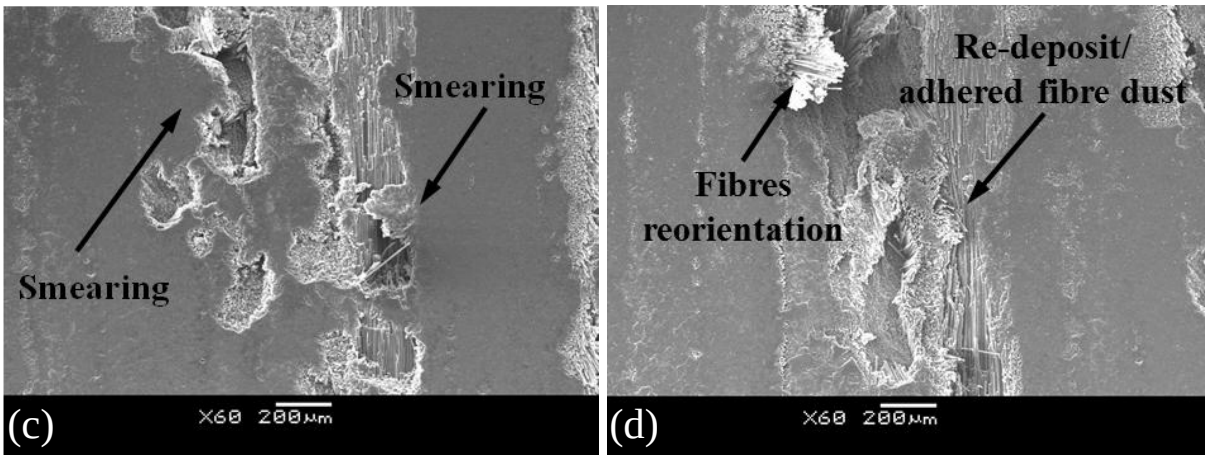


Figure 4.70: Cutting mechanism in machining of CFRP at various ply / fibre orientations [4]

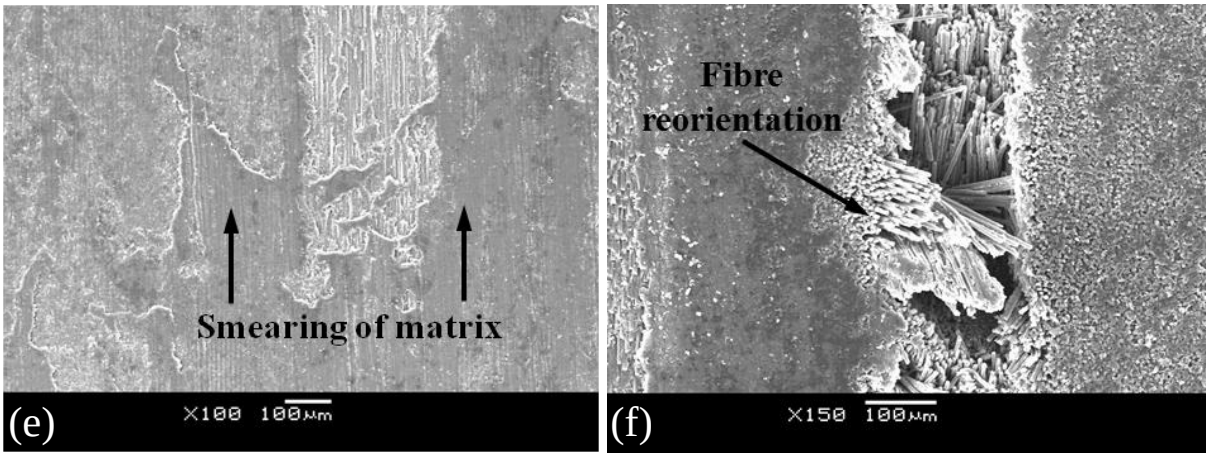
High resolution SEM micrographs of hole surfaces near the exit location (feed rate of 0.01 mm/rev) in selected tests are shown in Figure 4.71. In general, smearing of the matrix material (epoxy resin) and re-deposited / adhered fibre dust were prevalent in both first and last holes. This was most likely due to increased rubbing resulting from the prolonged contact time between the drill and hole surface when operating at the reduced feed rate. Fibre reorientation was also observed in the vicinity of the surface cavities, which was possibly due to bending and ploughing effects during the drilling process.



(a) First hole in Test 1 (Type 1 WP, 0.2mm/rev) (b) Last hole (hole 384) in Test 1



(c, d) Last hole (hole 384) in Test 3 (Type 3 WP, 0.2mm/rev)



(e, f) First hole in Test 5 (Type 2 WP, 0.4mm/rev)

Figure 4.71: Sample SEM micrographs at hole exit location under reduced feed rate operation (0.01 mm/rev)

4.5 Phase 2C: Evaluation of diamond coated and domed PCD tools when drilling CFRP at elevated / high cutting speeds

4.5.1 Tool wear and life

When operating at a cutting speed of 360 m/min, the CVD-diamond coated drill experienced catastrophic failure / fracture upon entry into the third hole, as shown in Figure 4.72. Drill fracture occurred towards the end of the cutting flutes (Figure 4.72(b)), which was possibly due to chatter / vibration at high rotational speed and tool deflection as well as the high thrust force (612 N) and torque (178 N.cm) levels. In contrast, the domed PCD drill showed gradual flank wear progressing up to 71 µm after 384 holes. This was most likely attributed to the shorter tool over-hang (~42 mm vs. 56 mm) as well as the superior cutting edge sharpness (4.6 µm cutting edge radius) and wear resistance of the PCD tool. Furthermore, torque in the first hole was ~75% lower when employing the domed PCD drill at a cutting speed of 360 m/min.

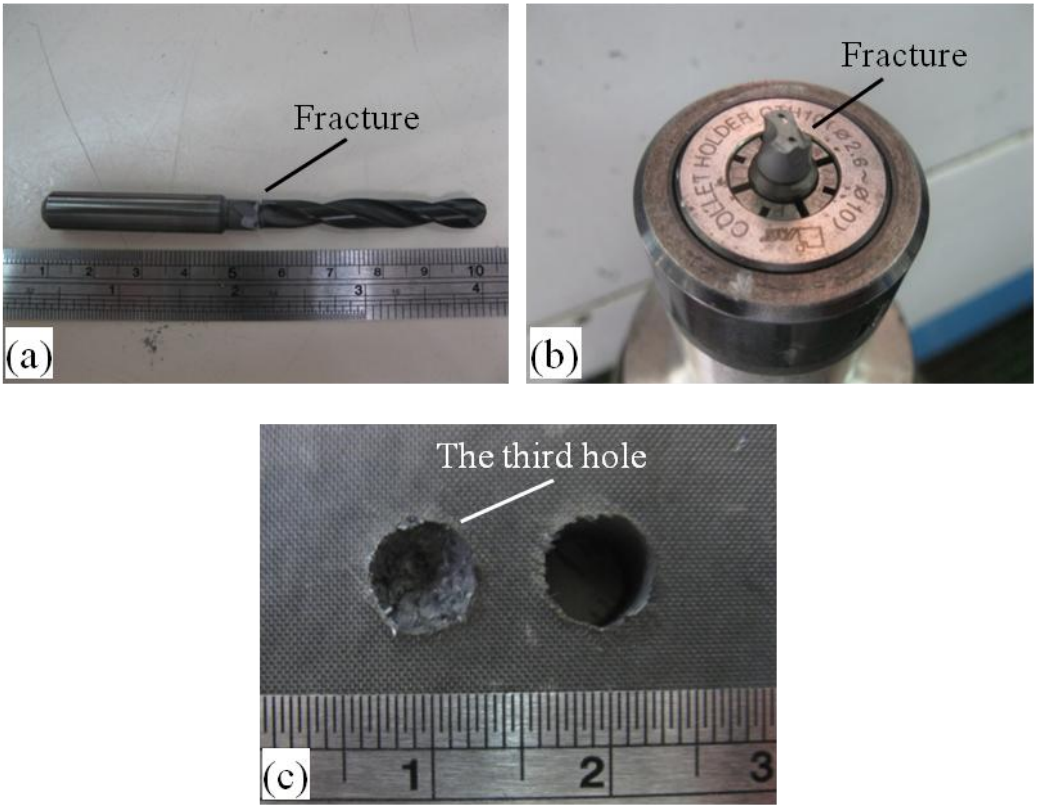


Figure 4.72: Tool fracture in (a) overview, (b) end view and (c) picture of the third drilled hole

Figure 4.73 shows tool wear scar images of CVD-diamond coated and domed PCD drills at test cessation after drilling at 280 (Test 3) and 360 m/min (Test 6) respectively. The

principal wear mode was abrasion / cutting edge rounding for both tool materials with no evidence of chipping. Maximum flank wear results for all trials are detailed in Figure 4.74, while the tool wear progression against number of drilled holes is outlined in Appendix C (Figure C3). In general, drill flank wear decreased with increasing cutting speed, where flank wear of the CVD-diamond coated drills at test cessation varied from 117 µm in Test 1 (180 m/min) to 86 µm in Test 3 (280 m/min). Similarly, flank wear of the domed PCD drills after 384 holes was ~10% lower when operating at 360 m/min compared to 180 m/min.

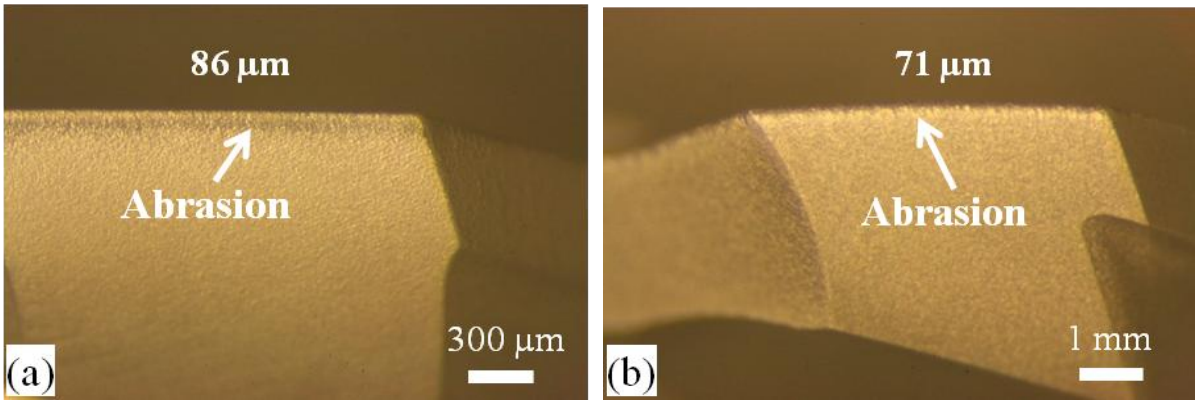


Figure 4.73: Tool wear scar at the cutting speed of (a) 280 m/min with diamond coated tool and (b) 360 m/min with domed PCD tool

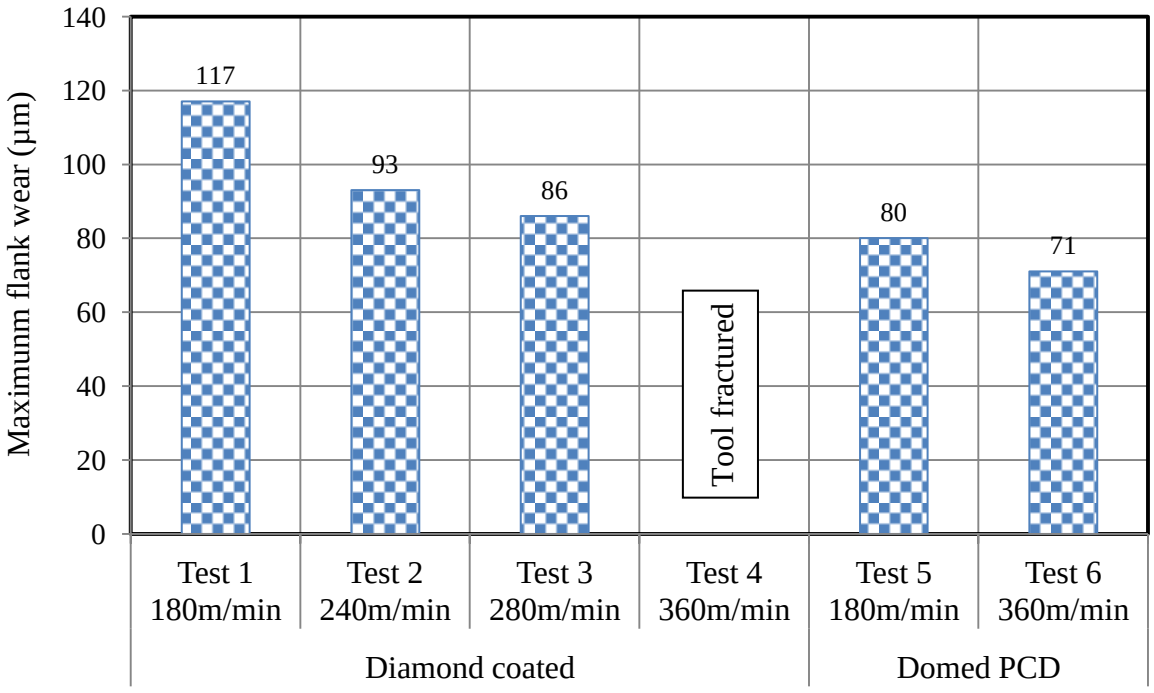


Figure 4.74: Maximum flank wear values at test cessation in all tests

4.5.2 Thrust force and torque

Figure 4.75 displays maximum the thrust force and torque results at the first and last holes in all trials, while the associated progression curves are detailed in Appendix C (Figure C4). For the first hole, both thrust force and torque values generally increased with cutting speed irrespective of tool materials. This was most likely due to elevated chatter / vibration and tool deflection. At the cutting speed of 360 m/min, thrust forces / torque in the first hole increased by 92.7% / 433% and 87.8% / 131.5% when drilling with CVD-diamond coated WC and domed PCD drills respectively, in comparison to tests at 180 m/min. However, no apparent trend in thrust force and torque variation was observed for the last holes drilled using the CVD-diamond coated tools, although thrust forces in Test 3 were lower (by up to 73N) compared to results in Test 1 (180 m/min). Despite lower tool wear levels, thrust force and torque were up to ~20% higher when using domed PCD drills over the CVD-diamond coated WC tools at test cessation. This was likely attributed to the tendency of fibre dust adhering onto the flutes of the PCD drills, thereby hindering swarf extraction, see Figure 4.76.

Typical / sample thrust force and torque signal profiles obtained when drilling CFRP at cutting speeds >180 m/min are shown in Figure 4.77. Signs of chatter / vibration was evident when utilising CVD-diamond coated WC drills in both Tests 2 (240 m/min) and 3 (280 m/min), see Figures 4.77(a) and 4.77(b), which was possibly a consequence of high tool wear levels / large initial cutting edge radius (23.8 µm). A ‘ringing’ sound was also audible during drilling but which gradually dissipated as the trial progressed, in line with the signals recorded at test cessation, see Figure 4.77(b). This was not present in trials involving domed PCD tools even at the higher cutting speed of 360 m/min, see Figures 4.77(c) and 4.77(d). Thrust forces however showed a decrease trend as the drill progressed deeper into a hole, which was likely due to a reduced flow of chilled air towards the bottom of the workpiece, leading to possible degradation in workpiece strength.

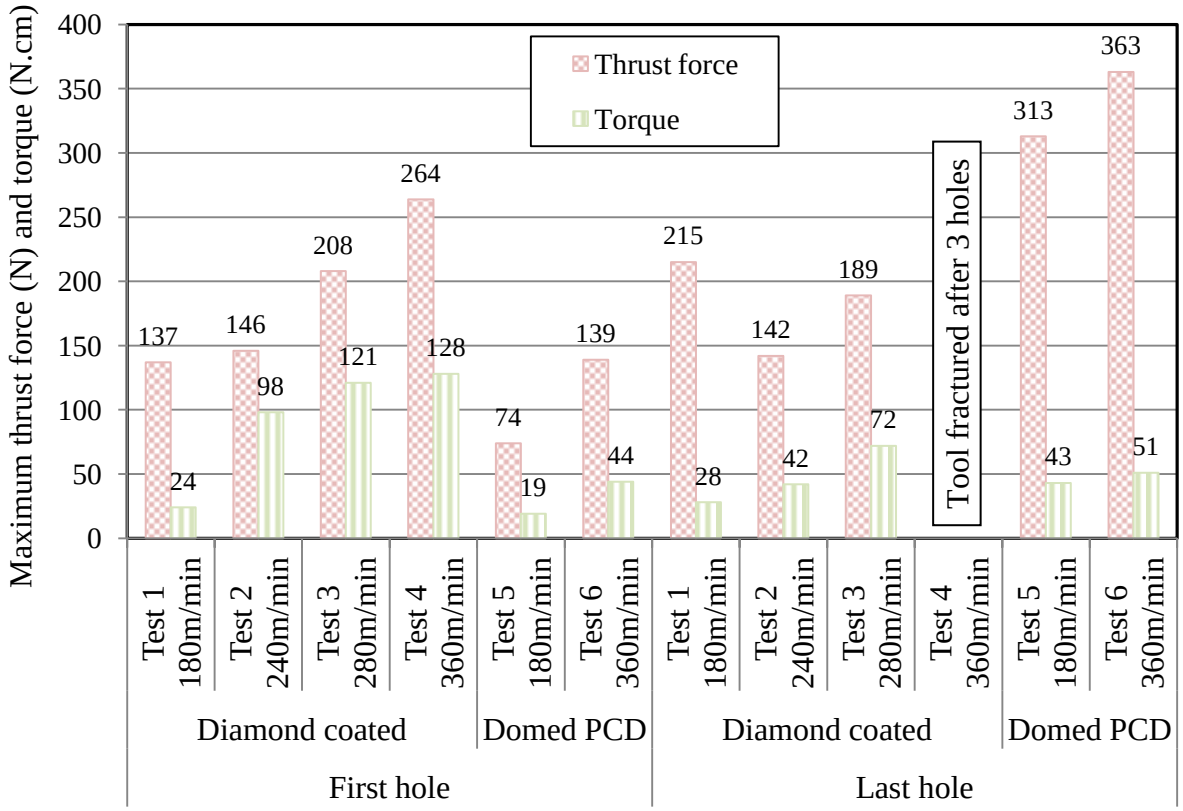


Figure 4.75: Maximum thrust force and torque values recorded at the first and last holes in all tests

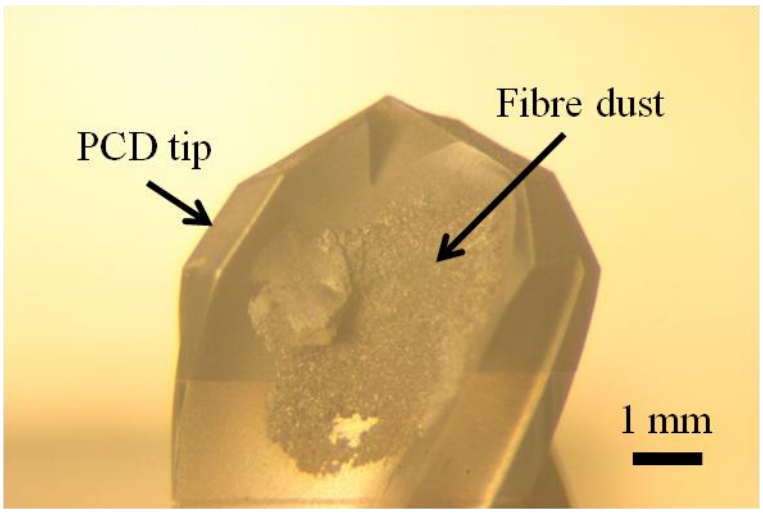
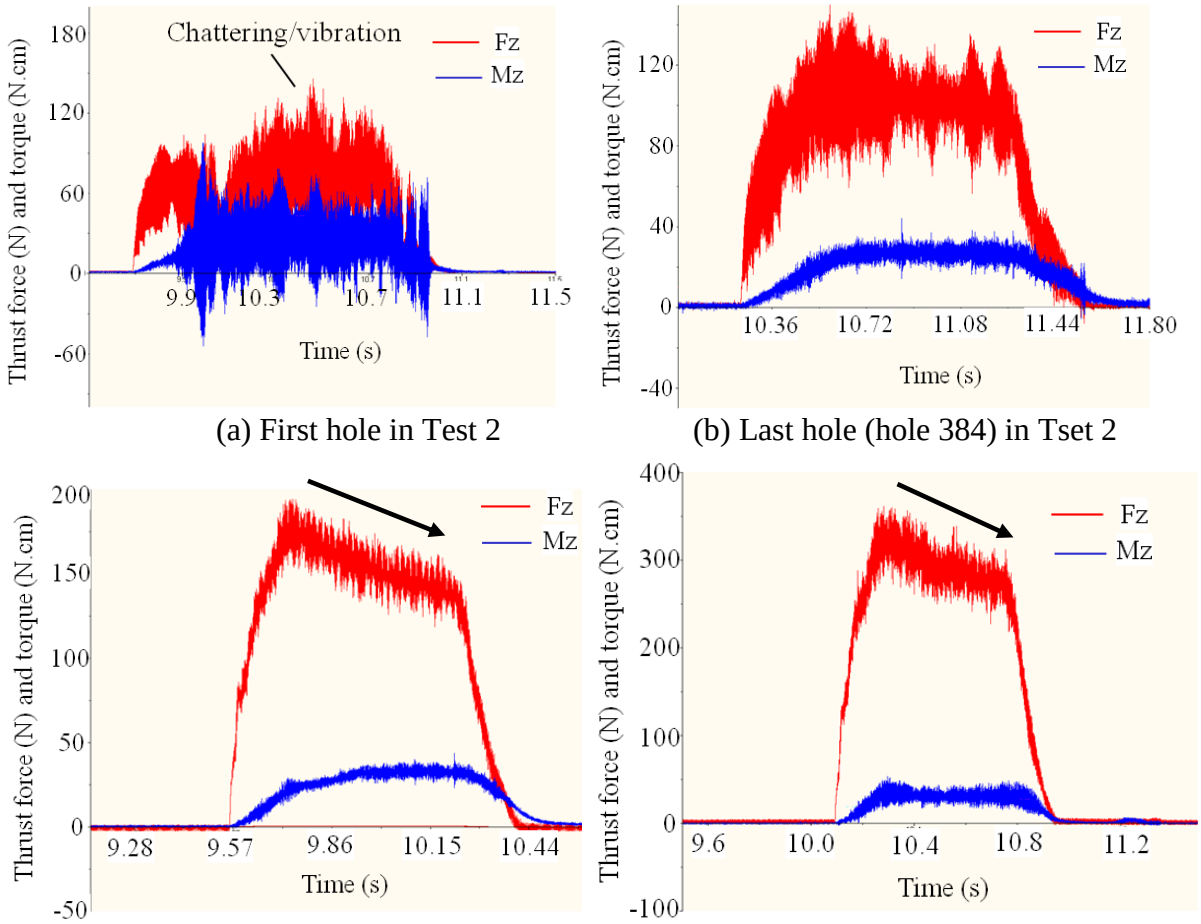


Figure 4.76: Micrograph showing fibre dust adhering to drill flute



(a) First hole in Test 2 (b) Last hole (hole 384) in Tset 2

(c) Hole 64 in Test 6 (d) Last hole (hole 384) in Test 6

Figure 4.77: Thrust force and torque profiles recorded at various cutting conditions

4.5.3 Hole entry and exit quality

Figure 4.78 details hole entry and exit for the first and last holes in all trials. The holes drilled with new domed PCD tools showed superior edge quality at both the entry and exit positions, which attributed to the low thrust force levels (<140N) and sharp cutting edge. Except for Test 4, only minor damage in the form of delamination and uncut fibres were observed at the entrance of the last hole drilled, which was due to the increasing flank wear / cutting edge radius and thrust force levels as drilling progressed. For trials utilising the CVD-diamond coated tools, uncut fibres were apparent at the exit location even from the first hole, irrespective of the cutting speed, although the damage was marginally more severe in Test 1 (180 m/min). Similarly, uncut fibres and minor delamination was also evident at the exit of the last holes drilled with the domed PCD tools.

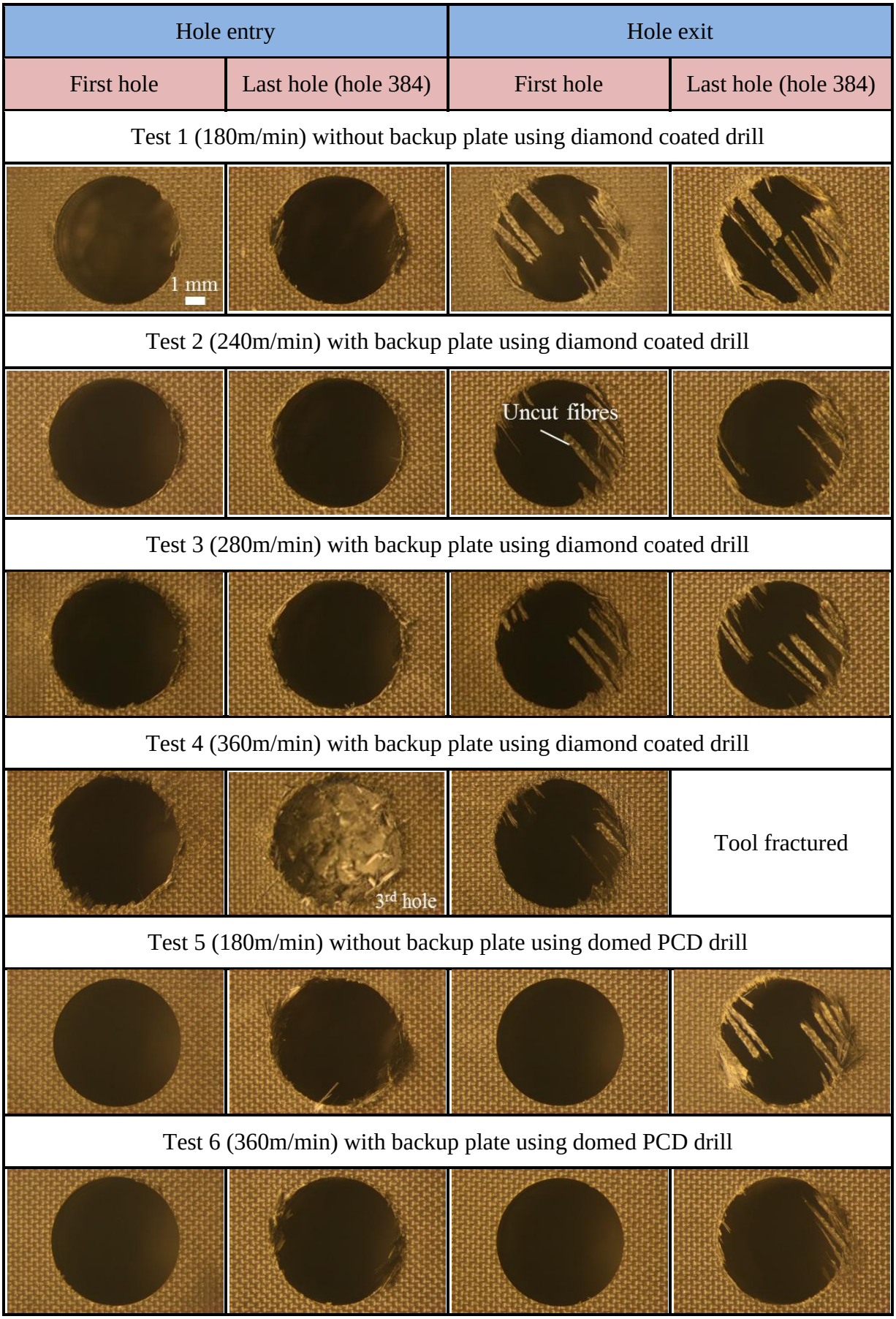


Figure 4.78: Hole entry and exit quality for the first and last holes in all tests

4.5.4 Hole roundness and cylindricity

Figure 4.79 presents out of roundness and cylindricity data for the first and last holes drilled in all trials. Both parameters were found to increase with cutting speed even in the first hole irrespective of tool material, possibly due to drill run out / deflection being more pronounced at elevated rotational speeds. This was similarly observed for the last holes produced with the CVD-diamond coated drills. In general, the domed PCD drills generated holes with significantly superior form accuracy, with out of roundness and cylindricity of the first hole not exceeding 10 and 13 µm respectively. In contrast, corresponding holes machined with CVD-diamond coated WC drills at 280 m/min showed an out of roundness of 68.98 µm and cylindricity of 79.68 µm. Selected hole roundness (measured near hole entrance) and cylindricity profiles at test cessation is detailed in Figure 4.80. Holes with typical gear / wave profiles were observed when using CVD-diamond coated WC tools, which was likely the result of process chatter / vibration seen previously in the thrust force and torque signals. In addition, the majority of holes machined with the diamond coated WC drill exhibited a bell-shaped form (larger at the top than the bottom). Conversely, holes drilled using the domed PCD tools, typically demonstrated concentric profiles as well as near cylindrical form / shape, see Figures 4.80(b) and 4.80(e) respectively.

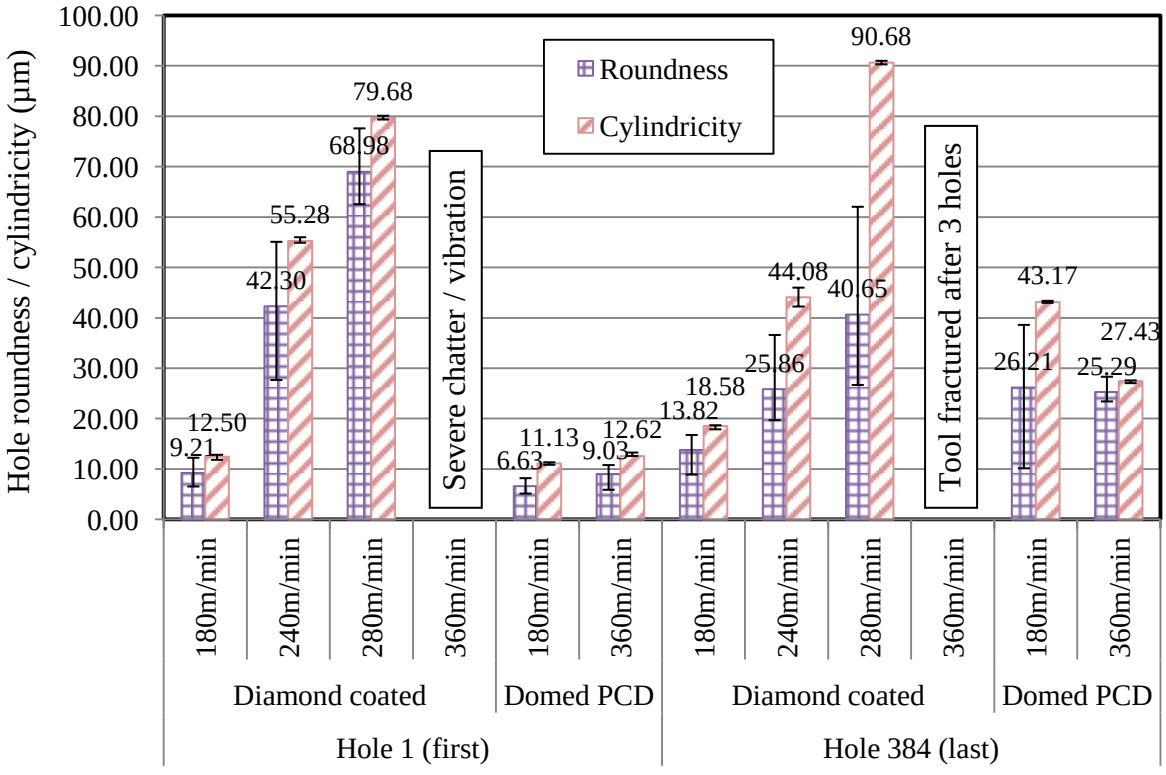
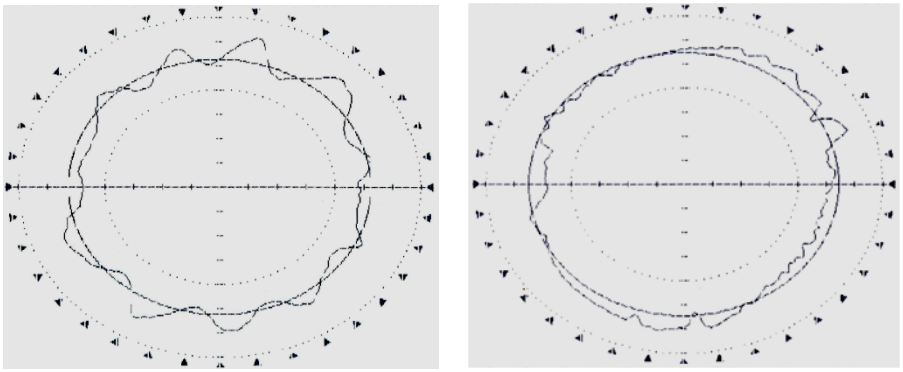
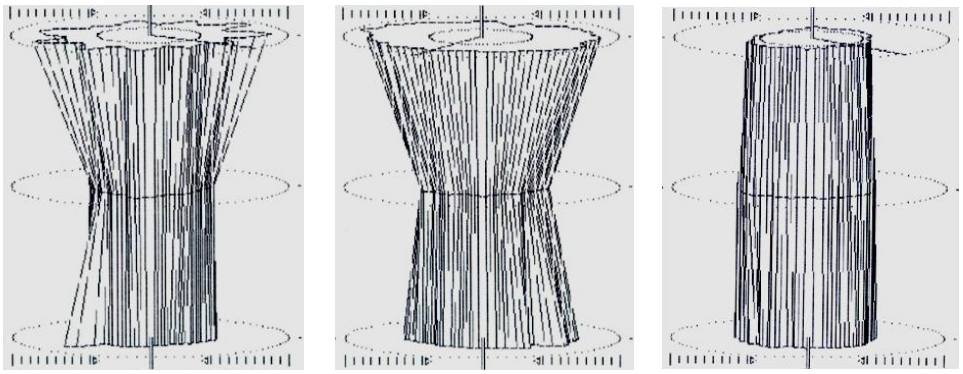


Figure 4.79: Out of roundness and cylindricity values at the first and last holes in all trials



Out of roundness: 30.15 µm 22.25 µm

(a) Test 2 (b) Test 6



Cylindricity: 42.15 µm 90.35 µm 27.25 µm

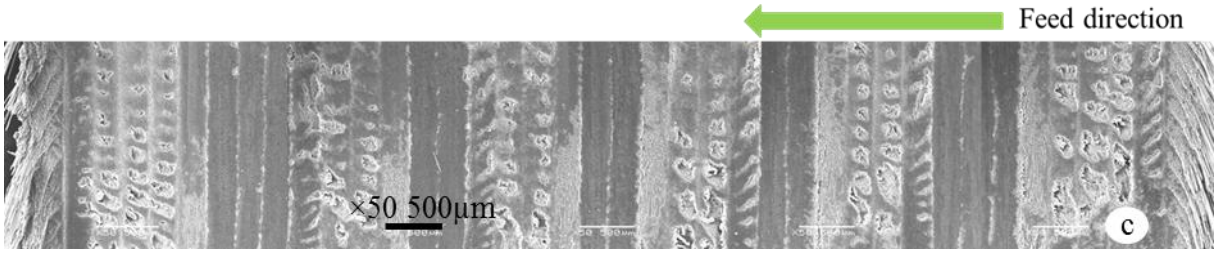
(c) Test 2 (d) Test 3 (e) Test 6

Figure 4.80: Sample out of roundness (1.5 mm beneath hole entrance) and cylindricity profiles measured at last hole (hole 384)

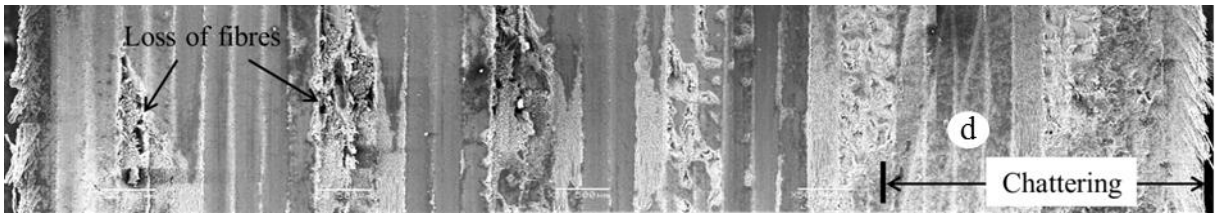
4.5.5 Hole surface integrity analysis

Figure 4.81 shows SEM micrographs of surfaces from the last hole machined with CVD-diamond coated WC drills at cutting speeds of 180 (Test 1) and 240 m/min (Test 2). Similar to results in Phase 2B, cavities / damage typically occurred at plies in the 135º direction. Increasing cutting speed to 240 m/min generally led to cavities / fibre pull out occurring over large areas of the hole. At the hole entry in Test 2 (240 m/min), evidence of chatter / vibration was characterised by the presence of feed marks extending to a length of ~2.5 mm. Figure 4.82 shows high magnification SEM micrographs of hole surfaces drilled using CVD-diamond coated WC tools at various cutting parameters. For both the first and last holes (hole 384), re-deposited / adhered fibre dust was typically observed near the hole entrance when cutting speed was >180 m/min. Conversely, However, fibre dust was largely absent from holes machined with domed PCD drills even at the higher cutting speed of 360 m/min. The difference in surface quality between the first and last holes at the exit location

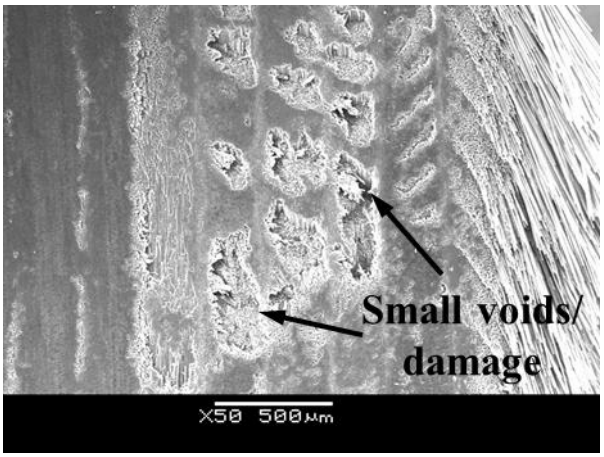
was negligible, as shown in Figures 4.83(a) and 4.83(b), possibly due to the relatively low level of flank wear (86 µm). Minor discontinuous cavities / voids were also observed at entry and exit positions of the first hole drilled with domed PCD tools, which further deteriorated as the trial progressed, see Figures 4.83(c) to 4.83(f).



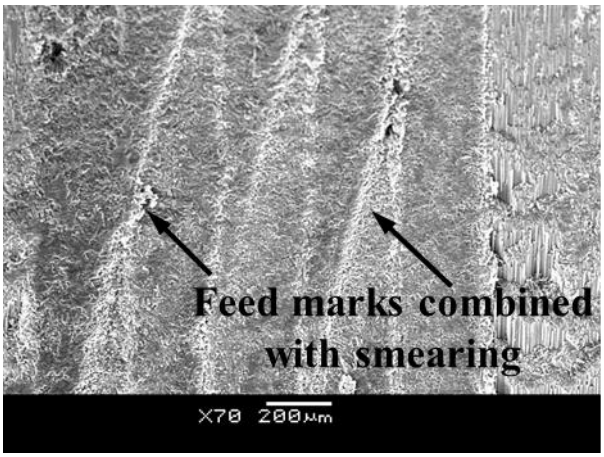
(a) Last hole (hole 384) in Test 1



(b) Last hole (hole 384) in Test 2

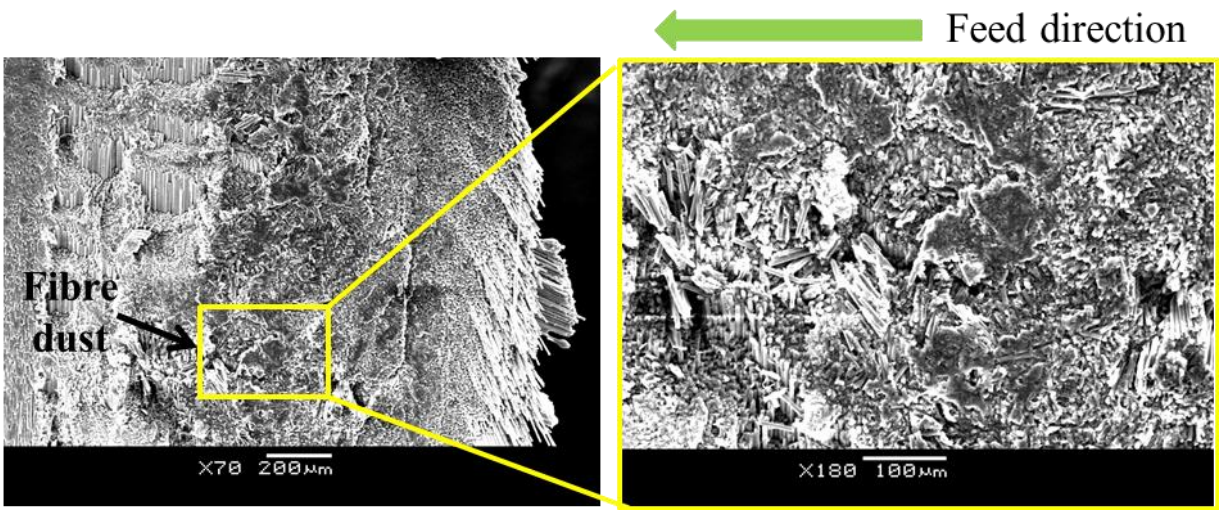


(c) Last hole (hole 384) in Test 1

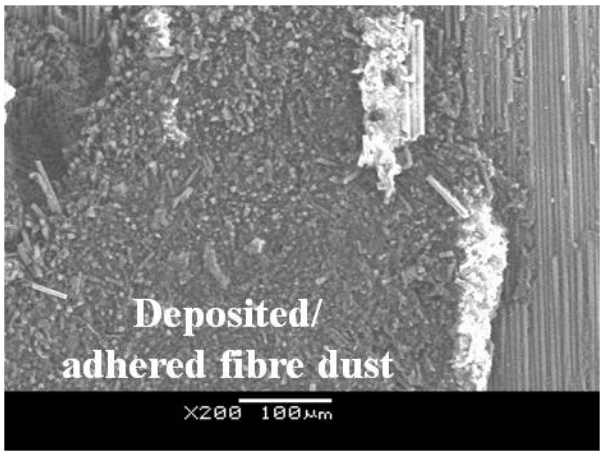


(d) Last hole (hole 384) in Test 2

Figure 4.81: SEM micrographs taken at the last hole (hole 384) in Tests 1 and 2



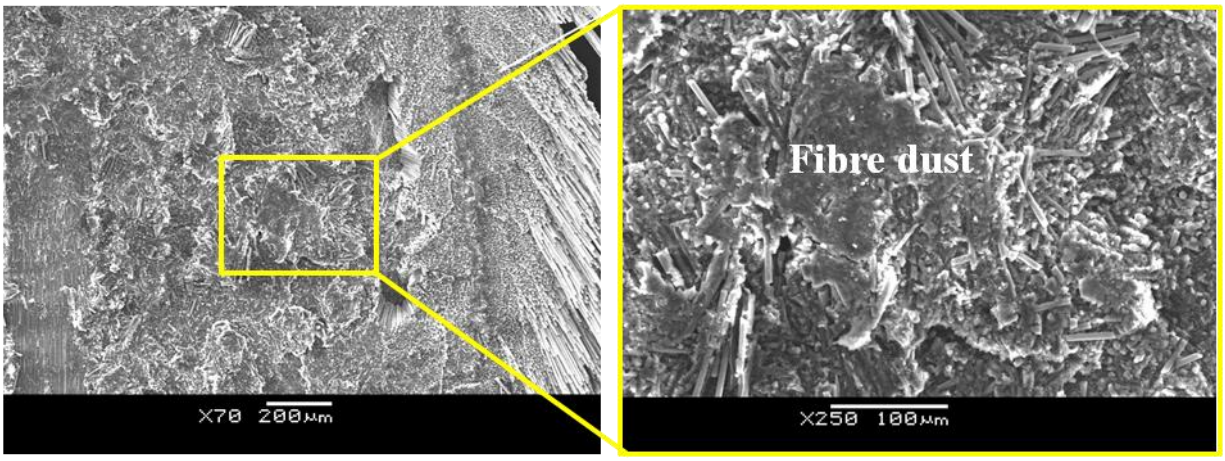
(a) Last hole (hole 384) in Test 2 (240 m/min)



(b) Fist hole in Test 3 (280m/min)

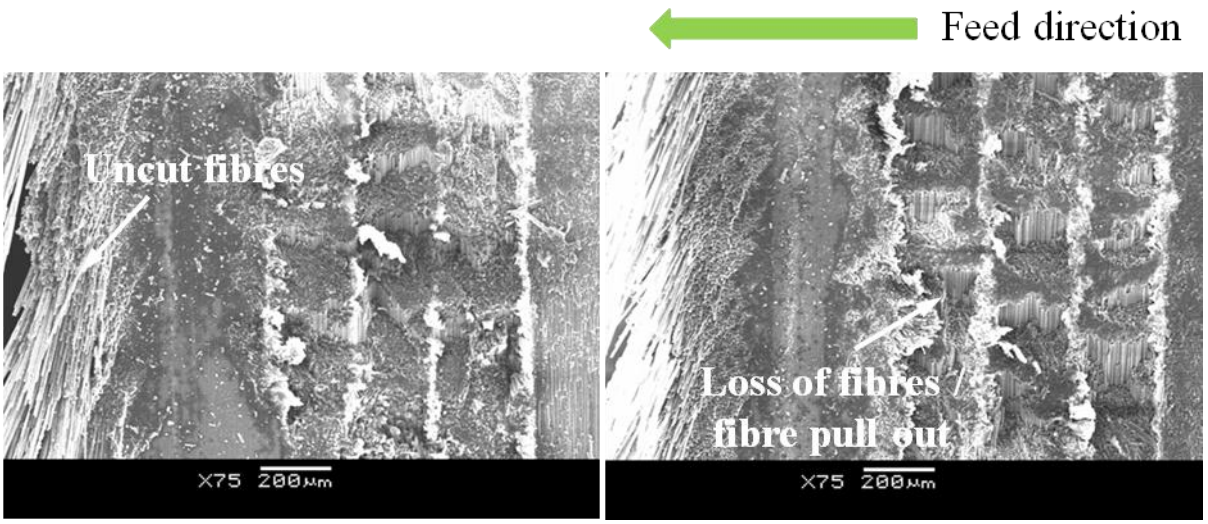


(c) Last hole (hole 384) in Test 3

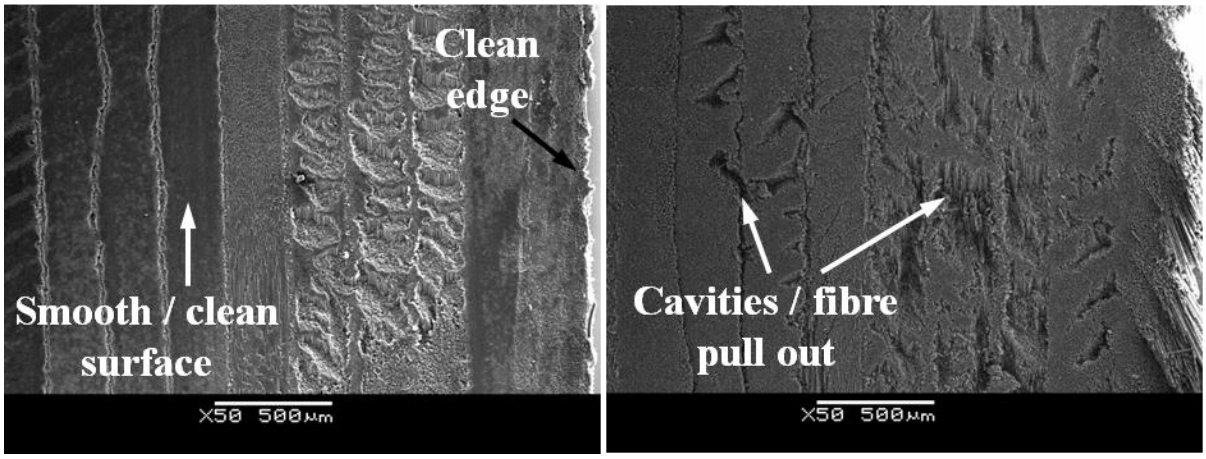


(d) Last hole (hole 384) in Test 3

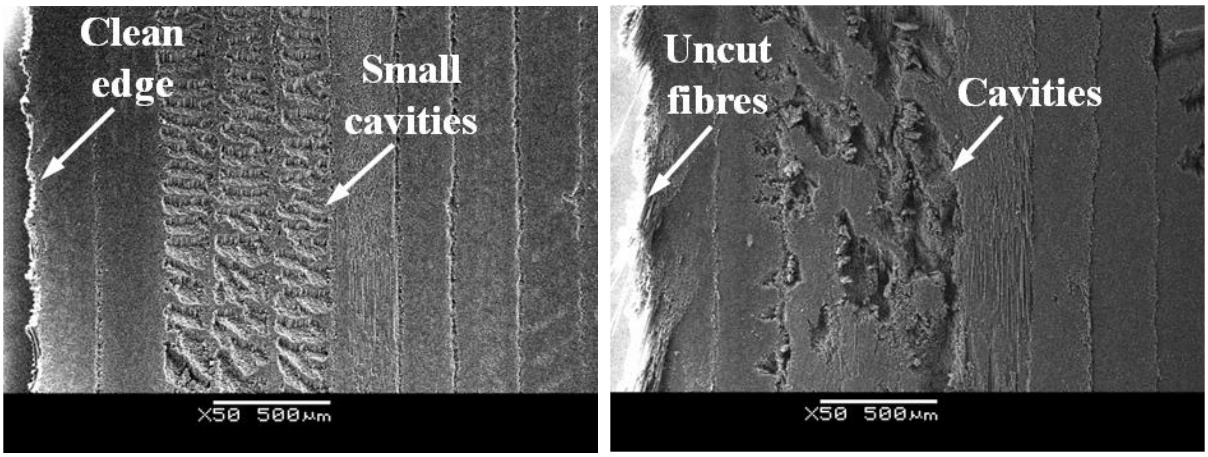
Figure 4.82: Sample SEM micrographs of hole surface machined with CVD-diamond coated tools



(a) First hole exit in Test 3 (280 m/min) (b) Last hole (hole 384) exit in Test 3



(c) First hole entry in Test 6 (360 m/min) (d) Last hole (hole 384) entry in Test 6



(e) First hole exit in Test 6 (360 m/min) (f) Last hole (hole 384) exit in Test 6

Figure 4.83: Sample SEM micrographs of hole entry and exit

4.6 Phase 3A: Preliminary / benchmarking trials in drilling MMCs with different tool materials / coatings

4.6.1 Tool wear and life

Figure 4.84 shows tool flank wear progression against number of holes drilled for all tests. For both uncoated and coated drills, tool life was less than 10 holes (VB_{max} > 300µm) irrespective of operating conditions, although marginally better performance was observed when operating at higher feed rates (0.2 mm/rev in Tests 2 and 4). In contrast, both trials involving the brazed PCD tools produced 300 holes, with corresponding maximum flank wear of 64 µm and 58 µm in Tests 5 and 6 respectively. This was attributed to the significantly higher hardness of PCD (~5,000-8,000HV) providing greater resistance against the abrasive SiC particles compared to the WC and hardmetal coatings (~2,000HV). Additionally, the superior thermal conductivity of PCD (560W/mºC compared to 100W/mºC for K10 WC) was expected to provide more effective heat dissipation from the cutting zone which further extended tool life [144]. For both uncoated and coated WC tools, increasing feed rate reduced tool wear, which was most likely due to lower the contact time between tool and workpiece material.

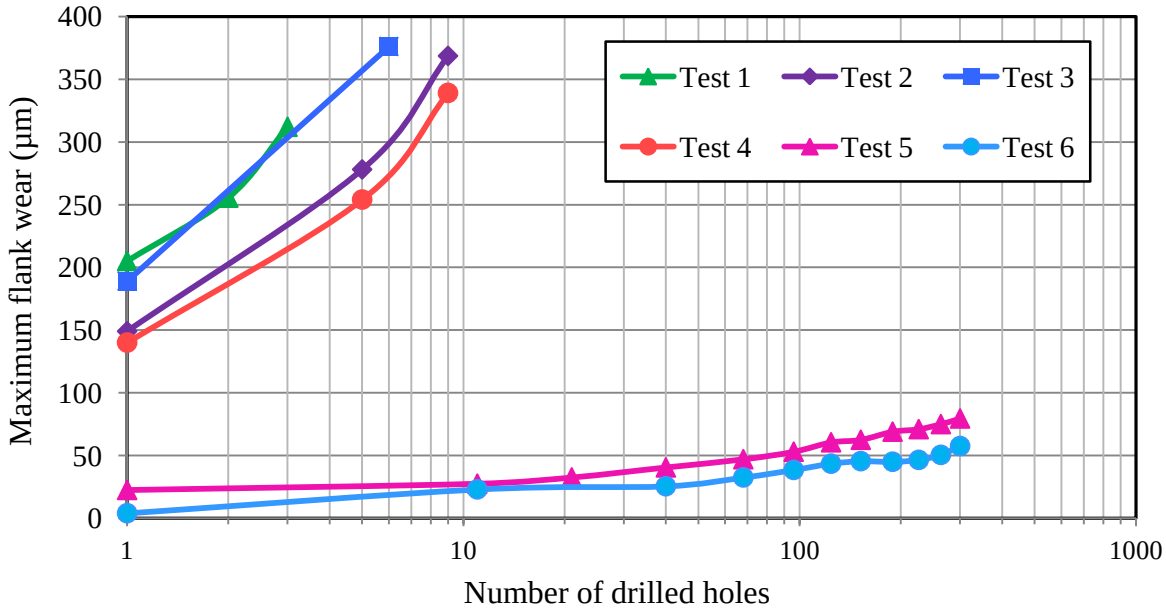


Figure 4.84: Flank wear progression against number of drilled holes in all tests

Figures 4.85 details optical micrographs of drills in the new condition as well as after drilling the first and last holes in all tests. Severe cutting edge rounding and flank wear was observed on the WC drills even after the first hole due to abrasion by the SiC particles. No obvious signs of built up edge or adhered materials was evident on any of the uncoated or coated WC tools, which was most likely due to the use of high pressure through tool coolant

environment. In contrast, considerable workpiece adhesion / BUE was apparent on the PCD drills, which was probably the result of insufficient cutting fluid / lubricant (supplied externally) arriving at the cutting zone. Wear along the cutting edge / flank face of the PCD drills however were found to be relatively uniform following removal of the adhered material / BUE by soaking in 25% NaOH solution for ~1 min, which is shown in Figures 4.86(a) and 4.86(b) for Tests 5 and 6 respectively.

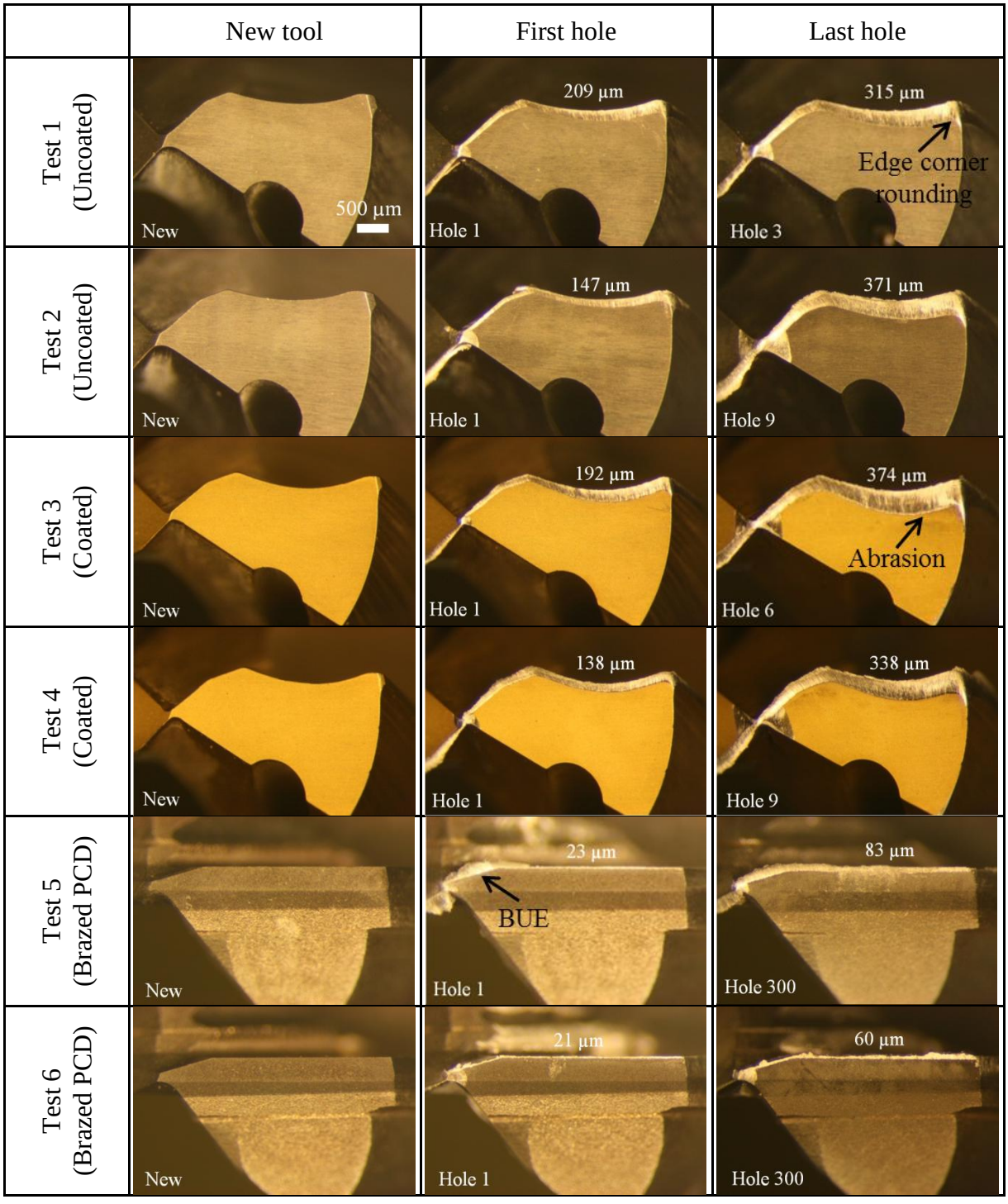


Figure 4.85: Tool wear scar at new tool, the first and last holes (hole 300) in all tests

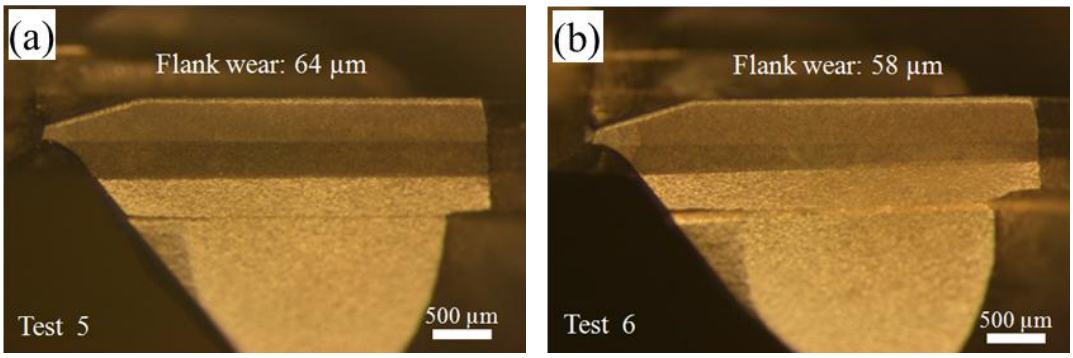
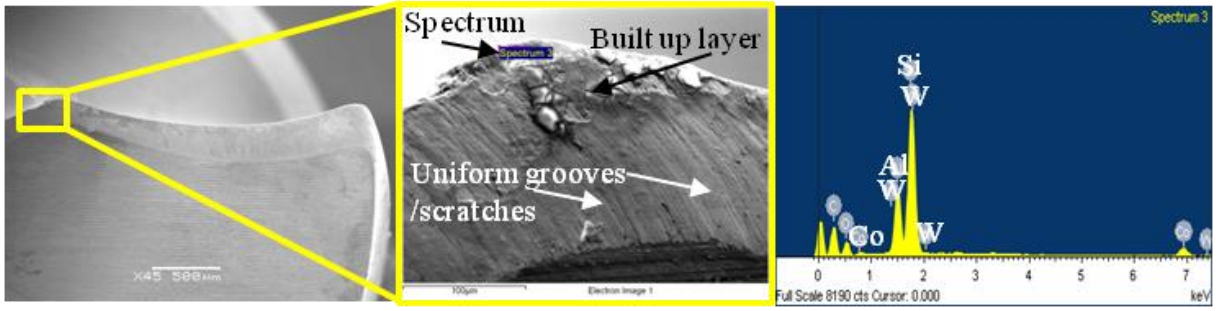
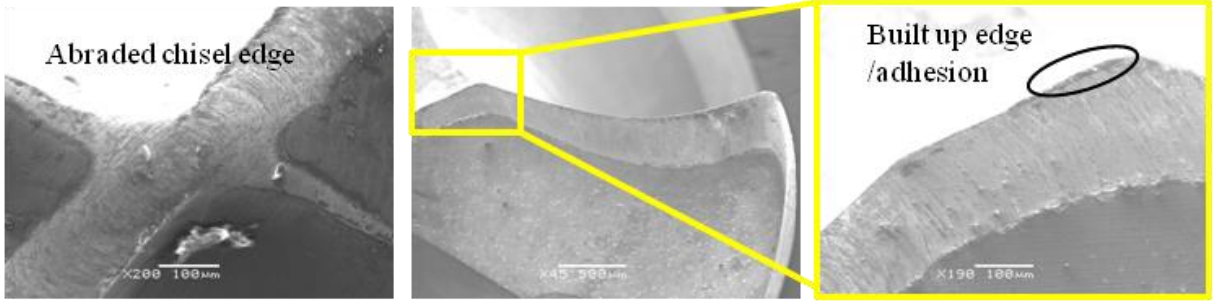


Figure 4.86: Tool wear scar following soaking in 25% NaOH solution to remove the BUE / workpiece adhesion in (a) Test 5 and (b) Test 6

Further in-depth analysis of the uncoated WC drills using SEM revealed the presence of built up layer (BUL) rather than BUE on the cutting edge, which was verified by subsequent EDS measurements, see Figure 4.87(a). Grooves / scratches were prevalent on the tool flank face, which was indicative of abrasion as the primary wear mechanism. Although there was substantially less adhered material on the coated WC tools, the chisel section was shown to be severely abraded / worn, see Figure 4.87(b). No sign of spalling or delamination of the coating however was seen at the boundary between the worn and unworn regions of the drill flank face.



(a) SEM and EDS analysis of uncoated drill in Test 1 (Uncoated / 80 m/min / 0.1 mm/rev)

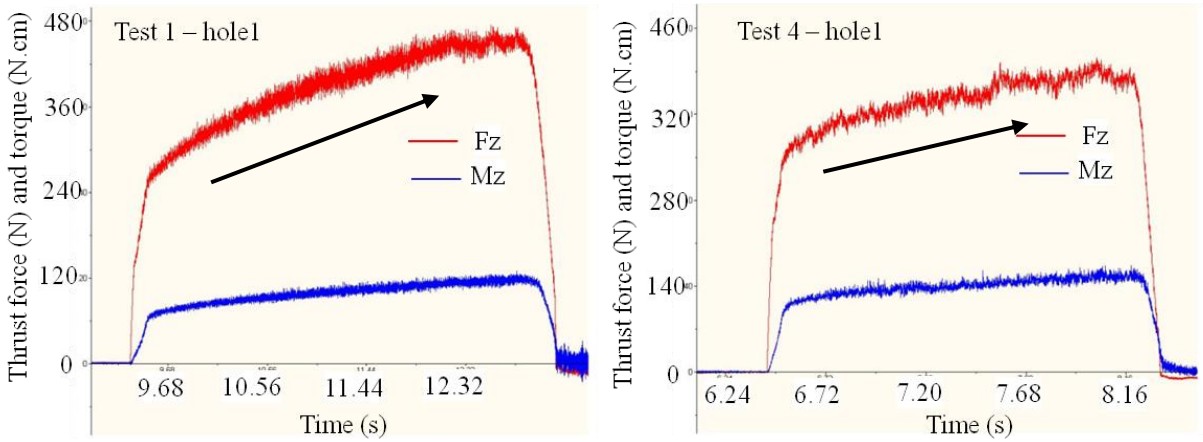


(b) SEM analysis of coated drill in Test 3 (TiAlN+TiN coated / 80 m/min / 0.1 mm/rev)

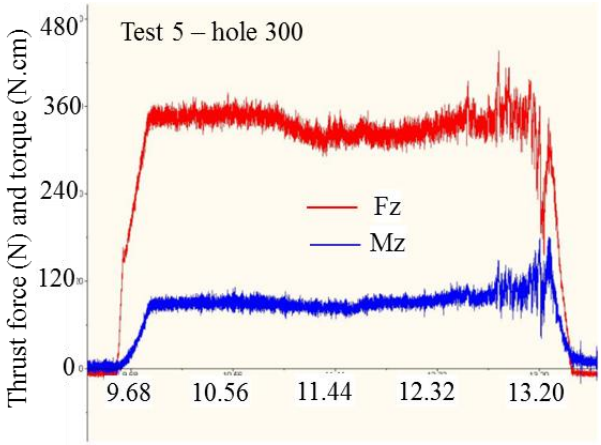
Figure 4.87: SEM and EDS analysis of worn cutting lips for (a) Test 1 and (b) Test 3

4.6.2 Thrust force and torque

For uncoated and coated drills, thrust force and torque significantly increased (up to ~100%) even within the first hole irrespective of drilling conditions, see thrust force and torque profiles for Tests 1 and 4 in Figures 4.88(a) and 4.88(b) respectively. Conversely, the thrust force and torque signals for the domed PCD drills were generally stable, with the minor increase at the hole exit probably due to the lack of coolant / lubricant at this location, see Figure 4.88(c).



(a) First hole in Test 1 (b) First hole in Test 4



(c) Last hole (hole 300) in Test 5

Figure 4.88: Thrust force and torque profiles at various cutting conditions

The evolution of maximum thrust force and torque values against tool life are shown in Figure 4.89. For uncoated and coated WC drills, thrust forces and torque increased rapidly (by up to ~87% and ~180% respectively) over test duration compared with results recorded at the first hole irrespective of operating conditions, which suggested very rapid rates of tool wear. When utilising brazed PCD tools however, thrust forces and torque were approximately constant over the entire test duration (300 holes). The stable values reflect the relatively low tool wear levels observed with the PCD drills (~60 μm).

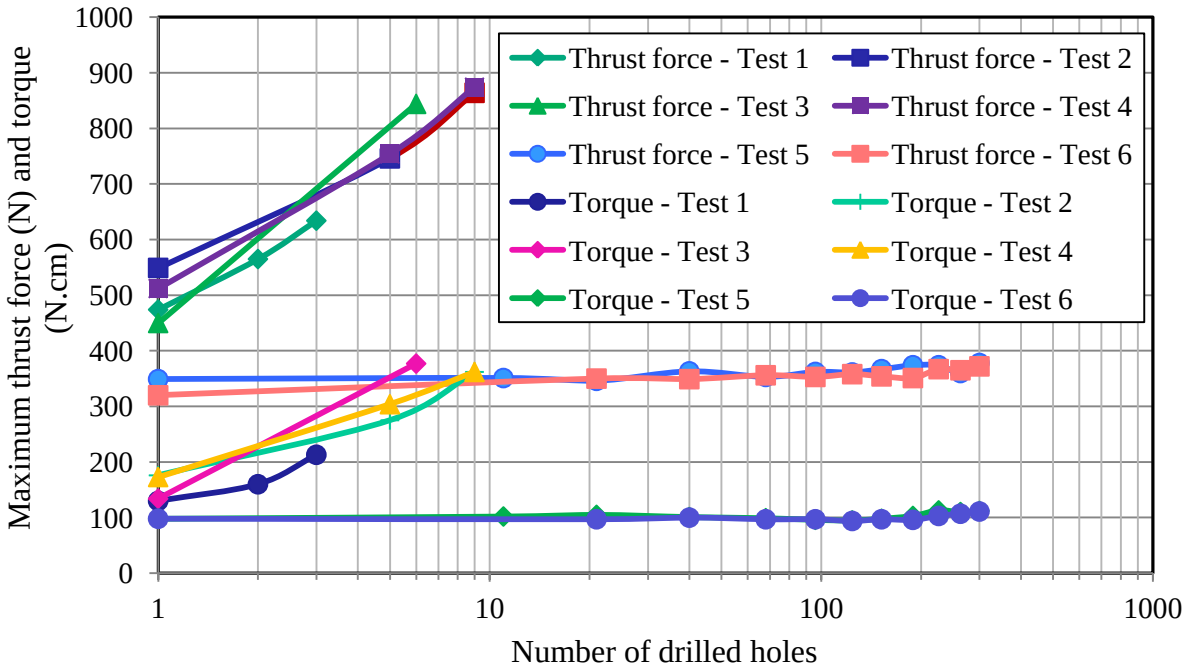


Figure 4.89: Maximum thrust force and torque against number of drilled holes

Figure 4.90 details thrust force and torque values recorded at the first and last holes in all tests. For the first hole, the maximum thrust force in Tests 2 and 4 was higher (~15%) compared with Tests 1 and 3, which was attributed to the higher feed rate applied in the former. At test cessation, thrust force increased by 34%, 57%, 88% and 71% in Tests 1, 2, 3 and 4, respectively, while a rise of up to 8% and 16% was recorded for Test 5 and 6 due to lower tool wear (~60 μm).

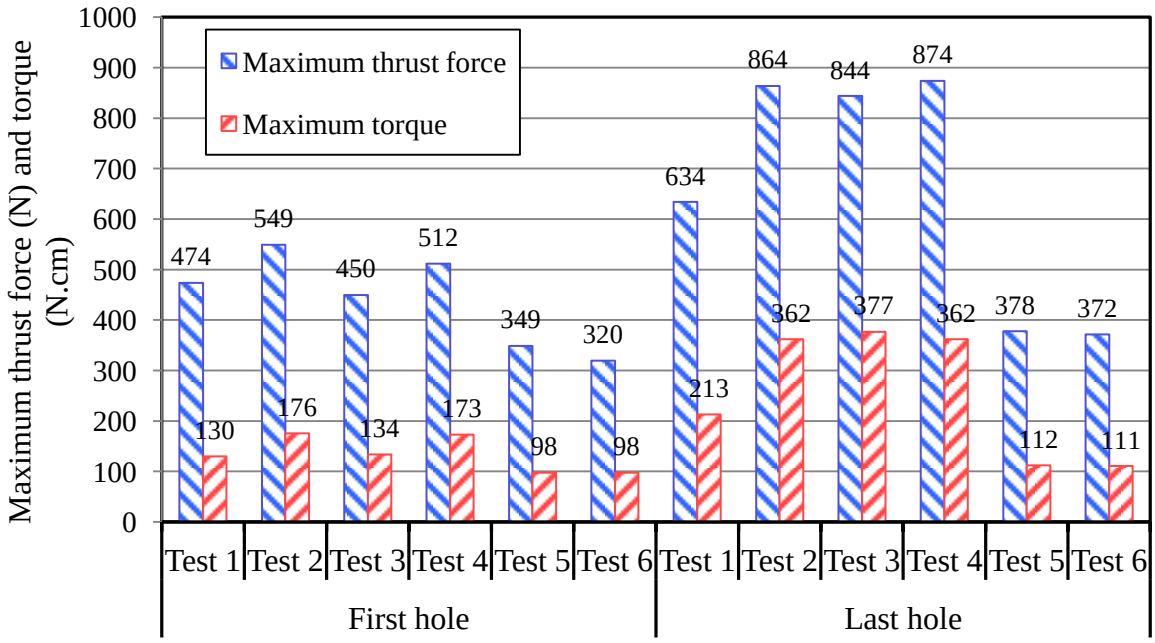


Figure 4.90: Maximum thrust force and torque for the first and last hole

4.6.3 Hole entry and exit quality

In general, uniform burrs (without caps) were obtained at the hole exit when employing uncoated and coated tools irrespective of process parameters, while both the entry and exit edges were free from burring when utilising brazed PCD drills, see Figure 4.91 for hole edge quality at test cessation. When machining with new tools (first hole), minimal burring or damage was seen at the hole entry location however fracture of the exit burrs was typical when using worn uncoated and coated WC drills, as shown in Figure 4.92. This was possibly due to the low ductility of the strain hardened workpiece material (< 4%) [7, 207].

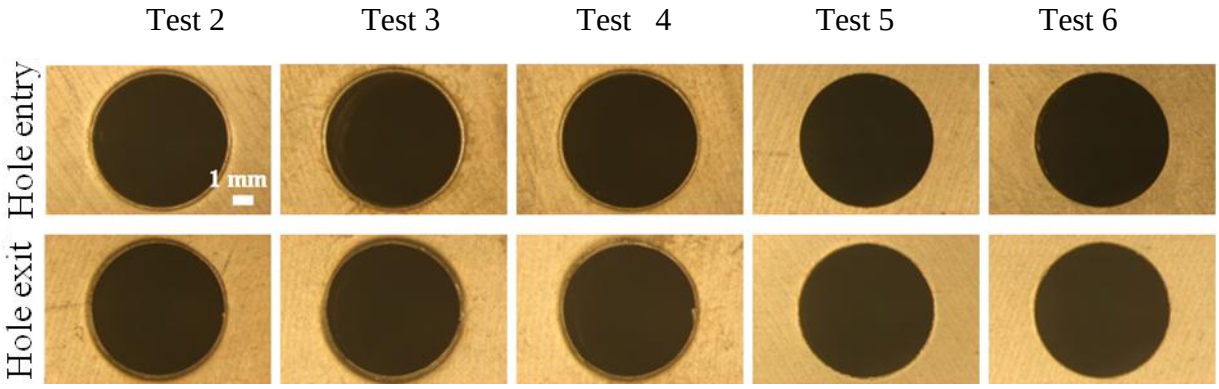


Figure 4.91: Hole edge quality for the last hole drilled

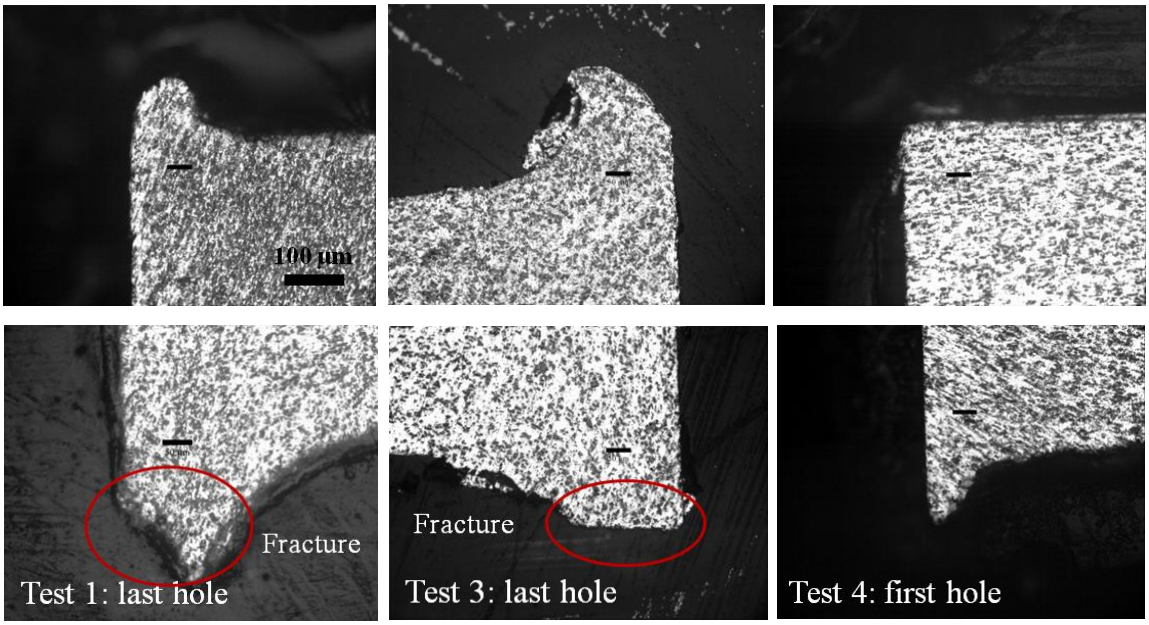


Figure 4.92: Burr morphology at hole entry and exit of the hole

4.6.4 Chip analysis

Figure 4.93 shows the various types of collected chips following each trial. Typically, uncoated and coated drills generated fan-shaped chips irrespective of cutting parameters, while the PCD tools produced shorter, needle-like swarf. Due to the material's low ductility,

the chips were unable to withstand the severe deformation during the drilling process, with a tendency to fracture under tension to form fan-shape swarf [208]. An example of the crack initiation can be seen in Figure 4.94 for Test 2. As for the different chip shape when utilising PCD drills, this was attributed to the presence of BUE along the cutting edges, which caused uneven chip flow and subsequently severe up-curling leading to the generation of needle-like chips [208, 209].

Uncoated T-type	**TiAlN+TiN coated M-type**	**Brazed PCD CX31**
Test 1 (80 m/min, 0.1 mm/rev)	Test 3 (80 m/min, 0.1 mm/rev)	Test 5 (160 m/min, 0.1 mm/rev)
		
Test 2 (80 m/min, 0.2 mm/rev)	Test 4 (80 m/min, 0.1 mm/rev)	Test 6 (160 m/min, 0.2 mm/rev)
		

Figure 4.93: Chips / swarf produced following each test

Further SEM analysis showed the presence of cavities / voids on the back surface of chips generally produced by coated and uncoated WC drills, see Figure 4.94, which suggested that pull out of SiC particles from matrix material occurred during drilling process. This was probably the result of the high tool wear rates leading to dull cutting edges. Cracks seen commencing from the smaller section of the chip was due to uneven flow over the blunt or rounded edge of the drill. Similarly, the saw-tooth profile at the top edge of the chips were most likely caused by the rounded / blunt cutting edge corner, while the lamella-like structures observed on the inner surface of the chips were due to shear localisation [209]. In

terms of the needle-like swarf, the underside surfaces were generally defect free except for some evidence of smeared material while the top edge was continuous. A schematic describing chip formation in drilling is shown in Figure 4.95.

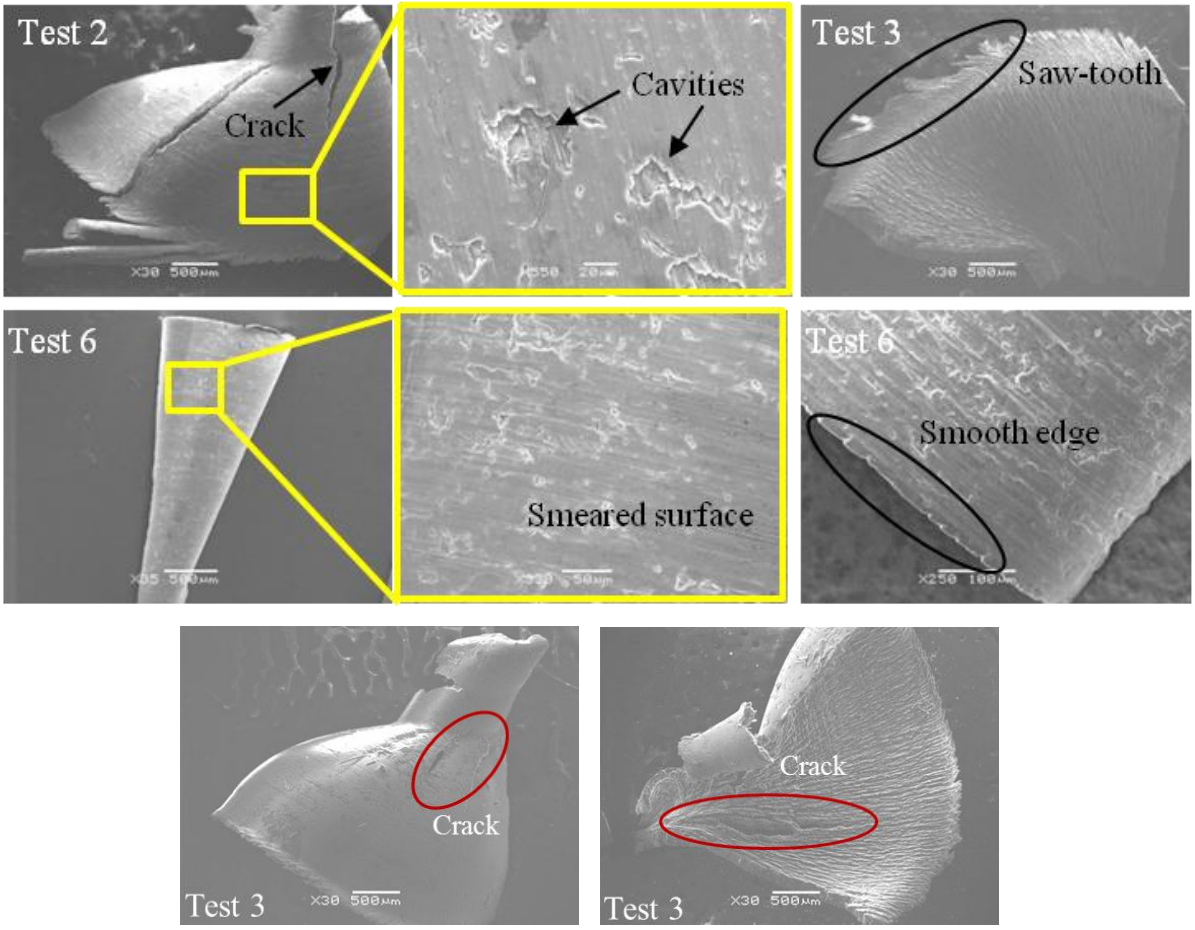


Figure 4.94: SEM micrographs of chip morphology following different drilling tests

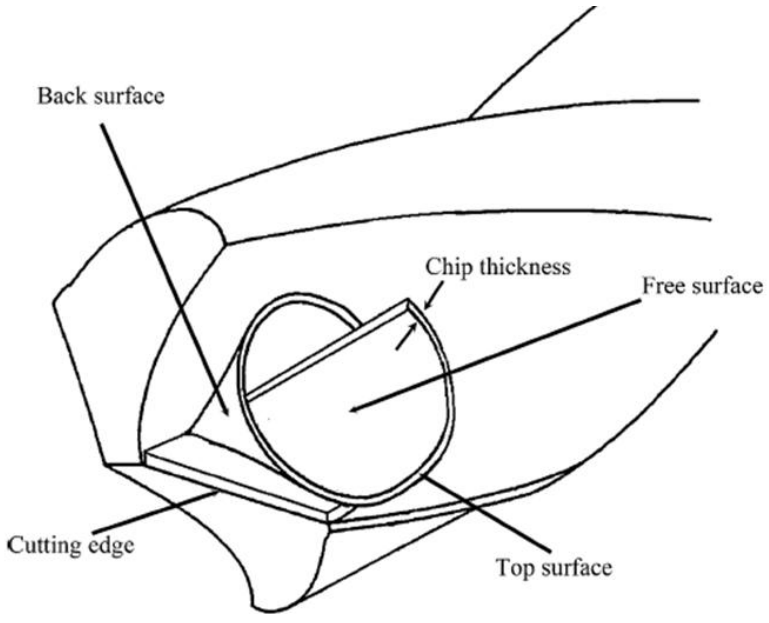


Figure 4.94: Schematic of chip formation in drilling [209]

4.6.5 Hole geometrical accuracy

Hole diameter results are presented in Figure 4.96. Most of the holes were oversized irrespective of tool material or operating conditions, with the exception of the last hole drilled in Test 4 which was undersized by 21µm. The deviation from the nominal diameter was possibly due to fabrication tolerances during tool manufacture. For brazed PCD tools, the change in hole diameter after 300 holes was minimal with a maximum reduction of 5µm.

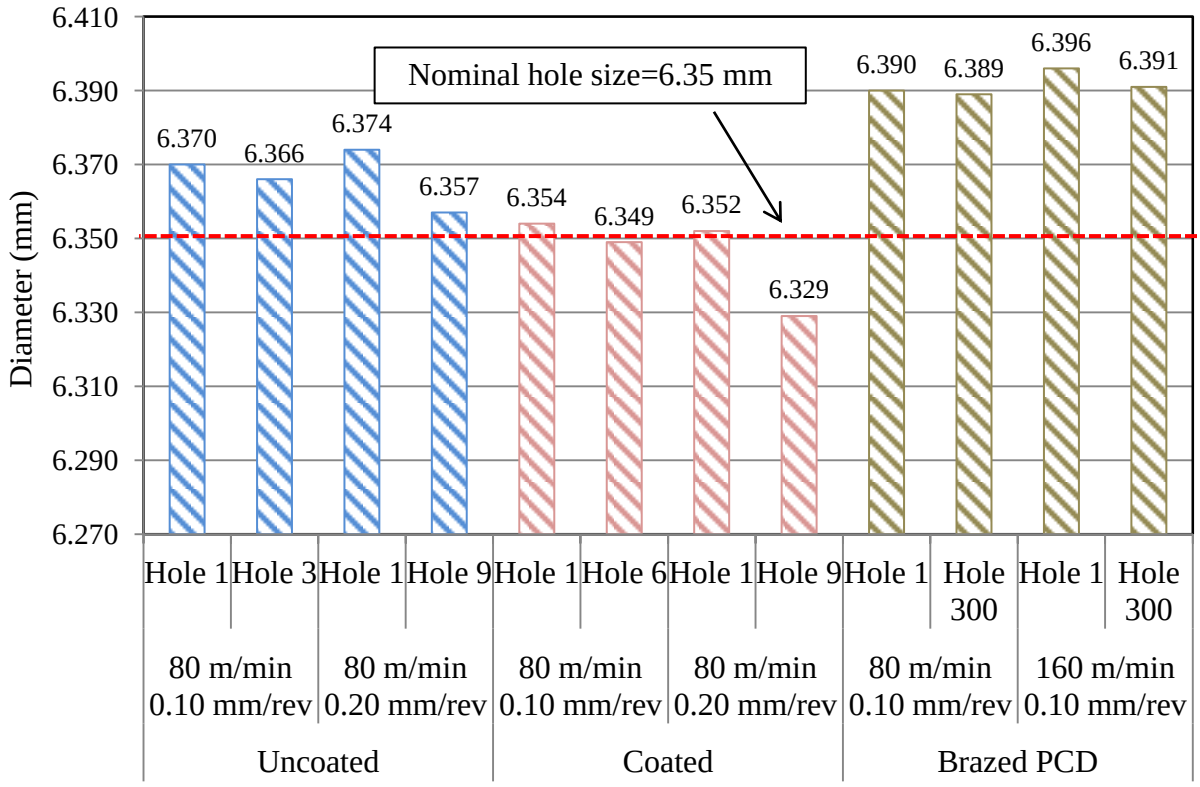


Figure 4.96: Hole diameter results for the first and last holes in all tests

Hole geometrical accuracy measurements in terms of out of roundness and cylindricity are detailed in Figure 4.97. Surprisingly, the roundness of the first hole produced by the uncoated and coated drills was better compared with those machined using PCD tools. This could have been due to increased burnishing / honing effect of SiC particles trapped between tool and drilled hole caused by the application of internal high pressure coolant [210]. Similarly, the cylindricity of the first hole produced using the carbide drills was generally lower compared to those machined with PCD drills. Increasing feed rate did not appear to produce any benefits in terms of both roundness and cylindricity. With the PCD tools, higher cutting speed however led to lower hole out of roundness and cylindricity levels.

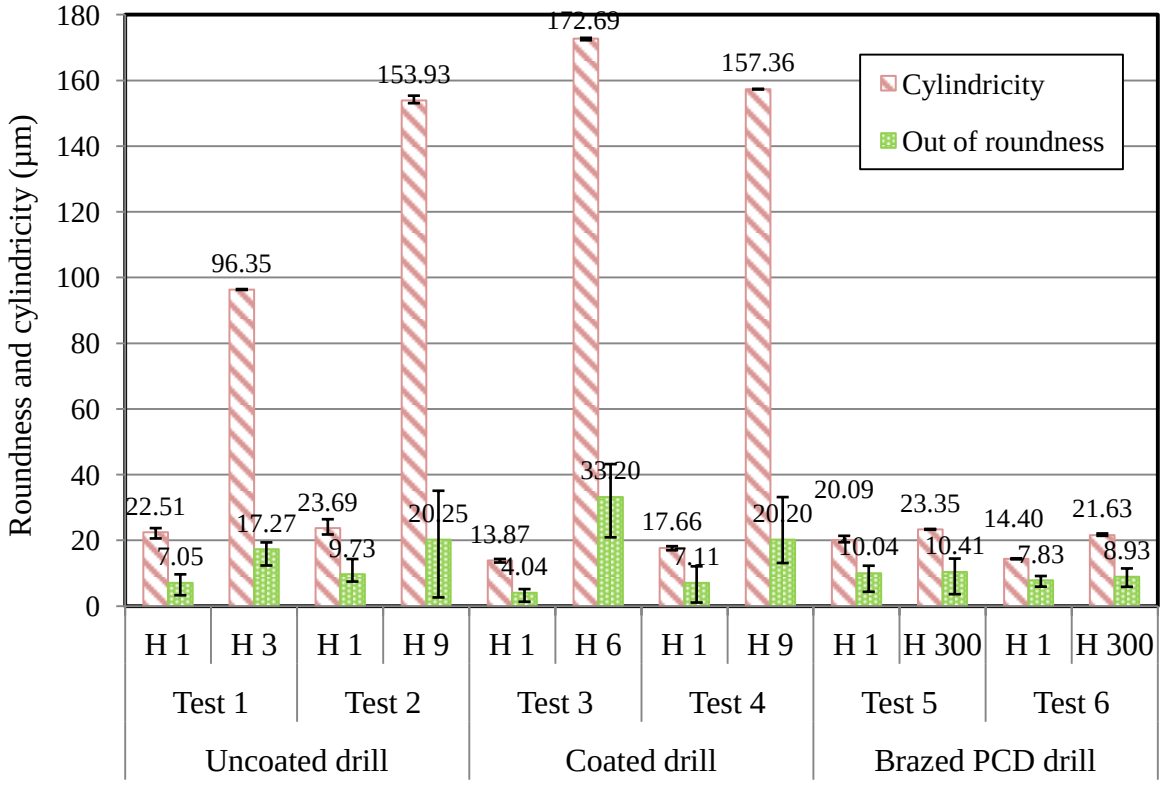
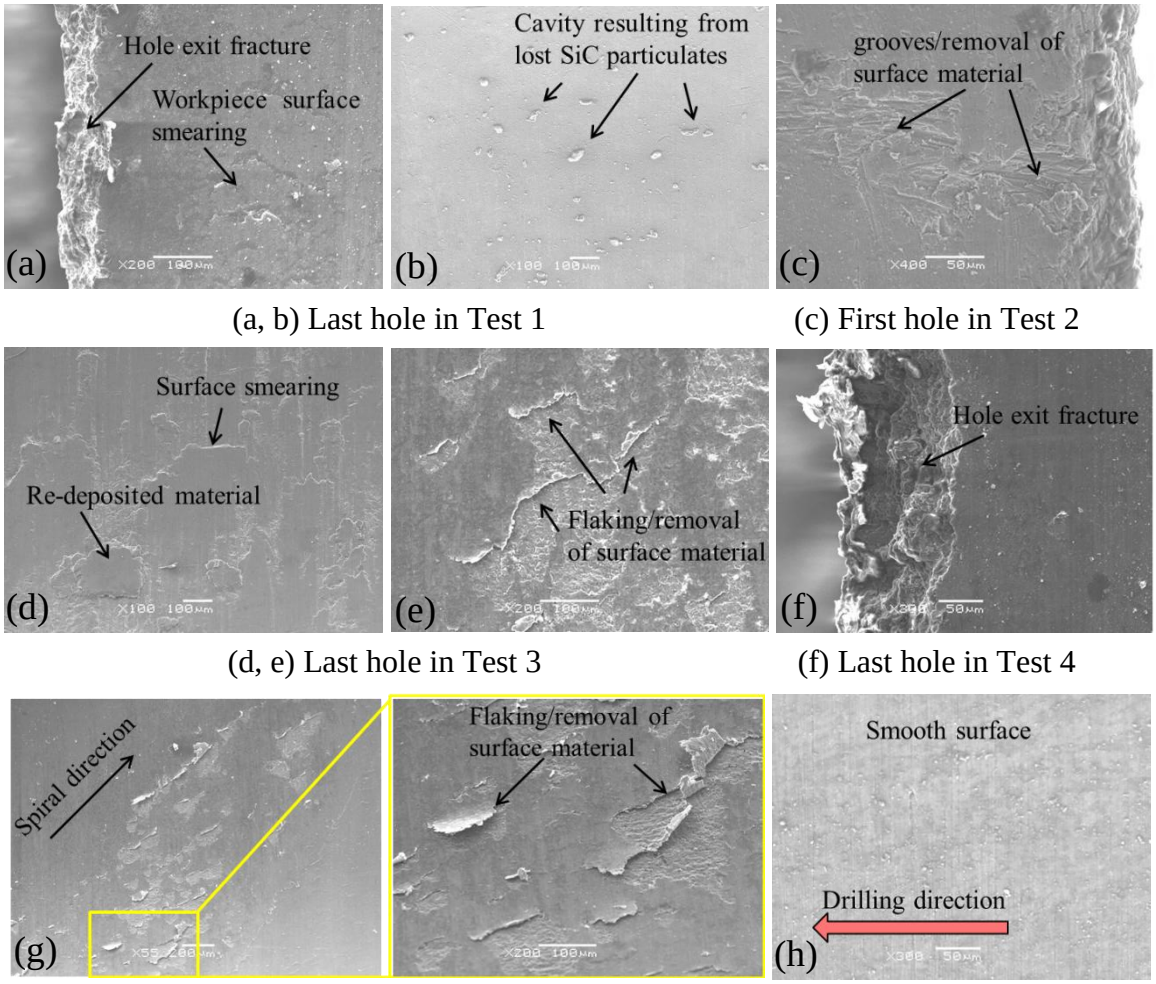


Figure 4.97: Hole out of roundness and cylindricity measurement results (H: hole)

4.6.6 Hole surface integrity analysis

Figure 4.98 shows SEM images of machined hole surfaces from various tests. In terms of hole surface integrity, a high incidence of surface defects comprising cavities / voids, workpiece smearing and surface material flaking was observed when employing uncoated / coated WC drills caused by extensive tool wear and poor swarf / chip extraction process. Hole exit fracture was prevalent at the last hole (see Figures 4.98(a) and 4.98(f)), which was more pronounced when operating at the higher feed rate (0.2 mm/rev). This was most likely attributed to the low ductility of strain hardened MMC workpiece material. In contrast, the surfaces produced with the PCD tools were relatively smooth with no obvious signs of damage even after 300 holes. Figure 4.99 presents cross-sectioned hole subsurface micrographs from selected tests. The subsurface damage observed generally corresponded to hole surface defects, with pits and folded / adhered material seen when using uncoated and coated WC drills while surfaces produced with brazed PCD tools were generally free of major defects.



(a, b) Last hole in Test 1 (c) First hole in Test 2

(d, e) Last hole in Test 3 (f) Last hole in Test 4

(g) Last hole in Test 4 (h) Last hole in Test 6

Figure 4.98: SEM of machined hole surface quality

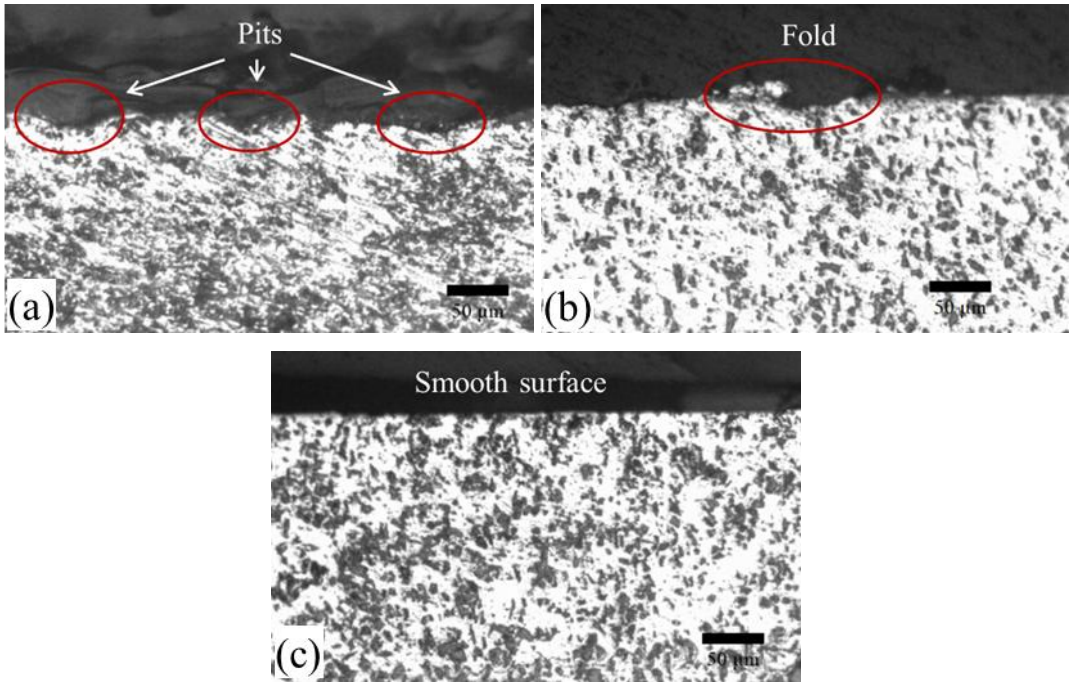


Figure 4.99: Micrographs of hole subsurface at the last holes in (a) Test 1, (b) Test 3 and (c) Test 6

4.7 Phase 3B: Evaluation of PCD tools and cutting parameters when drilling MMCs

4.7.1 Tool wear and life

Figure 4.100 shows tool flank wear progression versus number of drilled holes in all trials. All of the tests reached 306 holes and demonstrated similar trends with respect to steady increase / progression of flank wear with a maximum of 92 µm recorded in Test 7. The best performance in terms of tool wear (40 µm) was obtained when cutting with flood coolant (3 bar) using the brazed PCD drill at 80 m/min and feed rate of 0.2 mm/rev. Generally, brazed PCD tools exhibited lower flank wear compared with domed PCD drills, most likely due to the protection offered by higher levels of built up edge (BUE) in the former. This was in agreement with the observations of Ciftci et al. [123] when turning MMC's. Tool wear scars after the first and last holes (prior to and following removal of BUE / adhered material) are presented in Figure 4.101. Adhered material/BUE was apparent even after the first hole and prevalent in all trials involving brazed PCD drills. This was probably due to insufficient cutting fluid / lubricant arriving at the cutting zone together with poor extraction of the small needle-like chips (discussed in 5.7.4). Surprisingly, BUE formation was negligible along the cutting lips when using domed PCD tools irrespective of cutting parameters. This was possibly attributed to the optimised tool geometry and superior heat dissipation with the domed PCD drill. After removal of the BUE / adhered material, tool flank wear was revealed to be generally uniform. Abrasion was the primary tool wear mode with no signs of chipping / fracture. Figure 4.102 shows the top view of the drills in Tests 2 and 6 at test cessation. Adhered material was evident at the chisel edge / drill centre irrespective of tool configuration, due to the relatively low cutting speeds near the drill centre point.

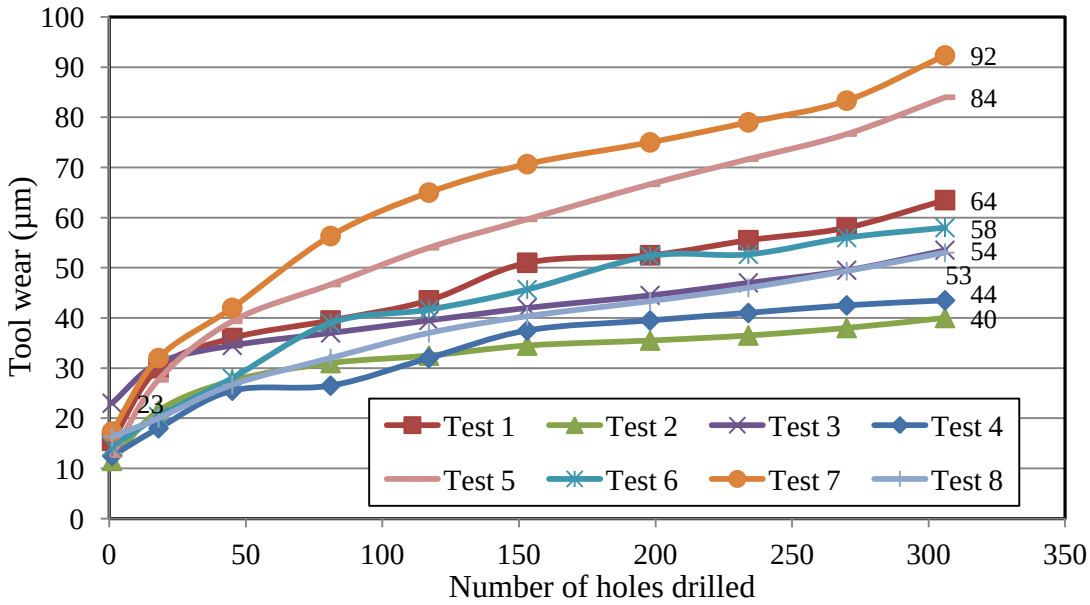


Figure 4.100: Tool wear progression in all trials

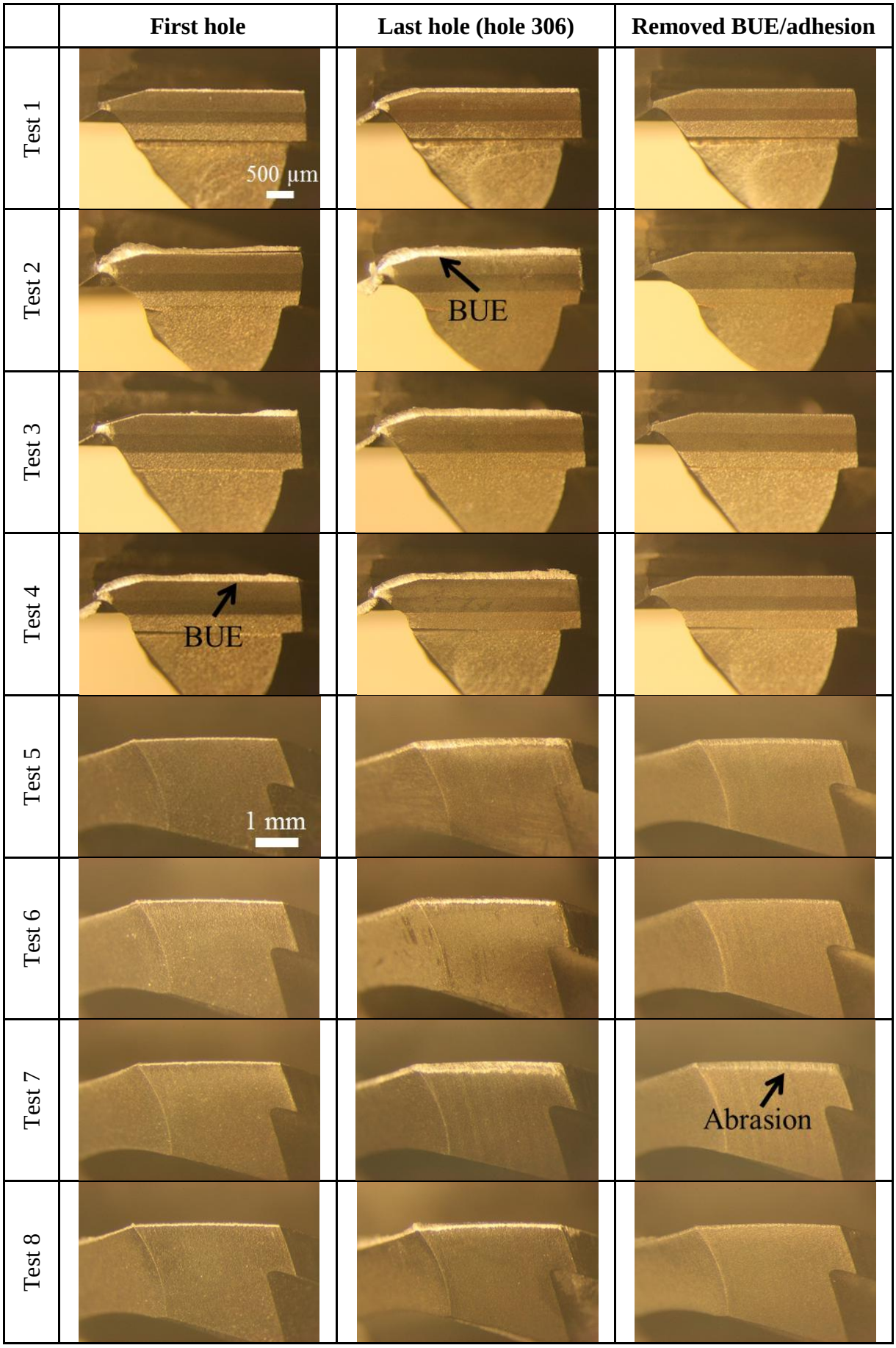


Figure 4.101: Tool wear scar for the first and last hole in all tests

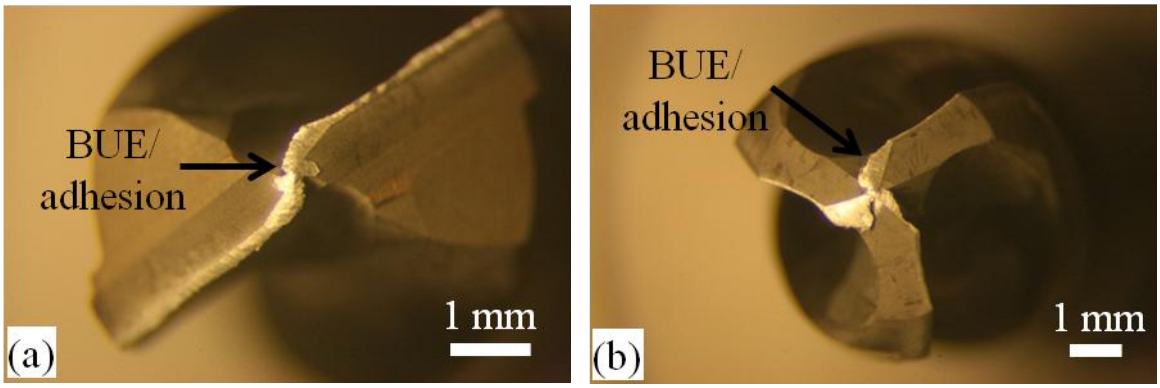


Figure 4.102: Top view of drills at test cessation in (a) Test 2 and (b) Test 6

Figure 4.103 shows the main effects plots for maximum flank wear at test cessation with associated ANOVA results detailed in Table 4.6. Lower flank wear was obtained when using the brazed PCD drill at high feed rate (0.2 mm/rev), as both factors were found to be significant at the 5% level. As feed rate increased, the contact time between the drill and workpiece material decreased, resulting in relatively lower cutting temperature and tool wear. The relatively low level of tool wear achieved with brazed PCD drills was partlly attributed to BUE formation, albeit with a likely detrimental influence on hole quality. This is discussed in the following sections. Statistical analysis showed that tool material and feed rate were the main contributing factors with corresponding PCR's of 36.57% and 50.26% respectively.

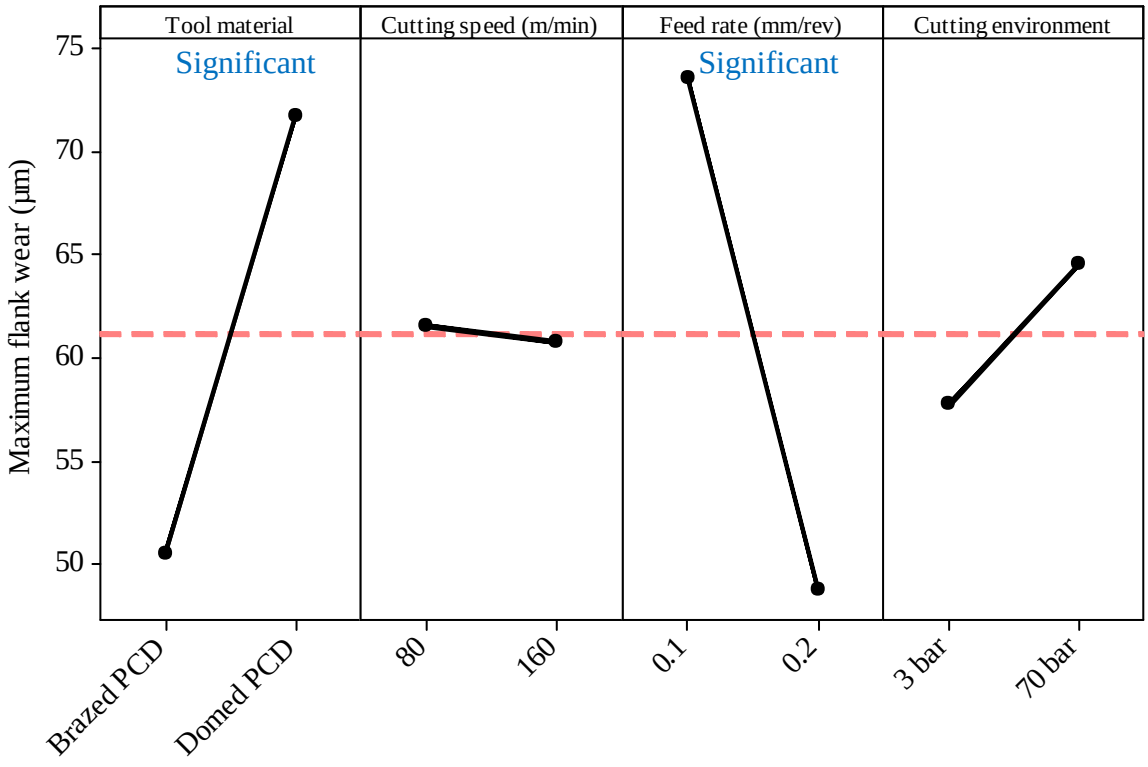


Figure 4.103: Main effects plot for maximum flank wear

Table 4.6: ANOVA results for maximum flank wear

Factor	DF	Seq SS	Adj MS	F	P	PCR
Tool material	1	903.12	903.12	20.78	0.020*	36.57%
Cutting speed (m/min)	1	1.12	1.12	0.03	0.882	0.00%
Feed rate (mm/rev)	1	1225.12	1225.12	28.19	0.013*	50.26%
Cutting environment	1	91.12	91.12	2.10	0.243	2.03%
Error	3	130.38	43.46			11.14%
Total	7	2350.87				

4.7.2 Thrust force and torque

Figure 4.104 details the maximum thrust force and torque values recorded following the first and last holes drilled in all trials. In general, thrust force and torque were highly dependent on the feed rate. For both the first and last holes, the values generated at high feed rate (0.2 mm/rev) were considerably higher (up to 337 N and 64 N.cm) compared to those at low feed rate (0.1 mm/rev) with equivalent cutting speed, regardless of cutting environment and tool material. The maximum thrust force (767 N) and torque (167 N.cm) was recorded in Test 6 when using a domed PCD drill at 80 m/min and feed rate of 0.2 mm/rev with high pressure coolant (70 bar). This was possibly attributed to the high feed rate applied together with efficient cooling resulting in lower cutting temperatures thereby minimising any thermal softening effects. Last hole thrust force and torque was substantially higher (by 57% and 46% respectively) compared with results recorded at the first hole in Test 7 due to the relatively high flank wear level of 92 µm. Domed PCD drills generally produced higher thrust forces and torque compared with brazed PCD tools due to the comparably longer cutting edge length in the former. Further details of thrust force and torque progression against number of drilled holes are presented in Appendix C.

Main effects plots in relation to thrust force and torque for the last holes are shown in Figures 4.105 and 4.106 respectively, while the corresponding ANOVA calculations are presented in Tables 4.7 and 4.8. Detailed results for the first holes (thrust force and torque) are presented in Appendix C. In general, main effects plots and ANOVA results for thrust forces at the first and last holes followed a similar trend, as feed rate had an overriding effect with high PCR's of 81.55% and 57.20% respectively. Statistical analysis also highlighted that feed rate had a significant impact on torque for both the first and last holes, with PCR's of 95.22% and 76.84% respectively. In terms of results at test cessation (last hole), tool material had an overriding influence on thrust force and torque with corresponding PCR's of 29.40% and

17.34%, while the effect on the results recorded at the first holes was marginal. Surprisingly, cutting speed and cutting environment were not statistically significant at the 5% level, which was possibly attributed to the large contribution of tool material and feed rate variables.

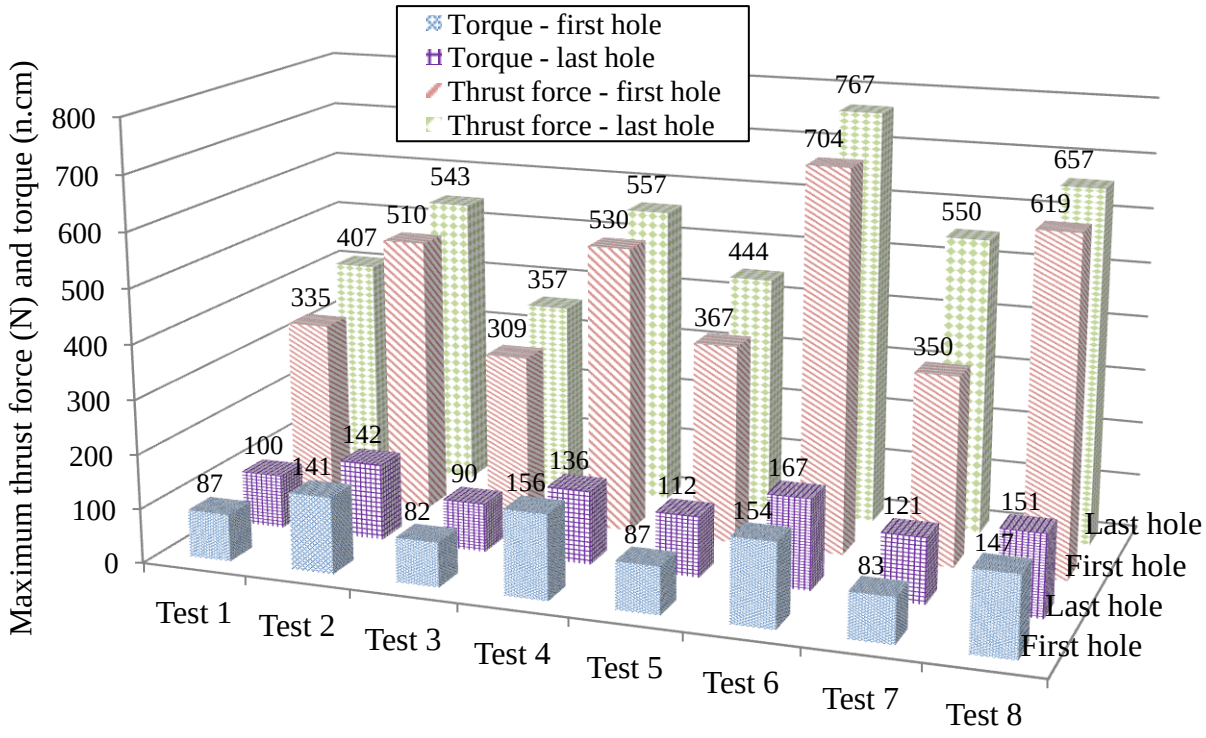


Figure 4.104: Maximum thrust force and torque values recorded at the first and last holes

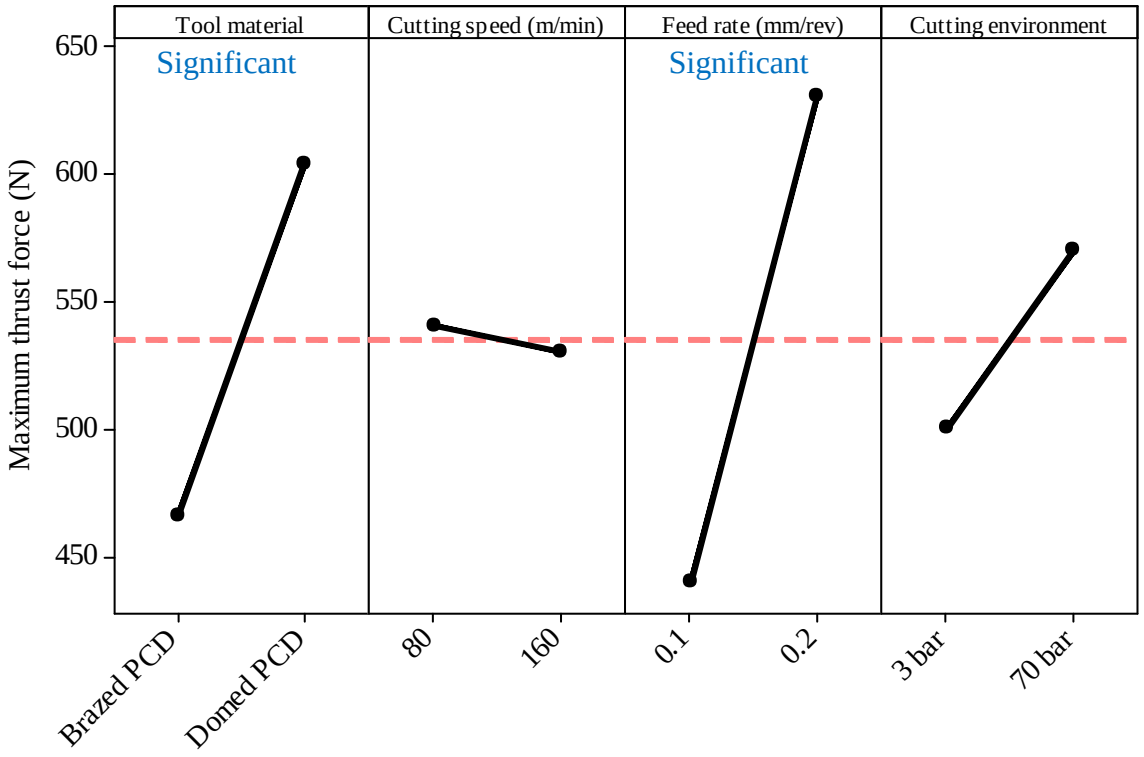


Figure 4.105: Main effects plot for maximum thrust force at the last hole (hole 306)

Table 4.7: ANOVA results for maximum thrust force at the last hole (hole 306)

Source	DF	Seq SS	Adj SS	F	P	PCR
Tool material	1	38364	38364	27.93	0.013*	29.40%
Cutting speed (m/min)	1	200	200	0.15	0.728	0%
Feed rate (mm/rev)	1	73344	73344	53.40	0.005*	57.20%
Cutting environment	1	9800	9800	7.14	0.076	6.70%
Error	3	4121	1374			6.70%
Total	7	125829				

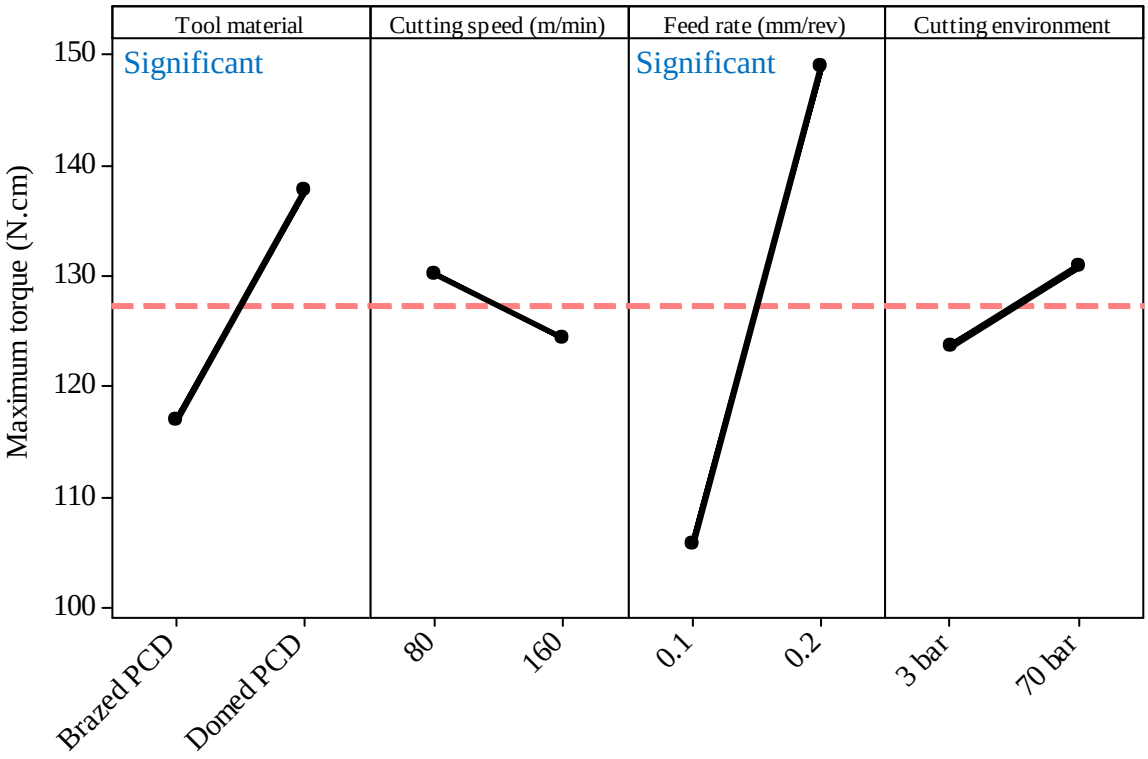


Figure 4.106: Main effects plot for maximum torque at the last hole (hole 306)

Table 4.8: ANOVA results for maximum torque at the last hole (hole 306)

Source	DF	Seq SS	Adj SS	F	P	PCR
Tool material	1	861.1	861.1	38.92*	0.008	17.34%
Cutting speed (m/min)	1	66.1	66.1	2.99	0.182	0.91%
Feed rate (mm/rev)	1	3741.1	3741.1	169.09*	0.001	76.84%
Cutting environment	1	105.1	105.1	4.75	0.117	1.71%
Error	3	66.4	22.1			3.20%
Total	7	4839.9				

4.7.3 Burr size and morphology

In general, hole edge quality at the entrance location was good with no evidence of major damage or burring regardless of drill condition, see details in Appendix C. Hole exit quality for both the first and last holes is presented in Figure 4.107. Limited / marginal damage in the form of burr formation was seen for all the first and last holes drilled with brazed PCD tools, while roll-back / rollover burrs were prevalent at the last holes when using domed PCD drills. The condition was exacerbated in Tests 7 due to comparably high tool wear (92 µm). The burrs however were fragile and discontinuous, hence they were easily removed. The possible reason for generating roll-back burrs was due to rubbing at the margins of the drill together with a small point angle (60º) and low efficiency of coolant access towards the bottom of the hole [211]. Similar burr formation was also previously reported by Dornfeld et al. when wet drilling Ti-6Al-4V [212].

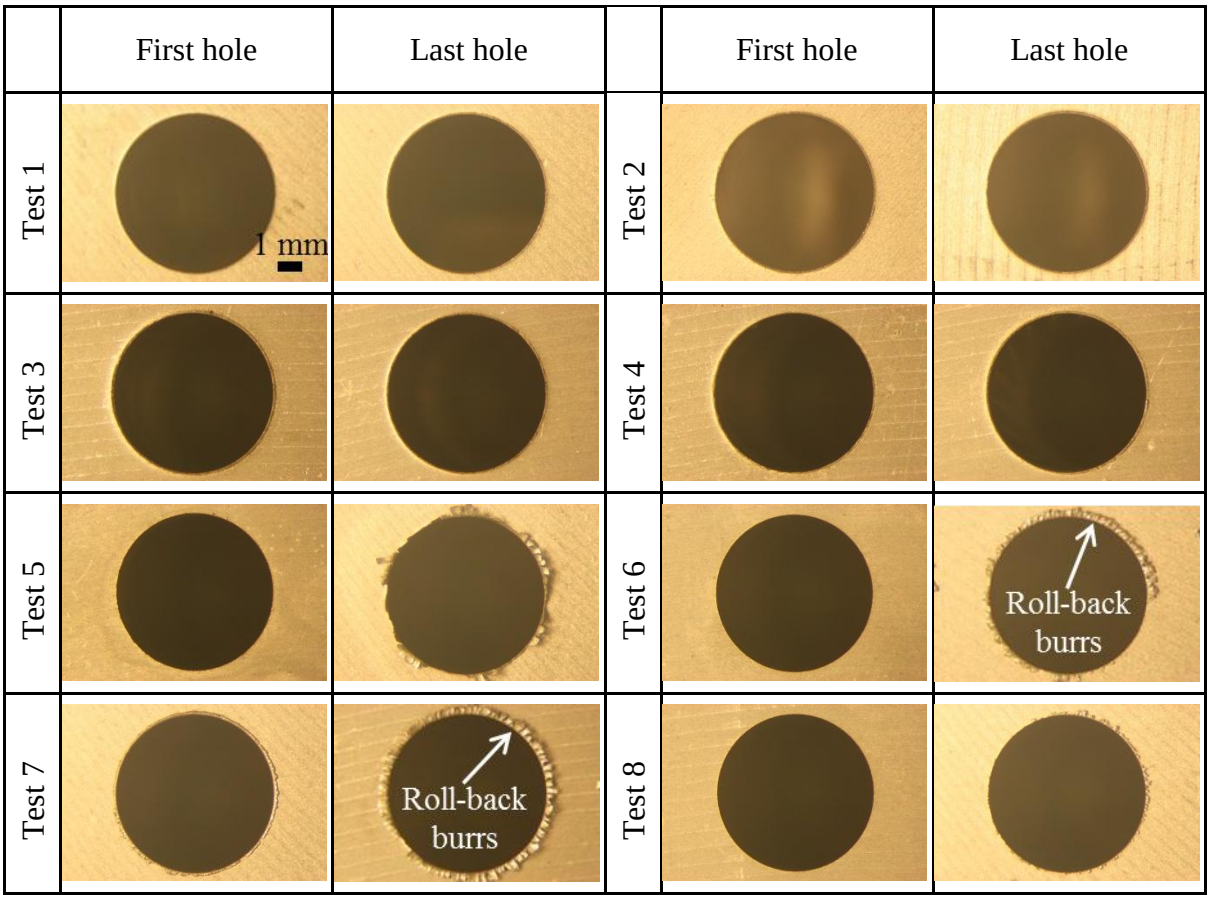
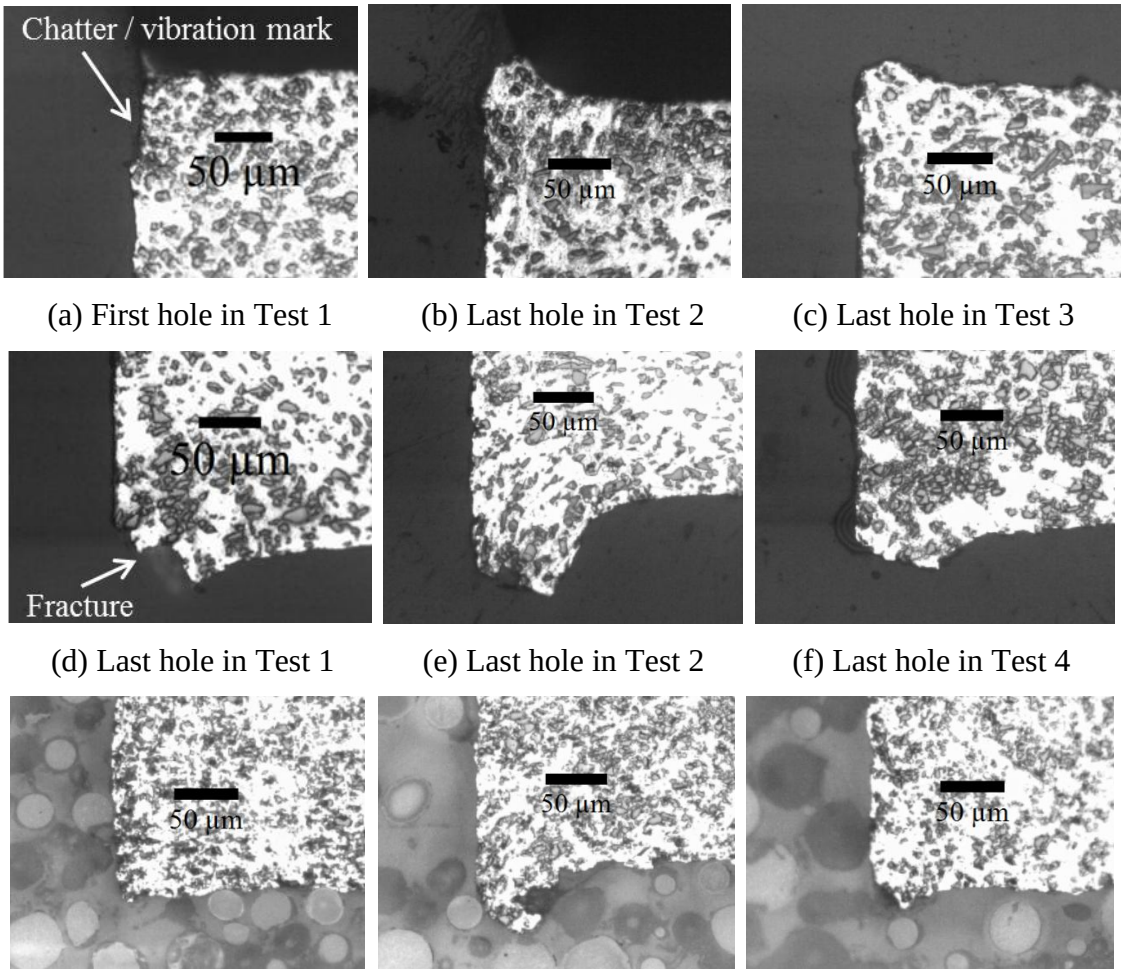


Figure 4.107: Hole exit quality in all tests

Sample micrographs of cross-sectioned holes for further analysis of burr formation / morphology is shown in Figure 4.108. Chatter marks up to ~50 µm in length were seen at hole entry for the first holes in Tests 1 and 3, see Figure 4.108(a). This was possibly due to

tool deflection / chatter. For last holes drilled using worn tools, entrance burr height was generally up to ~30 µm when using brazed PCD tools, while domed PCD drills generated near burr free holes over the trial duration. Similarly, hole exit burring was more severe when drilling with brazed PCD tools and was present even in the first hole. Exit burr height of up to ~130 µm was observed in Test 2 as shown in Figure 4.108(e). Burr fractures were also commonly seen when utilising the brazed PCD tools due to the low ductility of MMC (< 4%) [7, 207]. In contrast, domed PCD tools were superior in minimising burr formation, as burr height did not exceed ~60 µm for the last holes drilled. However, it was difficult to identify any clear relationship between burr size and cutting parameters, due to the incidence of burr fracture and the relatively fragile roll-back burrs produced by domed PCD drills.



(a) First hole in Test 1 (b) Last hole in Test 2 (c) Last hole in Test 3

(d) Last hole in Test 1 (e) Last hole in Test 2 (f) Last hole in Test 4

(g) First hole in Test 6 (h) Last hole in Test 7 (i) Last hole in Test 8

Figure 4.108: Micrographs of burr formation at hole entry and exit

4.7.4 Chip morphology

Figure 4.109 shows the various types of chips obtained in each test. In general, short (~3 mm) needle-like chips were produced when using brazed PCD drills regardless of operating parameters and cutting environment. This was most likely due to the formation of BUE, which was prevalent when employing brazed PCD tools. The BUE led to uneven chip flow resulting in severe up-curling swarf. Similar chip formation was also found by Akhavan Farid et. al [209] when drilling of Al–Si alloys. In contrast, various types of chips were produced when using domed PCD drills. Long and short spiral swarf were found in Tests 5 and 8, while fan-shape chips were seen in Tests 6 and 7. The long spiral swarf generally mimicked the contoured shape of the drill flute and was occasionally seen to be attached / entangled on the drill. Fan-shaped chips were generated possibly due to the application of high pressure coolant (70 bar), which facilitated chip evacuation together with an efficient supply of cutting fluid to the machining zone. The benefit of applying high pressure coolant in machining aluminium alloys was also outlined by several other researchers [132, 213]. When using low pressure flood environment (3 bar), the relatively poor transport of the fluid to the drill lips leads to higher cutting temperatures and increase in workpiece ductility / material softening. The generation of long spiral chips further exacerbated the situation as it impeded heat dissipation and clogged the drill flutes preventing the flow of cutting fluid. Figure 4.110 shows examples of the long spiral chips collected from Test 8. These were typically ~45 mm in length with curled / deformed swarf at one end. Generally, short / discontinuous chips are preferred when drilling, as they can be easily cleared from the cutting zone and helps with heat dissipation [144].

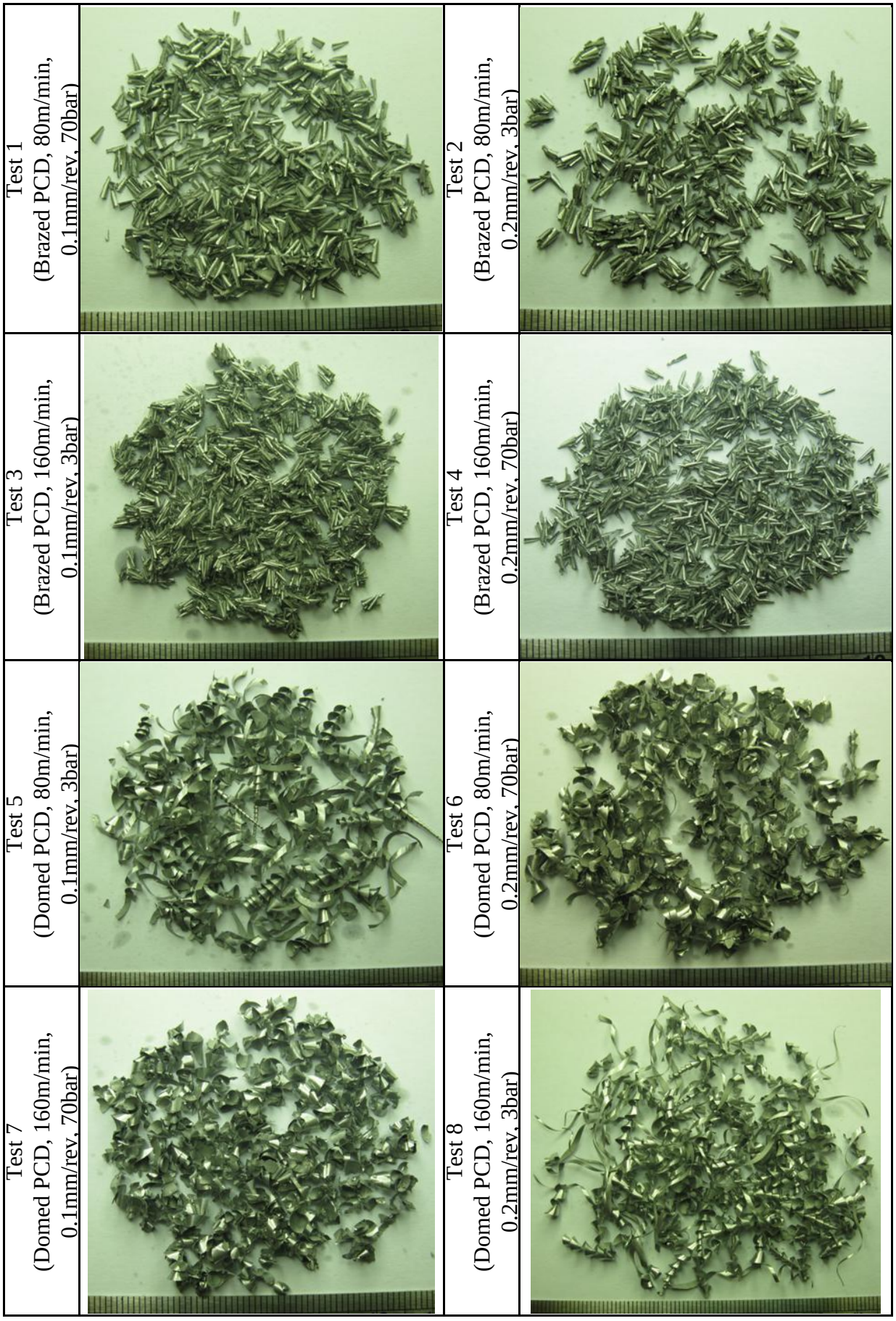


Figure 4.109: Chip morphology in all tests

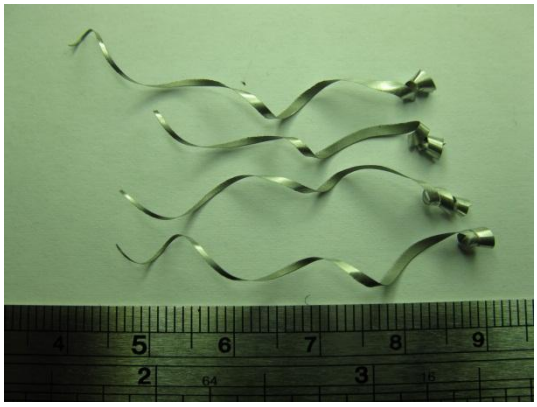


Figure 4.110: Sample long spiral chips generated in Test 8 (dome PCD, 160 m/min, 0.2 mm/rev and 3 bar low pressure flood)

4.7.5 Hole size and geometrical accuracy

Hole diameter and geometrical accuracy in terms of out of roundness and cylindricity were measured at hole 1 (first hole), 153 and 306 (last hole), with results presented in Figures 4.111, 4.112 and 4.113 respectively. All tests produced oversized holes even at test cessation with respect to the various nominal hole sizes of the different tool materials (brazed PCD drill: 6.38 mm, domed PCD drill: 6.36 mm). Hole diameter variation between new and worn (at test cessation) drills were limited to within 8 µm in all trials, due to low tool wear levels and consistent edge sharpness. The smallest discrepancy of 2 µm was seen in Test 2, which corresponded to the lowest tool wear recorded among all the tests (40 µm). However, there was no apparent correlation between the hole diameter and cutting conditions, which was possibly due to limited number of drilled holes and small variations of 8 and 14 µm at test cessation when using brazed PCD and domed PCD drills respectively. In terms of geometrical error measurements, out of roundness was generally below 10 µm and cylindricity was limited to within 20 µm. Although there was some fluctuations at hole 153, both the roundness and cylindricity parameters improved as the tests proceeded, except for the last hole in Tests 1 and 3. The improvement was possibly due to cutting edge rounding and subsequent elimination of feed marks. Similar results were also observed by Shyha et al. [71] when drilling Al-CFRP-Ti stacks. The contrasting results recorded in Tests 1 and 3 were most likely due to chatter / vibration in the drilling process. The effect of chatter / vibration affected on hole surfaces was further analysed in the following section. Domed PCD drills generally outperformed brazed PCD tools in terms of hole geometrical accuracy, which was due to almost negligible BUE generation and stable cutting operation.

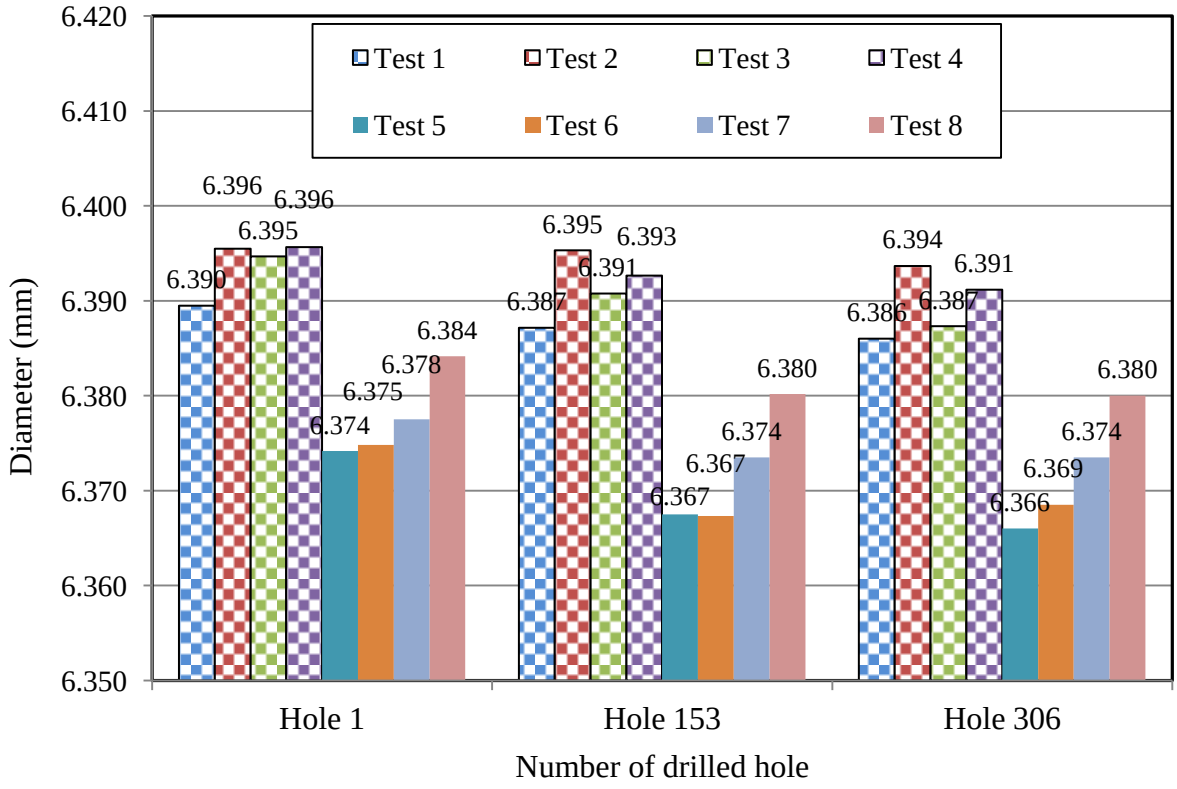


Figure 4.111: Hole diameter progression against number of drilled holes

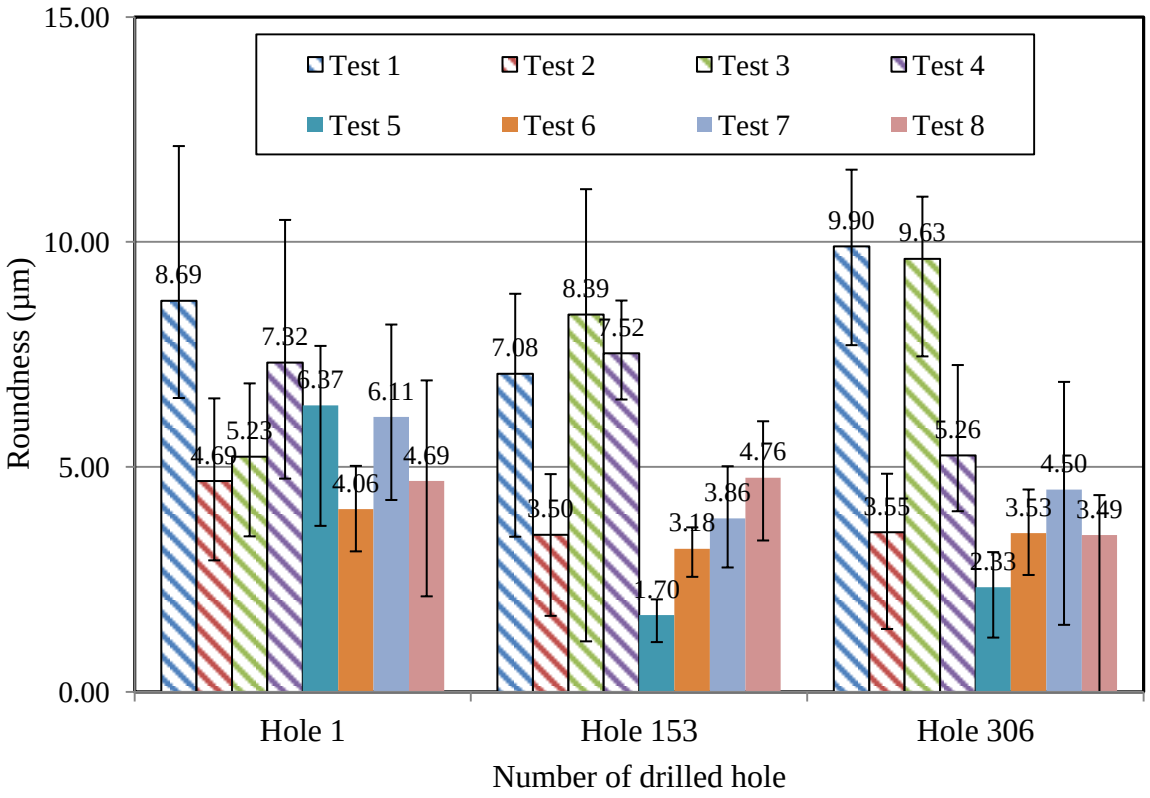


Figure 4.112: Out of roundness progression against number of drilled holes

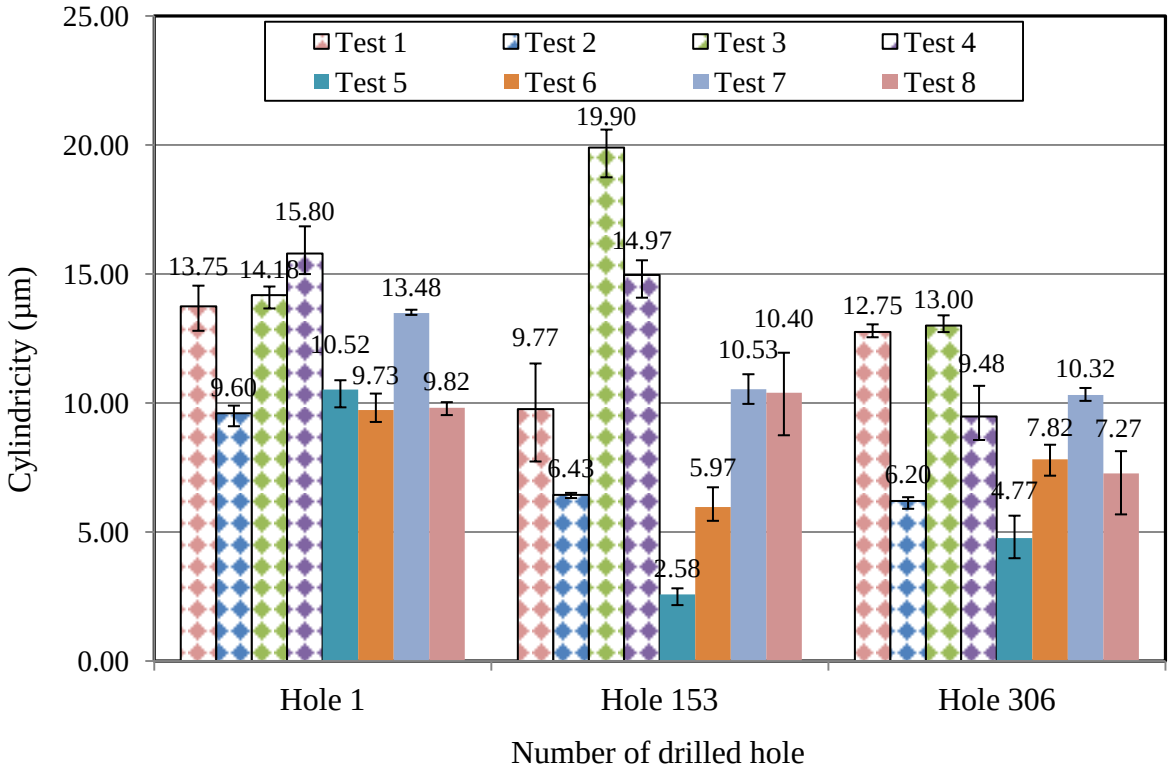


Figure 4.113: Cylindricity progression against number of drilled holes

4.7.6 Microhardness analysis

Figure 4.114 shows sample microhardness depth profile results following the first and last drilled holes, while details of all results are presented in Appendix C. In general, the microhardness increase was between 50 and ~60 $HV_{0.05}$ above the bulk hardness (~125 $HV_{0.05}$) irrespective of cutting parameters and extended up to ~100 µm beneath the machined surface. Limited discrepancy in microhardness levels was observed between the first and last holes drilled. The hardness increase was mainly due to strain hardening / plastic deformation caused by the drilling process. Such responses are not uncommon when machining MMCs materials and have been detailed by several researchers, with microhardness variations of 30-80 HV extending up to ~200 µm typically reported in both drilling and turning of MMC materials [133, 151-153].

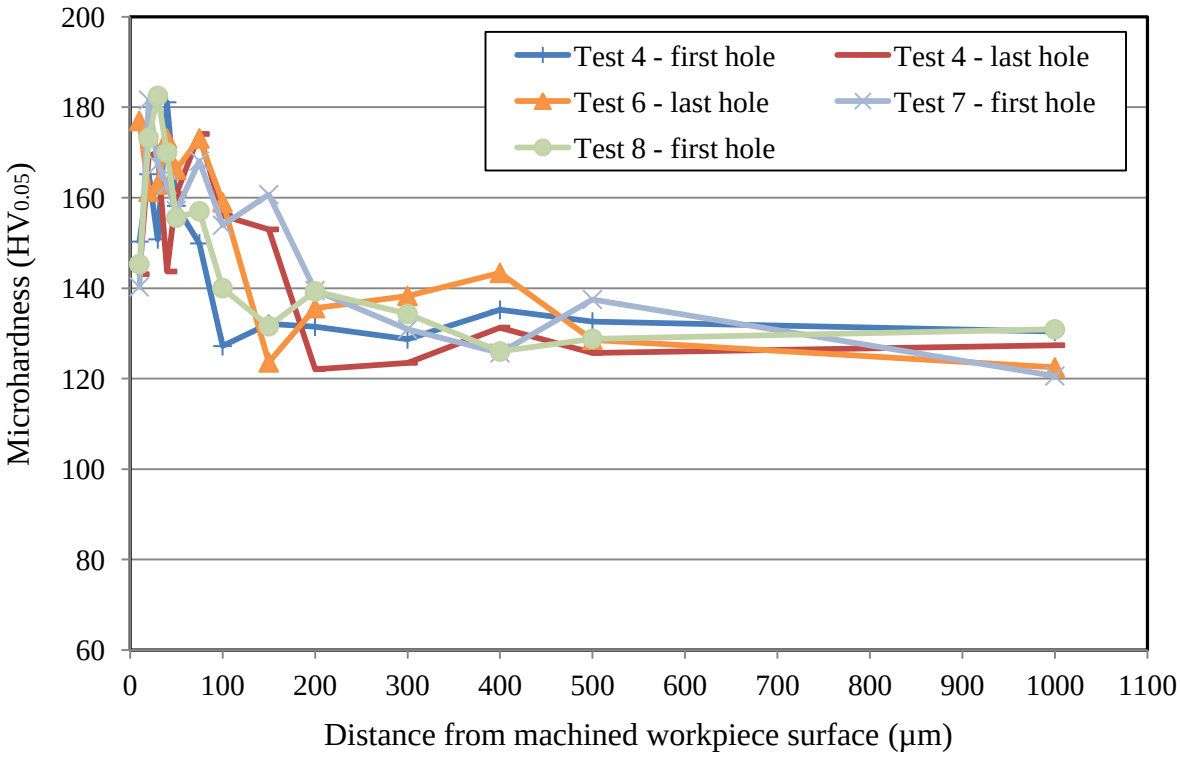


Figure 4.114: Microhardness results for both the first and last holes

4.7.7 Surface roughness analysis

Figure 4.115 details surface roughness values (Ra and Rt) for the first and last holes (hole 306) in all tests. In general, hole surface roughness was low, as Ra was less than 0.51 µm and Rt did not exceed 6.9 µm for all of the holes analysed. Better surface roughness in terms of both Ra (~0.15 µm) and Rt (~2.0±0.4 µm) was obtained in Tests 3 and 7 at the last hole when machining at a cutting speed of 160 m/min and feed rate of 0.1 mm/rev, while the trial carried out with low cutting speed (80 m/min) and elevated feed rate (0.2 mm/rev) in Test 6 experienced high Ra of up to 0.51 µm even at the first hole. Hole surface roughness improved in all tests as machining processed. This was possibly due to cutting edge corner rounding leading to minimisation of feed marks. The findings was in agreement with the results by Rattanakit [213] who reported similar observations when drilling aluminium alloys. According to the main effects plot shown in Figure 4.116 and ANOVA analysis, only feed rate was statistically significant and had an overriding effect on surface roughness Ra with a corresponding PCR of 68.18%. Although none of the other variables had a significant influence on Ra values of the last hole drilled, cutting speed had the second highest PCR of 12.85%. This was possibly due to the good wear resistance of PCD resulting in limited tool wear (< 92 µm) and consistent cutting edge sharp.

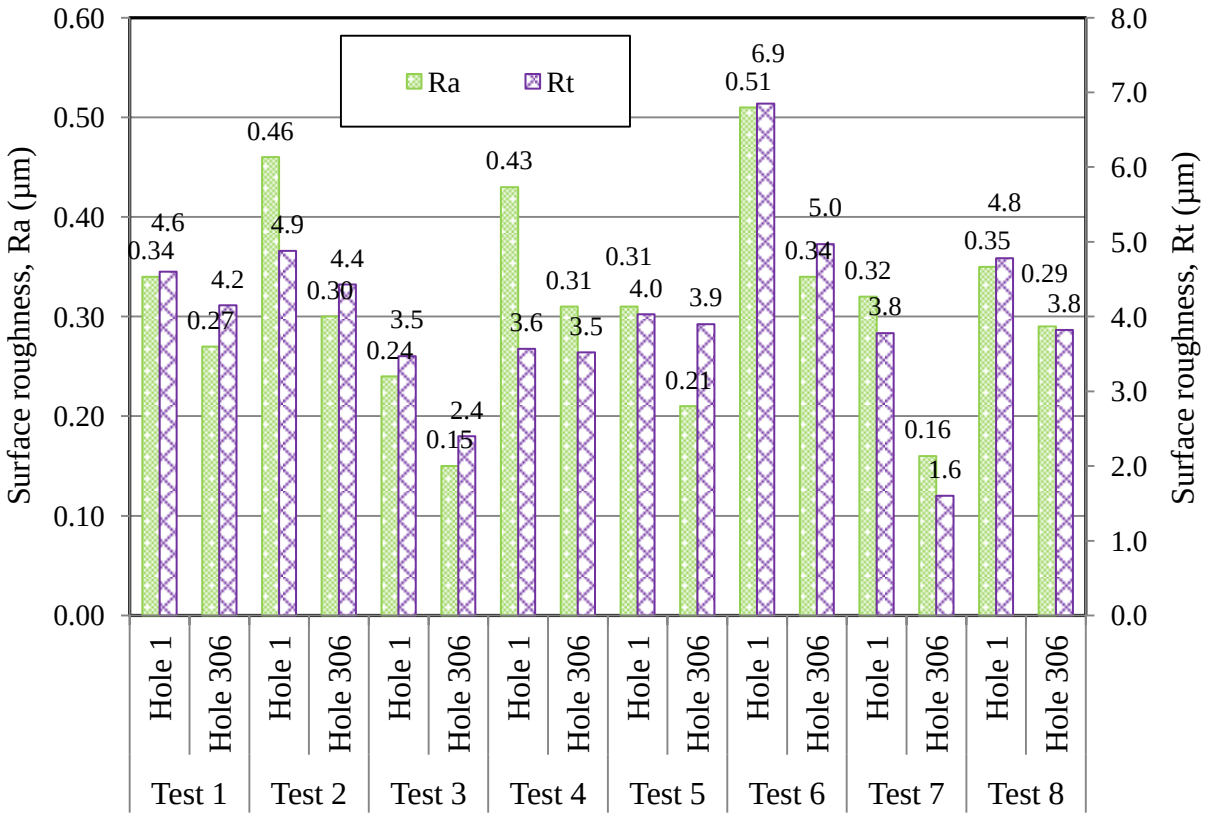


Figure 4.115: Surface roughness (Ra and Rt) measured at the first and last holes in all tests

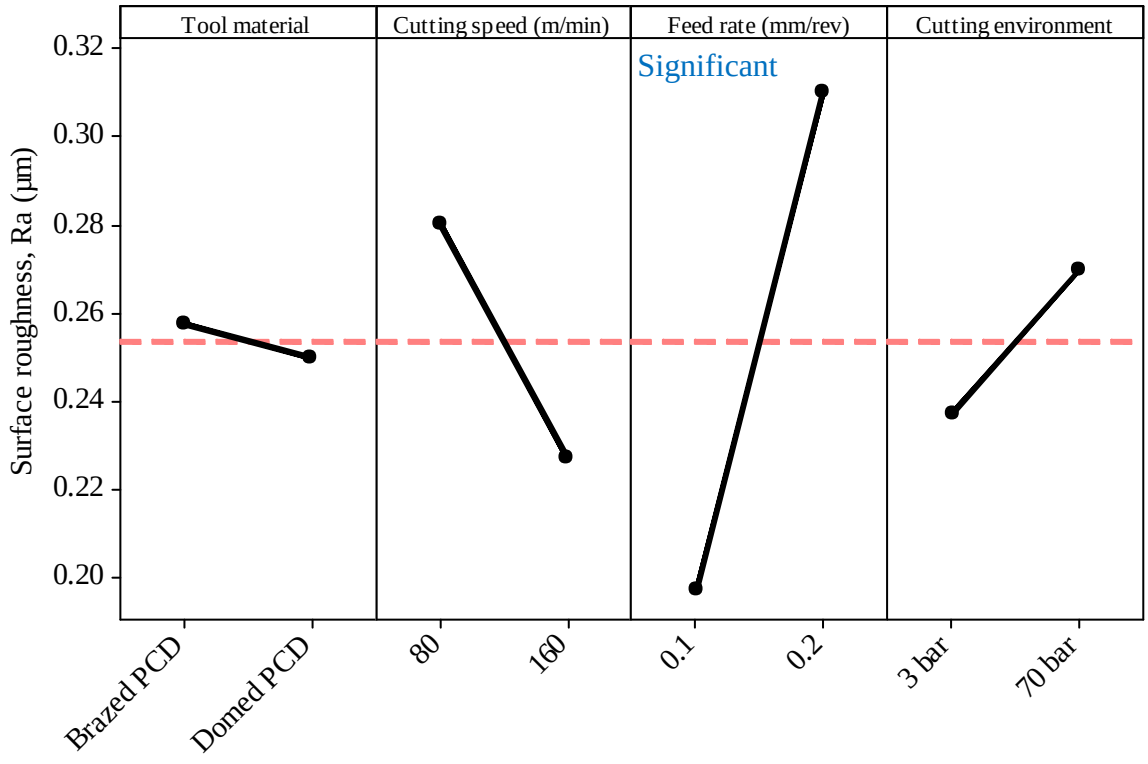


Figure 4.116: Main effects plot for surface roughness Ra measured at the last hole

4.7.8 Hole surface integrity analysis

Hole surfaces were generally smooth with limited damage in the form of smearing or voids / cavities in all tests when using brazed PCD drills, although vibration / chatter marks were observed in Tests 1 and 3. Figure 4.117(a) shows an overview of a typical inhomogeneous surface (over a length of ~ 4 mm) at the entrance of the first hole in Test 3 in comparison to a smooth surface produced in Test 7 with a domed PCD drill. Similar damage was observed in several holes from Tests 1 and 3, which were all located near the hole entrance. This mostly likely occurred during tool retraction, with a sharp ringing sound detected as the drill exited from the hole. Further SEM analysis showed that smearing together with adhered / deposited workpiece material were the main surface defects, see Figure 4.118 taken at the last hole in Test 3. The defects were possibly due to BUE and swarf clogging the drill flutes, similar to that shown in Figure 4.119. This was particularly evident when operating under flood coolant conditions. The curled / deformed and stacked chips likely caused chatter / vibration as well as drill deflection, which led to hole surface damage. This was also in line with variations in the recorded force / torque profile, as a sudden increase was observed when the drill exited the hole. Similar defects were not observed when using domed PCD tools regardless of the operating conditions with relatively damage free hole surfaces produced, see example in Figure 4.117(b).

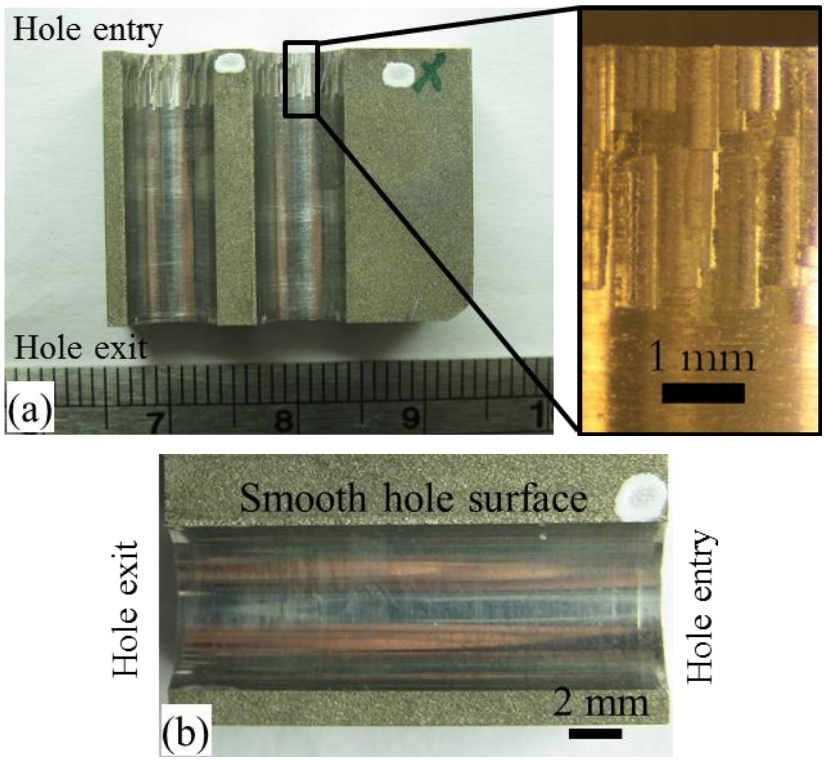


Figure 4.117: Overview of (a) the first hole surface in Test 3 using brazed PCD tool and (b) the last hole surface in Test 7 using domed PCD tool

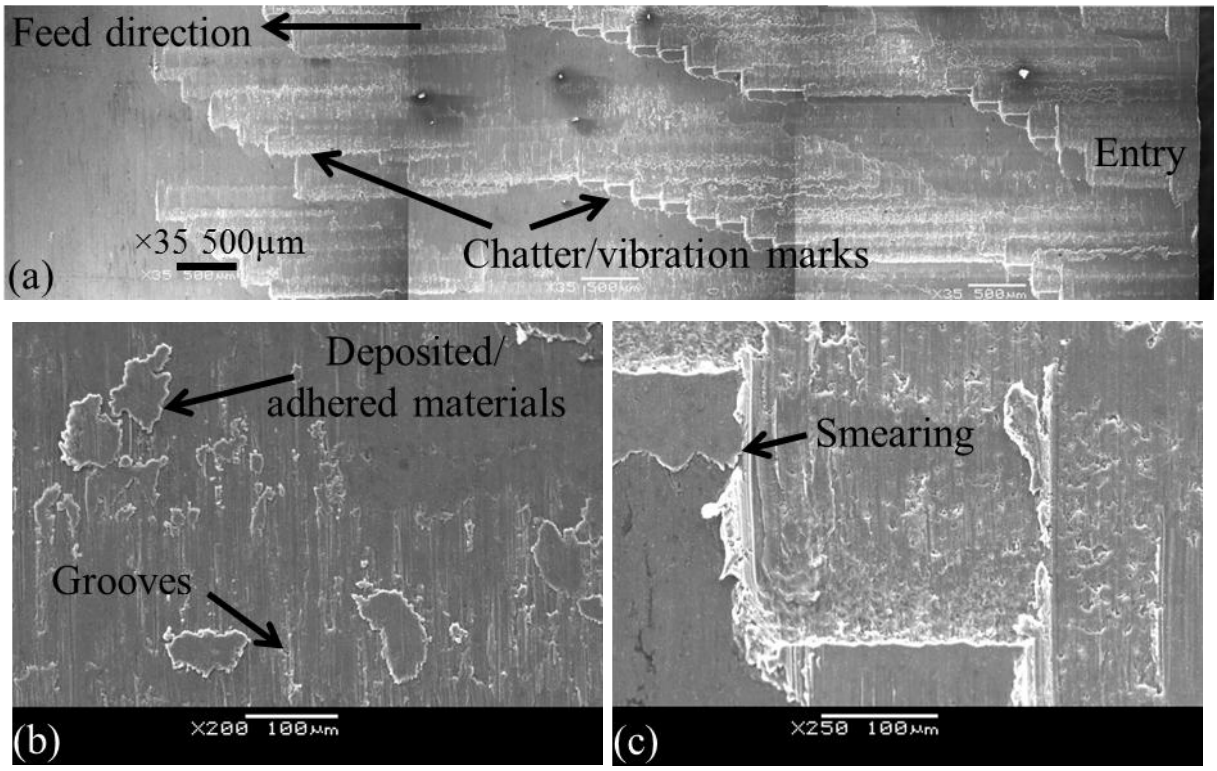


Figure 4.118: SEM micrographs of last hole (hole 306) surface in Test 3 with (a) overview and (b, c) higher magnification of hole surface

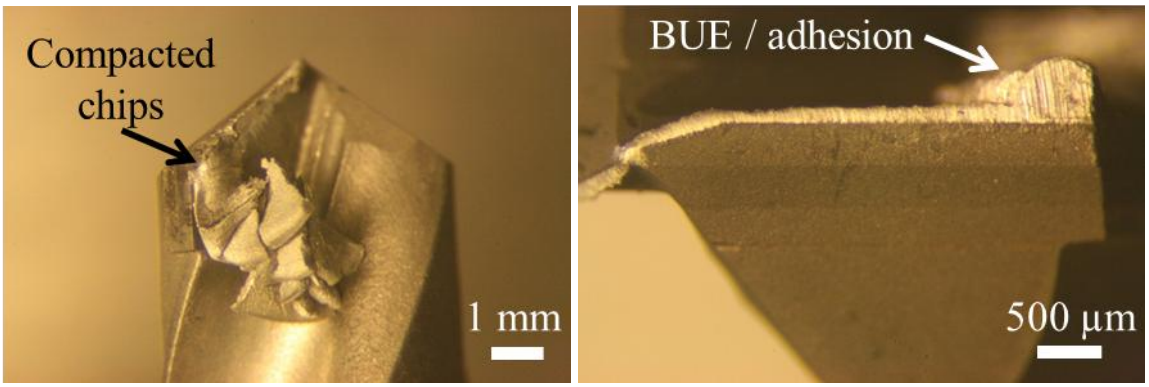


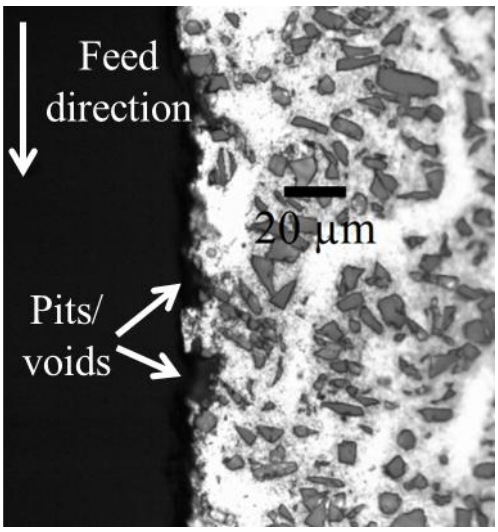
Figure 4.119: Sample pictures showing stacked / adhered chips / swarf at drill flute with (a) side view and (b) cutting lip at hole 234 in Test 3

Small cavities / voids with diameters of ~20µm were regularly observed in all trials especially at the last hole (hole 306), see SEM micrograph in Figure 4.120. This was due to pull out of SiC particles together with smearing of the matrix material. The dimensions of the porosities were in line with average size of reinforcement phase (15-20 µm). Figure 4.121 shows sample hole cross sectional micrographs taken along the feed direction. Loss of particles, folds / adhesion and smeared surfaces were observed in Tests 1 and 4 (see Figures 4.121(a) and 4.121(b)) when using brazed PCD tools. In constrast, comparatively smooth

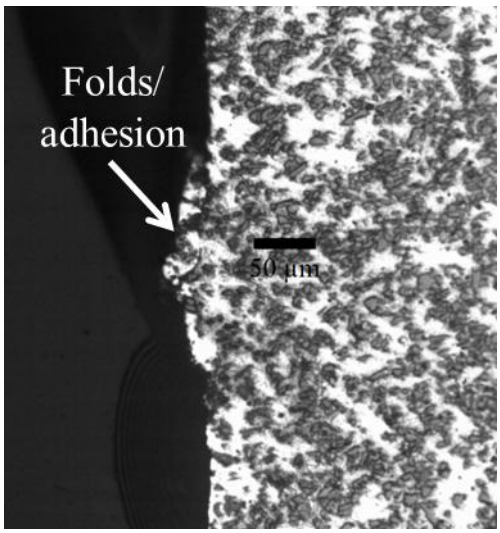
surfaces were seen when using domed PCD drills, due to the lack of BUE formation and superior cutting edge sharpness, see Figures 4.121(c) and 4.121(d).



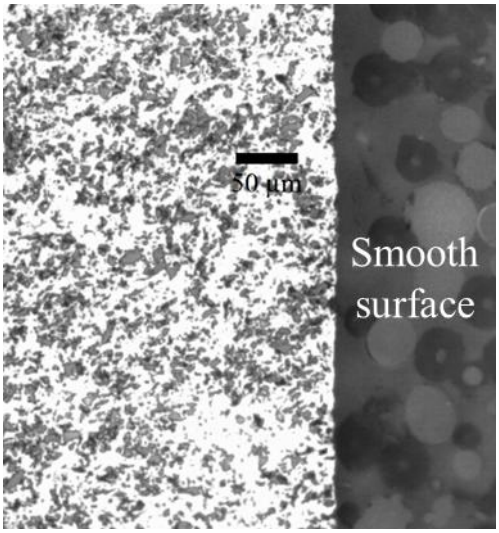
Figure 4.120: SEM micrograph observed at the last hole (hole 306) in Test 7



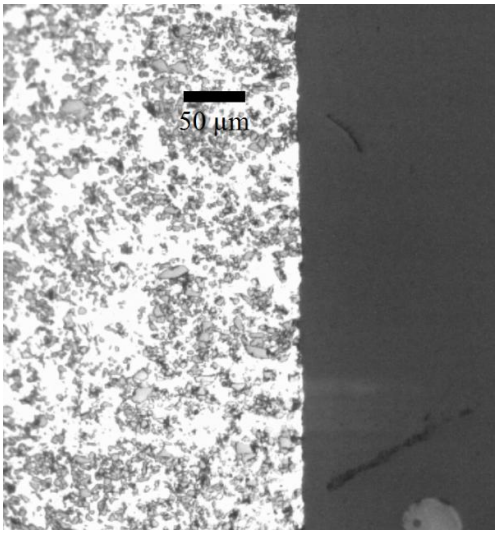
(a) Last hole in Test 1



(b) First hole in Test 4



(c) Last hole in Test 7



(d) First hole in Test 8

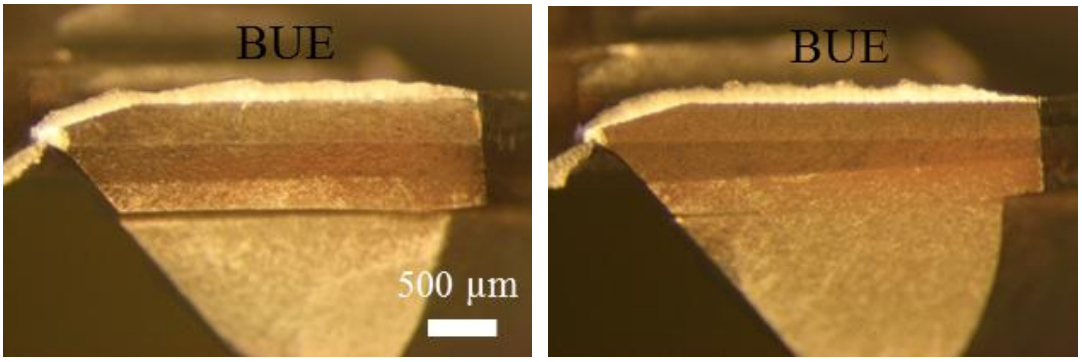
Figure 4.121: Sample micrographs observed at hole sections

4.8 Phase 3C: Drilling of MMCs using PCD tools at elevated / high cutting speeds

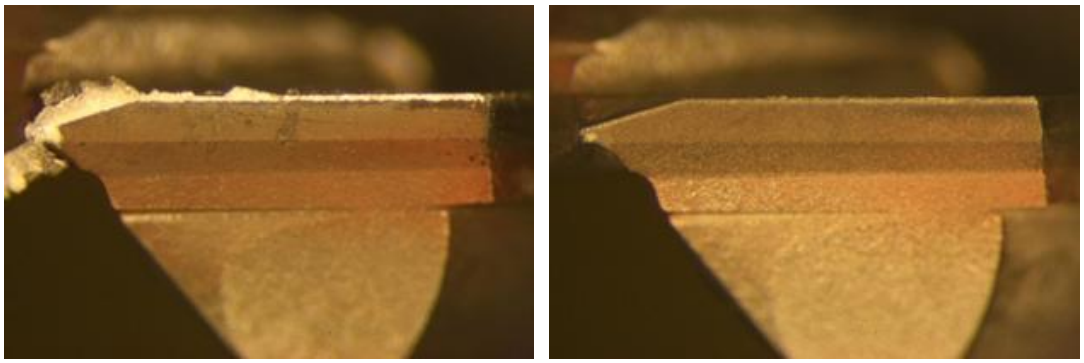
4.8.1 Tool wear / life, thrust forces and torque

Figure 4.122 shows sample micrographs of worn tools after drilling 300 holes (at test cessation) at various cutting speeds. Built up edge was prevalent in all trials and occurred mainly on the chisel edge and along the entire length of the cutting lip. A likely reason for this was the poor access / transport of coolant to the cutting zone especially at the bottom of the hole due to relatively thick (24 mm) workpiece. Lower levels of BUE was found in Test 4 when operating at the highest cutting speed (360 m/min), possibly due to the greater cutting temperatures generated. After soaking in 25% NaOH solution for ~1 min to remove the BUE / adhered materials, uniform flank wear was observed along the cutting edge, as shown in Figure 4.122(d). No chipping was observed in all trials with abrasion being the main tool wear mode due to the properties of the SiC particles. Figure 4.123 details maximum drill flank wear results at test cessation in all trials with detailed tool wear progression plots presented in Appendix C. All of the tests achieved the 300 hole criterion. Tool wear values were approximately similar between all tests with a maximum deviation of only 17 μm after drilling 300 holes. There was no apparent correleation between tool wear and cutting speed. This was possibly due to the stable layer of BUE observed and limited number of holes drilled.

The maximum thrust force and torque values at test cessation were also detailed in Figure 4.123, with the corresponding progression plot shown in Appendix C. The difference in thrust forces was limited to 14 N (~4% of the result recorded in Test 1) between all trials, possibly due to the constant feed rate applied together with the low level of tool wear (~70 μm) indicating the stable / consistent sharpness of the PCD drills. Maximum thrust force attained with worn tools (at test cessation) was 386 N in Test 2 (200 m/min) while torque values were constant at ~115 N.cm irrespective of cutting parameters.



(a) Last hole (hole 300) in Test 2 (b) Last hole (hole 300) in Test 3



(c) Last hole (hole 300) in Test 4 (d) After removal of BUE in figure (c)

Figure 4.122: Sample pictures of tool wear scar at test cessation

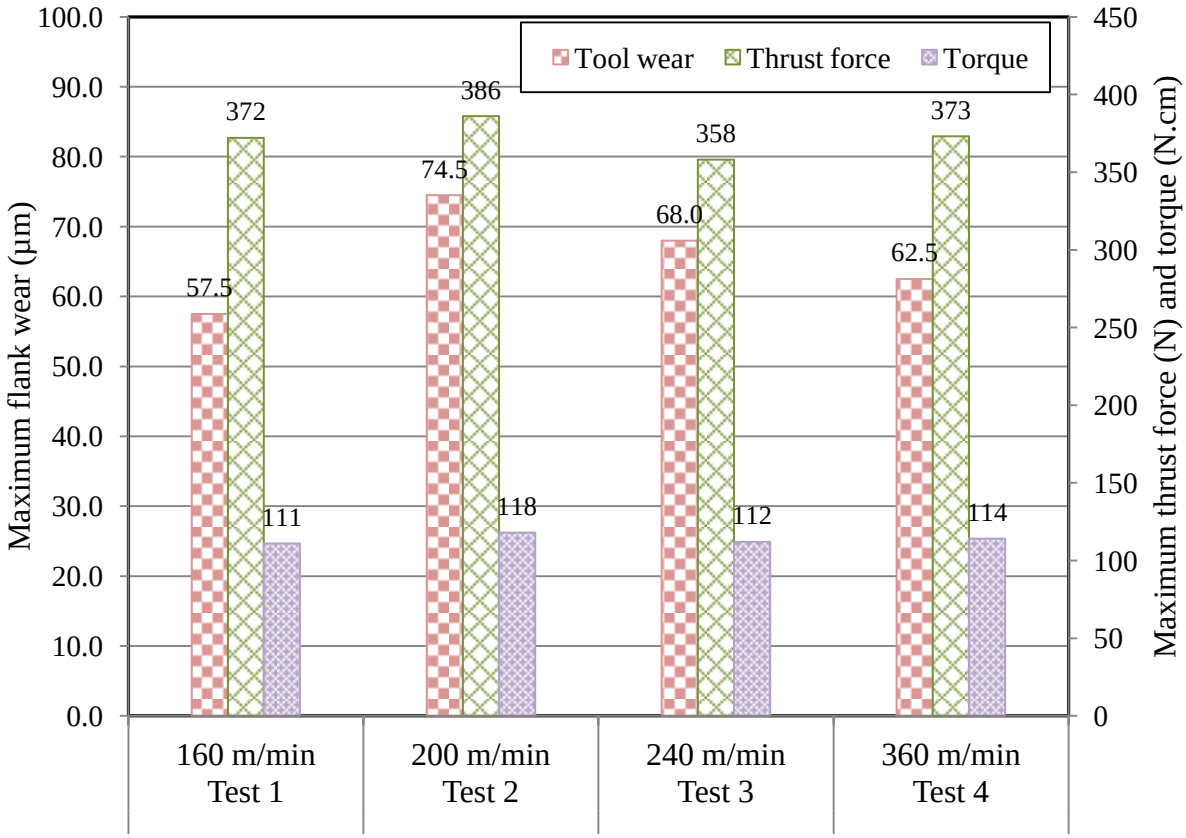


Figure 4.123: Maximum flank wear, thrust force and torque values at test cessation

4.8.2 Surface roughness analysis

Figure 4.124 details the results of surface roughness values including Ra, Rt, Rz and Rsk in all trials. In general, hole surface roughness was consistent and did not exceed 0.1 µm Ra in both the first and last holes regardless of cutting parameters. Drilling at higher cutting speeds (>160m/min) did not show any benefits / improvements in surface quality in terms of Ra. Surface roughness (Ra) showed a marginal improvement (~0.03 µm Ra) at the last hole compared with the first hole drilled. This was possibly due to the smaller feed marks as the radius of the cutting edge corner increased due to wear. Similar trends were also found in work by Rattanakit [213]. For the first hole, both Rt and Rz values increased with cutting speed possibly due to the increased tendency of SiC particle loss / pull out at elevated temperatures. This phenomenon was also observed for the last hole except in Test 3. A sample SEM micrograph showing the loss / pull out of SiC particles from Test 3 (240 m/min) is shown in Figure 4.125. The sample 2D topography trace recorded in Test 2 similarly revealed the presence of deep valleys on the hole surface, see Figure 4.126. Negative Rsk values up to -5.54 µm were found in all trials, suggesting a dominant peak topography with sharp / deep valleys, which was in agreement with observations from SEM microscopy and 2D topographic analysis.

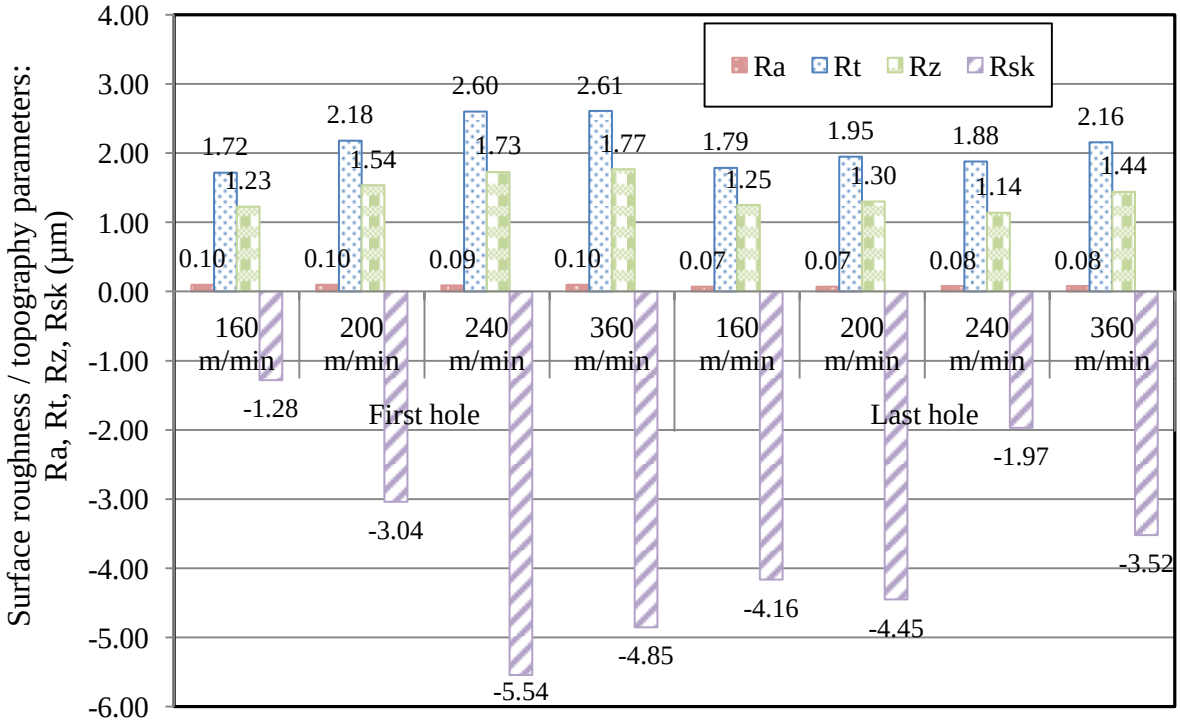


Figure 4.124 Hole surface roughness of Ra, Rt, Rz and Rsk measured at the first and last holes in all tests

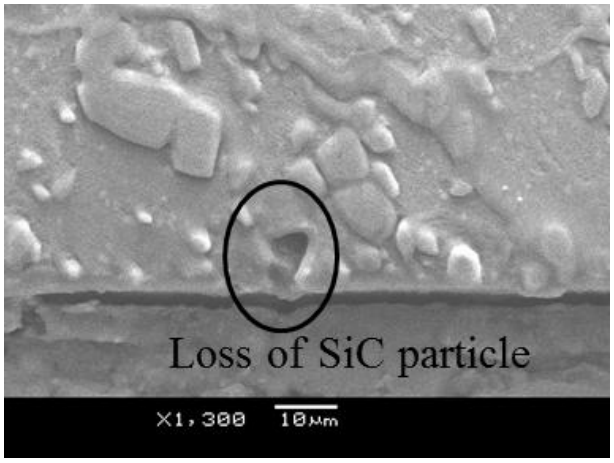


Figure 4.125: SEM micrograph observed at the last hole (hole 300) in Test 3

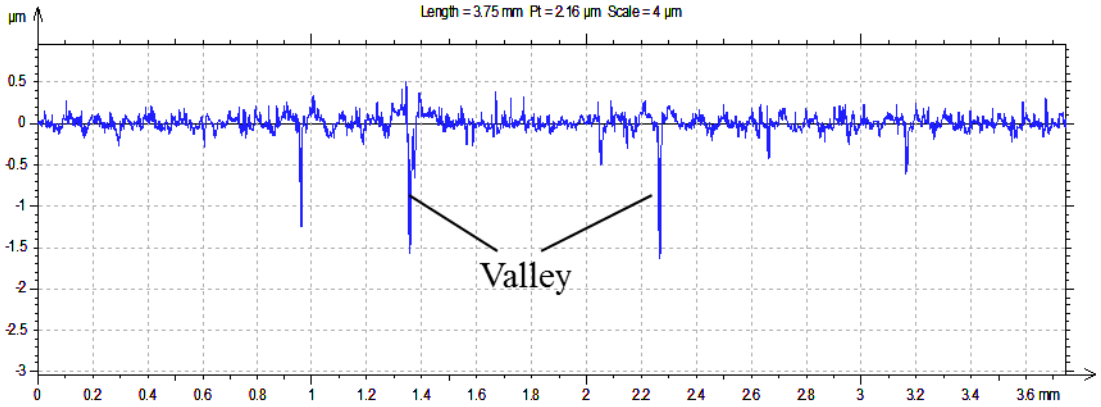


Figure 4.126: 2D topography trace recorded in Test 2 (200 m/min)

4.8.3 Microhardness analysis

Figure 4.127 shows Vickers' microhardness depth profile results for both the first and last hole (hole 300) in all trials. Observations showed the presence of a strain hardened layer up to a depth of ~80µm in both the first and last hole, irrespective of cutting parameters. The hardness increased by ~35$HV_{0.05}$ (~28%) above the bulk hardness (~125$HV_{0.05}$), which was partly due to the higher concentration of fine particles beneath the surface (~40 µm, detailed in section 4.8.6, see Figure 4.133(c)) and strain hardening / plastic deformation. Such trends are common when cutting metal matrix composite (MMC) and has been reported by several researchers [151-153]. Increasing cutting speed up to 360 m/min did not cause any substantial increase in subsurface microhardness compared with machining at 180 m/min. This was possibly due to the limited tool wear (~70 µm), suggesting consistent cutting edge sharpness when operating with high pressure coolant (70 bar).

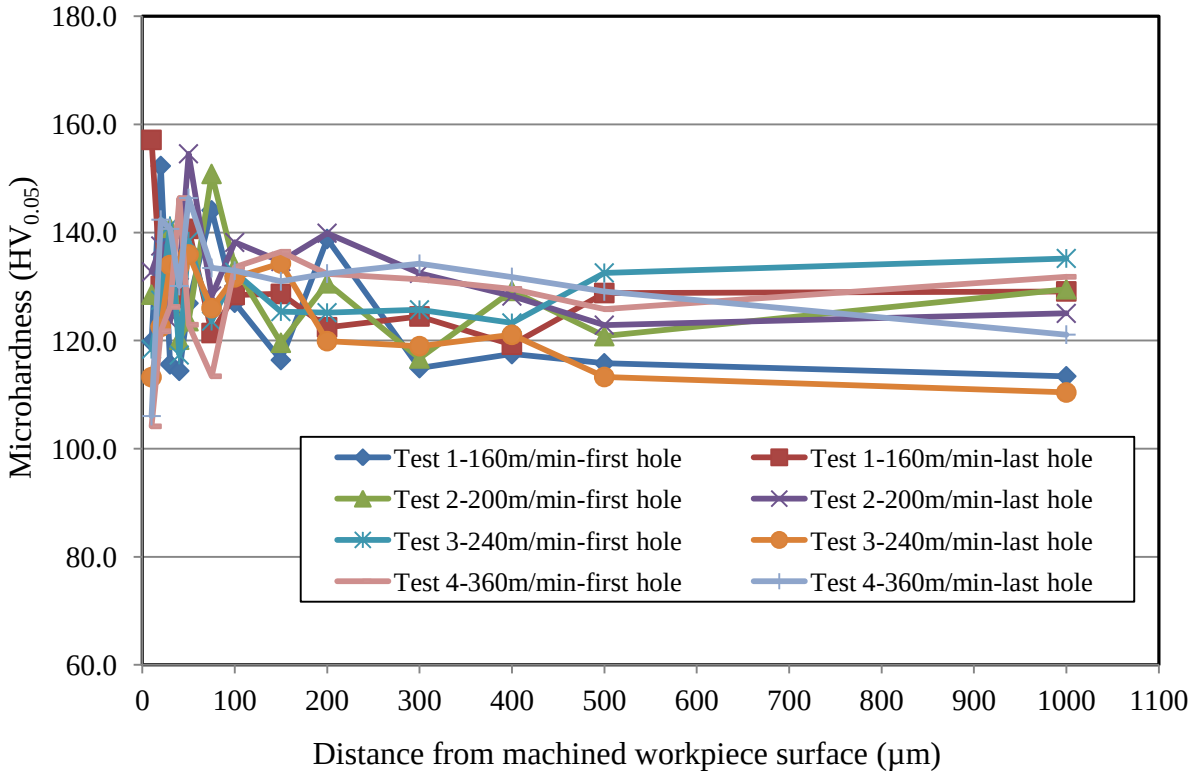


Figure 4.127: Microhardness profiles against distance from machined workpiece surface

4.8.4 Hole edge quality

Figure 4.128 presents exit hole edge micrographs for both the first and last hole in all trials. Similar results were attained compared with those in Phase 3B, the entry edges were free from burring irrespective of cutting parameters. Exit burrs were also absent, except for the test at 360 m/min due to limited flank wear (~70 µm) and consistent cutting edge sharpness. Irregular burrs occurred randomly at the hole exit in Test 4 (360 m/min) as shown in Figure 4.129. This was likely attributed in part to chatter / vibration at high cutting speeds and formation of BUE due to poor access of cutting fluid and lower cooling efficiency towards the bottom of the hole. The small chips generated could have also clogged of the drill flutes leading to restricted swarf evacuation.

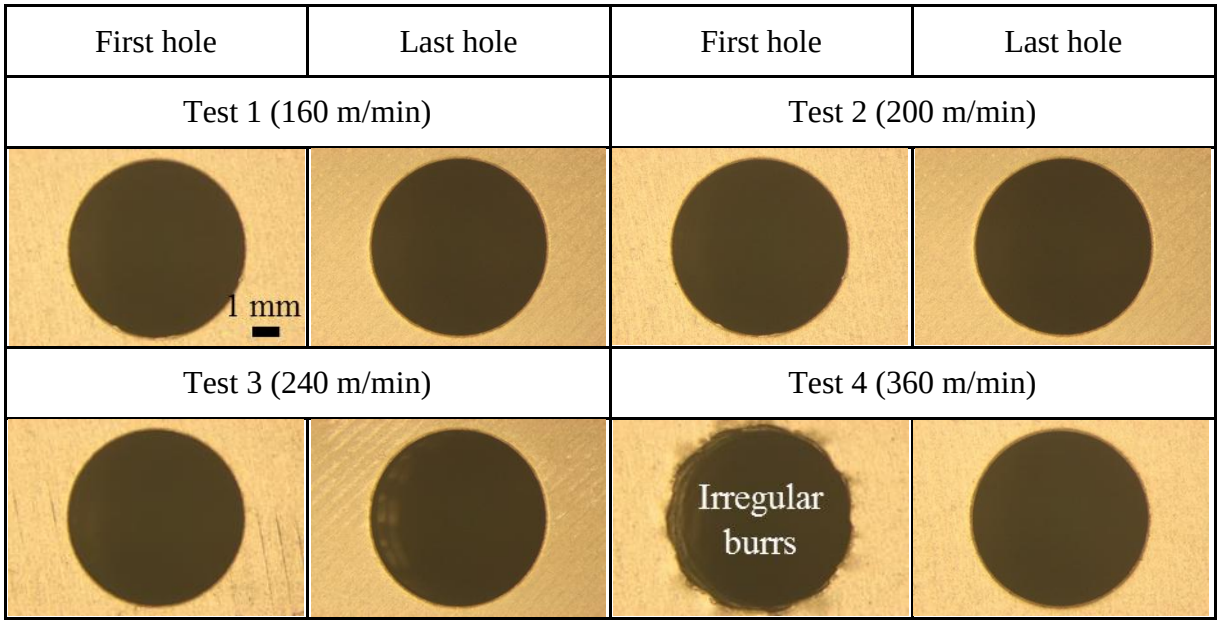


Figure 4.128: Hole exit quality at the first and last holes in all tests

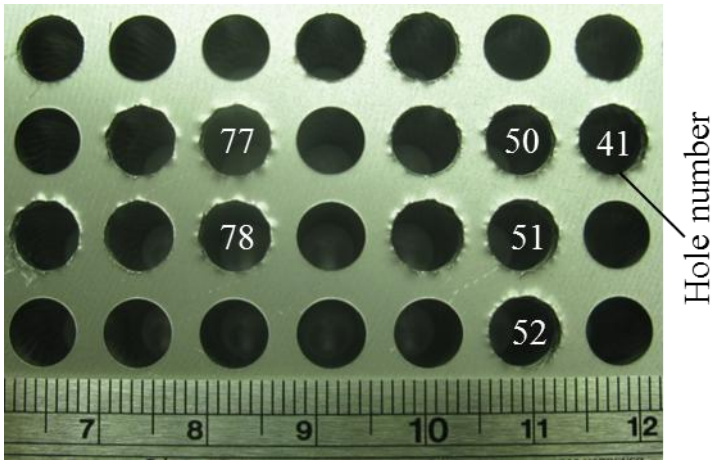
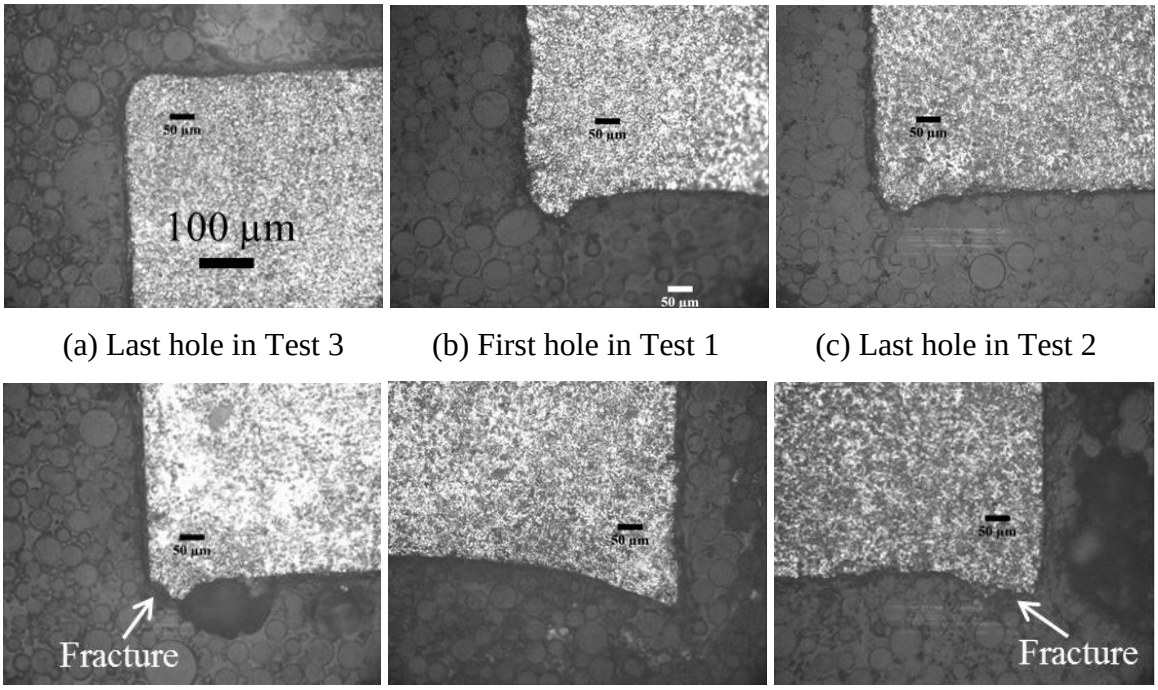


Figure 4.129: Irregular burrs observed at hole exit in Test 4 (360 m/min)

Figure 4.130 shows sample micrographs for burr formation of both hole entry and exit at various cutting speeds. In general, hole entry was consistently free of any major damage while uniform burrs without caps were obtained at the hole exit in all tests. Burr height was approximately 25 µm except for the first hole in Test 4 as chatter occurred. Fracture of the exit burr was seen at last hole (hole 300) in Tests 3 and 4 as shown in Figure 4.130(d) and 4.130(f) respectively. This was possibly due to low ductility of the strain hardened workpiece material together with poor flow of coolant to the cutting zone. There was no sign of increased burr size in hole 300 produced using brazed PCD drills when cutting speed increased from 160 to 280m/min, while irregular burrs were observed to form randomly when drilling at the highest cutting speed of 360 m/min.



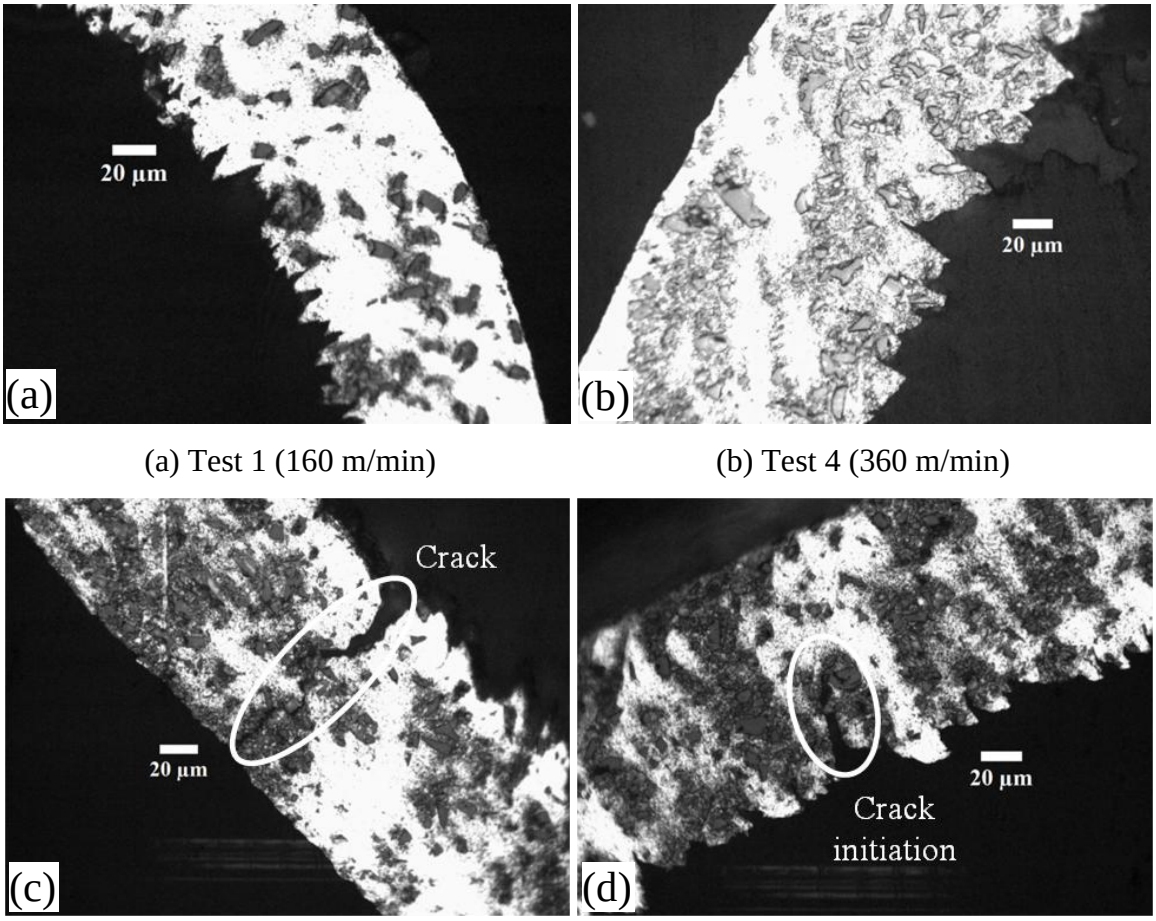
(a) Last hole in Test 3 (b) First hole in Test 1 (c) Last hole in Test 2

(d) Last hole in Test 3 (e) First hole in Test 4 (f) Last hole in Test 4

Figure 4.130: Sample micrographs of burr morphology at hole entry and exit

4.8.5 Chip morphology

In general, short needle-like chips were obtained in all trials. Further analysis using a high resolution microscope highlighted the formation of saw-tooth morphology at the cross-section of the top surface of all chips, as shown in Figure 4.131. At the higher cutting speed of 360m/min, the saw-tooth profile was more apparent although the frequency was reduced. Both the saw-tooth pitch and height were found to increase with cutting speed. This was in agreement with the results found by Akhavan et al. [209] when drilling Al-Si alloy at different cutting speeds (240-320 m/min). Cracks and crack initiation were observed at higher cutting speeds (360 m/min) as shown in Figure 4.131(c) and 4.131(d) respectively, due to severe plastic deformation and the low ductility of SiC reinforced aluminium MMCs (< 4%), while small voids were formed following the loss of SiC particles [7, 146, 207].



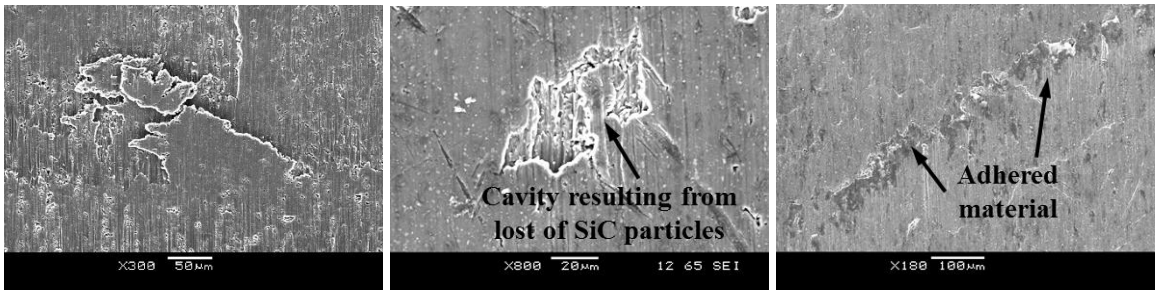
(a) Test 1 (160 m/min) (b) Test 4 (360 m/min)

(c-d) Test 4 (360 m/min)

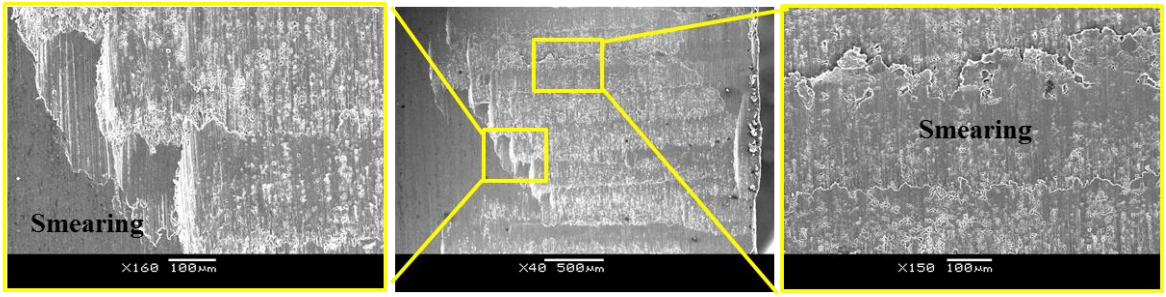
Figure 4.131: Chip morphology at the cross section observation

4.8.6 Hole surface integrity analysis

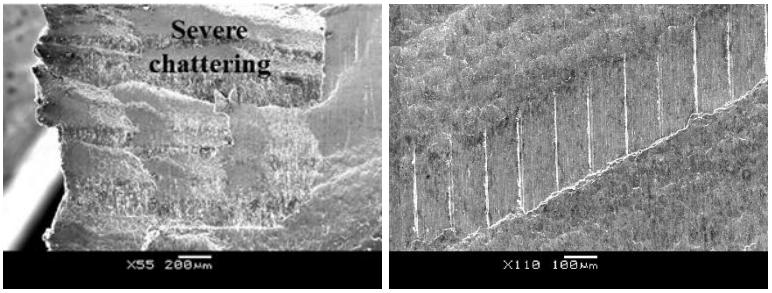
Figure 4.132 shows sample SEM micrographs of hole surfaces drilled at various cutting speeds. Grooves and smearing were visible on the surface, as shown in Figure 4.132(a). Small cavities (~20 µm in diameter) resulting from loss of particles / pull out were not uncommon in all trials. When increasing cutting speed to 280 m/min, chatter marks and smearing were observed at the entry of the last hole, which extended to ~ 3 mm in length. This was found to occur randomly over the test duration (300 holes), particularly during drill extraction from the hole, which was also usually accompanied by a ringing sound. The likely reason was attributed to the generation of BUE and tool deflection. Severe chatter / vibration was observed at / close to the hole exit when drilling at high cutting speed up to 360 m/min, as shown in Figure 4.132(e) and 4.132(f). This was possibly due to tool deflection and limited coolant transport to the bottom of the hole.



(a) Hole 128 in Test 2 (b) Last hole in Test 2 (c) Last hole in Test 3



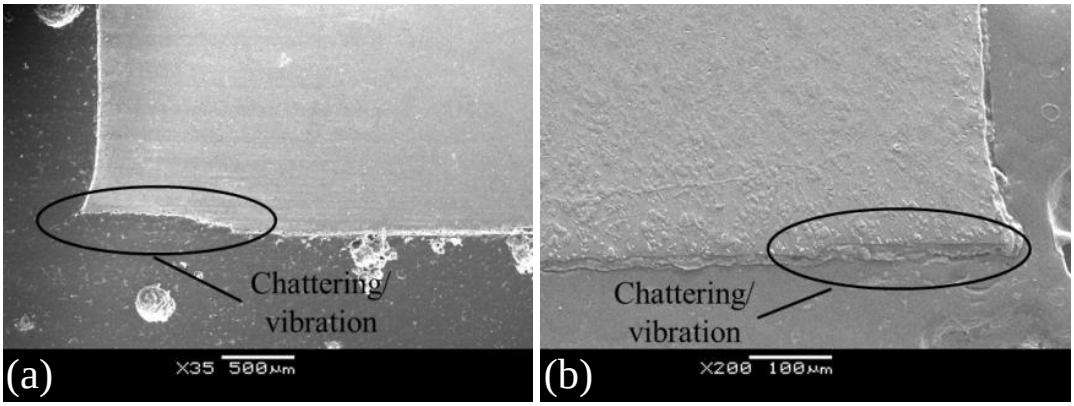
(d) Last hole in Test 3



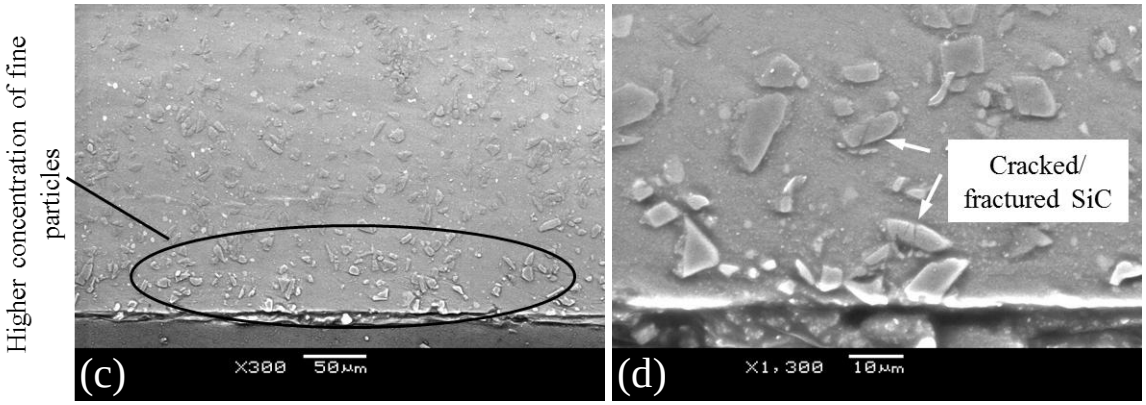
(e) First hole in Test 4 (f) Hole 65 in Test 4

Figure 4.132: SEM micrographs of hole surfaces

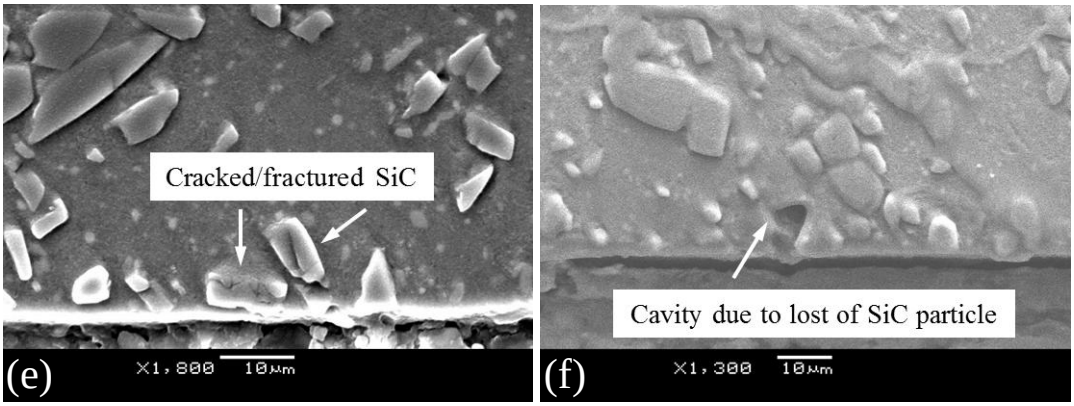
Some examples of workpiece subsurface damage are shown in Figure 4.133. A similar form of damage was present in all of the machined surfaces, being most severe in Test 4 especially at hole exit. A detailed examination revealed that chatter / vibration occurred at hole entry and exit in Tests 3 and 4, as shown in Figures 4.133(a) and 4.133(b) respectively. Shattered and cut particles can be generally identified on the surface, while fractured SiC particles were also prevalent up to a depth of ~15 µm beneath the machined surface, see Figures 4.133(d) and 4.133(e). It was likely that the high frequency of fractured / cracked particles was induced by ploughing of the cutting edge causing sudden tensile loading and exacerbated by the very brittle nature of the SiC material. High concentration of fine particles up to a depth of ~40 µm was observed (see Figure 4.133(c)) due to plastic deformation and resulted in subsurface hardening. Partial or complete SiC particles were also seen to be pulled out by the cutting tool and transported away with the chip or cutting fluid, leaving behind a void on the hole surface, see Figure 4.133(f).



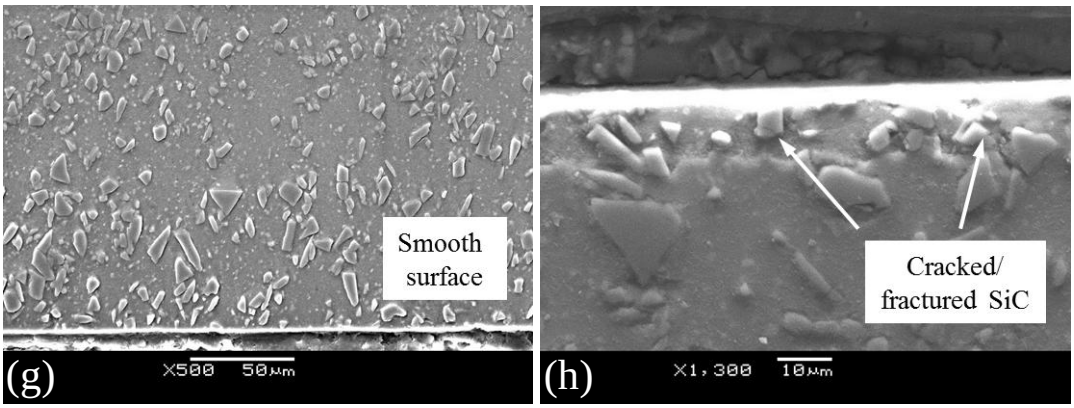
(a) First hole in Test 4 (b) Last hole in Test 3



(c-d) First hole in Test 1



(e-f) Last hole in Test 3



(g) Last hole in Test 3 (h) First hole in Test 4

Figure 4.133: SEM micrographs of machined subsurface

Chapter 5: CONCLUSIONS

5.1 Literature review

5.1.1 Drilling of CFRP

- While published research on the drilling of CFRP composites is extensive, the majority have reported experiments involving relatively low number of holes machined (<100). Cutting speeds varying from 20 to 80 m/min are usually employed, whereas feed rate values were generally lower than 0.3 mm/rev.
- The performance of uncoated tungsten carbide and hardmetal coated tools have been widely evaluated, while there have been limited investigations involving diamond coated and PCD drills to date.
- Dry cutting environment is commonly applied when drilling CFRP composites, with minimal trials conducted under chilled air or flood coolant conditions.
- While fibre pull out and matrix burning is prevalent drilling CFRP workpiece materials, hole entry / exit delamination and uncut fibres predominantly at the hole exit are the most common defects. Research has focused primarily on analysing the effect of cutting parameters on hole damage / defects, while corresponding data relating to fibre / ply orientation is scarce.
- Various non-conventional machining processes including laser machining, abrasive jet machining, vibration assisted machining and electrical discharge machining have been investigated for the cutting CFRP composites. However the high initial investment cost, low productivity together with limited improvement in surface finish of most non-conventional processes compared to conventional mechanical drilling have prevented industrial take-up.

5.1.2 Machining of MMC materials

- Literature relating to machining of MMCs is similarly extensive, although the majority have been focused on turning. Cutting tool materials / coatings assessed have encompassed uncoated tungsten carbides, hardmetal and diamond based coatings as well as PCD. While use of PCD inserts are widely utilised for turning of MMCs to improve productivity and surface finish, limited work on PCD tools has been reported in drilling operations.

- Use of flood and dry cutting environments is usually employed when machining MMCs, while trials involving high pressure coolant application is rarely reported.
- Research on drilling MMCs has focused primarily on the effect of cutting parameters on surface / subsurface damage and hole edge quality, with limited data corresponding to hole geometrical accuracy.
- Commonly observed issues when machining MMCs include high tool wear rate, formation of built up edge and adhered workpiece material on cutting tool tips as well as workpiece surface damage in the form of grooves, particle pull out, smearing and cavities.
- Laser assisted turning is the most common nonconventional technique used for machining MMCs, although complicated experimental setup and high investment costs are major drawbacks.

5.2 Experimental work – drilling of CFRP composites

5.2.1 Phase 1A: Influence of operating conditions and tool materials / coatings when drilling CFRP

- Swarf entanglement on the drill and adhesion of CFRP debris on the cutting flutes were prevalent when operating at a cutting speed of 90 m/min and feed rate of 0.05 mm/rev (Tests 1, 5 and 9) irrespective of tool materials / coatings. This was possibly due to higher temperatures generated when operating at low feed rate and dry condition.
- All tests involving the CVD-diamond coated drills achieved the 512 holes criterion, with flank wear ranging from 111 to 145 µm.
- With domed PCD tools, flank wear ranged from 73 to 96 µm, with the best performance seen in Test 12 (180 m/min, 0.1 mm/rev and dry condition). Abrasion was the main tool wear mode.
- Fibre dust / matrix burning was observed in Tests 1 and 4 using uncoated WC tools after drilling ~160 holes.
- The maximum thrust force in all trials did not exceed 310 N while torque was below 53 N.cm. These were typically lower compared to results reported in the literature. This was most likely due to the optimised double point angle geometry, with the top cutting lip acting as a pilot drill.

- Limited defects were observed at the entrance location even after drilling 512 holes when using CVD-diamond coated WC and PCD tools regardless of cutting parameters / conditions, while damage in the form of delamination, fuzzing and uncut fibres were predominant after ~100 holes when using uncoated tools.
- Uncut fibres and splintering / delamination were found at the exit of all holes using CVD-diamond coated WC tools. Conversely, holes machined with new domed PCD drills exhibited limited / marginal damage regardless of cutting parameters, while uncut fibres were prevalent at test cessation.
- Domed PCD tools generally produced lower delamination levels (33% and 10%) of the first and last hole respectively compared to CVD-diamond coated WC tools.
- Hole size error was up to 40 µm (~0.63%) when employing CVD-diamond coated WC tools (undersized), while domed PCD drills generated oversized holes with deviation limited to 17 µm after 512 holes. The best result was obtained in Test 10 with only a 4 µm deviation.
- In general, hole roundness and cylindricity values were constant except for results in Tests 5 and 9 (90 m/min, 0.05 mm/rev), which deteriorated significantly after ~320 holes.
- Fibre pull out resulting in voids / grooves were the main damage mode on hole surfaces. Ply orientation had a significant influence on hole quality with minimum defects on plies at 0º, 45º and 90º, while higher damage was seen at plies with 135º fibre orientaion.

5.2.2 Phase 1B and 2A: Evaluation of hole quality when drilling CFRP with variable feed rate operation

- In general, both thrust force and torque values increased with chilled air and flood coolant irrespective with cutting parameters. Maximum thrust force increased by up to 17.3% in flood condition compared with results drilled in dry condition.
- All tests achieved the 384 hole criterion with tool flank wear ranging from 114 (Test 5) to 193µm (Test 2). Tool-workpiece contact time increased by ~20% as feed rate increased from 0.1 (3.78s) to 0.3mm/rev (3.03s) for each hole.
- The maximum thrust force recorded was 591N at hole 384 in Test 6 (first stage of drilling), while at hole exit, thrust force remained stable at between 100 and 120N at a feed rate of 0.01mm/rev. Torque decreased by 61-78% when operating with the variable feed rate strategy.

- Feed rate was a significant factor affecting the entrance F_d of the first hole with a PCR of 87.9%. There was limited discrepancy between the exit delamination factors for the first and last holes due to the reduced feed rate of 0.01mm/rev used in all tests.
- Drilling with variable feed rate strategy improved surface quality at the hole exit section in terms of reduced fibre pull out and damage / voids.
- Measurement of hole diameter showed that all holes were generally undersized. The deviation from the nominal diameter was up to ~40 µm (~0.7%) at test cessation (hole 384).
- Even within the first hole, greater damage / voids were observed at the hole entry when operating at the principal feed rates (0.1-0.3 mm/rev) compared to the exit location, where the surface was almost smooth with limited damage were observed. For the last hole, damage / voids were seen over the entire surface including the exit location where reduced feed rate was employed.

5.2.3 Phase 2B: Influence of workpiece configuration / fibre orientation and high feed rates on hole quality when drilling CFRP

- The drill experienced catastrophic failure / fracture when operating at a feed rate of 0.6mm/rev as maximum thrust force was ~1304N. When operating at 0.2 and 0.4mm/rev feed rate, the wear progression followed a similar trend and all trials achieved 384 holes with maximum flank wear of 123 µm seen in Test 3 (Type 3 WP, 0.2 mm/rev) while the best performance was obtained in Test 4 (Type 1 WP, 0.4 mm/rev) with 102 µm flank wear.
- Abrasion and chipping (at drill corner) were the main tool wear modes.
- Thrust force values were between ~80 and 110 N, while torque values were typically constant (~30 N.cm) when drilling with the reduced feed rate (0.01 mm/rev).
- Uncut fibres and splintering were prevalent at hole entry when increasing feed rate to 0.4mm/rev even for the first hole. Hole exit was consistently smooth with minimal uncut fibres, due to the use of a support jig (with 7.0 mm diameter clearance holes) and reduced feed rate (0.01mm/rev).
- Uncut fibres / delamination mostly occurred at opposite quadrants of a hole with the critical cutting angles being in the range of $90^o \leq \theta < 180^o$, irrespective of exit ply orientations when drilling without a support jig.
- Surface roughness near the bottom of the hole was typically lower (maximum value recorded 4.04 µm Ra) compared with the top section in all tests due to the reduced

feed rate prior to the drill exiting the workpiece.Type 2 CFRP workpiece material produced the lowest Sa value (1.16 µm) at a feed rate of 0.4 mm/rev while Type 3 gave the highest roughness value (2.47 µm Sa) at test cessation.

- Surface defects in the form of grooves / cavities were generally observed at 135º plies irrespective of cutting parameters and tool condition, while those at 0º, 45º and 90º showed comparatively limited damage when utilising new drills. Due to the anisotropic nature of the material and influence of fibre direction on workpiece damage, 3D topographic / areal parameters are necessary for assessing machined surface quality in CFRP workpieces.
- In general, all tests produced oversized holes (>6.38 mm) with maximum variation at test cessation up to 10 µm. Surprisingly, drilling at high feed rate of 0.4 mm/rev did not deteriorate roundness levels as marginal variation was observed in all tests irrespective of the number of drilled holes. The effect of workpiece material type on roundness was not significant. Cylindricity results were similar to out of roundness data, with average value of ~15 µm recorded for the first hole which increased to ~23 µm at test cessation after drilling 384 holes.
- SEM observations showed smearing of matrix material and adhered / deposited fibre dust in the cavities when drilling with the lower feed rate (0.01mm/rev) near the exit location.

5.2.4 Phase 2C: Evaluation of diamond coated and domed PCD tools when drilling CFRP at elevated / high cutting speeds

- When drilling at 360 m/min with diamond coated tool, the drill fractured / broke at the third hole, due to chatter / vibration resulting in tool deflection at the hole entrance. For diamond coated tools, flank wear was lower by 21% (to 93µm) and 26% (to 86µm) after 384 holes when drilling at 240 and 280m/min respectively compared to operating at 180m/min (117µm), while there was only 9 µm difference when using domed PCD tools. Tool wear modes were confined to abrasion / cutting edge rounding without any signs of coating chipping.
- For the first hole, both thrust force and torque values generally increased with cutting speed irrespective of tool materials. At the cutting speed of 360 m/min, thrust force / torque at the first hole increased by 92.7% / 433% and 87.8 / 131.5% for diamond coated and domed PCD drill respectively in comparison with the corresponding values generated at the cutting speed of 180 m/min. For the last hole, the trend of thrust force

and torque produced by diamond coated tools was not apparent, they were however lower (up to 73 N) compared with the values generated at cutting speed of 180 m/min.

- Chatter / vibration was recorded and evident in both Tests 2 (240 m/min) and 3 (280 m/min) especially at the beginning of drilling stage when employing diamond coated drills. A ringing sound was also heard during machining but gradually reduced as the operation progressed.
- For diamond coated tools, increasing cutting speed to 280m/min led to incidence of uncut fibres at hole exit even with the use of a backup plate, although the number of uncut fibres were reduced compared with results in Test 1 (180 m/min). Surprisingly, small number of uncut fibres were still found at the last hole even drilling with domed PCD tool and high cutting speed up to 360 m/min.
- Chatter / vibration was observed until ~2.5 mm beneath the entrance surface at the cutting speed of 240 and 280 m/min. In this section, fibre dust was deposited / adhered on the hole surface.
- For both the first and last holes (hole 384) drilled with diamond coated tools, deposited / adhered fibre dust was typically observed at the hole entrance when cutting speed was elevated above 180 m/min. The hole surface was however comparably clean when using domed PCD tools even drilling at 360 m/min.

5.3 Experimental work – drilling of MMC materials

5.3.1 Phase 3A: Preliminary / benchmarking trials in drilling MMCs with different tool materials / coatings

- SEM micrographs of uncoated and coated tools at test cessation demonstrated that abrasion was the dominant tool wear mechanism when drilling MMC materials.
- PCD tools showed superior performance compared with uncoated and coated drills in terms of tool wear, productivity, hole quality and surface integrity. Uncoated and coated tools only lasted for ~10 holes, although increasing feed rate (to 0.2 mm/rev) gave slightly better tool life.
- Coated WC tools did not show any benefits when drilling MMC in comparison with uncoated tools.
- The tool wear of PCD drills was only ~60 μm after drilling 300 holes at the speed of 80 m/min. Increasing cutting speed to 160 m/min did not accelerate tool wear.

- Cavities / voids were observed over the internal hole surface and back surface of the chips when using coated and uncoated drills. It showed that SiC particles were ploughed / pulled out of the matrix material during drilling rather than sheared, due to the limited abrasion resistance and lower hardness of these tools in comparison with SiC particles.
- Fan-shaped chips were produced when using uncoated and coated drills irrespective of the cutting conditions employed, while brazed PCD tools generated needle-like chips.
- There was limited / marginal BUE on the cutting edge of coated and uncoated drills while BUL was evident on uncoated drills. This was possibly the benefits of using internal high pressure coolant which reduced temperature sufficiently.

5.3.2 Phase 3B: Evaluation of domed PCD tools and cutting parameters when drilling MMCs

- Brazed PCD tools generally exhibited lower flank wear compared with domed PCD tools, which was most likely due to the protection of built up edge (BUE). The best performance in terms of tool wear (40 µm) was obtained when cutting with flood coolant (3 bar) using brazed PCD drill at 80 m/min with a corresponding feed rate of 0.2 mm/rev.
- For both the first and last holes, the values generated at high feed rate (0.2 mm/rev) were considerably higher (up to 337 N and 64 N.cm) compared to those at low feed rate (0.1 mm/rev) with specific / same cutting speed regardless of cutting environment and tool material. The maximum thrust force (767 N) and torque (167 N.cm) in all trials was recorded in Test 6 when using domed PCD drill at 80 m/min and feed rate of 0.2 mm/rev with high pressure coolant (70 bar).
- Limited damage in the form of burr formation was seen for all the first and last holes drilled with brazed PCD tools, while roll-back burrs were prevalent at the last holes when using domed PCD drills. Burr fracture was common when using brazed PCD tools due to low ductility of MMC materials.
- Needle-like chips were produced when using brazed PCD drills regardless of cutting conditions and machining environment, while various types of swarf was generated when employing domed PCD tools regarding to different cutting parameters. Long and short spiral swarf were found in Tests 5 and 8, while fan-shape chips were seen in Tests 6 and 7 with high pressure coolant (70 bar).

- Hole diameter deviation produced between drills in new and worn (at test cessation) conditions was limited within 8 µm in all trials, due to low tool wear levels and consistent cutting edge sharpness. In terms of geometrical error measurements, out of roundness was generally below 10 µm and cylindricity was limited within 20 µm for all the drilled holes.
- Microhardness increase was between 50 and ~60 $HV_{0.05}$ in comparison with bulk hardness (~125 $HV_{0.05}$) irrespective of cutting parameters and extended up to ~100 µm beneath the machined surface for both the first and last drilled holes.
- In general, hole surfaces were consistently smooth, as Ra was limited within 0.51 µm and Rt did not exceed 6.9 µm for all the measurements.
- Hole surface was generally smooth with limited damage in the form of smearing and voids / cavities in all tests, while vibration / chattering marks were randomly observed when using brazed PCD tools. The marks were approximately 4 mm in length starting from hole entrance, which was possibly due to BUE and swarf clogging in the drill flutes.

5.3.3 Phase 3C: Drilling of MMC using PCD tools at elevated / high cutting speeds

- Tool wear, thrust force and torque were similar in all 4 tests as the deviation was only 17 µm, 14 N and 7 N.cm respectively after drilling 300 holes. Built up edge was apparent in all tests.
- Surface roughness of machined holes did not exceed 0.1 µm Ra in both the first and last holes regardless of cutting parameters. Drilling at higher cutting speed (>160 m/min) did not show any improvements in Ra.
- A strain hardened layer up to a depth of ~80 µm was observed in both the first and last hole in all tests. The hardness increase was ~35HV0.05 (~28%), which was partly due to higher concentration of fine particles near / beneath hole surface (up to 40 µm) as well as strain hardening / plastic deformation.
- Irregular burrs occurred randomly at hole exit at a cutting speed of 360 m/min, partly due to increased tool deflection and generation of BUE due to the lower cooling efficiency of the cutting fluid towards the bottom of the hole.
- At higher cutting speed of 360 m/min, the saw-tooth phenomenon became more apparent and the frequency was reduced. Both the saw-tooth pitch and saw height increased with cutting speed. Cracks and crack initiation were observed at high cutting speed of 360 m/min.

- SEM observations showed that SiC particles were mostly cut through with few cavities due to loss / pull out of particles, while fractured particles were prevalent up to a depth of ~15 μm beneath the machined surface.

5.4 Overall conclusions and recommended operating conditions

5.4.1 Drilling of carbon fibre reinforced plastic composite materials

- Uncoated carbide tools are not recommended for drilling CFRP due to rapid cutting edge rounding and flank wear (main tool wear modes). Drilling dry together with low feed rate (<0.05 mm/rev) and high cutting speed (>180 m/min) is likely to cause fibre dust / matrix burning.
- Use of chilled air is imperative when drilling composites to avoid fibre dust entangling on the drill and reduce the risk of matrix burning / degradation.
- Good correlation was observed between cutting edge radius and drilled hole surface quality. Cutting edge sharpness was more critical / significant for controlling surface damage in comparison to feed rate.
- Diamond coated WC and domed PCD tools showed superior performance in drilling CFRP, as the flank wear was only 111 and 73 μm respectively after drilling 512 holes (180 m/min, 0.1 mm/rev). Domed PCD tools showed considerable benefits over diamond coated tools in terms of consistent cutting edge sharpness and longer tool life (lower flank wear level).
- Variable feed rate drilling strategy is recommended in order to significantly improve hole exit quality. Use of principal feed rate up to 0.4 mm/rev in the first drilling stage and subsequently reduced to of 0.01 mm/rev in final 0.5 mm was demonstrated as the best combination in terms of tool wear and hole exit quality.
- The majority of hole damage in the form of fibre pull out / loss of fibres occurred at 135º fibre orientation.
- Domed PCD tools can be employed for high speed drilling (up to 360 m/min) to improve productivity, while chatter / vibration prevents use of CVD-diamond coated WC tools beyond ~180 m/min.
- Table 5.1 lists the recommended / preferred operating conditions for drilling CFRP composite materials.

Table 5.1: List of recommended / preferred operating parameters / strategy when drilling CFRP

Parameter / strategy	Value
Cutting environment	Chilled air
Tool material / coating	Diamond coated WC, domed PCD
Cutting speed	80-100 m/min for CVD-diamond coated WC tools, 180-240 m/min for domed PCD
Feed rate (variable)	0.2-0.4 mm/rev and 0.01 mm/rev in final 0.5 mm

5.4.2 Drilling of metal matrix composite materials

- Uncoated and coated WC tools lasted for only ~10 holes when drilling Al/SiCp MMCs irrespective of cutting parameters. The PCD tools showed superior performance in terms of tool wear, productivity, hole quality and surface integrity.
- Feed rate was the dominant factor affecting tool wear. Brazed PCD tools generally exhibited lower flank wear compared with domed PCD tools, as ~42 µm flank wear was recorded at a feed rate of 0.2 mm/rev irrespective of cutting speed (80-160 m/min).
- BUE covering the entire cutting lip was prevalent in trials using brazed PCD tools, while limited BUE was found on the domed PCD tools.
- High pressure cutting fluid (70 bar) did not provide any appreciable benefits in terms of hole quality compared to low pressure flood (3 bar) operation, although the former was essential for improving swarf evacuation and prevent chips adhering to the drill flutes.
- Brazed PCD drills outperformed domed PCD tools in terms of tool life, although there was no appreciable improvement in hole quality. Random vibration / chatter marks / defects however were observed when employing brazed PCD tools.
- Brazed PCD tools can be employed for high speed drilling (up to 360 m/min), while chatter / vibration in drilling process has to be controlled.
- Table 5.2 details the recommended / preferred operating conditions for drilling MMCs.

Table 5.2: List of recommended / preferred operating parameters / strategy when drilling MMCs

Parameter / strategy	**Value**
Cutting environment	High pressure flood (70 bar)
Tool material / coating	Brazed PCD, domed PCD
Cutting speed	160-200 m/min
Feed rate	0.1-0.2 mm/rev

Chapter 6: RECOMMENDATIONS FOR FUTURE WORK

Based on the results from the research, a number of areas have been identified as warranting further investigation. These include:

- Evaluation of vibration assisted drilling of CFRP as an alternative to improve process productivity as well as hole quality / surface integrity.
- Further development and optimisation of domed PCD drill geometry together with an evaluation of different PCD grades for machining CFRP and MMC composite materials.
- Application of finite element modelling (FEM) to simulate the drilling process of both CFRP and MMC composite materials in order to develop predictive capability.
- Further investigation of the influence of varying chilled air pressures and flow rates on performance when drilling CFRP.
- Measurement of temperature when drilling CFRP and MMC using different tool materials.

REFERENCES

[1] S. K. Mazumdar, *Composites manufacturing : materials, product, and process engineering*. Boca Raton, Fla. ; London: CRC Press, 2002.

[2] C. T. Herakovich, *Mechanics of fibrous composites*. New York: Wiley, 1998.

[3] R. M. Gill, *Carbon fibres in composite materials*. London: Iliffe for the Plastics Institute, 1972.

[4] J. Y. Sheikh-Ahmad, *Machining of polymer composites*, 1st ed. New York, NY: Springer, 2008.

[5] M. M. Schwartz, *Composite materials*. Upper Saddle River, N.J.: Prentice Hall PTR, 1997.

[6] J. P. Davim, *Machining : fundamentals and recent advances*. New York ; London: Springer, 2008.

[7] K. K. Chawla, *Composite materials : science and engineering*, 3rd ed. New York ; London: Springer, 2012.

[8] S. Hoa, *Principles of the manufacturing of composite materials*. Lancaster, PA: DEStech Publications, Inc., 2008.

[9] T. G. P. Gutowski, *Advanced composites manufacturing*. New York ; Chichester: John Wiley & Sons, 1997.

[10] C. Soutis, "Carbon fiber reinforced plastics in aircraft construction," *Materials Science and Engineering: A*, vol. 412, pp. 171-176, 2005.

[11] W. D. Callister, *Materials science and engineering : an introduction*, 5th ed. New York: Wiley, 2000.

[12] J. Lantrip, "New Tools Needed - new cutting tool materials are required for new generation airframes," *Cutting Tool Engineering*, vol. 60, 2008.

[13] S. Kalpakjian and S. R. Schmid, *Manufacturing processes for engineering materials*, 5th ed. Upper Saddle River, N.J.: Pearson Education, 2008.

[14] J. Pora, "Composite materials in the Airbus A380 - from history to future," *Proceedings of 13th International Conference on Composite Materials (ICCM-13), Beijing*, June 2001.

[15] C. Soutis, "Fibre reinforced composites in aircraft construction," *Progress in Aerospace Sciences*, vol. 41, pp. 143-151, 2005.

[16] "General Electric next generation turbofan: modle GEnx-1B." Available from: http://www.geaviation.com/engines/commercial/genx/genx-1b.html [Accessed: 20 Dec. 2013].

[17] A. Faraz, D. Biermann, and K. Weinert, "Cutting edge rounding: an innovative tool wear criterion in drilling CFRP composite laminates," *International Journal of Machine Tools & Manufacture*, vol. 49, pp. 1185-1196, 2009.

[18] W. O. Soboyejo and T. S. Srivatsan, *Advanced structural materials : properties, design optimization, and applications*. Boca Raton, FL: CRC Press, 2007.

[19] S. Rawal, "Metal-matrix composites for space applications," *JOM*, vol. 53, pp. 14-17, 2001.

[20] J. P. Davim, *Machining of metal matrix composites*. London: Springer, 2012.

[21] M. Taya and R. J. Arsenault, *Metal matrix composites : thermomechanical behavior*. Oxford: Pergamon, 1989.

[22] J. S. Shelley, R. LeClaire, and J. Nichols, "Metal-matrix composites for liquid rocket engines," *JOM*, vol. 53, pp. 18-21, 2001.

[23] J. Kunze and C. Bampton, "Challenges to developing and producing MMCs for space applications," *JOM*, vol. 53, pp. 22-25, 2001.

[24] D. Middleton, *Composite materials in aircraft structures*: Longman Scientific & Technical, 1990.
[25] R. Komanduri, "Machining of fiber-reinforced composites," *Machining Science and Technology*, vol. 1, pp. 113-152, 1997.
[26] W. Krenkel, *Ceramic matrix composites : fiber reinforced ceramics and their applications*. Weinheim: Wiley-VCH, 2008.
[27] A. R. Hyde, "Ceramic matrix composites," *Materials & Design*, vol. 11, pp. 30-36, 1990.
[28] S. V. Nair and K. Jakus, *High temperature mechanical behavior of ceramic composites*. Boston, Mass. ; Oxford: Butterworth-Heinemann, 1995.
[29] N. P. Bansal, *Handbook of ceramic composites*. Boston: Kluwer Academic Publishers, 2005.
[30] A. R. Hyde, "Ceramic matrix composites: high-performance materials for space application," *Materials & Design*, vol. 14, pp. 97-102, 1993.
[31] H. Ohnabe, S. Masaki, M. Onozuka, K. Miyahara, and T. Sasa, "Potential application of ceramic matrix composites to aero-engine components," *Composites Part A: Applied Science and Manufacturing*, vol. 30, pp. 489-496, 1999.
[32] W. Krenkel and F. Berndt, "C/C-SiC composites for space applications and advanced friction systems," *Materials Science and Engineering: A*, vol. 412, pp. 177-181, 2005.
[33] M. Rosso, "Ceramic and metal matrix composites: Routes and properties," *Journal of Materials Processing Technology*, vol. 175, pp. 364-375, 2006.
[34] H. Kaya, "The application of ceramic-matrix composites to the automotive ceramic gas turbine," *Composites Science and Technology*, vol. 59, pp. 861-872, 1999.
[35] A. Sommers, Q. Wang, X. Han, C. T'Joen, Y. Park, and A. Jacobi, "Ceramics and ceramic matrix composites for heat exchangers in advanced thermal systems--A review," *Applied Thermal Engineering*, vol. 30, pp. 1277-1291, 2010.
[36] R. Teti, "Machining of Composite Materials," *CIRP Annals - Manufacturing Technology*, vol. 51, pp. 611-634, 2002.
[37] A. M. Abrao, P. E. Faria, J. C. C. Rubio, P. Reis, and J. P. Davim, "Drilling of fiber reinforced plastics: A review," *Journal of Materials Processing Technology*, vol. 186, pp. 1-7, 2007.
[38] D. F. Liu, Y. J. Tang, and W. L. Cong, "A review of mechanical drilling for composite laminates," *Composite Structures*, vol. 94, pp. 1265-1279, 2012.
[39] R. Mishra, J. Malik, I. Singh, and J. P. Davim, "Neural network approach for estimating the residual tensile strength after drilling in uni-directional glass fiber reinforced plastic laminates," *Materials & Design*, vol. 31, pp. 2790-2795, 2010.
[40] R. Stone and K. Krishnamurthy, "A neural network thrust force controller to minimize delamination during drilling of graphite-epoxy laminates," *International Journal of Machine Tools & Manufacture*, vol. 36, pp. 985-1003, 1996.
[41] S. Abrate and D. A. Walton, "Machining of composite materials. Part I: Traditional methods," *Composites Manufacturing*, vol. 3, pp. 75-83, 1992.
[42] K.-H. Park, A. Beal, D. Kim, P. Kwon, and J. Lantrip, "Tool wear in drilling of composite/titanium stacks using carbide and polycrystalline diamond tools," *Wear*, vol. 271, pp. 2826-2835, 2011.
[43] S. Rawat and H. Attia, "Wear mechanisms and tool life management of WC-Co drills during dry high speed drilling of woven carbon fibre composites," *Wear*, vol. 267, pp. 1022-1030, 2009.
[44] M. K. N. Khairusshima, C. H. C. Hassan, A. G. Jaharah, A. K. M. Amin, and A. N. M. Idriss, "Effect of chilled air on tool wear and workpiece quality during milling of carbon fibre-reinforced plastic," *Wear*, vol. 302, pp. 1113-1123, 2013.

[45] M. Masuda, Y. Kuroshima, and Y. Chujo, "Failure of tungsten carbide-cobalt alloy tools in machining of carbon materials," *Wear,* vol. 169, pp. 135-140, 1993.

[46] Y. Karpat, B. Deger, and O. Bahtiyar, "Drilling thick fabric woven CFRP laminates with double point angle drills," *Journal of Materials Processing Technology,* vol. 212, pp. 2117-2127, 2012.

[47] D. Iliescu, D. Gehin, M. E. Gutierrez, and F. Girot, "Modeling and tool wear in drilling of CFRP," *International Journal of Machine Tools & Manufacture,* vol. 50, pp. 204-213, 2010.

[48] K. H. Park, P. Kwon, and D. Kim, "Wear characteristic on BAM coated carbide tool in drilling of composite/titanium stack," *International Journal of Precision Engineering and Manufacturing,* vol. 13, pp. 1073-1076, 2012.

[49] X. Wang, P. Y. Kwon, C. Sturtevant, D. Kim, and J. Lantrip, "Tool wear of coated drills in drilling CFRP," *Journal of Manufacturing Processes,* vol. 15, pp. 127-135, 2013.

[50] V. Franke, "Drilling of long fiber reinforced thermoplastics--Influence of the cutting edge on the machining results," *CIRP Annals - Manufacturing Technology,* vol. 60, pp. 65-68, 2011.

[51] W. Hintze, D. Hartmann, and C. Schütte, "Occurrence and propagation of delamination during the machining of carbon fibre reinforced plastics (CFRP) – An experimental study," *Composites Science and Technology,* vol. 71, pp. 1719-1726, 2011.

[52] I. El-Sonbaty, U. A. Khashaba, and T. Machaly, "Factors affecting the machinability of GFR/epoxy composites," *Composite Structures,* vol. 63, pp. 329-338, 2004.

[53] S. Rawat and H. Attia, "Characterization of the dry high speed drilling process of woven composites using Machinability Maps approach," *CIRP Annals - Manufacturing Technology,* vol. 58, pp. 105-108, 2009.

[54] U. A. Khashaba, I. A. El-Sonbaty, A. I. Selmy, and A. A. Megahed, "Machinability analysis in drilling woven GFR/epoxy composites: Part I - Effect of machining parameters," *Composites Part a-Applied Science and Manufacturing,* vol. 41, pp. 391-400, 2010.

[55] I. Shyha, S. L. Soo, D. Aspinwall, and S. Bradley, "Effect of laminate configuration and feed rate on cutting performance when drilling holes in carbon fibre reinforced plastic composites," *Journal of Materials Processing Technology,* vol. 210, pp. 1023-1034, 2010.

[56] I. S. Shyha, D. K. Aspinwall, S. L. Soo, and S. Bradley, "Drill geometry and operating effects when cutting small diameter holes in CFRP," *International Journal of Machine Tools and Manufacture,* vol. 49, pp. 1008-1014, 2009.

[57] I. Shyha, S. L. Soo, D. K. Aspinwall, S. Bradley, S. Dawson, and C. J. Pretorius, "Drilling of Titanium/CFRP/Aluminium Stacks," *Advanced Precision Engineering,* vol. 447-448, pp. 624-633, 2010.

[58] U. Heisel and T. Pfeifroth, "Influence of point angle on drill hole quality and machining forces when drilling CFRP," *Fifth CIRP Conference on High Performance Cutting (HPC),* vol. 1, pp. 471-476, 2012.

[59] R. Zitoune, V. Krishnaraj, B. Sofiane Almabouacif, F. Collombet, M. Sima, and A. Jolin, "Influence of machining parameters and new nano-coated tool on drilling performance of CFRP/Aluminium sandwich," *Composites Part B: Engineering,* vol. 43, pp. 1480-1488, 2012.

[60] W.-C. Chen, "Some experimental investigations in the drilling of carbon fiber-reinforced plastic (CFRP) composite laminates," *International Journal of Machine Tools & Manufacture,* vol. 37, pp. 1097-1108, 1997.

[61] R. Zitoune, M. El Mansori, and V. Krishnaraj, "Tribo-functional design of double cone drill implications in tool wear during drilling of copper mesh/CFRP/woven ply," *Wear,* vol. 302, pp. 1560-1567, 2013.

[62] K. Weinert and C. Kempmann, "Cutting temperatures and their effects on the machining behaviour in drilling reinforced plastic composites," *Advanced Engineering Materials,* vol. 6, pp. 684-9, 2004.

[63] K. Weinert, F. Brinkel, C. Kempmann, and K. Pantke, "The dependency of material properties and process conditions on the cutting temperatures when drilling polymers," *Production Engineering,* vol. 1, pp. 381-387, 2007.

[64] Y. Quan and L. Sun, "Experimental investigation on drilling temperature of composites," *International Journal of Machining and Machinability of Materials,* vol. 3, pp. 356-363, 2008.

[65] T. Yashiro, T. Ogawa, and H. Sasahara, "Temperature measurement of cutting tool and machined surface layer in milling of CFRP," *International Journal of Machine Tools & Manufacture,* vol. 70, pp. 63-69, 2013.

[66] E. Brinksmeier, S. Fangmann, and R. Rentsch, "Drilling of composites and resulting surface integrity," *CIRP Annals - Manufacturing Technology,* vol. 60, pp. 57-60, 2011.

[67] E. Brinksmeier and R. Janssen, "Drilling of multi-layer composite materials consisting of carbon fiber reinforced plastics (CFRP), titanium and aluminum alloys," *Cirp Annals-Manufacturing Technology,* vol. 51, pp. 87-90, 2002.

[68] M. Montoya, M. Calamaz, D. Gehin, and F. Girot, "Evaluation of the performance of coated and uncoated carbide tools in drilling thick CFRP/aluminium alloy stacks," *International Journal of Advanced Manufacturing Technology,* vol. 68, pp. 2111-2120, 2013.

[69] R. Zitoune, V. Krishnaraj, and F. Collombet, "Study of drilling of composite material and aluminium stack," *Composite Structures,* vol. 92, pp. 1246-1255, 2010.

[70] G. T. Smith, *Industrial metrology : surfaces and roundness*. London: Springer, 2002.

[71] I. S. Shyha, S. L. Soo, D. K. Aspinwall, S. Bradley, R. Perry, P. Harden, and S. Dawson, "Hole quality assessment following drilling of metallic-composite stacks," *International Journal of Machine Tools & Manufacture,* vol. 51, pp. 569-578, 2011.

[72] D. Kim and M. Ramulu, "Drilling process optimization for graphite/bismaleimide-titanium alloy stacks," *Composite Structures,* vol. 63, pp. 101-114, 2004.

[73] D. Kim and M. Ramulu, "Study on the drilling of titanium/graphite hybrid composites," *Journal of Engineering Materials and Technology-Transactions of the Asme,* vol. 129, pp. 390-396, 2007.

[74] M. Ramulu, T. Branson, and D. Kim, "A study on the drilling of composite and titanium stacks," *Composite Structures,* vol. 54, pp. 67-77, 2001.

[75] Z. J. Jin, Y. J. Bao, and H. Gao, "Disfigurement formation and control in drilling carbon fibre reinforced composites," *International Journal of Materials and Product Technology,* vol. 31, pp. 46-53, 2008.

[76] E. Aoyama, H. Nobe, and T. Hirogaki, "Drilled hole damage of small diameter drilling in printed wiring board," *Journal of Materials Processing Technology,* vol. 118, pp. 436-441, 2001.

[77] H. J. Zhang, W. Y. Chen, D. C. Chen, and L. C. Zhang, "Assessment of the exit defects in carbon fibre-reinforced plastic plates caused by drilling," in *Precision Machining of Advanced Materials*. vol. 196, pp. 43-52, 2001.

[78] G. DiPaolo, S. G. Kapoor, and R. E. DeVor, "An experimental investigation of the crack growth phenomenon for drilling of fiber-reinforced composite materials," *Journal of Engineering for Industry-Transactions of the Asme,* vol. 118, pp. 104-110, 1996.

[79] G. Caprino and V. Tagliaferri, "Damage development in drilling glass fibre reinforced plastics," *International Journal of Machine Tools & Manufacture,* vol. 35, pp. 817-829, 1995.

[80] E. Capello and V. Tagliaferri, "Drilling damage of GFRP and residual mechanical behavior - Part 1: Drilling damage generation," *Journal of Composites Technology & Research,* vol. 23, pp. 122-130, 2001.

[81] J. Campos Rubio, A. M. Abrao, P. E. Faria, A. E. Correia, and J. P. Davim, "Effects of high speed in the drilling of glass fibre reinforced plastic: Evaluation of the delamination factor," *International Journal of Machine Tools and Manufacture,* vol. 48, pp. 715-720, 2008.

[82] S. R. Karnik, V. N. Gaitonde, J. C. Rubio, A. E. Correia, A. M. Abrao, and J. P. Davim, "Delamination analysis in high speed drilling of carbon fiber reinforced plastics (CFRP) using artificial neural network model," *Materials & Design,* vol. 29, pp. 1768-1776, 2008.

[83] U. A. Khashaba, I. A. El-Sonbaty, A. I. Selmy, and A. A. Megahed, "Machinability analysis in drilling woven GFR/epoxy composites: Part II - Effect of drill wear," *Composites Part a-Applied Science and Manufacturing,* vol. 41, pp. 1130-1137, 2010.

[84] M. Ramulu, C. W. Wern, and J. L. Garbini, "Effect of fibre direction on surface roughness measurements of machined graphite/epoxy composite," *Composites Manufacturing,* vol. 4, pp. 39-51, 1993.

[85] O. Pecat, R. Rentsch, and E. Brinksmeier, "Influence of milling process parameters on the surface integrity of CFRP," *Fifth CIRP Conference on High Performance Cutting (HPC),* vol. 1, pp. 466-470, 2012.

[86] S. Abrate and D. Walton, "Machining of composite materials. Part II: Non-traditional methods," *Composites Manufacturing,* vol. 3, pp. 85-94, 1992.

[87] Y. Quan and W. Zhong, "Investigation on drilling-grinding of CFRP," *Frontiers of Mechanical Engineering in China,* vol. 4, pp. 60-63, 2009.

[88] J. Liu, D. Zhang, L. Qin, and L. Yan, "Feasibility study of the rotary ultrasonic elliptical machining of carbon fiber reinforced plastics (CFRP)," *International Journal of Machine Tools and Manufacture,* vol. 53, pp. 141-150, 2012.

[89] H. Wang, X. Qin, C. Ren, and Q. Wang, "Prediction of cutting forces in helical milling process," *The International Journal of Advanced Manufacturing Technology,* pp. 1-11, 2011.

[90] E. Brinksmeier, S. Fangmann, and I. Meyer, "Orbital drilling kinematics," *Production Engineering,* vol. 2, pp. 277-283, 2008.

[91] A. Sadek, M. Meshreki, and M. H. Attia, "Characterization and optimization of orbital drilling of woven carbon fiber reinforced epoxy laminates," *CIRP Annals - Manufacturing Technology,* vol. 61, pp. 123-126, 2012.

[92] V. Schulze, C. Becke, K. Weidenmann, and S. Dietrich, "Machining strategies for hole making in composites with minimal workpiece damage by directing the process forces inwards," *Journal of Materials Processing Technology,* vol. 211, pp. 329-338, 2011.

[93] K. Weinert and C. Kempmann, "Comparing Drilling and Circular Milling for the Drill Hole Manufacture of Fiber Reinforced Composites," *Production Engineering. Research and Development* 2005.

[94] B. Denkena, D. Boehnke, and J. H. Dege, "Helical milling of CFRP-titanium layer compounds," *CIRP Annals - Manufacturing Technology,* vol. 1, pp. 64-69, 2008.

[95] A. Riveiro, F. Quintero, F. Lusquiños, J. del Val, R. Comesaña, M. Boutinguiza, and J. Pou, "Experimental study on the CO2 laser cutting of carbon fiber reinforced plastic composite," *Composites Part A: Applied Science and Manufacturing,* vol. 43, pp. 1400-1409, 2012.

[96] J. P. Davim, N. Barricas, M. Conceição, and C. Oliveira, "Some experimental studies on CO2 laser cutting quality of polymeric materials," *Journal of Materials Processing Technology,* vol. 198, pp. 99-104, 2008.

[97] D. K. Shanmugam, F. L. Chen, E. Siores, and M. Brandt, "Comparative study of jetting machining technologies over laser machining technology for cutting composite materials," *Composite Structures,* vol. 57, pp. 289-296, 2002.

[98] D. Herzog, P. Jaeschke, O. Meier, and H. Haferkamp, "Investigations on the thermal effect caused by laser cutting with respect to static strength of CFRP," *International Journal of Machine Tools and Manufacture,* vol. 48, pp. 1464-1473, 2008.

[99] J. Wang, "A machinability study of polymer matrix composites using abrasive waterjet cutting technology," *Journal of Materials Processing Technology,* vol. 94, pp. 30-35, 1999.

[100] A. Alberdi, A. Suárez, T. Artaza, G. A. Escobar-Palafox, and K. Ridgway, "Composite cutting with abrasive water jet," *Procedia Engineering,* vol. 63, pp. 421-429, 2013.

[101] M. Ramulu and D. Arola, "Water jet and abrasive water jet cutting of unidirectional graphite/epoxy composite," *Composites,* vol. 24, pp. 299-308, 1993.

[102] J. Stock, M. F. Zaeh, and M. Conrad, "Remote Laser Cutting of CFRP: Improvements in the Cut Surface," *Physics Procedia,* vol. 39, pp. 161-170, 2012.

[103] X. Wang, L. J. Wang, and J. P. Tao, "Investigation on thrust in vibration drilling of fiber-reinforced plastics," *Journal of Materials Processing Technology,* vol. 148, pp. 239-244, 2004.

[104] S. Arul, L. Vijayaraghavan, S. K. Malhotra, and R. Krishnamurthy, "The effect of vibratory drilling on hole quality in polymeric composites," *International Journal of Machine Tools & Manufacture,* vol. 46, pp. 252-259, 2006.

[105] H. Hocheng and C. C. Hsu, "Preliminary study of ultrasonic drilling of fiber-reinforced plastics," *Journal of Materials Processing Technology,* vol. 48, pp. 255-266, 1995.

[106] J. Ramkumar, S. Aravindan, S. K. Malhotra, and R. Krishnamurthy, "An enhancement of the machining performance of GFRP by oscillatory assisted drilling," *International Journal of Advanced Manufacturing Technology,* vol. 23, pp. 240-244, 2004.

[107] J. Ramkumar, S. K. Malhotra, and R. Krishnamurthy, "Effect of workpiece vibration on drilling of GFRP laminates," *Journal of Materials Processing Technology,* vol. 152, pp. 329-32, 2004.

[108] L. B. Zhang, L. J. Wang, and X. Wang, "Study on vibration drilling of fiber reinforced plastics with hybrid variation parameters method," *Composites Part a-Applied Science and Manufacturing,* vol. 34, pp. 237-244, 2003.

[109] A. Sadek, M. H. Attia, M. Meshreki, and B. Shi, "Characterization and optimization of vibration-assisted drilling of fibre reinforced epoxy laminates," *CIRP Annals-Manufacturing Technology,* vol. 62, pp. 91-94, 2013.

[110] S. Jain and D. C. H. Yang, "Delamination-free drilling of composite laminates," *Journal of Engineering for Industry-Transactions of the Asme,* vol. 116, pp. 475-481, 1994.

[111] W. L. Cong, Q. Feng, Z. J. Pei, T. W. Deines, and C. Treadwell, "Rotary ultrasonic machining of carbon fiber-reinforced plastic composites: using cutting fluid vs. cold air as coolant," *Journal of Composite Materials,* November 2, 2011.

[112] W. L. Cong, Z. J. Pei, T. W. Deines, D. F. Liu, and C. Treadwell, "Rotary ultrasonic machining of CFRP/Ti stacks using variable feedrate," *Composites Part B-Engineering,* vol. 52, pp. 303-310, 2013.

[113] U. Teicher, S. Muller, J. Munzner, and A. Nestler, "Micro-EDM of carbon fibre-reinforced plastics," *Proceedings of the Seventeenth CIRP Conference on Electro Physical and Chemical Machining (ISEM)*, vol. 6, pp. 320-325, 2013.

[114] W. S. Lau, M. Wang, and W. B. Lee, "ELECTRICAL-DISCHARGE MACHINING OF CARBON-FIBER COMPOSITE-MATERIALS," *International Journal of Machine Tools & Manufacture*, vol. 30, pp. 297-308, 1990.

[115] H. Hocheng, Y. H. Guu, and N. H. Tai, "The feasibility analysis of electrical-discharge machining of carbon-carbon composites," *Materials and Manufacturing Processes*, vol. 13, pp. 117-132, 1998.

[116] Y. H. Guu, H. Hocheng, N. H. Tai, and S. Y. Liu, "Effect of electrical discharge machining on the characteristics of carbon fiber reinforced carbon composites," *Journal of Materials Science*, vol. 36, pp. 2037-2043, 2001.

[117] M. K. Brun, M. Lee, and F. Gorsler, "Wear Characteristics of Various Hard Materials for Machining Sic-Reinforced Aluminum-Alloy," *Wear*, vol. 104, pp. 21-29, 1985.

[118] S. Barnes, I. R. Pashby, and A. B. Hashim, "Effect of heat treatment on the drilling performance of aluminum/SiC MMC," *Applied Composite Materials*, vol. 6, pp. 121-138, 1999.

[119] M. Ramulu, P. N. Rao, and H. Kao, "Drilling of (Al2O3)p/6061 metal matrix composites," *Journal of Materials Processing Technology*, vol. 124, pp. 244-254, 2002.

[120] J. T. Lin, D. Bhattacharyya, and C. Lane, "Machinability of a Silicon-Carbide Reinforced Aluminum Metal-Matrix Composite," *Wear*, vol. 181, pp. 883-888, 1995.

[121] R. T. Coelho, S. Yamada, T. leRoux, D. K. Aspinwall, and M. L. H. Wise, "Conventional machining of an aluminium based SiC reinforced metal matrix composite (MMC) Alloy," *Proceedings of 30th International Matador Conference, Manchester, UK*. pp. 125-133, 1993.

[122] R. T. Coelho, S. Yamada, D. K. Aspinwall, and M. L. H. Wise, "The application of polycrystalline diamond (PCD) tool materials when drilling and reaming aluminium based alloys including MMC," *International Journal of Machine Tools and Manufacture*, vol. 35, pp. 761-774, 1995.

[123] I. Ciftci, M. Turker, and U. Seker, "Evaluation of tool wear when machining SiCp-reinforced Al-2014 alloy matrix composites," *Materials & Design*, vol. 25, pp. 251-255, 2004.

[124] I. Ciftci, M. Turker, and U. Seker, "CBN cutting tool wear during machining of particulate reinforced MMCs," *Wear*, vol. 257, pp. 1041-1046, 2004.

[125] J. Paulo Davim and A. Monteiro Baptista, "Relationship between cutting force and PCD cutting tool wear in machining silicon carbide reinforced aluminium," *Journal of Materials Processing Technology*, vol. 103, pp. 417-423, 2000.

[126] Y. Sahin, M. Kok, and H. Celik, "Tool wear and surface roughness of Al_2O_3 particle-reinforced aluminium alloy composites," *Journal of Materials Processing Technology*, vol. 128, pp. 280-291, 2002.

[127] Y. Sahin, "Preparation and some properties of SiC particle reinforced aluminium alloy composites," *Materials & Design*, vol. 24, pp. 671-679, 2003.

[128] M. El-Gallab and M. Sklad, "Machining of Al/SiC particulate metal-matrix composites. Part I: Tool performance," *Journal of Materials Processing Technology*, vol. 83, pp. 151-158, 1998.

[129] G. Tosun, "Statistical analysis of process parameters in drilling of Al/SiCp metal matrix composite," *International Journal of Advanced Manufacturing Technology*, vol. 55, pp. 477-485, 2011.

[130] G. Tosun and M. Muratoglu, "The drilling of Al/SiCp metal-matrix composites. Part II: Workpiece surface integrity," *Composites Science and Technology*, vol. 64, pp. 1413-1418, 2004.

[131] A. N. Haq, P. Marimuthu, and R. Jeyapaul, "Multi response optimization of machining parameters of drilling Al/SiC metal matrix composite using grey relational analysis in the Taguchi method," *International Journal of Advanced Manufacturing Technology*, vol. 37, pp. 250-5, 2008.

[132] S. Barnes and I. R. Pashby, "Through-tool coolant drilling of aluminum/SiC metal matrix composite," *Journal of Engineering Materials and Technology-Transactions of the Asme*, vol. 122, pp. 384-388, 2000.

[133] G. Tosun and M. Muratoglu, "The drilling of an Al/SiCp metal-matrix composites. Part 1: microstructure," *Composites Science and Technology*, vol. 64, pp. 299-308, 2004.

[134] E. Morin, J. Masounave, and E. E. Laufer, "Effect of Drill Wear on Cutting Forces in the Drilling of Metal-Matrix Composites," *Wear*, vol. 184, pp. 11-16, 1995.

[135] S. Basavarajappa, G. Chandramohan, and J. P. Davim, "Some studies on drilling of hybrid metal matrix composites based on Taguchi techniques," *Journal of Materials Processing Technology*, vol. 196, pp. 332-338, 2008.

[136] S. Basavarajappa, G. Chandramohan, J. P. Davim, M. Prabu, K. Mukund, M. Ashwin, and M. PrasannaKumar, "Drilling of hybrid aluminium matrix composites - Workpiece surface integrity," *International Journal of Advanced Manufacturing Technology*, vol. 35, pp. 1244-50, 2008.

[137] S. Basavarajappa, G. Chandramohan, J. P. Davim, M. Prabu, K. Mukund, M. Ashwin, and M. PrasannaKumar, "Drilling of hybrid aluminium matrix composites," *International Journal of Advanced Manufacturing Technology*, vol. 35, pp. 1244-1250, 2008.

[138] B. Mubaraki, S. Bandyopadhyay, R. Fowle, P. Mathew, and P. J. Heath, "Drilling studies of an Al_2O_3-Al metal matrix composite .1. Drill wear characteristics," *Journal of Materials Science*, vol. 30, pp. 6273-6280, 1995.

[139] T. Rajmohan, K. Palanikumar, and J. P. Davim, "Analysis of surface integrity in drilling metal matrix and hybrid metal matrix composites," *Journal of Materials Science & Technology*, vol. 28, pp. 761-768, 2012.

[140] T. Rajmohan, K. Palanikumar, and S. Prakash, "Grey-fuzzy algorithm to optimise machining parameters in drilling of hybrid metal matrix composites," *Composites Part B: Engineering*, vol. 50, pp. 297-308, 2013.

[141] J. Monaghan and P. Oreilly, "The drilling of an Al/SiC metal matrix composite," *Journal of Materials Processing Technology*, vol. 33, pp. 469-480, 1992.

[142] Y. Altunpak, M. Ay, and S. Aslan, "Drilling of a hybrid Al/SiC/Gr metal matrix composites," *International Journal of Advanced Manufacturing Technology*, vol. 60, pp. 513-517, 2012.

[143] A. R. Ahamed, P. Asokan, S. Aravindan, and M. K. Prakash, "Drilling of hybrid Al-5%SiCp-5%B4Cp metal matrix composites," *International Journal of Advanced Manufacturing Technology*, vol. 49, pp. 871-877, 2010.

[144] E. M. Trent and P. K. Wright, *Metal cutting*, 4th ed. ed. Boston ; Oxford: Butterworth-Heinemann, 2000.

[145] A. Pramanik, L. C. Zhang, and J. A. Arsecularatne, "Machining of metal matrix composites: Effect of ceramic particles on residual stress, surface roughness and chip formation," *International Journal of Machine Tools & Manufacture*, vol. 48, pp. 1613-1625, 2008.

[146] A. Manna and B. Bhattacharayya, "A study on machinability of Al/SiC-MMC," *Journal of Materials Processing Technology*, vol. 140, pp. 711-716, 2003.

[147] Y. Ozcatalbas, "Chip and built-up edge formation in the machining of in situ Al_4C_3-Al composite," *Materials & Design*, vol. 24, pp. 215-221, 2003.
[148] U. A. Dabade and S. S. Joshi, "Analysis of chip formation mechanism in machining of Al/SiCp metal matrix composites," *Journal of Materials Processing Technology*, vol. 209, pp. 4704-10, 2009.
[149] B. Griffiths, *Manufacturing surface technology : surface integrity & functional performance*. London: Penton, 2001.
[150] D. Novovic, R. C. Dewes, D. K. Aspinwall, W. Voice, and P. Bowen, "The effect of machined topography and integrity on fatigue life," *International Journal of Machine Tools & Manufacture*, vol. 44, pp. 125-134, 2004.
[151] M. El-Gallab and M. Sklad, "Machining of Al/SiC particulate metal matrix composites - Part II: Workpiece surface integrity," *Journal of Materials Processing Technology*, vol. 83, pp. 277-285, 1998.
[152] S. Kannan and H. A. Kishawy, "Surface characteristics of machined aluminium metal matrix composites," *International Journal of Machine Tools and Manufacture*, vol. 46, pp. 2017-2025, 2006.
[153] N. S. K. Reddy, S. Kwang-Sup, and M. Y. Yang, "Experimental study of surface integrity during end milling of Al/SiC particulate metal-matrix composites," *Journal of Materials Processing Technology*, vol. 201, pp. 574-579, 2008.
[154] N. Tomac, K. Tannessen, and F. O. Rasch, "Machinability of particulate aluminium matrix composites," *CIRP Annals - Manufacturing Technology*, vol. 41, pp. 55-58, 1992.
[155] Y. Wang, L. J. Yang, and N. J. Wang, "An investigation of laser-assisted machining of Al2O3 particle reinforced aluminum matrix composite," *Journal of Materials Processing Technology*, vol. 129, pp. 268-272, 2002.
[156] R. Bejjani, B. Shi, H. Attia, and M. Balazinski, "Laser assisted turning of Titanium Metal Matrix Composite," *Cirp Annals-Manufacturing Technology*, vol. 60, pp. 61-64, 2011.
[157] C. R. Dandekar and Y. C. Shin, "Laser-assisted machining of a fiber reinforced metal matrix composite," *Journal of Manufacturing Science and Engineering-Transactions of the Asme*, vol. 132, 2010.
[158] C. R. Dandekar and Y. C. Shin, "Multi-scale modeling to predict sub-surface damage applied to laser-assisted machining of a particulate reinforced metal matrix composite," *Journal of Materials Processing Technology*, vol. 213, pp. 153-160, 2013.
[159] P. N. Singh, K. Raghukandan, M. Rathinasabapathi, and B. C. Pai, "Electric discharge machining of Al-10%SiCp as-cast metal matrix composites," *Journal of Materials Processing Technology*, vol. 155, pp. 1653-1657, 2004.
[160] P. N. Singh, K. Raghukandan, and B. C. Pai, "Optimization by Grey relational analysis of EDM parameters on machining Al-10%SiCp composites," *Journal of Materials Processing Technology*, vol. 155, pp. 1658-1661, 2004.
[161] B. Mohan, A. Rajadurai, and K. G. Satyanarayana, "Electric discharge machining of Al-SiC metal matrix composites using rotary tube electrode," *Journal of Materials Processing Technology*, vol. 153, pp. 978-985, 2004.
[162] B. H. Yan, H. C. Tsai, F. Y. Huang, and L. C. Lee, "Examination of wire electrical discharge machining of Al_2O_3/6061Al composites," *International Journal of Machine Tools & Manufacture*, vol. 45, pp. 251-259, 2005.
[163] J. W. Liu, T. M. Yue, and Z. N. Guo, "An analysis of the discharge mechanism in electrochemical discharge machining of particulate reinforced metal matrix composites," *International Journal of Machine Tools & Manufacture*, vol. 50, pp. 86-96, 2010.

[164] M. A. Kadivar, J. Akbari, R. Yousefi, A. Rahi, and M. G. Nick, "Investigating the effects of vibration method on ultrasonic-assisted drilling of Al/SiCp metal matrix composites," *Robotics and Computer-Integrated Manufacturing,* vol. 30, pp. 344-350, 2014.

[165] C. S. Liu, B. Zhao, G. F. Gao, and F. Jiao, "Research on the characteristics of the cutting force in the vibration cutting of a particle-reinforced metal matrix composites SiCp/Al," *Journal of Materials Processing Technology,* vol. 129, pp. 196-199, 2002.

[166] H. Hocheng, N. H. Tai, and C. S. Liu, "Assessment of ultrasonic drilling of C/SiC composite material," *Composites Part a-Applied Science and Manufacturing,* vol. 31, pp. 133-142, 2000.

[167] P. J. Heath, "Developments in applications of PCD tooling," *Journal of Materials Processing Technology,* vol. 116, pp. 31-38, 2001.

[168] C. Murphy, G. Byrne, and M. D. Gilchrist, "The performance of coated tungsten carbide drills when machining carbon fibre-reinforced epoxy composite materials," *Proceedings of the Institution of Mechanical Engineers Part B-Journal of Engineering Manufacture,* vol. 216, pp. 143-152, 2002.

[169] S. Arul, L. Vijayaraghavan, S. K. Malhotra, and R. Krishnamurthy, "Influence of tool material on dynamics of drilling of GFRP composites," *International Journal of Advanced Manufacturing Technology,* vol. 29, pp. 655-662, 2006.

[170] J. P. Davim and F. Mata, "Chemical vapour deposition (CVD) diamond coated tools performance in machining of PEEK composites," *Materials & Design,* vol. 29, pp. 1568-1574, 2008.

[171] F. Mata, V. N. Gaitonde, S. R. Karnik, and J. P. Davim, "Influence of cutting conditions on machinability aspects of PEEK, PEEK CF 30 and PEEK GF 30 composites using PCD tools," *Journal of Materials Processing Technology,* vol. 209, pp. 1980-1987, 2009.

[172] J. Paulo Davim and F. Mata, "New machinability study of glass fibre reinforced plastics using polycrystalline diamond and cemented carbide (K15) tools," *Materials & Design,* vol. 28, pp. 1050-1054, 2007.

[173] J. P. Davim and P. Reis, "Machinability study on composite (polyetheretherketone reinforced with 30% glass fibre-PEEK GF 30) using polycrystalline diamond (PCD) and cemented carbide (K20) tools," *International Journal of Advanced Manufacturing Technology,* vol. 23, pp. 412-418, 2004.

[174] J. P. Davim, P. Reis, V. Lapa, and C. C. Antonio, "Machinability study on polyetheretherketone (PEEK) unreinforced and reinforced (GF30) for applications in structural components," *Composite Structures,* vol. 62, pp. 67-73, 2003.

[175] K. Palanikumar, "Application of Taguchi and response surface methodologies for surface roughness in machining glass fiber reinforced plastics by PCD tooling," *International Journal of Advanced Manufacturing Technology,* vol. 36, pp. 19-27, 2008.

[176] M. Ramulu, M. Faridnia, J. L. Garbini, and J. E. Jorgensen, "Machining of graphite epoxy composite materials with polycrystalline diamond (PCD) tools," *Journal of Engineering Materials and Technology-Transactions of the Asme,* vol. 113, pp. 430-436, 1991.

[177] M. Ramulu, P. Young, and H. Kao, "Drilling of graphite/bismaleimide composite material," *Journal of Materials Engineering and Performance,* vol. 8, pp. 330-338, 1999.

[178] S. Jahanmir, M. Ramulu, and P. Koshy, *Machining of ceramics and composites*. New York: Dekker, 1999.

[179] E. Kilickap, O. Cakir, M. Aksoy, and A. Inan, "Study of tool wear and surface roughness in machining of homogenised SiC-p reinforced aluminium metal matrix

composite," *Journal of Materials Processing Technology*, vol. 164-165, pp. 862-7, 2005.

[180] T. Ozben, E. Kilickap, and O. Cakir, "Investigation of mechanical and machinability properties of SiC particle reinforced Al-MMC," *Journal of Materials Processing Technology*, vol. 198, pp. 220-225, 2008.

[181] M. S. Karakas, A. Acir, M. Ubeyli, and B. Ogel, "Effect of cutting speed on tool performance in milling of B_4C_p reinforced aluminum metal matrix composites," *Journal of Materials Processing Technology*, vol. 178, pp. 241-246, 2006.

[182] O. Quigley, J. Monaghan, and P. Oreilly, "Factors affecting the machinability of an Al/SiC metal matrix composite," *Journal of Materials Processing Technology*, vol. 43, pp. 21-36, 1994.

[183] G. Castro, F. A. Almeida, F. J. Oliveira, A. J. S. Fernandes, J. Sacramento, and R. F. Silva, "Dry machining of silicon-aluminium alloys with CVD diamond brazed and directly coated Si3N4 ceramic tools," *Vacuum*, vol. 82, pp. 1407-1410, 2008.

[184] N. Muthukrishnan and J. P. Davim, "Optimization of machining parameters of Al/SiC-MMC with ANOVA and ANN analysis," *Journal of Materials Processing Technology*, vol. 209, pp. 225-232, 2009.

[185] R. K. Bhushan, S. Kumar, and S. Das, "Effect of machining parameters on surface roughness and tool wear for 7075 Al alloy SiC composite," *International Journal of Advanced Manufacturing Technology*, vol. 50, pp. 459-469, 2010.

[186] N. Muthukrishnan, M. Murugan, and K. P. Rao, "An investigation on the machinability of Al-SiC metal matrix composites using pcd inserts," *International Journal of Advanced Manufacturing Technology*, vol. 38, pp. 447-454, 2008.

[187] X. Ding, W. Y. H. Liew, and X. D. Liu, "Evaluation of machining performance of MMC with PCBN and PCD tools," *Wear*, vol. 259, pp. 1225-1234, 2005.

[188] S. Durante, G. Rutelli, and F. Rabezzana, "Aluminum-based MMC machining with diamond-coated cutting tools," *Surface & Coatings Technology*, vol. 94-5, pp. 632-640, 1997.

[189] Y. K. Chou and J. Liu, "CVD diamond tool performance in metal matrix composite machining," *Surface & Coatings Technology*, vol. 200, pp. 1872-1878, 2005.

[190] J. P. Davim, "Diamond tool performance in machining metal-matrix composites," *Journal of Materials Processing Technology*, vol. 128, pp. 100-105, 2002.

[191] Toray Industries (America), Inc. "Technical Data Sheet No. CFA-019." [online] Available at: http://www.toraycfa.com/pdfs/T800SDataSheet.pdf [Accessed: April 2012].

[192] Nex FlowTM Air Products Corp. "Frigid-XTM Tool Cooling System." [online] Available at: http://www.nex-flow.com/pdf_nex_flow/machine_tool_cooling_system .pdf [Accessed: March 2012].

[193] Kistler Instruments Ltd. "Data Sheet, Type 9123C, 5221B1, 5223B ." [online] Available at: http://www.kistler.com/mediaaccess/en-ex/000-121e-01.04.pdf [Accessed: April 2012].

[194] C. C. Tsao and H. Hocheng, "Taguchi analysis of delamination associated with various drill bits in drilling of composite material," *International Journal of Machine Tools and Manufacture*, vol. 44, pp. 1085-1090, 2004.

[195] A. T. Marques, L. M. Durão, A. G. Magalhães, J. F. Silva, and J. M. R. S. Tavares, "Delamination analysis of carbon fibre reinforced laminates: Evaluation of a special step drill," *Composites Science and Technology*, vol. 69, pp. 2376-2382, 2009.

[196] J. C. C. Rubio, A. M. Abrao, P. E. Faria, A. E. Correia, and J. P. Davim, "Delamination in high speed drilling of carbon fiber reinforced plastic (CFRP)," *Journal of Composite Materials*, vol. 42, pp. 1523-1532, 2008.

[197] Technical communication with Seco.

[198] Holemaking, Seco Tool Catalogue & Technical Guide, 2012.
[199] Extramet Corp. "Grades, EMT 100" [online] Available at: http://www.extramet.net/grades [Accessed: January 2014].
[200] Element Six Ltd. "PCD grades and characteristics" [online] Available from: http://www.e6.com/wps/wcm/connect/E6_Content_EN/Home/Materials+and+products/Synthetic+Polycrystalline+Diamond+%28PCD%29/ [Accessed: December 2013].
[201] H. Hocheng and C. C. Tsao, "Effects of special drill bits on drilling-induced delamination of composite materials," *International Journal of Machine Tools & Manufacture*, vol. 46, pp. 1403-1416, 2006.
[202] A. Velayudham, R. Krishnamurthy, and T. Soundarapandian, "Evaluation of drilling characteristics of high volume fraction fibre glass reinforced polymeric composite," *International Journal of Machine Tools and Manufacture*, vol. 45, pp. 399-406, 2005.
[203] M.-B. Lazar and P. Xirouchakis, "Experimental analysis of drilling fiber reinforced composites," *International Journal of Machine Tools and Manufacture*, vol. 51, pp. 937-946, 2011.
[204] P. J. Ross, *Taguchi techniques for quality engineering : loss function, orthogonal experiments, parameter and tolerance design*, 2nd ed. New York ; London: McGraw-Hill, 1996.
[205] A. Velayudham and R. Krishnamurthy, "Effect of point geometry and their influence on thrust and delamination in drilling of polymeric composites," *Journal of Materials Processing Technology*, vol. 185, pp. 204-209, 2007.
[206] V. Krishnaraj, A. Prabukarthi, A. Ramanathan, N. Elanghovan, M. Senthil Kumar, R. Zitoune, and J. P. Davim, "Optimization of machining parameters at high speed drilling of carbon fiber reinforced plastic (CFRP) laminates," *Composites Part B: Engineering*, vol. 43, pp. 1791-1799, 2012.
[207] O. Kolednik and K. Unterweger, "The ductility of metal matrix composites – Relation to local deformation behavior and damage evolution," *Engineering Fracture Mechanics*, vol. 75, pp. 3663-3676, 2008.
[208] K. Nakayama and M. Ogawa, "Basic rules on the form of chip in metal cutting," *Annals of the CIRP*, vol. 27, pp. 17-21, 1978.
[209] A. Akhavan Farid, S. Sharif, and M. Idris, "Chip morphology study in high speed drilling of Al–Si alloy," *The International Journal of Advanced Manufacturing Technology*, vol. 57, pp. 555-564, 2011.
[210] Y. Sahin, M. Kok, and H. Celik, "Tool wear and surface roughness of Al_2O_3 particle-reinforced aluminium alloy composites," *Journal of Materials Processing Technology*, vol. 128, pp. 280-291, 2002.
[211] J. C. Aurich, D. Dornfeld, P. J. Arrazola, V. Franke, L. Leitz, and S. Min, "Burrs-Analysis, control and removal," *CIRP Annals - Manufacturing Technology*, vol. 58, pp. 519-542, 2009.
[212] D. A. Dornfeld, J. S. Kim, H. Dechow, J. Hewson, L. J. Chen, "*Drilling burr formation in titanium alloy, Ti-6Al-4V*," *CIRP Annals - Manufacturing Technology*, vol. 48, pp. 73-76, 1999.
[213] R. Rattanakit, "Optimisation of the aluminium compressor impeller machining process," EngD thesis, *The University of Bimringham*, 2013.

APPENDIX A

Industrial collaborator's contact details

This project was conducted in collaboration with Seco Tools (UK) Ltd. and Element Six Ltd. Industrial partner contact details at the time of the research are as follows:

Company	**Contact details**
Seco Tools (UK) Ltd.	Mr. David Pearson Seco Tools (UK) Ltd. Springfield Business Park Alcester B49 6PU, UK Email: david.pearson@secotools.com
Element Six Ltd.	Dr. Wayne Leahy Element Six Ltd. Global Innovation Centre Harwell OX11 0QR, UK Email: wayne.leahy@e6.com

APPENDIX B

Summary of drills used in this project

Details of all the drills used in this project including tool materials / coatings, drill diameter and cost of each drill are shown below:

Phase and number of tools used	Drill description	Tool materials / coatings	Drill diameter	Cost per drill (including VAT)
Phase 1A & 2B & 2C (15 drills)	SD205A, C1 geometry	Diamond coated WC	6.38 mm	£248.00
Phase 2A (6 drills)	SD205A, C1 geometry	Diamond coated WC	6.00 mm	£210.00
Phase 1A (5 drills)	C1 geometry	Uncoated WC	6.38 mm	£76.20
Phase 3A & 3B & 3C (10 drills)	SD205, CX31 geometry	Brazed PCD	6.38 mm	£396.00
Phase 1A & 2C & 3B (10 drills)	CX1 geometry	Domed PCD	6.36 mm	£747.00
Phase 3A (2 drills)	SD205A, T geometry	Uncoated WC	6.35 mm	£91.50
Phase 3A (2 drills)	SD205A, M geometry	TiAlN+TiN coated WC	6.35 mm	£100.00

APPENDIX C

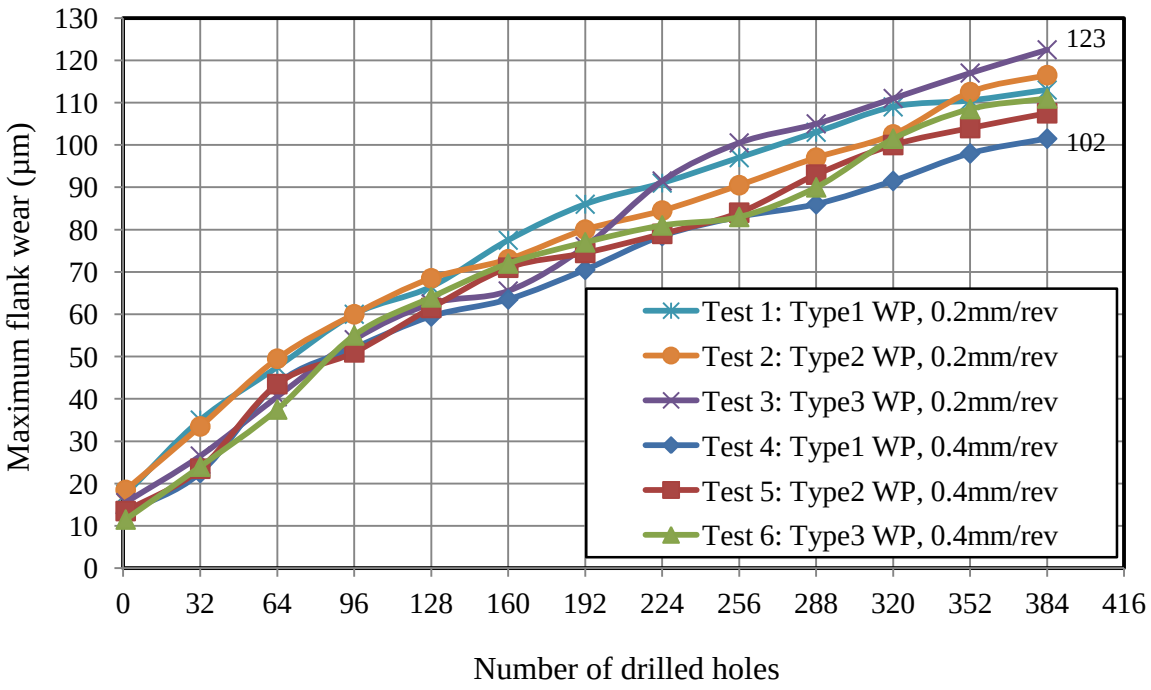


Figure C1: Flank wear curves against number of drilled holes in Phase 2B

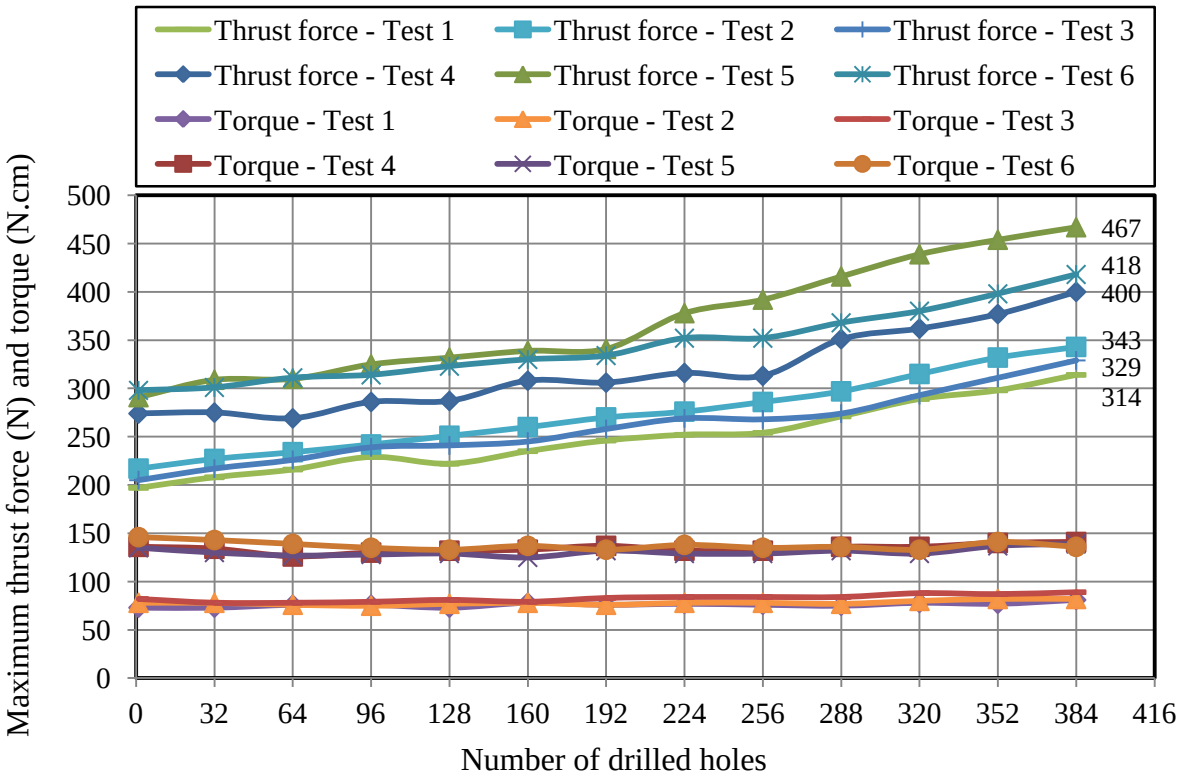


Figure C2: Thrust force and torque progression against number of drilled holes in the first stage of Phase 2B

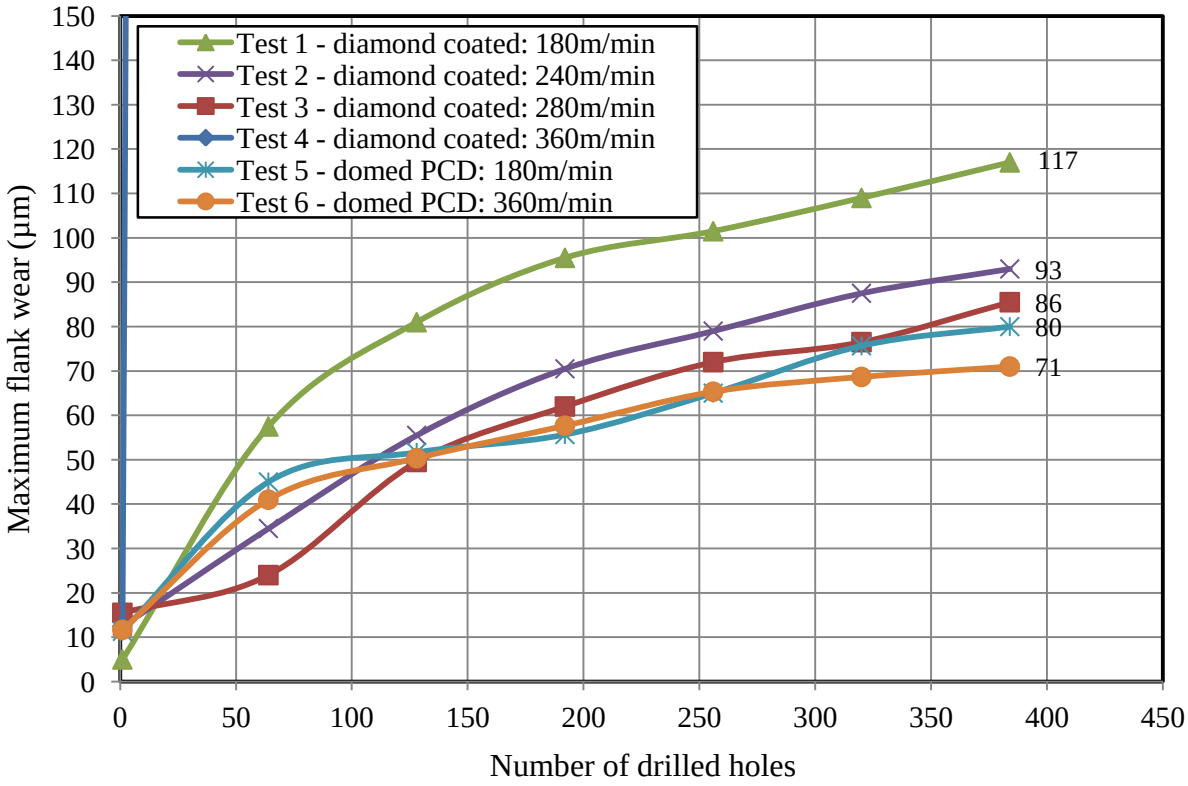


Figure C3: Tool wear progression against number of drilled holes in Phase 2C

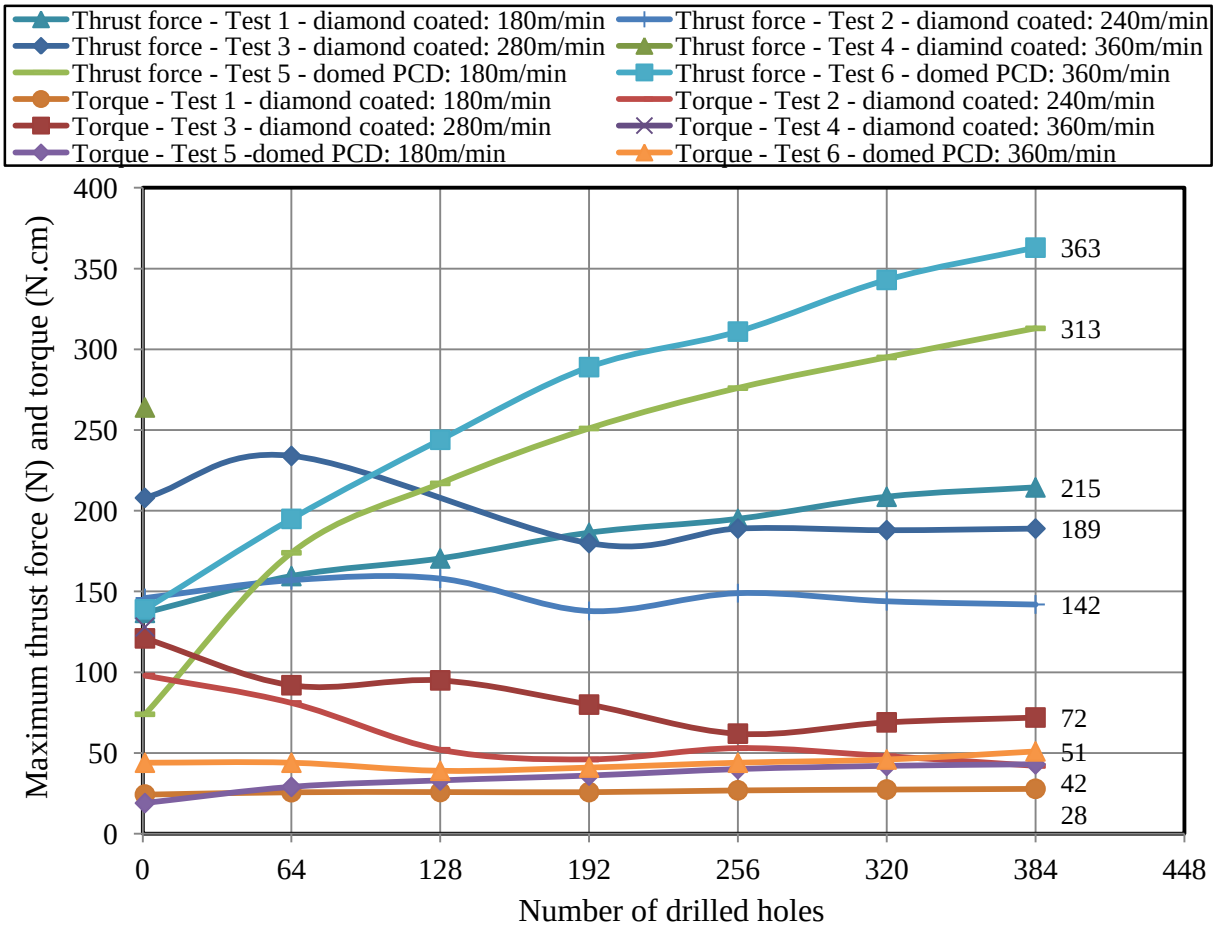


Figure C4: Thrust force and torque progression against number of drilled holes in Phase 2C

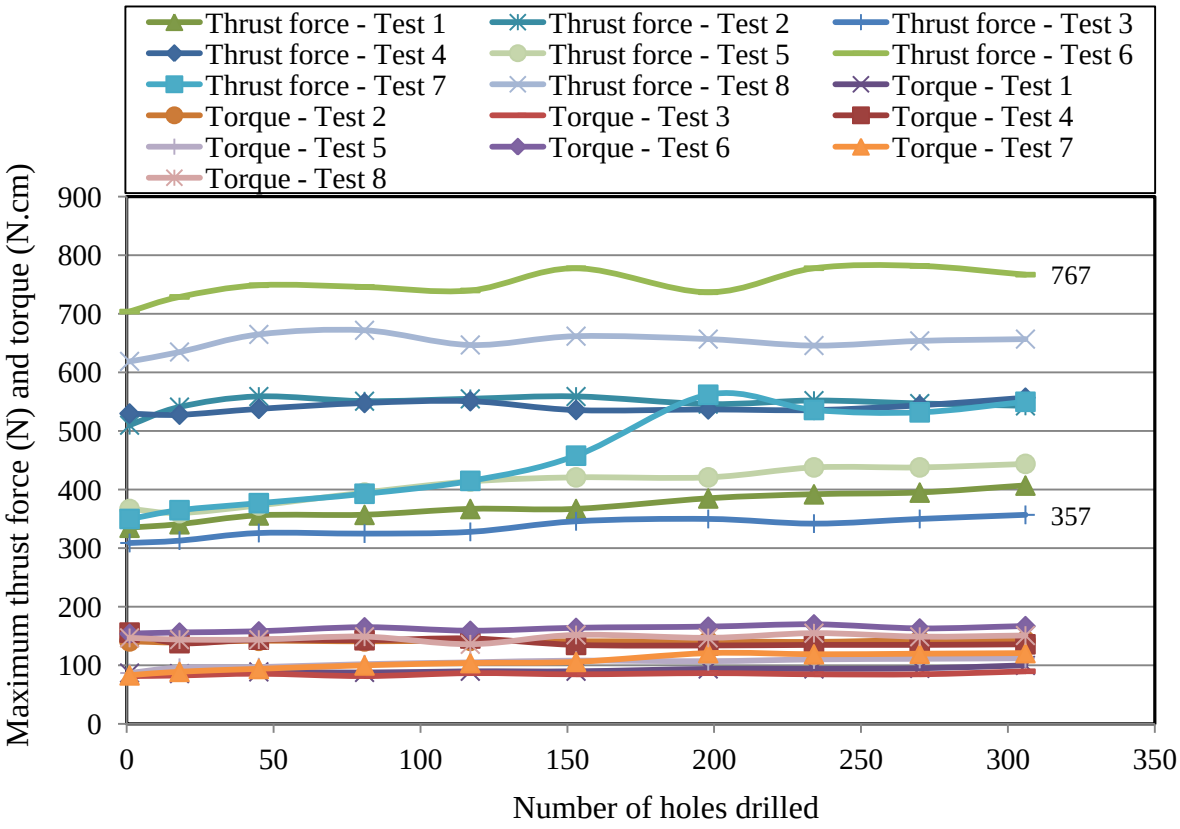


Figure C5: Maximum thrust force and torque progression against number of drilled holes in Phase 3B

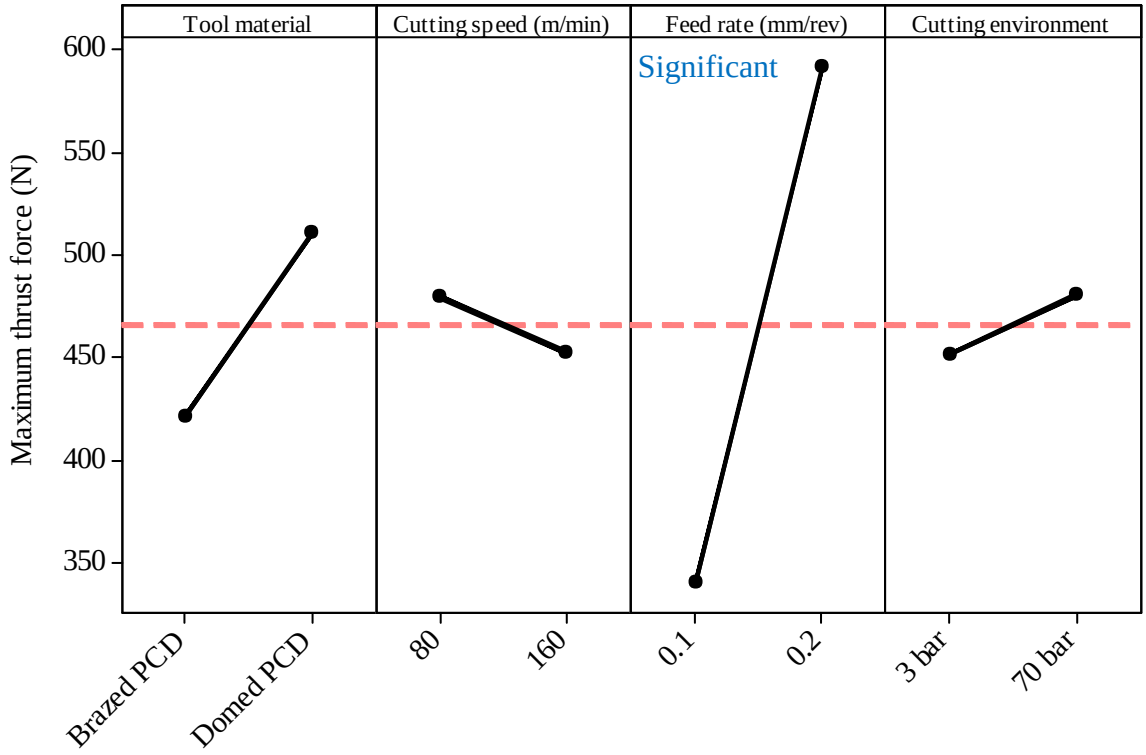


Figure C6: Main effects plot for maximum thrust force at the first hole in Phase 3B

Table C2: ANOVA results for maximum thrust force at the first hole in Phase 3B

Source	DF	Seq SS	Adj SS	F	P	PCR
Tool material	1	15842	15842	7.07	0.076	9.00%
Cutting speed (m/min)	1	1458	1458	0.65	0.479	0.00%
Feed rate (mm/rev)	1	125500	125500	55.99	0.005*	81.55%
Cutting environment	1	1624	1624	0.72	0.457	0.00%
Error	3	6725	6725			9.45%
Total	7	151150				

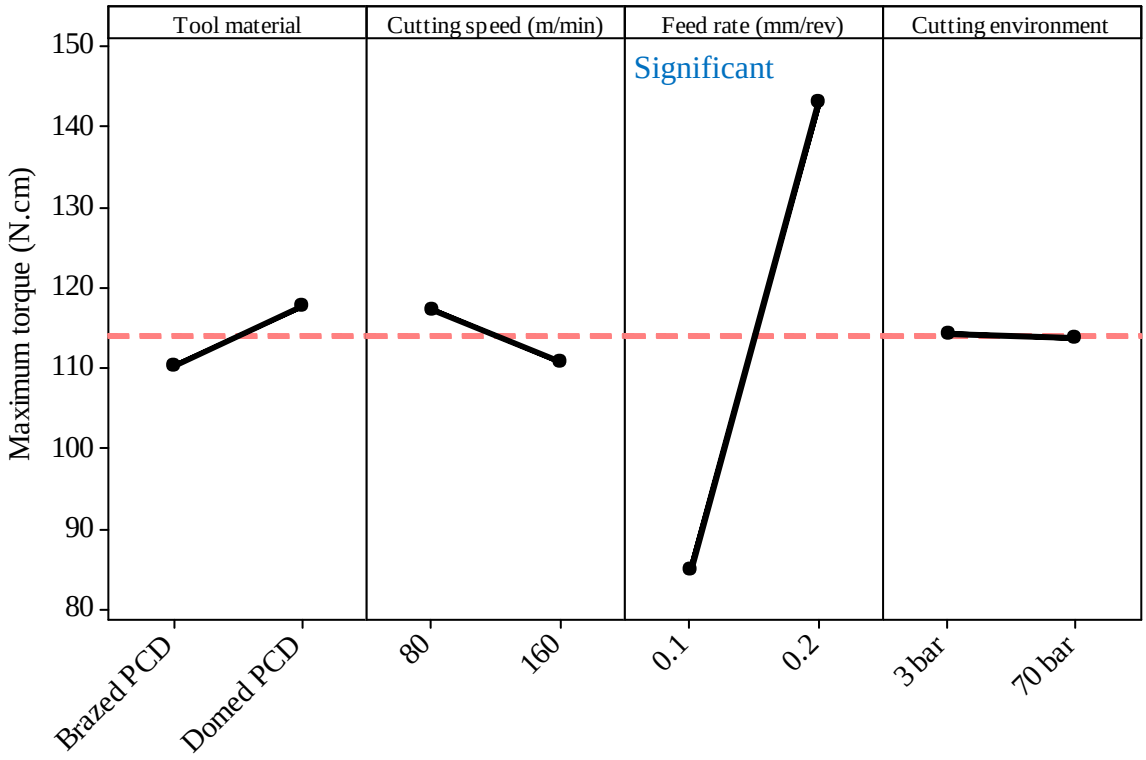


Figure C7: Main effects plot for maximum torque at the first hole in Phase 3B

Table C2: ANOVA results for maximum thrust force at the first hole in Phase 3B

Source	DF	Seq SS	Adj SS	F	P	PCR
Tool material	1	112.5	112.5	3.12	0.175	1.07
Cutting speed (m/min)	1	84.5	84.5	2.35	0.223	0.68
Feed rate (mm/rev)	1	6844.5	6844.5	190.12	0.001*	95.22
Cutting environment	1	0.5	0.5	0.01	0.914	0.00
Error	3	108.0	108.0			3.03%
Total	7	7150.0				

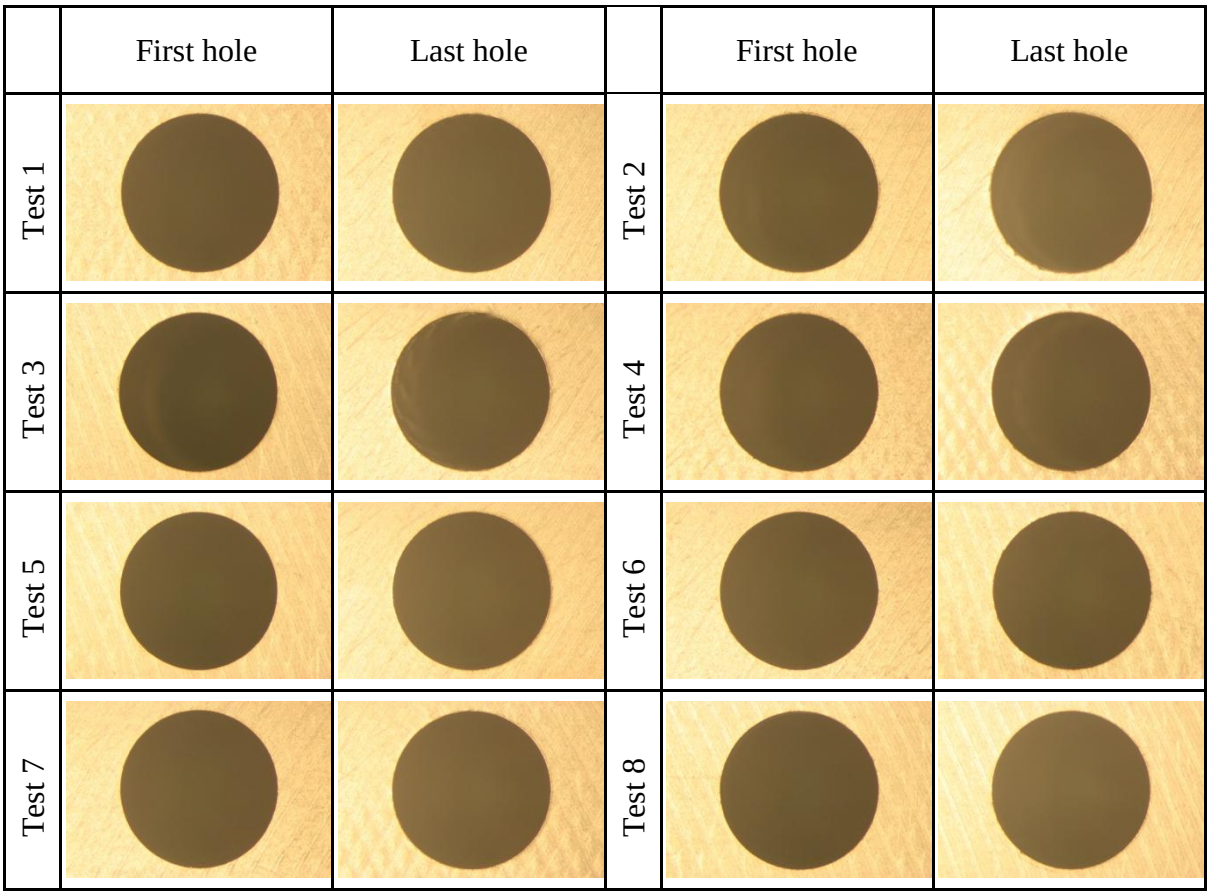


Figure C8: Hole entry quality in all tests in Phase 3B

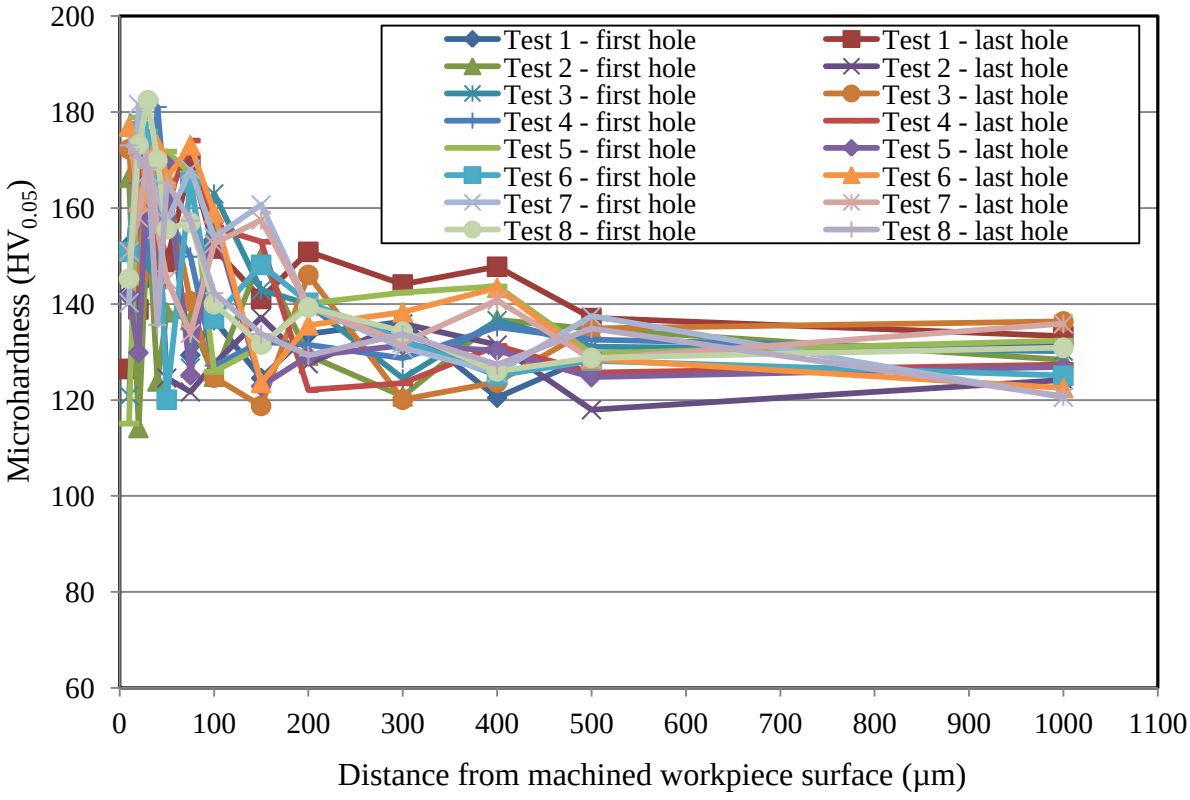


Figure C9: Microhardness results for both the first and last holes (Phase 3B)

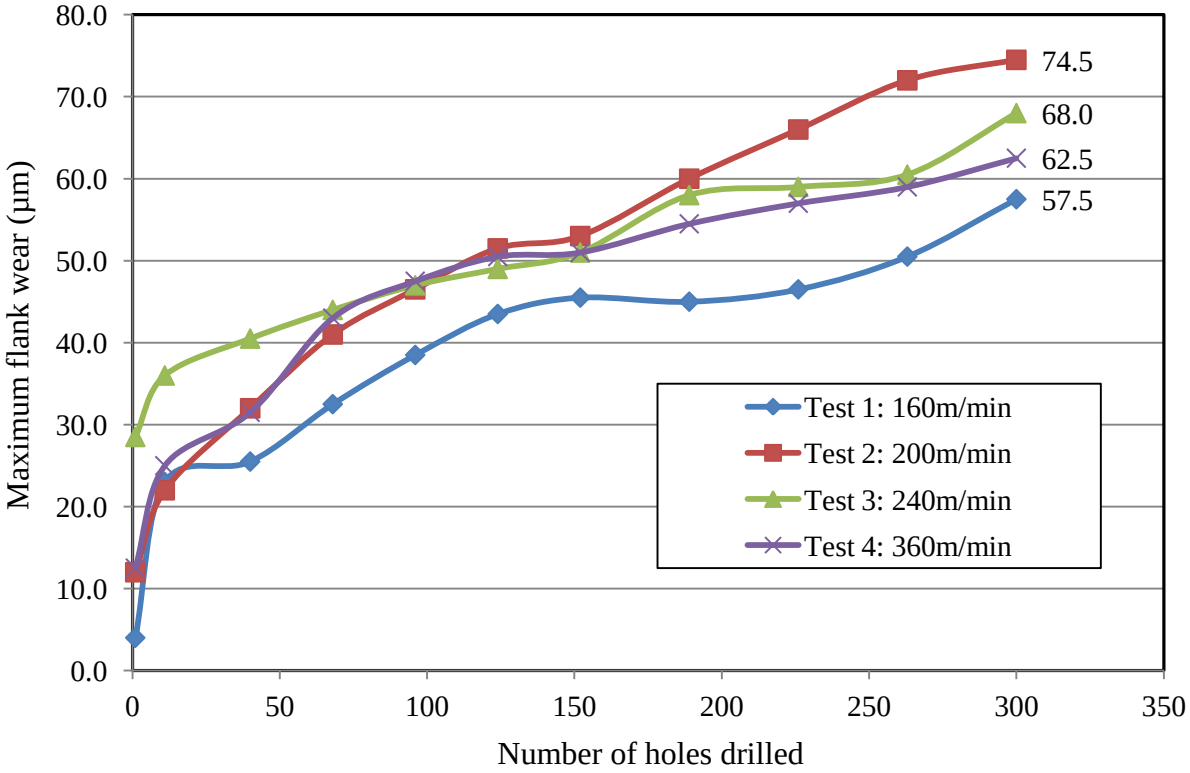


Figure C10: Tool wear progression against number of drilled holes in Phase 3C

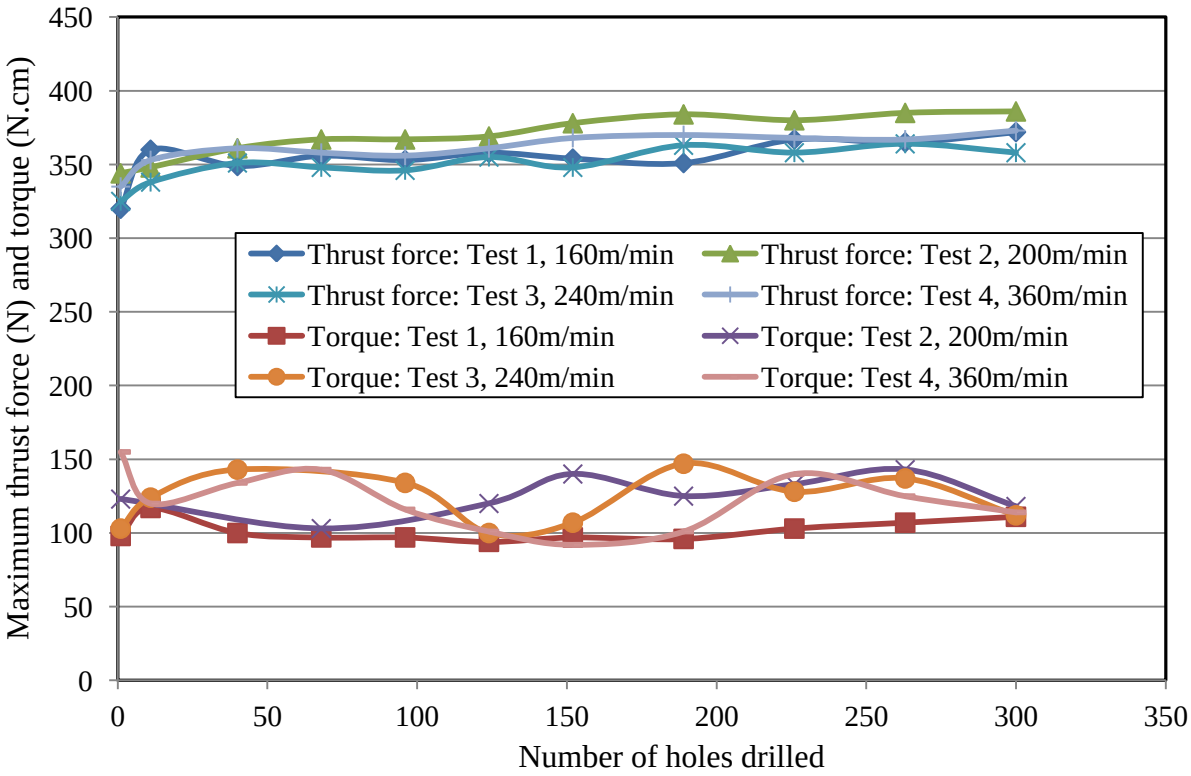


Figure C11: Maximum thrust force and torque progression against number of drilled holes in Phase 3C

APPENDIX D

List of publications

Paper published

M.J. Li, S.L. Soo, D.K. Aspinwall, D. Pearson and W. Leahy

Influence of workpiece configuration and varying feed rate operation on surface integrity when drilling carbon fibre reinforced plastic (CFRP) composites

Procedia CIRP, vol. 13, pp. 399-404, 2014.

M.J. Li, S.L. Soo, D.K. Aspinwall, D. Pearson and W. Leahy

The effect of operating parameters and tool materials on cutter wear/life and hole quality when drilling Al/SiC metal matrix composite (MMC)

Proceedings of the 30th International Manufacturing Conference (IMC30), University College Dublin, Ireland, September 3-4, 2013, pp. 355-364.

Papers under preparation

Influence of operating conditions and tool materials / coatings when drilling CFRP

To be submitted to Composites Part B: Engineering

Effect of fibre orientation and feed rate on surface integrity when drilling CFRP

To be submitted to Composites Science and Technology

Cutting performance and workpiece integrity when drilling CFRP at high speed

To be submitted to International Journal of Advanced Manufacturing Technology

Hole quality assessment when drilling MMC at elevated / high speed

To be submitted to International Journal of Machine Tools and Manufacture